THE UNIVERSITY OF READING

Molecular- genetic analysis of iron uptake in *E. coli*: Role and mechanism of Feo function and structural characterisation of target membrane protein transporter

A thesis submitted for the degree of Doctor of Philosophy

By

SALEM R. ARIAN AL-AIDY

School of Biomedical Sciences

Department/ Microbiology

Reading

United Kingdom

Supervisor: Prof. Simon C. Andrews

March 2020

Declaration

I confirm that this is my own work and that it has not been previously submitted for any dissertation or PhD degree at any other university or institution. The use of all materials from other sources has been properly and fully acknowledged. All drawings not cited are original artwork by the author.

SALEM R. AL-AIDY

Abstract

Iron is essential for the growth of nearly all bacteria. However, it is a dangerous metal because it has the ability to catalyse the generation of reactive oxygen species (ROS) through the Fenton chemistry. The oxidation status of iron in the environment is largely determined by pH and oxygen levels, with the poorly soluble ferric (Fe^{3+}) form persisting with high pH and high O_2, and the more soluble ferrous form (Fe^{2+}) favoured by low pH or low O_2. EfeUOB is a bacterial ferrous-iron transport system, induced by acidic pH aerobically, that exhibits maximal activity under low pH, low-iron conditions. The FeoABC system is also a ferrous-iron transporter, and is widespread in bacteria; it functions during low oxygen conditions, and unlike EfeUOB is not considered to be active aerobically. This study explores the differences in the activities of the two ferrous-iron transporters (Feo and Efe) of *E. coli* in their responses to environmental factors, in particular O_2 and hydrogen peroxide. *E. coli* mutants devoid of iron-transport systems were employed along with low-copy number plasmids, carrying either *efeUOB* or *feoABC* under control of their natural promoters or inducible surrogate promoters.

Results showed that the Feo system exhibits weak activity aerobically, and relatively-strong activity aerobically with reductant; in contrast, Efe shows weak anaerobic and strong aerobic activity. These effects were also apparent when the genes were under control of inducible P*ara* or P*rha* promoters. The difference in O_2 dependence of Feo and Efe appeared to be caused by their distinct responses to H_2O_2, with Feo being activated aerobically by exogenous catalase, and Efe being activated by provision of H_2O_2. ^{55}Fe uptake experiments supported the growth phenotype data, showing that Efe-mediated iron uptake requires H_2O_2 whereas Feo-mediated iron uptake requires the absence of H_2O_2. The results thus indicate that Feo-dependent iron uptake is sensitive to H_2O_2, rather than O_2 as reported previously. It is speculated that the H_2O_2-sensitivity of Feo results from peroxide-mediated oxidation of the three highly-conserved

Abstract

Cys residues in the permease (or 'Gate') domain of FeoB (the predominant Feo component). Indeed, alteration of these residues by site-directed mutagenesis (see below) led to complete loss of activity. Also, a convincing three-dimension model of the FeoB permease domain (based on a Gate-motif-containing nucleoside transporter) indicates that these three Cys residues are closely positioned and line the predicted uptake channel, and are thus well located to act as Fe^{2+} ligands. The H_2O_2 dependence of Efe correlates well with the reported peroxidase activity of EfeB (a periplasmic DyP-peroxidase), and the suggested ferrous-oxidation mechanism of EfeU-like ferric-permease iron-uptake systems (as established for Ftr1p/Fet3p of yeast). H_2O_2 assays clearly showed that the Efe system mediates consumption of H_2O_2 in a strain lacking catalases and alkylhydroperoxidase, further supporting the suggestion that H_2O_2 is required by Efe to oxidise iron prior to EfeU uptake.

Thus, the combined presence of EfeUOB and FeoABC allows ferrous-iron uptake under distinct conditions relating to peroxide abundance; this would thus explain the need for the combined presence of these two alternate ferrous-iron uptake systems in *E. coli* strains, and many other bacteria.

The requirement for FeoA (small, highly conserved, cytoplasmic SH3 protein) and FeoC (small, cytoplasmic winged helix-turn-helix [4Fe-4S] protein, with no apparent role in transcription control, particularly found to be associated with γ-Proteobacteria Feo systems) along with FeoB (cytosolic G-protein domain coupled to a permease domain), was also explored. FeoA was found to be essential, along with FeoB. Although, FeoC was not essential, it did consistently enhance activity of FeoAB under aerobic conditions, particularly with reductant. FLAG-tagged versions of Feo components were generated to enable estimation of their abundance in response to O_2 regime; the addition of the tags did not, generally, affect Feo activity but did enable detection by Western blotting. The results showed that FeoB levels are

Abstract

far higher anaerobically than aerobically – this effect was largely independent of FeoC and the FtsH protease, which contrasts with previous reports in *Salmonella*. .

Nine highly-conserved FeoB residues within the permease domain were altered by SDM. The FeoB-C403S, -C432S, -C677S and -E582Q variants failed to exhibit Feo-enhanced growth under iron restriction indicating an essential role for these residues. These four residues were found to be well positioned to act as Fe^{2+} ligands in a FeoB model structure. In contrast, the FeoB-E488Q mutant retained good Feo activity, although this was slightly reduced with FeoC aerobically, and slightly raised aerobically. This residue is predicted to be located in a cytosolic loop and thus may interact with the N-terminal G-protein domain. The FeoB-C772S/H773G and -C763S/C764S (residues in the C-terminal cytoplasmic subdomain of FeoB) variants showed greater Feo activity in the presence of FeoC, suggesting that this subdomain interferes with FeoC activation of Feo activity under aerobic conditions and that FeoC may interact with the C-terminal subdomain of FeoB. Further work is required to discover how FeoC activates Feo activity aerobically, how FeoB levels are reduced aerobically in an apparent post-translational fashion, whether the conserved FeoB Cys residues are indeed subject to oxidation and what factors influence FeoA activation of FeoB activity. The FeoB protein was overexpressed using a baculovirus system, purified to homogeneity in a monodisperse form and subject to crystallisation.

Dedication

I would like to dedicate all my humble effort,

To engineer of victory of Iraq Imam Ali al-Sistani, to whoever sacrificed for Iraq, to the spirit of my father and to my very kind and supportive mother - without my parents I would not be in a place like this, to my brothers and my sisters to my beloved wife Sagia and my four lovely daughters Yaqeen, Yasmeen, Zainab, Sama and little son Mohammed Reda: for all the care, encouragement and support they provided me with.

Acknowledgements

First, I would like to express my deepest gratitude to my wonderful advisor, Prof. Simon.C. Andrews, for giving me the opportunity to study and develop in his lab, for his guidance, for his endless support, and for the countless opportunities he has provided me with. I would also like to thank my thesis committee, Prof. Rob. Jackson and Dr. Sheila MacIntyre, for the input and support they have provided over the years. I am especially appreciative of Prof. Ian Jones, who provided me with protocols, material and reagents that helped propel my research forward in his lab (tissue culture and virology lab). I am especially appreciative of Dr. Isabel Moraes, who provided me with protocols and reagents that helped propel my research forward in her lab (Membrane protein purification, crystallisation and drug discovery). I would also like to thank the Harwell Complex Research NPL and MPL lab and Diamond light source (Oxford, Uk) for welcoming me when I joined their lab. I am extremely grateful to Dr. Isabel and Dr. Rosana Reis for all of their support throughout 2018, for her encouragement, for troubleshooting with me, for helping me to have a successful experment, and for always listening. I am also especially thankful to Tristan Kwan for his kindness, for his help, I am extremely grateful for the friendships that I started in University of Reading/ Biomedical sciences school. I am especially thankful to Dr. Liam McGuffin for his help in Bioinformatic and Emma Bartram for her help in creation of SDM mutants. I could not imagine going through graduate school with any other lab mate, I will sincerely miss working together. I would also like to thank Simon Feist for his help in Radio active material, for his advice, for all of the workouts, and being there for me through this whole experience.

A very special thank you to my furry family (Simon Iron Lab), Ameer, Aida, Sheama, Dhama, Entedar, Chris, Emma, Laura, Rana, Kang, Fawzi, Fawzia, Zara, Lewis, Ian Norton, Arvind, Amjed, Mohammed, Amer, Andrea, and Wafa their smiling faces made everyday happier. I would also like to thank my family. I am very grateful to my mother, father, brothers and sisters

for their love, encouragement, support, and the innumerable sacrifices they have made for me. Last, but certainly not least, I'd like to thank Sagia, my wife and best friend. She has been my biggest champion and supporter over the years. I could have never done this without her. I am extremely thankful to her for always supporting my dreams, for her sacrifices, for encouraging me everyday, for the home-cooked meals, for taking care of Sama and Mohamed Reda, for all of the weekends She spent in the help with me when we could have been doing anything else, for always making me laugh, for all of her endless patience, for always understanding, listening, and loving me unconditionally. A special thank you to my lovely daughter Yageen, Yasameen, Zainab, Sama and For my beautiful Son Mohammed Reda they make happiness, love for me and continued support, for their encouragement. A special thank you to my Country Iraq, Minsitry of higher Education, University of Wasit, College of Medicine for giving me the opportunity to study PhD and develop my Knowledge. Thank you for all my collegues in Wasit University and all friend who supported me.

Oral and poster presentations

1- Al-Aidy S., Andrews S.C. (2016): Role *efeUOB* and *feoABC* in ferrous-iron uptake: Postgragduate Symposium 1- Thursday 26 May 2016, URS Building. Reading University- Oral presentation.

2- Al-Aidy S., Andrews S.C. (2016): Molecular Analysis of the Mechanisms of Ferrous Iron Transport in *E. coli* The scientific Conference of Reading University-postgraduate research, Doctoral Research Conference 23 June 2016. Poster presentation

3- Al-Aidy S., Andrews S.C. (2016): The effect of pH, under oxic and anoxic conditions, on the ability of *efeUOB* and *feoABC* to support low-iron growth when expressed from inducible promoters: Research AWAY DAY-Tuesday 19 July 2016-Room G01, Building no. 22 on the London Road Campus. Poster presentation

4- Al-Aidy S., Andrews S.C. (2016): ^{55}Fe uptake by FeoABC and EfeUOB: Research day Symposium 1- Thursday 26 August 2016, Chemistry Building. Reading University- Oral presentation

5-Microbiology Society the 2016 Annual Conference will take place 3–6 April at the EICC in Liverpool

6- Al-Aidy S., Chris M., Andrews S.C. (2016): Infelounce H_2O_2 on two ferrous iron transport EfeUOB and FeoABC in *E. coli*: 10th International Biometals Symposium July 10 – 15, 2016 Dresden,Germany (**participated and I got the first prize poster award**)

7- Al-Aidy S., Andrews S.C. (2016): Effect of hydrogen peroxide on FeoABC system in *E. coli*: Metals in Biology BBSRC conference 19-20 December 2016, Durham

8- Al-Aidy S., Andrews S.C. (2017): FeoA and FeoB are required for Feo-mediated iron uptake, and FeoC is required for Ferrous uptake in *E. coli*: Postgragduate Symposium 2-Thursday 9 June 2017, URS Building. Reading University- Oral presentation

9- Al-Aidy S., Andrews S.C. (2017): Compartive charactrasation between two ferrous iron transporters in *E.coli*: Microbiology Society the 2017 Annual Conference will take place 3–6 April at the EICC in Edinburgh. Presented poster.

10- Al-Aidy S., Andrews S.C. (2017): FeoA and FeoC are essential components in FeoABC ferrous iron uptake system of the *E.coli O157*: Infections disease and public health in Surrey University February 27-29 June2017. Presented poster.

11- Al-Aidy S., Gareeb A., Andrews S.C. (2017): Comparative chractrasation between two ferrous iron uptake FeoABC and EfeUOB system in *E.coli:* SEVENTH CONGRESS OF THE INTERNATIONAL BIOIRON conference (BioIron 2017) May 7 – 11, 2017 UCLA Meyer & Renee Luskin Conference Center Los Angeles, California, USA. Presented poster.

12- Al-Aidy S., Andrews S.C. (2017): The EfeUOB transporter is essential for high-affinity acquisition of ferrous iron in *E.coli*. The scientific Conference of Reading University-postgraduate research, 20 June 2017. Presented poster.

13- Al-Aidy S., Andrews S.C. (2017): Influence of H_2O_2 on ferrous iron transport by EfeUOB and FeoABC in *E. coli:* Metalomics annual conference in Vienna, Austria 15-19 August 2017. Presented poster

14- Al-Aidy S., Andrews S.C. (2018): Effect of oxygen and FeoC-status on FeoB protein levels in FeoABC system: Microbiology Society the 2018 Annual Conference will take place 9–13 April at the EICC in Birmingham.

15- Al-Aidy S., Andrews S.C. (2018): Functional analysis of the iron uptake activity of the FeoABC sytem of *E.coli:* 11th International Biometals Symposium July 15 – 19, 2018 Ottawa,Canada. Presented poster.

16- Al-Aidy S., Andrews S.C. (2018): Functional analysis of ferrous iron transport in *E.coli*, the Feo. The Scientific Conference of Reading University-postgraduate research, 20 June 2018 (**participated and I got the first prize poster award**). Presented poster.

17- Al-Aidy S., Andrews S.C. (2019): The importance of nine conserved residues and the C-terminal sub-domain in Feo-mediated iron uptake in *E.coli.* Microbiology Society the 2019 Annual Conference will take place 10–11 April at the EICC in Beldast. Presented poster

18- I got the first prize award of PHD RESEARCHER OF THE YEAR FOR BIOMEDICAL SCIENCES 2018.

The Prize

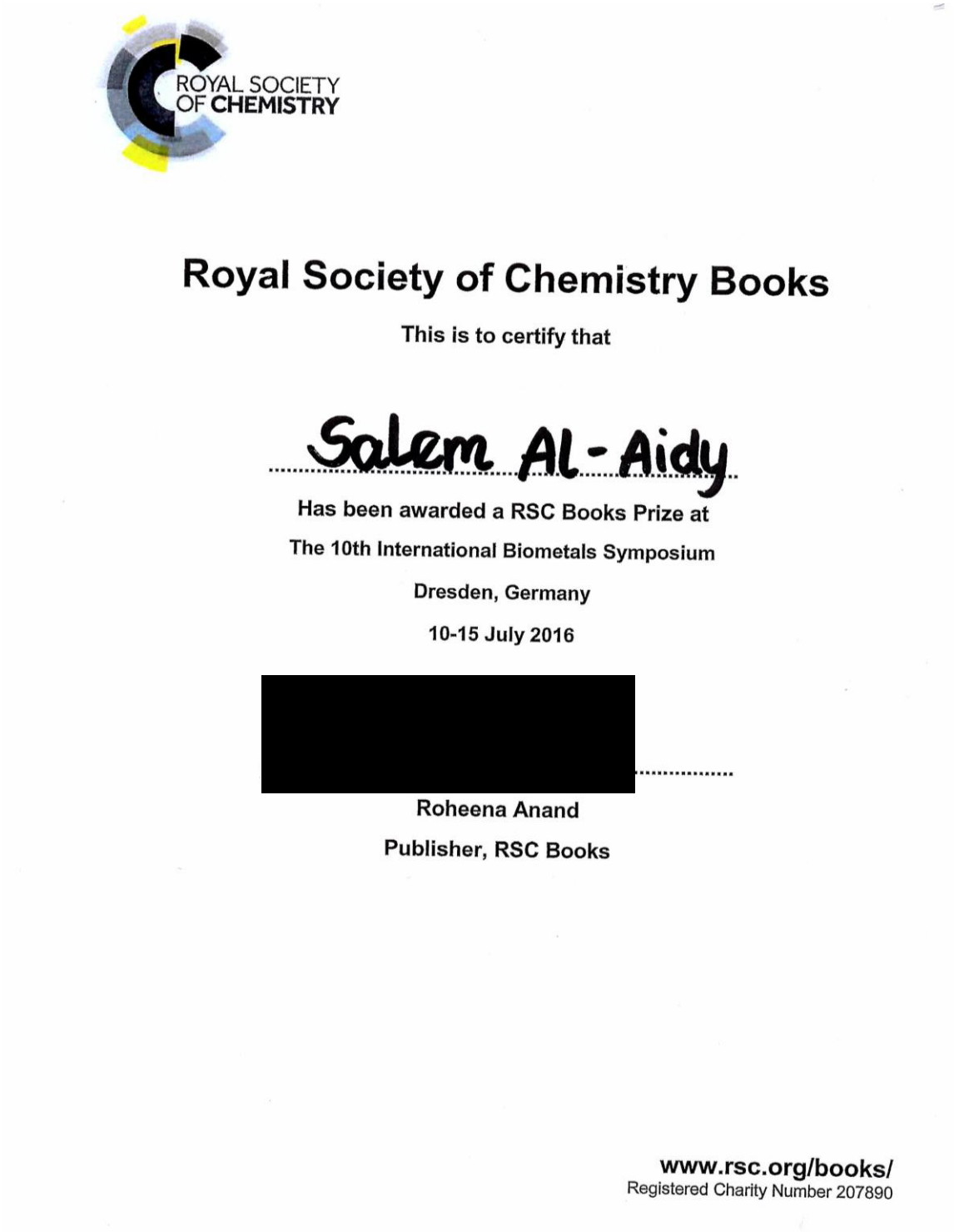

ROYAL SOCIETY OF CHEMISTRY

Royal Society of Chemistry Books

This is to certify that

Salem Al-Aidy

Has been awarded a RSC Books Prize at

The 10th International Biometals Symposium

Dresden, Germany

10-15 July 2016

[redacted]

Roheena Anand

Publisher, RSC Books

www.rsc.org/books/

Registered Charity Number 207890

University of Reading

School of Biological Sciences

PHD RESEARCHER OF THE YEAR FOR BIOMEDICAL SCIENCES

2018

SALEM AL-AIDY

IN RECOGNITION OF YOUR STRONG CONTRIBUTIONS AND ACHIEVEMENTS WITHIN THE DIVISION OF BIOMEDICAL SCIENCES AND BIOMEDICAL ENGINEERING AT

UNIVERSITY OF READING

[redacted]

[redacted]

Prof Robert W Jackson
Head of School
School of Biological Sciences
University of Reading

Dr Simon Clarke
Head of Research Division
Biological Sciences and
Biomedical Engineering
School of Biological Sciences
University of Reading

Contents

Lists of Figures

Lists of Figures

Lists of Figures

Lists of Figures

List of tables

Lists of Tables

Abbreviations

ABC	ATP-binding cassette
ATP	Adenosine triphosphate
Amp	Ampicillin
CHS	Cholestryl hemisuccinate
CMC	Critical micellar concentration
CSC	Critical solubilisation concentration
Conc	Concentration
CM	Cytoplasmic membrane
C12E8	Octaethylene glycol monododecyl ether
CD	Circular dichroism
CV	Column volume
DDM	n-Dodecyl b-D-maltopyranoside
Feo	Ferrous iron transport system
FNR	Fumarate and nitrate reductase
FUR	Ferric uptake regulator
GDI	GDP dissociation inhibitor
GDP	Guanosine diphosphate
GTP	Guanosine triphosphate
HTH	Helix turn helix
DLS	Dynamic light scattering
DDT	dithiotheritol
DTPA	Diethylene triaminepenta acetic acid
Dcytb	the duodenal cytochrome b

Abbreviations

DMT1	divalent-metal transporter-1
EDTA	Ethylene diamino tetra acetic acid
Ent	enterochelin
GFP	Green flourecent protein
HCP1	Haem Carrier Protein 1
Hb	Haemoglobin
IPTG	irsopropyl-thiogalactoside
IM	Inner membrane
LA	Luria-Bertani agar medium
LB	Luria-Bertani medium
LF	lactoferrin
OD	optical density
OD_{600}	Optical density at 600 nanometers
OMRP	outer membrane receptor proteins
OM	outer membrane
PCR	polymerase chain reaction
ROS	reactive oxygen species
M	marker
M9	minimal salts medium on 9 number
TF	transferrin
Tris	Tris (hydroxymethyl) amino methane

Chapter 1. Introduction

1.1. The properties of iron

Iron is an important micronutrient for life, essential for the survival of most organisms. It plays a crucial role in host-pathogen relationships (Andrews *et al*., 2003). It is the fourth most abundant element found in the Earth's crust (Cox *et al.*, 1994; Nam, 2007), and is the sixth most abundant element in the universe (McDonald *et al*., 2010). Naturally occurring iron consists of four isotopes: 5.845% of ^{54}Fe (theoretically very weakly unstable with a half-life over 3.1×10^{22} years), 91.754% ^{56}Fe, 2.119% of ^{57}Fe and 0.282% ^{58}Fe (Dauphas and Rouxel, 2006).

Iron is considered the most significant member of the transition metals; it is the 26th element in the periodic table and its d-orbital is not completely filled. Thus, iron is able to suffer rearrangement of its d-orbital electrons into various spin states, allowing iron to exist in different oxidation states, from –II (e.g. $Fe(CO)_4^{2-}$) to VI (e.g. FeO_4^{2-}). The Fe (II) (d^6) and Fe (III) (d^5), forms are the most common states of iron in biological systems. These various forms are readily inter-convertible allowing iron to contribute in redox reactions (Manahan, 2000).

Under physiological conditions, the reduced Fe^{2+} ferrous and the oxidised Fe^{3+} ferric forms are the most stable states of iron in biological systems. These forms are readily interchangeable allowing iron to metabolically recycle between oxidised and reduced forms which makes iron a useful electron carrier in biological redox reactions (Andrews, 1998). Fe^{3+} is soluble at low pH in aerobic environments whereas Fe^{2+} is more soluble at neutral pH, but is only stable under anaerobic conditions. Many years go, through evolution of the Earth, huge oxidation event was induced by the release of oxygen as a toxic waste product resulting from photosynthetic cyanobacteria leading to conversion of environmental ferrous iron (solubility 0.1 M at pH 7) to insoluble ferric iron (10^{-18} M at pH 7) resulting in inaccessibility of iron for living organisms. Consequently, aerobic organisms have developed various effective iron uptake and storage mechanisms for iron.

1.1.1. Effects of iron overload

Iron is a necessary micro-nutrient. It is essentialy obtained in trace amounts as acquisition of large amounts of iron is toxic, mainly due to the capability of free iron in the living cell to interact with oxygen and oxygen-reduction products to produce toxic products such as hydroxyl radicals ($OH^{\cdot}$) and superoxide (O_2^{-}), known as Reactive Oxygen Species (ROS) (Fig. 1.2) (Cornelis *et al*., 2011). ROS are reactive molecules and free radicals originating from molecular oxygen. ROS are produced as intermediates of metal catalyzed oxidation reactions. Oxygen has two unpaired electrons in separate orbits in its outer electron shell. This electron structure makes oxygen susceptible to radical formation. The sequential reduction of oxygen via the addition of electrons leads to the formation of several ROS: hydrogen peroxide (H_2O_2), superoxide ($\cdot O_2^{-}$), hydroxyl radical ($\cdot OH$), nitric oxide and hydroxyl ion (OH^-) (Figures 1.1).

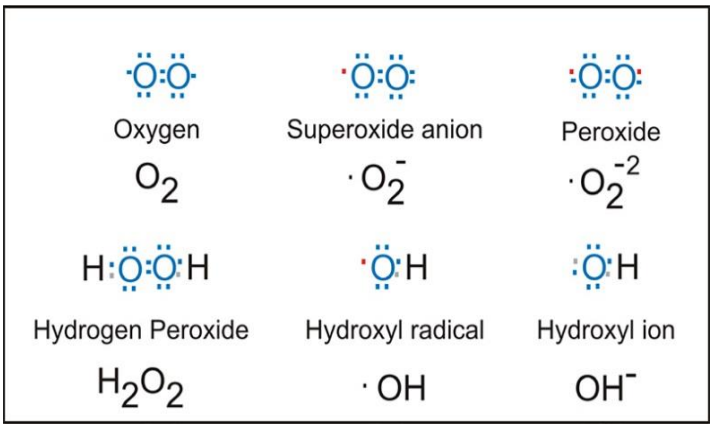

Figure 1.1: Electron structures of common reactive oxygen species. Each structure is provided with its name and chemical formula. The red dot designates an unpaired electron. (Kishmiri and Mankar, 2014)

When iron is present, Fenton chemistry can be activated andthis results in the production of highly ROS ($HO^{\cdot}$) producing an oxidative stress arising due to excess ROS or oxidants exceeding the capability of the cell to achieve an effective antioxidant response. Superoxide mediates the redox cycling of Fe(III) to Fe(II) (Eq III) which, in combination with Eq I, gives

the net Haber-Weiss reaction (Eq II) and the creation of the highly reactive $OH^{\cdot}$ radical catalysed by iron (Ratledge and Dover, 2000; Andrews *et al.,* 2003).

$Fe^{2+} + H_2O_2 \rightarrow Fe^{3+} + OH^- + \cdot OH$ (Eq. I)
$O_2^- + H_2O_2 \rightarrow \cdot OH + OH^- + O_2$ (Eq. II)
$Fe^{3+} + O_2^- \rightarrow Fe^{2+} + O_2$ (Eq. III) (Henle *et al.,* 1996).

Free radical toxicity is demonstrated by the ability of free radicals to irreversibly change and damage numerous cellular components such as pyrimidine and purine bases of DNA, [Fe-S] clusters, specific enzymes (by oxidation of co-factors and protein carbonylation) and amino acid residues (Cys and Met). Likewise, free radicals react with membrane lipids to introduce the free-radical chain reaction known as lipid peroxidation which reduces membrane fluidity, altering membrane properties and subsequently disrupting membrane-bound proteins significantly (Brooker, 2011).

To avoid the devasting affects of ROS, bacteria have established strong homeostatic mechanisms to keep intracellular ferrous levels within safe limits (Andrews *et al*., 2003). Bacteria can express genes which are required for enzymatic defence against ROS, like catalases, superoxide dismutases, alkylhydroperoxidases, peroxidide reductases and superoxide reductases that neutralise free radicals (de Orué Lucana1 *et al.,* 2012).There are three types of bacterial iron storage proteins, the DNA-binding proteins from starved cells (Dps),ferritins and bacterioferritins, which bacteria use to defend themselves from the effects of ROS, by limiting free iron availability. Dps, in particular, consumes H_2O_2 in the oxidation of ferrous iron generating water rather than ROS (Andrews, 2010).

1.1.2. Host iron withholding strategies

The human host limits access to necessary metals as a countermeasure directed at preventing invading pathogenic bacteria from obtaining such essential nutrients; this process is called “nutritional immunity”. Iron is necessary for nearly all bacterial pathogens, and by all

vertebrates, and thus restricting access to iron as a key metal exploits these requirements and serves as a potent defence against infection. The human adult contains an average of 3–5 g of iron. The majority (65–75%) is in the form of haem in haemoglobin, which is further contained within circulating red blood cells. This provides an additional barrier to access by pathogens. Free haemoglobin or haem released from erythrocytes are quickly bound to haptoglobin and haemopexin, respectively. Consequently, for bacterial pathogens to access this rich pool of iron, they need first to lyse erythrocytes, then remove haem from haemoglobin or haemopexin, then liberate the iron from the macrocyclic haem molecule. Furthermore, mammals diminish the concentration of free iron by increasing the level of iron-binding proteins such as lactoferrin and increasing iron storage. In the serum at physiological pH, extracellular ferrous form (Fe^{2+}) is oxidized to the insoluble ferric form which is bound by transferrin. Free ferric iron is also chelated by lactoferrin, a globular glycoprotein (similar to transferrin) that is present in secretions such as saliva, tears and breast milk. Also, transferrin in serum is never fully saturated with iron (Aisen *et al*. 2001) with only around 30–40% of its capability occupied; this ensures that the availability of free iron remains limited, as this protein is continuously capable of sequestering any extra iron that can arise in the blood or other fluids during infection to maintain constant iron-depletion conditions within the host (Skaar, 2010).

1.2. The role of iron in biological system

Living organisms can gain their nutrient requirement from the environment by passive diffusion, however, cannot do so for iron mainly because iron is accessible at very low concentration (10^{-18}M) at pH 7. It is therefore necessary for bacteria to obtain this element by utilizing active uptake systems (Ratledge and Dover, 2000). The significance of iron lies in its key role in many metabolic mechnisms such that it is required for growth of almost all organisms (Cornelis and Andrews, 2010). Iron is crucial to sustain essential cellular functions

and biological processes such as DNA biosynthesis, transport and storage of oxygen, photosynthesis, gene regulation and respiration, H_2 consumption and production, methanogenesis and N_2 fixation (Andrews *et al.*, 2003). For this reason, iron appears to be incorporated into many proteins where it generally acts as a cofactor (Table 1.1) (Andrews *et al*., 1998). Important iron-containing proteins in bacteria and humans are haem-containing proteins. Proteins containing haem participate in a range of metabolic functions including complex reactions such as oxygen activation carried out by cytochrome oxidase, and consumption of H_2O_2 by catalases and peroxide reductases (Joe and Hargeove. 2007). Iron always exists in its poorly soluble Fe^{3+} form at high pH (>7) under oxygenic conditions. Iron is also incorporated as Fe-S clusters and mono- and dinuclear ions. Iron thus provides a role as a cofactor for many proteins (Schaible and Kaufmann, 2004). For example, Fe-S clusters (Fig 1.2) abound in many redox enzymes, particularly membrane-bound respiratory systems (e.g. complex 1) where it is implicitly presumed that its major role is to mediate long-range electron transfer (Andrews *et al*., 2003; Faraldo-Gomez *et al*., 2003). Iron-sulphur clusters are common iron-containing molecules associated with fundamental life processes, they are present in many metallo-proteins like: ferredoxin, an electron transport protein; NADH dehydrogenase, involved in respiration; hydrogenases, that catalyse production or consumption of H_2 ; and nitrogenase, required for nitrogen fixation (Beinert, 2000). Three distinct forms of Fe–S clusters are commonly found. 2Fe-2S, 3Fe-4S and 4Fe-4S forms (Nakajima *et al*., 2010), where the latter is the most common form. The Fe^{2+}/Fe^{3+} oxidation potential spans from approximately -300 to +700 mV allowing iron to take part in a wide range of redox reactions.

Very few organisms do not depend on iron, these include *Lactobacillus* (Archibald, 1983; Weinberg, 1997), *Borrelia burgdorferi* that causes Lyme disease (Posey and Gherardini, 2000), and *Treponema pallidum* which causes syphilis. Despite the iron-independent status of the latter two, because of their compulsory lifestyle within cells they both rely on an iron-dependent host for survival (Andrews *et al*., 2003).

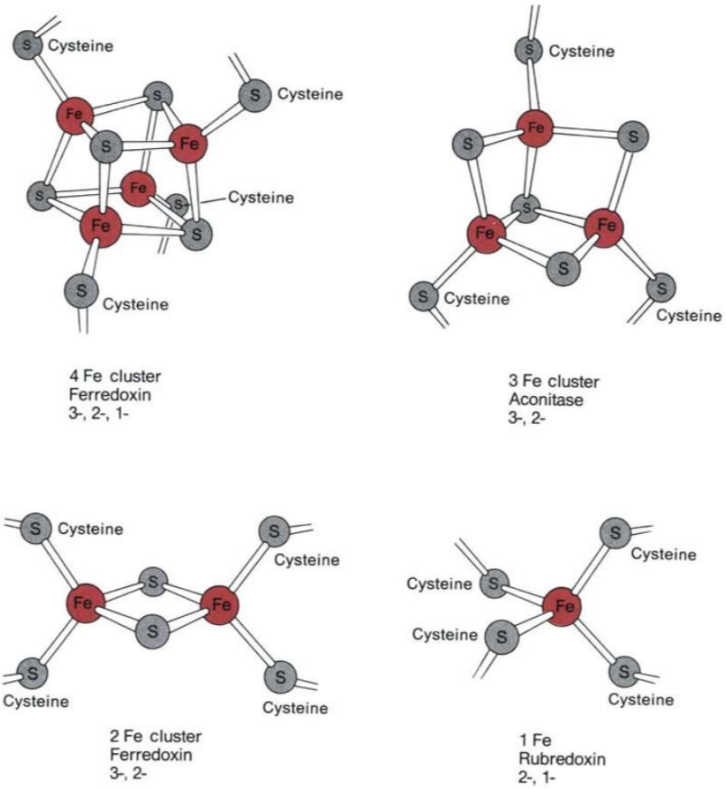

Figure 1.2. Structure of Fe-S clusters. Range of iron-sulphur clusters are shown (from Lippard and Berg, 1994).

Table 1.1. Biological processes of iron-containing proteins

Biological processes	Iron-containing proteins
Respiration	**Cytochromes, cytochrome oxidase and ferredoxins**
Amino-acid and pyrimidine biosynthesis	**Dihydrogenase, dihydro-orotate and glutamate synthetase**
The citric acid cycle	**Fumarase, aconitase and succinate dehydrogenase**
Degradation of hydrogen peroxide and superoxide	**Haem-catalases, peroxidase and iron-superoxide dismutase**
DNA synthesis .	**Ribonucleotide reductase**
Nitrogen fixation	**Nitrogenase.**
Gene regulation	**FNR, SoxR, CooA, PerR, Fur.**
Photosynthesis	**Light-harvesting complexes ferredoxin.**
Carbon fixation	**Methane monooxygenase**
Light-harvesting complexes ferredoxin.	**Photosynthesis**
Globins.	**Oxygen binding and NO detoxification**
FNR, SoxR, CooA, PerR, Fur.	**Gene regulation**

Adapted from (Andrews, 1998).

1.3. Mechanisms for resisting iron and ROS

To avoid the destructive effects of ROS (described above), many bacteria have developed strong homeostatic systems to keep intracellular Fe^{2+} concentration at safe levels (Andrews *et al*., 2003). The main strategy of bacterial defence against ROS involves consumption of oxygen species (superoxide and hydrogen peroxide) (Carrondo, 2003; Chiancone *et al*., 2004). Bacteria express a number of genes required for enzymatic defence against ROS (Nystrom-Lahti *et al*., 1996).

1.3.1. Iron and oxidative stress defence in Bacteria

Specific resistance to oxidative stress is mediated by a number of enzymes including catalase, peroxidase and superoxide dismutase (SOD). SOD is present in many bacteria and decreases intracellular superoxide (O_{2-}) to an acceptable level (Imlay and Fridovich, 1991). SOD catalyses the breakdown of superoxide to H_2O_2 and O_2. There are a number of types of SOD distinguished on the metal cofactor employed: nickel, copper-zinc, manganese or iron (van Vliet *et al*., 2002). Mutations causing loss of SOD lead to increased DNA damage and subsequent cell death (Carlioz and Touati, 1986; Farr *et al*., 1986; Nakayama, 1992). Such damage is exacerbated by iron, as cell-permeable iron chelators prevent cell death induced by superoxide (Imlay and Linn, 1988). *E. coli* has a regulatory system, SoxRS, that controls the response to superoxide and redox cycling agants. The *soxRS* genes are divergently transcribed and induce expression of oxidative stress defence (Chan and Weiss, 1987; Tsaneva and Weiss, 1990; Bauer *et al*., 1999) by a two-stage transcriptional activation. SoxS binds to the promoter regions of target genes inducing their expression (Amabile-Cuevas and Demple, 1991; Fawcett and Wolf, 1994; Li and Demple, 1994; Li and Demple, 1996). SoxR, a redox sensing protein, induces SoxS transcription in the presence of superoxide or redox-cycling agents (Tsaneva and Weiss, 1990; Amabile-Cuevas and Demple, 1991; Wu and Weiss, 1991; Nunoshiba *et al*., 1992; Wu and Weiss, 1992). SoxR also senses superoxide via an Fe-S centre which is normally reduced. Upon encountering superoxide, the iron sulphur centre becomes oxidise; only oxidised SoxR is capable of activating *soxS* transcription (Ding *et al*., 1996; Gaudu and Weiss, 1996; Bradley *et al*., 1997; Ding and Demple, 1997).

Peroxidases and catalases are produced by several bacteria and they function via converting H_2O_2 (produced by aerobic growth or superoxide dismutation) to H_2O (and O_2, for catalases). Inactivation of peroxides is important as they play a key role in the formation of hydroxyl radicals (see above). Most obligate anaerobes do not synthesise these enzymes, but almost all

aerobes and facultative anaerobes do (McCord *et al*., 1971). *E. coli* possesses two catalases, encoded by *katG* and *katE*. Hydroperoxidase I (HPI) is encoded by *katG* and is a bifunctional catalase-peroxidase. Encoded by *katE*, hydroperoxidase II (HPII) is a monofunctional catalase (Clairborne and Fricovich, 1979; Clairborne *et al*., 1979; Loewen *et al*., 1985).

Regulation of hydrogen peroxide induced oxidative stress responses is achieved in *E. coli* and *Salmonella* spp. by the transcription factor OxyR (Christman *et al*., 1985; Morgan *et al*., 1986; Storz *et al*., 1987). OxyR regulates a number of genes including *katG, ahpC* and *ahpF*. The genes *ahpC* and *ahpF* encode alkyl hydroperoxide reductase that reduces hydroperoxides to alcohols using NADP/NADPH as an electron donor (Storz *et al*., 1989; Altuvia *et al*., 1994; Zheng *et al*., 2001a; Zheng *et al*., 2001b). A pair of redox-sensitive Cys residues in OxyR sense oxidants directly. Upon exposure to H_2O_2, oxidised OxyR will induce transcription by interacting directly with RNA polymerase at cognate promoters to induce transcription (Zheng *et al*., 1998; Choi *et al*., 2001). As well as activating the expression of a number of genes, OxyR is subject to negatively autoregulation (Christman *et al*., 1989; Tartaglia *et al*., 1989) and is reduced, and therefore inactivated, by GrxA (glutaredoxin 1), a member of the regulon, allowing negative feedback (Zheng *et al*., 1998; Åslund *et al*., 1999). As well as OxyR, *E. coli* also regulates production of a small RNA, OxyS, upon exposure to H_2O_2. Abundant and stable, OxyS acts as a regulator, activating and repressing gene expression and reducing mutation rates (Altuvia *et al*., 1997).

1.3.1.1. Natural resistance-associated macrophage proteins (Nramp)

Nramp is a type of host protein that is generated by macrophages where it permits change in cellular iron concentrations (Wardrop and Richardson, 1999). Nramp1 acts to remove and obtain iron from transferrin (Tf), enhancing intracellular iron levels within the macrophage in response to infection by phagosomal pathogens (Skamene *et al*., 1998; Canonne-Hergaux *et al*.,

1999; Kuhn *et al*., 1999). The build up of iron within the macrophage results in the creation of toxic ROS (Zwilling *et al*., 1999).

Nramp1 (Slc11a1) influences the course of its infection by *Salmonella enterica* serovar Typhmurum and certain species of *Leishmania* and *Mycobacterium* (Atkinson *et al*., 1997; Blackwell *et al*., 2003). Even though these pathogens are taxonomically unrelated, they share the features of infecting macrophages, occupying phagolysosomes and relying on iron. Nramp1 is integrated into the phagolysosomal membrane and exports iron and other divalent ions out of this compartment, consequently diminishing iron availability for phagocytosed microbes (Jabado *et al*., 2000; Fritsche *et al*., 2007; Valdez *et al*., 2008). Mice with mutations in the Nramp1 gene are more susceptible to macrophage pathogens such as *S. typhimurium*.

1.4. Mammalian and iron system

In the mammalian system, iron nutrition requires iron uptake into the epithelial cells lining the duodenum and jejunum through active transport. Furthermore, iron absorbed into the blood directly if required e.g. for formation into erythrocytes, where it is transfered and bound to Tf, then passed into tissues, e.g. the bone marrow. If iron is not directly needed, it remains in the epithelial cells within ferritin (Crichton et al., 2002). The normal daily intake of iron in man is between 15-20 mg but only 1-2 mg is absorbed into the body. The proportion of dietary iron absorbed is regulated in response to various factors, in particular body iron status (i.e. the requirement of the body for iron). This homeostasis control helps to ensure that an adequate amount of iron is maintained to prevent complications such as anaemia, whilst avoiding toxic iron overlaod (Sherwood, 1997, Mu˜noz *et al*., 2012; Maukonen and Saarela, 2015).

1.4.1. Iron in the human host

Iron is essential for humans. Excessive iron will cause organ dysfunction through the creation of ROS whereas low, inadequate body iron levels will result in anaemia, reduced growth and cognitive development, and is a problem that is widespread, affecting half a billion people worldwide (Abbaspour *et al*., 2014). The typical amount of body iron is ~3–5 g, twothirds of which is incorporated into haemoglobin of red blood cells (RBC) which it is recycled every 120 days during RBC turnover. Most of the remainder (~20-30%) is stored in ferritin/haemosiderin, whereas only 1–2 mg of iron per day are absorbed in the intestinal tract and circulated in the blood. There is a sophisticated equilibrium of human body iron uptake for storage and transport. Several factors regulate body iron homeostasis including hepcidin. Hepcidin is a protein that in humans is encoded by the HAMP gene. It is a crucial regulator of the entry of iron into the circulation of the human body (Kohgo *et al*., 2008). Iron is not freely obtainable in the host environment, unlike elements such as nitrogen, carbon, magnesium, phosphate and potassium (Ratledge and Dover, 2000). In man, excess is stored as ferritin iron. The LIP (labile iron pool) is present within cells in order to facilitate biological actions involving iron atoms, and the LIP can become cytotoxic or carcinogenic when the concentration exceeds the protective capacity of ferritin. Most of the LIP is free ferric iron bound to citrate or adenosine diphosphate, and a small amount of LIP is reduced to ferrous iron, which can take part in the Fenton reaction (section 1.1.1). Iron toxicity is developed thorough the production of ROS (as discussed above) while increased iron concentrations may affect cell function by stimulating ROS (Harrison and Arosio, 1996). Free iron, non-Tf-bound iron, and labile plasma iron in the circulation, and the LIP within the cells, are responsible for iron toxicity. The characteristic features of advanced iron overload are failure of vital organs such as liver and heart in addition to endocrine dysfunctions. For the estimation of body iron, there are direct and indirect methods available. Serum ferritin is the most useful and widely available modality, even though its specificity is occasionally a problem. The

widely used application of iron chelators with high compliance resolves problems of organ dysfunction by excess iron and improves patient outcomes (Kohgo *et al*.,2008). In mammals, iron homeostasis is accurately controlled such that extracellular iron is made unavailable as host iron availability has a significant role in the relationship between the host and pathogen. For invasive pathogens, effective iron acquisition from the host is a pre-requisite.

Iron is transported in the blood by Tf (Ratledge and Dover, 2000). The basic characteristics of Tf and the related glycoproteins lactoferrin (Lf) and ovotransferrin (oTf) are that they are iron-binding proteins which are glycosylated, bi-lobed, monomeric proteins of around 80 kDa. They possess similar N- and C-terminal regions, each containing two domains which are isolated by an iron-binding cleft. Each protein reversibly binds two atoms of Fe^{3+} in combination with two bicarbonate anions, which permit coordination of the Fe^{3+} in the binding cleft (Abdallah & El Hage Chahine, 2000). In the intestine, iron may be presented as either Fe^{2+} or Fe^{3+} according to the pH and oxygen level. Inside the intestinal lumen the environment is anaerobic, which favours Fe^{2+} rather than Fe^{3+}. When closer to the intestinal mucosa, there is a more oxidative environment, resulting in an increase in Fe^{3+} (Wooldridge and van Vliet, 2005). On the surface of the intestine, iron can be reduced from Fe^{3+} to Fe^{2+} by the duodenal cytochrome b (Dcytb). The reduced iron is then taken up through intestinal cells by a permease, the divalent-metal transporter-1 (DMT1), which permits the passage of Fe^{2+} into the cytoplasm (Hentze *et al*., 2004, Schaible & Kaufmann, 2004).

Even though the sum of iron extracted from the diet is small, the regulation of the intestinal absorption of iron is serious because humans have no physiologic pathway for excretion. Enterocytes lining the absorptive villi close to the gastroduodenal junction are responsible for all iron absorption. Iron must pass from the gut lumen through the apical and basolateral membranes of the enterocyte to reach the plasma. Iron obtained from food is not bound to Tf, and there is no role for Tf within the lumen of the intestine. Instead, the low pH of the gastric effluent helps dissolve ingested iron and provides a proton-rich milieu. This facilitates enzymatic reduction of

ferric iron to its ferrous form by the brush border ferri reductase. DMT1 (formerly called Nramp2 or DCT1) transfers ferrous iron across the apical membrane and into the cell through a proton-coupled process (Fig 1.3). DMT1 is not specific to iron; it can transport a wide variety of divalent metal ions, including manganese, cobalt, copper, zinc, cadmium and lead. Haem iron is taken up by a separate process that is not well characterized (Srirama *et al*., 2008; Zheng and Monnot, 2012).

As Fe^{2+} passes into the blood, it is oxidized to Fe^{3+} by the intestinal membrane oxidase, hephaestin, or an oxidase found in plasma, ceruloplasmin, which permits binding to Tf, that then transports iron throughout the body. The absorption of iron from Tf by host cells takes place through receptor-mediated endocytosis. Ferri-Tf binds to the Tf receptor on the cell surface. Once internalized within endocytic vesicles, the vesicle is acidified, and iron is removed and released from Tf and then delivered to the cytoplasm by DMT1, where excess iron is stored through ferritin (Hentze *et al*., 2004).

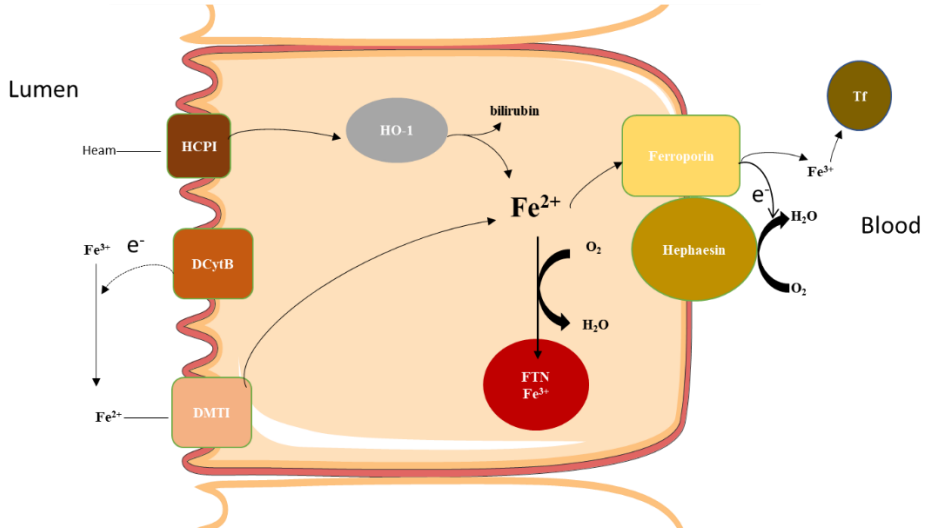

Figure 1.3: Summary of iron uptake from the gut lumen in warm-blooded vertebrates. It was suggested that dietary haem is taken up by the Haem Carrier Protein 1 (HCP1) and is subsequently oxidised by haem oxygenase 1 (HO-1) to give free Fe^{2+}; however, this suggestion is not now accepted (Latunde-Dada *et al*., 2006). Non-haem iron is reduced by DCytb, a cytochrome b reductase, at the cell surface, and is then taken up by DMT1, a Fe^{2+} transport protein. The ferrous iron taken up into the duodenal enterocyte is either kept in ferritin or delivered out of the cell through a complex of ferroporin with hephaesin, during which the iron is oxidised back to the ferric form. The ferric iron is inserted into Tf for transport in the blood (adapted from Edison *et al*., 2008).

1.4.2. The relation between iron and immunity

The association between microorganism virulence and iron was established in the 1960's (Bullen *et al*., 1967; Weinberg, 1978) when iron was found to play a crucial role in innate immune defence. One of the first innate immune responses to infection in mammalian hosts is to use regulatory strategies to control the level of bioavailable iron to invading organisms (nutritional immunity) by sequestration of iron into macrophages, enterocytes, hepatocytes and proteins (such as Tf) with a concomitant reduction of dietary iron absorption (Ganz, 2008; Chu *et al*., 2010; Coffey and Ganz, 2017). In response, bacteria use high-affinity sequestration and uptake systems to fulfill their iron requirements (Ganz, 2008). There are different opinions regarding the role of host iron sequestration merely as a bacteriostatic process that inhibits bacterial growth passively or as true component of the immune system (Brock *et al*., 1983;

Porto and Sousa, 2007). However, it has observed during infection neutrophils secrete Lf, following de-granulation of secondary specific granules, to actively sequester free iron and that in addition to iron chelation, Lf also has bactericidal properties (Kuby, 1997; Woodman *et al*., 2018). This clearly suggests an immunological role for iron sequestering molecules during a bacterial infection.

1.4.3. Iron acquisition by bacterial pathogens in the host

Typically, bacterial organisms (e.g. *Escherichia coli*) require 0.3–1.8 μM of iron for optimal growth, whereas the concentration of free iron is only 10^{-9} μM in mammalian blood (Vasil, 1999). Therefore, bacterial pathogens must employ strategies to circumvent nutritional immunity. Iron acquisition in bacterial pathogens can be generally divided into three major approaches: the production and use of iron-sequestering compounds or siderophores; haem uptake; and uptake of free Fe^{2+}. Siderophores are low molecular weight iron chelators which bind ferric iron with high affinity that surpasses that of Lf and Tf. This approach does not require direct contact as siderophores are free to diffuse within the external medium.

Haem acquisition systems typically involve the expression of cell surface receptors designed for haem either in free from or bound to proteins (haemoglobin, haemopexin and haemoglobin-haptoglobin), which pass haem through a membrane transport system into the cytoplasm (Figure 1.4). There are several well-characterized systems in Gram-negative bacteria, for example, the HemR-HemSTUV system in *Yersinia enterocolitica* (Stojiljkovic and Hantke, 1992), the HmuRSTUV system in *Yersinia pestis* (Hornung and Jones, 1996), ShuASTUV system of *Shigella dysenteriae* (Eakanunkul *et al*., 2005), and the PhuRSTUVW system in *Pseudomonas aeruginosa* (Lansky *et al*., 2006).

In addition, some Gram-negative pathogens e.g. *Neisseria* spp., *Morexella catarrhalis* and *Haemophilus influenzae* can produce receptors for host Fe-binding proteins such as Tf and/or Lf.

These TonB-dependent receptors mediate the uptake of Tf/Lf iron at the cell surface (Figure.1.4), without Lf/Tf internalisation (Cassat and Skaar 2013). *Actinobacillus pleuropneumoniae* mutants that lack the surface Tf receptors, TbpB and TbpA (responsible for extraction of iron from porcine Tf) are unable to generate pneumonia symptoms in pigs (Moraes *et al*., 2009) indicating that both receptor proteins are essential for survival within the porcine lung. Other pathogens, e.g. *Neisseria meninitidis*, are able utilise the host ferritin as an iron source (Larson *et al*., 2004).

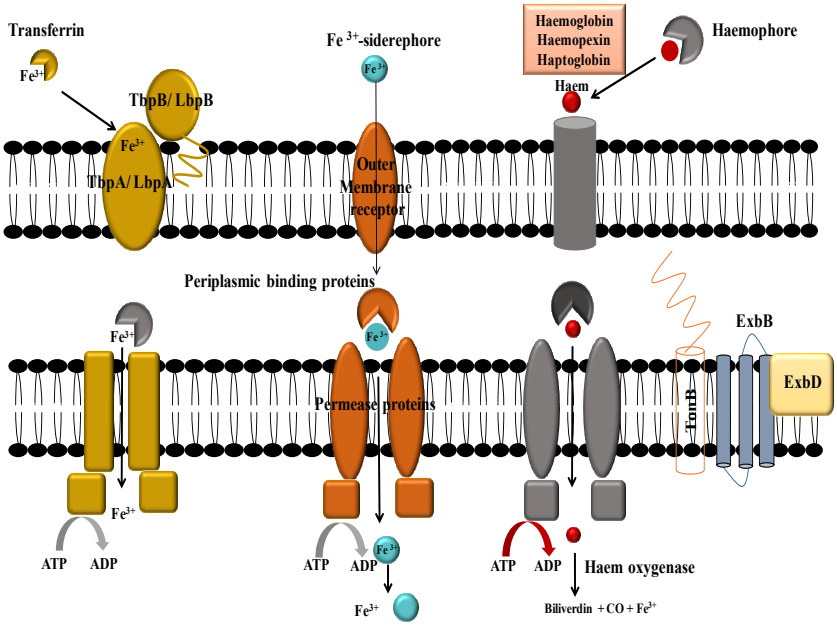

Figure 1.4: Schematic representation of ferric iron acquisition systems in Gram-negative bacteria. This schematic representation displays three uptake pathways for Tf/Lf, siderophores and haem. All these pathways require an outer membrane (OM) receptor, a periplasmic-binding protein and a cytoplasmic-membrane ABC transporter. Uptake through the OM receptors require energy derived from the TonB-ExbB-ExbD complex localised in the inner cytoplasmic membrane (not shown). Ferric iron is releases from siderophores in the cytoplasm as they are reduced into ferrous by the action of ferric reductase enzyme or degraded. Adapted from Andrews *et al*. (2003).

1.5. Bacterial Iron Upake and Pathogenicity

1.5.1. The relation between iron uptake and bacterial pathogenicity

Aerobically, iron has limited accessibility and can be toxic, because of ROS resulting from harmful Fenton chemistry (Touati *et al*.,2000). Large amounts of iron thus lead to protein, lipid and DNA damage that can cause cellular death. So, iron homeostasis is crucial in keeping the balance between meeting iron requirements and reducing iron-triggered toxicity. Iron homeostasis is maintained through numerous means: high-affinity transport systems, supply from iron stores such as bacterioferritin and ferritin, iron detoxification through redox stress-resistance, Fur-mediated down-regulation of iron-dependent proteins (iron rationing) and expression of non-iron dependent (replacement) isoenzymes when iron is inadequate (Andrews *et al*., 2003).

Pathogens use a number of mechanisms for acquisition of iron from the host, and the release of siderophores is considered to be the most important (Neilands, 1982; Andrews *et al*., 2003), since siderophores are able to extract iron from host proteins. However, the generation of siderophores is not necessary in some bacterial pathogens for iron acquisition. For instance, as indicated above, *Haemophilus influenzae* and *Neisseria* spp. use Tf and Lf directly from the host as a source of iron (Khan *et al.,* 2007).

The well-known bacterial siderophore enterochelin is generated by *E. coli* and *Salmonella* spp. However, in the human host it is bound to the host protein lipocalin 2 (Goetz *et al*., 2002) and this represents an important event in the innate immune reaction against bacterial infection (Flo *et al*., 2004). As a host defense strategy against the invading bacteria, the host immune response stimulates the transcription, translation and secretion of lipocalin 2, this reduces bacterial growth by sequestering certain iron encumbered siderophores (such as enterochelin) secreted by the bacteria to scavenge iron (Flo *et al*., 2004, Zughaier and Cornelis, 2018). Bacterial pathogens often respond to iron-scare conditions by upregulating iron-uptake systems and

virulence genes (Zughaier *et al*., 2014). Fur is the transcription factor that upregulates virulence factors in many bacteria in response to iron restriction (Ochsner and Vasil, 1996; Hassett *et al*., 1996). For example, in toxigenic strains of *E. coli* the lack of iron induces the production of enterotoxins (labile-toxin, shiga-toxin and shiga-like toxins 1 and 2) which illustrates the direct correlation between iron availability and expression of virulence factors (Calderwood and Mekalanos, 1987; Weinstein *et al*, 1988).

1.5.2. Heam as an iron source

As indicated above, iron can also be obtained by pathogenic bacteria directly from haem or from haem-bound to host proteins (Arnoux *et al*., 1999; Perry & Brubaker, 1979). For instance, enterohemorrhagic *E. coli* (EHEC) O157:H7 is able to take advantage of haem from haemoglobin (Torres & Payne, 1997). Some pathogenic bacteria, like *Serratia marcescens*, secrete haemophores (as mentioned above), which remove haem from haemoglobin and transport it to specific receptors on the surface of the bacterium allowing its iron to be liberated in the cytoplasm (once internalised) for utilisation by the pathogen.

The Has system (haemophore-dependent haem acquisition system) of *Y. pestis* (also found in other pathogens) is involved in haem and haemoglobin uptake. It is composed of the HasR receptor gene, the HasA haemophore gene, and genes (*hasDE*) encoding components of the HasA-devoted ABC transporter. Haem-loaded HasA supplies haem to the OM receptor HasR (Krieg *et al*., 2009), in addition, a TonB homologue called HasB, is required. After binding, haem is moved through the OM by a TonB-ExbB-ExbD dependent process by which energy derived from the pmf of the CM is transduced to the OM receptor (Benevides-Matos *et al*., 2008; Rossi *et al*., 2001). The HasA haemophore functions through association with the OM receptor HasR, for haem uptake. HasR can obtain free haem and Hb-bound haem directly without HasA assistance, but at lower affinity than when the HasA protein acts to deliver heam to HasR (Ghigo

et al., 1997). Although commensal *E. coli* K-12 lacks the capacity to uptake haem into the cell, more pathogenic strains such as *E. coli* O157 and *Shigella* can utilise haem as a source of iron (Cornellis and Andrews, 2010). In *E. coli* O157:H7 this ability requires a TonB-dependent OM receptor (69 kDa), which is the product of *chuA* (*E. coli* haem-utilization gene) induced in conditions of iron scarcity (Torres and Payne, 1997). The heam uptake system has features of the siderophore transporters and is composed of a TonB-dependent OM receptor, a periplasmic-binding protein and cytoplasmic-membrane ABC permease (ChuTUV) (Cornell and Andrews, 2010). The iron is released by haem degradation through the action of haem oxygenase (Genco and Dixon, 2001).

In *E. coli*, the periplasmic EfeB is reported to remove iron from haem which allows access to the liberated iron for growth (Létoffé *et al*., 2009).

1.5.3. Tf/Lf as an iron source

As indicated above, Gram-negative bacteria can utilise ferric iron from Tf and Lf independently of siderophores; the transporters involved have been identified in a number of pathogens including *H. influenza, N. gonorrheae* and *N. meningitidis* (Fig. 1.5). The uptake systems include OM receptors for Tf and Lf, TfR and LfR. The energy needed for traslocation Tf/Lf-iron across the OM are provided from the TonB system (Figure 1.4) (Anderson *et al*., 1994). The receptors consist of the two proteins TbpA and TbpB for TfR, and LbpA and LbpB for LfR. Iron is released from these compounds at the OM by the energy provided from TonB-ExbBD and the liberated iron is translocated by periplasmic Fbp (ferric binding protein) to an ABC permease which delivers iron to the bacterial cytosol (Chakraborty *et al*., 2013).

1.5.4 Ferri-siderophores

Bacteria are able to obtain iron using high affinity, siderophore-mediated, iron-uptake systems operating in conditions of iron restriction. Many bacteria, including *E. coli*, can obtain iron from siderophores that they do not synthesise: ferrichrome, hydroxamate, ferrichrysin, coprogen, rhodotorulate, ferrioxamine B and D are siderophores that are generated by other organisms but can be pirated by *E. coli* (Faraldo- Gomez and Sansom, 2003; Ratledge and Dover, 2000; Faraldo-Gomez and Sansom, 2003) (Fig. 1.5). Such siderophores are called exogenous siderophores or "xenosiderophores"(Matzanke *et al*., 1997). *E. coli* can also uptake iron in the form of ferric-citrate (Kammler *et al*., 1993), which is an environmentally common organic acid. Some bacteria can also generate more than one type of siderophore, for instance *Pseudomonas aeruginosa* produce both pyoverdin and pyochelin (Gasser *et al*., 2016).

1.5.4.1 Enterobactin-mediated iron uptake by *E. coli*

Enterochelin or enterobactin (Ent) is a catechol-type siderophore which is manufactured by most of the enteric bacteria. This siderophore possesses very high affinity for iron, is a cyclic trimer of 2, 3-dihydroxybenzoic acid (Cornelis and Andrews, 2010). It is a hexadentate molecule binding one Fe^{3+} atom using three pairs of neighboring OH groups carried by three benzene ring units. Ent is the most strongly iron-binding of all known siderophores (Weitl *et al*.,1979).

Biosynthesis of Ent in *E. coli* requires the products of 6 genes, *entA-F*, with seven additional genes coding for iron enterochelin uptake (*fepA-G*) and one for its secretion (*entS*). A further esterase gene (*fep*) encodes an enzyme required to break down the three ester bonds of Ent to enable iron release. 2, 3-dihydroxybenzoic acid (DHB) is an intermediate in Ent synthesis manufactured from isochorismate by EntC, -B and -A. Three serines are then combined with three DHB units by the EntD, -E and – F complex to form the trimeric Ent molecule. Importantly, enerobactin is not produced in conditions of iron availability, only in iron restriction, particularly

in high redox potential conditions. It has a strong ability to scavenge ferric iron from Tf, Lf (Hantke *et al*., 2003) and oTF at pH 7 with pM value equal to 36.7 (the negative logarithms of the free ion concentration). In *E. coli,* this type of siderophore cannot be used again after it has delivered iron to the bacterial cell because during iron release esterase breaks the cyclic triester bond in enterobactin complexes with Fe^{3+} leading to loss of the necessary ester bond to produce new complex with ferric iron. Many strains of *E. coli, S. flexneri* and *Klebsiella pneumoniae* that cause infections in animals, involving intestinal disorders, produce a second and unrelated siderophore, aerobactin (Wei & Murphy, 2016). Aerobactin is a secondary hydroxamate manufactured from citrate and lysine (Cornelis and Andrews, 2010; Chakraborty *et al*., 2013). Aerobactin differs from enterobactin as it is produced mainly by pathogens within the host where it scavenges iron from host cells and tissues (Torres *et al*., 2001). Although enterobactin is a more powerful siderophore allowing it to acquire iron from TF, unlike aerobactin it is not useful to pathogens within the host (Brock *et al*., 1991).

Many pathogenic strains, such as *Salmonella* species, uropathogenic *E. coli* (UPEC), avian pathogenic *E. coli* (APEC), *Klebsiella* strains and *S. dysentriae* have another sidrophore called salmochchelin (Muller *et al*., 2009). This sidrophore, first known in salmonella and named salmochelin, is a C-glucosylated enterobactin (Hantke *et al*., 2003). This sidrophore was noted in UPEC and *S. dysentriae* for its ability to evade the effect of lipocalin-2 by producing due to its glucoslylated nature (Fischbach *et al*., 2006). Salmochchelin synthesis and uptake requires the *iroBCDEN* genes.

1.5.4.2 The TonB-ExbB-ExbD system

The TonB-ExbB-ExbD complex acts to transfer the energy generated from the electrochemical gradient across the CM to the ferri-sidrophore OM receptor system for transport. TonB extends from the CM to the inner face of OM through the periplasm, and is complexed with ExbB and

ExbD which are attached in the CM (Postle and Larsen, 2007). TonB connects to the OM receptor bound to ligand, leading to conformational change in the receptor, which allows transfer of ligand to the periplasm. TonB appears to cycle between association and dissociation with the OM (Higgs *et al*., 1998). In *E. coli*, it seems that ExbB and ExbD function to cycle TonB between increased and decreased affinity for the OM receptor. ExbB is 26 kDa CM integrated protein and ExbD is a 17 kDa protein that like TonB has only one transmembrane helix and has a substantial periplasmic domain (Larsen *et al* 1999). The transmembrane domain of the TonB is responsible for interaction with ExbB and ExbD to form a transducing energy complex (Jaskula *et al*., 1994). However, the information of TonB interaction with the OM receptors is still ambiguous in spite of considerable investigation (Garcia-Herrero *et al*., 2007). The so called "TonB box" is a preserved 7 amino acid segment located at the N-terminal region of the plug domain of OM receptors (Noinaj *et al*., 2010). It is thought that the TonB box is the region of TonB interaction for inducing conformational changes in the OM receptors. A mechanical model of the TonB energy transduction is proposed whereby TonB remains in contact with the CM. Alternatively, a mechanism has been proposed, 'the shuttle mechanism', where the TonB N-terminal region exits the cytoplasmic membrane to deliver energy to the receptor of outer membrane (Larsen *et al*., 2003; Letain & Postle, 1997).

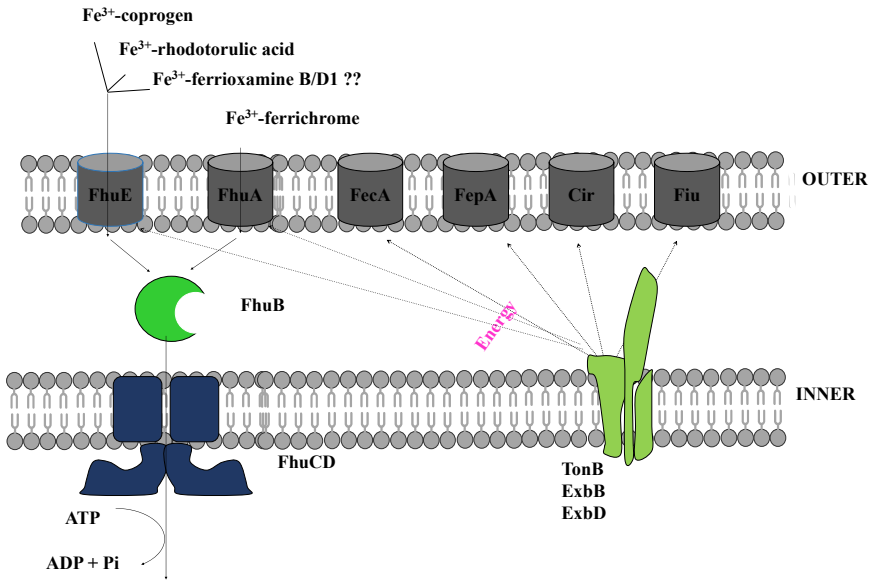

Figure 1.5: Diagram demonstrating iron acquisition of ferri-hydroxamates in *E. coli* K-12. This figure shows uptake through the OM receptors (FhuA and FhuE) requires energy derived from the TonB-ExbB-ExbD complex localised in the inner cytoplasmic membrane. The FecA, FepA, Cir and Fiu OM recpetors are also shown (but not the corresponding PBP-ABC permeases) which enable uptake of ferric citrate and catecholate siderophores. Adapted from Andrews *et al*, (2003).

1.5.5 Low-affinity iron transport

High-affinity iron transporters are not required when bacteria are grown in iron-copious conditions (5-10 µM iron) when high-affinity transport systems are repressed (Andrews *et al*., 2003). Iron reduction systems are thought to function in the acquisition of ferrous iron, and a few have been characterized (Small & O'Brian, 2011). In *E. coli* iron uptake mutants, ascorbic acid helps the absorption of iron, suggesting that reduction of ferric iron to ferrous iron assists iron uptake (Earhart, 1996).

E. coli has been shown to import ferrous iron by a low-affinity mechanism that is not well characterized but appears to include transporters used for other metals (e.g. the Mg^{2+} and Mn^{2+} transporters, CorA and MntH; Hantke, 1987). MntH is primarily involved in the high-affinity uptake of manganese, but also exhibits low affinity for Fe^{2+} ion (Kehres *et al* 2000). An additional low affinity iron transporter is ZupT. This system transports a variety of divalent

metals (Zn^{2+}, Fe^{2+}, Co^{2+} and possibly Mn^{2+}) and is generally expressed at low levels (Grass, *et al*., 2005). CorA, the transporter of magnesium, is also capable of Fe^{2+} uptake (Hantke, 1997).

1.5.6 Ferrous iron transport

1.5.6.1 FeoABC system transport

The Feo system was first discovered in *E. coli* K-12 as a ferrous-iron transport system (Kammler *et al*., 1993; Hantke, 1987). In this study, transport mutants were identified by streptonigrin treatment because of its ability to produce free radicals in the combined presence of iron and oxygen (Hantke, 1987). The gene was cloned and sequenced six years later when two open reading frames, *feoA* and *feoB*, were identified of the FeoABC system of *E. coli* K-12 (Kammler *et al*., 1993) (Fig. 1.6). The *feo* operon is now known to be composed of *feoABC* (Hantke, 2003). In *E. coli*, *feoA* encodes for a 75-residue hydrophilic protein of 8.4 kDa likely located in the cytoplasm, whereas *feoB* encodes a 773 residue polytopic transmembrane protein with a molecular weight of 84 kDa. The *feoC* gene encodes a cytoplasmic protein containing 78 amino acids and such genes are only found amongst the γ-Proteobacteria (Hantke 2003; Cartron *et al*. 2006). FeoB is believed to be the dominant transmembrane transporter, FeoC is involved in regulatory control of Feo levels and FeoA may interact with FeoB to control transport (Lau *et al*., 2013).

An *E. coli feoB* mutant displayed reduced colonization of the intestine of mice indicating a role in colonization and pathogenicity (Stojiljkovic *et al.*, 1993). It has been assumed that the reason for this is due to the inability of bacteria to absorb iron under the anaerobic conditions of the gut (Cartron *et al*., 2006; Robey & Cianciotto, 2002). A role in pathogenicity for *feoB* was also shown in *Legionella pneumophilia.* FeoB has been shown to be required by *H. pylori* for colonization of the gastrointestinal tract. Velayudhan *et al*. (2000) illustrated that *H. pylori* mutants for *feoB* were

unable to colonise the gastric mucosa of a mouse model, this infers that *feoB* has a significant role in iron uptake by *H. pylori* in the low pH, low-O_2 environment of the stomach. Feo plays an important role in colonization of the gut in several other bacteria (Andrews *et al*., 2003). the Feo system is regulated by Fur and Fnr. Fnr is a global regulator of anaerobic gene expression, it transcriptionally induces *feoABC* in *E. coli* in response to anaerobiosis (Kammler *et al*., 1993). Fnr is an oxygen sensor that stimulates transcription of the *feo* operon in the absence of oxygen (Kammler, Schon and Hantke 1993). The *feo* genes are constitutively activated; however, under anaerobic conditions the expression level is increased. *feo* is regulated by Fur and Fnr boxes (Kammler *et al*., 1993). Fur is commonly involved in regulation of iron homeostasis in Gram-negative bacteria, and also has a role in oxidative stress resistance. Fur generally acts as a transcriptional repressor, employing iron as co-repressor (Neto *et al*., 2009). When intracellular iron levels become high, expression of iron uptake systems is repressed by the Fur-Fe^{2+} complex. In contrast, Fur becomes inactive when iron levels fall below a certain threshold ~1-2 µM (Hidese *et al*.,2014). Fur is a transcriptional regulator of iron uptake genes in *E. coli* and many other bacteria (Bagg and Neilands, 1987). In anaerobic conditions, Fnr is a transcriptional activator of *feo* (Spiro and Guest, 1990). The Feo system is also controlled by a post-translational process in response to oxygen. FeoB is subject to proteolytic degradation by FtsH, but is protected by FeoC anaerobically. FeoC is an Fe-S protein that is itself degraded aerobically by Lon once its Fe-S cluster has been lost following exposure to oxygen (Kim *et al*., 2015) (Fig. 1.6).

Initially it was believed that FeoABC depends on ATP to drive iron uptake (Kammler *et al.*, 1993), however, studies have now illustrated that the FeoB protein contains a cytoplasmic domain acting as a G-protein that displays GTPase activity (Marlovits *et al*., 2002) which may drive the iron uptake process for FeoB.

The precise function of FeoA is not yet understood, however, it has similarity the C-terminal SH3 (Src-homology 3) domain of DtxR and IdeR (global iron regulators found in high G+C Gram-positive bacteria) (Andrews *et al*., 2003; Lau *et al*., 2013; Su *et al*., 2010). In *Vibrio cholerae*, all

three Feo components are essential for Feo function and FeoC was found to interact with the cytoplasmic domain of FeoB (Weaver *et al*., 2013).

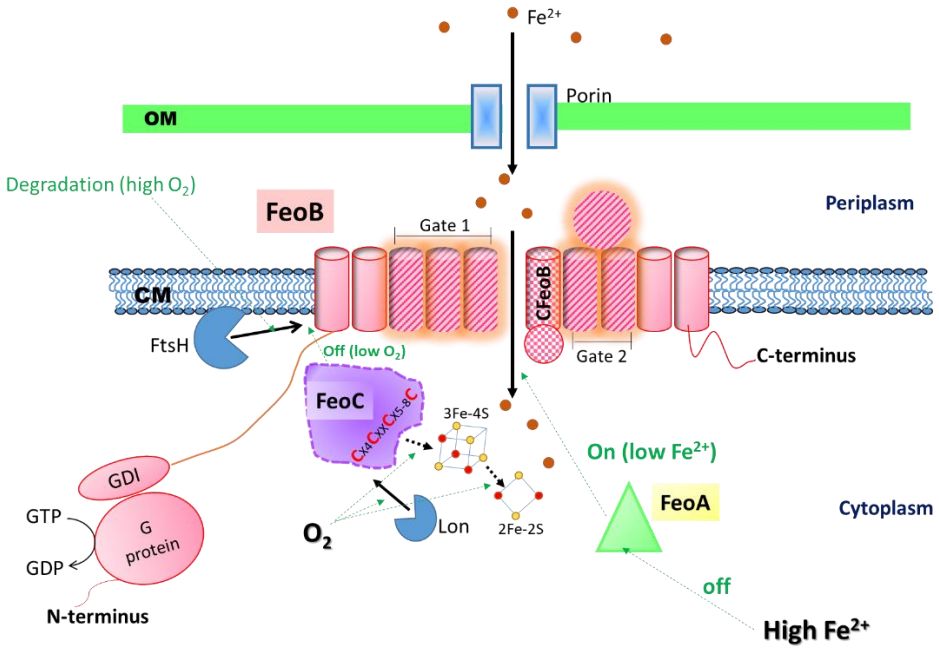

Figure 1.6. Schematic model of Feo-mediated ferrous transport in *E. coli*. Based on Cartron *et al*. (2006), Lau *et al*. (2013) and Kim *et al*. (2015). The striped transmembrane regions represents the Gate motifs while the dotted transmembrane regions represent the core CFeoB domain. The FeoB (pink) inner membrane protein takes up Fe^{2+} utilising its Gate motifs while the G-protein provides energy from GTP. FeoA (green) is speculatively shown as promoting FeoB activity under low iron conditions. FeoC (purple) is thought to bind to and protect FeoB from FtsH-mediated proteolysis, while the Fe-S cluster of FeoC regulates Lon-mediated FeoC proteolysis in an oxygen dependent manner. Thus, FeoC prevents FeoB turnover under anaerobiosis.

1.5.6.1.1 FeoA FeoA is a small Src-homology 3 (SH3)-like hydrophilic protein placed in CM, expected to act as a GTPase-activating protein (GAP) and/ or an Fe (II)-dependent repressor (Cartron *et al*., 2006). In a recent study, FeoA was shown to interact with FeoB in *S. enterica* (Kim *et al*., 2012) and is essential for Fe^{2+} uptake in both *S. enterica* and *V. cholerae in vivo* (Kim *et al*., 2012; Weaver *et al*., 2013). In *E. coli* it is suggested that FeoA possibly functions by interacting with the highly conserved core region in the transmembrane domain of FeoB, instead of a GAP as suggested earlier (Lau *et al*., 2011). FeoA was suggested to function

as a GTPase-activating protein operating on the FeoB N-terminal domain (NFeoB) (Cartron *et al*., 2006), but it is currently proposed to instead cooperate with the conserved core region of FeoB (Lau *et al*., 2013). FeoA has two α-helices, a β-barrel and interconnecting loop, with the general fold like a SH3 domain (Figure 1.7) (Sestok *et al*., 2018). It is this SH3 domain which proposes that FeoA may be included in triggering GTPases or G-protein interaction (Li, 2005; Lau et al., 2015). SH3 domains typically bind G-proteins through proline-rich sequences (PXXP), but the PXXP recognition site in FeoB is hidden in the protein core (Lau *et al*., 2013). A function for FeoA as a prokaryotic GAP is supported by the apparent abnormally slow rate of FeoB GTP hydrolysis (Su *et al*., 2010). Moreover, purified FeoA of *E. coli* does not impact the hydrolysis rate of the purified G-protein domain of FeoB (Cartron *et al*., 2006; Lau *et al*., 2013; Smith *et al*., 2018). Therefore, the function of FeoA remains an open question.

In 89% of bacterial Feo systems, FeoA and FeoB to exist together in a single cluster, suggesting their close proximal functioning with entwined roles (Lau *et al*., 2013; Lee, *et al*., 2007).
The requirement of Feo systems for FeoA differs among organisms. Knockout of the FeoA protein in *E. coli* resulted in reduction in function of Feo but did not eradicate it entirely, suggesting that FeoA augments FeoB activity rather than being essential for Fe^{2+} uptake (Kammler *et al*., 1993). In contrast, FeoA plays an essential function for Feo in *V. cholerae* (Weaver *et al*., 2013), although 20% of *feoB* loci do not include a *feoA* homologue (Cartron *et al*., 2006).

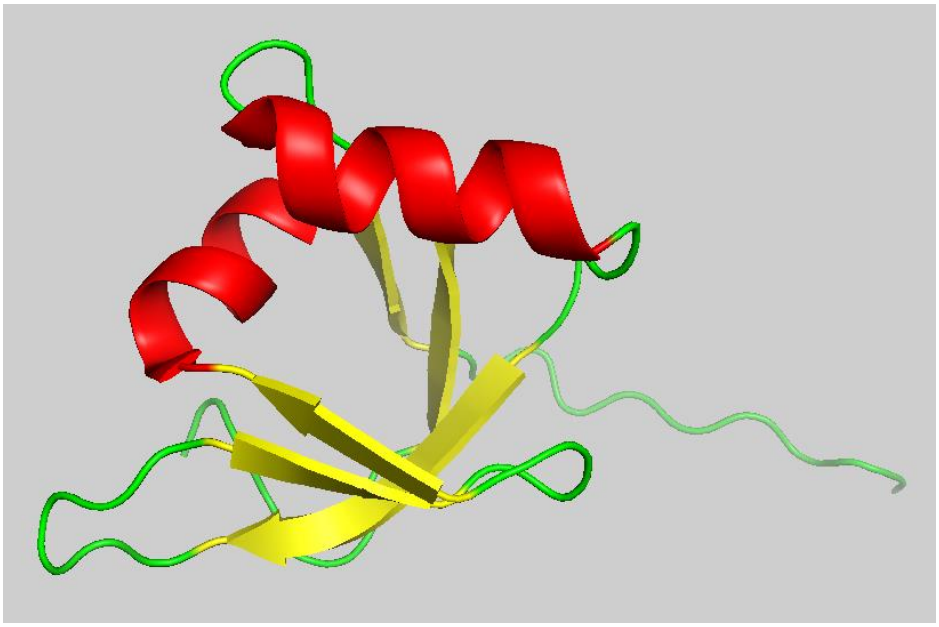

Figure 1.7: *E. coli* FeoA protein structure. β-strands as arrows (yellow), α-helices as coils (red). Image generated in PyMOL using PDB code 2LX9, shown in cartoon view. FeoA has a β-barrel topology like to that observed in the SH3 domain of the iron responsive prokaryotic transcription factor DtxR and eukaryotic GAPs.

1.5.6.1.2 FeoB

FeoB is a large protein with a cytosolic N-terminal domain and C-teminal integral membrane domain. The N-terminal domain can be divided into a Ras-like G domain and a helical S domain (Hung *et al*., 2010). The G domain is believed to supply energy for the transport process or to control the transport by sensing the energy state of the cell and moves to the transmembrane (Lau *et al*., 2013). The S domain may act as a switch between an open or closed state (Hung *et al*., 2012) The C-terminal region is a helical transmembrane domain that likely forms the function as a Fe^{2+} permease (Marlovits *et al*., 2002). FeoB is a multi-domain transmembrane channel protein, 773 residues in length and 84.6 kDa in volume. The GDP dissociation inhibitor domain (GDI), the cytoplasmic G-protein domain (NFeoB), and the transmembrane domain are the three main domains of FeoB (Cartron *et al*., 2006).

The G-protein domain includes five GTP binding motifs: the GTP α- and β-phosphate binding G1 (GxxxxGK(S/T)) domain, the magnesium and γ-phosphate binding G2 (T) and G3 (DxxG)

domains, the guanine nucleotide-binding G4 (NxxD) motifs, and the hydrogen bonding G5 (STRGRG) motifs (Figure 1.8) (Marlovits *et al*., 2002; Guilfoyle *et al*., 2009; Sprang, 1997; Hantke *et al*., 2003). The G-domain is critical for function of the Feo system; site-directed mutagenesis of the G-protein domain saw of loss of Fe^{2+} transport and overall Feo activity (Marlovits *et al*., 2002). Furthermore, the G-protein domain includes two regions which effect nucleotide binding and are related to effector protein regulation for signal transduction (Sprang, 1997).

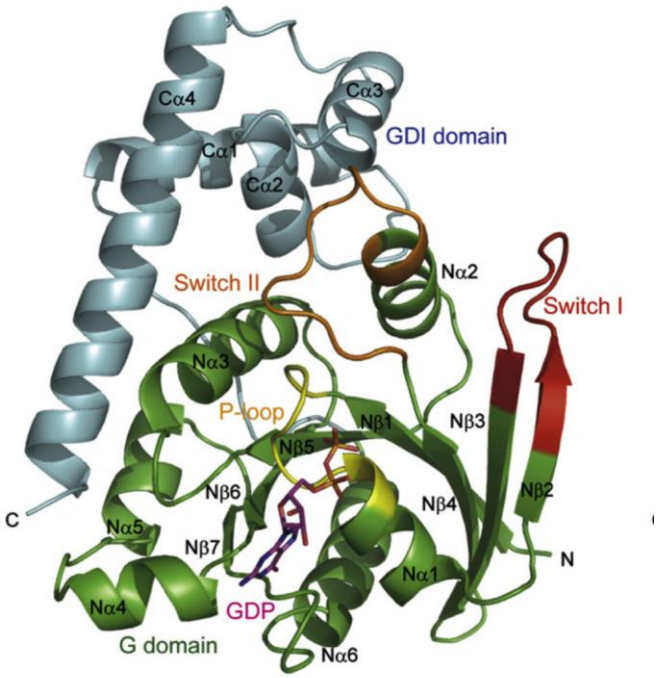

Figure 1.8: *E. coli* NFeoB displaying the G and GDI domains. The GDI domain (cyan), the P loop (yellow), switch I (red), and switch II (orange). The GDP-bound FeoB cytosolic domain structure in ribbon illustrations, with the G domain (green). GDP is displayed in a stick representation, with the carbon atoms highlited magenta. The secondary structure elements are labeled. Image generated in PyMOL using PDB code 5FH9, shown in cartoon view (Hattori *et al*., 2009)

The G-protein domain has the capability to bind Fe^{2+} at the ExxE motif; upon mutagenesis of this motif to AxxA, Fe^{2+} uptake was reduced. This indicates that Fe^{2+} uptake depends on these motifs however is not completely reliant, since Fe^{2+} uptake was not completely eliminated (Hung *et al*., 2010).

The GDI domain is ~100 residues long, hydrophilic, and cytoplasmic. Acting as a linker between the transmembrane domain and G-protein domain, the GDI domain interacts with a G-domain 'Switch' region to augment GTP binding. The close relationship between the G- and GDI-domains controls Fe^{2+} transport via the Feo system (Eng *et al*., 2008).

The transmembrane domain is ~500 residues long and is the least understood domain of the FeoB protein. This iron permease domain mainly helps to physically transport the Fe^{2+} ions to the cytoplasm (Lau *et al*., 2013). This domain has two Gate regions (as found in nucleoside transporters), likely to have opposing orientations in membrane, with three highly conserved Cys residues considered to act as Fe^{2+} ligands during uptake (Cartron *et al*., 2006). A FeoB full structural model was recently published, generated using homology modelling of the *P. aeruginosa* FeoB using the iron ferrous transporter as the homology model (Seyedmohammad *et al*., 2016). These studies suggested that FeoB possibly forms a homo-trimer generating a cysteine-lined central Fe^{2+}-transloaction pore, which is linked to a second central pore produced by G-domains. However, the quality of the model is poor, and the template used for the C-terminal domain displays low sequence similarity (22%) and did not include the duplicated Gate motifs, as as predicted for FeoB (Cartron *et al*., 2006). The concept that FeoB oligomerizes into a trimer is supported by previous work on the N-terminal domain of *E. coli* FeoB, which crystallised in trimeric form (Hung *et al*., 2012); though a further study indicates that FeoB is mainly monomeric in solution (Hagelueken *et al*., 2016).

The G-protein domain of FeoB FeoB was believed to bind ATP because of detected sequence homologies with ATPase binding sites (Kammler *et al*., 1993). Inhibitors of ATP synthesis/hydrolysis or a protonophores eliminated ferrous iron transport in *H. pylori* supporting this idea (Velayudhan *et al*., 2000). However, subsequent studies indicated that FeoB does not bind or hydrolyse ATP (Marlovits *et al*., 2002) and includes motifs reminiscent of GTP-binding G-proteins.

In the G-protein domain, there are two Switch regions (Figure 1.9). Switch regions of G-proteins are vital for nucleotide binding and for providing connection to the effectors of the associated signal transduction path way (Sprang, 1997; 2000).

Nucleotides induce conformation changes in the Switch regions leading to altered protein-protein interaction affinity for the G-domain and effector proteins, consequently, allowing signals to be controlled. For example, the G-protein bound with GTP will have a high affinity for an effector. Upon hydrolysis to GDP, the affinity will decline, and the effector will be released, eliminating the signal (Hilgenfeld, 1995; Hilgenfeld, 1995a). The G-domain of the *E. coli* FeoB plays an important role in iron transport since mutational studies show that changes in the G4 motif result in loss of transport activity of ferrous iron (Marlovits *et al*., 2002).

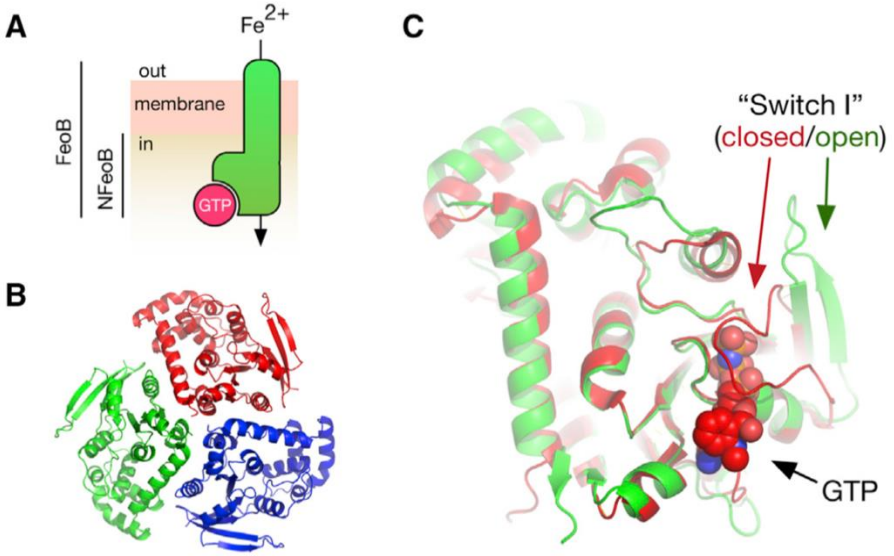

Figure 1.9. Structure of NFeoB from *E. coli* BL21. (A) Model of the domain structure of the 84 kDa membrane protein FeoB. (B) The crystallographic trimer of NFeoB from *E. coli* BL21 is presented as a cartoon model. (C) Structure of an NFeoB monomer. The position of the Switch I region (residues 25–40) is marked in its open (green arrow) and closed state (red arrow, PDB: 3LX5). A black arrow marks the GTP binding pocket with GTP displayed as spheres (Hagelueken *et al*., 2016).

The GTPase domain role has been the topic of significant discussion. Some would argue that FeoB is likely a GTP-gated pore, which regulates iron flow depending on the cell energy status (Seyedmohammad *et al*., 2016; Lau *et al*., 2016). Others suppose GTP activity provides energy to energetically pump Fe^{2+} through the inner membrane (Ash *et al*., 2010; Smith and Sestok, 2018). It has often been stated that the GTP-hydrolysis rate of FeoB's G-domain is too slow to support active transport (Seyedmohammad *et al*., 2014). The data on which this observation is based mainly originated from *in vitro* studies examining the GTPase activity of the G-protein domain (Smith and Sestok, 2018). Two studies have examined the GTPase activity of N-terminal FeoB with the C-terminal domain attached; one study found no proof to propose that GTPase activity differs from the values of other studies (Seyedmohammad *et al*., 2016). However, the most recent study showed that FeoB from *K. pneumoniae* can reach a hydrolysis level close to what would be estimated if it were driving active transport (Smith and Sestok, 2018). This particular study on FeoB originated from one species and does not provide definitive proof that FeoB transporters from all species are capable of hydrolysis at such a rate. It does, however, increase questions as to the dependability and exactitude of prior estimates of basal GTPase activity, therefore casting doubt on the disagreement that FeoB cannot be an active transporter due to its low rate of GTP hydrolysis.

The GDI domain of FeoB The binding region between the G-domain and the transmembrane domain was identified firstly as a GDP disconnection inhibitor (GDI) domain (Figure 1.10) (Eng *et al*., 2008). The GDI domain is hydrophilic and cytoplasmically located along with the FeoB G-domain. The amino acid sequences of this domain are not well conserved among diverse organisms, although its three-dimensional structure is (Hung *et al*., 2010). Eng and colllegues showed that the GDI domain stabilises binding of GDP by making specific interations with the switch I region of the G-protein domain (Eng *et al*., 2008). This indicates regulation of FeoB activity via GDI- and G-protein domain interaction (Eng *et al*., 2008).

The Gate motifs of FeoB The third main domain of FeoB is the transmembrane domain (Fig. 1.10), corresponding to residues 277-773 in the *E. coli* FeoB. It is predicted to include 8-10 transmembrane helices (TMHs) in the CM (Krogh *et al*., 2001). The transmembrane domain contins two Gate motifs that possess three highly conserved Cys residues which are essential to GTPase activity (Eng *et al*., 2008), suggesting coupling between GTPase activity and import activtiy. The four sequence elements (I-IV) of the Gate motif are conserved in the FeoB Gate motifs (Fig. 1.10), and two of the highly conserved Cys residues occupy identical positions in element IV of Gate I and 2 (Fig. 1.10). Several nucleoside transporter structures are solved (Johnson *et al*., 2012) and these show that the two Gate motifs are oppositely orientated in the membrane and are closely associated to form a transport channel at their interface within the membrane where the nucleotide is bound between the HP1 structural element of Gate 1 and the equivalent HP2 of Gate 2 (HP1 and 2 are 're-entrant' helix–turn–helix hairpins). The transport of nucleoside is driven by a sodium grandient (in *Vibrio cholerae*) and is thought to employ an 'elevator' mechanism (Fig. 1.11). This involves movement of the transport domain holding the solute away from one face of the membrane and towards the other, to mediate a switch between inward and outward facing conformations (Johnson *et al*., 2012). Given the similarities between the FeoB C-terminal domain and nucleoside transporters, a similar mechanism of transport can be anticipated.

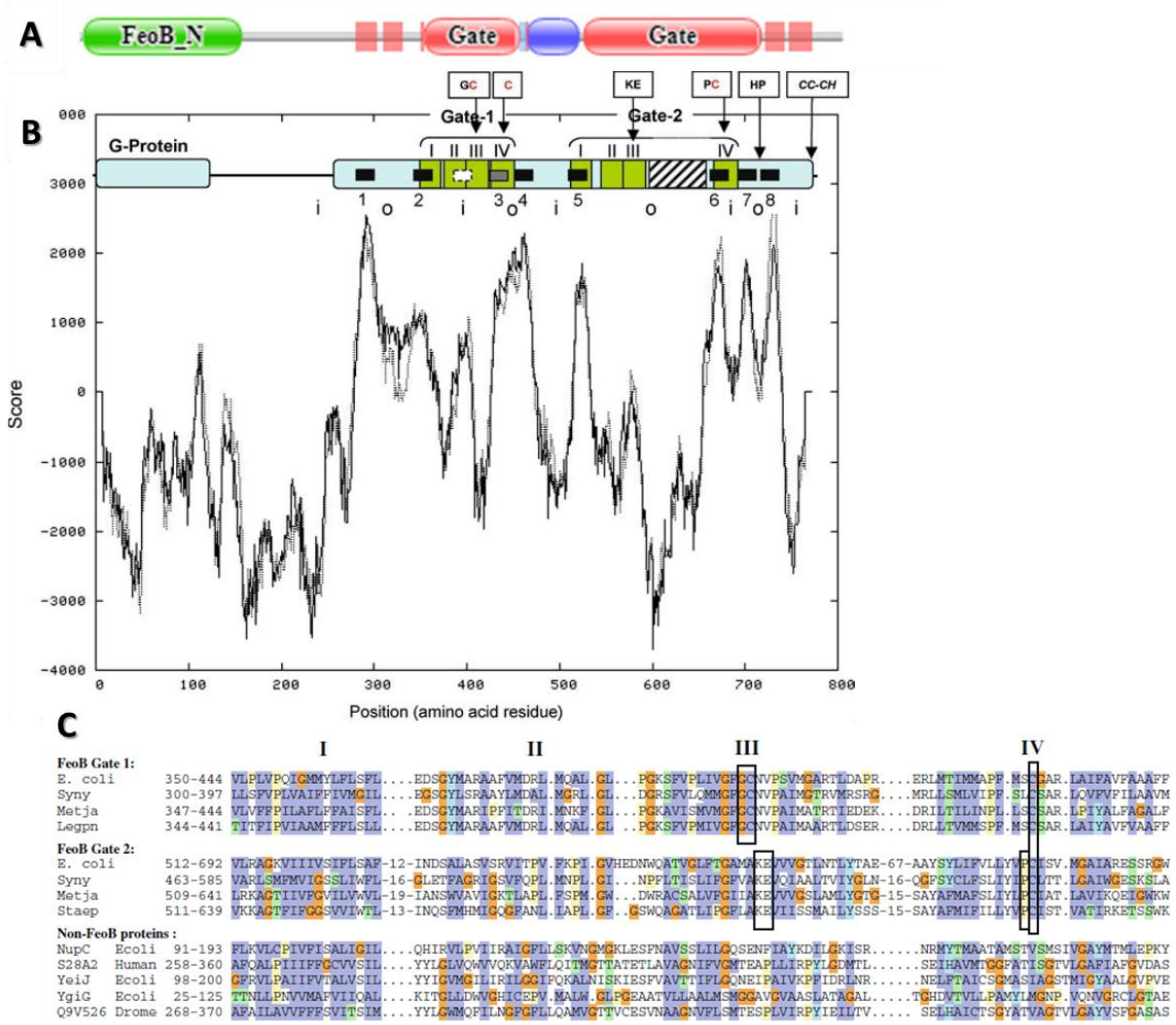

Figure 1.10. Gate motifs of FeoB of *E. coli*. (A) The domain organisation from Pfam, showing the two Gate motif domains and well conserved residues indicated. (B) The domain organisation shown with the hydrophobity plot for FeoB, indicating the two Gate motifs in green, predicted transmembrane helices in black bars (1-8) and topology, and the four elements of the Gate motif (I-IV). (C). Alignment of Gate motifs from FeoB proteins and nucleoside transporters, with the three highly conserved Cys residues in FeoB boxed. B and C from Cartron *et al*. (2006).

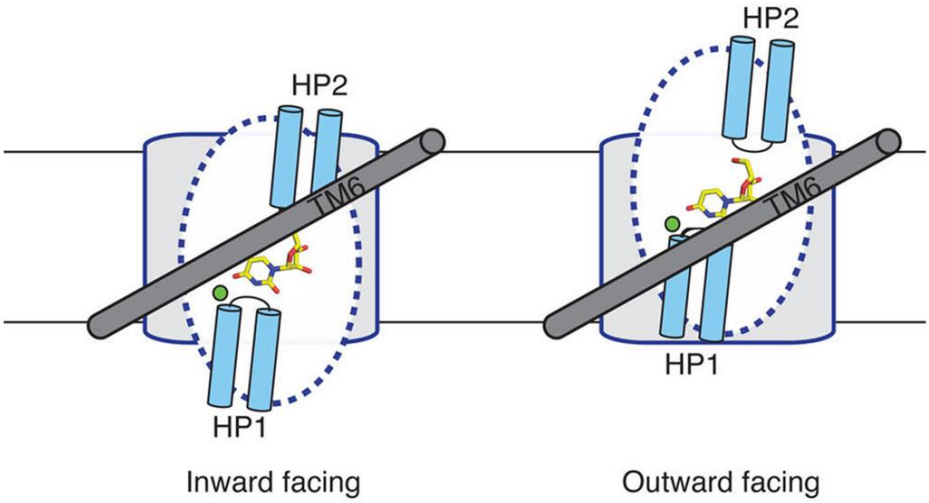

Figure 1.11. Suggested mechanism of nucleoside transport. TM6 is a major structural element of the scaffold region of the transporter that is envisaged to remain fixed in position within the membrane. It is also considered to form a hydrophobic barrier blocking access to the solute binding site from once face of the membrane, depending on the inward/outward facing conformation adopted. HP1 and 2 are from distinct, oppositely-oriented Gate motifs. From Johnson *et al.* (2012).

The C-terminus of FeoB The carboxy-terminal cytoplasmic protein of FeoB is a short region of just 270 - 773 membrane domain likely to act as the ferrous permease; residues. However, it is rich in well conserved Cys and His residues suggesting a role in metal interaction (Figure 1.10). However, this region is only consrved in the γ-Proteobacteria which might point to a role in FeoC interation (Cartron *et al*.,2006).

1.5.6.1.3 FeoC

FeoC is small, cytoplasmic and hydrophilic, containing a winged helix-turn-helix motif (Sestok *et al*., 2018) with a β-pleated hairpin between the second and third helices (Figure 1.11). Such motifs traditionally act as transcriptional repressors, with the third helix intercalating into the major groove of DNA to regulate transcription. The FeoC amino acid sequence displays four conserved Cys residues in the wing' region with a consensus sequence $CX_4CXXCX_{5\text{-}8}C$, that was predicted to provide binding sites for iron in the form of an iron-sulphur cluster, and indeed

a 4Fe-4S cluster has now been shown to be formed by FeoC from *Klebsiella pneumoniae* (Cartron *et al*., 2006; Hung *et al*., 2012; Hsueh *et al*., 2013). Consequently, FeoC was proposed to act as a [Fe-S]-dependent transcriptional regulator, directly regulating *feo* expression. However, FeoC of *Y. pestis* was shown not to control the *feo* promoter and no evidence has shown DNA binding activity of FeoC. Instead, it appears that FeoC functions at the post-translational level in controlling FeoB levels (Hung *et al*., 2010; Kim *et al*., 2013). FeoC protein enhances FeoB protein levels by protecting NFeoB from FtsH protease-mediated proteolysis in *S. enterica* (Kim *et al*., 2013). Furthermore, FeoC in *V. cholerae* interacts with the cytoplasmic domain of FeoB (Weaver *et al*., 2013). In *K. pneumoniae*, FeoC was found to bind with NFeoB with high affinity (Fig. 1.12) and may organise the [4Fe-4S] cluster to control Fe^{2+} through modulating G protein activity (Hung *et al*., 2010; Hsueh *et al*., 2013).

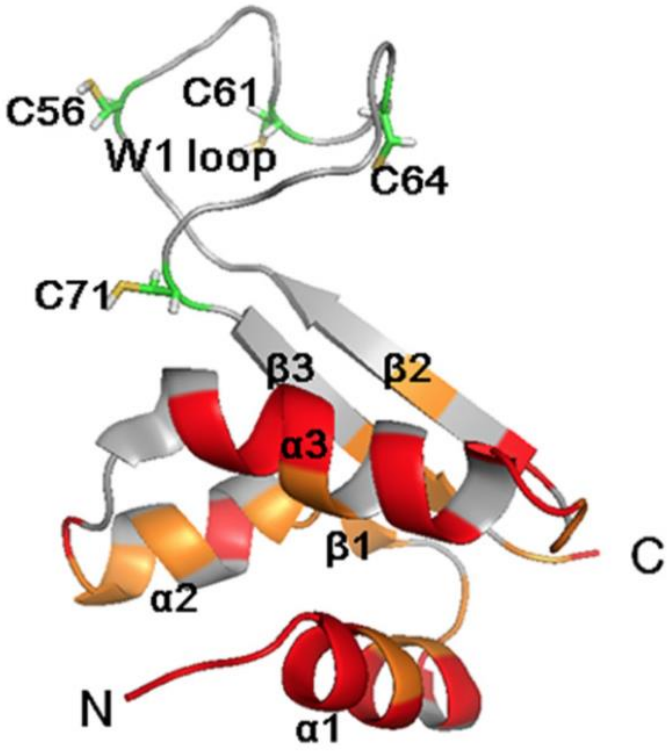

Figure 1.12. The NMR structure of FeoC of *Klebsella pneumoniae* with residues which are affected by binding to *Klebsella pneumoniae* NFeoB highlighted. Structural mapping of *Klebsella pneumoniae* FeoC residues perturbed by *Klebsella pneumoniae* N-FeoB. Residues with large chemical shift perturbations are colored red, and those with weaker perturbations are colored orange. Residues with resonances that were unperturbed are colored gray (Hung *et al*., 2012).

Along with transcriptional repression, FeoC has been found to shield FeoB against FtsH-mediated proteolysis by interaction with its N-terminal region (Figure 1.12) (Kim *et al*., 2013). Aerobically, FeoC is less prone to Lon-mediated proteolysis due to reduction of the Fe-S cluster. In anaerobic, iron-poor conditions, Fe^{2+} transport increases when FeoC protectively binds to FeoB. In aerobic conditions, the FeoC Fe-S cluster becomes oxidised, thus heightening its exposure to Lon-mediated proteolysis. In turn, FeoB becomes susceptible to FtsH-mediated proteolysis. Therefore, FeoC regulation can hinder FeoB accumulation and Fe^{2+} uptake when conditions switch from anaerobic to aerobic (Kim *et al*., 2015).

FeoC is found in γ-Proteobacteria and enhances FeoB activity. It was first proposed to be an iron-responsive transcription factor, as it contains a winged helix fold common to several DNA binding proteins and four conserved cysteine residues which provide a potential binding site for Fe-S clusters1 (Figure 1.13). Formation of Fe-S clusters at the proposed binding site has been confirmed in *K. pneumoniae*; these may be degraded in the presence of oxidising agents, changing FeoC conformation and thus activity (Hsueh *et al*., 2013). It therefore appears likely that FeoC regulates FeoB activity in response to the oxygen state of the cell. However, it has been shown that FeoC does not regulate transcription of the Feo operon in *Y. pestis* or *V. choerae* (Weaver *et al*.,2013; Fetherston *et al*., 2012), and no DNA binding activity has been detected to date (Hsueh *et al*., 2013).

There are currently two models for FeoC-mediated regulation at the post- translational level; FeoC may act as a G-protein regulator or as a protease inhibitor (Hsueh *et al*., 2013). The protease inhibitor model is based on the observation that the enzyme FtsH breaks FeoB down in the absence of FeoC (Kim *et al*., 2013). Binding of FeoC to the N-term of FeoB has been observed, and this interaction may prevent degradation (Kim *et al*., 2013). This model is supported by in vivo data, which the other two models lack (Hsueh *et al*., 2013).

Of the three Feo proteins, FeoC exhibits the greatest sequence diversity, and it is not yet clear whether FeoC has a conserved function across all γ-Proteobacteria (Hsueh *et al*.,2013).

1.5.6.1.4 Effect of Feo on the virulence of bactria

The importance of the Feo system for ferrous iron uptake occurs when access to oxygen is limited (Hantke, 1987). Under these conditions, the Feo system plays a significant role in bacterial virulence as has been demonstrated by deletion or mutation of the Feo genes for many pathogenic/non-pathogenic Gram-negative and -positive bacteria (Table 1.2). Feo is important for anaerobic/microaerophilic growth in the non-pathogenic bacterium, *E. coli* K-12, as well as in the pathogenic Gram-negative bacteria *C. jejuni*, *H. pylori*, *Porphyromonas gingivalis* and *V. cholerae* (Hantke, 1987); in these bacteria, *feo* mutants are not able to colonize the mouse intestine (Blaser, 1990; Forman *et al*., 1991; Stojiljkovic *et al*., 1993;Nomura *et al*., 1994; Raphael and Jones, 2003; Dashper *et al*.,2005). On other hand, mutants with defective ferric iron transport systems for the siderophore enterochelin (also known as enterobactin) or for dicitrate-iron are able to colonize the mouse intestine; thus, the ability of *E. coli* gut colonization is specifically dependent on uptake of ferrous iron (Stojiljkovic *et al*., 1993). Deletion of *feoB* in *H. pylori* resulted in inability for colonization of the gastric mucosa of mice (Table 1.2) (Velayudhan *et al.*, 2000). However, *C. jejuni* was first thought not to require FeoB for ferrous iron uptake (Raphael and Jones, 2003), but is now known to be important for the uptake of ferrous iron, gut colonization and intracellular survival (Naikare *et al*., 2006). Furthermore, FeoB is also needed for this pathogen's survival past the initial infectious stage, and hence in *C. jejuni* FeoB plays a significant role in intraepithelial and intramacrophage cell survival (Naikare *et al*., 2006). *feo* deletions in *V. cholerae* do not affect its colonization in the mouse model (Table 1.2) (Wyckoff *et al*., 2006). This means the *V. cholerae* has an additional ferrous iron transport pathway. Even though Feo might not affect colonization of *V. cholerae*, it is essential for iron homeostasis in this organism as inframe deletions of *feoA*, *feoB*, *feoC* all resulted in reduced iron acquisition (Weaver *et al.*, 2013). In *Streptococcus suis*, *Xanthomonas* species, *Francisella tularensis*, *Legionella pneumophila*, *Salmonella typhimurium* and

Pseudomonas aeruginosa, virulence also is not solely dependent on the Feo system. FeoA and FeoB have been found in *S. suis*, a Gram-positive swine pathogen, deletion of *feoB* remarkably attenuated its virulence in mice (Table 1.2) (Aranda *et al*. 2009). *S. suis* does not need iron for growth *in vitro*, which indicates that the main role of FeoB may be as a transporter for other divalent metal ions similar to other FeoB-like proteins that transport manganese (Aranda *et al*., 2009).

Table 1.2. Importance of the Feo system *in vivo*.

Organism	Pathogenic	Model	*feo* mutant virulent?	Colonization	Reference
E. coli O78 χ7122	yes	Chicken	Combination with another system of iron uptake	Blood	Sabri *et al*. 2008
S. typhimurium	yes	Mouse	Reduced	Intestine	Tsolis *et al*. 1996; Boyer *et al*. 2002
H. pylori	yes	Mouse	No	Gastric mucosa	Blaser, 1990; Forman *et al*., 1991; Nomura *et al*., 1994
S. flexneri	yes	Henle cells	Reduced during combination with anther system of iron uptake		Runyen-Janecky *et al*. 2003
V. cholerae	yes	Mouse	No	Stomach	Wyckoff *et al*., 2006
Y. pestis	yes	Mouse	Combination with anther system of iron uptake	Macrophages	Perry *et al*., 2007
C. jejuni	yes	Human and Porcine	No	Intestinal cells and macrophages	Raphael and Jones, 2003 Naikare *et al*. 2006)
S. suis	yes	Mouse	Reduced	Blood and membranes of brain and spinal cord	Aranda *et al*. 2009
E. coli K-12	no	Mouse	No	Intestine	Hantke, 1987; Stojiljkovic *et al*., 1993

1.5.6.2 EfeUOB iron transport

Many bacteria have a particular ferrous-iron uptake system with functional similarities to the Fet3p/Ftr1p system in yeast, fungi and algae (Askwith *et al*., 1997; Paronetto *et al*., 2001). Some bacteria (e.g. *E. coli* O157:H7) encode an elemental ferrous iron (EfeUOB) transport system recently found to act as a specific ferrous-iron uptake system (Grosse *et al*., 2006; Cao *et al*., 2007; Miethke *et al*., 2013). The *efe* operon of *E. coli* K-12 (formerly known as *ycdNOB*) is cryptic because of a single base-pair deletion in *efeU* resulting in a frameshift; however, the *efeO* and *efeB* genes are expressed and appear functional. Correction of the frameshift mutation generated a functional EfeUOB system (**E**lement **fe**rrous **u**ptake), whereas *efeUOB* of *E.coli* O157 lacks any frameshift mutation and appears fully functional (Cao *et al*., 2007).

EfeUOB is a three component ferrous-iron transporter found in pathogenic *E. coli* and many other bacteria (e.g. *Bacillus subtilis, Klebsiella pneumoniae, N. meningitidis*) (Baichoo *et al*., 2002; Grifantini *et al*., 2003; Ollinger *et al*., 2006). EfeU resembles Ftr1p of yeast, with seven predicted transmembrane helices (TMHs), two of these helices, carry the conserved REXXE motif (Fig. 1.12) of TMH 1 and 4 (Große *et al*., 2006). EfeU is thought to be located in the CM where it functions as a ferric permease (Rajasekaran *et al*., 2010). Indeed, its function has been reported to be as a ferric permease when incorporated in proteoliposomes (Grosse *et al*., 2006). One report indicates that EfeU is solely involved in iron acquisition, and EfeU-dependent growth is not affected by other divalent metal (Zn^{2+}, Pb^{2+} or Cu^{2+}) suggesting high iron selectivity for EfeU (Grosse *et al*., 2006). It is thought that this protein transfers ferric iron, oxidized from the ferrous form by EfeO and EfeB, through the CM, and it is thought that this oxidation step supplies the energy required for high affinity uptake by EfeU (Létoffé *et al*., 2009).

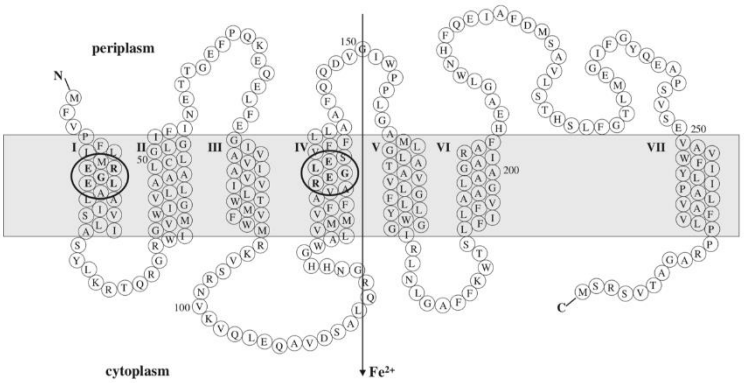

Figure 1.13. Topological medel of EfeU from *E. coli* Nissle 1917. Represented is a combinatory model derived from in silico and *in vivo* analysis of EfeU. Numbers (I-VII) denote putative transmembrane helices. Circles indicate conserved REGLE motifs of the OFeT family (Große *et al*., 2006).

EfeB is a periplasmic haem peroxidase (Cao *et al*., 2007, Goblirsch *et al*.,2011) that is exported into the periplasm by the Tat pathway (Twin arginine translocation). This is one of the only haem comprising protein seen to be secreted via this pathway (Zhang *et al*., 2015). EfeB is a periplasmic haem-containing DyP-like peroxidase (Sturm *et al.*, 2006). *In vitro,* EfeB has been noted to exhibit H_2O_2-dependent peroxidase activity at acidic pH with artificial substrates guaiacol or dianisidine; which has been found to occur in DyP as well (Sturm *et al.*, 2006). Liu and co-workers (2011) have reported the crystal structure of EfeB from *E. coli* O157 linked to haem. EfeB illustrating a unique haem-binding motif well conserved in this protein family. EfeUOB in *B. subtilis* can transport iron in both the ferrous and ferric forms (Miethke *et al*., 2013), whereas in *E. coli* the preferred substrate is Fe^{2+} (Cao *et al*., 2007). Figure 1.14 shows the crystal structure of EfeB (Liu *et al*., 2011). Although the function of EfeB has been proposed as a mediator for the oxidation of ferrous iron, consuming hydrogen peroxide as an electron acceptor, this suggested role remains to be experimentally proven (Zhang *et al*., 2015).

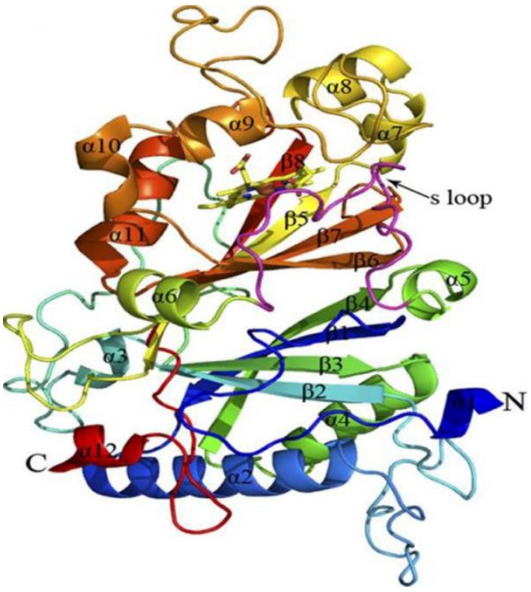

Figure. 1.14. The structure of haem-bound EfeB. This figure shows the structure of EfeB with the 12 α-helices and 8 β-strands labelled, forming a ferredoxin-like fold. The N- and C-terminus of the protein are indicated, and the bound haem is signified as a multi coloured stick structure. The monomer is composed of two domains with the haem moiety located in a hydrophobic pocket in the C-terminal domain. The S loop represents a 'switch' loop that interconnects the two domains and occupies space within the haem binding pocket. This loop is considered flexible and may facilitate substrate turnover (Liu *et al*., 2011).

EfeO (a M75 metalloprotease-cupredoxin hybrid protein) is periplasmic in *E. coli*; it consists of a C-terminal peptidase M-75 domain (Fig. 1.15) and an N- terminal cupredoxin (Cup) domain (Rajasekaran *et al*., 2010). Three of metal-binding sites are proposed within the protein proposed by modelling and sequence conservation analysis. One site is a predicted copper binding site in the cupredoxin domain, with a second site nearby predicted to favour ferric iron binding. A third site, thought to bind ferrous iron, is located in the M75 domain (Rjasekaran *et al*., 2010; 2009).

The Cup domain of EfeO is unique among the cupredoxin family as it appears to be the first to have a role in iron uptake in single-cupredoxin-domain format (Rjasekaran *et al*., 2010). The precise mechanism and role EfeO plays is ambiguous, but it is assumed that it binds ferrous iron in the periplasm which is consequently oxidized and then transferred to EfeU in the cytoplasmic membrane. The electrons resulting from this process are thought to transfer to the

H_2O_2-oxidised haem group of EfeB restoring it to its resting state (Figure 1.16) (Rjasekaran *et al*., 2010). The EfeUOB suggested mechanism is similar to that of the related Ftr1p-Fet3p system of yeasts where Fet3p acts as a multicopper oxidase in the reduction of oxygen to water and the oxidation of incoming ferrous iron to ferric iron, prior to translocation by the EfeB-like Ftr1p protein (Coa *et al*., 2007; Rjasekaran *et al*., 2010).

The ferroxidation stage may serve to provide energy to drive uptake and may also act to raise metal selectivity of the uptake mechanism. The EfeO M75 domain is homologous to alginate binding protein Algp7 (Fig 1.15), which is also a peptidase M75 family member. Both proteins contain the well conserved HXXE motif, thought to be involved in divalent-metal binding (Zn^{2+}/Fe^{2+}), although no metal was found binding in the crystal structure of Algp7 (Maruyama *et al*., 2011).

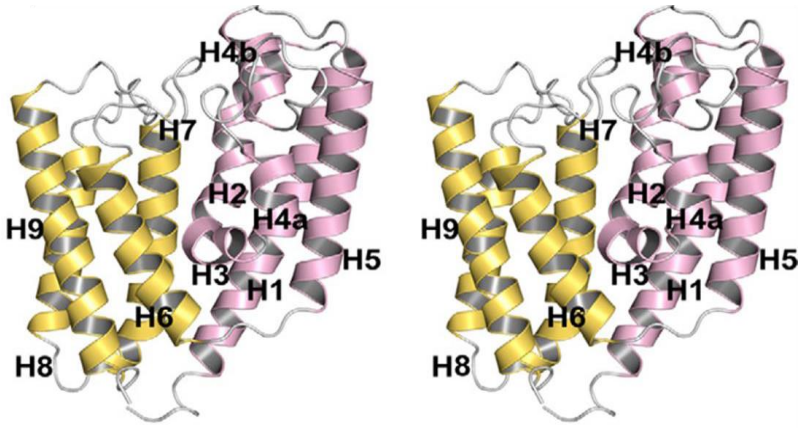

Figure 1.15. The structure of the EfeO homologue, Algp7. This figure illustrates the structure of the alginate binding protein Algp7 containing two up-and-down four α-helix bundles. Bundle A contains four major α-helices (H1, H2, H4a, H4b and H5) highlighted in purple, bundle B contains another set of 4 α-helices (H6, H7, H8 and H9) highlighted in yellow. A possible metal binding motif 115HxxE118 is situated in H4b of bundle A, at the open end of the cleft between the two bundles. The two bundles are hinged by a single loop between H5 and H6. Image from (Maruyama *et al*., 2011).

In *E. coli*, the Efe system is known to be produced under iron-starvation, low pH or in the presence of exogenous copper (Cao *et al*., 2007). The important discovery is induction of *efeUOB* under aerobic conditions (Cao *et al*., 2007), when pH and the amount of Fe^{2+} are low. The regulatory factor Fur and the two-component system CpxAR are required for iron- and pH-

dependent expression, respectively. The OmpR-like response regulator CpxR seems to repress the *efeUOB* promoter in its deactivated (de-phosphorylated) form. In response to low external pH, the sensor kinase CpxA phosphorylates CpxR and causes repression of *efeUOB*. *efeUOB* is also Fe^{2+}-Fur repressed. Fe^{2+}-Fur control is dependent on intracellular iron availability and Fur status (Cao *et al.*, 2007, McHugh *et al.*, 2003). The Efe system of *E. coli* is induced (~15 fold) by acidic conditions and 2.5 fold by low iron. The low pH induction is thought to be related to the stability of ferrous iron in these condition against oxygen-mediated oxidation. Expression of *efeUOB* of *E. coli* is not oxygen dependent (unlike *feo*), and it appears to function under both aerobic and anaerobic conditions, and it is considered to offer an aerobic option for ferrous-iron uptake as an alternative to the anaerobic option provided by Feo.

In the Gram-positive bacterium, *B. subtilis*, the Efe system has a dual mechanism for acquisition of iron, where it relies on extracellular conditions to allow acquisition of both ferrous and ferric iron (Miethke *et al.*, 2013). The binding protein EfeO and permease EfeU form a minimal complex for ferric-iron uptake; EfeB promotes growth under microaerobic conditions where ferrous iron is more abundant and EfeB is dispensable for direct ferric uptake via EfeUO (Miethke *et al.*, 2013).

The reason for the cryptic nature *efe* in the K-12 strain is unclear. The functional form of EfeUOB of *E. coli* was shown to provide a growth advantage under low pH, iron-restricted conditions in the presence of manganese as a competing metal suggesting that EfeUOB is not subject to Mn^{2+} inhibition (unlike Feo). This ability of EfeUOB to select Fe^{2+} over Mn^{2+} is consistent with studies showing that divalent metals (lead, copper, zinc) do not inhibit iron-mediated transport of EfeU (Grosse *et al.*, 2006).

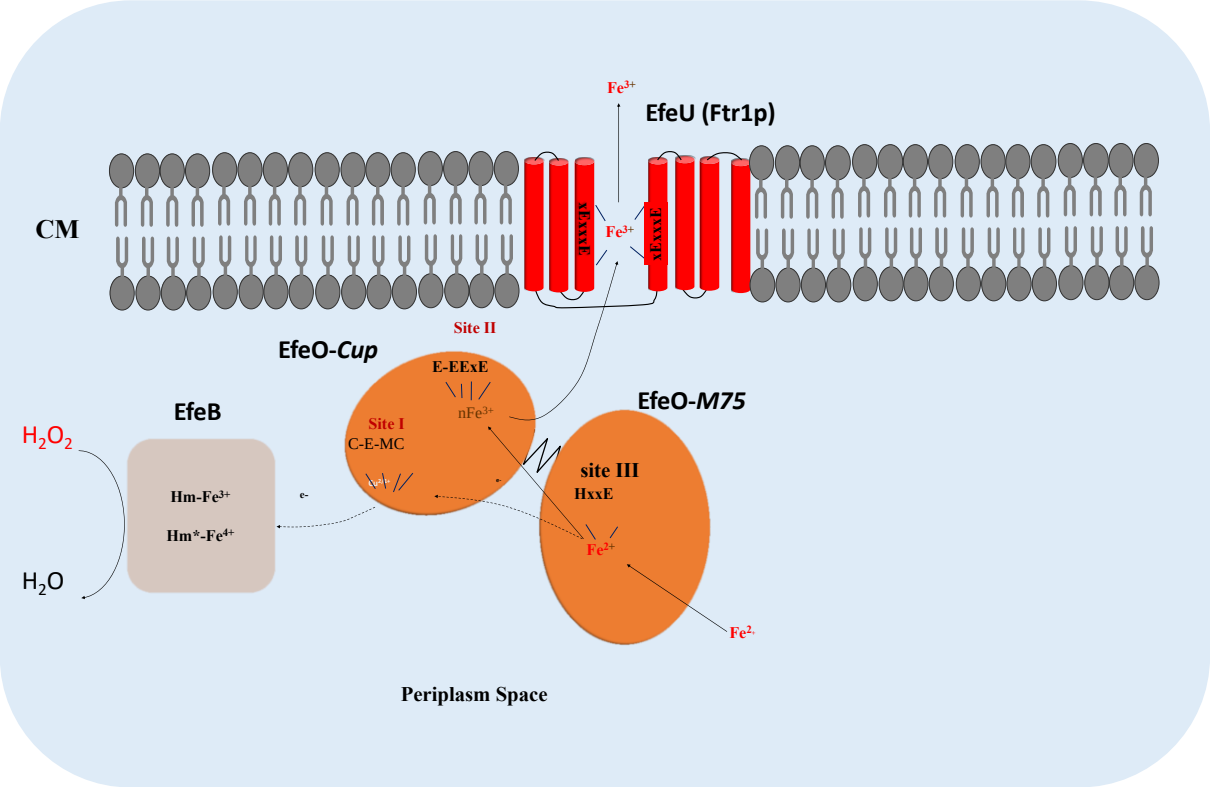

Figure 1.16. Schematic representation of the EfeUOB of *E. coli.* This figure illustrates a model for the EfeUOB system of *E. coli*. Ferrous iron initially binds to the periplasmic EfeO at the HxxE motif. Then $Fe^{2+}$is oxidized and the released electrons are transferred to the proposed copper site of the cupredoxin domain and then to the ferryl-haem group of EfeB to return it back to its resting ferric state. The oxidized iron is transported across the cytoplasmic membrane by the ferric-iron permease protein EfeU (Rjasekaran *et al*., 2010). Efe Fe^{2+}-uptake is thus driven by H_2O_2 through EfeB-mediate peroxidase activity.

1.5.6.3 MntH system

MntH, a CM bacterial protein, has a similar function to Nramp-1 in divalent cation transport in mammals, and is related to this protein. MntH was thought to be a transporter for both Mn^{2+} and Fe^{2+} in *E. coli* (Makui *et al.*, 2000). However, later studies proved that it has higher affinity to transport Mn^{2+} than other divalent cations (Kehres and Maguire, 2003). Kehres and co-workers (2000) reported that this protein may act as an Fe^{2+} transporter. MntH is encoded by a single gene, *mntH*, in *E. coli* and is regulated by MntR (manganese-sensitive transcription factor) that acts as a repressor for *mntH* conditions of Mn^{2+} availability (Patzer and Hantke 2001). This leads to homeostatic control of the MntH transporter in order to

maintain Mn^{2+} levels (Kehres *et al.,* 2000). Recent studies demonstrate that the binding site of this repressor is found associated with four genes, *mntH, mntR, yebN* (*mntP;* an Mn^{2+} efflux pump) and *dps* (Yamamoto *et al*., 2011).

In mammals the internal phagosomal environment presents engulfed pathogens with oxidative stress, low nutrients and low pH as well as an iron-restricted condition as a result of the transport activity of the 'host natural resistance-associated macrophage protein' (NRAMP-1). This transporter in the phagosomal membrane removes divalent cations out of the phagosome (Jabado *et al*., 2000; Papp-Wallace and Maguire 2006). This has a negative impact on many intracellular pathogens because they cannot get adequate amounts of these cations, which leads to its inability to survive in such condition (Anderson *et al.,* 2009).

1.5.6.4 ZupT system

ZupT was first identified as a Zn(II) transporter in *E. coli* (Grass *et al*., 2002), but later research demonstrated that Fe(II) can be transported by ZupT, along with Co(II), Zn(II) and Mn(II). ZupT is a CM protein belonging to a group of eukaryotic divalent ion transporters known as the ZIP family. ZupT mediates zinc uptake in *E. coli*. Growth of a *zupT* mutant was inhibited by EDTA at extremely decreased metal concentrations (Grass *et al*., 2002). *zupT* expression is not affected by metal ions as it is constitutively expressed (Grass *et al*., 2005). Its structure is similar to ZIP protein, composed of eight TMHs (Grass *et al*., 2005). ZupT has the same activity as MntH and Feo in the uptake of Fe^{2+}(Grass *et al*., 2005).

1.5.6.5 The Ftr1p system

Saccharomyces cerevisiae has two different plasma uptake systems for securing iron, a high-affinity system that uptake only iron and is encoded by two genes, FTR1 and FET3. Secondly, a low affinity system that assists in uptaking various metals such as cobalt and

cadmium, encoded by the FET4 gene (Figure 1.17) (Van Ho *et al*., 2002; Dix *et al*., 1994). Ferrireductase enzymes play crucial roles in both systems as they convert extracellular oxidised Fe^{3+} to the reduced Fe^{2+} which is the form transported (Askwith and Kaplan, 1997). The Ftr1p system requirements Fet3p for function. Fet3p is an extracellular, type one multi-copper oxidase that is bound to the CM by a single trans-membrane domain; it has three types of copper site including a type 1 site where ferrous oxidation using oxygen molecules takes place prior to transport via Ftr1p further transportation (Singh *et al*., 2006).

Ftr1p has seven conserved TMHs (like EfeU) containing two REXLE motifs located in TMH 1 and 4, the R and E residues of which are essential for iron permeation. Ftr1p also contains a DASE motif in extracellular loop six and a Glu in TMH3 that are essential for iron transport (Severance *et al*., 2004). The two motifs are thought to serve as iron binding sites whereas the conserved Glu residues in the RExxE motifs work as the direct ligands (De Silva *et al*., 1995). A third component required for Ftr1p function is Fre1p and/or Fre2p. These are flavin- and haem-containing NADPH dependent metalloreductases. Two are ferric/cupric reductases that function to reduce extracellular Fe^{3+} to the Fe^{2+} prior to transport via the Ftr1p/ Fet3p complex (Kosman, 2003). Transcription of these genes is controlled by the iron-sensing transcription factor Aft1p (Felice *et al*., 2005). Moreover, Ftr1p is copper controlled by the copper transcription factor Mac1p (Van *et al*., 2002). The mechanism of high-affinity iron uptake via this complex is thought to follow the sequence of ferrous form oxidation by Fet3p, then transfer of the ferric form directly to Ftr1p, followed by ferric form permeation through Ftr1p into the cytoplasm (Kwok *et al*., 2006).

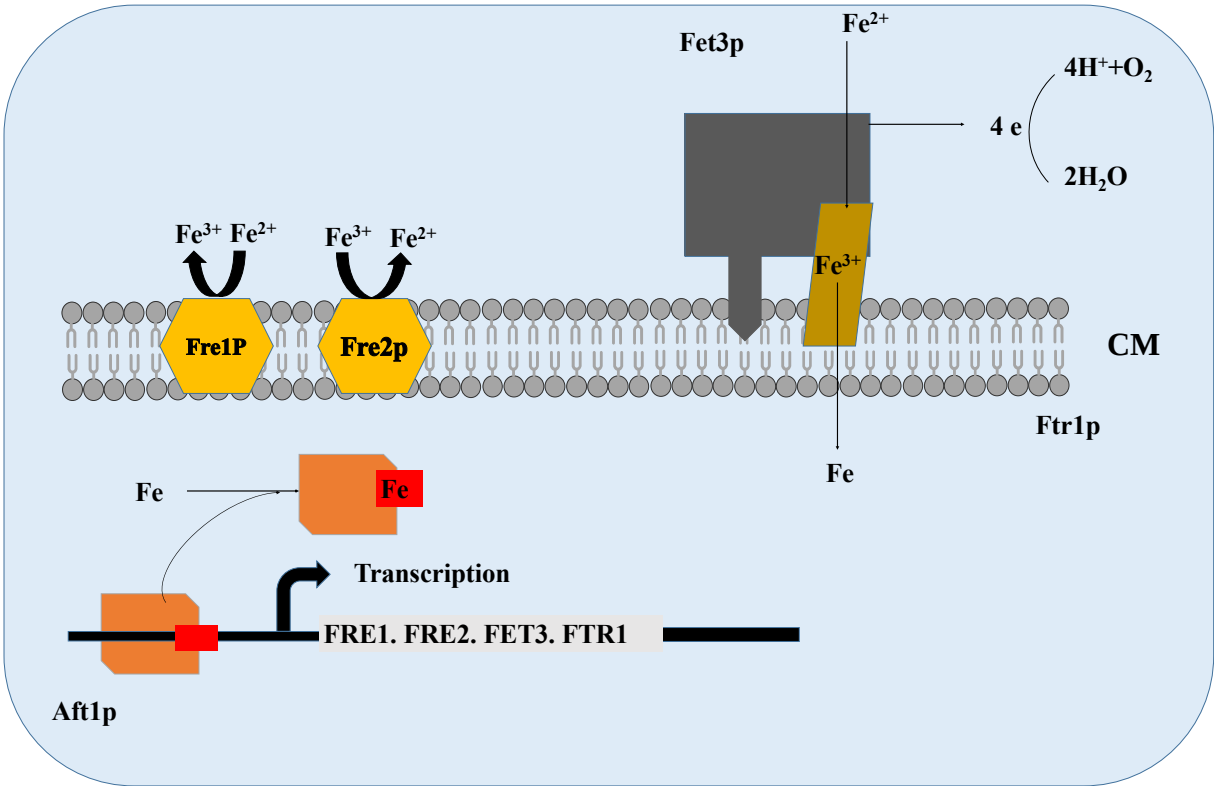

Figure 1.17: Schematic representation of iron uptake and regulation components in yeast. Ferric iron is reduced to ferrous by Fre1p and Fre2p -NADPH dependent reductases. Fe^{2+} is then oxidized to Fe^{3+} with O_2 as oxidant, by the activity of the multi-copper ferroxidase (Fet3p), that is associated with Ftr1p in the CM. Fe^{3+} is then transported into the cell via the Ftr1p permease. FRE1, FRE2, FET3, and FTR1 are transcribed depending on iron need by the transcriptional activator Aft1p. Adapted from Anthony *et al*. (2002).

1.6. Regulation of iron transport

1.6.1. Fur

Iron metabolism and transport in prokaryotes is usually related to its availability in the environment. Fur is a global regulator common in Gram-negative bacteria, that acts as a transcriptional repressor of iron-regulated promoters via its ferrous ion-dependent DNA binding activity (D'Autréaux *et al*., 2004; Lorenzo *et al*., 1999). However, there are examples where Fur activates expression and where the apo-form is capable of transcriptional control. In *E. coli*, Fur is responsible for the regulation of more than 90 genes (Hantke, 2001) involved in

many functions (McHugh *et al.*, 2003; Seo *et al*., 2014; Marcoleta *et al*., 2018, Sastry *et al*., 2019). The mechanism of iron uptake and iron consumption in bacteria is regulated in response to iron availability. It also controls the production of bacterial virulence factors such as shiga toxin in *Shigella dysenteriae* and haemolysin in *E. coli* (Ratledge and Dover, 2000). Fur regulates virulence factors in other bacteria also, e.g. endotoxin A in *Pseudomonas* (Crichton, 2009). *fur* mutation in bacteria causes overexpression of siderophore receptors in the OM and excretion of siderophores during iron availability. This shows that Fur plays a significant role for regulation of the biosynthesis of siderophores. Therefore, Fur is a major regulator of iron uptake in *E. coli*, particularly the enterobactin and ferrichrome transport systems (Earhart, 1996). In *E. coli*, Fur is a repressor for not only gene control for iron acquisition during iron abundance (<5 µM) (McHugh, 2003 ; Andrews *et al.*, 2003) but also control of genes which are responsible for non-iron acquisition functions such as methionine biosynthesis, respiration, the tricarboxylic acid cycle (TCA) cycle, glycolysis, flagella mobility, DNA packaging of phage, DNA synthesis, purine metabolism and redox stress resistance (McHugh *et al*., 2003). The *fur* mutant phenotype has been identified in many bacteria, including *Salmonella* and *E. coli*. *Salmonella fur* mutants are more sensitive in low pH environment (acid stress) (Foster and Hall, 1992). In *E. coli*, growth inhibition on non-fermentable carbon sources is observed due to respiration deficiency, and the *fur* mutants are also susceptibility to redox stress caused by high level of labile iron in their cytoplasm (Hantke, 1987). Fur binds to a Fur box, located between the predicted -35 and -10 boxes, as a pair of homodimers (Kammler *et al*., 1993; Brutscher *et al*., 2006). The binding of Fur to its ferrous iron co-repressor increases the affinity for its DNA binding site by ~1000-fold (Smith *et al*., 1996).

1.6.2. RyhB

The Fe^{2+}–Fur complex represses the *ryhB* gene, which encodes RyhB, a small non-coding RNA that controls expression of a subset of genes in *E. coli* in response to iron (Murphy and Payne, 2007). A number of genes in *E. coli* that are indirectly induced by Fur are negatively regulated by RyhB - these include as *acnA, bfr, sdh* and *sodB*. This indicates that Fur plays a key role in controlling such genes under iron sufficiency (Massé and Gottesman, 2002). RyhB thus mediates an 'iron rationing' or 'iron sparing' process whereby the iron needs of the cell are reduced under iron insufficiency.

1.7. Iron storage

Bacteria have iron reserves housed in iron-storage proteins, in case external iron provisions are ever limited, to avoid toxicity and counter poor iron solubility (Stojiljkovic *et al*., 1993). The three main types of storage proteins are the related bacterioferritins, ferritins and Dps proteins (Figure 1.18) (Ferreira *et al*., 2016; Velayudhan *et al*.,2000; Naikare *et al*., 2006). Ferritins and bacterioferritins support bacterial growth under iron-limited conditions, signifying their role as iron storage proteins (Pandey and Sonti, 2010). Most Dps proteins have DNA-binding capacity and primarily work to protect DNA from redox stress, with a secondary role being iron storage (Pandey and Sonti, 2010). All three types of iron storage protein share common features, including the same architecture, in that they are composed of homologous subunits arranged spherically to form a hollow 'cage' structure. Bacterioferritins and ferritins are larger in size than the Dps proteins. The Dps proteins are constructed from 12 subunits (12-mer) whereas the bacterioferritins and ferritins possess 24 subunits (24-mer); these subunits are similar in structure, maintaining a four-α-helix bundle fold with loops joining the helices (Fig. 1.18 C). The larger bacterioferritins and ferritins are ~500 kDa in size, possessing the capacity to house 2000-3000 iron atoms within their central cavity, whereas the Dps proteins are ~250

kDa in size and have a smaller storage space, holding only ~500 iron atoms (Andrews *et al*., 2003). These three proteins uptake soluble ferrous iron (Fe^{2+}) which is then oxidised to the insoluble ferric (Fe^{3+}) form via a ferroxidation step. In bacterioferritins and ferritins, this reaction occurs in internal ferroxidase centres located in the subunit centres. Contrastingly, in Dps proteins this step occurs at the two-fold boundary between adjacent subunits (Runyen-Janecky *et al*., 2003). Ferric iron is then retained in the cage cavity and as Fe^{3+} depositions build up, a ferrihydrite or amorphous ferric phosphate core forms (Andrews *et al*., 2003)

The bacterioferritins are haem-containing and it is thought that the haem groups provide a route for electrons to reduce the iron core for release of iron from stores (Andrews *et al.*, 2003). *E. coli* has four ferritins: bacterioferritin (Bfr), Dps and two non-haem bacterial ferritins (FtnA and FtnB). Dps proteins utilise H_2O_2-as oxidant whereas ferritins and bacterioferririns are able to use O_2 as oxidant for core formation. Harmless water is the major reduction product (Le Brun *et al*., 2010; Haikarainen and Papageorgiou, 2010).

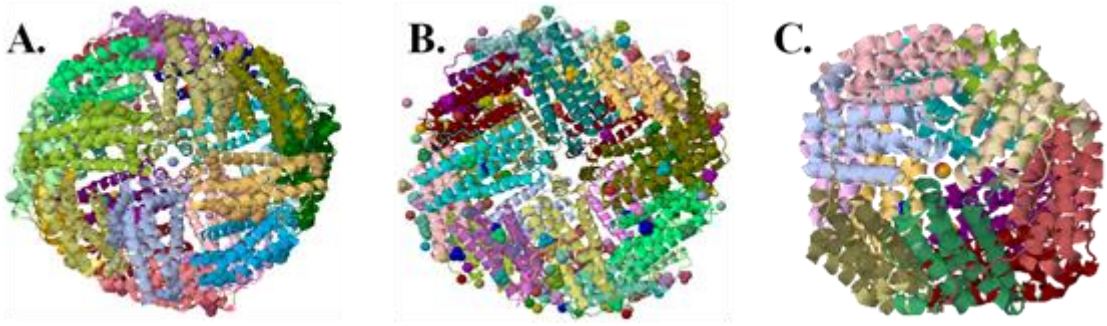

Figure 1.18: Iron storage proteins. A: Crystal structure of 24-meric bacterioferritin from *Mycobacterium tuberculosis*, shown in cartoon view, biological assembly generated in PISA software using PDB code 2WTL; **B:** Crystal structure of 24-meric ferritin from *E. coli*, shown in cartoon view, biological assembly generated in PISA software using PDB code 4REU; **C:** Crystal structure of 12-meric Dps from *Mycobacterium smegmatis*, shown in cartoon view, biological assembly generated in PISA software using PDB code 4M35.

1.8. Aims of this research:

Iron is an essential for nutrient most microorganisms, however, the availability of iron from the environment is limited by the low solubility of the oxidized form that prevails aerobically. To overcome these difficulties, bacteria employ three major strategies to achieve iron balance: high-affinity absorption of iron; iron rationing; and iron storage (Andrews *et al*., 2003). The absorption of iron is the most a crucial strategy for the survival of bacteria under low iron and bacteria normally possess multiple routes for iron acquisition that are of various types (reviewed above); these tend to be specific to either ferrous or ferric iron (Andrews *et al*., 2003).

A common route for bacterial iron uptake involves the ferrous-specific FeoABC system (Dashper *et al*., 2005). Feo-like systems are present in 1076 bacterial species within the Pfam database (containing 2754 species in total), suggesting it has a 39% occurrence. Within the Archaea, the occurrence rate is even greater at 62%. However, some bacteria (e.g. *E. coli*) possess another (or additional) high affinity iron transport system, EfeUOB. This system is less common (583 and 15 EfeU homologues in the Bacteria and Archaea, respectively; 21 and 14% occurrence, respectively), but nevertheless is well represented in the Proteobacteria (38%), Actinobacteria (39%) and Cyanobacteria (65%). The Feo and Efe systems are entirely unrelated yet fulfill the same purpose as ferrous uptake systems. Feo is an anaerobic/microaerobic transporter, whereas Efe is dependent on low pH and aerobic conditions. Thus, Feo and Efe are active under two distinct environmental conditions that each allow ferrous iron stability. However, it is unclear why two systems are required; why Feo only functions under low O_2 regime whereas Efe only functions effectively at low pH and is able to cope with the presence of oxygen at atmospheric levels.

The aim of this work is to further characterize the more recently discovered bacterial iron transporter, EfeUOB, and to compare it with the better known FeoABC system. The specific aim is to more fully determine the environmental requirements for Feo and Efe iron uptake activity and to correlate such requirements to the different mechanisms used by these two systems to transport ferrous iron. It is anticipated that this research will indicate the reasons for two distinct types of ferrous iron transporter in bacteria. *E. coli* will be used as the model.

The **first hypothesis** to be tested is that Feo only operates anaerobically because it is intrinsically sensitive to H_2O_2. It is postulated here that this sensitivity to peroxide is caused by the presence of two highly conserved Cys residues (one each in Gate motifs I and II) within the permease domain. These Cys residues are anticipated to act as iron ligands within the uptake channel of FeoB, and are thus expected to be exposed to solvent and to H_2O_2, when present. Oxidation to sulfenic or sulfinic acid will likely inactivate FeoB rapidly; such inactivation is unlikely to be reversed by sulfenic acid reduction (by the periplasmic DsbG, that reduces sulfenic acid Cys derivatives (Depuydt *et al*., 2009) since FeoB resides in the membrane and so these residues would probably be inaccessible to repair pathways. It is hypothesised that this inactivation process is a design feature of FeoB ensuring rapid shutdown of ferrous-iron uptake under conditions of potential redox stress.

A **second hypothesis** to be tested is that Efe activity is dependent of H_2O_2. Thus, Efe is expected to be able to substitute for Feo aerobically (at low pH) when peroxide levels are relatively high (due to endogenous generation by aerobic metabolic processes). Thus, the overarching hypothesis to be tested is that Feo and Efe are both required due to their distinct responses to H_2O_2, with Feo being specifically inactivated H_2O_2 and Efe activity being driven by H_2O_2.

A third hypothesis is that the FeoB permease domain is structurally and mechanistically akin to that of the nucleoside transporters. This possibility will be investigated by structural characterisation of FeoB. The bottleneck in FeoB membrane protein structure determination is the expression, purification and the crystallisation, and requires that the membrane protein can be purified to monodispersity (Carpenter *et al.* 2008). Thus, in the present work I aim to further evaluate the role and mechanisms of the FeoB membrane embedded domain by X-ray crystallography.

Chapter 2. Materials and Methods

2.1. Water

The qH_2O used was ultra-purified by ion exchange and reverse osmosis (18.2 Ω) using a Barnstead system.

2.2. Bacterial growth conditions

All media were purchased from Difco, Melford, Oxoid, Fisher or Sigma, unless stated otherwise. *Escherichia coli* strains were routinely cultured aerobically at 37 ºC in Lysogeny broth (LB) medium or M9 minimal salts medium (Smith & Bidochka, 1998; Sambrook and Russell, 2001). Liquid cultures were incubated with shaking (200-250 rpm, G10 Gyrotory Shaker, New Brunswick Scientific Co., U.S.A.) for 14-16 h (overnight). Media (routinely stored at 4 ºC) were supplemented with antibiotics where necessary to select for strains carrying recombinant plasmids. For plasmid DNA isolation, *E. coli* cultures were incubated for 14-16 h in LB, with appropriate antibiotic (Sambrook and Russell, 2001).

2.3. Storage of bacterial strains

E. coli strains were routinely stored at -80 ºC in cryo-tubes as glycerol stocks (Sambrook and Russell, 2001). Bacteria were recuperated from frozen stocks (preserved on dry ice) by scraping cells from the surface of the frozen culture followed by incubation on LB agar. Resultant single *E. coli* colonies were grown overnight in LB liquid cultures and cells were harvested by centrifugation (at 5000 × *g* for 5 min at room temperature, Eppendorf centrifuge 5810 R). *E. coli* cells were re-suspended in 0.5 ml of fresh LB broth of M9 medium and mixed with an equal volume of sterile 38% (v/v) glycerol and frozen rapidly in dry ice.

2.4. Sterilisation

Reagents were of analytical grade and sterilisation, where required, was achieved by autoclaving at 121 ºC, 15 lb/inch^2 for 15 min. All media were stored long-term at 4 ºC except 'Super Optimal broth with Catabolite repression' (SOC) which was aliquoted and stored at -20 ºC. Antibiotics were added to media that had been cooled to 55 ºC or below; Petri dishes were supplied by Sterilin. Antibiotics and any other solutions requiring sterilisation by filtration were passed through a 0.22 μm filter membrane using either Stericups (Millipore) with a vacuum pump (Fisher Scientific) or Pall Life Sciences acrodisc syringe filters with BD Plastipak 5 ml or 10 ml syringes (Becton, Dickenson and Company, U.K.). Glassware used in microbiological procedures was sterilised by dry heat (150 ˚C for 2 to 2.25 h). For all iron-restricted growth, acid-washed glassware was used.

2.5. Microbiological growth media

Standard media recipes were prepared as previously described (Sambrook and Russell, 2001).

2.5.1. Luria-Bertani (LB) medium: 1% (w/v) Bacto-tryptone, 0.5% (w/v) Bacto-yeast extract and 0.5% (w/v) NaCl, adjusted to pH 7.2 with 5 M sodium hydroxide. Solid medium was made by addition of 1.5% (w/v) Bioagar (15 g/L, Biogene Ltd.) prior to sterilisation.

2.5.2. M9 minimal salts medium: M9 minimal salts medium was prepared with 1 × M9 salts (Sigma), 0.4% (w/v) sterile glucose, 0.1 mM $CaCl_2$, 2 mM $MgSO_4$, 0.001% thiamine in sterile qH_2O. The $MgSO_4$ and $CaCl_2$ solutions were prepared and sterilised separately and added last to the medium. M9 minimal salts agar was produced by adding 1.5% (w/v) Bioagar to the qH_2O prior to sterilisation (Smith and Bidochka, 1998; Sambrook and Russell, 2001).

2.5.3. SOC medium: SOC medium is a nutrient-rich medium that enables optimized recovery of transformation and electroporation cells. This was prepared with 2% (w/v) bacto-tryptone,

0.5% (w/v) bacto-yeast extract, 0.05% (w/v) NaCl, 2.5 mM KCl and 10 mM $MgCl_2$, adjusted to pH 7.0 with 5 M NaOH and sterilised. Filter-sterilised glucose was added to give 20 mM final concentration. After sterilization, the final volume was adjusted with sterile qH_2O (Hanahan, 1983).

2.6. Chemicals

All chemicals were of analytical grade or higher and were purchased from Bio-Rad Fluka, Fisher, Melford or Sigma unless otherwise stated.

2.6.1 Phosphate Buffered Saline (10 × PBS): 136 mM NaCl, 27 mM KCl, 0.015 M KH_2PO_4 and 0.08 M Na_2HPO_4 in qH_2O. The buffer was adjusted to pH 7.4 with 2 M HCl. The final volume was adjusted with qH_2O and the buffer was sterilised.

2.6.2. Tris-borate-EDTA (TBE) Electrophoresis Buffer: 0.04 M Tris (tris(hydroxymethyl)aminomethane) and 1 mM EDTA in qH_2O. The buffer was adjusted to pH 7.8 with glacial acetic acid and the final volume was adjusted with qH_2O. The buffer was sterilised.

2.6.3 Tris-borate-EDTA (TBE) 5X Electrophoresis Buffer. In qH_2O: 5.4% (w/v) Tris base, 2.75% (w/v) boric acid, 2% (v/v) EDTA. For use in agarose gel electrophoresis, TBE 5X was diluted to 0.5X before use.

2.6.4. Tris-buffered Saline (TBS) Buffer

In qH_2O: 0.242% (w/v) Tris base, 2.92% (w/v) NaCl. The pH was adjusted to 7.5 via the dropwise addition of NaOH (aq).

2.6.5. Tris-buffered Saline with Tween 20 (TTBS) Buffer

In qH_2O: 0.242% (w/v) Tris Base white crystalline powder (Fisher Scientific), 2.924% (w/v) NaCl(s), 0.05% (v/v) Tween 20. The pH was adjusted to 7.5 via the dropwise addition of NaOH (aq).

2.6.6. Resolving Gel Buffer

In qH_2O (for 1.5 M buffer): 18.6% (w/v) Tris base. The pH was adjusted to 8.8 via the dropwise addition of NaOH (aq).

2.6.7. Stacking Gel Buffer

In qH_2O (for 1 M buffer): 12.1% (w/v) Tris base. The pH was adjusted to 6.8 via the dropwise addition of NaOH(aq).

2.6.8. Running Buffer

In qH_2O: 0.305% (w/v) Tris base, 1.44% (w/v) glycine, 0.1% (w/v) sodium dodecyl sulphate (SDS).

2.7. Enzymes

All restriction enzymes were purchased from Promega, New England Biolabs or Fisher Scientific. DNA polymerase and Quick ligase were purchased from Bioline and Fisher Scietific. All the enzymes were used according to the manufacture's instruction with the appropriate buffers (1 µg DNA with 1 µl restriction enzyme in 20 µl reactions).

2.8. DNA size marker and protein size markers

GeneRuler^{TM} 1 kb DNA ladder from Fisher Scientific was used to determine the size and quantity of DNA following gel electrophoresis and Page-ruler pre-stained protein ladder from Thermo Scientific was used for SDS-PAGE gels and western blotting (see Fig. 2.1 below).

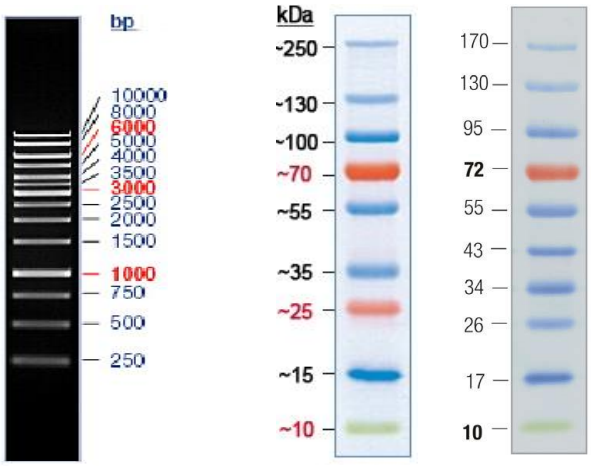

(A) **(B)**

Figure 2.1. A. DNA marker. GeneRuler 1kb ladder (250-10000 bp) from Fermentas (Fisher Scientific) was used to estimate the size and quantity of DNA. B. PageRuler™ protein plus prestained protein marker. Thermo Scientific Protein Ladder is a mixture of nine (9) blue-, orange- and green-stained proteins (10 to 250 kDa) for use as size standards in protein electrophoresis (SDS-PAGE and Western blotting).
Source: http://2009.igem.org/wiki/images/3/3f/Generuler s_1kb_marker_Fermentas.jpg

2.9. Antibiotics

Antibiotics were prepared as described (Table 2.1) with those dissolved in water being filter sterilised through a sterile 0.22 µm membrane (Whatman) and stored at -20 ˚C. Ampicillin and kanamycin were dissolved in water and sterilised by filtration through a sterile 0.22 µm membrane (Whatman) and stored at -20 ˚C. Those antibiotics prepared in ethanol were assumed sterile by virtue of the solvent used.

Table 2.1. Antibiotics used in this study.

Antibiotic	Mode of action	Uses	Working Strength
Ampicillin (100 mg/ml stock in q H_2O)	Gram negative bacterial. Inhibits cell wall peptidoglycan synthesis at the transpeptidation step	Selection and maintenance of *E. coli* strain carrying the β-lactamase gene	100 µg/ml
Chloramphenicol (50 mg/ml in ethanol)	Bacteriostatic, inhibits 50 S ribosomal elongation	Selection and maintenance of *E. coli* strains carrying the *cat* gene	50 µg/ml
Kanamycin (50 mg/ml stock in q H_2O).	Interacts with 30S subunit of bacterial ribosomes and inhibits translocation during protein synthesis	Selection and maintenance of *E. coli* strains carrying the *kan* gene.	25-50 μ g/mL

2.10. Centrifugation

A Biofuge benchtop Microcentrifuge (MSE) was used to centrifuge volumes smaller than 1.5 ml, a Biofuge benchtop centrifuge (Centaur) was used for centrifugation of 2.5-50 ml samples at room temperature. A benchtop BR401 refrigerated centrifuge (Denley) was used for centrifugation of 2.5-50 ml samples at 4 ºC. An ultra centrifuge was used for centrifugation of membrane protein samples.

2.11. Bacterial strains and plasmids

The bacterial strains and plasmids used and constructed during this study are listed in Table 2.2.

Table 2.2. Bacterial strains and plasmids. All strains are *E. coli* K-12, unless otherwiswe indicated.

Bacterial Strain	Characteristics	Reference/Source
Sakai 813 (*E. coli* O157 *stx*$^-$)	Sakai Δ*stx1A*, Δ*stx2A*::*kan*	(Zhang et al., 2004)
***E. coli* W3110 (*E.coli* K-12)**	Wild-type F$^-$ λ$^-$ Δ(*rrnD-rrnE*)1 *rph*$^-$ (defective *efe* system)	Chris Rensing
***E. coli* LC106**	MG1655: Δ *ahpCF'* *kan*::*'ahpF* Δ (*katG17*::Tn*10*)1 Δ (*katE12*::Tn*10*)1	L.Seaver (2004)
***E. coli* MG1655**	Wild-type F- λ$^-$ *ilvG rfb-50 rph-1*	Lab stock
TUV93-0 (*E. coli* O157 *stx*$^-$)	EDL933 Δstx1A, Δstx2A	(Campellone *et al*, 2002)
***E. coli* JC28**	W3110, Δ*fecABCDE*, Δ*zupT*, Δ*mntH*, Δ*entC*, Δ*feoABC*.	Cao *et al*., 2007
***E. coli* JC32-1**	W3110, Δ*fecABCDE*, Δ*zupT*, Δ*mntH*, Δ*entC*, Δ*feoABC* Δ*efeU*	Lab stock
***E. coli* JC32-2**	W3110, Δ*fecABCDE*, Δ*zupT*, Δ*mntH*, Δ*entC*, Δ*feoABC* Δ*efeU*	Lab stock
***E. coli* JC33**	W3110, Δ*fecABCDE*, Δ*zupT*, Δ*mntH*, Δ*entC*, Δ*feoABC* Δ*efeO*	Lab stock
***E. coli* JC34**	W3110, Δ*fecABCDE*, Δ*zupT*, Δ*mntH*, Δ*entC*, Δ*feoABC* Δ*efeB*	Lab stock
***E. coli* TOP10**	*E. coli* F$^-$ *mcrA* Δ *(mrr*$^-$ *hsdRMS mcrBC)* φ80*lacZ*Δ*M15* Δ*lacX74 nupG recA1 araD139* Δ*(ara-leu)7697 galE15 galK16 rpsL* (Str^R) *endA1* λ$^-$	Sambrook *et al.*, 2001
***E. coli* BL21(λDE3)**	F$^-$, *ompT*, *hsdSB*, (rB$^-$, mB$^-$), *dcm*, *gal*, λ DE3.	Promega
***E. coli* BW25113**	F$^-$ Δ (*araD-araB*)*567* Δ *lacZ4787*(::*rrnB*- 3) λ$^-$ *rph-1* Δ (*rhaD-rhaB*)*568 hsdR514*	Lab stock
***E. coli* Stellar**	F$^-$, *ara*, Δ(*lac-proAB*)[Φ80d *lacZ*Δ*M15*], *rpsL*(*str*), *thi*, Δ(*mrr-hsdRMS-mcrBC*), Δ*mcrA*, *dam*, *dcm*	Clontech
***E. coli* S17**	λ*pir*, RP4-2(Km::*Tn*7,Tc::Mu-1), *pro-82*, *recA1*, *endA1*, *thiE1*, *hsdR17*, *creC510*	Lab stock
E. coli* JC28 Δ*ftsH	W3110, Δ*fecABCDE*, Δ*zupT*, Δ*mntH*, Δ*entC*, Δ*feoABC* Δ*ftsH*	This study
E. coli* JC32 Δ*ftsH	W3110, Δ*fecABCDE*, Δ*zupT*, Δ*mntH*, Δ*entC*, Δ*feoABC* Δ*efeU* Δ*ftsH*	This study
***E. coli* AR3289**	W3110, *sfhC21*, z*ad220*::*Tn*10	Tatsuta *et al.* (1998)
***E. coli* AR3291**	W3110, Δ*ftsH*3::*kan* s*fhC21*, *zad220* ::*Tn*10	Tatsuta *et al.* (1998)
***E. coli* JW1224-1**	BW25113 Δ*galU*::*kan*	Baba *et al.* (2006)
***E. coli* JW1224-2**	BW25113 Δ*galU*::*kan*	Baba *et al*. (2006)

2.12. Plasmids

All plasmid stocks were maintained at -20 ºC in qH_2O. Plasmid details are listed in Table 2.3.

Plasmid name	Genotype	Antibiotic resistance	Source / Reference
pBADara	Is a plasmid. An arabinose inducible promoter; *araC*, pBR322-derived expression vectors.	Amp^R	Guzman *et al*., (1995)
pBADrha	Rhamnose induced expression vector, ori_{p15}*rhaR rhaS* P_{rhaB} Cm^r	Cm^R	Ford *et al*., (2014)
pBADrha-*efeUOB*^{O157}	pBADrha plus *efeUOB* system from *E. coli* O157:H7	Cm^R	This work
pBADrha-*feoABC*	pBADrha containing the *E. coli feoABC* operon	Cm^R	This work
pBADrha-*efeU*OB*$^{K-12}$	pBADrha plus *efeUOB* 'corrected' system from *E. coli*	Cm^R	This work
pBADara-*efeUOB*^{O157}	pBADara plus *efeUOB* system from *E. coli* O157:H7	Amp^R	This work
pBADara-*feoABC*^{O157}	pBADara plus *feoABC* system from *E. coli* O157:H7	Amp^R	This work
pBADara-*efeU*OB*$^{K-12}$	pBADara plus *efeU*OB* system from *E. coli*	Amp^R	This work
pBADara-*feoAB*^{O157}	pBADara plus *feoAB* system from *E. coli* O157:H7	Amp^R	This work
pBADara-*feoA*^{O157}	pBADara plus *feoA* gene from *E. coli* O157:H7	Amp^R	This work
pBADara-*feoB*^{O157}	pBADara plus *feoB* gene from *E. coli* O157:H7	Amp^R	This work
pBADara-*feoC*^{O157}	pBADara plus *feoC* gene from *E. coli* O157:H7	Amp^R	This work
pBADara-*feoBC*^{O157}	pBADara plus *feoBC* system from *E. coli* O157:H7	Amp^R	This work
pBADrha-*feoAB*^{O157}	pBADrha plus *feoAB* system from *E. coli* O157:H7	Cm^R	This work
pBADrha-*feoA*^{O157}	pBADrha plus *feoA* gene from *E. coli* O157:H7	Cm^R	This work
pBADrha-*feoB*^{O157}	pBADrha plus *feoB* gene from *E. coli* O157: H7	Cm^R	This work
pBADrha-*feoC*^{O157}	pBADrha plus *feoC* gene from *E. coli* O157:H7	Cm^R	This work
pBADrha-*feoBC*^{O157}	pBADrha plus *feoBC* gene from *E. coli* O157:H7	Cm^R	This work

pBADara-HisTAG-*feoA*^{O157}	pBADara plus HisTAG-*feoA* gene from *E. coli* O157:H7	Amp^R	This work
pBADara-*feoA*^{O157}-HisTAG	pBADara plus *feoA*- HisTAG gene from *E. coli* O157:H7	Amp^R	This work
pBADara-*feoB*^{O157}-HisTAG	pBADara plus *feoB*- HisTAG gene from *E. coli* O157:H7	Amp^R	This work
pBADara-HisTAG *feoB*^{O157}	pBADara plus HisTAG *feoB* gene from *E. coli* O157:H7	Amp^R	This work
pBADara-*feoAB*^{O157}-HisTAG	pBADara plus *feoAB*-HisTAG gene from *E. coli* O157:H7	Amp^R	This work
pBADara-HisTAG-*feoAB*^{O157}	pBADara plus HisTAG-*feoAB* genes from *E. coli* O157:H7	Amp^R	This work
pBADara-HisTAG-*feoBC*^{O157}	pBADara plus HisTAG-*feoBC* gene from *E. coli* O157: H7	Amp^R	This work
pBADrha-FlagTAG-*feoA*^{O157}	pBADrha plus FlagTAG-*feoA* gene from *E. coli* O157: H7	Cm^R	This work
pBADrha-*feoA*^{O157}-FlagTAG	pBADrha plus *feoA*-FlagTAG gene from *E. coli* O157:H7	Cm^R	This work
pBADrha-*feoB*^{O157}-FlagTAG	pBADrha plus *feoB*-FlagTAG gene from *E. coli* O157:H7	Cm^R	This work
pBADrha-FlagTAG *feoB*^{O157}	pBADrha plus FlagTAG *feoB* gene from *E. coli* O157:H7	Cm^R	This work
pBADrha-*feoAB*^{O157}-FlagTAG	pBADrha plus *feoAB*-FlagTAG gene from *E. coli* O157:H7	Cm^R	This work
pBADrha-FlagTAG-*feoAB*^{O157}	pBADrha plus FlagTAG-*feoAB* genes from *E. coli* O157:H7	Cm^R	This work
pBADrha-FlagTAG-*feoBC*^{O157}	pBADrha plus FlagTAG-*feoBC* gene from *E. coli* O157:H7	Cm^R	This work
pHSG-*efeUOB*^{O157}	pHSG576 plus *efeUOB* from *E. coli* O157:H7	Cm^R	Salunkhe (2016)
pHSG-*efeU*OB*^{K12}	pHSG576 plus *efeUOB* system from *E. coli* K-12		Lab stock Cao *et al.* (2007)

pHSG-*feoABC*^{O157}	pHSG576 plus *feoABC* operon from *E. coli* O157:H7	Cm^R	Salunkhe (2016)
pHSG576	Low copy number plasmid, *lacZ*$^{\alpha}$, Cam^R.	Cm^R	Takeshita *et al*., (1987)
pJET1.2	Cloning vector	Amp^R	Fermentas
pET21a	Over-expression vector Amp^R, *lacI*, pBR322 ori	Amp^R	Novagene (lab stock)
pET21a-*feoB*	pET21a plus *feoB* from *E. coli* O157:H7	Amp^R	This study
pTri-Ex 1.1	Insect, bacterial, and mammalian vector for expressing proteins with a C- terminal HSV-8xHis cassette.	Amp^R	Novagene
pTri-Ex-HisTAG-*feoB*	pTri-Ex vector carrying N- terminal his tagged *feoB* from *E. coli O157*	Amp^R	This study
pTri-Ex-*feoB*- His TAG	pTri-Ex vector carrying C- terminal his tagged *feoB* from *E. coli O157*	Amp^R	This study
pTri-Ex-*feoB*	pTri-Ex vector carrying *feoB* from *E. coli O157*	Amp^R	This study
pTri-Ex-*feoB*- Flag TAG	pTri-Ex vector carrying C- terminal his tagged *feoB* from *E. coli O157*	Amp^R	This study
pTri-Ex-*feoB*-eGFP	pTri-Ex vector carrying N- terminal his tagged *feoB* from *E. coli O157*	Amp^R	This study
pCP20	Knockout plasmid 9.4 kb, temperature-sensitive replication and thermal induction of FLP synthesis.	Cm^R and Amp^R	(Datsenko and Wanner, 2000)
pKD3	Plasmid for gene disruption., containing FRT-flanked *cat* gene from pSC140	Amp^R and Cm^R	Mori *et al.*, 2000
pKD4	Tempreture sensitive replication (*repA101*st); encoding lamda *red* genes (*exo*,*bet*,*gam*). Derived from pINT-ts, containing *araC-ParaB*. Also, Amp^R contains the tL3 terminator this plasmid can be cured of strain with growth at 37-42° C	Amp^R	Lab stock

2.12.1. pHSG576 vector

pHSG576 is a low-copy plasmid encoding chloramphenicol resistance (Takeshita *et al*., 1987). This plasmid carries the PolI-independent pSC100 origin of replication (Camps and Loeb, 2003). Restriction maps of pHSG576, pHSG576-*feoABC*^{O157}, pHSG576-*efeU*OB*$^{K-12}$ and pHSG576-*efeUOB*^{O157} illustrating the multiple cloning site, Cam^R locus and *lacZ* gene are provided in the Appendix.

2.12.2. pBADara vector

pBADara is described as a low-copy number plasmid. The pBADara plasmids are pBR322-derived expression vectors designed for regulated expression and encoding ampicillin resistance. It includes an arabinose inducible promoter (P_{BAD}) and *araC*, the regulatory gene. The regulatory protein, AraC, is provided by the pBADara vectors allowing regulation of P_{BAD}. Induction of expression occurs in the presence of L-arabinose, whilst expression from P_{BAD} is turned off in the absence of L-arabinose producing very low levels of transcription from P_{BAD} (Lee *et al*., 1981; Lee *et al.*, 1987). Restriction maps of pBADara pBADara-*feoABC* pBADara-*efeUOB*^{O157} and pBADara-*efeU*OB*-K-12 are provided in the Appendix.

2.12.3. pBADrha vector

pBADrha is a plasmid encoding chloramphenicol resistance. A rhamnose inducible promoter is utilised from pSCrhaB2 (Cardona & Valvano, 2005; Ford *et al*., 2014) to allow controlled expression. The plasmid carries P_{rhaB}, a rhamnose inducible promoter; *rhaR* and *rhaS*, regulatory genes of the rhamnose promoter; the *rrnB*T1T2 transcriptional terminator; M13*ori* (an M13 origin of replication allowing generation of single-stranded DNA); and p15A*ori* (a p15A origin of replication). Restriction maps of pBADrha, pBADrha-*feoABC*, pBADrha-*efeUOB*^{O157} and pBADrha-*efeU*OB*-K-12 are provided (Appendix).

2.12.4. pTriEx 1.1 vector

pTriEx-1.1 is a plasmid conferring ampicillin resistance. It contains an IPTG-inducible promoter and is designed to allow rapid characterization of target genes in multiple expression systems. pTriEx™-1.1 can be used to test expression in insect cells, vertebrate cells and, *E. coli*. Expression in vertebrates is achieved via a promoter consisting of a CMV immediate early enhancer linked to the β-actin promoter from chicken. Insect cells expression is enabled by baculovirus sequences that mediate generation of baculoviruses via the BacVector™ System.

This requires the use of baculovirus-infected insect cells where expression is then dependent on the p10 promoter. In *E. coli*, expression is dependent on a T7*lac* promoter and requires T7 RNA polymerase producing strain to be used as host (e.g. BL21(DE3) pLacI), enabling IPTG induction. A restriction map of pTriEX1.1-*feoB* is provided (Appendix).

2.13. Cloning methods

2.13.1. Preparation of plasmid DNA

A single colony from *E. coli* carrying the plasmid was inoculated into 5 ml LB containing the suitable antibiotic and incubated overnight at 37 ºC with shaking at 250 rpm. Then the cells were harvested, and plasmid DNA was detected by a GeneJET™ plasmid Miniprep kit (Thermo Scientific) according to the manufacturer's instructions. The fragment size was confirmed by gel electrophoresis. All plasmids were eluted in qH_2O and stored at -20 ºC.

2.13.2. Polymerase chain reaction (PCR)

A BioLabs Q5® High Fidelity DNA polymerase kit was utilized for DNA amplification. Each 20 µl PCR reaction contained the following components: 4 µl of 5x GC buffer, 0.4 µl of 10 mM dNTPs, 1.5 µl of 0.5 µM primers, 0.6 µl of 3% DMSO, 1-2 µl DNA (60-100 ng/µl) and up to 20 µl sterile qH_2O. Hi Fi DNA polymerase enzyme was also used according the manufacturer's instructions (Clontech). PCR was performed using 30 thermal PCR cycles, typically using the regime below unless indicated otherwise:

Initial denaturation	**98 ˚C, 3 min**	**1 cycle**
Denaturation	98 ˚C, 30 s	30 cycles
Annealing	61-71 ˚C, 30 s	
Extension	72 ˚C, 5 min	
Final Extension	72 ˚C, 5 min	1 cycle

2.13.3. Purification of PCR products

PCR products were purified using the GeneJET^{TM} PCR Purification Kit (Thermo Fisher Scientific), according to company instructions. One volume of binding buffer was added to the PCR product, up to 800 µl of the re-suspension solution was transferred to the GeneJET^{TM} purification column which was then centrifuged for 1 min. 700 µl of wash buffer were added and the column was then centrifuged again for 1 min. The column was centrifuged for 1 min, then 35 µl of qH_2O were added and the column was centrifuged for 1 min at 1000 rpm. The DNA was then stored at -20 ºC.

2.13.4. Restriction digestion

DNA digestion of PCR products and vectors was generally performed in 20-35 µl volumes containing 50-100 ng/µl DNA, 2 µl of 10x FastDigest Buffer and 0.5 µl of appropriate restriction enzymes. The mixture was incubated in water bath at 37 ºC for about 20-30 min. The digested DNA was purified using PCR product purification kit (Thermo Fisher Scientific).

2.13.5. Colony PCR

Colony PCR was used as a method to detect the absence or presence of insert DNA in plasmid constructs in multiple colonies. This was performed by designing primers annealing to the cloning-site flanking regions of the selected plasmid. Reactions consisted of a 25 µl volume

containing 2.5 µl 10x Dream TaqTM DNA polymerase buffer, 0.5 µl 10 mM dNTPs, 1 µl 10 µM forward primer, 1 µl 10 µM reverse primer, 1 µl $MgCl_2$, 18.7 µl qH_2O and 0.3 µl Dream TaqTM DNA polymerase, added on ice to a 0.2 µl PCR tube. The desired colony was then touched using a sterile fine yellow tip attached to a Gilson pipette set to 20 µl, which was heated to 99 °C 2 min, then a 5 µl volume of colony suspension was taken, which was added to the PCR reaction mixture. The mixture was then mixed and microcentrifuged for 20 sec. PCR amplifications were performed in an Eppendorf Mastercycler® gradient PCR machine: initial heating step at 95 °C for 3 min; 35 cycles with 1 min at 95 °C (denaturation), 1.5 min at 45 °C (annealing) and 1 min at 72 °C (extension); a final extension step at 72 °C for 5 min. The PCR reactions were cooled to 4 °C and reactions were analysed for the appropriate plasmid insert by agarose gel electrophoresis (section 2.20).

2.13.6. Confirmation cloning or deletion by PCR

Taq DNA polymerase (Thermo Fisher Scientific) was used according to the company protocol to carry out the PCR reaction with a Master cycler gradient thermal cycler (Eppendorf) machine. Each reaction was performed in a 25 µl volume containing: 2.5 µl of Dream Taq buffer, 0.5 µl of 10 µM dNTP, 2 µl of 10 µM forward and reverse primers, 1 µl $MgCl_2$, 1 µl of purified DNA template, 18.8 µl of q H_2O and finally 0.2 µl of DNA polymerase was added to start the reaction.

The programme for fragment amplification was as follow: an initial denaturing step at 95 °C for 3 min, 95 °C for 30 sec, followed by 35 cycles at 95 ºC for 30 sec (denaturing), 60-66 °C for 30 sec (annealing), and then 72 °C for 10 min for the extension step. Then followed by 30 cycles at 95 ºC for 30 sec and finally a 72 ˚C at 5 min and hold 4 ˚C. The PCR product was purified according to the manufacturer's instructions using a GeneJET PCR purification kit (Thermo Fisher Scientific) and stored in -20 ˚C.

2.13.7. Ligation reactions

Ligation of the purified *efeUOB* PCR product and the pBAD vector was performed using Fusion cloning (Thermo Fisher Scientific) following the sticky-end cloning protocol. The total volume was 20 µl: 10 µl of 2x reaction buffer, 1 µl (25-50 ng/µl) PCR product, 1 µl (50-100 ng/µl)cut plasmid DNA, 7 µl qH_2O and 1 µl (200 units or 50 ng/µl) T4 DNA ligase. The mixture was incubated at room temperature for 5 min and stored at -20 $^{\circ}$C for transformation.

For classical ligation reactions, the purified PCR product and pBAD vector were quantified and digested with the appropriate restriction enzymes before use in ligation reactions. All DNA digestions of PCR product and vector were generally performed in 10 µl total volume containing 1 µl (30ng/ µl) DNA, 7.5 µl qH_2O, 1 µl fast digestion buffer and the 0.5 µl of the appropriate restriction enzymes. The mixture was incubated for 15 min to 1 h in 37 ºC. The digested and purified PCR products and vector were ligated together in a volume of 10 µl containing 70-100 ng of the digested PCR product and 100-200 ng of the digested plasmid (to give a ~3:1 molar ratio), 1X T4 ligase buffer (Fermentas) and 3 U of T4 ligase (Thermo Fisher Scientific). Sticky-end ligations were incubated at room temperature for 10 min whereas sticky end ligations were incubated for 1 h. In both cases, 2-3 µl was used for transformation of 200 µl of chemically competent cells.

2.14. Gene knockout

2.14.1. Lambda (λ) Red disruption system

ftsH gene knockout in *E. coli* JC32 strain was made using the Wanner method (Datsenko and Wanner, 2000). This method relies upon the presence of a low copy, temperature sensitive "helper" plasmid encoding components of the homologous recombination system found in bacteriophage λ. These components are called Exo (a 5'- 3' exonuclease, which processes along

double-stranded DNA), Bet (a single-stranded DNA-binding protein, which is able to anneal complementary single strands) and Gam (an inhibitor of host RecBCD exonucleases). Expression of these genes is under the control of an arabinose-inducible promoter (pBAD). When cells carrying the plasmid are grown in the presence of arabinose, exogenously applied linear DNA is able to undergo homologous recombination with the bacterial chromosome. In this way, it is possible to generate an in-frame gene deletion using a PCR product.

2.14.2. Primer design

Primers were designed to anneal at the 4th codon and the penultimate codon of the target gene, (Table 2.4), allowing generation of an in-frame deletion with minimal downstream effects. The 5' end of each primer (between 45-48 nucleotides) was according to the target gene, whereas the 3' end of each primer was designed to amplify the chloramphenicol resistance cassette encoded by pKD3. This plasmid was selected for use due to the fact that it bears very little similarity to the *E. coli* genome and so potential generation of unwanted side product was reduced.

2.14.3. PCR amplification of *cat* cassette

The plasmid pKD3 was used as a template for PCR so that linear DNA encoding the Cm^{R} cassette could be generated. PCR was carried out as described in Section 2.13.2 and the product was purified as described in Section 2.13.3.

2.14.4. Induction and preparation of host cells

Cells carrying the pKD46 plasmid were grown in LB (containing antibiotics as appropriate) at 30 °C, 250 rpm for 4 h. At this point, arabinose was added to a final concentration of 10 mM in order to induce expression of the homologous recombination system. The cells were incubated under the same conditions for 1 h and then harvested by centrifugation at 4,000 rpm for 20 min at 4 °C. The cell pellet was then aspirated and re-suspended in 1 ml ice cold qH_2O. The cells were then centrifuged at 13,000 rpm for 1 min, the supernatant was removed, and the pellet was re-suspended in the same volume of ice-cold water. This washing process was repeated five times in total, after which the cells were re-suspended in a volume of ice-cold water approximately double that of the pellet. The cells were then aliquoted into pre-chilled electroporation cuvettes and incubated on ice for 15 minutes prior to use.

2.14.5. Electroporation with linear DNA

About 1-2 µg of the linear PCR amplified DNA were added to each electroporation cuvette and mixed by pipetting. The cell/DNA mixture was then electroporated. The cells were incubated at 30 °C for 1-2 h and subsequently spread on solid medium containing chloramphenicol (8 µg/ ml). The plates were then incubated at 37 °C overnight. Next day, single colonies were selected for further work and propagated on L-agar plates containing (34 µg/ ml) chloramphenicol.

2.15. Cloning of *efeUOB*^{O157}, *efeUOB*$^{K-12}$ and *feoABC*^{O157} DNA fragments into the pBADrha vector using In-Fusion Cloning

For cloning *efeUOB*^{O157}, *efeUOB*$^{K-12}$ and *feoABC*^{O157}, PCR was employed using a high-fidelity polymerase with primers providing a *Nde*I site at the start codon and a *Sal*I site just downstream of the stop codon. Primers used are indicated in Table 2.4; these where dissolved in sterile qH_2O

to give 100 pmol/µl as a stock which was diluted 1:10 to get 10 pmol/µl as a working primer solution. These were stored at -20 ºC. The primers were designed according to the procedures in the manual of In-Fusion® HD Cloning Kit User. PCR reaction mixtures of 25 µl were assembled on ice and were composed of 5 µl 5x reaction buffer, 0.5 µl of 10 mM dNTPs, 1.25 µl each of forward and reverse primer, 1 ng to 1 µg of template DNA and 0.25 µl (0.2 U/µl) of DNA polymerase, made to the final volume with sterile distilled water. Each PCR fragment was purified using the GeneJet PCR purification kit (Thermo Fisher Scientific) then cloned into the equivalent sites of pBADrha (vector linearized with *Sal*I and *Nde*I restriction enzymes), according to the Quick-Fusion Cloning Kit protocol. To generate pBADrha-*efeUOB*^{O157}, pBADrha-*efeUOB*$^{K-12}$ and pBADrha-*feoABCO*^{157}, Fusion cloning reactions were prepared: 10 µl final volume with insert to vector molar ratio 2:1, ~50 ng of vector DNA, 1 µl of Fusion Enzyme and 2 µl 5x Fusion Buffer. This reaction was incubated for 30 min at 37 °C. Following this, 2-3 µl of each reaction was transformed into Stellar competent cells (Section 2.15). Resulting transformants were picked using a sterile loop and grown overnight in LB and L-agar containing the appropriate antibiotic (Cm^R at 50 µg/ml) for plasmid extraction and analysis by restriction mapping (double digestion by *Sal*I and *Nde*I restriction enzyme), followed by final confirmation by sequencing.

2.16. Cloning of *efeUOB*^{O157}, *efeUOB*$^{K-12}$ and *feoABC* DNA fragments into the pBADara vector using Fusion Cloning Reaction

For cloning *efeUOB*^{O157}, *efeUOB*$^{K-12}$ and *feoABC*, PCR was employed using a high-fidelity polymerase with primers (Table 2.5) providing a *Nco*I site at the start codon and a *Hin*dIII site just downstream of the stop codon. Each PCR fragment was purified and cloned into the equivalent sites of pBADara (vector linearized with *Nco*I and *Hin*dIII restriction enzymes). Following the cloning reaction and subsequent transformation, transformants were selected on L-agar containing the appropriate antibiotic (Amp at 100 µg/ml) and extracted plasmids where

analysed by restriction mapping (double digestion by *Nco*I and *Hin*dIII), followed by final confirmation by sequencing. All other details are as above (Section 2.15).

2.17. Elimination of the Kanamycin resistance cassette

The kanamycin resistance cassette was removed as part of the strain construction process, and the flanking Flippase recognition target (*frt*) sites were used in order to do so. The method used to delete the antibiotic resistance gene is described by Cherepanov and Wackernagel (1995). Strains from which kanamycin resistance genes needed to be removed were transformed with pCP20 plasmid (Table 2.3). This is an ampicillin and chloramphenicol resistant plasmid that has temperature sensitive replication and thermal induction of FLP synthesis (Cherepanov and Wackernagel, 1995). The transformed cells were plated onto LB solid medium containing ampicillin and incubated overnight at 30 °C. A few colonies were selected, plated on LB agar and incubated overnight at 44 °C in order to delete the kanamycin resistance cassette from the bacterial chromosome. Single colonies were picked and streaked onto LB agar, LB agar plus ampicillin and LB agar plus kanamycin, and grown overnight at 30 °C. The mutants that grew only on LB agar (without any additional antibiotics) were those that had the kanamycin cassette removed and had also lost the plasmid. The deletion of the kanamycin resistance genes was confirmed by colony PCR (Section 2.13.6).

2.18. Primers

Oligonucleotides primers were designed using Vector NTI *Express* or manually, and ordered from Eurofins (formally MWG) or Sigma. All primers used in this study are listed in Tables 2.4-2.10.

Table 2.4. Primer designed for amplification of *E. coli* O157:H7 EDL933 for In-Fusion cloning.

Primer Name	Primers Forward/Reverse (5′ → 3′)	Res. Enzyme site	Primer length (nt)	Tm (°C)	GC (%)
pBADaraEfeUOB-K12^{F}	GAGGAATTAACCATGGATTGTGTGATGTGGATTGG	*Nco*I	35	67.9	41
pBADara-EfeUOB-K12^{R}	AAAACAGCCAAGCTTTTAAACCCGCAATAACGCGCTTCC	*Hin*dIII	39	68.99	50
pBADaraEfeUOB-O157^{F}	GAGGAATTAACCATGTTTGTTCCGTTTCTCATTATGTTGCGC	*Nco*I	42	77.11	42
pBADara-EfeUOB-O157^{R}	AAAACAGCCAAGCTTTTAAACCCGCAATAACGCGCTTCC	*Hin*dIII	39	68.99	50
pBADara-FeoABC-O157^{F}	GAGGAATTAACCATGCAATACACTCCAGATACTGCG	*Nco*I	36	64.13	48
pBADara-FeoABC-O157^{R}	CAAAACAGCCAAGCTTTTAACGCAGCGCCCAGCG	*Hin*dIII	34	67.40	67
pBADRhaEfeUOB-K12^{F}	GCAGGATCACATATGGATTGTGTGATGTGGATTGGC	*Nde*I	36	65.69	46
pBADRhaEfeUOB-K12^{R}	TGCCTGCAGGTCGACTTAAACCCGCAATAACGCGCTTCC	*Sal*I	39	68.99	50
pBADRhaEfeUOBO157^{F}	GCAGGATCACATATGTTTGTTCCGTTTCTCATTATGTTGCGC	*NdeI*	42	70.11	40
pBADRhaEfeUOBO157^{R}	TGCCTGCAGGTCGACTTAAACCCGCAATAACGCGCTTCC	*SalI*	39	68.99	50
pBADRhaFeoABCO157^{F}	GCAGGATCACATATGCAATACACTCCAGATACTGCG	*Nde*I	36	64.13	48
pBADRhaFeoABCO157^{F}	TGCCTGCAGGTCGACTTAACGCAGCGCCCAGCG	*Sal*I	33	68.99	50

Table 2.5: Primer designs for the infusion cloning of the Feo system (*feoABC*) into pBADara and pBADrha.

Primer Name	Primers Forward/Reverse (5′ → 3′)	Restriction Enzyme Site	Primer Length (nt)	Tm (°C)	G+C Content (%)
F-pBADAraFeoA	GAGGAATTAACCATGCAATACACTCCAGATACTGCG	*Bam*HI + *Hind*III	36	66.3	45.83
R-pBADAraFeoA	CAAAACAGCCAAGCTTTTAACAGGAAACCGCTTCCACTTC	*Bam*HI + *Hind*III	40	68.2	45.83
F-pBADAraFeoB	GAGGAATTAACCATGAAAAAATTAACCATAGGCTTAATTGG	*Bam*HI + *Hind*III	41	65.4	27.59

R-pBADAraFeoB	CAAAACAGCCAAGCTTTTAATG GCAATCACCGGTGGT	*BamH*I + *Hind*III	37	68.4	47.62
F-pBADAraFeoC	GAGGAATTAACCATGGCTTCAC TTATTCAGGTGCGTG	*BamH*I + *Hind*III	36	70.8	45.83
R-pBADAraFeoC	CAAAACAGCCAAGCTTTTAACG CAGCGCCCACCACTC	*BamH*I + *Hind*III	37	84.5	61.9
F-pBADAraFeoAB	GAGGAATTAACCATGCAATACA CTCCAGATACTGCG	*Bam*HI + *Hind*III	32	66.3	45.83
R-pBADAraFeoAB	CAAAACAGCCAAGCTTTTAATG GCAATCACCGGTGG	*BamH*I + *Hind*III	36	67.9	50
F-pBADAraFeoBC	GAGGAATTAACCATGAAAAAA TTAACCATAGGCTTAATTGG	*Bam*HI + *Hind*III	41	65.4	27.59
R-pBADAraFeoBC	CAAAACAGCCAAGCTTTTAACG CAGCGCCCACCACT	*Bam*HI + HindIII	36	72.1	60
F-pBADRhaFeoA	AGCAGGATCACATATGCAATAC ACTCCAGATACTGCG	*Nde*I + HindIII	37	66.3	45.83
R-pBADRhaFeoA	TGCCTGCAGGTCGACTTAACAG GAAACCGCTTCCACTTC	*Nde*I + *Hind*III	39	68.2	45.83
F-pBADRhaFeoB	GCAGGATCACATATGAAAAAA TTAACCATAGGCTTAATTGG	*Nde*I + *Hind*III	37	65.4	27.59
R-pBADRhaFeoB	TGCCTGCAGGTCGACTTAATGG CAATCACCGGTGGT	*Nde*I + *Hind*III	36	68.4	47.62
F-pBADRhaFeoC	GCAGGATCACATATGGCTTCAC TTATTCAGGTGCGT	*Nde*I + *Hind*III	36	68.7	45.83
R-pBADRhaFeoC	TGCCTGCAGGTCGACTTAACGC AGCGCCCACCACTC	*Nde*I + *Hind*III	36	73.5	61.9
F-pBADRhaFeoAB	GCAGGATCACATATGCAATACA CTCCAGATACTGCG	*Nde*I + *Hind*III	36	68.7	45.83
R-pBADRhaFeoAB	TGCCTGCAGGTCGACTTAATGG CAATCACCGGTGGTGCT	*Nde*I + *Hind*III	39	68.7	45.83
F-pBADRhaFeoBC	GCAGGATCACATATGAAAAAA TTAACCATAGGCTTAATTGGTA ATCC	*NdeI* + *Hind*III	47	69	28.57
R-pBADRhaFeoBC	TGCCTGCAGGTCGACTTAACGC AGCGCCCACCAC	*Nde*I + *Hind*III	34	71.7	63.16

Table 2.6: Primer designs for the In-Fusion cloning of the Feo system (*feoABC*) into pBADara and pBADrha with His- and Flag TAGs for *feoABC* genes products

Primer Name	Primers Forward/Reverse (5′ → 3′)	Restriction Enzyme Site	Primer Length (nt)	Tm (°C)	G+C Content (%)
F-pBADara-HisTAG-FeoA	CTAACAGGAGGAATTAACCATGGCTCACCACCATCACCATCACCATCACCAATACACTCCAGATACT	*BamH*I + *Hind*III	67	74	46
R-pBADara-HisTAG-FeoA	GCCAAAACAGCCAAGCTTTTAGTGATGGTGATGGTGATGGTGGTGACAGGAAACCGCTTCCACTTCT	*BamH*I + *Hind*III	67	76	49
F-pBADara-HisTAG-FeoB	AGGAGGAATTAACCATGGCTCACCACCATCACCATCACCATCACAAAAAATTAACCATAGGCTTAATTGG	*BamH*I + *Hind*III	70	71	40
R-pBADara-HisTAG-FeoB	GCCAAAACAGCCAAGCTTTTAGTGATGGTGATGGTGATGGTGGTGATGGCAATCACCGGTGGTG	*BamH*I + *Hind*III	64	77	52
F-pBADrha-FlagTAG-FeoA	TCAGCAGGATCACATATGGATTATAAAGATGATGATGATAAACAATACACTCCAGATACTGCGTGG	*Nde*I + *Hind*III	66	68	38
R-pBADrha-FlagTAG-FeoA	AGGTCGACTCTAGAGGATCCTTATTTATCATCATCATCTTTATAATCACAGGAAACCGCTTCCACTTC	*Nde*I + *Hind*III	68	69	40
F-pBADrha-FlagTAG-FeoB	TCAGCAGGATCACATATGGATTATAAAGATGATGATGATAAAAAAAAATTAACCATAGGCTTAATTGGT	*Nde*I + *Hind*III	69	65	29
R-pBADRha-FlagTAG-FeoB	CAGGTCGACTCTAGAGGATCCTTATTTATCATCATCATCTTTATAATCATGGCAATCACCGGTGGTG	*Nde*I + *Hind*III	67	70	42
F-Pet21-HisTAG-FeoB	TCGAGTGCGGCCGCAAGCTTATGCACCACCATCACCATCACCATCACAAAAAATTAACCATAGGCTTA	*Hind*III +*EcoR*I	68	76	47
R-Pet21-HisTAG-FeoB	TGGGTCGCGGATCCGAATTCTTAGTGATGGTGATGGTGATGGTGGTGATGGCAATCACCGGTGGTGCT	*Hind*III +*EcoR*I	68	79	54
R-Pet21-FeoB	CGGATCCGAATTCTTAATGGCAATCACCGGTGGTGCTG	*Hind*III +*EcoR*I	38	71	53
FWDeGFP	TCAAAGGAGATATACCATGGCTGTGAGCAAGGGCGAGGAGCTGTTCACC	*Nco*I	49	78	63
Rev-eGFP	ACCAATTAAGCCTATGGTTAATTTTTTCTTGTACAGCTCGTCCATGCCGAGAGT	-	54	74	56
FWD-FeoB	ACTCTCGGCATGGACGAGCTGTACAAGAAAAAATTAACCATAGGCTTAATTGGT	-	54	61	26
Rev-Histag-FeoB	TGATGGTGATGGTGGTGCTCGAGTTAGTGATGGTGATGGTGATGGTGGTGATGGCAATCACCGGTGGTGCTGGCTGCG	*Xho*l	78	67	46

Table 2.7. Primer designed for full sequencing of *efeUOB*^{O157} and *feoABC* in *E. coli* O157.

Primer Name	Primers; Forward/Reverse (5′→3′)	Primer Length	Tm	GC (%)
pBADara^{F}	ATGCCATAGCATTTTTATCC	20	45.6°C	35%
pBADara^{R}	TCTGATTTAATCTGTATCAGG	21	46.5°C	33%
pBADrha^{F}	CTTTCCCTGGTTGCCAATG	19	51.1°C	53%
pBADrha^{R}	AAGCTTGCATGCCTGCAGGT	20	53.8°C	55%
pBADara-efeUOBO^{157F}	ATTTTTGGCTATCAGGAAGC	20	60.2°C	40%
pBADara-efeUOBO^{157F}	TCACCGGTTTCCACCGTCTG	20	70.9 °C	60%
pBADara-efeUOBO^{157F}	CTACATTGCGCCCGATAATC	20	64.5 °C	50%
pBADara-efeUOBO^{157F}	GCAGGAAAAAGACCGACTCC	20	65.3 °C	55%
pBADara-efeUOBO^{157R}	CCTTTCGGGTTAGTCAGCAG	20	64 °C	64%
pBADara-efeUOBO^{157R}	TTCACGCCGTTTTTATCTTC	20	62 °C	40%
pBADara-efeUOBO^{157R}	TGTTCTTTCAGCGGCGTTCT	20	67.4 °C	50%
pBADara-feoABC^{157F}	CGACATTGCCGAGAAGCAAA	20	68.7°C	50%
pBADara-feoABC^{157F}	CGACATTGCCGAGAAGCAAA	20	68.7°C	50%
pBADara-feoABC^{157F}	CAATCCGGCGGAATTTAACC	20	67.3°C	50%
pBADara-feoABC^{157R}	GCTGGTTAAATAAGGTTGTC	20	55.9°C	40%
pBADara-feoABC^{157R}	GGGTGTTGCTTACCACATCA	20	63.9°C	50%
pBADara-feoABC^{157R}	CCAGGTCTGGATAATCAGGC	20	63.8°C	55%
pBADara-feoABC^{157R}	CCGATAACCACGATGTTAAA	20	60.3°C	40%
pBADRha-*efeUOBO*^{157F}	GCGAAGTCGCCGTCTGGTTT	20	70.9°C	60%
pBADRha-*efeUOBO*^{157F}	GAAAAAGCATTGTTTGGCG	19	63.5°C	42%
pBADRha-*efeUOBO*^{157F}	TCTTGGCGGCTACATTGC	18	65.4°C	55%
pBADRha-*efeUOBO*^{157R}	CAGCAGGAAAAAGACCGACT	20	63.7°C	50%
pBADRha-*efeUOBO*^{157R}	CAGCAGACCGCAGGTCATAT	20	65.6°C	55%
pBADRha-*efeUOBO*^{157R}	CTTCATACTGCATAATGC	18	51.9°C	38.9
pBADRha-*efeUOBO*^{157R}	CTCGAAACTGAATCAAGCGT	20	62.4°C	45%
pBADRha-*feoABC*^{157F}	ATTGATGCTCTGTCGGCG	18	65.6°C	55%
pBADRha-*feoABC*^{157F}	GTTTGTGATGGACCGCCTGA	20	68.7°C	55%
pBADRha-*feoABC*^{157F}	AGATGAAACCTGGCAGAGCC	20	65.9°C	55%
pBADRha-*feoABC*^{157R}	CCTGATGATCGGTGGTGG	18	65.8°C	61%
pBADRha-*feoABC*^{157R}	CTTACCACATCACAGATGGC	20	61.1°C	50%

pBADRha-*feoABC*^{157R}	ATGGTAGACCGGCAGCTCCA	20	69.4°C	60%
pBADRha-*feoABC*^{157R}	CCACGATGTTAAACAGGATA	20	58.1°C	40%
pBADara^{F}	ATGCCATAGCATTTTTATCC	20	45.6°C	% 35
pBADara^{R}	TCTGATTTAATCTGTATCAGG	21	46.5°C	33%
pBADrha^{F}	CTTTCCCTGGTTGCCAATG GC	21	51.1°C	53%
pBADrha^{R}	AAGCTTGCATGCCTGCAGGT	20	53.8°C	55%
pHSG567^{F}	CGTTTTACAACGTGA	15	41.1°C	40%
pHSG567^{R}	GAAATTGTTATCCGCT	16	44.13°C	38%

Tabel 2.8: The primers used to introduce mutations in *feoB*. The altered codons are highlighted in yellow.

Primer name	Primer sequence	Primer lenght	TM	GC %
Cys403Ser F	5'CTGATCGTCGGTTTCGGTTCTAACGTACCGTCGGTAAT-3'	38	79.2	62
Cys403Ser R	5'ATTACCGACGGTACGTTAGAACCGAAACCGACGATCAG-3'	38	79.2	62
Cys432Ser F	5'-GCACCGTTTATGTCCTCTGGCGCGCGTCTGGCT-3'	33	81.1	64
Cys432Ser R	5'- AGCCAGACGCGCGCCAGAGGACATAAACGGTGC-3'	33	81.1	64
Glu488Gln F	5'- ACGCCGTTTGTCATGCAGCTGCCGGTCTACC-3'	29	80.2	62
Glu488Gln R	5'- GGTAGACCGGCAGCTGCATGACAAACGGCGT -3'	29	80.2	62
Cys677Ser F	5'-TCCTGCTGTATGTACCATCTATCTCGGTGATGGGAGC-3'	37	80.2	61
Cys677Ser R	5'-GCTCCCATCACCGAGATAGATGGTACATACAGCAGGA-3'	37	80.2	61
Glu582Gln F	5'-GGTGCAATGGCGAAACAGGTGGTGGTGGGTACGC-3'	34	81.8	61
Glu582Gln R	5'-GCGTACCCACCACCACCTGTTTCGCCATTGCACC-3'	34	81.8	61
Glu687S* F	5'-GAGCCATCGCCCGTTAATCAAGCCGTGGCTG-3'	29	80.2	62

Glu687S* R	5'-CAGCCACGGCTTGATTAACGGGCGATGGCTC-3'	29	80.2	62
Cys762Ser /Cys763Se r F	5'-CCGCAAGTCGGTAAGTAGTAGCAGCGCAGCCAG-3'	31	78.4	61
Cys762Ser /Cys763Se r R	5'- GTCGGTAAGTAGTGCTGCTGCAGCCAGCACC-3'	31	78.4	61
Cys772Ser /His773Gl n F	5'ATCATCATCTTTATAATCCTGGCTATCACCGGTGGTGCTGG-3'	39	79	48
Cys772Ser /His773Gl n R	5'-CATCATCTTTATAATCAGCCAGATCACCGGTGGTGCTGG-3'	39	79	48

2.9: Primer designs for the infusion cloning of the FeoB gene into pTriEx 1.1 and pOPINE vector with insert C-terminal Flag-TAG, His-TAG or N-terminl-His TAG and N-terminal eGFP

Primer Name	Primers Forward/Reverse (5′ → 3′)	Res. Enzyme site	Primer length (nt)	Tm (°C)	GC (%)
pTriX-Flag-FeoB^F	TCAAAGGAGATATACCATGGCTGATTATAAAGATGATGATGATAAAAAAAAATTAACCATAGGCTTAATTGGT	*Nco*I	73	72	29
pTriX-FeoB^R	TGGTGATGGTGGTGCTCGAGTTAATGGCAATCACC	*Xho*I	35	77	51
pTriX-His-FeoB^F	TCAAAGGAGATATACCATGGCTCACCACCATCACCATCACCATCACAAAAAATTAACCATAGGCTTAATTGGT	*Nco*I	73	79	40
pTriX-FeoB^R	TGGTGATGGTGGTGCTCGAGTTAATGGCAATCACC	*Xho*I	35	77	51
pTriX-FeoB^R	TCAAAGGAGATATACCATGGCTAAAAAATTAACCATAGGCTTAATTGGT	*Nco*I	33	67	30
pTriX-His-FeoB^R	TTAGTGATGGTGATGGTGATGGTGGTGCTCGAGATGGCAATCACCGGTGGTGCTGG	*Xho*I	56	70	48
POPINE-FeoB-3C-EGFP^F	CAAAGGAGATATACCATGG*ATGAAAAAATTAACCATAGGCTTAATTGG*	*Nco*I	43	69	33
POPINE-FeoB-3C-EGFP^R	TCCACTTCCAGTTTAAA*CATGGCAATCACCGGTGGTG*	*Pme*I	33	74	48

Table 2.10: Primer designs for gene knockout and confirmation of gene deletion

Gene	Primers Forward/Reverse (5′ → 3′)	Tm	GC %	Length(nt)
FWD-ftsH	ACCGGGAGATTTCAGACGAAAGTTT	64.93	44	25
Rev-ftsH	AAGAGTTTCATGATGTTATCCCTGG	60.39	40	25
FWD-Kan	TATAAATGGGCTCGCGATAATGTCG	62	45	25
Rev-Kan	TCGGGCTTCCCATACAATCGATAGATT	63	42	27
FWD Locus deletion from ftsH	ATGGATGGCTTCGAAGGTAACGAA	61	46	24
Rev-Locus deletion from ftsH	GAACATCTGGCAAGCCGACCACAA	65	54	24
FWD-FeoABC	AGCCACATCAACATTGAGTCAGAT	60.74	42	24
REV-FeoABC	TGTGTATTAGCGAGTTTTCATCCCT	65.7	40	25
FWD-efeU	TTCCGCTTGTGTTTTTCTTTGCCGT	68.95	44	25
REV-efeU	CCACGCTCAACTGCAATGCGTTAC	68.39	54	24
FWD-mntH	CTATCAGAGAAATCACCACAATCCA	60.18	40	25
REV-mntH	TGCGTCTTATCAGGCCTACAAACC	64.74	52	25
FWD-zupT	ATACGCTTGTTCGGCGGAGTAAGAA	66.50	48	25
REV-zupT	CTTAAACAGTACGAGAGAAGAGACAGCC	62.01	46	28
FWD-entC	ACCTCAAGAGTTGACATAGTGCGCG	66.42	52	25
REV-entC	GAATGTCGGTCAGCGGCAAATCCT	69.83	54	24
FWD-FecABCD	TCTATTACGCGGTACTGGATAAACA	59.77	40	25
REV-FecABCD	TCTTTCAGAGTCCGGAAAAGTTCA	62.54	42	24
FWD-FTSH-KNOCKOUT	ACAGTTGTAATAAGAGGTTAATCCCTTGAGTGACATG GCGAAAAACCTAATACTCTGGCTGGTCATTGCCGTTGT GCTGATGTCAGTATTCCAGAGCTGTGTAGGCTGGAGCT GCTTC	72	47	118
REV-FTSH-KNOCKOUT	TCGGTACAAATACAGTCATCTGATGCGGGAACTTACTT GTCGCCTAACTGCTCTGACATGGTGTTACCCGGGTTCG GCGTACGCGGTTCATCAACCCATATGAATATCCTCCTT AGT	85	49	117
FWD-post-ftsH	CACCTTGATGAGTTCATGGTGCTCTAAC	69	46	28
Rev-post-ftsH	AACCCAGCTTAAGCACAAAATCAGGTGTGAT	72	42	31
FtsH-invF	5’GTAGCGATCGCCCAAAGGCTCCTCGTCCGGTTGATG AACC-3’	63	57	21
FtsH-invR	5’GTAGCGATCGCCTCGCTGGGCCCAAAGCTCTGGAAT ACT-3’	62	40	25
CmFtsH-F	GTAGCGATCGCGCTTTGGGCCCAGCGAGTGTGTAGGC TGGAGCTGCTTCGAA	73	47	53
CmFtsH-R	GTAGCGATCGCACCGGACGAGGAGCCTTTGGATGGTC CATATGAATATCCTCCTTAGTTCC	67	43	62

2.19. In-Fusion® cloning

An In-Fusion® Cloning Kit from Clontech Laboratories, Inc. was used for Gibson assembly cloning. The In-Fusion cloning kit fuses DNA fragments (e.g. PCR-generated sequences and linearized vectors), efficiently and precisely, by recognizing a 15 bp overlap at the ends of the fragments. This 15 bp overlap was created by designing primers for amplification of the desired sequences. The kit includes exonuclease for generating sticky ends, a DNA polymerase to fill gaps in annealed fragments and a DNA ligase to seal nicks.

2.19.1. Primers designed for In-Fusion® HD cloning

The 5′ end of every In-Fusion primer was designed to possess 10-15 nucleotides that are homologous to those at one end of the DNA fragment to which the amplification product will be joined. Also, primers were designed to allow cloning into pBADara at the *Nco*I and *Hin*dIII restriction sites, pBADrha at the *Nde*I and *Sal*I sites and pTriEX1.1 at *Nco*I and *Xho*l.

2.19.2. In-Fusion cloning procedure

Approximately 2 µl (10-100 ng) of the gel purified PCR product (e.g. insert) were mixed with 1 µl of around 20-100 ng of the linearized vector, 1 µl of 5X In-Fusion HiFi Enzyme Premix, 2 µl 5X In-Fusion Reaction buffer and the total reaction volume was adjusted to 10 µl using qH_2O, then the reaction components were mixed. Subsequently, the reaction mixture was incubated for 15-30 min at 37 °C and then holding on ice for transformation.

2.19.3. In-Fusion transformation procedure using Stellar™ competent cells

Stellar™ competent cells (Clontech) were used for transformation with 2 µl of the In-Fusion reaction mixture (added to 50 µl Stellar™ competent cells). Each transformation reaction was placed into a separate tube and the volume was adjusted to 1000 µl with a nutrient-rich SOC

medium. Each diluted transformation reaction was spread on a separate LB plate containing a desired concentration of an appropriate antibiotic for the cloning vector and all plates were then incubated overnight at 37 °C. Next day, individual isolated colonies were picked up from each transformation plate. Later, plasmid DNA was isolated using GeneJET^{TM} Plasmid Miniprep Kit (Thermo Fisher Scientific). To determine the presence of insert, the DNA was analysed by restriction digestion.

2.20. Agarose gel electrophoresis

Nucleic acids were routinely analysed using agarose gel electrophoresis (Sambrook and Russell, 2001). Agarose gels were prepared by dissolving SeaKem LE Agarose (Cambrex Bio Science Rockland Inc., Rockland, ME, USA) in TBE buffer to 0.8-2.0% (w/v) depending on the range of fragment sizes being separated. Gel Red (10 µg/ml, Thermo Fisher Scientific) was added to molten agarose (cooled to 55 ºC) to achieve a final concentration of 0.5 µg/ml. Horizontal BioRad gel electrophoresis tanks were used. Gels were cast in casting trays with a gel comb depending on gel size inserted to a depth of 5-7.5 mm. After the gel had set it was placed in a gel electrophoresis tank and covered with TBE buffer (section 2.6.3). DNA samples were mixed with 5× gel loading buffer (5× TBE buffer, 15% v/v glycerol, 0.3% w/v orange G) to give a final concentration of ×1 prior to loading into wells created by the removal of the gel comb.

2.21. Plasmid 'miniprep' isolation

1 ml of an overnight cell suspension were centrifuged at 13,000 g for 8 min and 100 µl of buffer 1 (50 mM Tris-HCl, 10 mM EDTA, 100 ug/ml RNase A, pH 8.0) were added to each cell pellet and mixed by vortexing. 200 µl of buffer 2 (1% SDS, 0.2 M NaOH) were added to each tube and mixed by inversion. Tubes were placed on ice for 5 min, 150 µl of ice-cold buffer 3 (3 M potassium acetate, pH 5.5) were added to each tube and mixed as before and placed on ice for

another 5 min. Samples were centrifuged at 13,000 g for 5 min, the supernatant was transferred to a new tube. 400 µl of isopropanol were then added to each tube which was mixed vigorously and left to stand in room temperature for 2 min. The samples were centrifuged as before, the supernatant was discarded, 200 µl absolute ethanol were added to each tube and mixed by inversion. Samples centrifuged as before, the supernatant was discarded and the tubes with open lids were left at 37 ºC. 20 µl of TE buffer (10 mM Tris-HCl, 1 mM EDTA, pH 8.0) were added to each tube followed by mixing cell pellet and mixed. Samples were finally stored at -20 ºC (according to the BioLab manufacture's protocol).

Plasmids were also isolated by using Thermo Scientific GeneJET^{TM} Plasmid Minipreps (Fermentas). One colony carrying the desired plasmid was inoculated in 2.5 ml LB containing a selective antibiotic and incubated overnight at 37 °C on a shaker (250 rpm). The entire overnight culture was centrifuged at 13,000 rpm for 5 min at room temperature, supernatant was discarded. Pellet was resuspended in 250 µl of Resuspension Solution (containing RNase A) and vortexed until no cell clumps remained. Bacterial suspension was centrifuged as before, 250 µl of Lysis Solution were added to the pellet and mixed thoroughly by inverting the tube 4-6 times until the solution became viscous and slightly clear. Neutralization Solution (350 µl) was added to the sample and immediately mixed thoroughly as described before. The sample was then centrifuged as before for 5 min to pellet cell debris and chromosomal DNA. Supernatant was carefully transferred to the GeneJET spin column and centrifuged for 1 min, flow-through was discarded and column backed into the same collection tube. Plasmids in the collection tube was washed twice by 500 µl of Wash Solution (diluted with ethanol) and then centrifuged as above for additional 30-60 sec to remove residual Wash Solution. The final step of the plasmid isolation was adding 50 µl of the Elution Buffer to the centre of GeneJET spin column membrane to elute the plasmid DNA. The collection tube was incubated at the room

temperature for 2 min prior plas centrifugation. The eluted, purified plasmid DNA was then stored at -20 ℃ for future work.

2.22. Plasmid DNA digestion

Digestion of plasmid DNA was generally performed in 20 µl volumes containing 4 µl (60-100 ng/µl) DNA, 10X react buffer and appropriate restriction enzymes (1-5 U). The mixture was incubated at 37 ˚C for up to 60 min without shaking. Reactions were halted by cooling on ice prior to further processing.

2.23. Quantification of DNA and determination of DNA concentration

The concentration of the plasmid DNA was determined using the Nanodrop spectrophotometer. 2 µl of plasmid DNA were placed onto the spectrophotometer's pedestal and the absorbance of the sample at 260 nm was used to determine DNA concentration**.** Purified chromosomal DNA was diluted in qH_2O and quantified using absorption at 260 nm (A260). A single A260 unit of double-stranded DNA is ~50 µg/ml in qH_2O. Purity was measured using the ratio of absorbance at 260 and 280 nm (A260/A280) in a Nanodrop system; a ratio of 1.8 to 2.0 indicated pure DNA. Where the sample absorbance ratio was less than 1.8 contamination with protein or aromatic substances may have occurred, while a ratio of above 2.0 indicated possible RNA contamination.

2.24. Transformation of bacterial cells

Competent cells were prepared and transformed following standard protocols (Ausubel *et al.*, 1992; Sambrook and Russell, 2001).

2.24.1. Preparation of competent *E. coli* cells

Chemically competent *E. coli* cells were prepared from a single bacterial colony used to inoculate 3-ml LB liquid medium which were incubated overnight 14-16 h (Sambrook and

Russell, 2001). Broths were then diluted 1/50 into 50 ml of fresh LB broth. These were incubated in an orbital shaking incubator at 37 ºC, and 250 rpm until the culture reached mid-exponential phase until the OD at 600 nm (OD600) had reached 0.4-0.5. The OD was measured by spectrophotometry at determined intervals (Ultrospec 10, GE Healthcare, Cell Density Meter with 1.6 ml disposable cuvettes, Sarstedt). Cells were harvested (at 4000 rpm for 15 min at 4 ºC), washed once in an equal volume of ice cold 50 ml 0.1 M $CaCl_2$ and re-suspended then placed on ice for 15 min and centrifuged again under similar conditions. The supernatant was discarded, and the cells were re-suspended in 30 ml of ice-cold 0.1 M $MgCl_2$ and incubated on ice for 10 min. Cells were centrifuged again as previously and pellet was re-suspended in 4 ml of ice-cold 0.1 M $CaCl_2$ with 20% (v/v) glycerol. Cells were aliquoted into 200 µl in each ependroph and stored at -80 ºC.

2.24.2. Heat-shock transformation of *E. coli*

Plasmid/DNA-fragment ligation reactions or plasmid DNA were used to transform chemically competent *E. coli* cells using heat shock transformation (Sambrook and Russell, 2001). All tubes (1.5 ml, Eppendorf) were pre-chilled on ice and chemically competent cells were defrosted on ice for around 3 min. Purified DNA (1 to 25 ng), up to 4 µl of any ligation reaction or appropriate control, were placed in a pre-chilled tube, mixed gently with 50 µl of competent cells and incubated on ice for 20 min. Cells were heat-shocked at 42 ºC for 45-50 sec and subsequently transferred to ice for 2 min. Room temperature SOC (125 µl) was mixed with the cells which were then incubated at 37 ºC for 1 h. Transformants were grown by overnight incubation on LB agar plates supplemented with the appropriate antibiotics (Table 2.1). A second protocol was also followed in which 1 µl of DNA (25-50 ng/µl) (plasmid or ligation reaction) were added to 100 µl competent cells and mix gently by rolling. The cells were incubated on ice for 30 min and then were heat-shocked at 42 ˚C for 1 min. The mixtures were placed on ice again for additional 5 min. 0.7 ml of pre-warmed LB were added to the cells and

they were then incubated at 37 ˚C for 60 min. After incubation, the cells were harvested by centrifugation for 5 min and 900 µl of supernatant were discarded. The pellet was re-suspended in the remaining supernatant and the suspension was spread onto LB agar containing the appropriated antibiotic(s). Plates were incubated overnight at 37 ˚C and single colonies were selected for further experimental use.

2.24.3. Preparation of competent cells for electro-transformation

Electroporation allows the entry of exogenous DNA by utilizing a high-intensity electric field to permeablise the bacterial cell membranes. Electroporation in *E. coli* is divided in to two steps. Firstly, *E. coli* electro-competent cells were prepared using sucrose treatment to permeabilise the membrane, and in the second step is the electroporation process was performed with electro-competent cells mixed with DNA subject to an electric shock (Cadoret *et al*., 2014). Although a large proportion of the cells are killed during this electrical pulse, many surviving cells take up the exogenous DNA.

From an overnight culture obtained in LB at 37 °C under shaking conditions, fresh LB rich medium was inoculated at an OD600 of 0.05 and the culture incubated at 37 °C with shaking (250 rpm). When the OD600 reached 0.5–0.6, the culture was harvested by centrifugation for 10 min at 5000 g. After discarding the supernatant, the bacterial pellet was gently re-suspended in an equal volume of a cold 300 mM sucrose solution. Next, the bacterial suspension was centrifuged for 10 min at 5000 g in a pre-cooled centrifuge (4 °C). Cells were re-suspened in 0.5 volume of a cold 300 mM sucrose solution and centrifuged for 10 min as above. Finally, cells were suspended in 0.01 volumes of cold sucrose and used directly for electro-transformation. Using Bio-Rad Gene Pulser® Cuvettes, 40 µl of cell suspension were gently mixed with up to 5 µl of a DNA solution at 0.1–1 µg/ml. The DNA-bacteria mixture was subjected to a pulse of 2,500 V and 200 µF (for 4-5 sec) (using a BioRad 2510 electroporator);

950 µl of pre-warmed LB medium were added, and the cells were incubated, standing, at 37 °C for at least 4 h before being spread on selective LB agar plates and then incubated at 37 °C for 24 h.

2.25. Phenotypic studies

2.25.1. Phenotypic analysis with *E. coli* JC28 and JC32 mutant strain and wild type

In all the phenotypic studies, the bacteria were grown under aerobic conditions in M9 minimal medium supplemented with 0.4% (w/v) glucose.

2.25.1.1. Aerobic growth

To prepare an overnight culture, a single bacterial colony was inoculated into 3 ml of M9 minimal medium (Buhler *et al*., 1998), containing 0.4% glucose (as a source of carbon), 0.5 mM $MgSO_4 \cdot 7H_2O$ and 0.1% thiamine, 10 µM ferric citrate (pH adjusted with 1 M NaOH to 7). Bacteria were grown overnight at 250 rpm, 37 ºC in a Sanyo Gallenkamp orbital shaker. The overnight culture was centrifuged at 4,000 rpm, 4 ºC for 15 min in bench-top centrifuge to pellet the cells. The pellet was then re-suspended in 5 ml of 0.9% NaCl (with 0.01 M EDTA, pH 8.0) or minimal medium and re-centrifuged as before in order to wash the remaining iron from the cell surface. The pellet was again re-suspended in 5 ml of 0.9% NaCl or minimal medium and the OD600 of 1 ml of the suspension was measured using a Helios α Unicam spectrophotometer. This OD was used to calculate the volume of culture that should be added to fresh liquid minimal medium to give a starting OD of 0.01. The growth was performed in 'iron poor' minimal M9 medium with 0.4% glucose. For iron replete conditions, 10 µM ferric citrate was added but for iron restricted conditions, 1-4 µM DTPA (diethylene triamine penta acetic acid) was added as a ferric-iron chelator. All glassware was acid washed.

2.25.1.2. Anaerobic growth

Cells were inoculated in 5 ml M9 medium for overnight growth, as above. Cells were harvested by centrifugation (5000 rpm 4 ℃ 10 min) and the supernatant discarded. The pellet was re-suspended in 5 ml of fresh M9 medium and the OD600 of the cell suspension was measured. A volume of culture was added to 25 ml of M9 to give a starting OD of 0.02. This was transferred to a sterile 25 ml syringe equipped with needle. The air in the syringe was expelled using the plunger and the syringe-plunger-needle was imbedded into a rubber bung. Bacterial growth was allowed to grow at 37 ˚C without shaking where growth was monitored by measuring the OD_{600nm} from the culture released from each syringe every 2 h.

2.26. Hydrogen peroxide sensitivity test

2.26.1. H_2O_2 sensitivity test of *E. coli* strains on M9 plates and broth

One colony of JC28 or JC32 complemented with plasmids carrying *efeUOB* or *feoABC* were inoculated in 3 ml M9 medium and incubated overnight at 37 ℃ and 250 rpm. A specific volume of the overnight culture was adjusted to give an initial OD_{600} of 0.01; this was then kept on ice. A serial (x10, x100, 1000 and x10000) dilution was be made using ice cold M9. Then, 5 µl of each suspension was spot-inoculated on M9-agar with or without 100, 200 or 300 µM H_2O_2, to test the effect of hydrogen peroxide on the mutant strains in comparison with the vector control. Plates were grown at 37 ℃ and growth monitored; results were photographically recorded.

2.26.2. Effect of *efeUOB* and *feoABC* on liquid culture growth of *E. coli* with H_2O_2

The phenotypic effects under different H_2O_2 conditions were assessed using a Bioscreen microbiology growth curve analysis system. Single colonies of strains of interest were

inoculated from M9 plates into 3 ml M9 medium and incubated overnight at 37 °C. After the incubation, the overnight cultures were diluted to get suspensions of 0.01 $OD_{600\ units}$ (in M9 with 0, 100, 200 or 300 µM H_2O_2, with/without catalase) and then 300 µl from each solution were added into the well of sterile Bioscreen C (Honeycomb®) plate. The plate was then placed in the Bioscreen machine to measure OD values in the wells during growth every 1 h over a 24 h period, whilst shaking at 37 °C. Up to 200 wells could be measured in parallel.

2.27. Mutagenesis method

Mutagenesis allows a modification of genetic information. Such modifications can occur unexpectedly in nature or may be introducted by a mutagenic agent. On a molecular basis, these mutations include nucleotide substitutions, deletions, insertions and recombinations. Site-directed mutagenesis (SDM) methods such as Quickchange (Liu and Naismith, 2008), Kunkel mutagenesis (Kunkel, 1985), modified PCR (Cadwell and Joyce, 1992) and inverse PCR (Dominy and Andrews, 2003) allow a defined mutation to be engineered into DNA.

2.27.1. Generation of mutant plasmids by SDM

Site directed mutagenesis was carried out using the Aglient QuikChange II XL Site-Directed Mutagenesis kit; the protocol is described below. The pBADara plasmid with a *feoAB* insert and pBADrha with a *feoAB*-Flag TAG were used.

2.27.2. Thermal cycling: 2.5 µl of 10x reaction buffer, 0.5 µl of dNTP mix, 1.5 µl of QuikSolution and pBADara plasmid containing the *feoAB* genes were added to Eppendorf tubes, alongside 5 ng of the forward and reverse primers encoding the desired mutation (Table 2.8). 0.1 µl of the supplied HF DNA polymerase and water to a final volume of 25 µl were dispensed into each tube. A positive control was also set up, using primers and template DNA provided with the kit. All reactions were subjected to thermo cycling using the parameters outlined in the manual.

The amount of plasmid DNA used, and annealing temperatures, were varied to optimise the reaction for each mutant. 5 ng of DNA and an annealing temperature of 60 ˚C led to the successful generation of mutants containing the Cys432Ser mutation. The amount of template DNA was increased to 75 ng per reaction and the PCR annealing temperature to 68℃ to improve the efficiency of the reaction for the other two cysteine mutants. Site directed mutagenesis of all three Glu residues was carried out using 25 ng of pBADara plasmid and an annealing temperature of 68℃. Also, site directed mutagenesis of two Cys/Cys and Cys/His residues was carried out using 25 ng of pBADrha plasmids and an annealing temperature of 68℃

2.27.3. Digestion of template DNA: The original plasmid was digested using 0.5 µl of *Dpn*I in each tube. The tubes were centrifuged for one minute and then incubated at 37℃ for 1 h.

2.27.4. Transformation: The mutant plasmids were used to transform XL10-Gold ultracompetent cells (see Table 2.4) supplied with the kit. Eppendorf tubes were pre-chilled, and 45 µl of cells dispensed into each. 2 µl of β-mecaptoethanol were added and the tubes were incubated on ice for 10 min, with gentle mixing every 2 min. 2 µl of the mutated plasmid samples were each added to one tube and mixed by swirling. Following a 30-min incubation on ice, the samples were heat shocked at 42℃ for 30 sec. 0.5 ml of pre-warmed SOC medium were added to the tubes, which were then left at 37℃ for 1 h. The contents of each tube were transferred onto two ampicillin containing plates, which were left overnight at 37℃. The following next day the plates were checked for the presence of colonies and transferred to the cold room.

2.27.5. Plasmid isolation and digestion: Plasmids were isolated using the GeneJET Miniprep Plasmid kit. 5 ml volumes of LB broth containing 100 µl/ml of ampicillin were

innoculated with colonies obtained in Section 2.5.3. These were left overnight at 37℃ with shaking.

The following morning the cultures were transferred into 15 ml Falcon tubes and centrifuged for 20 min. The supernatants were discarded, and the pellets resuspended in 250 µl of resuspension solution. The resuspended pellets were moved to an Eppendorf tube; 250 µl of lysis buffer were then added and mixed by inversion of the tubes. After 3-4 min, 350 µl of neutralisation solution were added to the Eppendorfs to prevent damage of the plasmid DNA. The contents of the tubes were mixed by invertion several times, and the tubes were centrifuged for 5 min. The supernatants were transferred to GeneJET spin columns and centifuged for 1 min. Flow-through was thrown away and the columns were replaced in the collection tubes. 500 µl of wash solution were added to each column and the tubes were centrifuged for 1 min; flow through was discarded and the wash step repeated. The columns were transferred to fresh Eppendorf tubes. 50 µl of water were added as an elutant. The Eppendorfs were left at room temperature for 2 min before being centrifuged for a further 5 min. The columns were discarded, and the solutions tested for the prescence of the plasmids by gel electrophoresis.

Plasmids were subjected to a single restriction digest with *Hin*dIII (Section 2.13.4) and the banding patterns determined by agarose gel electrophoresis to confirm their identity (Section 2.20). Sanger sequencing of the mutated regions was performed by Eurofins.

Table 2.11: The primers used for sequencing of the plasmids obtained from the site directed mutagenesis reactions.

Primer name/residues to be sequenced	Primer sequence
Cys403Ser/Cys432Ser F	5'-TCTCCTTCCTTGAGGACTCC-3'
Cys403Ser/Cys432Ser R	5'-GCATATACAGCGAGAAGACC-3'
Glu488Gln/Glu582Gln R	5'-CGGATTGAACTCTTCGTCC-3'
Cys677Ser/Glu687S* F	5'-GGCGTGATGGATCAGAAATTCG-3'

2.28. Transduction using P1 phage

Transduction is a mechanism discovered by Zinder and Lederberg (1952) that mediates the, horizontal transfer of bacterial DNA fragments from donor bacteria to the recipient bacteria via bacteriophage. There are two types of transduction, specialized and generalized. The specialized transduction the phage (e.g. lambda) is limited to the ability to carry only particular genes that are next to the insertion sequence site, which can be incorporated into its DNA as a hybrid molecule. In generalized transduction, phage can transfer pieces of host genome of length up to that of the phage chromosome. This transduction occurs when new phage is being generated during infection and a transducing phage particle is produced by packaging any bacterial DNA fragment instead of phage DNA. This DNA can be transferred to the recipient cell by the transducing phage particle upon infection, but the recipient bacterium cannot be lysed by the transducing phage because this phage does not carry its own genetic material. Integration of the donor DNA into the recipient chromosome occurs by homologous recombination.

2.28.1. Isolation and purification of P1 phage from stock

P1 was isolated from the P1*vir* stock (10 µl stock from Gary Sawers [Germany] diluted in 200 µl P1 dilution fluid) by preparing x10 dilutions from 10^{-1} to 10^{-10}. Then, 0.1 ml from an overnight culture of *E. coli* W3110 were combined with 0.1 ml of P1 phage for all dilutions. These phage-bacteria mixtures were incubated at 37℃ for 15 min, and then was mixed with 2.5 ml soft agar 50℃ and pour on agar plate. After 6 h incubation, the plaque forming units were calculated. Next, in order to isolate single plaques, the plate showing discrete individual plaques was selected. From this plate, four plaques were picked up by using sterile 1 ml blue pipette tips and each was transferred into an individual microfuge tube containing 1 ml of P1 dilution fluid (0.1% peptone, 0.03 % NaCl, 10 mM Tris, 0.5 mM MgSO4, pH 7.8) plus two drops of chloroform. This mixture was mixed briefly and left for 1 h at room temperature. Following this step, tubes were micro-centrifuged for 10 min at 12000 *g*. Finally, the supernatant was transferred into a sterile microfuge tube and stored at 4℃ after adding one drop of chloroform. The concentration of P1 phage was expected to be 10^5-10^6 pfu/ml by this method. In order to increase concentration, the protocol for construction of P1 transducing phage was followed by infecting 'wild type' bacteria (W3110) with this phage lysate (~10^5-10^6 pfu/ml). The concentration of P1 lysate was expected to be ~ 10^8-10^9 pfu/ml by this method.

2.28.2. Phage lysate preparation

P1 transduction was performed as described in Miller (1992). One colony of donor strain was inoculated into 5 ml LB and incubated on a shaker (250 rpm) for several hours at 37℃. After overnight incubation, P1 phage stock was aerated under the flame of a Bunsen burner to evaporate chloroform away. Then a wide range of phage concentrations, from 10^1 to10^9 pfu/ml, was prepared by diluting in P1 dilution buffer. A 1-3 ml volume of donor cell culture was centrifuged, and the pellet resuspended in 5 ml of broth (LB) in a 100 ml flask. Then, 5 ml of

phage buffer were added and 100 µl (>10^9 pfu/ml) of stock lysate (P1, propagated on W3110). Then the flask was incubated with slow shaking (approximately 50 rpm) at 30 °C for 2-4 h until lysis was complete (giving a perfectly clear solution). Finally, the lysate was filter sterilised and the phage titre determined, which should be 10^9 to 10^{10} pfu/ml. This was stored at 4 ºC under chloroform.

2.28.3. Phage transduction

An overnight culture of the recipient bacteria in 20 ml LB broth was harvested by centrifugation (5,000 rpm, 10 min). The pellet was resuspended in 1 ml LB broth. In 20 ml sterile Universals, samples and controls were prepared follows: 500 µ1 recipient cells (or no cells), 1 ml LB with 10 mM $CaCl_2$, 0 to 500 µ1 of phage lysate.

The mixtures were incubated without shaking at 37 °C for 25 min, followed by a 15 min on an orbital shaker at the same temperature. Then, 1 ml ice cold 0.02 M sodium citrate were added, and the samples were left on ice for 5 min. The cells were harvested as above, and the supernatant thoroughly removed. The pellet was resuspended in 1 ml of ice cold 0.02 M sodium citrate and left on ice for 30 min to 2 h. Aliquots of 100 and 200 µl were then spread on to LB agar plates containing selective antibiotic and 0.05% sodium citrate. After incubation of plates at 37 °C for 90 min, the plates were overlayed with 5 ml of LB top agar (100 ml LB broth + 0.7g Bacto agar containing selective antibiotics). Plates were further incubated for 24-48 h at the required temperature until transductant colonies (typically 10-100 per plate) appeared. These were tested for detecting identity by colony PCR.

2.28.4 Calculation of P1 levels (by P1 titration)

The collected lysate was diluted in dilution fluid to prepare x10 dilution series. Then a sensitive strain was grown in LB to log phase. The diluted phage lysate (100 µl) was then mixed with 400 µl of the sensitive strain culture. 50 µl of 1 M $CaCl_2$ were then added and the mix left on the bench for at least 15 min. Phage top agar was melted and cooled to 50 °C, and then 5 ml were added to the phage mixture. This was rapidly mixed at 50 ˚C and then immediately poured over a pre-warmed bottom agar plate. Once set, the plates were incubated overnight at 37℃. After incubation the plaques were counted and the plaque forming units per ml were calculated.

2.29. Protein work

2.29.1 Sample preparation

Liquid protein samples were mixed with an equal volume of 2x SDS-loading buffer, while cell pellets (0.5 OD units) were suspended in 100 µl of 1x sample-loading buffer (50 mM Tris-HCl pH 6.8, 2% w/v SDS, 0.1% w/v Bromophenol Blue, 100 mM dithiothretiol, 10% v/v glycerol, in qH_2O). All samples were heated to 100 °C for 5 min and micro-centrifuged for 10 min.

2.29.2. SDS-polyacrylamide gel electrophoresis (SDS-PAGE)

Electrophoresis was in 15% polyacrylamide slab gels using the Bio-Rad Mini Protein II system. The 15% SDS-polyacrylamide gels contained 5 ml Tris-HCI (0.5 M, pH 8.8), 10 ml 30 % w/v acrylamide (Bio-Rad), 0.2 ml 10 % w/v SDS, 0.07 ml 10% fresh w/v ammonium persulphate, 0.015 ml TEMED and 0.7 ml qH_2O. The gel was cast and, once set, the stacking gel applied to the top. The stacking gel was made up of 2.5 ml Tris-HCL (0.5 M, pH 6.8), 1.5 ml 30% w/v acrylamide, 0.035 ml 10 % w/v SDS, 0.01 ml (fresh) 10% w/v ammonium persulphate, 0.015 ml TEMED and 4.9 ml qH_2O. 10-20 µl of denatured protein sample were loaded per well in a

polymerized polyacrylamide gel. The gel was resolved at 30 mA per gel in SDS-PAGE running buffer (25 mM Tris, 192 mM glycine, 0.1% w/v SDS) for 1 h. Following SDS-PAGE, gels were either stained or further processed for Western blotting. For visualisation of total protein, Coomassie blue stain (1.2 mM Coomassie Brilliant Blue R-250, 50% (v/v) methanol, 10% (v/v) glacial acetic acid) was applied for 2 h. The stain was removed and the gel washed with cold water to remove excess stain. The gel was then submerged in de-stain (10% v/v acetic acid, 30% v/v methanol) initially for 30 min and then for an additional 2 h minimum, until the gel had little or no blue background remaining. Upon complete de-staining, the gel was equilibrated in water, and recorded using a G-Box (Syngene).

2.29.3. Western blotting by semi-dry method

Samples for Western blotting were treated as in Section 2.21.4 but were not stained with Coomassie blue; after gel electrophoresis the gel with separated protein was removed from the glass plates, equilibrated in 1x Tris-glycine transfer buffer for 15 min and transferred to a polyvinylidene fluoride (PVDF) membrane. The PVDF membrane was prepared by soaking in methanol for 10 sec, followed by pure water for 2 min and 15 min in 1x Tris-glycine transfer buffer. A Bio-Rad Trans Blot SD semi-dry transfer cell was used to transfer protein from the SDS-PAGE gel to the PVDF membrane. A transfer buffer-soaked sheet of filter paper was applied to the anode of the transfer cell, ensuring that all air bubbles were removed, followed by the prepared PVDF membrane, the equilibrated SDS-PAGE gel and a final sheet of transfer buffer-soaked filter paper. The cathode was attached, and proteins transferred for 1-2 h with a continuous 60 volts.

Following transfer, the PVDF membrane and the SDS-PAGE gel were removed from the transfer apparatus. On some occasions, the PVDF membrane was stained with Ponceau S (0.1% w/v Ponceau S in 1% v/v acetic acid) to ensure that proteins had been transferred to the membrane. Ponceau S was applied directly to the membrane and shaken for 5 min; excess stain

was removed with washing with 5% acetic acid or water. The stain is reversible and blocking of the membrane was commenced after visualisation of bound proteins to the membrane. In addition, the post-transfer polyacrylmide gel was stained with Coomassie blue to determine the efficiency of the transfer.

The PVDF membrane was blocked with 5% dried skimmed milk powder in Tris buffered saline (TBS: Tris 50 mM at pH 7.6, 150 mM NaCl) for 1 h at room temperature with shaking or over-night at 4 °C. Blocking reagent was removed through washing three times for 5 min each with 0.01% skimmed milk powder and 0.05% Tween 20 in TBS. After washing, primary polyclonal antibody was applied at 1:500 dilution to the membrane and shaken at room temperature for 1 h. The wash step was repeated and secondary antibody (anti-rabbit IgG at 1:3000) was applied for 1 h with shaking. The wash step was repeated and one BCIP/NBT (5-bromo-4-chloro-3-indolyl-phosphate and nitro blue tetrazolium; Sigma-Aldrich) tablet was dissolved in 10 ml of qH_2O. This was applied to the membrane and left to develop for 5-10 min. Following development of the stain, the membrane was washed 10 times with PBS and dried at 50 °C.

2.29.3 Protein detection by Western blotting - dry method

Proteins separated by SDS-PAGE were transferred to a nitrocellulose membrane by electroblotting at 60 V for 1 h. Following transfer, the membrane was washed in 1x TBS (20 mM Tris, 500 mM NaCl, pH 7) for 10 min on a shaking platform. The membrane was then blocked in blocking solution (1% BSA-TBS) for 1 h at room temperature or overnight at 4 ˚C while shaking gently. After blocking, the membrane was washed twice in TTBS (20 mM Tris, 500 mM NaCl, 0.05% Tween 20, pH 7.0) for 10 min for each wash. The membrane was then probed with the primary antibody diluted in antibody buffer (1% BSA-TTBS) and incubated for 1 h at room temperature. Following three 10 min washes in TBST, membranes were

incubated for 1 h with the secondary antibody conjugated to horseradish peroxide (HRP) or alkaline phosphatase diluted in antibody buffer. Finally, membranes were washed three times for 10 min each in TBS to remove excess tween detergent followed by signal detection using either ChemiFastChemiluminescence Substrate (Syngene) according to the manufacturer's instructions or BCIP tablets (Sigma). Results were visualised and recorded using a G:BOX Chemi (Syngene) with GeneSys software.

2.29.4. Protein production and analysis

2.29.4.1 Small-scale protein overproduction

For initial expression analysis, an overnight culture was prepared by inoculating a single colony of *E. coli* BL21/λDE3 carrying a suitable plasmid for protein expression (pET21a, pTriEx) from a freshly streaked plate into 5 ml L-broth containing the appropriate antibiotic. A 50 ml volume of pre-warmed LB (in 250 ml sterile flask) was inoculated with 0.5 ml of overnight starter culture (1:100 inoculum: broth ratio). The OD600 was taken at regular times to determine when the culture reached an OD of 0.5 to 0.6 at which point the culture was induced by the addition of IPTG (isopropyl ß-D-1-thiogalactopyranoside) to 1 mM, which induces T7 RNA polymerase allowing transcription and translation of the T7 promoter driven vector.

Samples were taken at regular time points after induction with IPTG (one before induction, every 1 h for 4-6 h and one sample after overnight growth). Samples were taken to a standardized volume of 0.5 OD units and were pelleted by centrifugation at 13,000 rpm for 5 min. The supernatant was removed, and dry pellets were stored temporarily at -20 °C. All samples were re-suspended in 100 µl of 1x SDS sample loading buffer and denaturated by incubation at 37 °C for 30 min. A 10-20 µl aliquot of each denaturated, centrifuged sample was loaded per well. Following electrophoresis and staining, Gene Tools software (Gene*Sys*) was

used to determine the percentage expression of the recombinant protein in the whole cell extract and approximate molecular weight of the expressed protein.

2.29.4.2. Cell lysis and protein extraction

2.29.4.2.1. Cell disruption using French Press

Cell pellets from large-scale overexpression were subjected to lysis using a French Pressure Cell (20,000 psi). The lysis procedure was repeated twice. Following that, cells were centrifuged using rotor SS34 (8 x 50 ml) at 17,000 rpm for 20 min. All components of the French pressure cell were maintained at 4 °C to minimize potential protein degradation. The supernatant was retained for further purification work.

2.29.4.2.2. Sonication

Sonication was performed using Sonic Vibra-cell sonicator system to effectively lyse cells for further application. Cells to be lysed were first defrosted and re-suspended in 50 mM PBS pH 7.4, 500 mM NaCl and 1% NP-40 detergent. Next, lysozyme was added at 1 mg/ml and incubated on ice for 30 min. Sonication was then performed at 80% amplitude with a run time of 10 min.

2.29.5. Protein purification process

2.29.5.1. Nickel-affinity chromatography

Nickel-affinity chromatography was used as a purification protein technique. Previous to separation of recombinant protein, the nickel affinity chromatography column was washed with two column volumes of degassed 20% ethanol to remove all contamination; all solutions to be applied to all chromatography columns were degassed via exposure to a negative pressure achieved through vacuum pressure. The column was stripped of bound nickel by washing with two column volumes of 0.5 M EDTA (pH 8.0) followed by two column volumes of qH_2O. The

stripped column was re-charged with nickel via washing with two column volumes of 0.5 M $NiSO_4$ followed by two column volumes of qH_2O to remove unbound nickel. The column was then equilibrated by washing first with one column volume of buffer Binding buffer (B1) (20 mM PBS, 500 mM NaCl, 20 mM imidazole and 0.1% Tween 20 or Triton X-100, pH 7.4) then three column volumes of buffer elution buffer (A1) (B1 with 500 mM imidazole). The protein-sample was then loaded onto the buffer A1 equilibrated nickel affinity column. Excess un-bound protein was removed from the column with washing with two column volumes of buffer A1, from which the flow through was collected for subsequent SDS-PAGE analysis. All subsequent elution was collected as 7 ml fractions in plastic test tubes, and the UV absorbance measured throughout. A further two column volumes of buffer A1 was used to wash residual unbound protein from the column; the UV reading of the eluent was set to zero and a linear gradient of 0-100% of buffer B1 were applied over eight column volumes. To ensure all protein was eluted, a further two column volumes of buffer B1 was applied followed by two column volumes of buffer A1 and two column volumes of 30% ethanol to preserve the column. Volumes of 10 µl for all collected fractions displaying elevated UV absorbance suggesting presence of purified recombinant protein were analysed by SDS-PAGE.

2.29.5.2. Dialysis and concentration of protein samples

Protein samples at different stages of purification were dialyzed thoroughly to remove any unwanted salt molecules or low mass contaminants. Dialysis membrane tubing of molecular weight cut off (MWCO) 30 kDa was employed from Fisher Scientific. The dialysis tubing was first boiled in qH2O containing a small amount of EDTA to ensure the tubing was sterile. Any extra dialysis tubing not used following boiling in EDTA and washing was stored in 30% ethanol at 4 °C. Appropriate lengths of dialysis tubing were cut and sealed at one end; the tubing was then subjected to a leak test first by filling with qH_2O. The water was subsequently tipped out and the tubing gently squeezed to remove any excess, the protein sample was then placed

carefully into the tubing and the other end was tightly sealed to ensure the protein was contained. Sealed tubing was placed in 500 ml of the appropriate buffer, which was gently stirred on a magnetic stirrer using a small-size flea. Dialysis was performed at 4 °C; the buffer was changed twice after at least 6 h of dialysis.

Following purification, recombinant protein from liquid chromatography was concentrated using a Vivaspin 20 (5,0000 and 100,000 MWCO) (SatoriusStedim Biotech) centrifugal concentrator according the manufacturer's instruction. Chromatography eluent was loaded into the upper compartment of the concentrator and cool centrifuged at 3250 g for 20 min at 4 °C (Eppendorf 5804R with A-4-44 rotor), the flow through from the column was kept and analysed by SDS-PAGE to ensure the absence of the recombinant protein. Eluent was continually applied to the top of the concentrator until the required concentration of protein was achieved.

2.29.5.3. Determination of protein concentration

Protein concentration was determined according to the dye-binding method of Bradford (1976) using a prefabricated assay from Bio-Rad Laboratories (Hercules, CA) and bovine serum albumin (BSA) as protein standard. Standards were prepared by diluting bovine serum albumin (BSA) in a series ranging from 0.025 to 5 µg/ml. Volumes of 10 µl for each duplicate BSA dilution (standards) and 10 µl of each protein sample (unknowns) were added into a 96-well microtiter plate, followed by adding 190 µl of 1x Bio-Rad protein assay dye reagent. PBS (50 mM pH 8) solution was used as blank. The absorbance was measured at 595 nm using a microtiter-plate reader. Using measurements obtained from the standards, a standard curve was created, from which the protein concentration was calculated. The protein concentration was also assessed using Nandrop ND-1000 (Nanodrop Technologies) which measures the absorbance of 2 µl of protein sample at 280 nm after detecting molar extiaction coefficient

factor from data base. Both data from Nanodrop and Bradford assay were compared to ensure consistency and accuracy.

2.30. Cell culture

2.30.1. *Sf*9 cell line

Sf9 insect cells originated from *Spodoptera frugiperda* as a Fall Armyworm derived from pupal ovarian tissue. The *Sf9* cell line was used for protein expression and baculovirus amplification. The cells were cultured in suspension in conical polycarbonate flasks with vented caps (Corning®, CLS430421-50EA) in BioWhittaker Insect-XPRESSTM medium with the addition of 2% (v/v) foetal bovine serum (FBS – Biosera, FB-1001), 100 μg/ml penicillin, 100 μg/ml streptomycin (Gibco®, InvitrogenTM, 15140-122) and 2.5 μg/ml amphotericin B (Fungizone® – Gibco®, 15290-026) at 28 °C on Innova 4430 incubator shaker (New Brunswick Scientific) at 110 rpm. The culture was passaged at the density of $2.5x10^6$ cells/ml.

2.30.2. *Ao*38 cell line

Ascalapha odorata is a cell line from the egg of the Black Witch moth, a large moth in central and North America, it was used as a source for the insect cell line *Ascalapha odorata* Ao38. This cell line was used for protein expression. The *Ao*38 cell line was sustained as for *Sf*9. This insect cell line is an essential component in the manufacture of recombinant proteins in the Bac-Med system and *Ao*38 new cell lines increase both quantity and quality of protein production (Smagghe *et al*., 2009; Hashimoto *et al.,* 2010).

2.30.3. Baculovirus expression

To visualize mCherry and GFP expression in cells the baculovirus *Autographa californica* multiple nuclear polyhedrosis virus (AcMNPV) expression system was used with vectors encoding the full sequence of HCoV-HKU1 mCherry+frameshift+eGFP and mutations thereof. The baculovirus DNA was prepared from a cloned copy of the genome, a bacmid, in which sequence coding for the essential ORF1629, was deleted. Viable baculovirus was rescued by homologous recombination of bacmid DNA with the transfer vector containing a complete ORF1629 gene sequence and the gene of interest (Zhao *et al*., 2003).

The baculoviral expression system was utilised to generate recombinant baculoviral stocks and recombinant proteins in *Ao*38 and *Sf*9 insect cells. The procedure used for baculoviruses as expression vectors relies on the high yield of recombinant proteins in insect cell lines because of strong virus gene promoters and similar post-translational modification to those in mammalian cells (Kelly *et al*., 2007; Zhao *et al*., 2003).

2.30.4. Transfection of *Sf*9 cells and production of recombinant baculovirus

*Spodoptera frugiperda Sf*9 cells at 40% confluency were transfected in monolayer in a 6-well format using Lipofectin reagent (Invitrogen) and attached to a 6 well plate (NUNC) and incubated at 20 ℃ for 30 min to allow the cells to attach to the well. A transfection mix was prepared according to the company protocol by combining of 400 ng Bac-Mid (5 µl) (Invitrogen) with 500 ng of the transfer vector comprising the desired gene, made up to final volume of 12 µl with qH_2O, then gently mixed with 12 µl of Lipofectin mix (8 µl of Lipofectin (Invitrogen) and 4 µl of sterile water) and incubated at room temperature for 15-30 min. The cell line was washed two times with 1 ml of serum-free insect cell medium (BioWittaker) which was then replaced with 2 ml of serum-free medium. 24 µl of the transfection mixture (lipid-DNA complex) were added to each well. The plates were incubated overnight at 28 ˚C then

the medium was replaced with 2% FCS insect cell medium. The cell line plates were incubated further for an additional 4-5 days at 28 °C, then all the cells and culture medium were harvested and centrifuged at 4000 rpm for 10 min. The supernatant which contains the recombinant baculovirus (P0) was transferred to sterile Eppendorf tube and stored at 4 °C for further passage. Subsequently, recombinant viruses were passaged twice in 6-well plates containing fresh adherent *Sf9* cells at 50% confluence, and infected by P0 to prepare passage one (P1) and after 3-4 days incubation the supernatant was transferred to sterile a Eppendorf tube and stored at 4 °C for further passage. The same processing was used to prepare passage two (P2). The infected cell pellet was analysed for the expression of fusion proteins of interest by SDS-PAGE and Western blotting.

2.30.5. Small scale protein expression using the recombinant baculovirus system

The small-scale protein expression was performed through infection of a 6-well plate (NUNC) which was pre-seeded with $1x10^6$ *Sf*9 or *Ao*38 cells and incubated at room temperature for 30 min to allow the cells to attach. The cell line was washed two times with 1 ml of insect cell serum-free medium (BioWittaker) which was then replaced with 2 ml of Insect Xpress medium with L-glutamine (BioWittaker) supplemented with 2% for *Sf*9 cells or 1% *Ao*38 cells in foetal calf serum (FCS). Then, 100 µl of a high titre stock of the recombinant baculovirus, typically passage 2 or 3, were added to the wells, which were incubated for 5 days at 28 °C. Fluorescence protein expression was checked during the incubation by using a digital inverted microscope (Fisher). Afterward, all the cells and culture media were harvested and centrifuged at 4000 rpm for 10 min. The cell pellets were used for fluorescence microscopy and Western blot.

2.31.6. Protein expression using the baculovirus expression system

Small scale protein expression was carried out in a monolayer culture in a 6 well format with the relevant recombinant baculovirus. Each well was seeded with $0.9x10^6$ cells and incubated at 28 °C for 30 min so the cells adhered to the well surface as a monolayer. Then, 200 µl of the recombinant baculovirus were added to the appropriate well and incubated for 72 h at 28 °C. The cells and culture media were harvested by centrifugation at 13000 rpm for 5 min. Cell pellet and supernatant were collected separately, subjected to analysis by SDS-PAGE and by Western blot. Medium-scale protein expression was performed in a 1 l suspension culture of *Sf*9 insect cells in a 3 l Erlenmeyer flask format with the relevant recombinant baculovirus. Each flask was seeded with $0.5x10^6$ cells per ml. Cells were infected with 30 ml of the appropriate recombinant baculovirus and incubated for a further 72 h. Then a viable count using 0.4% Trypan blue was used to estimate the number of dead cells before harvesting.

Large scale protein production was carried out using 5 l suspension culture of *Ao*38 insect cells in a 10 l wave Biotech fermenter bag format. A 5 l wave Biotech fermenter bag was filled with serum free medium supplemented with 2% foetal calf serum and antibiotics and inoculated with exponentially growing *Ao*38 insect cells to an initial density of $0.5x10^6$ cells per ml. The bag was housed in the wave Bioreactor and incubated for 12 to 24 h to allow the cell density to reach $1x10^6$ cells per ml, whereupon recombinant baculovirus expressing pTriEX-FeoB was added. The infected culture was incubated at 28 °C with rocking under aeration for a further 72 h before harvesting by centrifugation. A viable count was performed using 0.4% Trypan blue to estimate the number of dead cells before harvesting. The cells was harvested by centrifugation at 5000 rpm for 45 min at 4 °C.

2.31. Fluorescent size exclusion chromatography (FSEC)

110 µl of each sample (before and after IMAC purification) were applied to a 1.5 ml Superdex® 200 Increase 10/300 GL GE Healthcare, (column L × I.D. 30 cm × 10 mm, 8.6 µm particle size) for small-scale preparative purification for obtaining milligram amounts of highly size-homogenous target protein at the polishing stage of the purification procedure. This was linked to a Shimadzu prominence system with 487/512 nm fluorescence detection (Shimadzu Corp., Kyoto, Japan). The flow rate was 0.75 ml/min. The FSEC was performed in running buffer of n-dodecyl-β-D-maltoside (DDM) (50 mM phosphate buffer pH 7.0, 0.03% DDM(n-dodecyl-β-D-maltoside)). The flow rate was 1 ml/min. All detergents were added to the FSEC running buffer at the concentration of ~3x their respective critical micelle concentration (CMC).

2.31.1. Target GFP-fusion construct for FSEC assay

FeoB *E. coli* membrane protein-GFP fusion constructs was generated in this work. The *feoB-GFP-6His* coding sequence was cloned into a pTriEx1.1-vector at the *Nco*I/*Xho*I sites to allow expression of a FeoB-GFP-6His fusion was used primers in (Table 2.7) was used overlapping PCR amplification method for cloning strategy.

2.31.2. Sample preparation for FSEC

5.5 ml lysis buffer (filtered 50 mM phosphate buffer pH 7.5, 2 mM $MgCl_2$, 100 µg/ml DNase, EDTA-free cocktail protease inhibitors [Roche Molecular Systems, CAI], 0.006% CHS [Cholesteryl Hemisuccinate TRIS salt]) were added to 10 ml lysis buffer, and the cells were thawed on ice. After rotation mixing, the dissolved the pellet (from 50 ml of cell culture) was mixed on a rotory shaker for10 min. The cells were lysed using four cycles of freeze-thawing at -20 °C, followed by mixing (pipetting up and down). For solubilisation with different

detergents, 360 µl of crude lysate were mixed with 40 µl 5% detergent stock in a 96 x 2 ml deep-well plate (Axygen Scientific, CA). The mixture was incubated on a plate shaker with orbital shaking for 2 h at 4 °C (all detergents were from Ana trace, OH). Debris was pelleted by ultra-centrifugation for 1 h at 30000 rpm in a benchtop centrifuge with plate inserts. The supernatant was transferred to the new tubes. Then 110 µl of supernatant were added to a chromacal 03-FISV vial (ThermoFisher), which was then was applied to a UFLC SHIMAZU RF-20AXS (Ultra fast liquid chromatography) system. 200 µl of every sample was also transferred to a regular, rounded-bottomed 96-well plate and saved for FSEC. Cell pellets were freeze-thawed directly in the 24-well growth plate before proceeding to solubilisation. These samples were also centrifuged to remove debris, but not filtered, before injection onto the column.

2.31.3. Measurement of protein concentration

The protein concentration was determined utilising the Beer-Lambert law by measuring the absorption of the protein solution with light at a wavelength of 280 nm with a Lambda 40 spectrophotometer (Perkin-Elmer, Waltham, USA). The extinction coefficient of each protein was calculated with the PROTPARAM tool of the EXPASY proteomics server (http://www.expasy.ch). PROTPARAM calculates the protein extinction coefficient from the amino acid sequence in conjunction with calculated values of tyrosine and tryptophan residues (Edelhoch, 1967; Pace *et al*., 1995).

2.31.4. Large-scale protein expression in *Ao*38 insect cell

Large-scale protein expression was performed in a 1 l suspension culture of *Ao38* insect cells in a 3 l Erlenmeyer flask format with the relevant recombinant baculovirus. Each flask was

seeded with $0.5x10^6$ cells per ml. cells were infected with 10% of the appropriate recombinant baculovirus and incubated for a further 72 h. Then a viable count using 0.4% Trypan blue estimated the number of dead cells before harvesting. The cell culture was harvested by centrifugation at 5000 rpm for 45 min at 4 °C.

A 3 l wave Biotech fermenter bag was filled with serum free medium supplemented with 1% foetal calf serum and antibiotics and inoculated with exponentially growing *Ao38* insect cells to an initial density of $0.5x10^6$ cells per ml. The bag was housed in the wave Bioreactor and incubate for 12 to 24 h to allow the cell density to reach $1x10^6$ cells per ml, whereupon recombinant baculovirus was added. The infected culture was incubated st 28 °C with rocking for a further 72 h before harvesting by centrifugation. A viable count was performed using 0.4% Trypan blue to estimate the number of dead cells before harvesting. The protein was harvested by centrifugation at 5000 rpm for 45 min at 4 °C. After collecting, pellets were transferred to 50 ml tubes, centrifuged briefly, overlayed with 1 ml buffer (50 Tris pH 7.5, 150 mM NaCl) to avoid drying, and then frozen at -80 °C.

2.31.5. Manual cell lysis (Harwell Complex Research)

All components of the manual pressure cell press were maintained at 4 °C minimise potential protein degradation processes upon cell lysis. Once assembled the pressure cell press was used to lyse cells, with a total of 2-3 passes through the pressure cell to ensure maximum cell lysis. Debris was removed by centrifuging at 100,000 g at 4 °C for 1 h and the supernatant was quickly decanted and retained for loading onto a protein purification column used ultrasound cool centrifugaton.

2.31.6. Large-scale protein purification

Pellets were resuspended for membrane preparation in lysis buffer (50 mM Tris pH 7.5, 150 mM NaCl, 1 mM TCEP, 20 mM mannitol, 1 mM $MgCl_2$, 50 µg/ml DNase, EDTA-free cocktail protease inhibitors). All steps of lysis and membrane preparation were performed at 4 °C. Cells were homogenised in 100 ml lysis buffer with 0.5% MNG detergent using a Dounce homogeniser, followed by incubation for 2 h at 4 ˚C with gentle shaking. The lysate was transferred to a new tube for centrifugation for 1 h at 38,000 g in a Beckman JA25.50 rotor. Then, the lysate was filtered using a 0.2 µm pore membrane. The supernatants were transferred to a Beckman Ti45 ultracentrifuge rotor and centrifuged at 100,000 *g* for 1 h.

The supernatant was incubated at 4 °C with Ni^{2+}-charged Profinity IMAC resin (0.5 ml bed volume) for 1 h with gentle rotation and the loaded on a gravity flow column (Bio-Rad). After washing with 100 ml washing buffer one (50 mM Tris pH 7.5, 500 mM NaCl, 20 mM imidazole, 20 mM mannitol, 1 mM TECP, 0.05% MNG detergent), the column washed with 100 ml washing buffer 2 (50 mM Tris pH 7.5, 150 mM NaCl, 30 mM Imidazole, 20 mM mannitol, 1 mM TECP, 0.05% MNG detergent). Protein was eluted with 100 ml elution buffer (50 mM Tris pH 7.5, 150 mM NaCl, 300 mM imidazole, 20 mM mannitol, 1 mM TECP, 0.05% MNG detergent). Elutate was applied to a 1.5 ml SuperoseTM 6 Increase 10/300 GL column (GE Healthcare Bio-Sciences) linked to an AKTA Purifier. Fractions were collected in 50 ml Falcons and the main peaks were pooled, concentrated to 5-10 mg/ml using Vivspin concentration devices (Sartorius, Gottingen, Germany), flash-frozen and saved for subsequent structural and functional studies.

2.31.7. Protein desalting

To remove imidazole from the purified protein sample, the protein was filled into pre-wetted dialysis tubing (Medicell International Ltd., London, UK), with a molecular weight cut off (MWCO) of 10 kDa. The protein solution in the tube was dialysed against 2 l of dialysis buffer for 16 h at 4 °C. If a target proved unstable, PD-10 desalting columns (GE Healthcare, Amersham, UK) were used instead of dialysis. These columns were equilibrated with 25 ml of Dialysis buffer Buffer A (20 mM Tris pH 7.5, 150 mM NaCl, 1 mM TECP, 20 mM mannitol, 0.05% DDM). The protein sample was applied to the column in 2.5 ml and eluted with 3.5 ml Buffer A. After the removal of imidazole, the solution was centrifuged at 3000 *g* for 20 min. Fractions representing the main peaks were pooled, concentrated to 5-10 mg/ml using Vivaspin concentration devices, flash-frozen and saved for subsequent structural and functional studies.

2.31.8. Size exclusion chromatography (SEC)

SEC was used as the final protein purification step as well as to assess the monodispersity of the protein sample. Before being applied to a gel filtration column, the protein solution was concentrated in a 100 kDa MWCO Vivaspin concentrator until a final volume of 500 µl was reached. The sample was then applied with a 500 µl loop onto a Superdex 200 10/300 gel filtration column (GE Healthcare, Little Chalfont, UK), which was pre-equilibrated with Washing Buffer (20 mM Tris pH 7.5, 150 mM NaCl, 0.05% DDM, 1 mM TECP, 20 mM mannitol). The target was eluted with 1.5 column volumes (36 ml) of Buffer A and collected in 1 ml fractions. SEC runs were performed on an ÄKTA purifier. Fractions were analysed by SDS-PAGE analysis and checked by Dynamic light scattering (DLS), also known as photo correlation spectroscopy or quasi-elastic light scattering. This is a simple yet powerful method that measures and characterises particles in solution. It correlates the Brownian motion of

("spherical") particles with their sizes. Brownian motion is merely the random movement of particles due to their encounters with the solvent molecules that surround them, the larger the particles, the slower the Brownian motion and vice versa. Brownian movement is also dependent on the medium viscosity and temperature and the samples containing protein were pooled and concentrated for use in crystallisation trials.

2.31.9. Cell lysis and membrane preparation

To lyse the cells, the frozen cell pellets were thawed on ice and resuspended in 50 mM Tris pH 7.5 using 50 ml of buffer per 10 g of *Sf9* or *Ao38* cells. Complete protease inhibitor tablets (Roche Diagnostics Ltd., Burgess Hill, UK) (1 per 100 ml) and 10 mg of DNAse (Sigma-Aldrich), 1 mM TCEP, 20 mM mannitol, were added. Cell lysis was performed for small volumes using a French pressure cell (Thermo Scientific, Waltham, USA) at 13000 psi in three passes. Larger volumes were lysed using a constant flow Cell Disrupter. Three passes (20000 psi) broke the cell walls. Following lysis, the cell debris was sedimented by centrifugation at 1 h at 380000 g.

2.31.10. Solubilisation of membrane proteins

The target proteins need to be isolated from their membranous host using detergents. In this study, Maltose-neopentyl glycol (MNG) detergent (Anatrace, Maumee, USA) was used for all solubilisations. Samples were thawed on ice and diluted in Lysis Buffer I (50 mM Tris-HCl pH 7.5 and 150 mM NaCl, 1 mM $MgCl_2$, ~1 mg DNase and protein inhibitor), using 50 ml for 20 g of wet cells. Assuming an extinction coefficient of 1 at 280 nm, the total protein concentration was measured, and the membrane suspension diluted to reach a final concentration of 40 mg/ml. A 10% (w/v) solution of MNG in the above buffer was added dropwise with stirring until a

final concentration of 1.5% (w/v) MNG was reached. The protein solution was gently stirred for 2-16 h at 4 °C. The insolubilized material was sedimented by ultracentrifugation for 50 min at 380000 *g*. The target protein-detergent complex was thus released to the supernatant along with other membrane proteins that were solubilised by MNG. The desired membrane protein could then be purified from this solution using the following purification methods.

2.31.11. Immobilised metal-affinity chromatography (IMAC)

In this work a histidine-Tag attached to the membrane protein was used, comprising eight histidine residues (His6) provided by the pTriEX1.1-*feoB*-His-Tag construct, for purification with immobilised metal affinity chromatography (IMAC). The aromatic ring of the imidazole side chain of the histidines binds to a Ni^{2+} ion that is immobilised with a linker to the column matrix, such as nitriloacetic acid (NiNTA). A concentration gradient of imidazole is employed to elute the target protein off the column. The following describes the protocol for membrane protein purification based on the IMAC method used in this study.

Any precipitation was removed by centrifugation at 5,000 g for 30 min. The supernatant was filtered (0.22 μm) and loaded (2 ml/min) onto a pre-equilibrated (Lysis buffer) 5 ml Histrap column (GE Healthcare, Amersham, UK). The column was washed with three column volumes (cv) of Wash buffer one and Wash buffer two followed by a step elution buffer, which was composed of four steps of increasing imidazole concentrations. Steps were performed on an ÄKTA purifier with Buffers 1 and 2 (3 ml/min). In the first two concentration steps of 20 and 30 mM (each 3 cv) non-specific binding proteins were eluted followed by target elution (5 cv) with 300 mM imidazole. The final step of 500 mM (5 cv) was used to clean the column of any remaining proteins. The eluate was collected in 2 ml fractions for the first two imidazole steps and in 1 mL fractions during target elution. The collected fractions were examined by SDS-PAGE.

Table 2.12: Buffers and required materials employed for IMAC purification. Lysis buffer was also employed to equilibrate desalting columns and for gel filtration columns.

Buffers & Materials	Composition	Comments
Washing buffer one	20 mM Tris-HCl (pH 7.5) 150 mM NaCl, 1 mM TCEP, 20 mM mannitol, 20 mM imidazole 0.05% (w/v) MNG	Sterilised by filtration
Washing buffer two	20 mM Tris-HCl (pH 7.5) 150 mM NaCl, 1mM TCEP, 20 mM mannitol, 30mM imidazole 0.05% (w/v) MNG	Sterilised by filtration
Elusion Buffer	20 mM Tris-HCl (pH 7.5) 500 mM NaCl, 1 mM TCEP, 20 mM mannitol, 300 mM imidazole 0.05% (w/v) MNG	Sterilised by filtration
5 mL HisTrap-column	NiNTA	Supplied by GE Healthcare
Äkta Purifier	Fast Protein Liquid (FPLC) Chromatography	Supplied by GE Healthcare

2.31.12. Mass spectrometry

Mass-spectrometry was collaboration with Dr. Nicholas Michael, CAF (Technical Specialist, Mass Spectrometry, Department of Chemistry, Harborne Building, The University of Reading).

2.32. Static light scattering (SLD)

Static light scattering is used to characterise membrane proteins in detergent solution. Determination of the oligomeric state or the subunit stoichiometry of integral membrane proteins in detergent solution is notoriously difficult, because the amount of detergent (and lipid) associated with the proteins is usually not known. Only two classical methods (sedimentation equilibrium centrifugation and static light scattering) can measure directly the

absolute molecular mass of a protein present in a protein/detergent micelle, without any assumption on the amount of detergent bound, or the shape of the proteins. This experiment was done with collibration with membrane protein Lab(MPL) and National Phisic lab(NPL) Harweel Complex research, Oxford,UK.

2.32.1. Dynamic light scattering (DLS)

Purity and homogeneity of a protein can be determined by standard laboratory techniques. However, the aggregation and polydispersity of a protein is determined by DLS or SAXS. This can confirm whether soluble proteins are monodisperse and folded. DLS was used under different conditions, to assess the stability of the protein in different buffers and in the presence of various ligands or so-called additives. Such screening was used to select the best conditions for FeoB protein stability. The beam from a solid-state diode laser (Coherent Model 2020), operating at 532 nm with vertically polarized light, was focused onto the sample cell through a temperature-controlled chamber filled with refractive-index-matching toluene. The incident and scattered beams were polarized with Glan and Glan-Thompson polarizers with extinction coefficients higher than 10^{-6} and 10^{-7}, respectively. The sample solutions were filtered through 0.45 filters (Millipore) directly into pre-cleaned light scattering cells of highest quality. Dynamic Light Scattering (DLS) Results from the DLS measurements show that hydrodynamic (DDM). radius (Rh) of the pure DDM micelles is around 4.5 nm while the PDC micelle is around 6.9 nm. The in situ DLS experiments were carried out at 293 K using a SpectroLight 610 (XtalConcepts GmbH, Hamburg, Germany) instrument. 2 µl of each sample were pipetted onto a 72-well Terasaki plate Hamburg, Germany) and covered with parawas filled each well from cassette by 100 µl paraffin oil then added 2 µl from protein sample then checked the protein by light scattering analyses.

2.32.2 Small-angle X-ray scattering (SAXS)

ASXS is intensities from dilute macromolecular solutions contain global structural information averaged over orientations and types of components in the sample, which, in the absence of interactions can be expressed as a linear combination. SAXS is far more sensitive to changes in the global structure than to changes due to binding of small ligands alone, and this distinguishes SAXS-based screens from affinity-based techniques such as isothermal titration calorimetry (ITC). SAXS Measurements. Preliminary and production screening sessions were conducted at Diamond beamlines, using the automated sample changer setup8 to simplify measurement on 96-well plates. The plate geometry was leveraged to conduct 6 or 8-point titrations spanning apoprotein to 1:1 mixtures, at 50 μM protein concentration and 40 μl final volume. This work was help as Charllee PhD student.

2.33. Crystallography of FeoB

FeoB protein was prepared for crystallisation screening by concentration using a 100 kDa Vivspin device (Sartorius) and final protein concentration was typically 8-10 mg/ml. Concentrated protein (1 μl) was used to set up crystal screen trays using both lipid cupic and sitting drop methods (Landau and Rosenbusch, 1996; Martin Caffrey, 2014). A variety of screens were used in the laboratories of Dr I. Moraes and R. Reis (Harwell Complex Research, Diamond Light Source, Oxford, UK). The screens used are listed below (Table 2.14). It should be noted that initial screens (at Diamond using LCP) were chosen because they had been specially designed for membrane proteins.

Table 2.13: The commercially available crystallisation screens employed for the hanging drop method.

Screen	Manufacturer
MemGold BN149-1-41	Molecular Dimensions Ltd., Newmarket, UK
MemGold2 BNO82-1-64-1-41	Molecular Dimensions Ltd., Newmarket, UK
MemSys BNO81-1-33	Molecular Dimensions Ltd., Newmarket, UK
CS II (HR2-112)	Hampton Research, Aliso Viejo, USA
CS I (HR2-110)	Hampton Research, Aliso Viejo, USA
MemMeso BNO29-1-87	Molecular Dimensions Ltd., Newmarket, UK

In all cases, the plates were checked regularly, and care was taken to avoid crystal degradation by excessive plate handling.

2.34.1. Crystallisation experiments

2.34.1.1. Initial screening

Protein samples were subjected to sparse matrix screens in concentrations from 4.7– 12 mg/ml. Initial screening was performed at 22 ℃ using the sitting-drop vapour-diffusion method. The reservoir contained 50 µl and drop volumes (1:1 ratio of protein and reservoir solution) ranged from 500 nl to 1 µl. 96-well plates (MRC, SwissSci, Neuheim, Switzerland) for initial screens were prepared through dispension of reservoir solution by a Hamilton Microlab Star robot (Hamilton Bonaduz AG, Switzerland) and then stored at 4 ℃, until required. The drops of crystallisation experiments were set up automatically with a Cartesian Honeybee nanoliter dispensing system (Genomic Solutions Ltd., Huntington, UK). Initial 96-well screening plates were integrated into a Rhombix Crystal Plate Imager (Thermo Scientific Waltham, USA) for automatic monitoring or checked by microscope. All trays were incubated at 22 °C. Trays were

checked for signs of crystal formation after one, three, five, seven, ten and fourteen days and weekly thereafter. The commercial screens used for initial screening are listed in Table 2.12.

2.34.2. LCP crystallisation

This is considered a novel concept for the crystallization of membrane proteins. Lipidic cubic phases (LCP) is crystallization method as bi-continuous cubic phases consisted of monopalmitolein (1-monopalmitoleyl-rac-glycerol, C16:1c9, or MP, Sigma) or monoolein (1-monooleoyl-rac-glycerol, C18:1c9, or MO, Sigma) with water or appropriate buffers. Micellar type cubic phases contained palmitoyl-lysophosphatidylcholine (Avanti Polar Lipids) and water/buffer. The preparations were thermostated at 20 ˚C in the dark throughout crystallization.

2.34.3 Fluorescence Dye-Based Diferential Scanning Fluorimetry (DSF) and CPM Assay

Membrane-bound and purified recombinant FeoB protein was assayed to determine the effect of temperature on membrane protein cysteine residue activity. The protocol utilises a real-time PCR machine. The thiol-specific fluorochrome, N-[4-(7-diethylamino-4-methyl-3-coumarinyl) phenyl]maleimide (CPM), binds to buried Cys residues exposed upon denaturation which results in enhanced fluorescence (Yeh *et al*., 2006; Alexandrov *et al*., 2008; Liu *et al*., 2010). The assay can be performed in low volume and allows the effects of buffers, detergents and ligands on protein stability to be measured, and indicates the overall integrity of the folded state.

The fluorescence dye-based differential scanning fluorimetry (DSF) method, likewise known as protein thermal-shift assay or ThermoFluor, is a simple yet powerful tool that was initially

advanced to screen protein stability in the presence of small ligands (fragments) in early drug discovery platforms (Lo *et al*., 2004; Zucker *et al*., 2010; Sjuts et al., 2019). Currently, it is a well-established approach to assess the stability of soluble (Vedadi *et al*., 2010) and membrane proteins (Kohlstaedt *et al*., 2015) in the presence of different buffer formulations, detergents, and small molecules.

The DSF technique is based on the association with protein stability and its Gibbs free energy of unfolding (DGu). In other words, as temperature rises, protein stability reduces, and it starts unfolding. When the amount of unfolded protein equals the amount of folded protein, the value of DGu becomes zero and the system has reached what is known as the "melting point" temperature (Tm). In the DSF method, the fluorescence intensity is plotted as a function of the temperature. As a result, a sigmoidal curve is generated where the inflection point of the curve is the Tm value.

2.35. ^{55}Fe Transport Assay

Transformants of *E. coli* (JC28 and JC32) were grown overnight in 5 ml 0.4% glucose M9 medium, from which approximately 1 ml was used to inoculate 50 ml of fresh medium supplemented with 1 µM DTPA (diethylenetriaminepentaacetic acid) in a 250 ml flask (to give a starting OD_{600} of 0.02) under aerobic condition with addition of the required antibiotic, 2 mM ascorbic acid, 100 mM MES pH 6 or 100mM TAPS pH 8, and 0.2% arabinose. Cells were allowed to grow until mid-exponential phase was achieved (OD_{600}nm 0.1~0.15), at which time cells were harvested. Induced cells were harvested by centrifugation (5000 x g 4 °C 10 min). The cell pellet was washed once in uptake buffer (Chelex 100 treated 1×M9 salts, 100 mM MES pH 6 or 100 mM TAPS pH 8, 0.4% glucose, 0.001% vitamin B1, 0.2 mM $CaCl_2$, 2 mM $MgSO_4$, 1 µM DTPA, 2 mM ascorbate), and then resuspended in 3 ml of transport buffer (~0.1 µM iron) and retained on ice and the supernatant discarded, the cells were washed with 10 ml

cold transport buffer (TB: 50 mM MES pH 6, 0.4% glucose, 0.2 mM $CaCl_2$, 2 mM $MgCl_2$, 2 mM ascorbate). The cell pellet was re-suspended in TB. The resuspended cells were placed in a 3 ml reaction chamber with gentle stirring at 37 °C. Uptake reactions were initiated by adding 4 µCi $^{55}FeCl_3$ (Perkin-Elmer Life and Analytical Sciences) combined with various quantities of $^{56}FeSO_4$ to give the desired final level of total iron. When Fe^{2+} was required, the required quantities of $^{55}FeCl_3$ and $^{56}FeSO_4$ were diluted together into 20 µl of 1 M ascorbic acid. When Fe^{3+} was required, $^{55}FeCl_3$ and ^{56}Fe-dicitrate. Samples of 250 µl were taken at each time point and 250 µl of cell suspension were removed from the reaction cell at each assay time point, and were immediately filtered through a 0.22 µm Whatman filter, followed by washing with 10 ml cold wash buffer (100 mM sodium citrate, 0.2 mM $CaCl_2$, 2 mM $MgCl_2$) then 10 ml cold EDTA buffer (WB: 10 mM EDTA pH 8.0). Each washed filter was added to 4 ml Ultima Gold XR scintillant (Perkin Elmer) and inverted until dissolved. All samples were left for 24 h to allow for a reduction in background chemi-luminescence, before liquid scintillation counting (0.2 – 6.2 KeV) with a Beckman LS-6500 multi-purpose scintillation counter for 3 min per sample.

The diluted cells were filtered through a 0.2 µM nitrocellulose membrane (Whatman) followed by washing with 10 ml of 10 mM EDTA. The membrane was then placed into a scintillation vial (VWR International, UK) with 3 ml of scintillation cocktail ULTIMA GOLD XR (Perkin-Elmer). The radioactivity was measured using a Beckman LS6500 liquid scintillation counter (Beckman Coulter, Fullerton, CA) in the energy region of 0.0-10.0 keV to give optimal efficiency (higher radioactivity and lower background). Control experiments was performed with cell-free uptake buffer and the resulting cell-free data was subtracted from the uptake data to correct for low level background binding of ^{55}Fe to the membrane. Three OD units of cells were diluted into 3 ml pre-warmed (37 ^{o}C) TB in a reaction cell, and maintained with continual stirring. ^{55}Fe was added at time zero to initiate the uptake reaction. Results were standardised per mg of protein determined via a Bradford assay on the original cell suspension (see Appendix

for standard curve). Additions of hydrogen peroxide and catalase (*Micrococcus lysodeikticus*) were made just prior to addition of the ^{55}Fe.

The effect of anaerobiosis was examined by inoculation of 50 ml of fresh M9 (starting OD 0.02) under anaerobic conditions with antibiotic, 2 mM ascorbic acid, 100 mM MES (pH 6), 0.2% arabinose and 1 µM DTPA. Cells were allowed to grow until mid-log phase, at which time cells were harvested by centrifugation (5000 x g 4 °C 10 min). Other details are as above except that dissolved oxygen was removed from all solutions by de-gassing by bubbling of nitrogen gas through solutions for 20 min. 3 ml of degassed transport buffer were used with in the reaction cell, which was sealed with an o-ringed plunger to maintain a reduced oxygen environment. The removal of oxygen ensured the cessation of oxidative respiration, therefore preventing hydrogen peroxide generation – thus removing the reduction substrate for iron import.

Where required, 200 µM hydrogen peroxide was introduced via hypodermal syringe injection through the O-ringed sealed plunger at T_0. Then 250 µl of cell suspension were removed from the reaction cell at each assay time point, and were immediately filtered through a 0.22 µm Whatman filter, followed by washing with 10 ml cold wash buffer (100 mM sodium citrate, 0.2 mM $CaCl_2$, 2 mM $MgCl_2$) then 10 ml cold EDTA buffer (WB: 10 mM EDTA pH 8.0). Each washed filter was added to 4 ml Ultima Gold XR scintillant (Perkin Elmer) and inverted until dissolved. All samples were left for 24 h to allow for a reduction in background chemi-luminescence, before liquid scintillation counting (0.2 – 6.2 KeV) with a Beckman LS-6500 multi-purpose scintillation counter for 3 min per sample.

2.36. Hydrogen peroxide assay

Measurements of hydrogen peroxide concentrations were made with Amplex Red (Thermo). Transformants of JC32 or LC106 were used, or *E. coli* W3110. These were grown 5 ml 0.4% glucose M9 medium (starting OD 0.05), and when the OD_{600} reached ~0.4 (mid log) inducer

was added (0.2% rhamnose) and growth continued for 1 h after which the cells were harvested and washed once with 10 ml cold WB(Wash buffer: 100 mM sodium citrate, 0.2 mM $CaCl_2$, 2 mM $MgCl_2$), then twice with TB (Transport buffer: 50 mM MES pH 6, 0.4% glucose, 0.2 mM $CaCl_2$, 2 mM $MgCl_2$, 2 mM ascorbate) followed by dilution to 1 OD units/ml. For each measurement of H_2O_2 concentration, 100 µl of cell-free solution were added to 100 µl Amplex Red reagent and absorbance at 560 nm determined, then compared to a standard curve generated with known concentrations of H_2O_2. For each assay, a measurement prior to addition (Pre) of 15 µM H_2O_2 (T0) was made to ensure endogenous H_2O_2 concentrations were minimal, then every 2 min after H_2O_2 addition during the assay. When used, desferrioxamine was added prior to addition of cells or iron. The pH of TB was adjusted as required.

2.37. Bioscreen and FLUOstar assays

The colonies obtained were plated onto M9 plates and left at 37℃ for 2 days to allow acclimatisation to the less nutrient-rich medium. Overnight cultures were made by inoculation of 5 ml of M9 minimal medium (non- pH adjusted) containing 2 µl/ml 10 µM ferric citrate and 100 µl/ml ampicillin (100 µg/ml) and 50 µl/ml of 50 µg/ml chloramphenicol for double transformants) with colonies selected from these plates. The following morning, the cultures were transferred to Falcon tubes and centrifuged at 5000 rpm for 5 min, and the supernatants discarded. The pellets were resuspended in 5 ml of iron-free M9 medium. The wash step was repeated, the supernatants discarded, and the pellets resuspended in 2 ml of M9 iron depleted medium (pH 6, 7 or 8). This ensured any residual iron was removed from the cultures.

0.4% glucose M9 medium (pH 6, 7 or 8) was prepared for inoculation. Ampicillin and arabinose were added to final concentrations of 100 µg/ml and 0.2%; bacteria containing pBADrham-*feoC* were incubated in medium also containing 50 µg/ml chloramphenicol or 100 ug/ml

ampicillin, and 0.2% rhamnose or 0.02% arabinose. Various additives were also included in some cases: 0.5 μM DTPA, 2 mM ascorbic acid, 10 μM ferric citrate.

The medium was dispensed into tubes. The overnight cultures were used to inoculate the medium prepared; the volume of inoculate used was calculated to ensure that the samples had a starting OD of 0.01. These were then loaded in triplicate into 100 well plates and incubated in the Bioscreen reader at 37℃ with continuous shaking for 24 hours. OD readings (600 nm) were taken and recorded hourly.

2.38. Anaerobic growth

Anaerobic growth was achieved using syringes. The bacterial strains and the transformants to be tested were grown overnight aerobically at 37 °C. Next day, the OD_{600} was measured used to calculate the volume of culture to be added to fresh 0.4% glucose M9 medium to give a starting OD of 0.01. The culture was then drawn into 20 or 50 ml syringes, any trapped air expelled and the needle inserted into a bung to prevent any oxygen from entering. Growth was at 37 °C for 24-36 h without agitation. growth was measured by expulsion of samples for OD measurement every 2 h. Other growth conditions are as above.

2.39. Spot assay

E. coli strains harbouring the desired plasmid were grown in 3 μl LB overnight at 37 °C with 250 rpm shaking. The OD_{600} of each culture was measured and 0.01 OD of cells were transferred into 0.5 ml sterile Eppendorf tubes: 10 μl of cells were then serially diluted into 90 μl of M9 until a dilution of 10^{-7} was achieved. M9 plates with various additions(Results not shown) from were prepared and 5 μl of each dilution of culture were applied to the agar. The culture was allowed to absorb into the agar, after which the plates were inverted and incubated

at 37 °C overnight. The growth on the plates was recorded using a G-Box imager system (Gene*Sys*).

2.40. Scanning Electron Microscope (SEM) for microorganism

In order to determine the cell morphology of the *E. coli ftsH* mutant, SEM was used. In SEM, the electron beam is used as a source of illumination as it has a much greater resolving power than the ordinary light microscope as the wavelength of the beam is much smaller (Sousa and Leapman, 2012). An electron-dense stain allows the surface characteristics of the sample to be visualised. The wildtype and mutant were first grown in 0.4% glucose M9 medium to mid exponential phase, and then were harvested and washed twice with 5 mM PBS buffer (pH 7). The washed cells were resuspended in the same buffer PBS at cell density of 10^8 CFU/ml and incubated at 37 °C for 30 min. After incubation, cells were centrifuged and pellets were fixed overnight with 2% (w/v) paraformaldehyde, 2.5% (v/v) glutaraldehyde fixative in 5 mM HEPES buffer at 4 °C. Then the pellets were dehydrated through a graded ethanol series at room temperature, and finally by with CO_2 and coated with gold in a sputter coater. Cells were examined and photographed with a FEI Quanta scanning electron microscope operating at 20 kV (Dr. P. Harris and A. Kaur). Experiments were conducted in triplicate and at least six cells from six fields of microscopic view were photographed.

Chapter 3: Role *efeUOB* and *feoABC* in ferrous-iron uptake

3.1 Introduction

E. coli K-12 encodes two distinct ferrous-iron uptake systems, encoded by the *feoABC* operon and the *efeUOB* operon (Cartron *et al*., 2006; Cao *et al*., 2007). *E. coli* also possesses ferric reductase activity that acts extracellularly to convert ferric to ferrous iron and thus facilitates ferrous iron transport by raising the levels of the soluble, ferrous form (Cowart, 2002), although the nature of this is little understood. Also, ferrous iron can be taken up by *E. coli* using the NRAMP-like transporter (MntH) and the ZIP transporters (ZupT). The former system appears to act primarily as a Mn^{2+} transporter (Kehres *et al*., 2000), and the latter has specificity for a variety of divalent metals (Grass *et al*., 2005). Thus, Fe^{2+} transport in *E. coli* occurs both aerobically and anaerobically, but is induced anaerobically or by low pH, as well as by low iron.

In *E. coli* and many other bacteria, the *feoABC* operon consists of three adjacent genes, *feoA*, *feoB* and *feoC* encoding FeoA, FeoB and FeoC respectively. These are transcribed from a Fe^{2+}-Fur and FNR-regulated promoter upstream of *feoA*. In *E. coli* O157:H7, the 'elemental ferrous' iron transport system (EfeUOB) was the first example of a bacterial Ftr1p like system involved in iron uptake, and was identified as a highly specific ferrous iron transport system (Cao *et al*., 2007; Grosse *et al*., 2006).

3.1.1 Objective of this chapter

FeoABC provides an advantage for *E. coli* under anaerobic iron-restricted conditions (Hankle, 1987), whereas EfeUOB provides a growth advantage under iron-restricted, aerobic, reducing conditions, at low pH in the presence of a competing metal (Cao *et al*., 2007). There is no clear

understanding on the ecological niche in which EfeUOB offers an advatage, and therefore the relevant natural environmental conditions where EfeUOB supports growth remain to be established. Understanding the distinct environmental conditions under which FeoABC and EfeUOB provide advantage (or disadvantage) can provide insight into the respective roles of these two systems in aerobic and anaerobic growth. In particular, elucidation of the basis of any distinct dependency on O_2 and/or acidic conditions would enhance understanding of the purposes and limitations of the Efe and Feo systems. To progress such understanding, the effect of *feoABC* or and *efeUOB* complement on growth *E. coli* JC28 under iron-restiction, with and without oxygen, was examined to allow the following questions to be addressed:

What are the growth conditions where a functional FeoABC system provides an advantage to *E. coli* JC28 and are they similar/different than those in which EfeUOB can provide an advantage?

Can EfeUOB provide an advantage to *E. coli* JC28 in its natural genetic context under conditions where Feo cannot?

Ultimately, the aim is to find possible reasons why bacteria such as *E. coli* have two different dedicated ferrous iron transport systems (EfeUOB and FeoABC) as opposed to one (FeoABC)?

3.2 Complementation of *E. coli* wildtype and iron-uptake mutant (JC28) with pHSG-*efeUOB* or pHSG-*feoABC* plasmids

3.2.1 Preparation of plasmids encoding the *efeUOB* and *feoABC* operons

In order to study the functions of the *efeUOB* and *feoABC* operons of *E. coli*, plasmids containing the entire *efeUOB* or *feoABC* operons of *E. coli* O157:H7 in the low-copy number

pHSG576 plasmid (Table 2.3) were employed. These plasmids carry the entire operons of both gene sets including the promoter regions, and were already available from laboratory stocks.

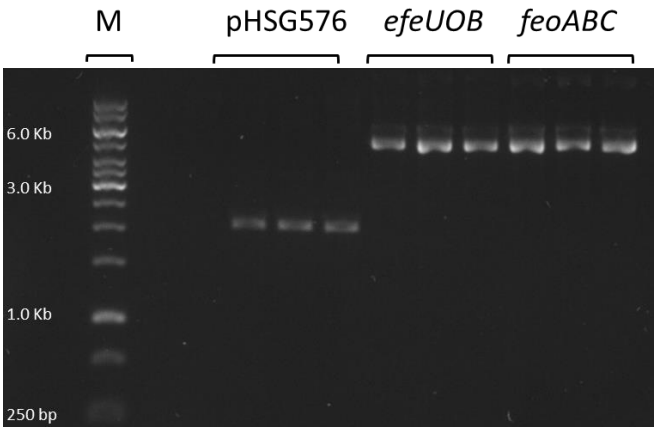

Figure 3.1 Analysis of pHSG-*efeUOB*^{O157}, pHSG-*feoABC*^{O157} and pHSG576 DNA by agarose gel electrophoresis. The gel contained 0.5x TBE and was 0.7% agarose. The 1 kb Ladder (Fermentas) was used as a marker. 4 µl of each 50 µl plasmid preparation (three isolates for each type) were loaded with loading dye (see Methods 2.13.3) in undigested form. The gel was strained with Gel Red, according to the manufacturer, and visualized by UV-transillumination.

DNA of the required plasmids was transformed into competent TOP10 and then plasmid DNA was extracted from Cm^R transformant colonies using a plasmid mini-prep kit (Section 2.21); these plasmid preparations were then analysed by agarose gel electrophoresis (Fig 3.1). The pHSG-*efeUOB*^{O157} and pHSG-*feoABC* ^{O157} plasmids thus identified were ~twice the size of the pHSG576 vector without insert, as expected. The plasmid preparations were subjected to further analysis by double restriction enzyme digestion with *Eco*RI and *Hin*dIII for pHSG-*efeUOB*^{O157} and *Eco*RI, *Bam*HI and for pHSG-*feoABC* ^{O157} (Fig 3.2 & 3.3).

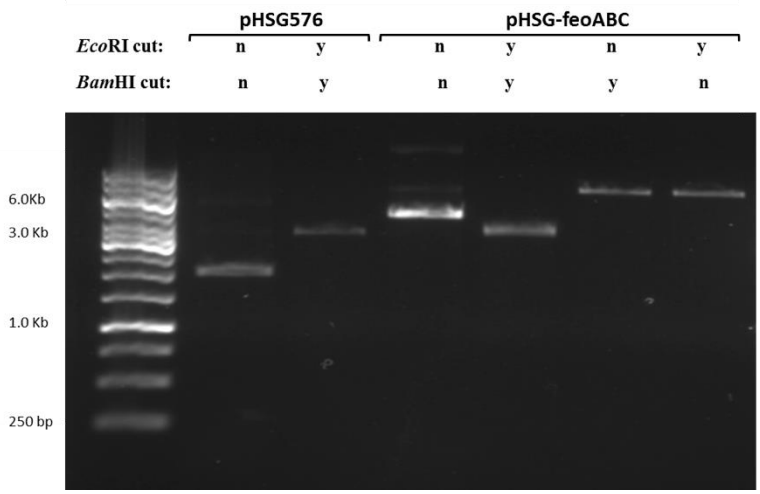

Figure 3.2 Confirmation of pHSG576 and pHSG-*feoABC* plasmids by restriction digestion. Agarose gel electrophoresis was as in Fig 3.1. Digestion with *Eco*RI and *Bam*HI was as described in Methods Section 2.22.

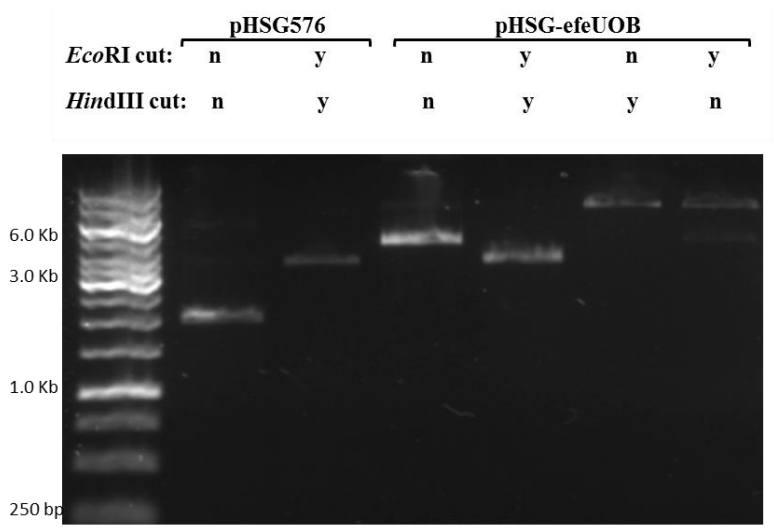

Figure 3.3. Confirmation pHSG-*efeUOB* and pHSG576 plasmids by restriction digestion. Details are as for Fig 3.2 except that *Eco*RI and *Hin*dIII were used for digestion, and just two pHSG-*efeUOB* isolates were analysed.

The pHSG-*feoABC* plasmid had an expected size of 6692 bp, and is expected to give fragments of 3.2 (vector) and 3.7 kb (insert) upon digestion. The pHSG-*efeUOB* plasmid is 6238 bp and is expected to give 3.2 and 3 kb (insert) bands. The digestion patterns obtained match those

expected although the two bands generated are not distinct on the gels. However, both plasmids had been previously confirmed by complete nucleotide sequence analysis (Salunkhe, 2016).

3.2.2 Phenotypic analysis of *E. coli* wildtype and JC28 carrying the pHSG-*efeUOB* or pHSG-*feoABC* plasmids aerobically

The *feoABC* and *efeUOB* plasmids isolated above (and the vector, pHSG576) were used to transform the wildtype (W3110) and JC28 (a mutant of *E. coli* K-12, strain W3110, lacking Fe uptake capacity; *feoABC*, *efeU*, *mntH*, *fec*, *ent*, *zupT*). JC28 is defective for growth under iron restriction since it has no known routes for iron uptake in minimal medium (Cao *et al*., 2007). Growth comparisons were carried out using a Bioscreen apparatus to confirm the iron-restriction phenotype of JC28 and to confirm the ability of cloned *efeUOB*^{O157} and *feoABC*^{O157} to complement the poor growth of JC28 under low Fe. The wild type *E. coli* W3110 strain, and JC28, transformed with the three relevant plasmids above. Growth was compared in 0.4% glucose M9 medium with/without 10 µM ferric citrate or 1, 2, 4 µM DTPA (iron chelator) and Cm (for tranformants only). The experiment was carried out aseptically. Medium was prepared in acid washed glassware. The Bioscreen growths were at 37 ˚C, for 24 h with shaking, and automated recording of OD at 600 nm.

To initiate growth, overnights culture were propagated using inocula from M9 agar plates with (transformants) or without (non-transformants) Cm, in 3 ml M9 medium with/without 10 µM ferric citrate (overnight 37 ˚C, 250 rpm). The JC28 cultures required longer than the wildtype for overnight growth (36-40 h) when pre-cultured without iron. All overnight growths were in triplicate. Pre-cultures were washed with fresh M9 medium to remove iron before use as inocula to initiate growth comparisons in the Bioscreen apparatus.

3.2.2.1. *E. coli* W3110 is subject to iron restriction in M9 medium

This experiment was carried out to confirm the impact of iron on the growth of *E. coli* (W3110) under sufficient growth conditions, and to show that iron-restricted growth can be achieved. The growth curve of *E. coli* (wild type) in this study was determined using an iron-limited minimal (M9) medium, and the same medium supplemented with 10 µM ferric citrate (iron-sufficient medium). As expected, the OD under low iron was below that attained under iron-sufficient conditions in wild type, with a ~twofold lower final OD_{600} achieved with no additions, a ~3.5 fold reduction with 1 µM DTPA, and almost complete inhibition by DTPA at 2 µM. This confirms that iron restriction can be achieved for the growth of *E. coli*.

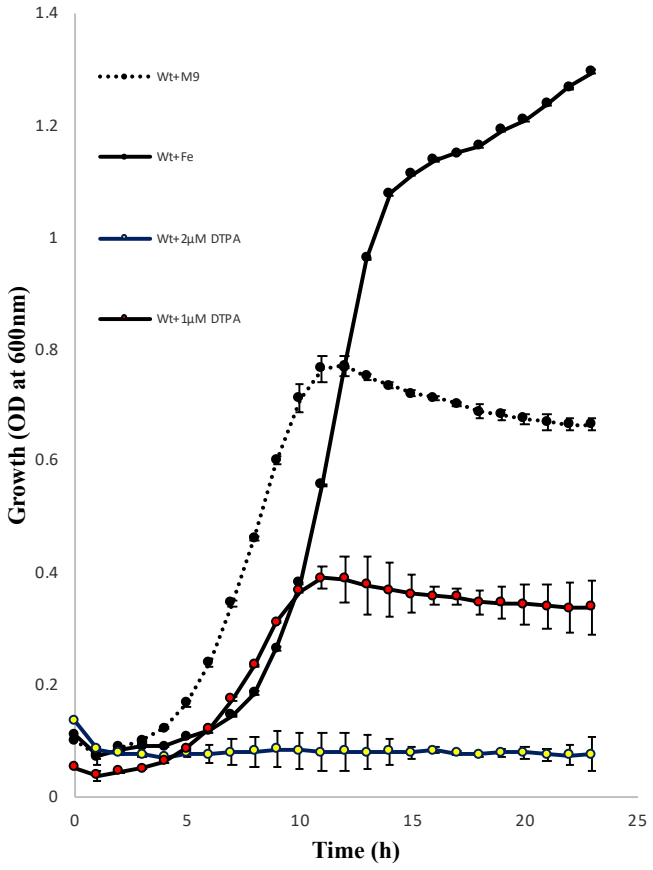

Figure 3.4. Wild type W3110 growth curve in minimal medium with and without ferric citrate or DTPA Strains were grown aerobically in acid-washed flasks containing 0.4% glucose in M9 minimal medium with or without 10 µM ferric citrate, or 1-2 µM DTPA. Precultures were grown in the same medium (with iron), washed and used to give a starting OD of 0.01. Values illustrated are avareges of two independent growths. Error bars presented the standard deviations.

3.2.2.2. Compaison of the effect of iron regime on the growth of the wildtype and iron transport mutant (JC28)

Initially, the growth of the wildtype and JC28 strains were compared under high and low iron regime to confirm the low-iron growth defect of JC28 specifically when iron was not included in the pre-culture. Growth results showed that the wildtype and JC28 strains carrying the vector both grew well in M9 medium with added iron in pre-culture and post-culture. However, there was a major difference when the iron supplement was absent from the pre-culture but present in the postculture with the mutant strain exhibiting a major growth lag with respect to the wildtype (~12 h) likely caused by lack of iron-uptake capacity, although similar maximum OD levels were achieved in wild type and mutant (Fig 3.6). When iron was present in the preculture, but absent in the post culture, a similar lag phase was seen together with a reduced final OD (~0.8 cf. 0.6 OD units). When iron was absent from both the preculture and postculture, the overall growth of the JC28 strain was greatly diminished showing more than a threefold reduction in maximum OD (Fig 3.5). These results confirm that JC28 has a major iron-restricted growth defect (Cao *et al*. 2007) but show that it can achieve good growth under iron sufficiency, albeit with a delay with respect to the wildtype under some conditions. Growth of both strains was greatly affected by no iron addition to the pre-culture and post-culture, with JC28 showing very little apparent growth and W3110 only able to achieve a fourfold increase in OD over the 24 h period of analysis. This suggests that the M9 growth medium had very little available iron such that inclusion of no additional iron was sufficient to impose severe iron restriction on the wildtype (as well as the JC28 strain).

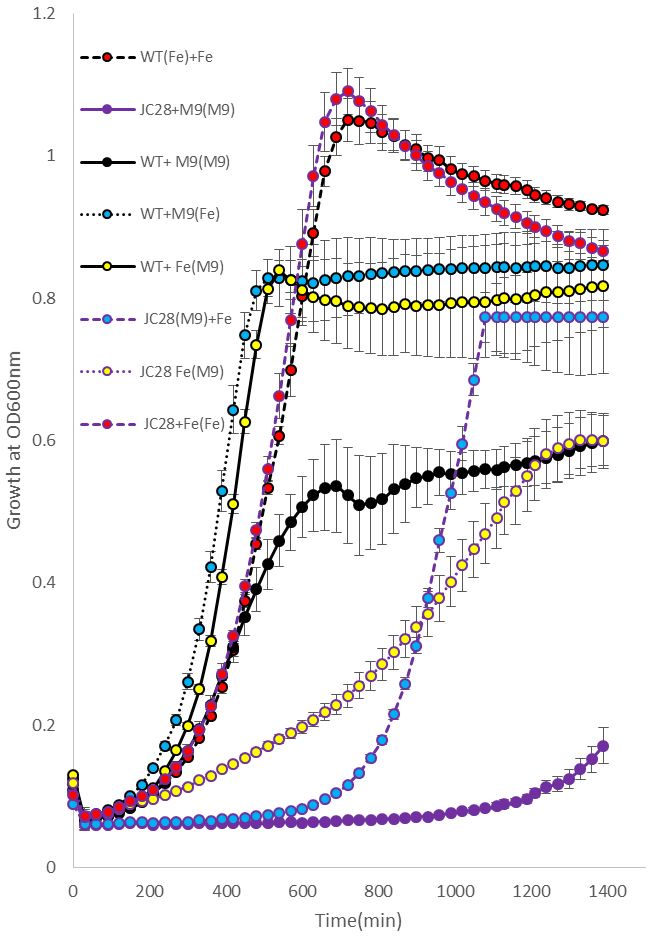

Figure 3.5. Growth of wildtype and iron transport mutant (JC28) under low and high iron. Strains used were W3110 (pHSG576) and JC28 (pHSG576). Medium was 0.4% glucose in M9 medium (plus 50 µg/ml chloramphenicol), either with 10 µM ferric citrate or no additions. Other details are as for Fig. 3.4.

3.2.2.3. Effect of *efeUOB* and *feoABC* complementation on iron-restricted growth of the iron-transport mutant (JC28)

Having confirmed the low-iron growth defect for JC28, the next requirment was to determine whether the pHSG-*feoABC*^{O157} and pHSG-*efeUOB*^{O157} plasmids could complement the low-iron restricted growth of JC28. JC28 carrying the aforementioned plasmids or the vector were therefore grown overnight in low-iron M9 medium and then use to inoculate low-iron M9 medium for growth comparison (Fig. 3.6). A clear growth advantage was observed for the

efeUOB transformant over the vector control, with a 3.5-fold greater increased OD at 24 h (Fig. 3.6). This result matches that of Cao *et al.* (2007) who reported an enhanced iron-restricted growth for the JC28 strain when complemented with a functional version of *efeUOB* in low-copy number. Somewhat surprisingly, complementation with *feoABC* also resulted in improved low-iron growth, but only by ~twofold, suggesting that *feoABC* is less effective at supporting low iron growth of JC28 than is the case for *efeUOB*. This finding presumably relates to the aerobic growth conditions employed here which would disfavour *feo* expression and function. However, it should be noted that the conditions employed were not optimal for *efeUOB* expression and function since neither acidic pH nor reductant were utilised

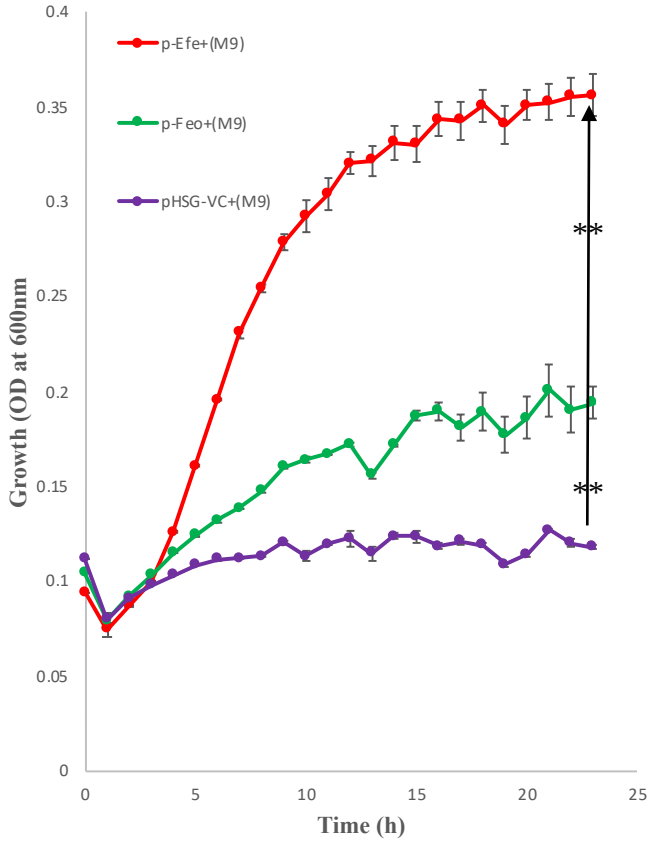

Figure 3.6. Effect of complementation of the iron transport mutant (JC28) with *efeUOB* and *feoABC* during growth under low-iron conditions. JC28 carrying either pHSG576, pHSG-*efeUOB* or pHSG-*feoABC* was grown overnight in M9 medium without iron, and was then inoculated into the same medium (no iron) for growth comparison in a Bioscreen apparatus. Other details are as in Fig. 3.4 & 3.5. Representative result from three repeats independent experiments; values are avareges of three independent growths. Error bars presented the standard deviations. Statistically significant differences (P<0.01) as determined by Graph Prism One way Anova and significant differences are indicated at 24 h.

The experiment above (Fig. 3.6) was repeated twice more and similar results were obtained (not shown). However, when iron was included in the preculture, *feo* gave an improved growth advantage (but this still remained less so than with *efe*). (Fig. 3.7) This difference in the impact of *feo* on low-iron growth of JC28 suggests that the effect of the Feo system is strongly influenced by slight changes in the growth conditions (e.g. residual iron concentrations and oxygen tension).

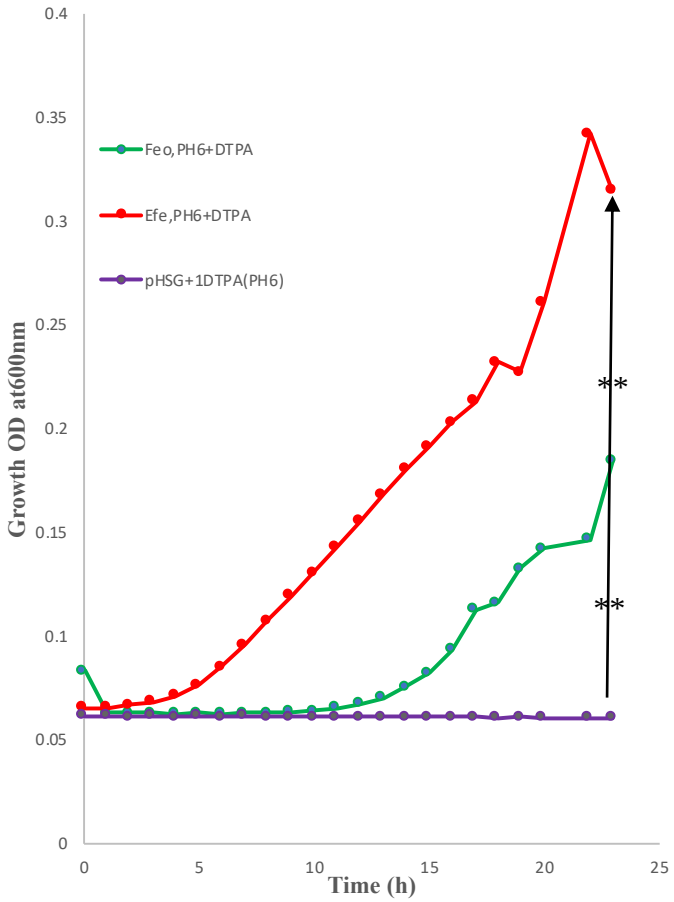

Figure 3.7. Comparison of low-iron growth of *E. coli* JC28 complemented with *feoABC* or *efeUOB*, with inocula propagated with iron. Strains were *E. coli* JC28 transformants containing pHSG576, pHSG-*efeUOB*^{O157} or pHSG-*feoABC*^{O157} precultured in M9 minimal medium with iron and then compared for growth in the same medium without iron. Other details are exactly as in Fig. 3.6. The results shown is representative of three repeats. Values illustrated are avareges of three independent growths. Error bars presented the standard deviations. Statistically significant differences ($P<0.01$) as determined by Graph Prism One way Anova and are indicated at 24 h.

To further explore the ability of EfeUOB and FeoABC to support low-iron growth aerobically, the experiment was repeated with DTPA in the post-culture medium to exacerbate the low iron conditions (Fig. 3.8). The vector control failed to grow under these conditions, whereas both *feo* and *efe* provided clear growth advantages achieving final ODs of ~0.2 and 0.35, respectively. This result further indicates that FeoABC supports low iron growth of JC28 under aerobic conditions, but not as strongly as EfeUOB. This finding somewhat contradicts previous work suggesting that FeoABC is subject to rapid degradation aerobically and is dependent on anaerobic induction for expression (Kim *et al*., 2012, Weaver *et al*., 2013).

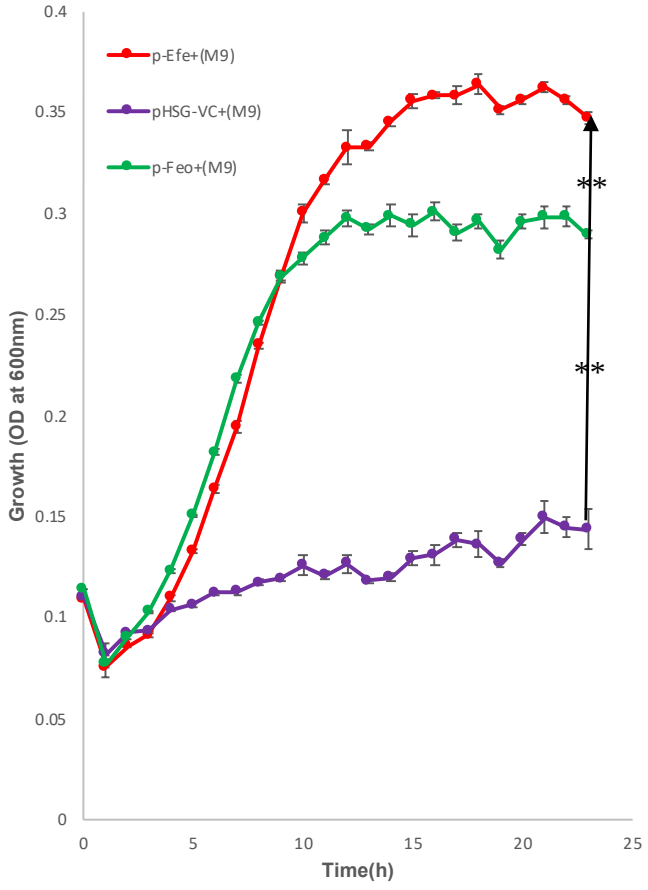

Figure 3.8. Comparison of growth of *E. coli* JC28 complemented with *feoABC* or *efeUOB*, with both inocula iron sufficient and cultures propagated under low iron conditions with 1 µM DTPA. Strains were *E. coli* JC28 transformants containing pHSG576, pHSG-*efeUOB*^{O157} or pHSG-*feoABC*^{O157} precultured in M9 minimal medium with iron and then compared for growth in the same medium with 1 µM DTPA. Statistically significant differences (P<0.01) as determined by Graph Prism One way Anova and significant differences are indicated at 24 h. Other details are exactly as in Fig. 3.6.

Having shown that the low-iron growth of the JC28 strain is enhanced by *efeUOB* and *feoABC* complementation, the effect of iron supplementation was tested; it was anticipated that there would be little benefit of complementation for JC28 when iron levels are sufficient. Indeed, the results (Fig. 3.9 & 3.10) show that JC28 growth is greatly enhanced by iron supplementation (as indicated above, Fig. 3.5) and that the presence of *efe* or *feo* has little effect on the final growth density obtained. In addition, the results in Fig. 3.9-10 confirm that EfeUOB-enhances growth of JC28 under low-iron conditions (a 2.6-fold greater growth at 24 h over the vector control; Fig. 3.10) and that FeoABC also enhances such growth, but to a lesser degree (by 1.3 fold; Fig. 3.10). Thus, the results confirm those generated previously showing that *efeUOB* more greatly stimulated JC28 low-iron growth than does *feoABC* (Fig. 3.9 & 3.10).

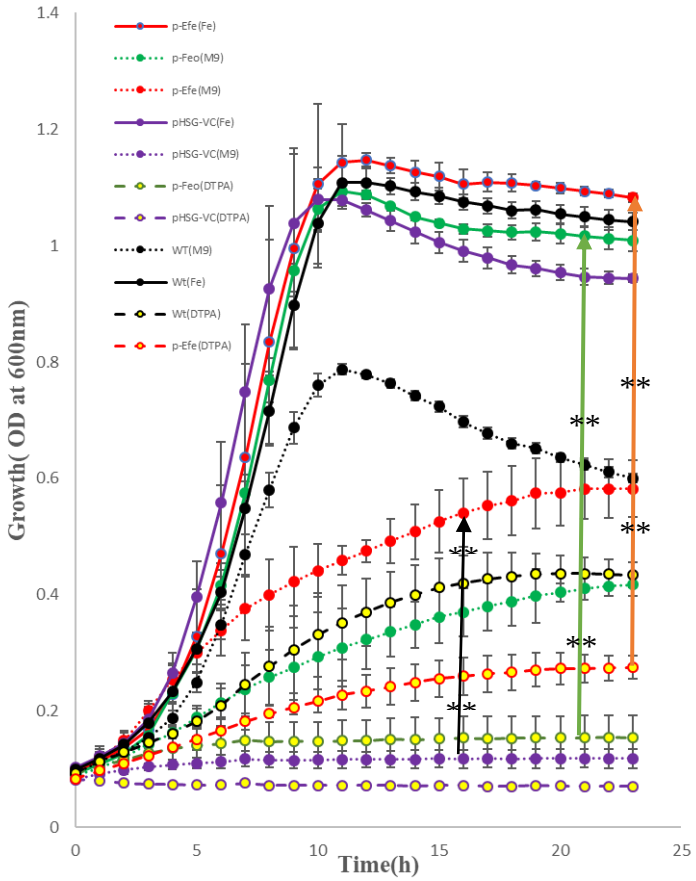

Figure 3.9. Growth of *efeUOB* or *feoABC* complemented iron transport mutant (JC28) and the wildtype under iron supplementation. Precultures were generated without iron supplementation in M9 medium. Strains were JC28 carrying either pHSG576, pHSG-*efeUOB* or pHSG-*feoABC*, or the plasmid-free wildtype (W3110). Growth was with or without 10 μM ferric citrate or 1 μM DTPA. Values illustrated are avareges of three independent growths. Error bars presented the standard deviations. Statistically significant differences as determined by graph Prism One-way Anova and significant differences are indicated at 24 h ($p < 0.05$). Other details are as for Fig 3.6.

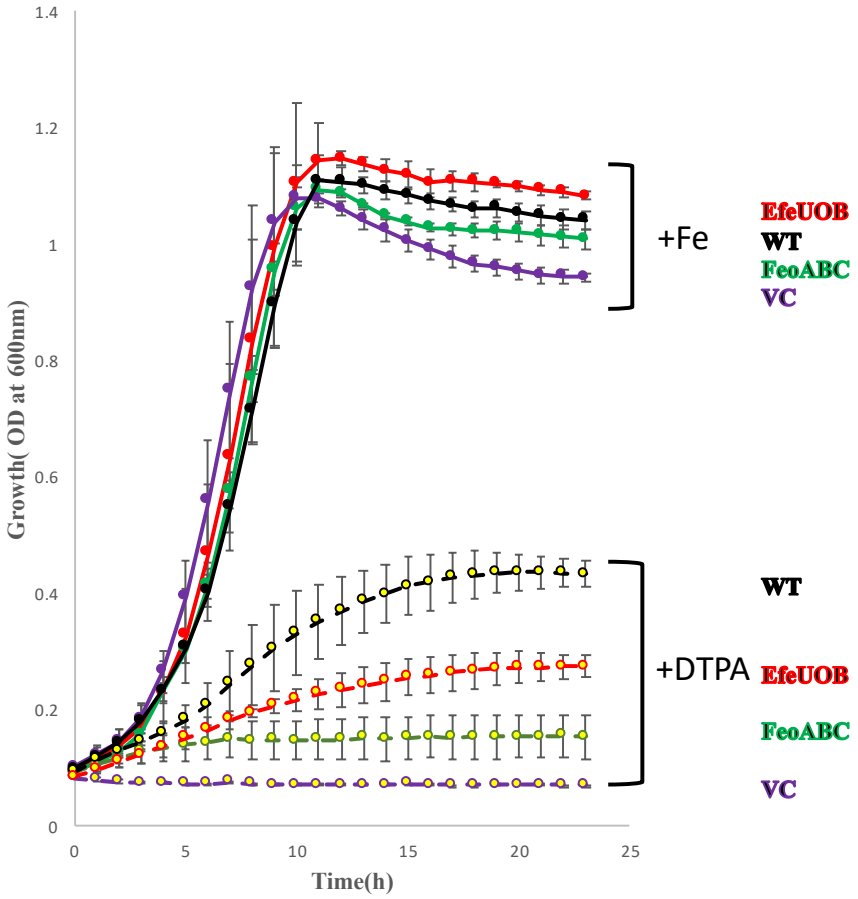

Figure 3.10. Growth of *efeUOB* or *feoABC* complemented iron transport mutant (JC28) under low iron or with iron supplementation. The results shown here are a repeat of those in Fig. 3.10 (except for the exclusion of the M9 growth data).

3.2.2.4. Provision of plasmid-borne *efeUOB* and *feoABC* does not greatly enhance the iron-restricted growth of the wildtype

The results above clearly establish that the Efe and Feo systems enhance the aerobic, low-iron growth of JC28. In order to determine whether the growth enhancement elicited by Efe requires the absence of alternative iron-uptake systems, the effect of *efeUOB* (and *feo*) complementation of the wildtype was examined. *E. coli* K-12 possesses a cryptic frame-shift mutation in the *efeU* gene so it is possible that provision of $efeUOB^{O157}$ will increase its iron-restricted growth through complementation of the chromosomal *efeU* defect.

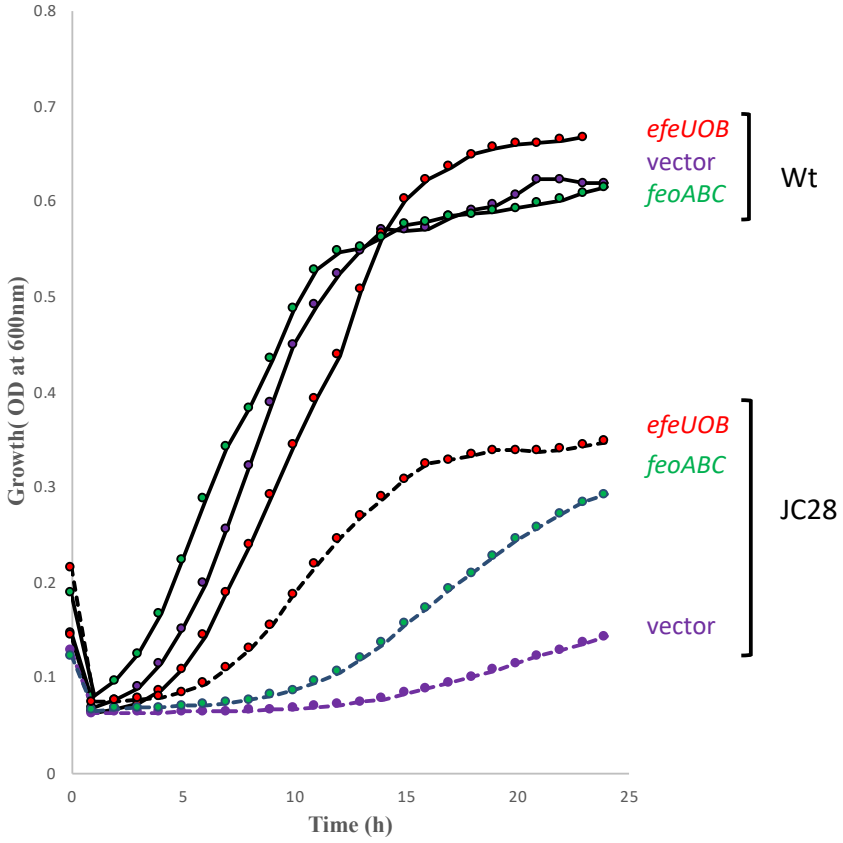

Figure 3.11. Comparison of growth of wildtype and iron-transport mutant (JC28) complemented with *feoABC* or *efeUOB* under low iron conditions. Strains used were W3110 (solid lines) and JC28 (dashed lines) carrying pHSG576, pHSG-*efeUOB*^{O157} or pHSG-*feoABC*^{O157} precultured in M9 minimal medium without iron and then compared for growth in the same medium. All other details are as in Fig. 3.6.

Comparison of the growth of the wildtype and JC28 transformants under low-iron conditions shows that provision of plasmid-borne *feoABC* has little impact on the maximum growth yield of the wildtype, in contrast to effect on the mutant (Fig. 3.11). However, the Feo system did slightly decrease the lag phase of the wildtype (by ~1 h). However, there was a greater lag time (1-2 h) for the *efe*-complemented W3110 transformant, and a higher final OD. Thus, the presence of functional Efe may slightly slow growth under low iron, but could also increase final culture density slightly. These results are in contrast to those seen for the JC28 strain where both Efe and Feo conferred a clear growth advantage under low-iron conditions. Thus,

any growth advantage provided by EfeUOB in the wildtype under low-iron conditions is relatively weak and far less substantial than that seen for JC28 (Fig. 3.11).

3.2.2.5. Comparison of the effect of pre-cultures with or without iron on subsequent growth

The iron-restricted growth studies reported above were largely performed without iron included in the pre-culture. This was expected to impose a greater degree of iron restriction on the subsequent sub-culture through elimination of the potential to store iron, thus ensuring that iron provision during bacterial subculture would entirely depend upon uptake systems, and would not benefit from iron stores. To test the impact of iron stores laid down in preculture, growth comparisons were performed using inocula generated under high- and low-iron conditions (Fig. 3.12).

Precultures produced under high iron, which were then subcultured under high iron, showed better growth than precultures generated under low iron before subculturing under high iron (Fig. 3.12 & B). This effect was only apparent for the JC28 strain, the wildtype gave similar results under high iron subculture with or without iron in the preculture. This suggests that the wildtype is able to acquire sufficient iron from the medium when iron is abundant and so does not gain a notable advantage from iron stores during iron-sufficient growth.

Two of the JC28 transformants show a marked decrease in growth under high iron when iron had not been included in the pre-culture, in comparison to when iron had been included (Fig. 3.12). In particular, the JC28 vector control showed a 4 h increase in lag phase in the absence of iron in preculture, as well as a lower maximum culture density (0.72 cf. 0.93; Fig. 3.12B). The presence of *efeUOB* and particularly *feoABC* was able to reverse this extended lag-phase

effect by 4 and 6 h, respectively (Fig. 3.12B). Thus, even under iron-sufficient conditions, the JC28 vector control exhibits a growth defect that is largely reversed by preculture under high iron, indicating that it relies on iron stores to compensate for its poor iron transport capacity (even under 'iron-sufficient' conditions). However, the provision of Feo (and also to a degree Efe) appears to reduce the dependence of the JC28 strain on the preculture conditions. These results suggest that under high-iron conditions Feo (and Efe, to a lesser degree) provides the JC28 strain with a clear advantage if opportunity to deposit iron stores is not provided in the preculture.

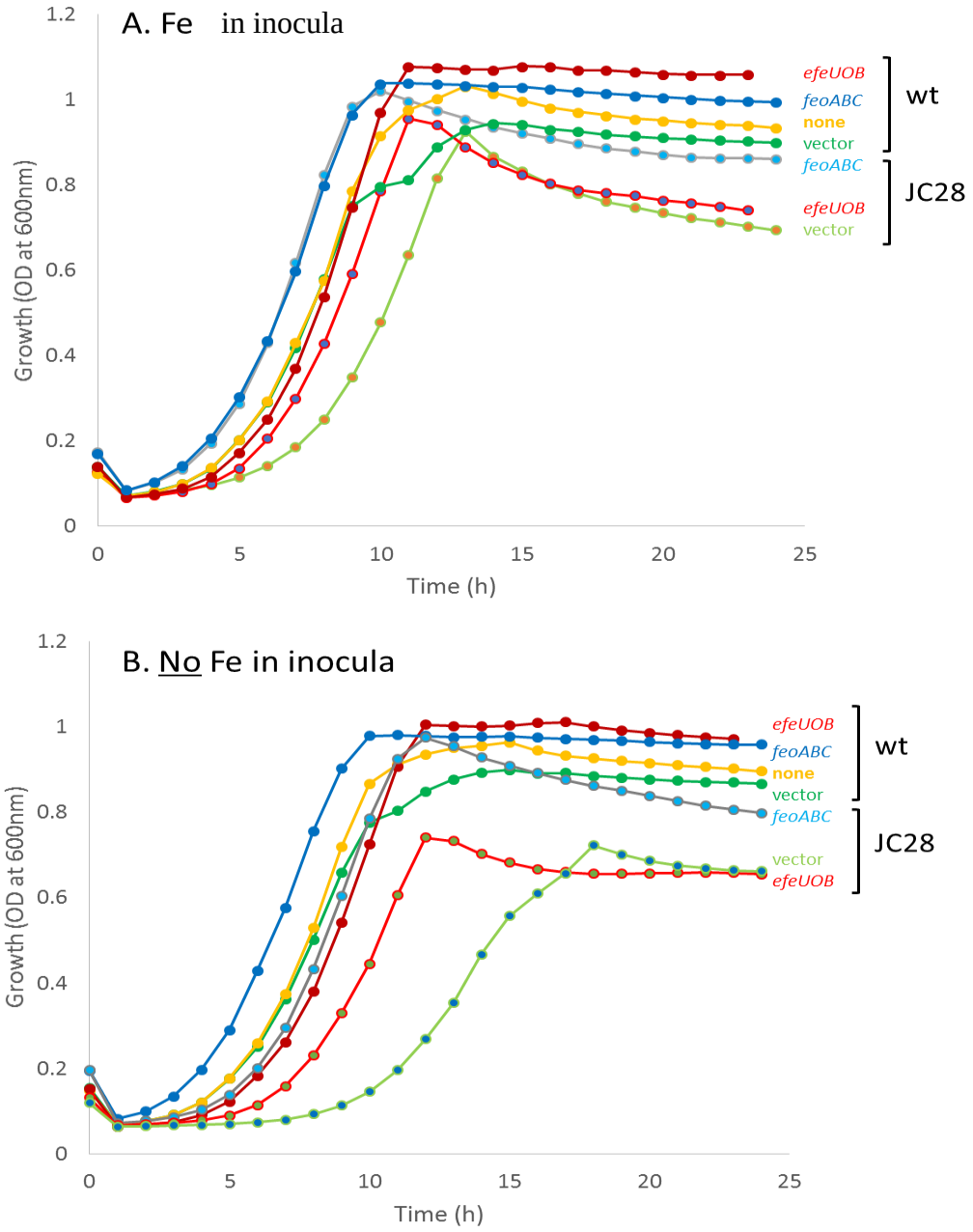

Figure 3.12. Comparison of the effect of *feoABC* and *efeUOB* complementation on iron-sufficient growth of the wildtype (W3110) and JC28 following high- (A) and low-iron (B) preculture. Strains used were W3110 and JC28 carrying pHSG576, pHSG-*efeUOB*^{O157} or pHSG-*feoABC*^{O157} precultured in M9 minimal medium with (A) or without (B) 10 µM ferric citrate and then compared for growth in the same medium (with 10 µM ferric citrate). Plasmid-free W3110 was also included. All other details are as in Fig. 3.6.

The above experiment was repeated, but with subcultures under low rather than high iron. Under these conditions, pre-stored iron is expected to be more valuable since the subsequent

subculture is iron restricted which limits exogenous iron supply. Thus, such low-iron precultures might be expected to enhance the phenotype of the JC28 strain and the complementing effects of *feo* and *efe*.

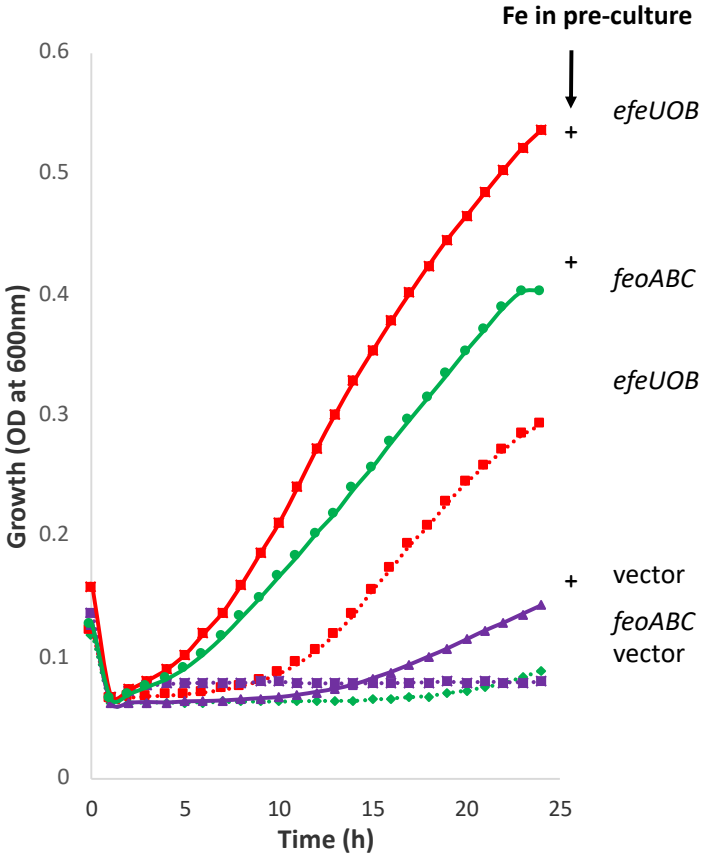

Figure 3.13. Effect of preculture with or without iron on subsequent low-iron growth of the complemented iron-transport mutant (JC28). JC28 carrying either pHSG576, pHSG-*efeUOB* or pHSG-*feoABC* was grown overnight in M9 medium either with or without 10 µM ferric citrate (as indicated). Subsequent growth was measured in M9 medium lacking iron supplementation. Other details are as in Fig. 3.5.

The growth comparisons (Fig. 3.13) show a clear growth enhancement in all cases for precultures with iron in comparison to those without iron (2-14 fold raised final density). For iron-supplemented precultures, the *efeUOB* and *feoABC* complemented JC28 strains showed a 15- and 1.5-fold greater growth yield than the vector control (respectively). However, for the iron-supplemented inocula, the *efeUOB* and *feoABC* complemented strains showed a 6.7- and

4.7-fold greater final growth density. Thus, *efeUOB* provides a greater growth enhancement for non-iron-supplemented precutures, whereas *feoABC* provides somewhat weaker advantage under such conditions. This differential effect could be related to the greater efficiency of Efe as an iron transporter (with respect to Feo) under the aerobic conditions employed enabling Efe to more effectively drive growth under iron sufficiency in the absence of iron stores, as suggested above.

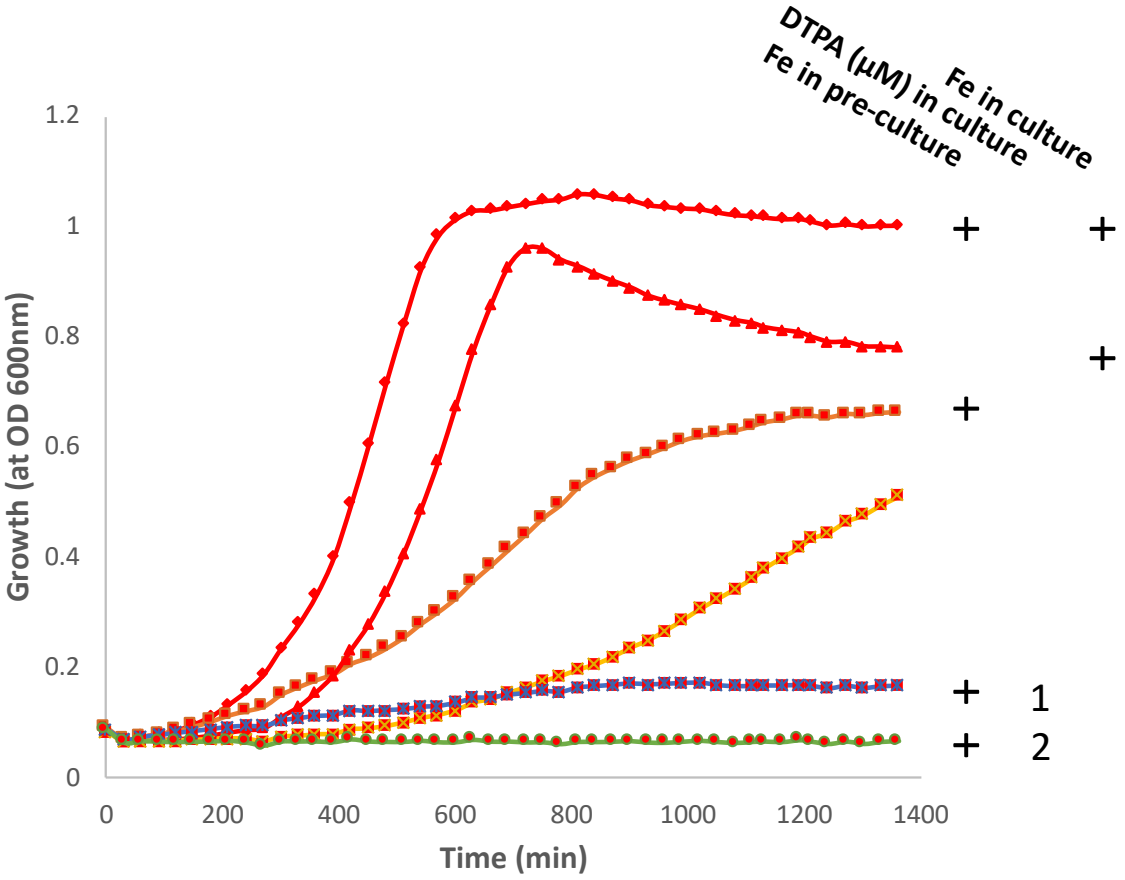

Figure 3.14. The effect of iron supplementation in the inoculum and/or in the culture on growth of *E. coli* JC28 complemented with *efeUOB*^{O157}. The strain employed was JC28 complemented with pHSG-*efeUOB*. Iron (when present) was 10 μM ferric citrate. DTPA was also included in the culture in some cases (as indicated). Other details are as in Fig. 3.5.

The effects of iron-in-the-preculture were further explored for JC28 complemented with *efeUOB* (Fig. 3.14). The results clearly demonstrate that iron in the preculture enhances the

growth of this strain and also show that the presence of iron stores do not overcome the iron-limiting impact of the chelator DTPA, which abolishes iron-limited growth with 2 µM DTPA even though iron was included in the preculture (Fig. 3.14).

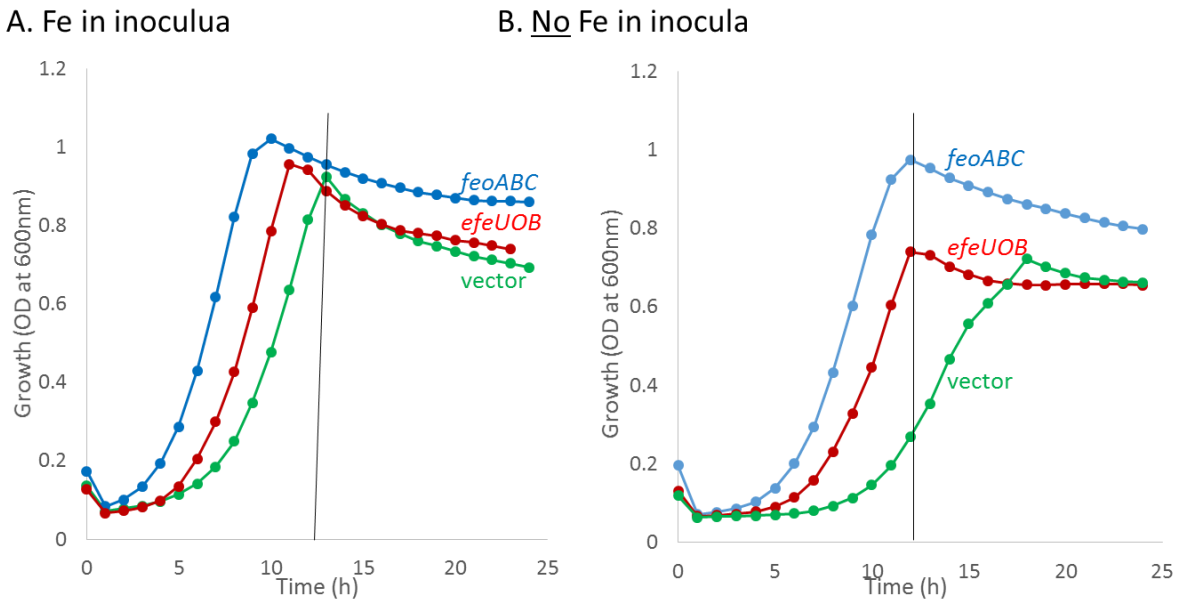

Figure 3.15. Effect of iron in the inocula on subsequent high-iron growth of JC28 complemented with *feoABC* or *efeUOB*. Strains were *E. coli* JC28 transformants containing pHSG576, pHSG-*efeUOB*^{O157} or pHSG-*feoABC*^{O157} precultured in M9 minimal medium with (A) or without (B) 10 µM ferric citrate, and then compared for growth in the same medium with 10 µM ferric citrate. The 12.5 h time point is indicated by a blue vertical line highlights the delayed growth of the 'no Fe inocula' cultures. All other details are as in Fig. 3.6.

The data presented in Fig. 3.12 are re-presented in Fig. 3.15 to emphasize the how presence or absence of iron in the preculture affects the growth of the JC28 transformants under iron sufficiency. The impact of lack of iron in precultures is clearly greater for the vector control that lacks any dedicated iron uptake system even though iron is available at 'sufficient' levels in the medium.

3.4. Effect of low oxygen regime on FeoABC- and EfeUOB-dependent low-iron growth enhancement of JC28

Previous work indicates that the EfeUOB system may function anaerobically since it is not subject to oxygen-dependent expression control (Cao *et al*., 2007). In addition, EfeUOB was able to support low-iron growth anaerobically, albeit modestly (Cao *et al*., 2007). The data presented above indicates that the FeoABC system supports aerobic growth of JC28, despite previous reports indicating that it is an anaerobic/microaerobic system (Cartron *et al*., 2006). Thus, to determine whether FeoABC is more effective than EfeUOB anaerobically, the capacity of the *efeUOB* and *feoABC* plasmids used above to complement low-iron growth of JC28 was tested under low-oxygen regime.

In order to determine whether the presence of either *feoABC* or *efeUOB* enhances growth of JC28 under iron-deficient conditions anaerobically, the JC28-complemented strains were grown, as described above, in M9 minimal medium. Low-oxygen conditions were achieved using either cultures contained within syringes equipped with needles inserted into rubber bungs, or with an anaerobic/microarobic FLUOstar microplate system

3.4.1. Anaerobic growth condition

Initially, the three plasmid-bearing (pHSG-*feoABC*, pHSG-*efeUOB* and pHSG576) JC28 strains were grown aerobically with 10 µM ferric citrate overnight. Starting cultures were then prepared with an initial OD of 0.01 with or without 10 µM ferric citrate or 1 µM DTPA, and growths were performed under fermentative anaerobic conditions in syringes.

A significant growth difference was observed under iron-sufficient and -deficient conditions for the vector control (Fig. 3.16), with virtually no growth observed under iron restriction (Fig. 3.16B) and a diminished growth (cf. the *feo*- and *efe*-bearing strain) under iron sufficiency (Fig

3.16A). This suggests that either FeoABC or EfeUOB can support anaerobic iron-deficeint growth of JC28, and that ferrous-iron uptake systems are required for strong growth of JC28 even under iron-sufficient conditions. Importantly, under anaerobiosis, both FeoABC and EfeUOB clearly supported growth of JC28; this was the case under both low and high iron conditions. However, FeoABC enabled a better growth than EfeUOB, particularly under iron deficiency (Fig. 3.16B) where the *feoABC* complemented strain showed a 2.5-fold greater final OD than the *efeUOB* complemented strain. Thus, in contrast to the observation under aerobic conditions, *feoABC* was more effective than *efeUOB* in promoting low-iron growth. This finding supports the primary role of FeoABC as an anaerobic ferrous-iron transporter and thus is consistent with previous findings (Weaver *et al*., 2013). The DTPA had little impact on growth anaerobically, possibly because it is a ferric-iron chelator and iron would be expected to be found largely in its reduced form anaerobically.

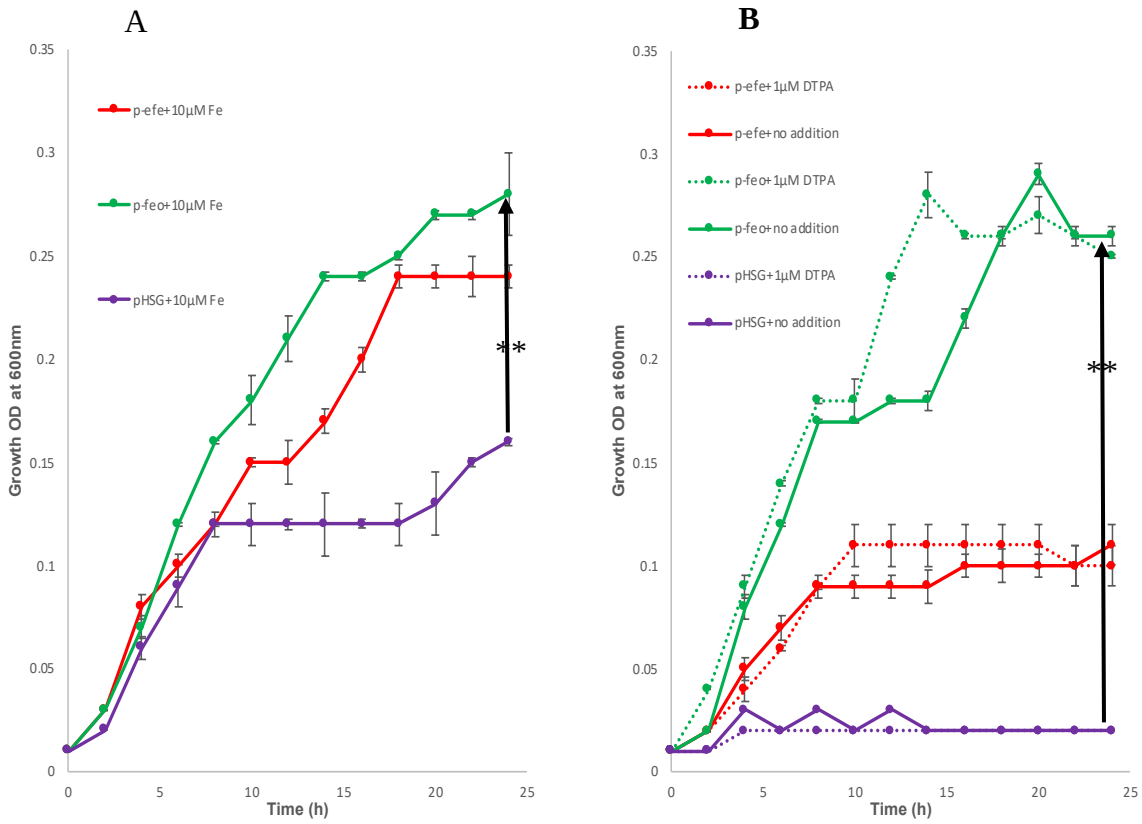

Figure 3.16: Anaerobic, fermentative growth of JC28 complemented with *efeUOB* or *feoABC* in glucose-containing M9 medium under high and low iron availability using anaerobic syringes. Strains were grown anaerobically in 50 ml syringes in M9 medium (with glucose). Precultres were in the same medium with 10 µM ferric citrate. **A**. M9 containing 10 µM ferric citrate. **B**. no addition or 1µM DTPA (dashed lines). The strains employed were: JC28(pHSG576), JC28(pHSG-*feoABC*) and JC28(pHSG-*efeUOB*). Dotted lines, 1 µM DTPA; solid line, no additions. Values presented are averages of three independent growths, each assayed in duplicate. Statistically significant differences (P<0.01) were determined by Graph Prism One-way Anova and significant differences are indicated (P<0.01). Error bars show standard deviations.

Cao *et al*. (2007) previously showed that *efeUOB* could support the low-iron anaerobic growth of JC28. However, here a comparison with *feoABC* complementation clearly demonstrates a preference for FeoABC as a route for iron uptake anaerobically, and EfeUOB as a route aerobically. The above experiment was repeated using the microtitre plate system under low oxygen regime (M9 with 0.4% glucose with and without DTPA with MES or TAPS buffer) at pH 6 and 8, and similar results were obtained (Fig. 3.17-3.18) under anaerobic low-iron

conditions as those obtained using syringes (Fig. 3.16), with both *feoABC* and *efeUOB* promoting low-iron growth of JC28, but the effect for *feoABC* was ~2.5-fold greater (Fig. 3.17).

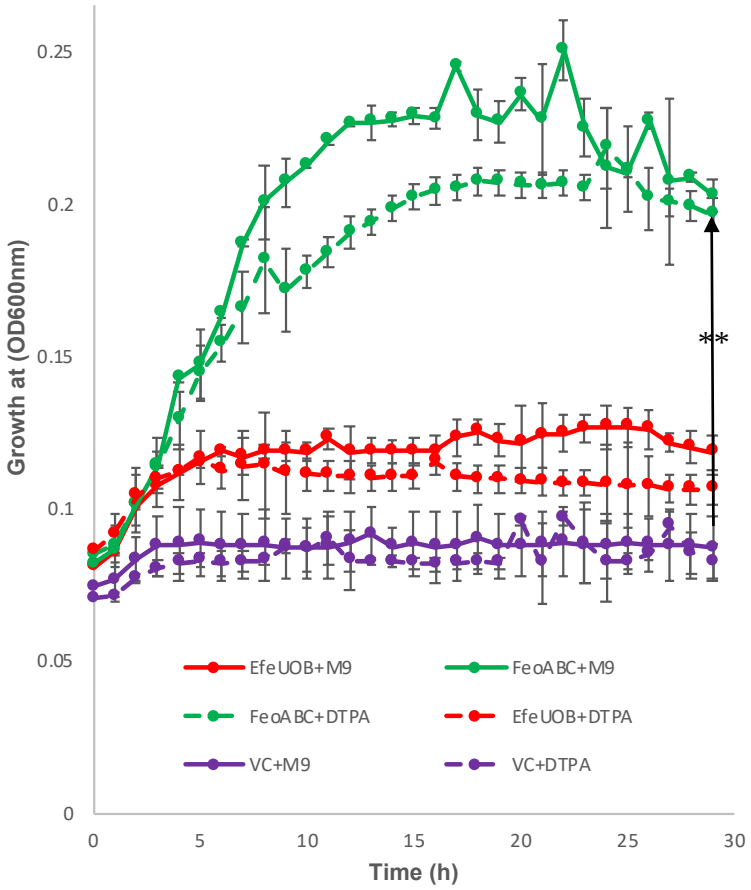

Figure 3.17: Low-oxygen, fermentative growth of JC28 complemented with *efeUOB* or *feoABC* in glucose-containing M9 medium under low iron availability, using a FLUOstar microplate system at pH 6. Strains were grown in microtitreplates in M9 medium (with glucose). Precultres were in the same medium with 10 μM ferric citrate. Growths were with (dashed lines) or without (solid lines) 1 μM DTPA. The strains employed were: JC28(pHSG576), JC28(pHSG-*feoABC*) and JC28(pHSG-*efeUOB*). Other details are as in Fig. 3.16. Values presented are averages of three independent growths, each assayed in duplicate. Statistically significant differences ($P < 0.01$) as determined by Graph Prism Two way Anova and significant differences are indicated at 24 h. Error bars show standard deviations.

The effects seen at pH 6 and 8 were similar (Figs. 3.21 & 3.22), although growth for the *feo*-complemented strain was better by ~twofold at pH 8.

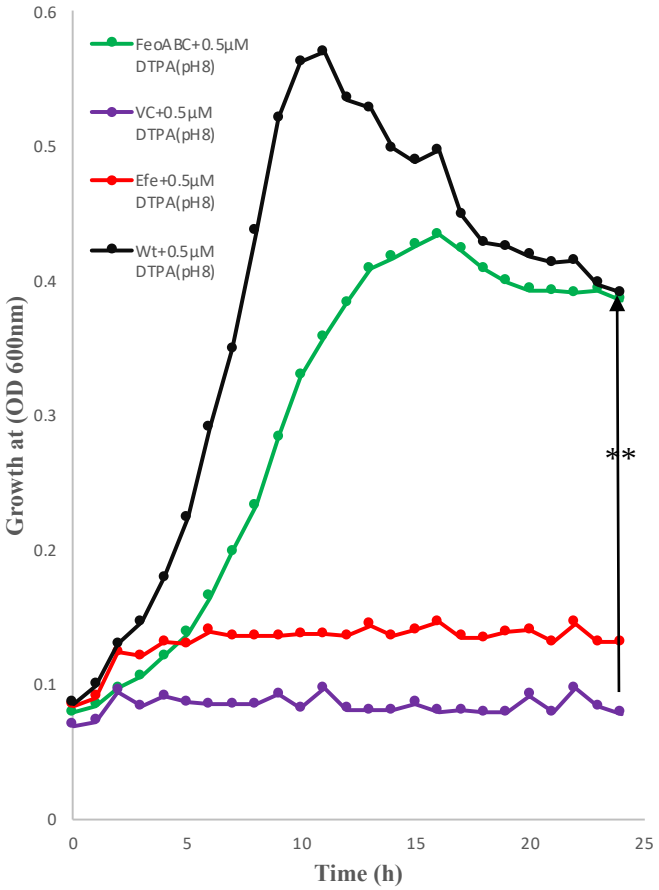

Figure 3.18: Effect of microaerobiosis on EfeUOB and FeoABC complemented inJC28 and wild type at pH 8. The strain employed was JC28 and WT (Strains were grown anaerobically in M9. DTPA was also included in the culture in some cases (as indicated). Other details are as in Fig. 3.21. Values presented are averages of two independent growths, each assayed in duplicate. Error bars show standard deviations. Statistically significant differences (P< 0.01) were determined by Graph Prism Two way Anova and significant differences are indicated at 24 h.

3.5. Conclusion

In conclusion, this preliminary work has confirmed the iron-restricted growth defect of the JC28 strain and its usefulness as a tool to investigate the roles of FeoABC and EfeUOB in iron uptake. The ability of the *efeUOB* low-copy number plasmid to enhance aerobic iron-restricted growth of JC28 is also confirmed (Cao *et al*. 2007). The low-copy-number *feoABC* plasmid also enhanced the aerobic growth of JC28, particularly when iron was included in the preculture. The effect of Feo was less than that of Efe and was variable in the absence of iron in the preculture. It is likely that the aerobic conditions of growth employed are more suited to Efe activity than to Feo activity (*feo* is known to be anaerobically induced and aerobically degraded whereas Efe activity and expression appears little affected by oxygen; Liu *et al*. 2011; Cao *et al*. 2007). Iron in the preculture was shown to enhance the growth of the JC28 strain even under subsequent iron sufficiency, an effect that was most notable for the vector control and can be interpreted as being caused by a greater reliance on iron stores for this strain due to its lack of high-affinity iron uptake capacity.

Under anaerobic conditions, the impact of the Feo and Efe systems was reversed. Feo promoted low-iron growth more strongly than Efe, although Efe supported iron-resticted growth somewhat. This observation matches the evidence in the literature indicating that the Feo system functions anaerobically, partly due to expression control by FNR (Lau *et al*., 2016). The *feo* and *efe* plasmids had little impact on growth of the wildtype under the conditions employed here, which is consistent with the iron-uptake proficient genetic status of this strain.

The above preliminary work has thus established the growth conditons and strains that are required for future work on the role of factors such as effect on the activities of the Efe and Feo systems, which will form the basis of the next set of experiments (Chapter 4).

The earlier report on EfeUOB function in *E. coli* (Cao *et al*., 2007) showed a phenotype under low iron both aerobically and anaerobically, as well as at both low and high pH. However, this phenotype was obtained in an *E. coli* K-12 strain lacking all other known iron transporters (JC28) and the effect was enhanced at low pH. In a wildtype background, a phenotype could only be observed for *efeUOB* under low iron, low pH, with reductant and Mn^{2+} (Cao *et al*., 2007), indicating that other iron transporters (such as Feo) obscure any iron-uptake activity of EfeUOB under other conditions (e.g. high pH, absence of Mn^{2+}). This therefore justifies the use of JC28 as the host strain selected for the EfeUOB and FeoABC comparison studies.

In summary, the phenotypes observed here for the *feoABC* and *efeUOB* complementations support previous work suggesting that FeoABC and EfeUOB operate under distinct environmental conditions, with FeoABC operational mainly in the absence of oxygen with EfeUOB functioning primarily aerobically. However, it remains unclear whether this difference in activity in response to oxygen is dependent on expression control, or to fundamental biochemical differences in the respective mechanisms of operation of the two ferrous-iron transport systems. This is further investigated in the following chapter.

Chapter 4. The effect of pH, under oxic and anoxic conditions, on the ability of *efeUOB* and *feoABC* to support low-iron growth when expressed from inducible promoters

4.1 Introduction

Previous work (above) with *efeUOB* and *feoABC* operons of *E. coli* O157 utilised the operons under control of their natural promoters. These promoters are subject to iron control (Fur mediated) as well pH (for *efe*, CpxAR) and oxygen (for *feo*, Fnr) regulation. Replacing the natural expression control of these systems with an easily controllable regulation system will allow the biochemical properties of the corresponding iron transporters to be divorced from any transcriptional regulatory control. To achieve this, the *efeUOB* and *feoABC* operons were introduced into the pBADrha and the pBADara vectors, under control of a rhamnose or arabinose inducible promoter, respectively. The resulting constructs were used to complement JC32 (*E. coli* strain carrying six mutations eliminating the main routes of iron uptake in minimal medium, similar to JC28) in the presence of inducer and under a range of environmental conditions (e.g. aerobic and anaerobic). This work will reveal to what degree Feo is able to operate aerobically and whether Efe can be fully functional anaerobically if appropriately expressed.

Growth experiments were performed in triplicate and were repeated twice unless stated otherwise.

4.2. Preparation of inducible *efeUOB* and *feoABC* constructs

4.2.1. Amplification of the *efeUOB*^{O157}genes

EfeUOBrha^{F} and EfeUOBrha^{R} primers (Table 2.4) were used to amplify a 3238 bp *efeUOB* fragment of the *E. coli* O157 EDL933 chromosome with High Fidelity Phusion® DNA polymerase (Hot start; Thermo Fisher Scientific). The amplified fragment was of the expected size, and was purified and then re-analysed by agarose gel electrophoresis to confirm recovery of the amplified fragment (Fig 4.1). A fragment of the expect size (~3238 bp) was thus generated for cloning into pBADrha.

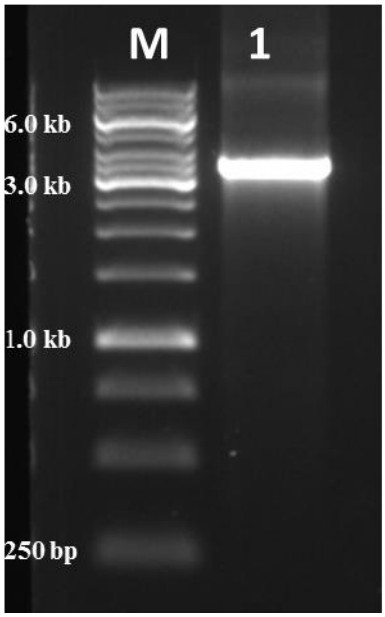

Figure 4.1: Gel electrophoretic analysis of the *efeUOB*^{O157} PCR product for insertion into pBADrha. Electrophoresis was performed using a 0.6% agarose TBE gel. Purified PCR product (2 µl) was loaded with 6 µl qH_2O and 2 µl loading dye in lane 1. 1 µl GeneRuler® 1 kb ladder (Fermentas) diluted in 9 µl qH_2O and 2 µl loading dye was loaded as marker in lane M.

A similar approach was used for amplification of a PCR product for cloning into pBADara, except that the primers employed were EfeUOBara^{F} and EfeUOBara^{R} (Table 2.4; Fig. 4.2).

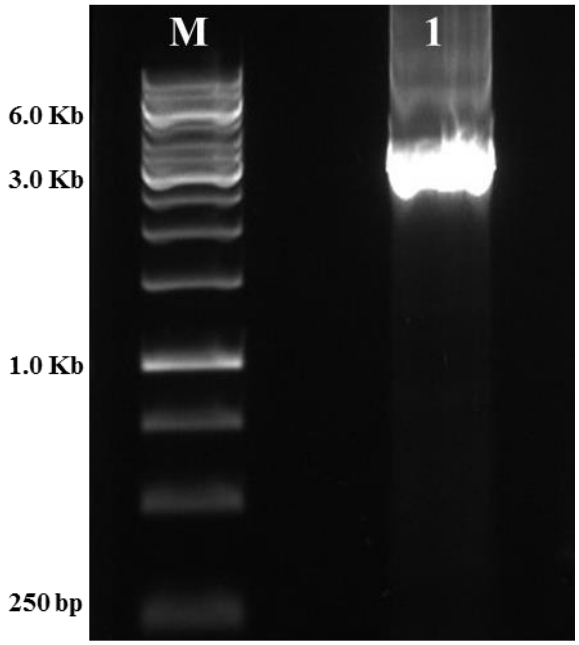

Figure 4.2: Gel electrophoretic analysis of the purified *efeUOB*^{O157} PCR product for cloning into pBADara. See Fig 4.1 for details.

4.2.2. Cloning of *efeUOB*^{O157} into pBADara

The plasmid pBADara (4102 bp) carries the rapidly and efficiently repressed (particularly in *ara*$^{+}$ strains) P*araBAD* promoter. It is likely that *ara*$^{+}$ strains lower the concentration of inducer as they grow since they can metabolize arabinose and use it as a carbon source, which leads to a higher degree of repression. The Amp^{R} pBADara vector can be used to provide cloned genes at a copy number that resembles that of the natural condition (Gunzman *et al*., 1995).

Cloning was achieved using the In-Fusion kit (Clontech) with pBADara digested with the restriction endonucleases *Nco*I and *Hin*dIII (37 ºC for 5 min, followed by incubation at 65 ºC for 15 min to inactivate the enzymes) and then purified by PCR clean-up (Sections 2.13.4). Following confirmation of the recovery of the digested plasmid by electrophoresis, the digested vector DNA was incubated together with the PCR product using the In-Fusion cloning kit, according to the manufacturer's instructions (Section 2.19.3). After transformation into

competent *E. coli* TOP10, Amp^R transformants were selected on agar plates. In this way, 62 Amp^R colonies were obtained and 5 were selected for plasmid isolation. The resulting plasmid DNA was analysis by electrophoresis; four gave single plasmid bands which migrated at ~4.6 kb, as was expected (Fig. 4.3).

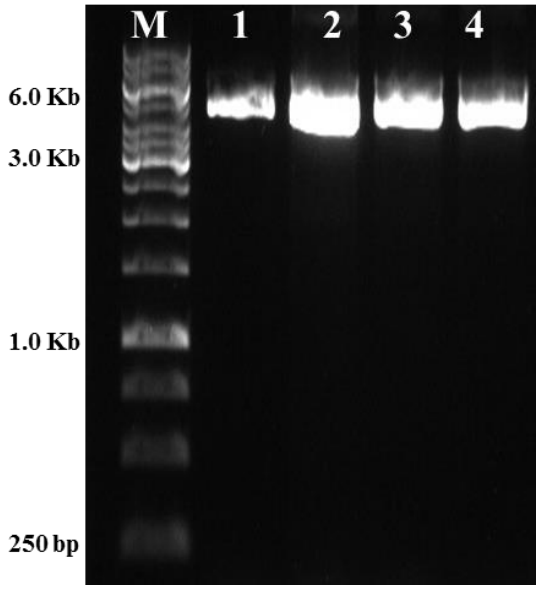

Figure 4.3: Analysis of pBADara-*efeUOB*^{O157} isolates by agarose gel electrophoresis. The gel contained 0.5x TBE and was 0.6% agarose. The 1 kb Ladder (Fermentas) was used as a marker. 4 µl of each 50 µl plasmid preparation (four isolates) were loaded with loading dye (see Methods 2.13) in undigested form. The gel was strained with Gel Red, according to the manufacturer, and visualized by UV-transillumination. Lane M contains marker.

4.2.3. Cloning of *efeUOB*^{O157} into pBADrha

The In-Fusion Cloning Kit (Clontech) was also used for cloning of the *efeUOB*^{O157} PCR product (~3238 bp, generated with EfeUOBrha^F and EfeUOBrha^R primers; Table 2.4; data not shown) into pBADrha, as described above. 117 Cam^R *E. coli* TOP10 transformants were obtained, 3 of which were selected for plasmid 'miniprep' isolation (Section 2.21). These plasmids were analysed by electrophoresis and the expected mobility was observed (at ~6.2 kb).

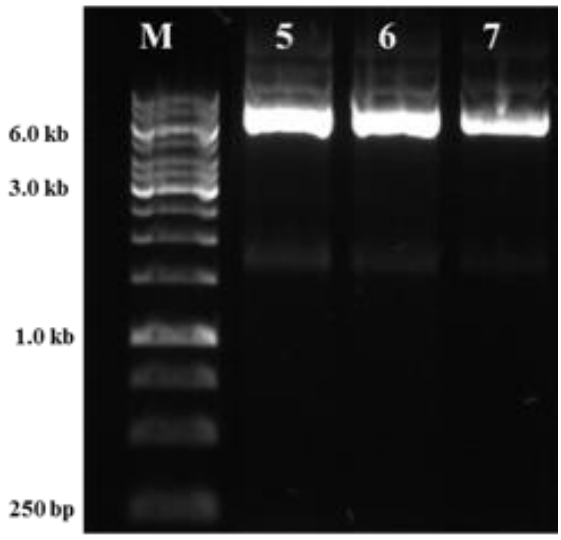

Figure 4.4: Analysis of pBADrha-*efeUOB*^{O157} isolates by agarose gel electrophoresis. Details are as for Fig. 4.3.

4.2.4. Confirmation of identity of pBADrha-*efeUOB*^{O157} and pBADara-*efeUOB*^{O157} by restriction digestion

One pBADrha-*efeUOB* candidate plasmid (#1) was digested with *Sal*I and *Nde*I restriction enzymes to release the insert, if present. Electrophoresis revealed two bands matching the sizes expected for the insert (3238 bp) and vector (6.1 kb), together with a higher band likely to be the linearised plasmid (~9.3 kb) (Fig. 4.5). Similar results were obtained for #2 (not shown). Thus, the cloning was apparently successful.

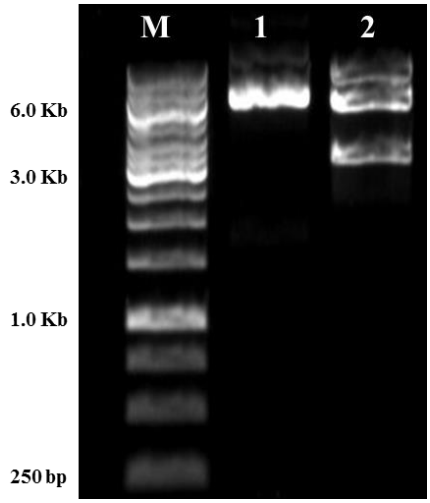

Figure 4.5. Confirmation of pBADrha-*efeUOB*^{O157} plasmid #1 by restriction digestion. Agarose gel electrophoresis was as in Fig 4.3. Digestion with *Sal*I and *Nde*I was as described in Methods Section 2.14.

One pBADara-*efeUOB* candidate plasmid (#1) was digested with *Bam*HI and *Hin*dIII restriction enzymes to release the insert, if present. Electrophoresis revealed three bands (1.1, 2.3 and 3.9 kb) for the double digest (along with a partially-cut band at ~5 kb) and two bands (2.3 and 5.0 kb) for the single digest with *Bam*HI, as expected (Fig. 4.6), thus confirming that the PCR fragment had been successfully cloned.

The pBADara-*efeUOB*^{O157} and pBADrha-*efeUOB*^{O157} plasmids generated above (see Appendix for plasmid maps) where further confirmed by nucleotide sequencing using a set of primers designed to enable complete sequence determination of the inserts on both strands. The primers employed whereas shown in Table 2.5. The assembled sequence data showed complete coverage of the cloned inserts with no errors with respect to the template sequence (see Appendix).

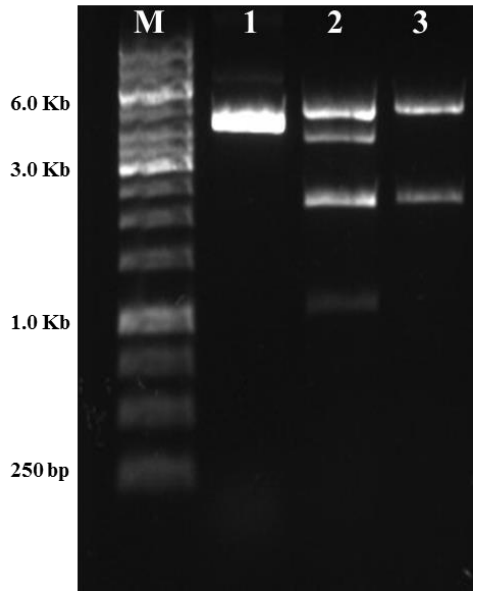

Figure 4.6. Confirmation of the pBADara-*efeUOB*^{O157} plasmid by restriction digestion. Agarose gel electrophoresis was as in Fig 4.4. Lane 2, plasmid DNA digested by *Bam*HI and *Hin*dIII; lane 3, plasmid DNA digested by *Bam*HI only, lane M, marker.

4.2.5. Amplification of the *feoABC*^{O157} operon for cloning into pBADrha using In-Fusion technology

The *feoABC* operon of *E. coli* O157 was amplified as above using *feoABC*rha^{F} and *feoABC*rha^{R} primers (Table 2.4) to give a 2896 bp fragment. Electrophoretic analysis of the resulting PCR product indicated that the expected fragment had been generated (Fig. 4.7).

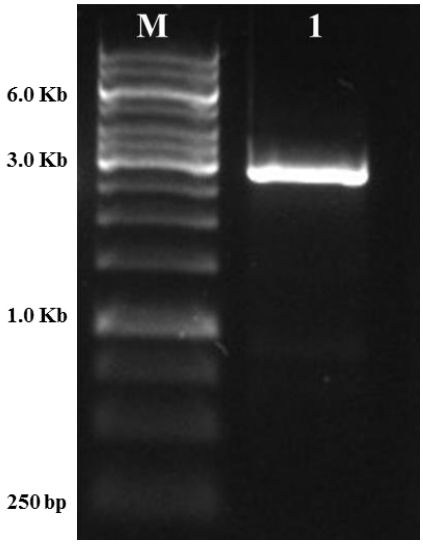

Figure 4.7: Gel electrophoretic analysis of *feoABC* PCR product for cloning into pBADrha. Electrophoresis was performed using a 0.6% agarose TBE gel. Lane 1, 2 µl of the PCR reaction; Lane M, the GeneRuler 1 kb ladder.

4.2.6. Cloning of *feoABC*^{O157} into pBADrha

The purified *feoABC* fragment thus obtained was combined with pBADrha using an In-Fusion reaction (as above), which was then used for transformation giving 67 Cam^R transformants. Plasmid 'miniprep' isolation was performed on ten, and five were found to have a low mobility matching that anticipated for the required construct (mobility equivalent to ~6.2 kb) (see Fig. 4.8 for plasmid isolate #5).

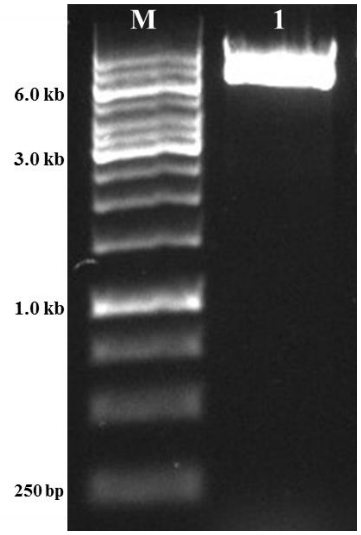

Figure 4.8: Analysis of a pBADrha-*feoABC*^{O157} isolate by agarose gel electrophoresis. See Fig. 4.4 for details (1 indicates uncut DNA for isolate #5).

4.2.7. Digestion of pBADrha-*feoABC*^{O157}

Three candidate plasmids were double digested with *Nde*I and *Sal*I to test for the presence of the insert. Locations of the *Nde*I and *Sal*I sites in the pBADrha-*feoABC*^{O157} clone are illustrated in the Appendix. Electrophoresis revealed that all three plasmids (#2, 5 and 10) gave two bands matching those of the insert (~2.8 kb) and vector (6.1 kb) (Fig. 4.9). One of these plasmids (#2) was selected for further study; this was designated pBADrha-*feoABC*^{O157} and confirmed by sequencing (as described above) (see Appendix for sequence data summary).

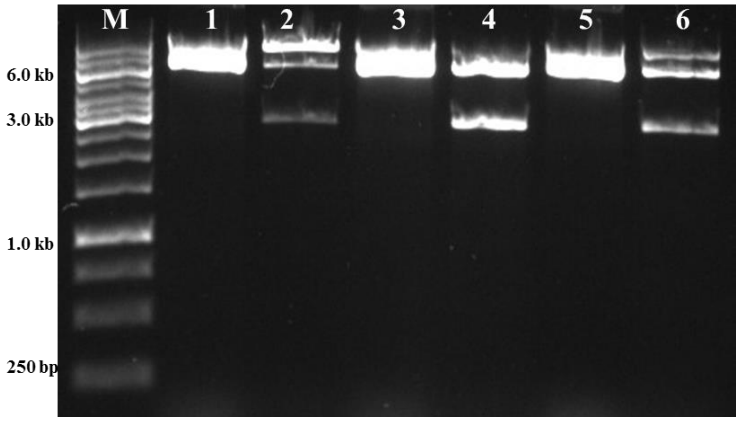

Figure 4.9. Confirmation of pBADrha-*feoABC*^{O157} plasmids by restriction digestion. Agarose gel electrophoresis was as in Fig 4.4. Digestion with *Sal*I and *Nde*I was as described in Methods section 2.22. Two bands of 2.9 kb (insert) and 6100bp (vector) were expected.

4.2.8. Amplification of the *feoABC*^{O157} genes for cloning into pBADara

The *feoABC* operon was also cloned into pBADara. This would allow co-expression of *feo* and *efe* using the compatible pBADara and pBADrha vectors. FeoABC-ara^{F} and FeoABC-ara^{R} primers (Table 2.4) were used to amplify a 2896 bp fragment from the chromosomal DNA of *E. coli* O157, as described above. This was subsequently purified (Fig. 4.10) for cloning into pBADara.

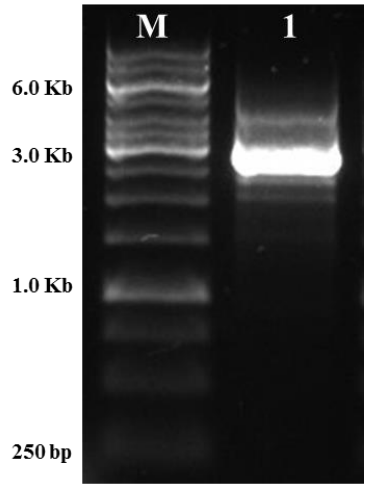

Figure 4.10: Gel electrophoretic analysis of the *feoABC* purified PCR reaction product. See Fig. 4.4 for details. '1' indicates the purified PCR product.

4.2.9. Cloning of *feoABC* into pBADara vector

The *feoABC* PCR product was cloned into pBADara as described above. In-Fusion cloning products were used to transform *E. coli* Stellar competent cells resulting in 38 Amp^{R} transformants. Four were selected for plasmid extraction. These were analysed by electrophoresis and all four displayed mobility matching that anticipated for the required construct (Fig. 4.11) and so were further analysed by restriction digestion.

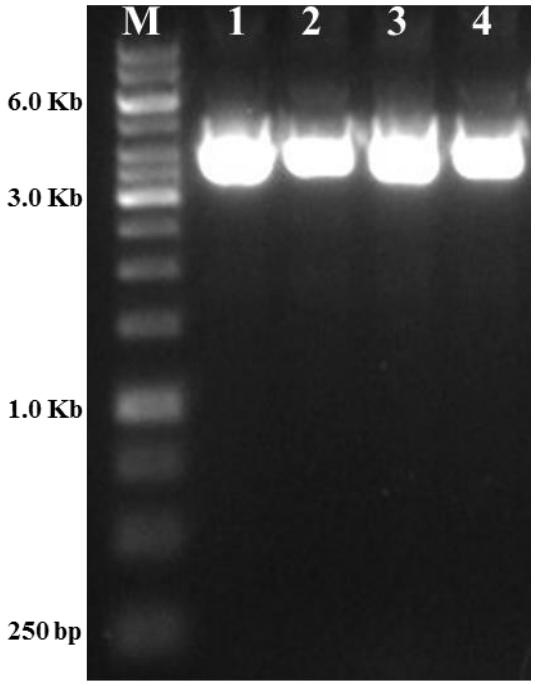

Figure 4.11: Analysis of pBADara-*feoABC*^{O157} candidate plasmids by agarose gel electrophoresis. See Fig. 4.4 for details. Plasmid isolates #1-4 are indicated in lanes 1-4.

4.2.10. Confirmation of pBADara-*feoABC* by restriction digestion

One candidate plasmid (#1) was digested with *Hin*dIII restriction enzyme to confirm the cloning. Electrophoresis revealed a major band that matched the expected size (~7.0 kb) of the insert and vector (Fig. 4.12). This plasmid was designated pBADara-*feoABC* and was confirmed by sequencing, as above (no errors were detected; see Appendix for summary).

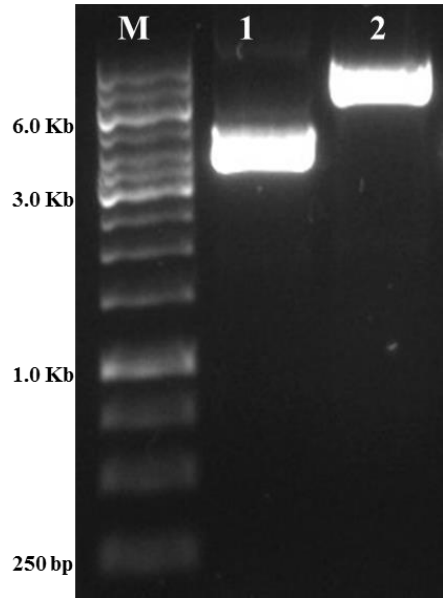

Figure 4.12: Gel electrophoretic analysis of pBADara-*feoABC* by restriction digestion. Digestion was with *Hin*dIII. Electrophoresis was as in Fig. 4.4. Lane 1, undigested isolate #1; lane 2, digested isolate #1.

4.2.11. Amplification of *efeU*OB*$^{K-12}$ operon

The above cloning experiments have generated four new plasmids: two pBADara plasmids, one carrying *feoABC* and the other *efeUOB*; and two pBADrha plasmids, one carrying *feoABC* and the other *efeUOB* (see Appendix for plasmid maps). Thus, it is now possible to examine the iron transport activities of FeoABC and EfeUOB under specific growth conditions without interference from environmental control of expression (other than that imposed by arabinose and rhamnose).

To provide an additional comparator to confirm data obtained with the *efeUOB*^{O157} clones, it was considered desirable to also clone the *efeUOB* operon of *E. coli* K-12, in the same vectors. Since the *E. coli* K-12 *efeUOB* operon is cryptic (due to a frame-shift in *efeU*), the 'corrected' *efeU*OB* version was employed for cloning purposes (see Cao *et al*., 2007).

The *efeU*OB*$^{K-12}$ operon was amplified from pHSG-*efeU*OB*$^{K-12}$ using two pairs of *efeU*OB*$^{K-12F}$ and *efeU*OB*$^{K-12R}$ primers (Table 2.4) to give a ~3.5 kb fragment (as described above). Electrophoretic analysis of the resulting PCR product is shown in Fig 4.13.

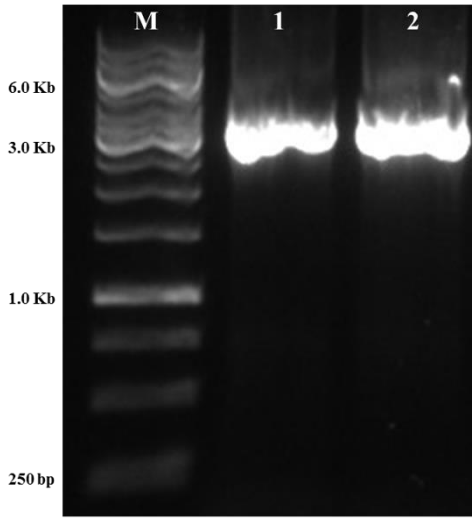

Figure 4.13: Gel electrophoretic analysis of the *efeU*OB*$^{K-12}$ PCR reaction products. Lane 1, the PCR product destined for cloning into pBADrha; lane 2, the PCR product destined for cloning into pBADara. Other details are as in Fig. 4.4.

4.2.12. Cloning of the e*feU*OB*$^{K-12}$ products into pBADrha and pBADara

In-Fusion cloning was used for cloning of the e*feU*OB*$^{K-12}$ PCR products, as before. Reaction products were transformed into *E. coli* TOP10 cells resulting in 92 Cam^R and 36 Amp^R transformants for the pBADrha and pBADara clonings, respectively. Four from each were selected for plasmid extraction. These were analysed by electrophoresis and one of each was selected that had mobility matching that anticipated for the required construct (Fig. 4.14) and was further analysed by restriction digestion (see below).

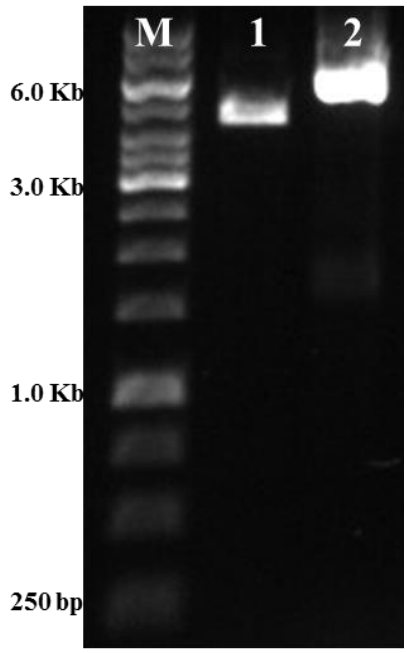

Figure 4.14: Analysis of pBADrha-e*feU*OB*$^{K-12}$ and pBADara-e*feU*OB*$^{K-12}$ candidate plasmids by agarose gel electrophoresis. Lane 1, pBADara-e*feU*OB*$^{K-12}$ #1; and lane 2, pBADrha-e*feU*OB*$^{K-12}$ #1. Lane M, marker. Other details are as for Fig. 4.4.

4.2.13. Confirmation of pBADara-e*feU*OB*$^{K-12}$ by restriction digestion

Plasmid isolate #1 was digested with *Bam*HI and *Hin*dIII to confirm the cloning. Electrophoresis revealed three major bands that matched the expected sizes (~1.0, 2.2 and 4.0 kb; Appendix; Fig. 4.15). This plasmid was designated pBADara-e*feU*OB*$^{K-12}$ and its identity was confirmed by sequencing (only the forward and reverse vector primers were used; data not shown).

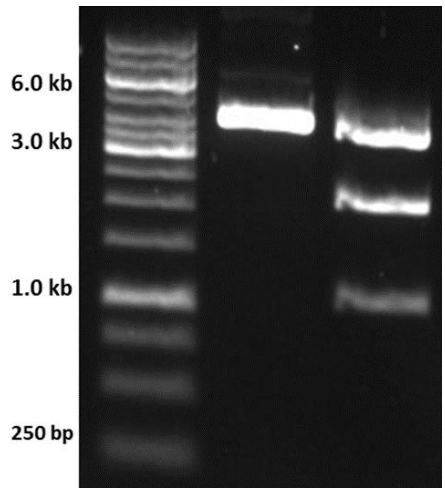

Figure 4.15: Gel electrophoretic analysis of *Hin*dIII and *Bam*HI digested pBADara-*efeU*OB*$^{K-12}$. Lane 1, 2 µl undigested plasmid #1; lane 2, 4 µl DNA digested with *Hin*dIII and *Bam*HI; lane M, GeneRuler 1 kb ladder. With full digestion, three bands of ~1, 2 and 4 kb were expected, as observed.

4.2.14. Confirmation of pBADrha-e*feU*OB*$^{K-12}$ by restriction digestion

One candidate plasmid (#1) was digested with *Nde*I and *Sal*I restriction enzymes to release the insert (Appendix). Electrophoresis revealed two major bands that matched the expected size (~3.2 kb for the insert; ~6.1 kb for the vector; see lanes 2-5 in Fig. 4.16). Three of these plasmids (#1-3) were confirmed by sequencing (vector specific F and R primers only, thus far) and were designated pBADrha-e*feU*OB*$^{K-12}$ #1-3.

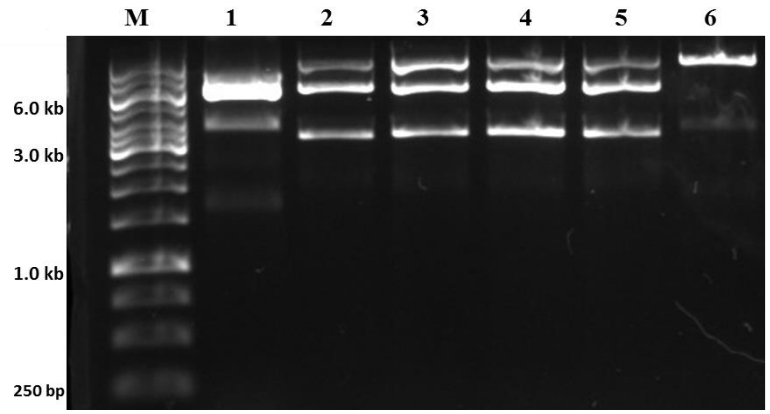

Figure 4.16: Gel electrophoretic analysis of restriction digested pBADrha-*efeU*OB*$^{K-12}$ candidate plasmids. Four plasmids (#1-4) were subject to *Nde*I and *Sal*I restriction digestion (lanes 2-5, respectively). Lane 1, undigested plasmid #1 DNA; lane 6, *Nde*I digestion plasmid #1 DNA; lane M, GeneRuler 1 kb ladder. With single digestion, a 9.0 kb band was expected and observed.

4.3. Phenotypic confirmation of the complementation of *efeO* and *efeB* mutants with pBADrha or pBADara constructs

To investgate the effect of the two different vector systems on low-iron growth, growth of JC32 (as JC28 but with an *efeU* deletion) transformants carrying pBADara-*efeUOB*^{O157} or pBADrha-*efeUOB*^{O157} was directly compared at a range of inducer concentrations (Fig. 4.17). The results show that *efeUOB* induction enhances low-iron growth in an inducer-concentration-dependent fashion for both plasmids. This indicates that the pBAD cloned *efeUOB* locus is subject to inducer controlled expression and encodes a function EfeUOB system.

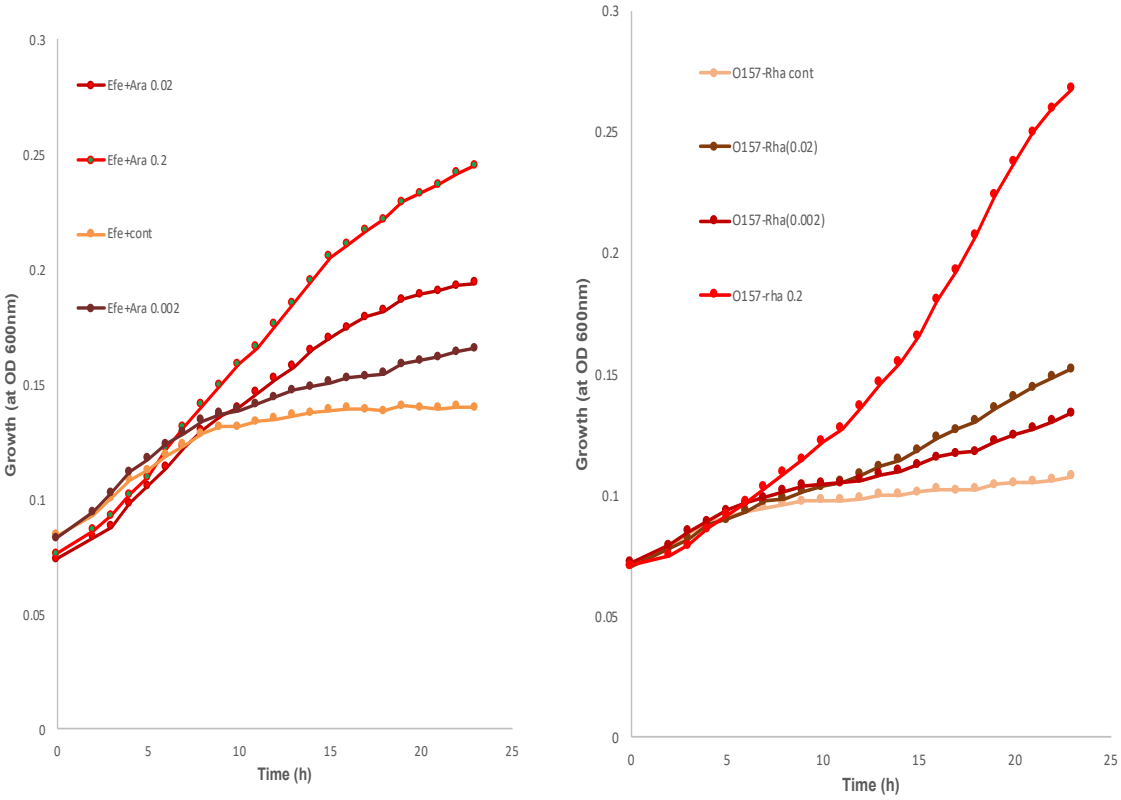

Figure 4.17: Effect of inducer low-iron growth of *E. coli* JC33 with pBADrha-*efeUOB*^{O157} or pBADara-*efeUOB*^{O157} under aerobic conditions. 300 µl bacterial cultures were grown aerobically in M9 medium with 0.4% glucose, rhamnose (0.002 ,0.02 or 0.2%), 1 µM DTPA and antibiotic (chloramphenicol, 50 µg/ml; or ampicillin, 100 µg/ml) in 100 well Bioscreen plates. The strains employed were JC32 transformed with plasmids pBADrha-*efeUOB*^{O157} or pBADara-*efeUOB*^{O157}. Each growth curve is the average of three replicates. Precultures were grown overnight in the same medium (no inducer, no DTPA) with 10 µM ferric citrate, and were washed prior to use as inocula to give a starting OD of 0.01. Different concentration of inducer (0.2-0.002%) was added to the medium this did not affect the growth of the complemented vector control (data not shown).

Western blotting was used to determine whether the EfeO and EfeB proteins were expressed in the JC33 and JC34 mutants complemented with the pBAD-*efeUOB*^{O157} plasmids. The *efeO* status of the complemented JC33 mutants was first tested, by Western blotting (Fig. 4.18). The results show the present of the EfeO protein (size 41 kDa) in the complemented JC33 mutants in the presence of inducer (Fig. 4.18). This confirms that the *efeO* gene is expressed in JC33 complemented with *efeUOB*. The EfeO protein was present in the wildtype but was not obvious in the vector-only-containing JC33 mutant (which has Δ*efeO* status), as expected. This confirms that the Western blotting is specific for EfeO and that the complementation enables EfeO production. In general, there was more EfeO observed with higher inducer levels. To quantify such effects, the immune-reactive bands were analysed using ImageJ software and comparison of their densities indicated that there is up to a 2.4 fold increase in EfeO levels upon induction by high (rather than low) arabinose levels (7.3 density at 0.02% and 3.04 density at 0.002%), but there was only a 1.2-fold increase in EfeO levels upon induction by high (rather than low) rhamnose levels (6.5 density at 0.02% and 5.4 density at 0.002% concentration) (Fig. 4.17). This suggests that expression of the *efeUOB* operon is only weakly regulated by levels of inducer. It should be noted that the cultures used were in stationary phase and ideally expression should be measured throughout growth to determine induction effects. Furthermore, the effect of no inducer was not considered, and should be in future work.

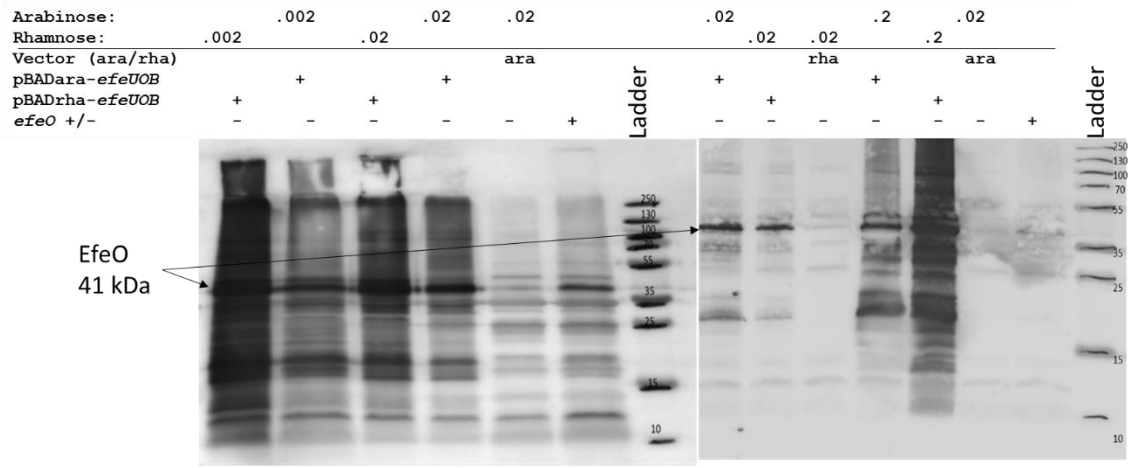

Figure 4.18. Western blot analysis of EfeO. Growth was performed in M9 containing 100 μg/ml ampicillin or 50 μg/ml chloramphenicol at 37 °C. 0.002-0.2% rhamnose or arabinose were added (as indicated) and cultures grown overnight. Whole-cell samples (0.05 OD units) were fractionated by SDS-PAGE (15% acrylamide) before anti-EfeO Western blotting. The ladder was Prestained Protein Ladder (Thermo Fisher Scientific). Strains were W3110 and JC33 (*efeO*$^{+}$ and $^{-}$, respectively). Strains carried either pBADara-*efeOUB*^{O157} or pBADrha-*efeUOB*^{O157}, or pBADrha or pBADara (vector only JC33 'control'), as indicated. In all cases, the western blots were repeated once, and similar results obtained.

The western blots below (Fig. 4.19) show the EfeB status of JC34 transformants carrying pBADara-*efeUOB* or pBADrha-*efeUOB*. Results show the presence of EfeB in wildtype and JC34 (Δ*efeB*) complemented with the pBAD-*efeUOB* plasmids, confirming the induction of *efeB* in the presence of inducer. However, EfeB was absent in JC34 carrying vector only, which confirms that the pBADara-*efeUOB* and pBADrha-*efeUOB* plasmids drive expression of *efeB* (as well as *efeO*, as shown above). Thus, the pBAD-*efeUOB* plasmids allow the production of EfeO and EfeB in the presence of inducer, and also support aerobic, low-iron growth.

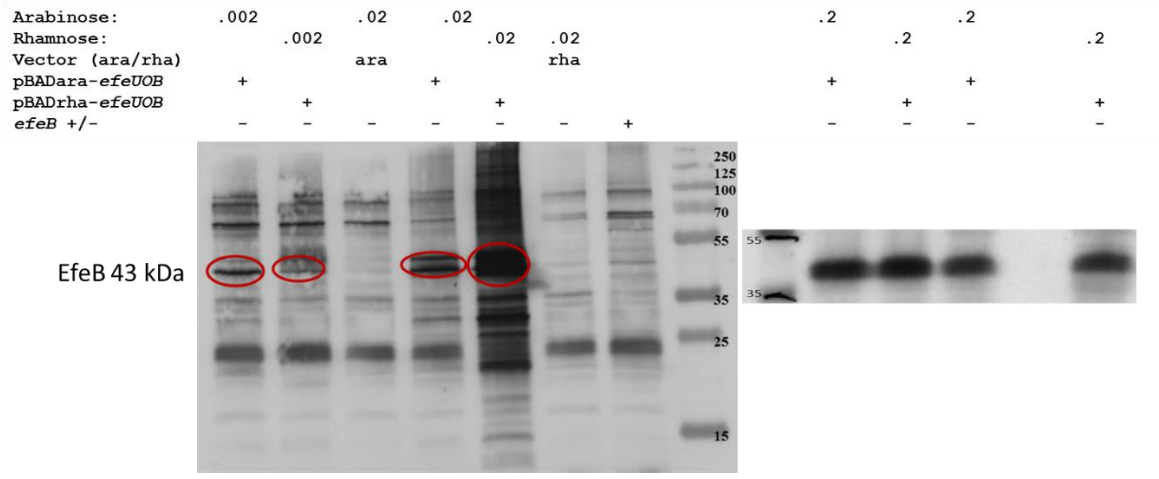

Figure 4.19. Western blot analysis of the EfeB status of complemented JC34. Details are as above except that JC34 (Δ*efeB*) was used in place of JC33, and the antiserum used was anti-EfeB.

Densitometry (as above) indicated a 3.5-fold induction of EfeB by high arabinose, relative to low arabinose (17.2 OD at 0.02% cf. 4.8 OD at 0.002%). In addition, there was a 7.5-fold increase in EfeB levels upon induction by high levels of rhamnose (68.3 cf. 9.5 OD at 0.02% cf. 0.002% rhamnose, respectively) (Fig. 4.19). Thus, EfeB levels appear to be quantitatively regulated by inducer concentration (more so than EfeO levels) indicating that the *efeUOB* operon is subject to quantitative regulatory control by the inducers.

The whole-cell samples obtained above were also analysed for their protein composition by SDS-PAGE (Fig. 4.20). Surprisingly, a protein band simlar in size to EfeO or EfeB (41-43 kDa) was enhanced in the JC33 with pBADara-*efeUOB* suggesting a relatively high degree of expression for the *efeUOB* operon in this case. Note that AraC is just 33.4 kDa and no such band (41-43 kDa) was observed in the vector control.

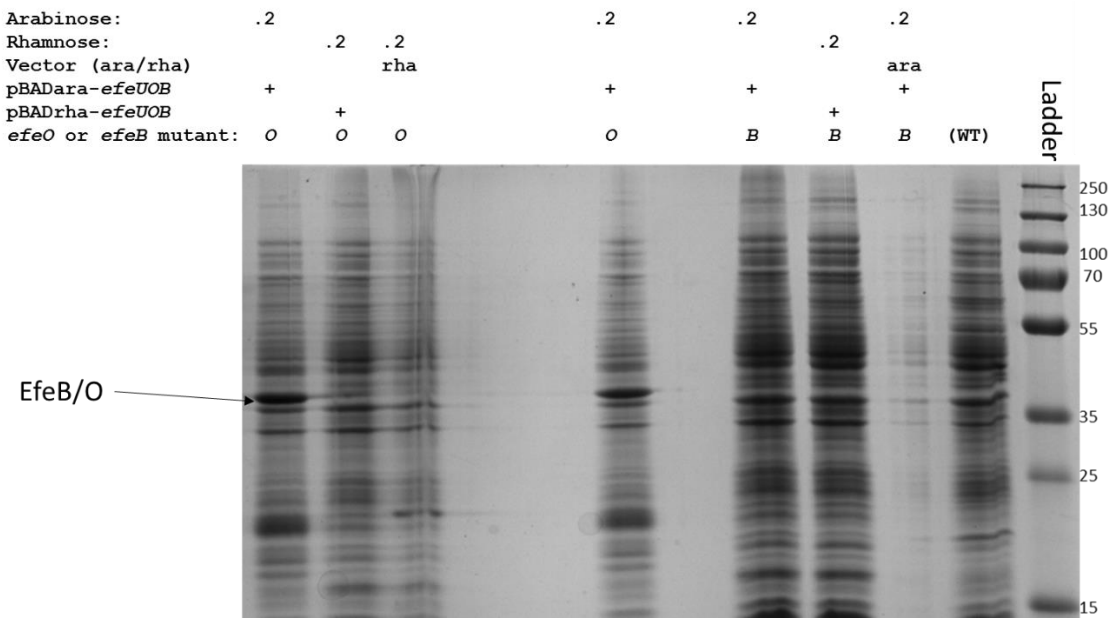

Figure 4.20. SDS-PAGE showing EfeO and/or EfeB may be visible within whole-cell extract when expressed from the pBADara-*efeUOB*^{O157} plasmid. Strains were JC33 (*efeO*) and JC34 (*efeB*) with the vectors indicated, or the wildtype (W3110)**.** Other details are as above. Arabinose and rhamnose were at 0.2%, where present. Note: this experiment has only been performed once so far, and will be repeated to confirm the results obtained.

In summary, induction of the *efeUOB* genes from the pBAD plasmids with arabinose or rhamnose was successful, as indicated by the raised levels of EfeB and EfeO. The successful induction of the *efeUOB* operon now allows analysis of the effect of *efeUOB* on iron-limited growth under various environmental conditions, without complications arising from expression effects (i.e. caused by Fur or CpxAR control).

No antibodies were available for FeoABC components, so such no western blot analysis on *feoABC* expression could be performed here (but see Chapter 8). Also, see below for effect of inducer levels on *feoABC* complementation.

4.4. Effect of induction of *efeUOB* and *feoABC* on growth under iron-sufficient and -restricted conditions

4.4.1. Induction of *efe* or *feo* increases iron-restricted growth of JC32

To further determine the ability of the Efe and Feo systems to operate as iron transporters under various environmental conditions, the pBAD plasmids constructed above were used to transform *E. coli* JC32 and then the ability of the cloned *feo* and *efe* systems to support iron-restricted growth was tested upon induction. Initially, this work was performed using glucose M9 minimal medium under aerobic conditions. Experiments were also performed with and without inducer to establish that promotion of iron-restricted growth requires induction of expression of *feo*, as well as *efe*

pBADara-*efeUOB*^{O157}, pBADrha-*efeUOB*^{O157}, pBADrha-*feoABC*^{O157}, pBADara-*feoABC*^{O157}, pBADara and pBADrha were transformed into JC32 and the resulting transformants were maintained aerobically on minimal medium (iron free) agar plates with antibiotic and as seed stocks in glycerol. Fresh isolated transformant colonies of JC32 were inoculated into 5 ml of 0.4% glucose M9 medium containing 50 µg/ml chloramphenicol or 100 µg/ml ampicillin, supplemented with 10 µM ferric citrate, and were incubated over-night at 37 °C with 250 rpm shaking. The overnight cultures were washed with M9 medium and re-suspended again in M9 to a final OD_{600} of 0.01. Growth tests were in 0.4% glucose M9 medium with/without inducer and either 20 µM ferric citrate, DTPA (generally at 1 µM) or no other additions. Culture volumes of 300 µl of were aliquoted into each well of a one hundred well plate. The optical density of each well of these was read every hour over a 24 h period of incubation at 37 °C with continuous shaking.

All growths were performed in triplicate and averages are reported. Error bars are not generally shown, for the purposes of clarity.

The growth curves obtained with the pBADrha vectors show that both *efe* and *feo* support growth under low iron conditions with inducer (Fig. 4.21 & 4.22), and that good reproducibility was obtained. The effect is particularly clear when neither iron nor DTPA are included; the *efe* and *feo* transformants reach max ODs of 0.52 and 0.32, respectively, ~2.5 and 1.5 fold greater than the vector control (OD 0.20; Fig. 4.21). This result is similar to that seen with the pHSG plasmids, although greater growth enhancement is seen with the pBAD vectors. Greater growth was also seen in the presence of iron for the induced *efe* and *feo* systems, although the effect was weaker (~1.2 fold increase at 14 h). With 1 µM DTPA, there was very little sign of growth for the vector control but both the *efe* and *feo* transformants grew, albeit weakly (maximum OD of 0.3). A key observation is that the *efeUOB* pBAD plasmid contuinues to provide a greater growth enhancement than the *feoABC* pBAD plasmid, indicating that the greater capacity of EfeUOB to support low-iron growth aerobically (cf. FeoABC) is not solely due to anaerobic expression control.

Similar results were obtained with the pBADara vectors (Fig. 4.23). The *efeUOB* plasmid again gave the greatest growth improvement for JC32. Thus, *efeUOB* conferred stronger low–iron growth on JC32 in both pBADrha and pBADara formats. The data thus suggest that Efe is a more effective iron transporter than Feo under aerobic conditions and that this effect is unrelated to differences in their promoter-mediated expression.

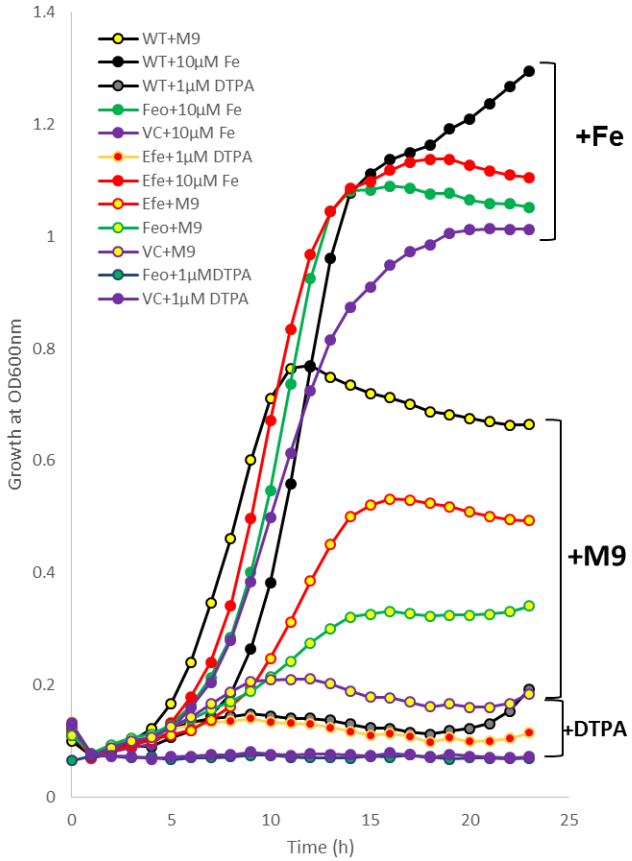

Figure 4.21: Effect of pBADrha-*efeUOB*^{O157} and pBADrha-*feoABC*^{O157} on aerobic iron-sufficient and iron-restricted growth of *E. coli* JC32. 300 µl bacterial cultures were grown aerobically in M9 medium with 0.4% glucose, 0.02% rhamnose and chloramphenicol (50 µg/ml) in 100 well Bioscreen plates. The M9 medium contained either 20 µM ferric citrate, 1 µM DTPA or no additions. The strains employed were: JC32 transformed with plasmids pBADrha, pBADrha-*efeUOB*^{O157}or pBADrha-*feoABC*^{O157}. Each growth curve is the average of three replicates. Precultures were grown overnight in the same medium with 10 µM ferric citrate, and were washed prior to use as inocula to give a starting OD of 0.01.

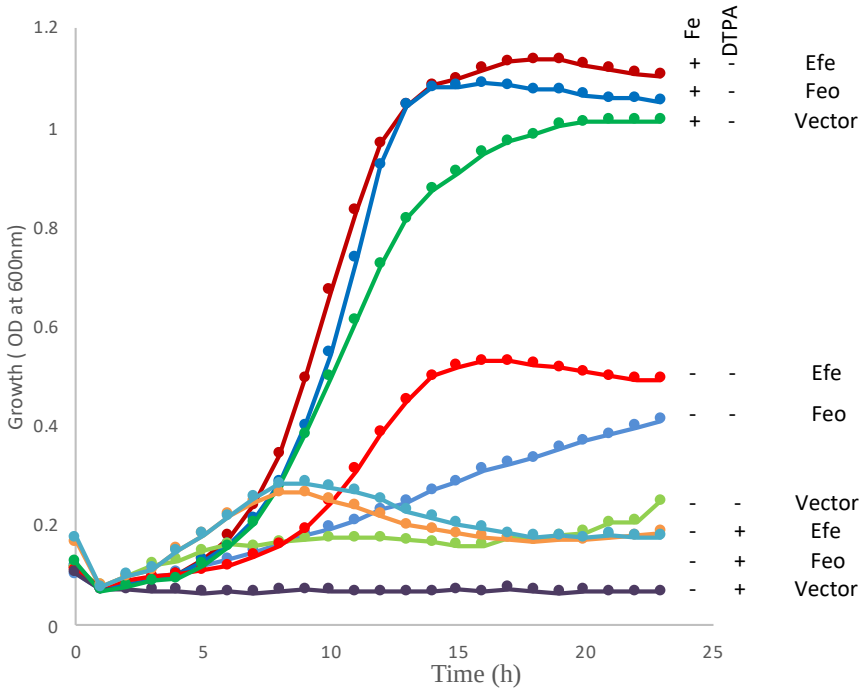

Figure 4.22: Effect of pBADrha-*efeUOB*^{O157} and pBADrha-*feoABC*^{O157} on aerobic iron-sufficient and iron-restricted growth of *E. coli* JC32. As above – a repeat experiment (but lacking the wildtype) illustrating reproducibility.

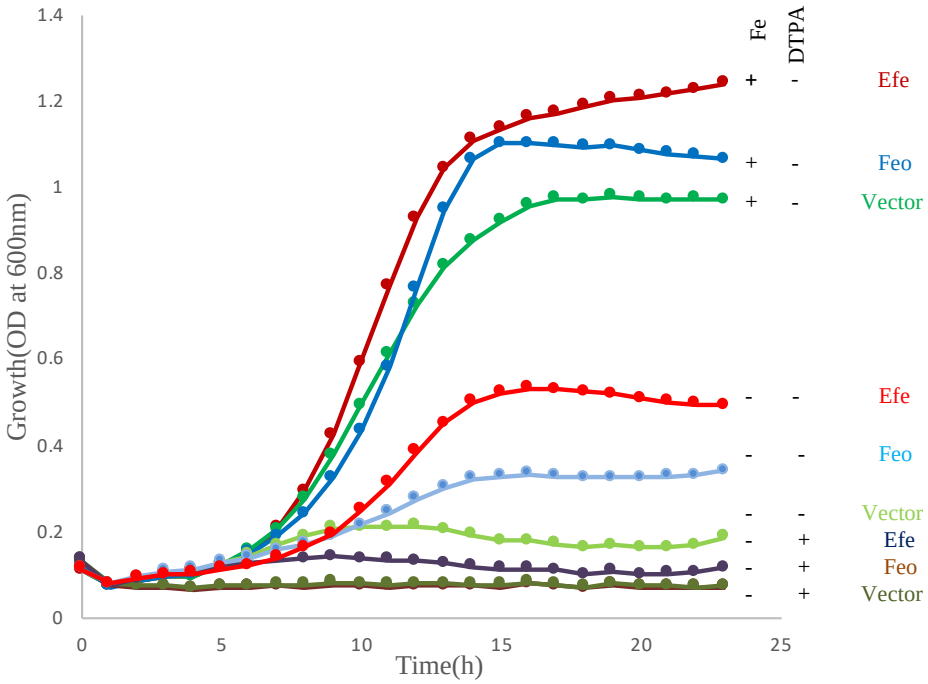

Figure 4.23: Effect of pBADara-*efeUOB*^{O157} and pBADara-*feoABC*^{O157}on aerobic iron-sufficient and iron-restricted growth of *E. coli* JC32. Details were as for Fig. 4.21 except that the medium included 0.02% arabinose and ampicillin (100 µg/ml) in place of rhamnose and chloramphenicol, and the pBADara plasmids were used in place of pBADrha.

4.4.2. The *efe*- and *feo*-mediated increase in iron-restricted growth requires inducer

Having illustrated that the low-iron growth of the JC32 strain is increased by *efe* and *feo* in the presence of inducer, particularly under low iron conditions, it was considered necessary to determine whether this effect is reliant on the presence of the inducers, rhamnose and arabinose (although this has already been shown above for the *efeUOB* system, this has not yet been completed for the *feoABC* system). Thus, the growth experiments were repeated with and without inducer.

For both expression systems, the absence of inducer resulted in either no growth advantage for the *efe* and *feo*-containing plasmids under low iron conditions, or a very modest growth increase (with respect to vector) (Figs. 4.24 & 4.25). Thus, it is clear that the inducers are indeed required to enable both the *efe* and *feo* systems to exert any substantial growth advantage, as was expected. Therefore, it can be presumed that the corresponding promoters are under significant regulatory control in response to arabinose or rhamnose.

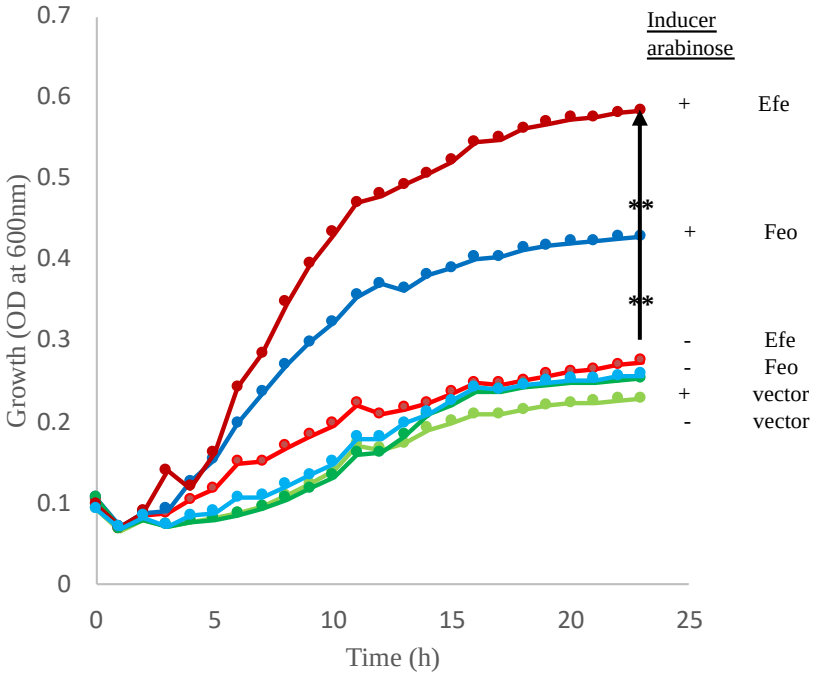

Figure 4.24: Effect of arabinose inducer on pBADara-*efeUOB*^{O157} or pBADara-*feoABC*^{O157} aerobic iron-restricted growth of *E. coli* JC32. Details are as above (Fig. 4.21) except for the exclusion of arabinose where indicated. Statistically significant differences with and without inducer (P<0.01) were determined by Graph Prism One way Anova and significant differences are indicated above at 24 h.

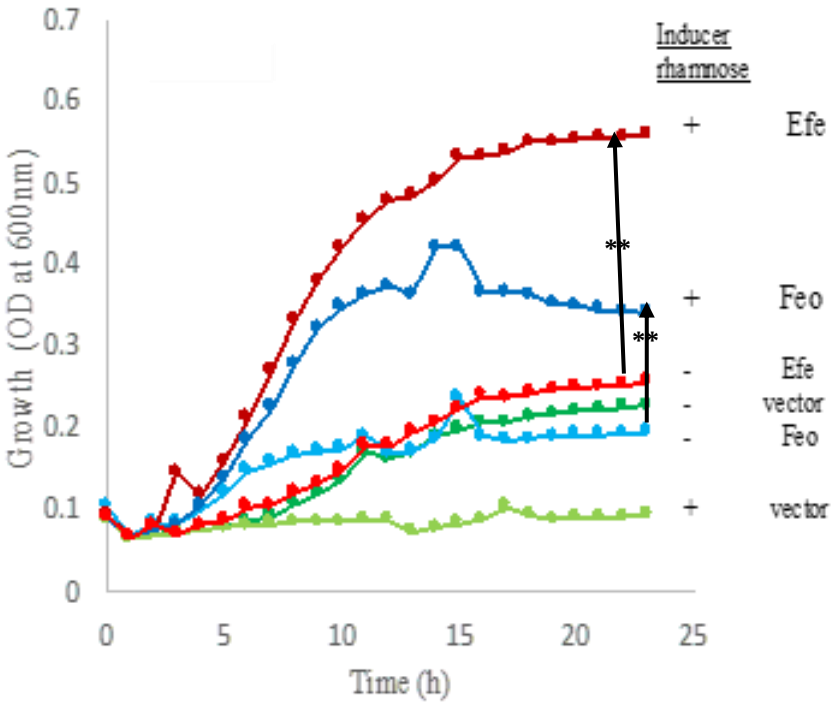

Figure 4.25: Effect of rhamnose inducer on pBADrha-*efeUOB*^{O157} or pBADrha-*feoABC*^{O157} in aerobic iron-restricted growth of *E. coli* JC32. Details are as above (Fig. 4.21) except for the exclusion of rhamnose where indicated. Statistically significant differences with and without inducer (P<0.01) were determined by Graph Prism One way Anova and are indicated at 24 h.

Additional experiments were performed on the effect of inducer under iron sufficiency and with DTPA for the *efe* system (Fig. 4.26). For both the pBADara and pBADrha systems, inducer caused a major increase in growth rate (and final OD) with 1 µM DTPA. Arabinose decreased the doubling time from ~5 to ~2 h (in the 5-10 h time period; Fig. 4.26). A similar increase in doubling time in the presence of 1 µM DTPA was seen with induction by rhamnose (Fig. 4.27).

When iron was included, the effect of arabinose was only slight, causing a modest delay in growth (0.5-1 h) and a slightly higher maximum OD (1.0 cf. 0.9). Similar effects were observed with induction by rhamnose (data not shown).

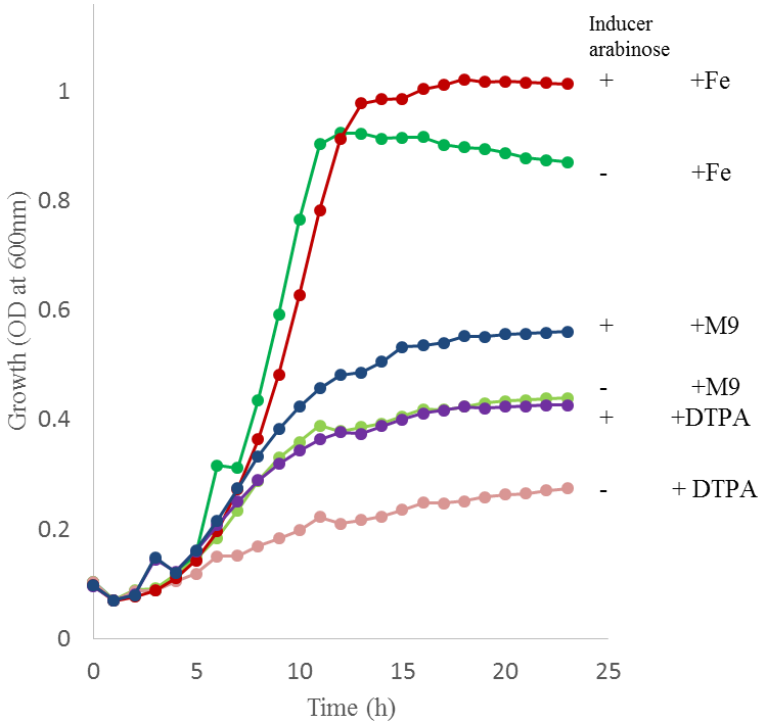

Figure 4.26: Effect of arabinose inducer on pBADara-*efeUOB*^{O157} in aerobic iron-sufficient and iron-restricted growth of *E. coli* JC32. Details are as for Fig 4.21 except that inducer was excluded as indicated. Where present, ferric citrate was at 10 µM, and DTPA was at 1 µM.

The effect of the inducers on iron sufficient growth and growth with 1 µM chelator was also explored for the *feo* system, and similar results were obtained (data not shown) indicating the

need for inducer in order to achieve maximum complementation activity for *feoABC*. For the pBADara vector, control experiments showed no influence of the inducer under iron sufficient or deficient conditions, or with chelator (Fig. 4.27). This strongly indicates that the improved growth seen for induction of *feo* and *efe* with arabinose is caused by the increased expression of the cloned genes. Similar results were obtained for the pBADrha vector (data not shown). Thus, under low-iron and inducing conditions, the JC32 transformants carrying pBAD-*efeUOB* and pBAD-*feoABC* clearly showed a better growth compared to JC32 transformants carrying only the vector. The above results support the role of *efeUOB* and *feoABC* as iron transport systems (since the pBAD-*efeUOB* and pBAD-*feoABC* plasmid increased the growth of the JC32 strain which lacks iron transport capacity). Furthermore, the above results suggest that *efeUOB* provides JC32 with a greater iron-restricted growth advantage than *feoABC* under the aerobic growth conditions employed and that both *efeUOB* and *feoABC* are subject to induction.

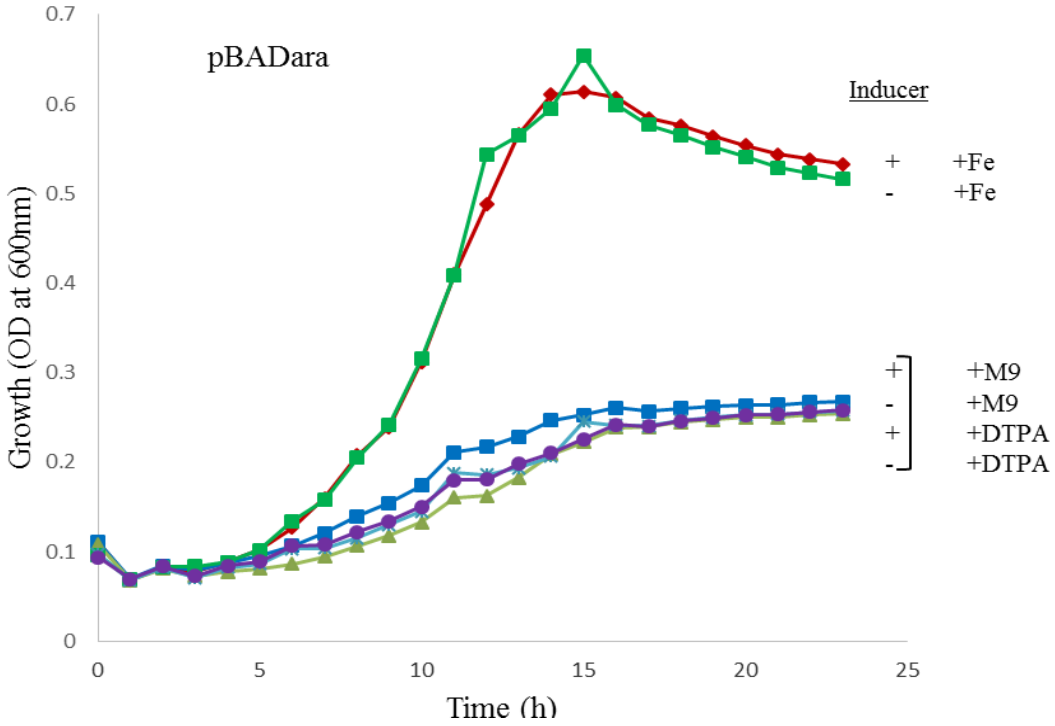

Figure 4.27: Effect of arabinose inducer on aerobic iron-sufficient and iron-restricted growth of *E. coli* JC32 with pBADara. Details are as described above.

4.5. Effect of pH on iron-restricted growth of JC32 carrying inducible *efeUOB* or *feoABC* operons

In order to determine whether pH has any impact on the low-iron growth of JC32 carrying inducible *feoABC* or *efeUOB* systems, the JC32 transformants were tested for their growth properties in glucose-containing M9 medium at acidic (pH 6) and alkaline (pH 8) pH. Since *efeUOB* is strongly induced by low pH, it remains possible that the greater iron-uptake associated with EfeUOB at low pH is simply related to its expression control. This possibility can now be tested. In addition, as ferrous iron is more stable at low pH, it is possible that both EfeUOB and FeoABC provide a greater low-iron growth benefit under acidic conditions where ferrous iron might predominate over ferric iron.

As before, growth experiments were performed in a Bioscreen C system under aerobic conditions and a FLUOstar plate reader under anaerobic/microaerobic conditions and pH was maintained using a 100 mM buffer.

4.5.1. Aerobiosis

Results again showed that induction of *feoABC* or *efeUOB* in JC32 enhanced iron restricted growth. This effect was observed at both pH 6 and 8 (Fig. 4.28). However, the degree of *efeUOB*- and *feoABC*-mediated growth enhancement under low-iron conditions was far greater at pH 6 than pH 8 (2.3 and 3.3 fold higher final ODs achieved for the complemented strains than for the vector control at pH 6 with 1 μM DTPA, whereas at pH 8 the growth was very weak with DTPA and growth differences were modest in the absence of DTPA at ~1.3 fold; Fig. 4.29). Further, EfeUOB enabled better growth that FeoABC at pH 6 under low iron, but there was little difference between the benefit provided by the systems at pH 8 (Fig. 4.29). These results are consistent with the notion that EfeUOB is better equipped than FeoABC to

transport ferrous iron aerobically, and that both EfeUOB and FeoABC provide greater benefit at acidic than alkaline pH as ferrous iron is likely to be more readily available.

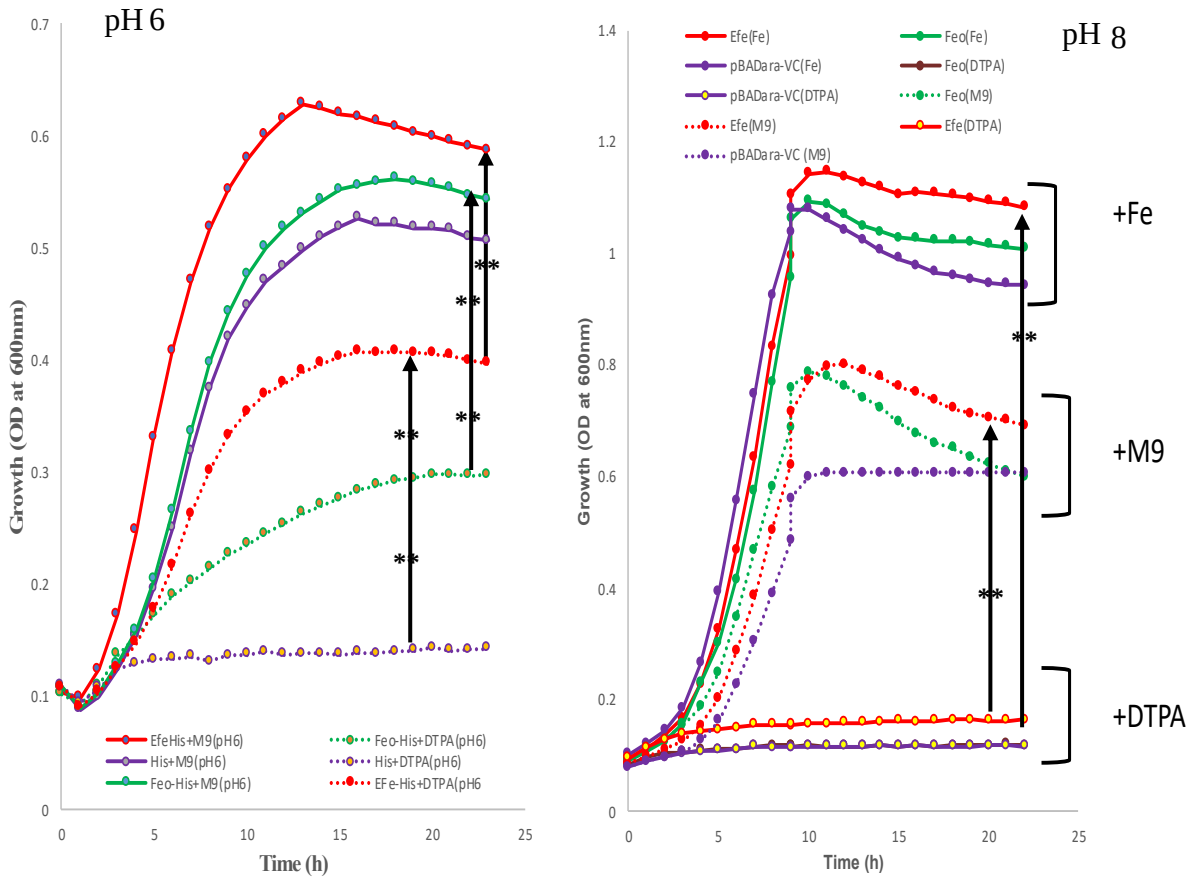

Figure 4.28: Effect of pBADara-*feoABC*^{O157} and pBADara-*efeUOB*^{O157} complemented JC32 on aerobic, iron restricted growth in M9 medium at pH 6 and pH 8. Strains were grown aerobically with continuous shaking in Bioscreen C system in M9 medium containing 0.4% glucose with 1 µM DTPA, 10 µM ferric citrate or no addition, under alkaline or acidic pH, with 0.02% inducer. The pH was maintained using 100 mM TAPS or MES. Other details are as in Figure 4.21. Equivalent high growth was seen for all strains with added iron at pH 6; these data are omitted above. (note: His is pBADara (vector control). Statistically significant differences (P<0.01) as determined by Graph Prism One way Anova are indicated.

Similar results were seen with the pBADrha-*feoABC*^{O157} and pBADrh-*efeUOB*^{O157} plasmids (Fig. 4.29). The low-iron growth differences between the complemented strains and the vector control were greater at pH 6 than pH 8, and the EfeUOB system promoted low iron growth

more so than the FeoABC system at pH 6. However, at pH 8 the EfeUOB system did not appear to be superior to the FeoABC system in promoting low iron growth (Fig. 4.29). These results thus support the findings and conclusions made above.

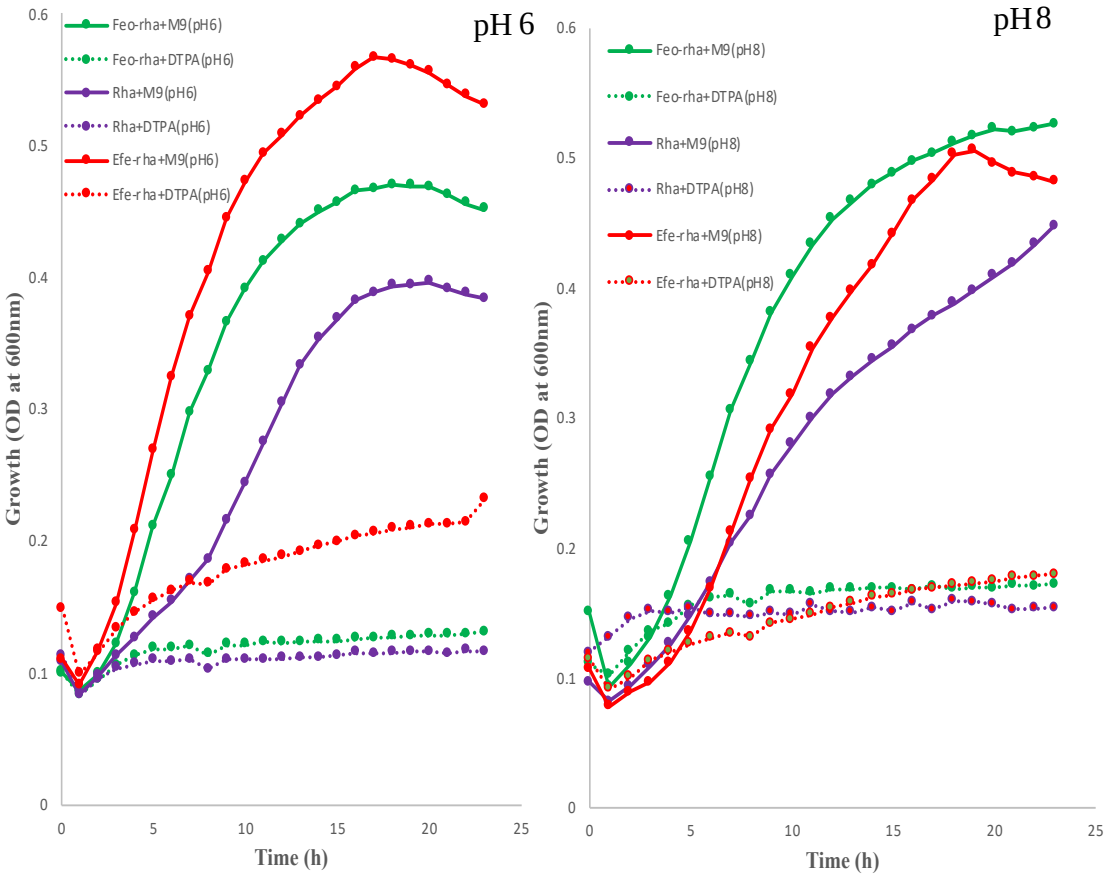

Figure 4.29: Effect of pBADrha-*feoABC*^{O157} and pBADrha-*efeUOB*^{O157} complemented JC32 on aerobic, iron restricted growth in M9 medium at pH 6 and 8. Details are as above except for the plasmids and inducer employed.

4.5.2 Low-oxygen growth conditions

In order to determine whether the pH affects observed aerobically are reiterated anaerobically, the experiments described above were repeated using anaerobic/microaerobic growth conditions. It is possible that low-oxygen conditions will support the availability of ferrous over ferric iron such that low-iron growth would no longer be influenced by pH (6 versus 8).

The results show that under low O_2 regime at pH 6 the FeoABC system provides a greater low-iron growth advantage than EfeUOB (Fig. 4.30). This effect was particularly strong in the case of the pBADara vector. Indeed, the FeoABC system was able to restore low-iron growth at anaerobic, low pH to levels that are similar to those of the wildtype (Fig. 4.30).

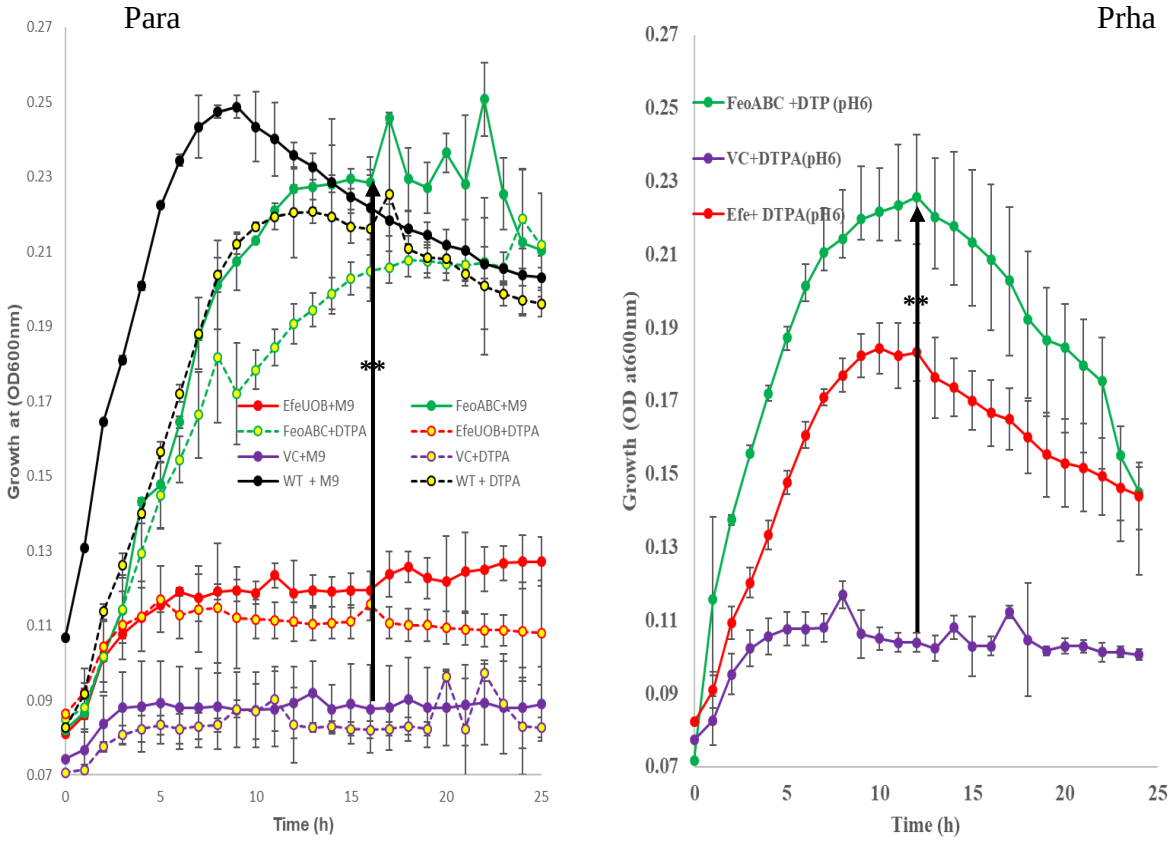

Figure 4.30: Effect of pBAD-*feoABC*^{O157} and pBAD-*efeUOB*^{O157} plasmids on <u>anaerobic</u>, iron-restricted growth of JC32 in M9 medium <u>at pH 6</u>. Strains were grown anaerobically in M9 medium containing 0.4% glucose with 0.5 µM DTPA. The strains employed were W3110 ('WT') and JC32 with pBADara-*feoABC*^{O157} and pBADara-*efeUOB*^{O157} or pBADara (left), or with pBADrha-*feoABC*^{O157} and pBADrha-*efeUOB*^{O157} or pBADrha (right). 100 mM MES buffer was used to maintain a pH of 6. Values presented are average of three independent growths. Statistically significant differences ($P<0.05$) as determined by Graph Prism One way Anova are indicated.

When the experiment was repeated at pH 8, the difference between FeoABC- and EfeUOB-mediated low-iron growth was more dramatic. The FeoABC system stimulated growth considerably (>fourfold) with respect to the vector control, whereas EfeUOB stimulated growth

weakly (1.2-fold or less; Fig. 4.30). This effect was seen for both the pBADara and pBADrha formats. Indeed, the FeoABC system was able to increase low-iron anaerobic growth at pH 8 to a degree that matched that achieved by the wildtype. This suggests that the anaerobic low-iron growth of the wildtype is largely enabled by the FeoABC system, particularly at high pH.

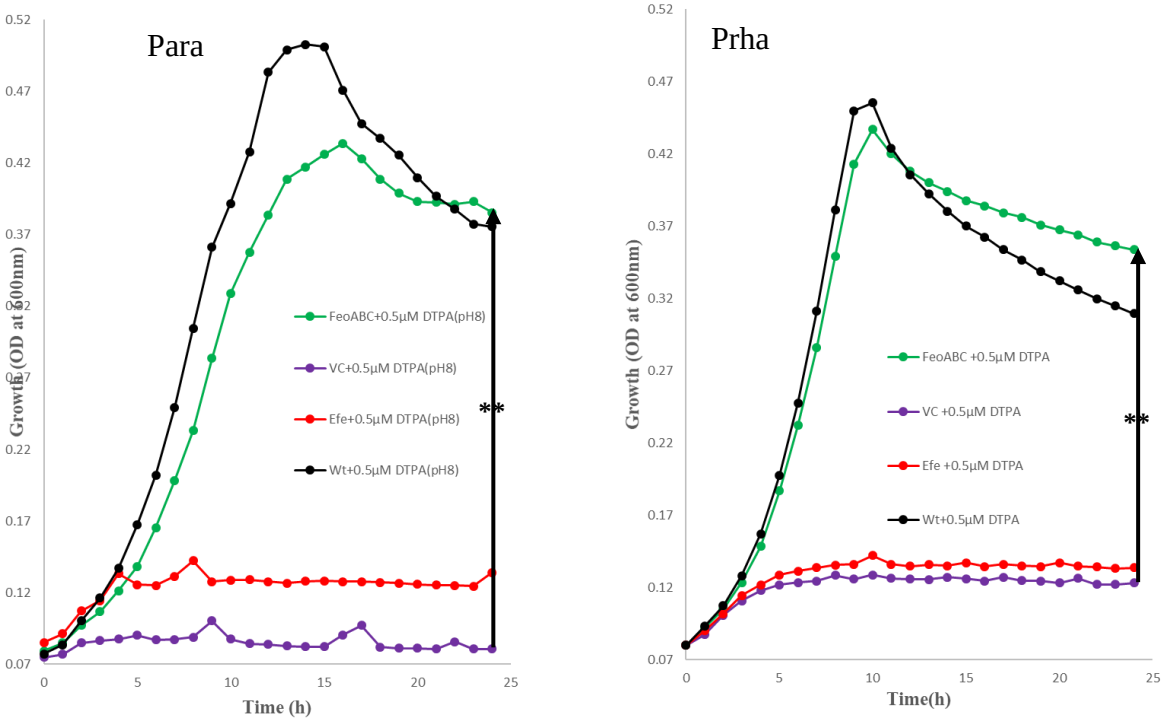

Figure 4.31: Effect of pBAD-*feoABC*^{O157} and pBAD-*efeUOB*^{O157} plasmids on <u>anaerobic</u>, iron-restricted growth of JC32 in M9 medium <u>at pH 8</u>. Details are as for Fig. 4.30 except that 0.5µM DTPA was employed and the pH was maintained at 8 with a 100 mM TAPS buffer. In addition, the wildtype was omitted. Statistically significant differences (P<0.01) as determined by Graph Prism One way Anova are indicated at 24 h.

The influence of low pH (6) on low-iron anaerobic growth for JC32 with *efeUOB* or *feoABC* was further explored using the 'corrected' *efeU*OB*$^{K-12}$ system (Fig. 4.32). Results are similar to those obtained before (Fig. 4.30) except that the differences between EfeUOB and FeoABC dependent low-iron growth are greater and similar to those seen at pH 8. This difference between the results in Figs. 4.30 and 4.32 likely relates to the technical difficulties associated

with maintaining consistency between growth conditions (in particular, iron availability) on a day to day basis.

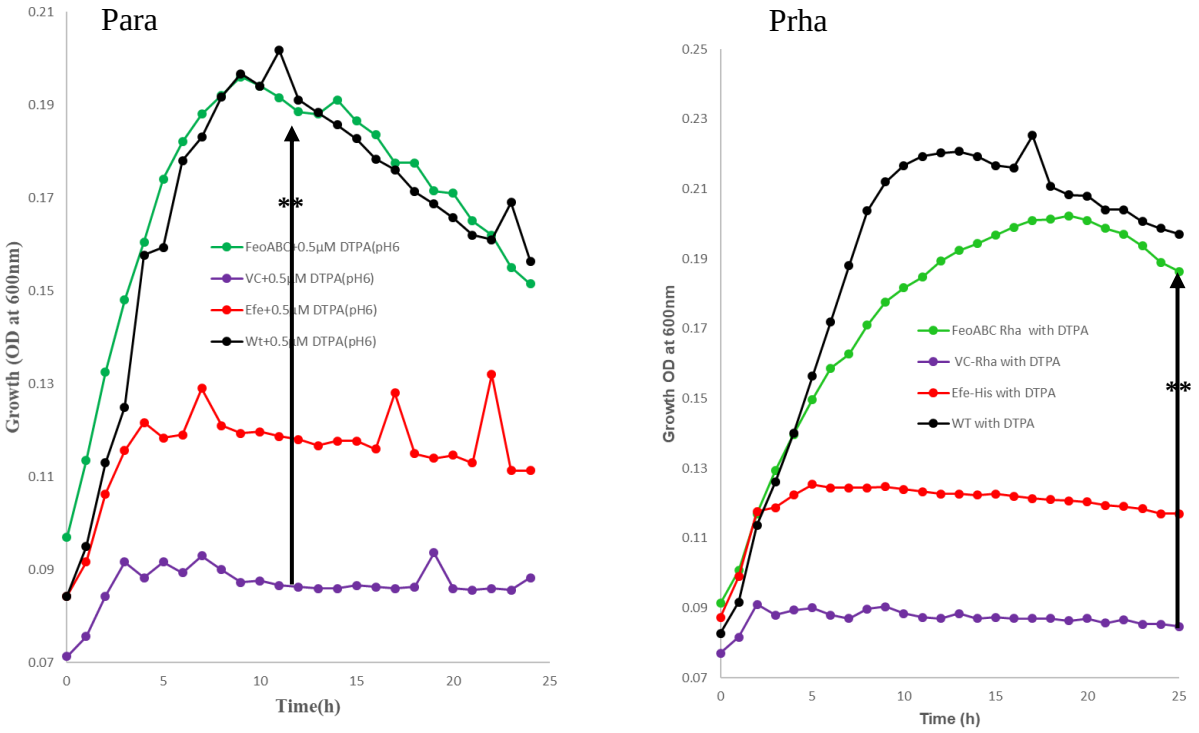

Figure 4.32: Effect of pBAD-*feoABC*^{O157} and pBAD-*efeUOB*$^{K-12}$ plasmids on anaerobic, iron-restricted growth of JC32 in M9 medium at pH 6. Details are as in Fig. 4.31 except for use of the K-12 systems indicated. Statistically significant differences (P<0.01) as determined by Graph Prism One way Anova are indicated at 24 h.

To investigate the effect whether the sufficient iron condition observed anaerobically, the experiments described above were repeated using anaerobic/microaerobic growth conditions. It is possible that low-oxygen conditions will support the availability of ferrous over ferric iron such that low-iron growth would no longer be influenced by pH (6 versus 8).

The results show that under low O_2 regime at pH 6 and 8 the EfeUOB and FeoABC system provides a greater high-iron growth advantage than vector control (Fig. 4.34). This effect was particularly strong in the case of the pBADara vector. Indeed, the EfeUOB system was able to

restore high-iron growth at anaerobic, low pH and high pH to levels that are slightly similar to those of the FeoABC (Fig. 4.33).

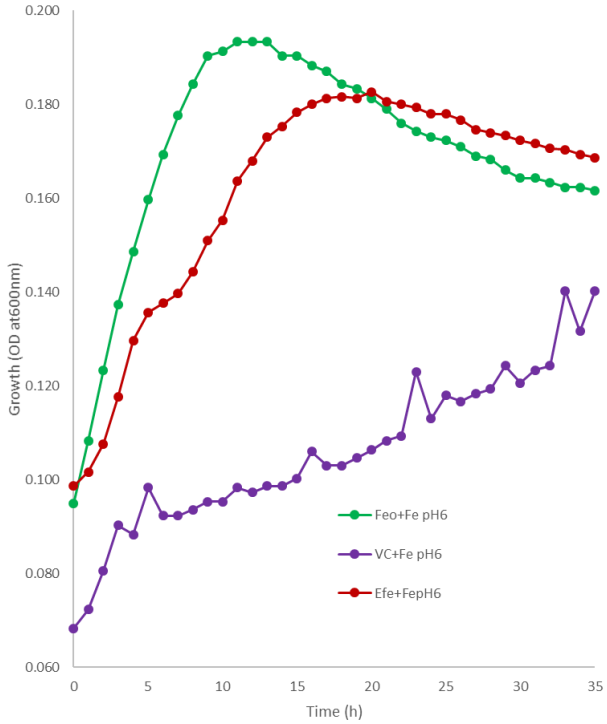

Figure 4.33: Effect of pBAD-*feoABC*^{O157} and pBAD-*efeUOB*^{O157} plasmids on anaerobic, iron-sufficient growth of JC32 in M9 medium at pH 6 . Details are as for Fig. 4.31 except that 10 μM ferric citrate was employed, and the pH was maintained at 6 a 100 mM MES buffer.

4.5.3 Anaerobic growth conditions

A further set of anaerobic experiments were performed (under conditions of fermentation) using syringes to maintain completely oxygen-free conditions (Methods 2.39). The experimental conditions were otherwise as above. These conditions were used in order to determine whether completely anaerobic conditions might negatively influence the impact of EfeUOB under low-iron growth conditions at pH 6 or 8.

The results obtained were similar to those presented above (Section 4.5.2) with greater low-iron, anaerobic growth stimulation by FeoABC than by EfeUOB (Figs. 4.34 & 4.35) at both pH 6 and pH 8. These results thus confirm those obtained above indicating that EfeUOB is far less effective at supporting the anaerobic low-iron growth of *E. coli*, at both high and low pH, than FeoABC.

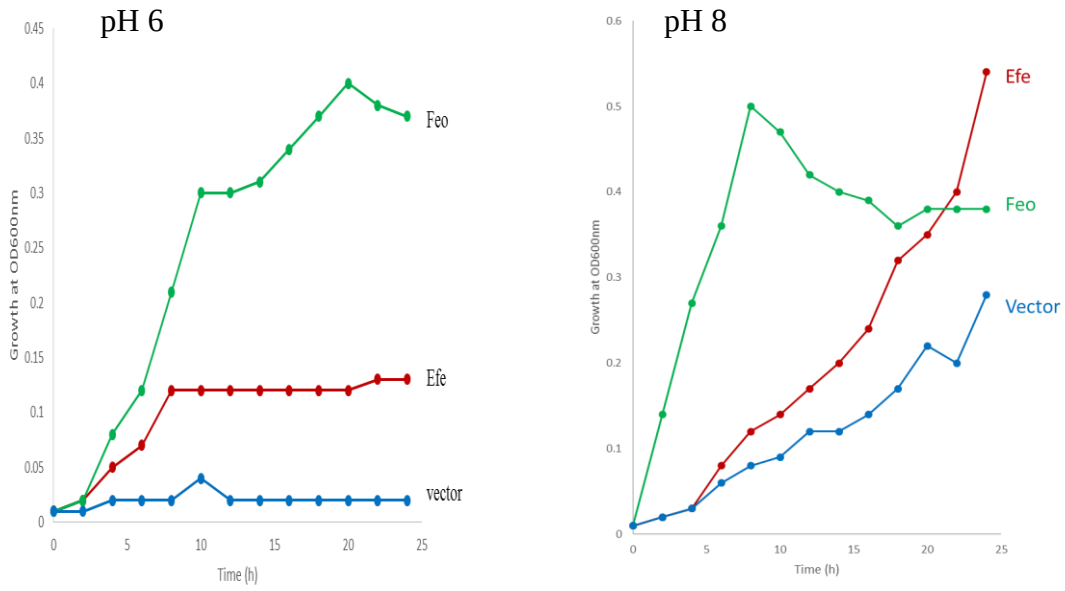

Figure 4.34: Effect of pBADara-*efeUOB*^{O157} or pBADara-*feoABC*^{O157} plasmids on anaerobic, iron-restricted growth of JC32 in M9 medium at pH 6 or 8 using syringes. Details are as for Fig. 4.31. The medium contained inducer and antibiotic (no iron or chelator were added). The pH was maintained at 6 or 8 with a 100 mM MES or TAPS, respectively. Data represent the mean OD values of duplicates.

In summary, the results obtained here show that the anaerobiosis dependence of Feo activity is not solely related to its transcriptional control by Fnr, but is also dependent upon factors beyond transcriptional control. The mechanism by which O_2 influences Feo activity is unclear but could be at least partly related to the FtsH-dependent proteolytic degradation of FeoB stimulated by oxygen (Kim *et al*., 2013). EfeUOB displays much weaker anaerobic activity than FeoABC, but both systems utilise ferrous iron as primary substrate, and anaerobic conditions would be expected to favour ferrous iron availability. Thus, it is unlikely that differences in ferrous iron

availability would explain why EfeUOB is poorly effective anaerobically. Similarly, it is unlikely that the relatively poor aerobic performance of FeoABC is related to ferrous iron availability. However, these observations would be consistent with the view that EfeUOB is dependent on the presence of peroxide (a product of aerobic metabolism) for its activity whereas FeoABC is subject to inhibition by peroxide. This hypothesis will be further explored in subsequent chapters.

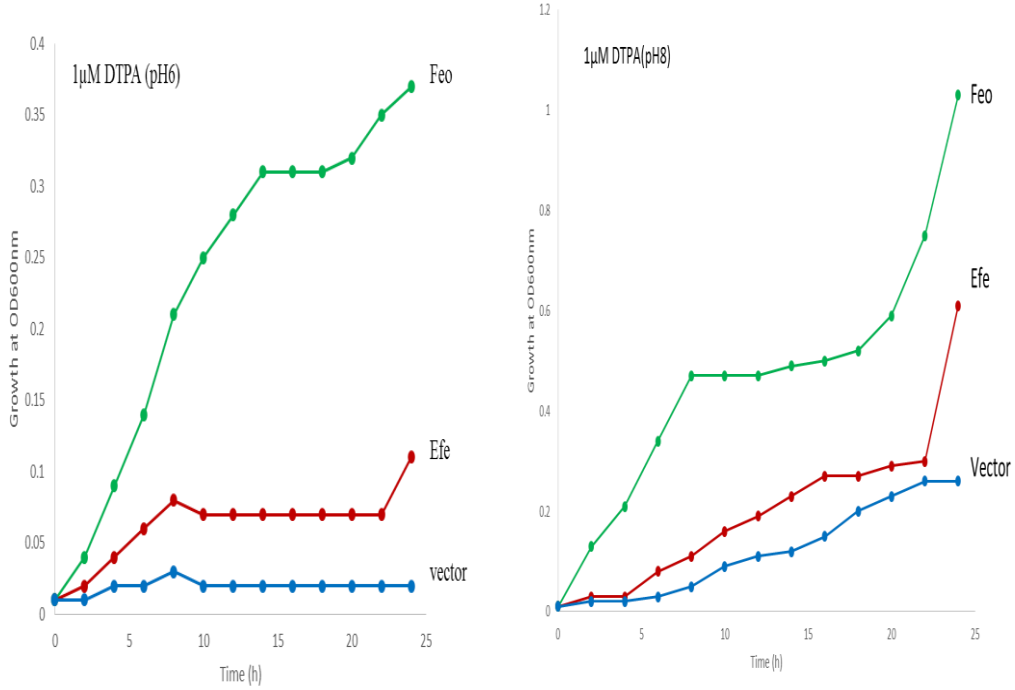

Figure 4.35: Effect of pBADara-*efeUOB*^{O157} or pBADara-*feoABC*^{O157} plasmids on anaerobic, iron-restricted growth of JC32 in M9 medium with 1 µM DTPA at pH 6 or 8 using syringes. Details are as for Fig. 4.34 except for the use of 1 µM DTPA.

4.6. Summary and Brief Discussion

Iron is a significant factor for microorganism growth and survival. Iron is found in two main states, the ferric and ferrous forms. In aerobic circumstances, iron is commonly present in the oxidized and relatively insoluble ferric form. It is understood that the ferrous iron is prevalent under oxygen limited conditions, such as the lumen of the human gut, and may also persist at low pH. The study of bacterial Fe^{2+} acquisition systems should thus contribute to knowledge and insight on bacterial strategy for competing for iron under iron-restricted conditions where ferrous iron might be stable, such as the anaerobic intestine or in acidic phagolysosomes.

The main focus of this chapter was to divorce the promoter-controlled low-pH and anaerobic dependence of EfeUOB and FeoABC, respectively, from their observed physiological preference for such environmental conditions as ferrous iron transporters.

feoABC expression is subject to FNR induction anaerobically, and Fur repression under high iron. It is also reported to be regulated post-translationally in response to oxygen by FeoC. Thus, FeoC protects FeoB against aerobic degradation by FtsH. However, it should be stressed that this regulatory role on the FeoABC system, as seen in *S. enterica*, was not observed in *E. coli* or *V. cholerae* (Weaver *et al*., 2013; Kim *et al*., 2013), although it would be unexpexcted for FeoC to function differently in *E. coli* and *S. enterica*.

The results obtained in Chapter 3 show that aerobically, the iron-uptake activity provided by *feoABC* (from pHSG576) is much lower than that provided by *efeUOB*. However, this effect could arise from the negative aerobic controlling elements (Fnr and FeoC) that would provide an impact under the aerobic conditions employed (Cao *et al*., 2007). Thus, by providing the *feoABC* system with arabinose and rhamnose inducible promoters, such influences can be eliminated.

For both pHSG-*efeUOB*^{O157} and pHSG-*feoABC*, control by Fur remains relevant. Ferrous iron is known to predominant under acidic and reducing condition. It is reasonable to suggest that

ferrous iron transport would have an important role under acidic, aerobic conditions. EfeUOB is an acid inducible and CpxR-regulated ferrous transporter known to be functional in *E. coli* O157:H7 (Cao *et al*., 2007). In this thesis, EfeUOB was shown to increase growth under iron-starvation but not under rich-iron conditions. Consequently, the data obviously indicate an important role for Efe under iron depletion, as shown previously (Cao *et al*., 2007). This EfeUOB-dependent advantage was clearly shown to be stronger at low pH than at high pH. This result correlates well with the observation that EfeO is induced under acidic conditions (Maurer *et al*., 2005) although no acidic stimulus for *efeU* was shown by GroBe *et al*. (2006). The effect of low pH on low-iron growth of *E.coli* JC28 complemented with *efeUOB*, as illustrated here, is considered to be due to the fact that, aerobically, Fe^{2+} is stable against oxidation at acidic condition. However, as *efeUOB* is subject to transcriptional induction by CpxAR, it remained possible that the enhanced role of EfeUOB at low pH is expression related, rather than dependent on substrate availability or any pH-dependent mechanistic effect on the transporter. However, it should be noted that the *B. subtilis efeUOB* operon is believed utilise Fe^{3+} when Fe^{2+} is not available (Ollinger *et al*., 2006).

In this chapter, the inducible plasmids, pBADrha and pBADara, where used to generate *feoABC* and *efeUOB* constructs to enable controlled expression of these operons in the absence of any environmental control (iron, pH, oxygen), other than that imposed by the specific inducer. This thus allowed examination of the ability of Feo and Efe to support low-iron growth without interference from expression effects relating to the growth conditions employed. Thus, the effect on growth of the biochemical activities of the transporters could be studied under aerobic and anaerobic conditions, at low and high pH. The related *E. coli* strains JC28 and JC32 were used as hosts, as they carry mutations in iron transport system, including *feoABC* and *efeU*, with JC32 possessing a deletion in *efeU* whereas JC28 carried a frameshift mutation in *efeU*. The results showed that, aerobically, both the *feo* and *efe* plasmids support low-iron growth of the

mutant strain, in comparison to the vector control. In addition, the Efe system gave a greater growth increase than Feo, reflecting the anaerobic preference for Feo. Western blotting showed that the inducible *efeUOB*-containing plasmids increased production of EfeB and EfeO in response to inducer – strongly suggesting that any phenotypic effect exerted by the pBAD-*efeUOB* plasmids should be subject to inducer regulation. Indeed, the addition of inducer was required for the effects of the *efe* and *feo* plasmids to be well exhibited – this suggests that both systems are indeed induced by arabinose and rhamnose from the corresponding vectors. The aerobic low-iron growth enhancement of EfeUOB was greater at low pH, which suggests that the previously observed low pH preferences of EfeUOB is not entirely related to pH-transcription control. However, FeoABC also showed a low pH preference in some cases (Fig. 4.49), which suggests that the low pH effect observed might be related to ferrous iron availability.

Anaerobically, EfeUOB provided only a modest increase in low-iron growth, and this was largely pH independent. However, FeoABC gave a strong increase in low-iron growth anaerobically which suggests that FeoABC is better suited mechanistically to ferrous iron uptake anaerobically than EfeUOB. It is speculated that this difference is related to FeoC-dependent oxygen degradation of FeoABC and the suggested requirement of EfeUB for peroxide as oxidant of ferrous iron to drive iron uptake via the Ftr1p-like EfeU permease. This effect could also arise from sensitivity of key Cys residues in FeoB to oxidation.

The clear growth improvement provided by the *efe* and *feo* pBAD plasmids (in contrast to the vector control) shows that both operons generate active systems that support low iron growth, presumably by driving ferrous-iron uptake. Thus, these plasmids can be employed in further work on the environmental requirements for Feo and Efe activity. These findings support a role for *efeUOB*^{O157} and *feoABC*^{O157} in iron uptake and thus match the findings made previously

(e.g. GroBe *et al*., 2006; Cao *et al*., 2007; Weaver *et al*.,2013). Therefore, Efe and Feo function will next be analysed by testing their response to hydrogen peroxide and catalase (reported in Chapter 5).

Chapter 5. Influence of H_2O_2 on the two dedicated ferrous-iron uptake systems (FeoABC and EfeUOB) of *Escherichia coli*

5.1. Introduction

The Enterobacteriaceae are facultative anaerobes and require iron in micro-molar concentrations (Guerinot *et al*., 1994). Enterobacteriaceae include species pathogenic for humans such as *Shigella, Salmonella, Yersinia* and pathogenic *E. coli* strains; these bacteria must be able to acquire iron over a wide range of oxygen concentrations within the host (Clements *et al*., 2012). The oxidation state and availability of iron are highly impacted by the amount of oxygen in the surroundings, as well as pH. The capacity of bacteria to sense and respond to the concentration of both oxygen (or redox stress) and iron have important outcomes in preventing either iron starvation or iron toxicity. Depending on oxygen levels and pH, iron is present in one of two distinct forms, Fe^{2+}or Fe^{3+}, and bacteria utilise different uptake systems for the transport of iron for the ferrous and ferric forms. *E. coli* O157 uses two distinct systems for ferrous iron transport, EfeUOB and FeoABC, the former functioning anaerobically and the latter aerobically at low pH. Since iron has the ability to mediate the production of toxic reactive oxygen species (ROS) (Touati, 2000), its metabolism is often co-ordinately regulated in response to ROS (Imlay, 2013). In *E. coli*, this is largely achieved through the regulation of Fur by SoxRS and by OxyR (Zheng *et al*., 1999; Pomposiello and Demple, 2001; Jang and Imlay, 2010). It should be noted that there are several examples of alternative isoenzymes in *E. coli* that are generated according redox-stress or aerobic status (e.g. aconitases A and B).

The results in Chapters 3 and 4 show that the iron-uptake activities of EfeUOB and FeoABC display opposite preferences for aerobiosis and anaerobiosis. One possible reason for this difference is that the two systems are adapted to respond to aerobic conditions in a fashion that limits the potential for iron-dependent redox stress. The hypothesis suggested here is that the

EfeUOB Fe^{2+}-uptake system is driven by H_2O_2 through EfeB-mediate peroxidase activity. Thus, this system would only be expected to function well aerobically when H_2O_2 production would occur as a result of aerobic metabolism. The weak EfeUOB activity seen anaerobically (Chapters 3 and 4, and Cao *et al*., 2007) could arise as a result of peroxide production within the culture media prior to anaerobiosis (Anjem *et al*., 2009; Jang and Imlay, 2010). FeoABC may be inhibited by H_2O_2 rather than oxygen per se, possibly through peroxide oxidation of the conserved Cys residues in the two Gate motifs of FeoB (Fig 5.1). Such a mechanism of inactivation would ensure that FeoABC does not continue to take up iron when *E. coli* becomes subject to a sudden exposure for peroxide. This proposed opposite responses of EfeUOB and FeoABC to peroxide would adequately explain the observed aerobic/anaerobic preferences of the two systems.

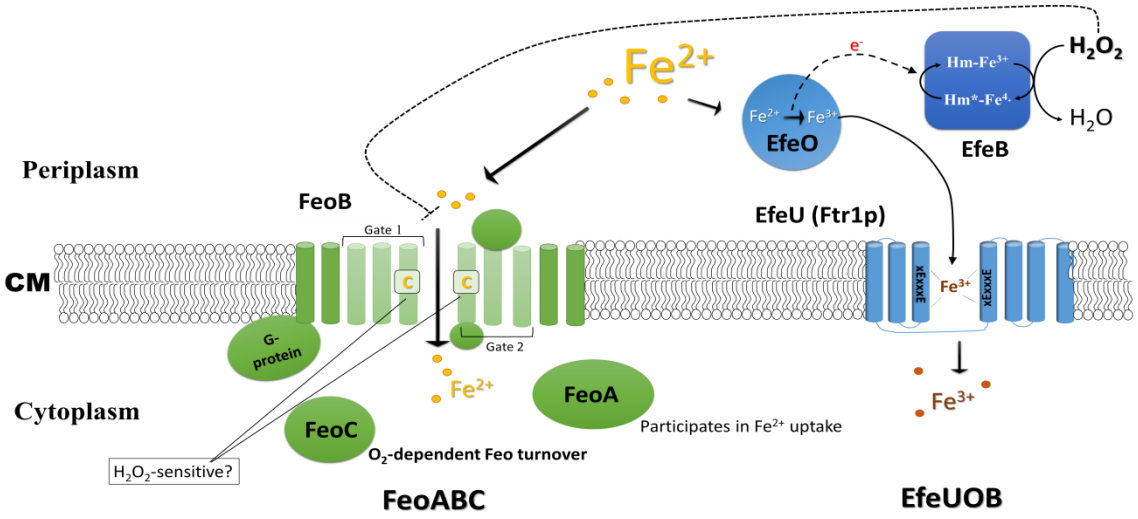

Figure 5.1. Schematic representation of the EfeUOB and Feo systems of *E. coli.* This figure illustrates a model for the EfeUOB and Feo systems of *E. coli*. Ferrous iron initially binds to the periplasmic EfeO at the HxxE motif. Then $Fe^{2+}$is oxidized and the released electrons are transferred to the proposed copper site of the cupredoxin domain and then to the ferryl-haem group of EfeB to return it back to its resting ferric state. The oxidized iron is transported across the cytoplasmic membrane by the ferric-iron permease protein EfeU (Rjasekaran *et al*., 2010). Efe Fe^{2+}-uptake is thus driven by H_2O_2 through EfeB-mediate peroxidase activity. Feo may be inhibited by H_2O_2, possibly through peroxide oxidation of conserved Cys residues in the FeoB Gate motifs I and II.

In order to determine whether the distinct responses of FeoABC and EfeUOB to oxygen are indeed peroxide dependent, this chapter explores the influence of H_2O_2, under low and high pH, with/without oxygen, on EfeUOB- or FeoABC-dependent low-iron growth.

5.2. Effect of H_2O_2 or catalase on growth of JC28 complemented with pHSG-*efeUOB*, pHSG-*feoABC* or pHSG576 under aerobic conditions

5.2.1 Introduction

The Efe system includes a haem-peroxidase periplasmic component (EfeB) predicted to act as an electron acceptor for ferrous iron oxidation during Efe-mediated iron uptake and to use H_2O_2 as oxidant to dispose of electrons received from Fe^{2+} oxidation, thus enabling the feroxidation process. Therefore, the ferrous iron uptake reaction of Efe should be dependent on the presence of hydrogen peroxide if the above hypothesis is correct. This possibility was tested here by growth of *E. coli* JC28 *efe* or *feo* transformants with H_2O_2 or catalase using a Bioscreen C apparatus for growth of bacteria under aerobic conditions. Single colonies of JC28 transformants with pHSG-*efeUOB*, pHSG-*feoABC* or pHSG576 (vector control) were taken from M9 plates for inoculation into 5 ml of M9 liquid medium (with iron). The cultures were incubated overnight at 37 °C and 250 rpm, and cells were then washed and diluted in fresh medium give a final OD_{600} of 0.01. Growth was then monitored in 100-well plates using a Bioscreen, using 300 µl volumes of low-Fe M9 medium in each well, over a 24 h period, whilst shaking at 37 °C. Growth conditions were varied by inclusion/exclusion of the following additions: 20 µM DTPA, 16 µM $MnCl_2$, 2 mM ascorbic acid, 100 mM MES (pH 6), 100 mM MOPS (pH 7), 100 mM TAPS (pH 8), and various concentrations of H_2O_2 or catalase. The presence of 16 µM Mn, 20 µM DTPA and 2 mM ascorbate at pH 6 was previously shown to

generate a strong growth advantage for *efeUOB*-containing wildtype *E. coli* (Cao *et al*., 2007) and so these conditions were selected for use here.

Since the pHSG576 constructs were used here, the *efeUOB* and *feoABC* genes remained under control of their native promoters/operators.

5.2.2 Results

Initially, the impact of H_2O_2 or catalase addition was tested on the growth of JC28 complemented with pHSG-*efeUOB* or pHSG-*feoABC* under low pH (6) and iron-restriction conditions (Fig. 5.2). Addition of 200 µM H_2O_2 gave a 17% growth enhancement for the pHSG*efeUOB*^{O157} strain with respect to the condition without addition (at 24 h, $P < 0.05$; Fig 5.2A). Similar results were seen with the pHSG*efeUOB*^{K12} strain (Fig. 5.2B). For the vector control however, addition of 200 µM H_2O_2 resulted in reduced growth by ~2.8 fold with respect to the no-addition control (Fig. 5.2D). In contrast, when catalase was added in place of hydrogen peroxide, neither the vector control nor *efe* complemented strains could grow well over 24 h (Fig. 5.2). This was a surprise, and it remains unclear why growth of the vector control would be affected by catalase since this would be expected to have either no effect or a slightly beneficial effect (through depletion of peroxide). Thus, the poor growth of the *efe*-containing strain with catalase is not due to loss of Efe function caused by depletion of peroxide, and the reason for this effect remains unclear.

For JC28 complemented with pHSG-*feoABC*, growth was diminished by 200 µM H_2O_2, although a similar effect was seen for the vector control suggesting that the lower growth is related to peroxide toxicity rather than a direct effect on iron uptake (Figs. 5.2C & D). However, with catalase growth was greatly increased (by ~1.8 fold at 24 h with respect to the non-addition control; Fig. 5.2C), unlike for the vector control and pHSG*efeUOB* strains were growth was diminished (Fig. 5.2), indicating that the ability of Feo to promote low-iron growth is enhanced

when hydrogen peroxide levels are lowered. This result is consistent with EfeUOB-dependent iron uptake being promoted by hydrogen peroxide and FeoABC-dependent iron uptake being inhibited by peroxide. It also matches previous (Kammer *et al*., 1993) indicating that Feo is only functional anaerobically or micro aerobically. Indeed, these results would indicate that the lack of Feo activity when oxygen is abundant is related to peroxide inhibition, which would also explain why the *feoABC* operon is anaerobically induced.

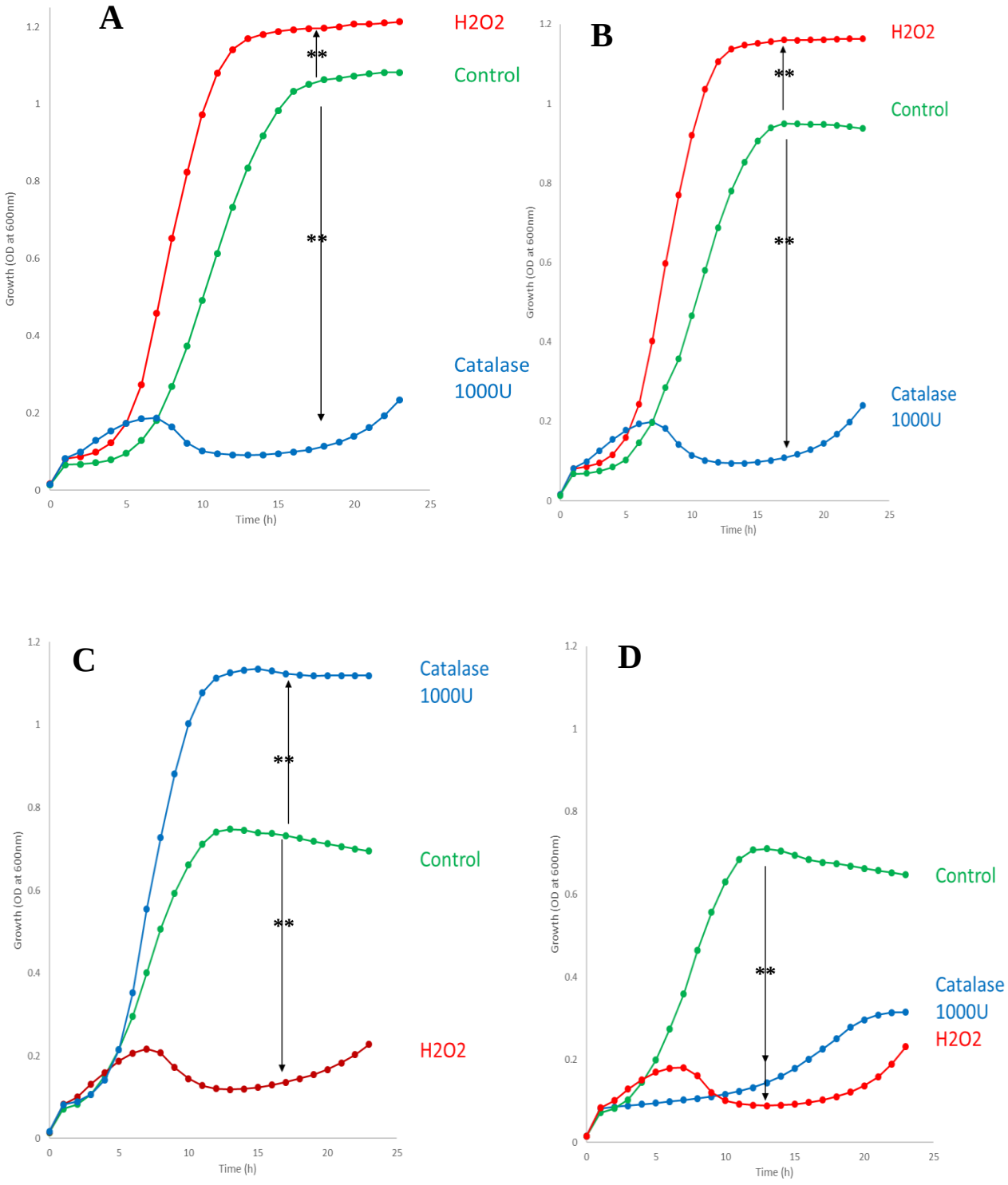

Figure 5.2. Effect of peroxide and catalase on FeoABC and EfeUOB^{O157}-dependent growth under low-iron conditions at pH 6. Strain used was JC28 with pHSG-*efeUOB*^{O157}. Medium was 0.4% glucose in M9 medium at pH 6 (plus 50 µg/ml chloramphenicol), with 16 µM $MnCl_2$, 20 µM DTPA, 100 µM MES (pH 6) and 2 mM ascorbic acid. Growth was at 37 ˚C in a Bioscreen apparatus (300 µl

volumes) with constant shaking at 250 rpm. Values are averages of three biological replicates, each performed as technical triplicates. Pre-cultures were grown overnight in 0.4% glucose M9 medium with iron citrate (37 ˚C, 250 rpm). Starting cell density of all Bioscreen cultures was adjusted to OD_{600} 0.01. 200 µM H_2O_2 or 1000 U/ml catalase (*Micrococcus lysodeikticus*) were added as indicated. Statically significant difference ($P<0.05$) as determined by Graph Prism One-way Anova at 24 h of growth is indicated. Effect of peroxide and catalase on (**A**) $EfeUOB^{O157}$-, (**B**) $EfeU*OB^{K-12}$-, (**C**) $feoABC^{O157}$-, and (**D**) pHSG576-dependent growth under low-iron conditions at pH 6**.**

The effect of catalase and peroxide addition was compared for all four transformants carrying pHSG576-derived plasmids in a single set of growth experiments (Fig. 5.3). The results confirm that only the *feo*-complemented strain is favoured by the provision of catalase, growth of the other strains is very weak with catalase (confirming the results above). In contrast, only growth of the *efe*-complemented strain is supported upon addition of peroxide, again confirming the data above. Peroxide inhibited growth for both the Feo strains and vector control by ~5 fold compared with the Efe-complemented strain. Catalase increased growth of the Feo-complemented strain by 4.6-fold at 24 h, whereas the vector control and Efe-complemented strain showed a reduced growth with catalase (Fig. 5.3).

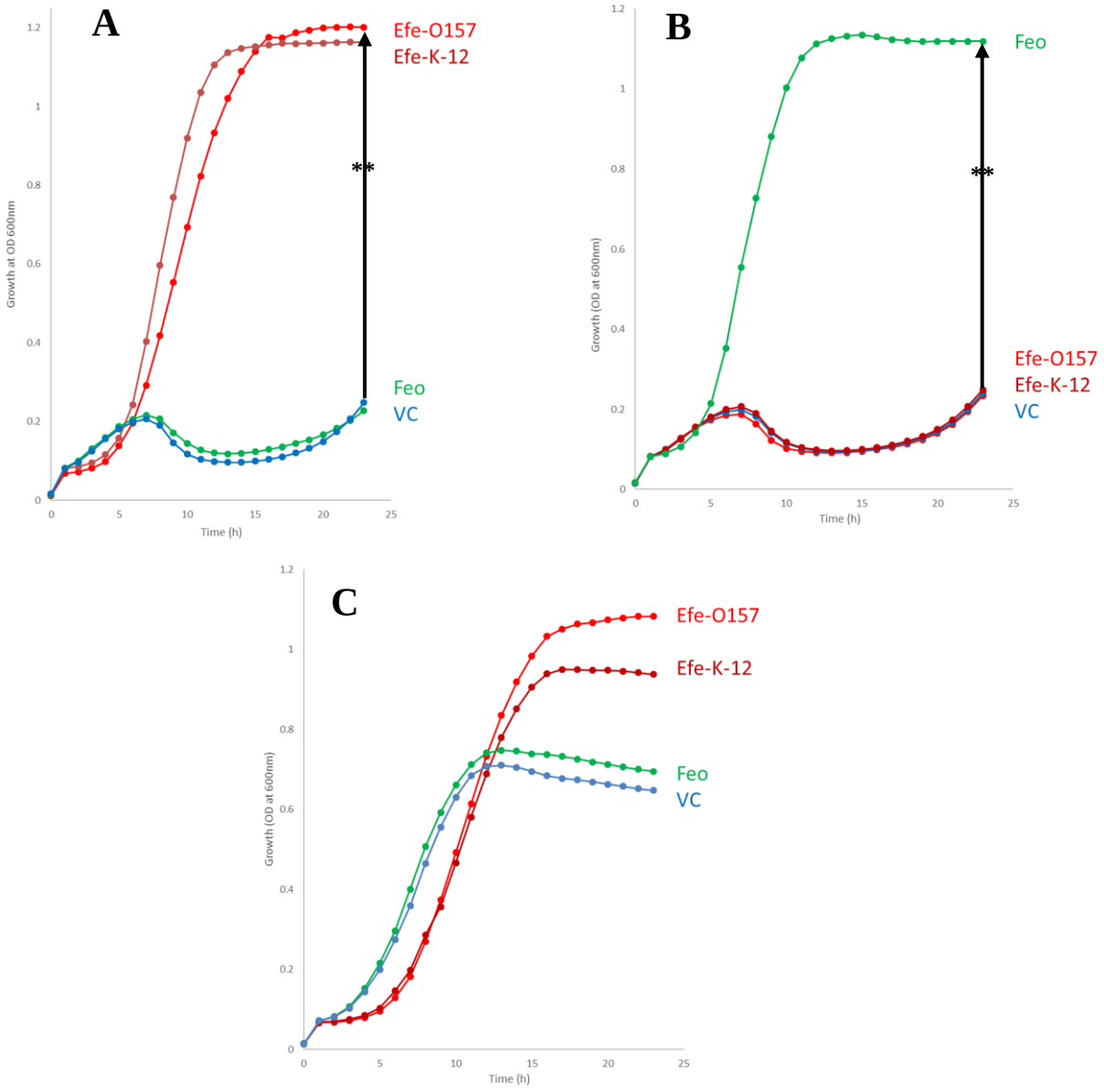

Figure 5.3. Effect of H_2O_2 and catalase on low-iron growth at pH 6 for *E. coli* JC28 transformed with pHSG-*efeU*OB*$^{K-12}$, pHSG-*efeUOB*^{O157} and pHSG-*feoABC*^{O157}. Details are as for Fig. 5.2 with JC28 transformed with pHSG576, pHSG-*efeU*OB*$^{K-12}$, pHSG-*efeUOB*^{O157} and pHSG-*feoABC*^{O157}. **A. H_2O_2** was at 200 µM; **B. catalase** was 1000U/ml. **C. no addition** as a control. Statistically significant differences (P<0.01) as determined by Graph Prism One way Anova are indicated at 24 h.

5.3. Analysis of the effects of a range of H_2O_2 and catalase levels on iron-restricted growth of *efeUOB* or *feoABC* complemented JC28

The above work showed opposite effects of hydrogen peroxide on EfeUOB- and FeoABC-dependent low-iron growth of JC28. The pH employed was 6, where *efeUOB* is known to be well expressed and give a strong growth advantage (Cao *et al*., 2007). In the work below, growths were repeated with a range of concentrations of peroxide and catalase to determine whether the effects of these agents are quantitative. Other conditions remained unchanged.

The results in Fig. 5.4A show that as the level of H_2O_2 was raised (20-160 μM) the degree of growth inhibition of the *feoABC*-complemented strain was increased. The greatest relative degree of growth inhibition was seen with addition of 20 μM H_2O_2 (~2.3 fold at 24 h; Fig. 5.4A), with higher concentrations causing smaller increments in inhibition. However, the results in Fig. 5.4B show that as the level of H_2O_2 was raised (20-160 μM) the degree of growth enhancement of the *efeUOB*-complemented strain was increased. The greatest relative degree of growth enhancement was seen with addition of 160 μM H_2O_2 (~1.4 fold at 24 h; Fig. 5.4B), with higher concentrations causing smaller increments in enhancing. On the other hand, the vector control showed inhibited growth with addition of 20 μM H_2O_2 (~2.4 fold at 13 h; Fig. 5.4C), with higher concentrations causing smaller increments in inhibition.

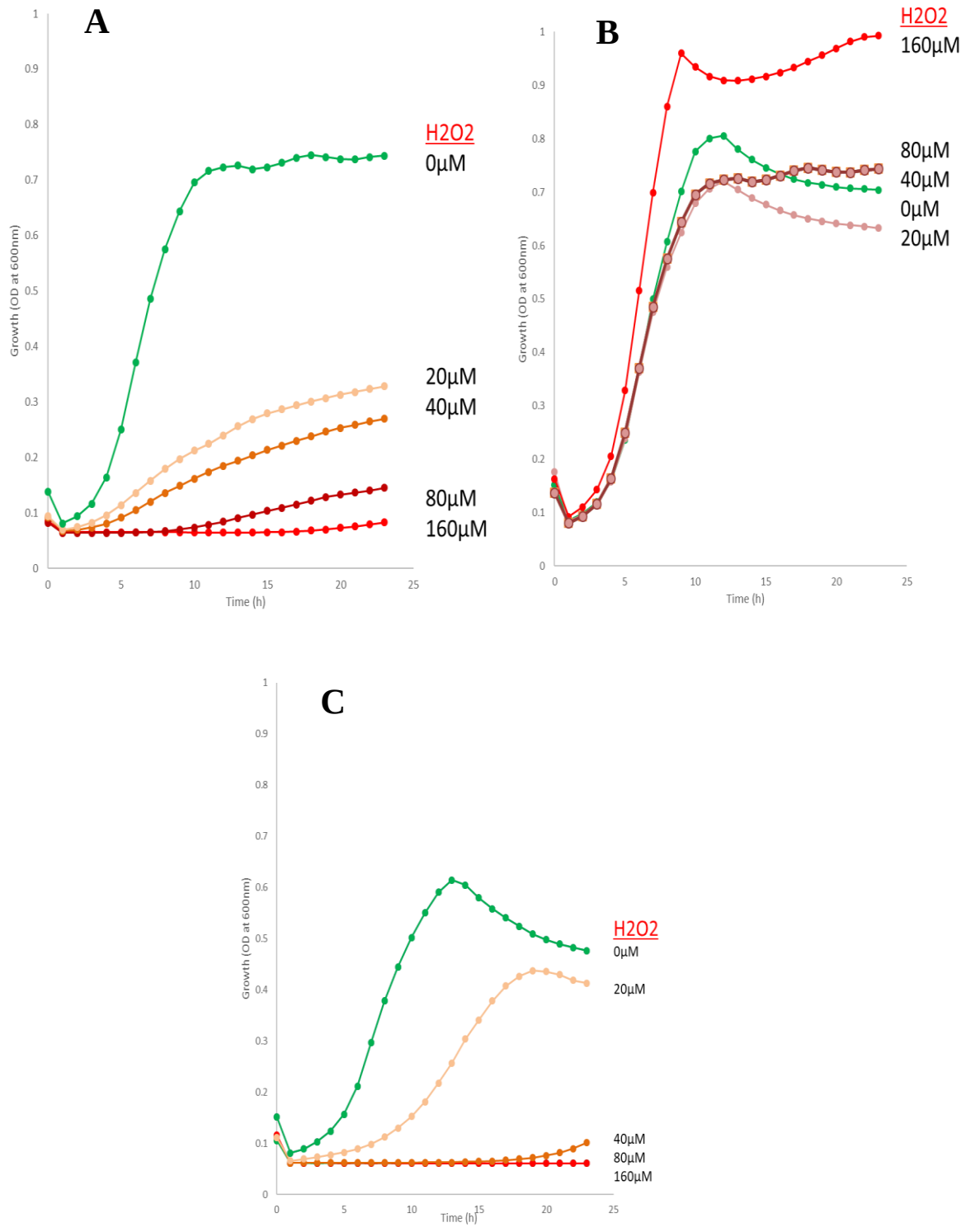

Figure 5.4. Effect of H_2O_2 concentration on low-iron growth at pH 6 of *E. coli* JC32 transformed with (A) pHSG-*feoABC*^{O157}, (B) pHSG-*efeUOBC*^{O157} or (C) vector only. Details are as above in Fig. 5.2 except for the range H_2O_2 concentrations, which were as indicated.

In response to increasing catalase concentrations at pH 6, the *feoABC* transformant displayed a concentration-dependent increase in iron-restricted growth (Fig. 5.5). This well matches the results obtained previously supporting the view that peroxide inhibits Feo-dependent iron uptake aerobically. This effect could either be a direct effect on the transport process, or a regulatory impact on *feo* expression (or Feo proteolytic turnover). In contrast, the vector control was sensitive to catalase (Fig. 5.5C) at pH 6 with a quantitative decrease in growth displayed with increasing catalase addition. This is similar to the effect observed before (Section 5.2) and it remains unclear how catalase is causing the observed growth reduction for the vector control. However, as Feo clearly provides a major growth advantage under iron restriction, with catalase, this supports the suggestion that FeoABC-dependent iron uptake is subject to peroxide inhibition.

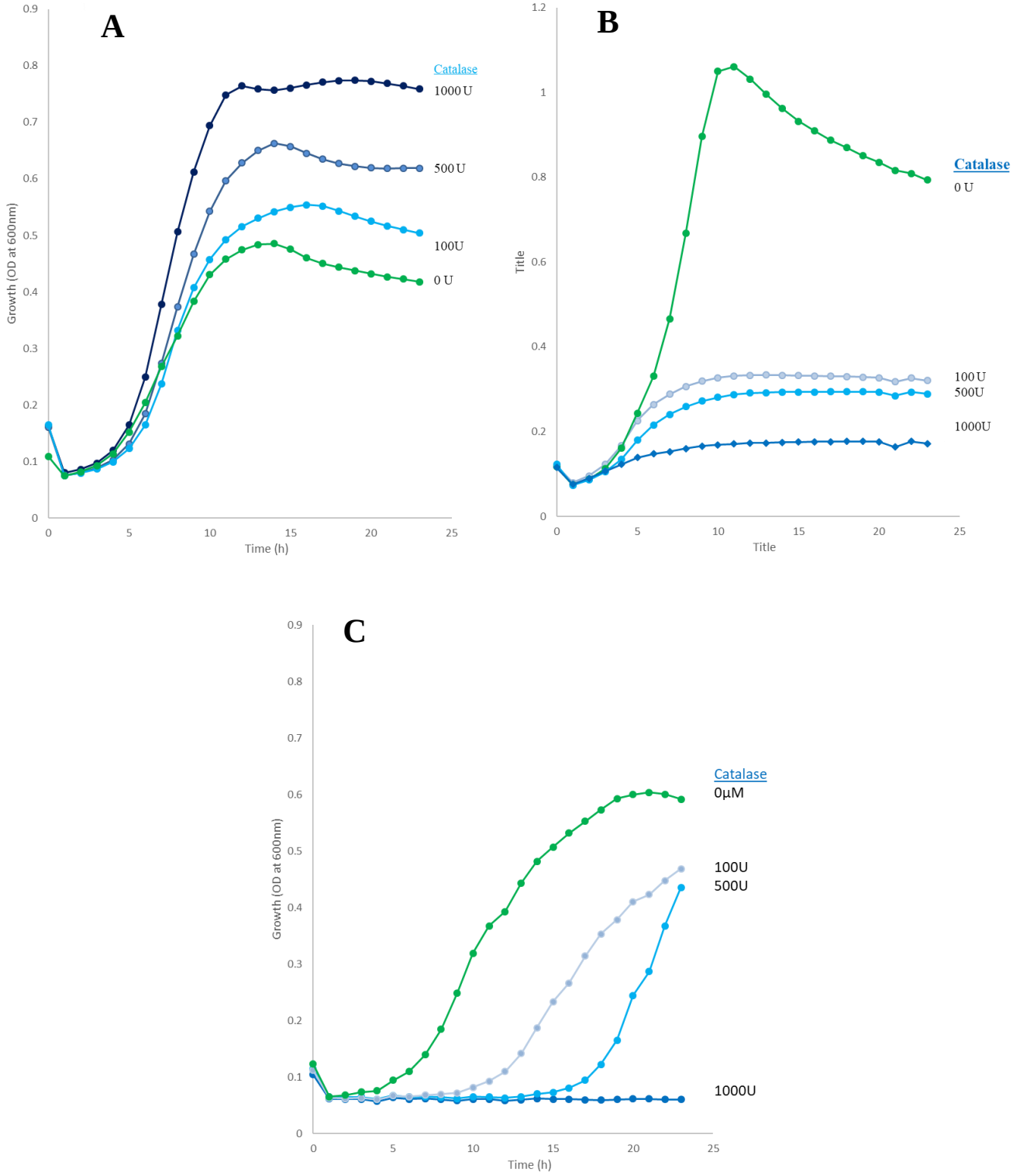

Figure 5.5. Effect of catalase concentration on low-iron growth at pH 6 of *E. coli* JC32 transformed with (A) pHSG-*feoABC*^{O157} , (B) pHSG-*efeUOBC*^{O157} or (C) vector cononlytrol. Details are as in Fig. 5.2 but with a range of catalase levels used (100-1000 U/ml). Buffer was 100 mM MES (pH 6).

5.4. Effect of hydrogen peroxide and catalase on JC32 (JC28 lacking *efeU*), complemented with inducible forms of *feoABC* or *efeUOB*

5.4.1 Introduction

The experiments described above show that Feo- and Efe-supported iron-restricted growth responds distinctly to peroxide in the medium. Since the above work was performed with the *feo* and *efe* operons under control of their native promoters, any effect of peroxide might be caused by changes in expression. For this reason, the *feo* and *efe* operons were placed under control of controllable promoters (as described above) that would not be expected to respond to environment conditions of relevance (pH, redox, iron). This allows the above experiments to be repeated under circumstances were expression effects can be well controlled. Furthermore, the JC28 strain used previously was replaced with a derivative (JC32) lacking *efeU* (deletion of the ferric permease gene) in order to ensure no biological effect would be exerted by any chromosomally expressed EfeU.

Thus, the response of the Efe and Feo iron-transport systems to H_2O_2 and catalase was further explored using the pBADara/rha vectors under inducing conditions.

5.4.2. Effect of EfeUOB^{O157} complementation on aerobic iron-restricted growth with H_2O_2 or catalase

The results show a modest impact of peroxide at pH 6 in increasing the growth of the *efeUOB*^{O157} transformants (Figs. 5.6A & B), and thus resemble the results obtained with the *efeUOB* operon under control of its native promoter (Chapter 4). This modest increase contrasts greatly with the dramatic growth inhibition caused by peroxide seen for the vector control under the same conditions (Fig. 5.4C). Thus, peroxide caused a clear increase in low-iron growth for

the *efeUOB* transformants with respect to the vector control. This finding further supports a role for peroxide in stimulating EfeUOB dependent low-iron growth and indicates that the effect is not caused by peroxide-mediated transcriptional control of *efeUOB*.

In contrast to peroxide, catalase almost entirely eliminated growth of the *efeUOB*^{O157} transformants, which reflects findings made with the vector controls.

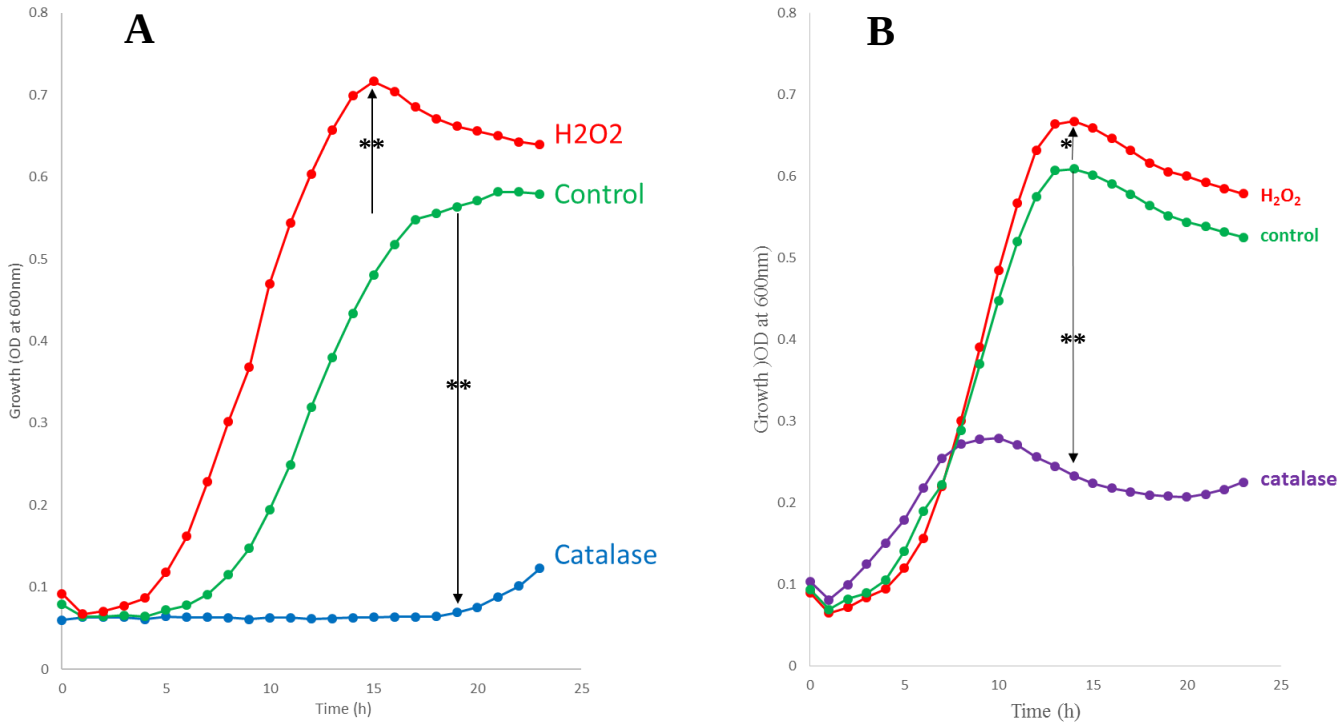

Figure 5.6. Effect of H_2O_2 and catalase on growth of *E. coli* JC32 transformed with (A) pBADrha-*efeUOB*^{O157} or (B) pBADara-*efeUOB*^{O157}. Strains were grown aerobically in low-iron conditions on M9 medium with 100 mM MES (pH 6), 0.4% glucose with 16 µM $MnCl_2$, 20 µM DTPA and 2 mM ascorbic acid. **A.** Strain was JC32 with pBADara-*efeUOB*^{O157}. Arabinose was included as inducer. Data represent the mean OD values of triplicates. H_2O_2 addition, 200 µM; catalase addition, 1000 U. **B.** Strains were grown as in A, except for use of pBADrha-*efeUOB*^{O157} in place of the pBADara plasmid, and the inclusion of rhamnose in place of arabinose. Appropriate antibiotic was included. A plate reader was used for growth at 37 °C for 24 h with shaking every 5 min. Statistically significant differences ($P<0.01$) as determined by Graph Prism One way Anova are indicated at 16 h.

5.4.3 Effect of 'corrected' *efeUOB* from *E. coli* K-12 complementation on aerobic iron-restricted growth with H_2O_2 or catalase

In order to test whether the 'corrected' EfeU*OB system of *E. coli* K-12 could also stimulate low-iron growth when induced from pBADara, and show a response to peroxide, the pBADara-*efeU*OB*$^{K-12}$ complemented JC32 strain was tested as described above. A similar result was obtained (Fig. 5.6 A & B) showing that the EfeUOB systems of the K-12 and O157 strains exhibit similar peroxide dependencies that are independent of transcriptional control effects.

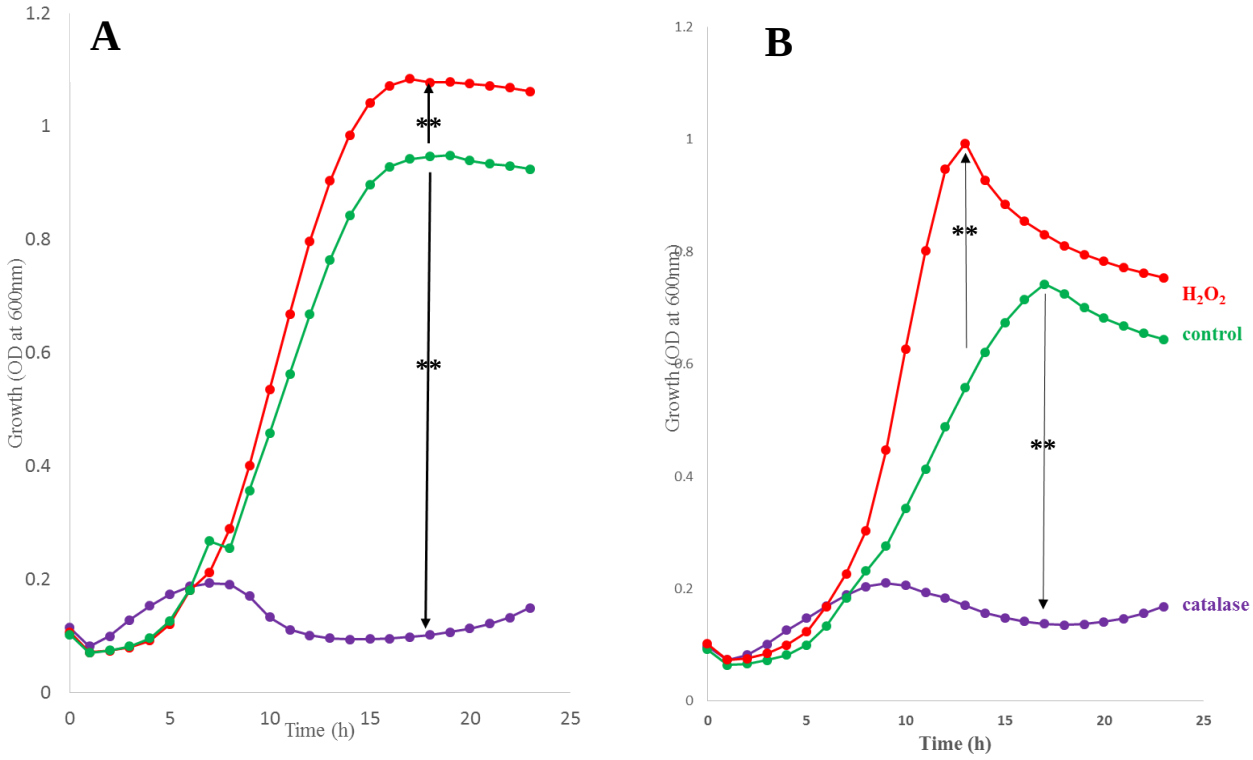

Figure 5.7. Effect of H_2O_2 and catalase on growth of *E. coli* JC32 transformed with (A) pBADrha-*efeU*OB*$^{K-12}$ or (B) pBADara-*efeU*OB*$^{K-12}$. Conditions were as above except for the use of pBADrha-*efeU*OB*$^{K-12}$ or pBADara-*efeU*OB*$^{K-12}$ Relevant inducer was included. Significant differences are indicated at 19 h growth compared.

5.4.4 Effect of *feoABC* complementation on aerobic iron-restricted growth with H_2O_2 or catalase

The results with the pBADara-*feoABC* transformant at pH 6 were again similar to those obtained with the pHSG576 constructs (Figs. 5.7A & B). Catalase raised growth under iron restriction in a quantitative fashion whereas peroxide prevented growth. Thus, as for EfeUOB, it can be concluded that the effects of peroxide on Feo-dependent low iron growth are not related to alterations in expression (although could be related to Feo turnover).

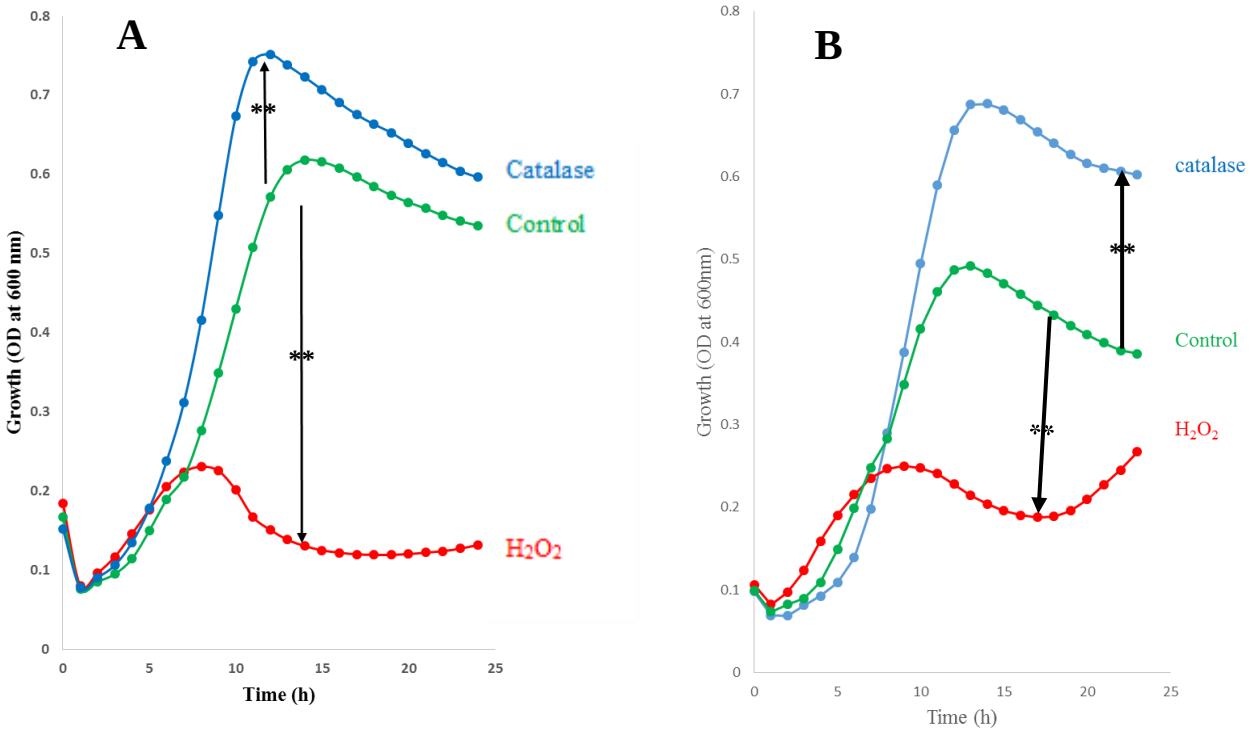

Figure 5.8. Effect of H_2O_2 and catalase on growth of *E. coli* JC32 transformed with (A) pBADrha-*feoABC*^{O157} or (B) pBADara-*feoABC* ^{O157}. As above, but with pBADrha-*feoABC*^{O157} or pBADara-*feoABC*^{O157}. H_2O_2 addition, 200 µM; catalase addition, 1000 U. Statistically significant differences ($P<0.01$) are indicated at 13 h.

5.4.5. Effect of pBAD-vector control on aerobic iron-restricted growth with H_2O_2 or catalase

Addition of catalase or H_2O_2 to the cultures of JC32 carrying pBADara under iron restriction resulted in growth inhibition (Fig. 5.7A & B), as was the case previously with JC28 carrying pHSG576. Similar results were obtained with pBADrha with peroxidase and slightly difference with catalase. Thus, the low-iron growth increase seen for the pBAD-*efeUOB* transformants with peroxide, and for the pBAD-*feoABC* transformants with catalase, are mediated by the presence of the corresponding ferrous-iron transporters.

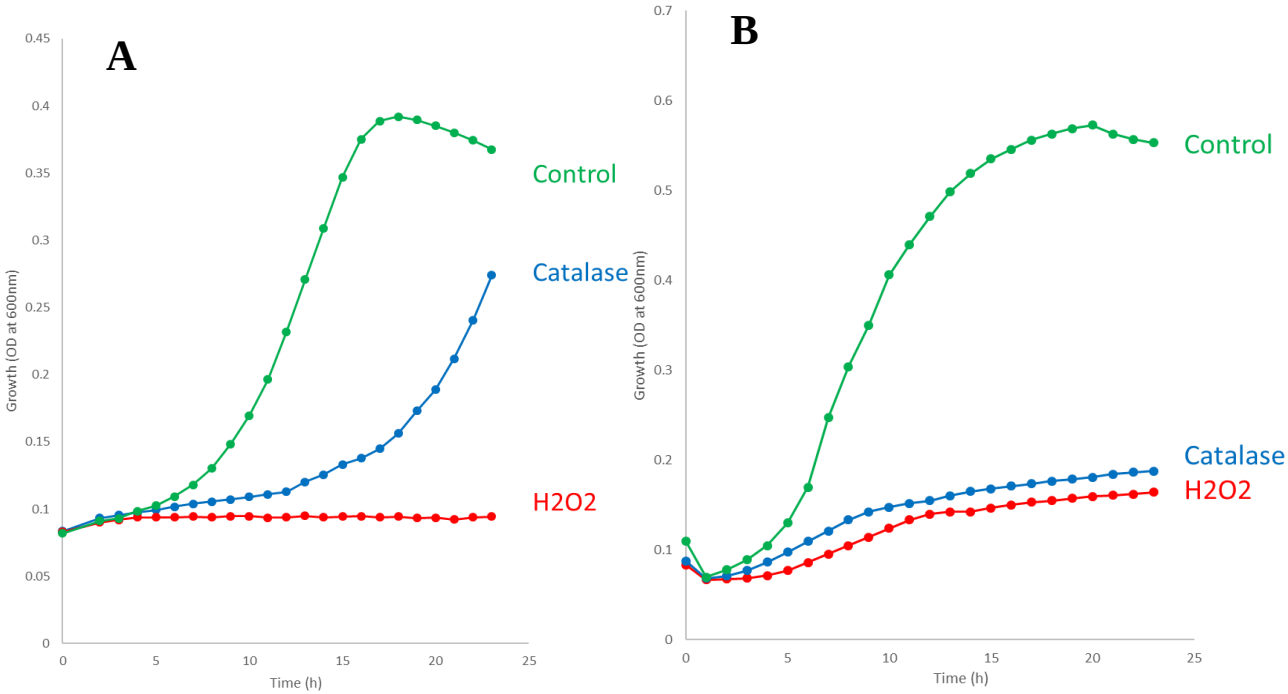

Figure 5.9.: Effect of H_2O_2 and catalase on growth of *E. coli* JC32 transformed with pBADrha (A) or pBADara (B). As above, but with pBADrha or pBADara. H_2O_2 addition, 200 µM; catalase addition, 1000 U.

5.5. Analysis of the effects of a range of H_2O_2 and catalase levels on iron-restricted growth of *efeUOB* or *feoABC* cloning into inducible promotor pBADrha and pBADara complemented JC32

The above work showed with low copy pHSG765 vector opposite effects of hydrogen peroxide on EfeUOB- and FeoABC-dependent low-iron growth of JC32. The pH employed was 6, where *efeUOB* is known to be well expressed and give a strong growth advantage, In the work below, growths were repeated with a range of concentrations of peroxide and catalase to determine whether the effects of these agents are quantitative into inducible promotor. Other conditions remained unchanged.

The results in Fig. 5.8A show that as the level of H_2O_2 was raised (20-160 μM) the degree of growth inhibition of the *feoABC*-complemented strain was increased. The greatest relative degree of growth inhibition was seen with addition of 20 μM H_2O_2 (1.3 fold at 24 h; Fig. 5.10A), with higher concentrations causing smaller increments in inhibition. However, the results in Fig. 5.10B show that as the level of H_2O_2 was raised (20-160 μM) the degree of growth enhancement of the *efeUOB*-complemented strain was increased. The greatest relative degree of growth enhancement was seen with addition of 160 μM H_2O_2 (~1.4 fold at 15 h; Fig. 5.10 B), with higher concentrations causing smaller increments in enhancing. On the other hand, vector control shown inhibition growth with addition of 20 μM H_2O_2 (~1.6 fold at 24 h; Fig. 5.10C), with higher concentrations causing smaller increments in inhibition.

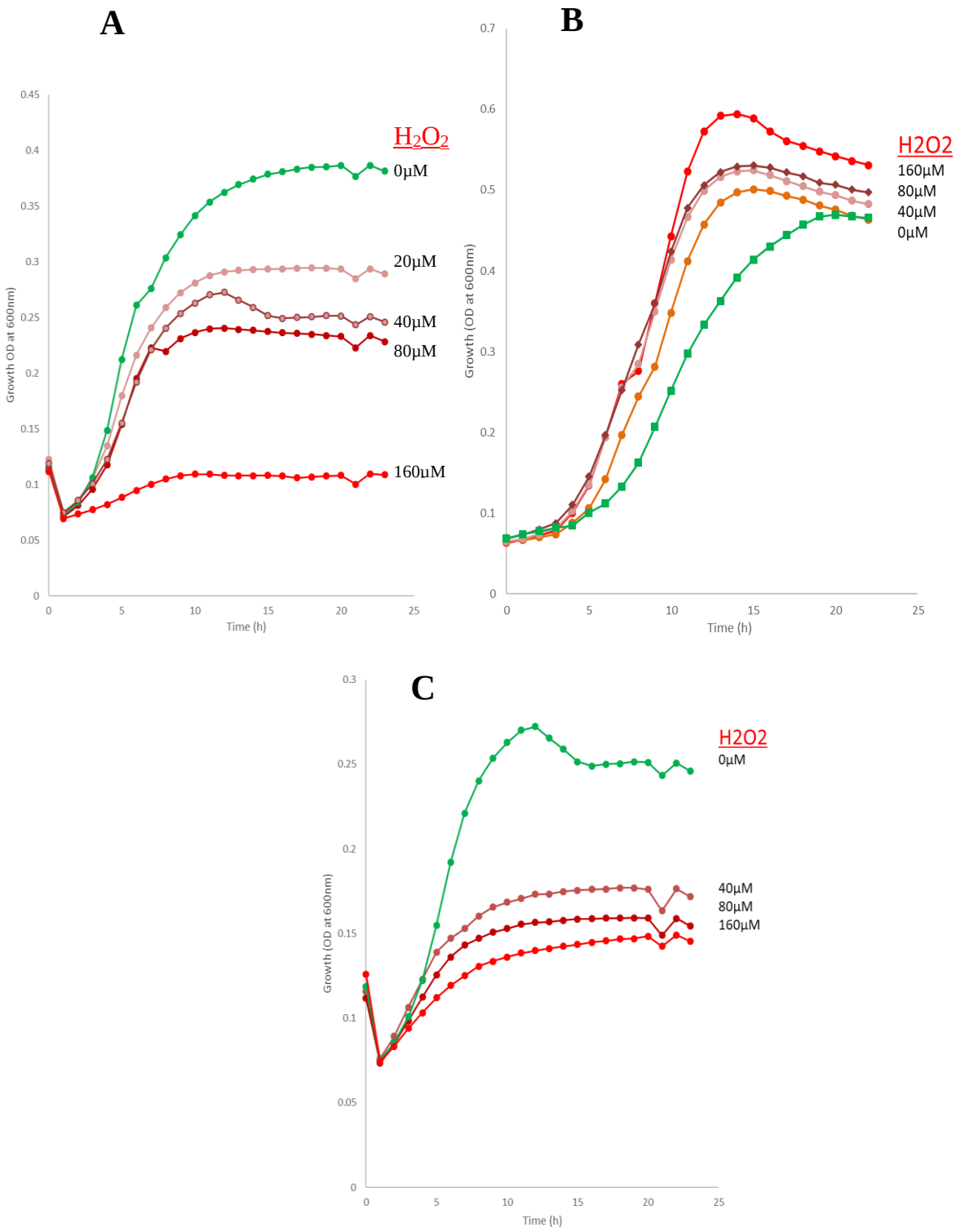

Figure 5.10. Effect of H_2O_2 concentration on low-iron growth at pH 6 of *E. coli* JC32 transformed with (A) pBADara-*feoABC*^{O157} , (B) pBADara-*efeUOBC*^{O157} or (C) pBADara vector control. Details are as above in Fig. 5.2 except for the range H_2O_2 concentrations, which were as indicated, and use of a kinetic plate reader to perform and measure growth (with shaking every 5 min).

As previous experiment used range concentration from catalase(100-1000U/ml) in response to increasing catalase concentrations at pH 6 with low copy number plasmid in this experiment used inducible plasmid, the *feoABC* transformant gave a concentration-dependent increase in iron-restricted growth (Fig. 5.11A) similar with results above. This well matches the results obtained previously supporting the view that peroxide inhibits Feo-dependent iron uptake aerobically. This effect could either be a direct effect on the transport process, or a regulatory impact on *feo* expression. On the other hand, the vector control was sensitive to catalase (Fig. 5.11C) at pH 6 with a quantitative decrease in growth displayed with increasing catalase addition. This is similar to the effect observed before (Section 5.2D). However, as Feo clearly provides a major growth advantage under iron restriction, with catalase, this supports the suggestion that FeoABC-dependent iron uptake is subject to peroxide inhibition.

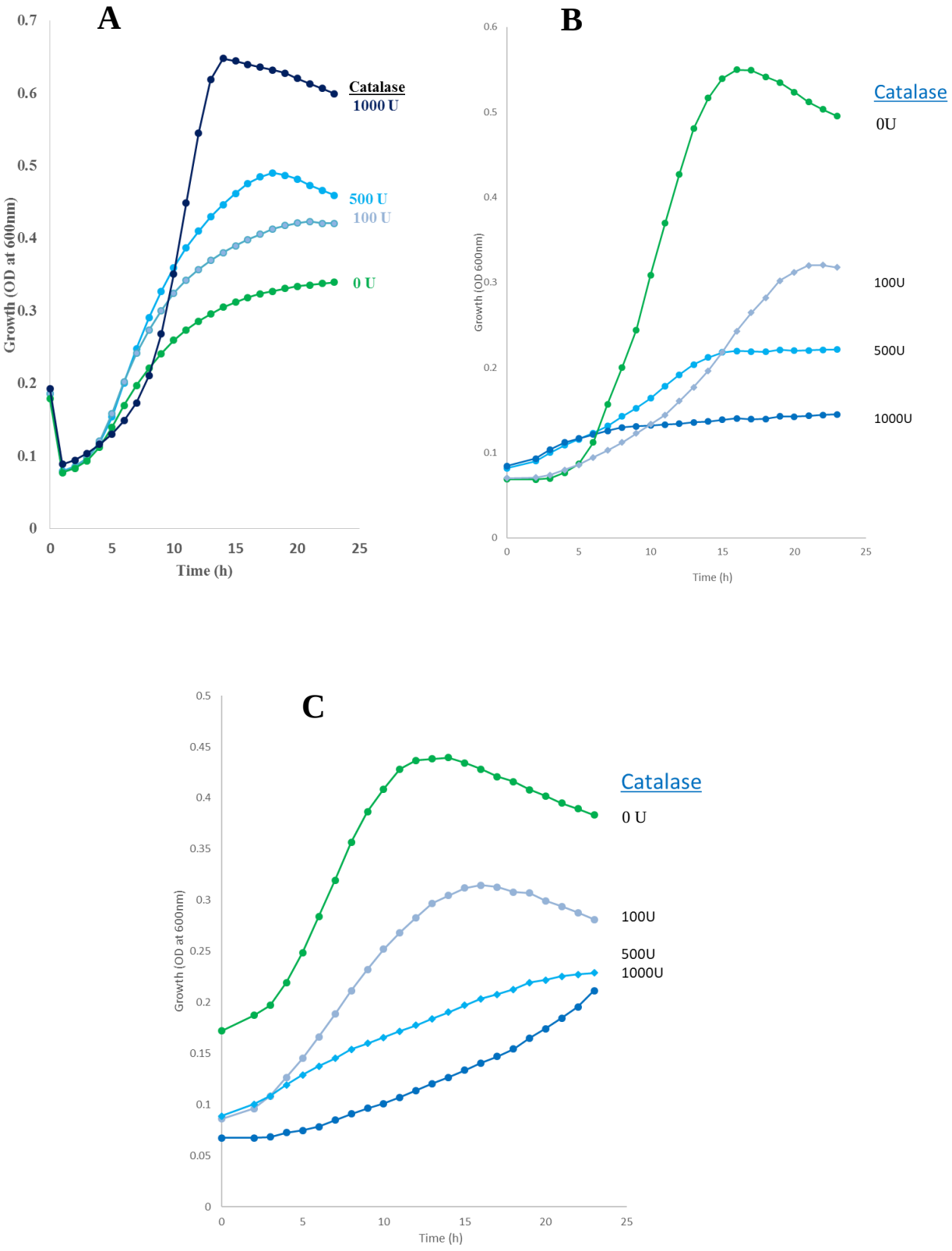

Figure 5.11. Effect of catalase concentration on low-iron growth at pH 6 of *E. coli* JC28 transformed with (A) pBADara-*feoABC*^{O157} , (B) pBADara-*efeUOBC*^{O157}, (C) pBADara vector control. Details are as in Fig. 5.2 but with a range of catalase levels used and use of a plate reader for growths with shaking every 5 min. Buffer was 100 mM MES (pH 6).

5.6. Effect of chromosomal *efeO* mutation on pBAD-borne *efeUOB*- mediated growth enhancement under under Fe-restriction

Since the JC32 and JC28 strains retain copies of *efeO* and *efeB,* the impact of lack of chromosomal *efeO* on pBADara-*efeUOB*^{O157} dependent enhanced growth under low iron conditions was tested – it was considered possible that a greater growth enhancement might be observed (for the *efeUOB* plasmid) since the chromosome of JC33 carries two *efe* mutations (*efeU* frameshift mutation; Δ*efeO*::*kan*) such that expression of both *efeU* and *efeO* would be entirely dependent on complementation. Results obtained (Fig. 5.12) indicate that a similar growth advantage was achieved as that seen for the corresponding JC32 transformants, with a similar response to peroxide and catalase. Thus, the vector borne *efeUOB* system has no/little requirement for the chromosomally encoded EfeO. As similar findings were obtained to those seen previously for both the pBADara-*feoABC* and –*efeUOB* JC33 transformant (Figs. 5.12-13), the results serve to further confirm the contrasting effects of peroxide on Efe and Feo-dependent low iron growth. In contrast, the vector control was sensitive to H_2O_2 (Fig. 5.14) at pH 6 with a quantitative decrease in growth displayed with catalase addition.

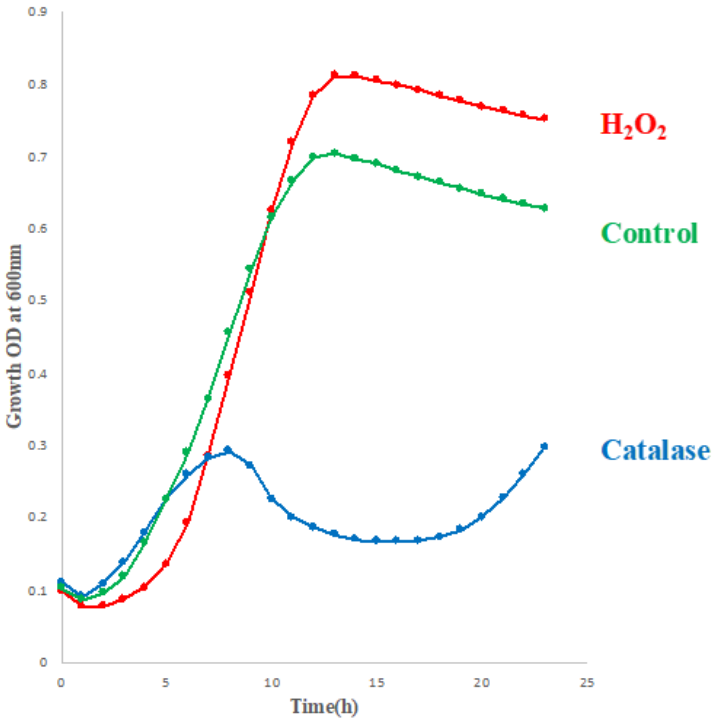

Figure 5.12. Effect of H_2O_2 and catalase on growth of *E. coli* JC33 transformed with pBADara-*efeUOB*^{O157}. Strains were grown as above aerobically in M9 medium with 100 mM MES (pH 6), 0.4% glucose with 16 µM $MnCl_2$, 20 µM DTPA and 2 mM ascorbic acid. Data represent the mean OD values of triplicates. H_2O_2 addition, 200 µM; catalase addition, 1000 U.

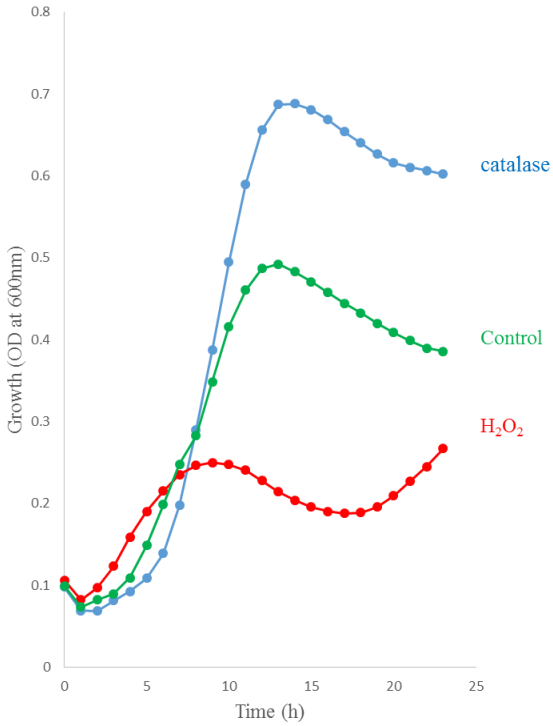

Figure 5.13. Effect of H_2O_2 and catalase on growth of *E. coli* JC33 transformed with pBADara-*feoABC*. Details are as above except for the use of pBADare-*feoABC*.

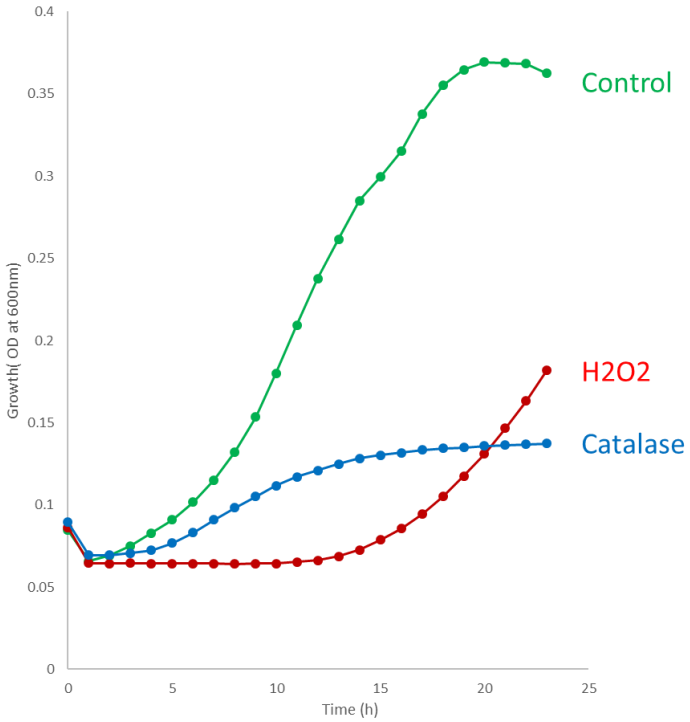

Figure 5.14. Effect of H_2O_2 and catalase on growth of *E. coli* JC33 transformed with pBADara. Details are as above except for the use of pBADara as a control.

5.7. Effect of pH on H_2O_2- and catalase-influenced Efe- and Feo-supported low-iron growth

Here, the impact of pH of the peroxide-sensitivities of Feo- and Efe-supported low-iron growth is considered. The Efe system is acid induced and the experiments above suggest that Efe functions more effectively at low pH. Results below again show that Efe activity is promoted by peroxide whereas Feo acitivity is inhibited by peroxide (Fig. 5.15). Overall, the response to peroxide (catalase and H_2O_2) was stronger for both Feo and Efe at pH 6 than at pH 8. This might reflect the pH dependence of aerobic ferrous iron stability. To confirm that the effects seen are specific to Feo and Efe activity, vector control data must be considered (Fig. 5.16). This demonstrates that, at pH 7, the greater growth of the *feo*-complemented strain with catalase (Fig. 5.15C) is not observed for the control (5.16B), and that the lower growth of the *efe*-

complemented strain with catalase (Fig. 5.15D) and higher growth with peroxide (Fig. 5.15D) is also not observed for the vector control (Fig. 5.16B). This indicates that the Feo- and Efe-specific peroxide effects described above (at pH 6) are also exhibited at pH 7. At pH 8, the vector control showed a reduced growth with catalase (Fig. 5.16C) whereas the *feo*-complemented strain showed an enhanced growth (Fig. 5.15E). The vector control also showed a reduced growth with peroxide whereas the *efe*-complemented strain continued to show an enhance growth (Fig. 5.15F). These findings indicate that the Efe/Feo peroxide effects are also relvant at pH 8.

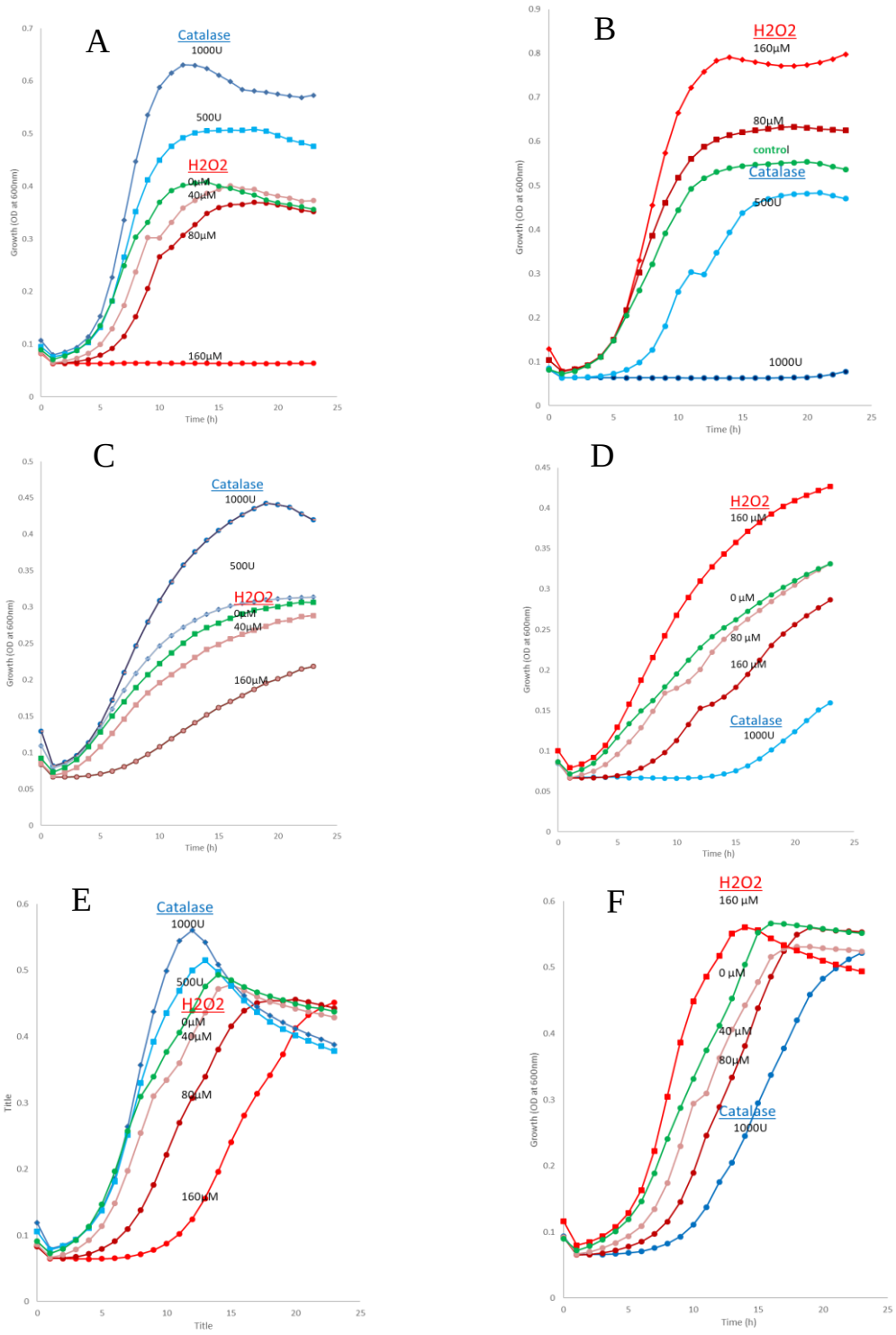

Figure 5.15.A Effect of H_2O_2 and catalase on growth of *E. coli* JC32 transformed with pBADara-*feoABC* (A, C, E) or pBADara-*efeUOB* (B, D, F) at pH 6-8. pH 6 (A, B), pH 7 (C, D), pH 8 (E, F). Strains were grown aerobically in M9 medium with 100 mM MES, MOPS or TAPS (pH 6, 7 or 8 respectively), 0.4% glucose with 16 µM $MnCl_2$, 20 µM DTPA and 2 mM ascorbic acid. Data represent the mean OD values of triplicates.

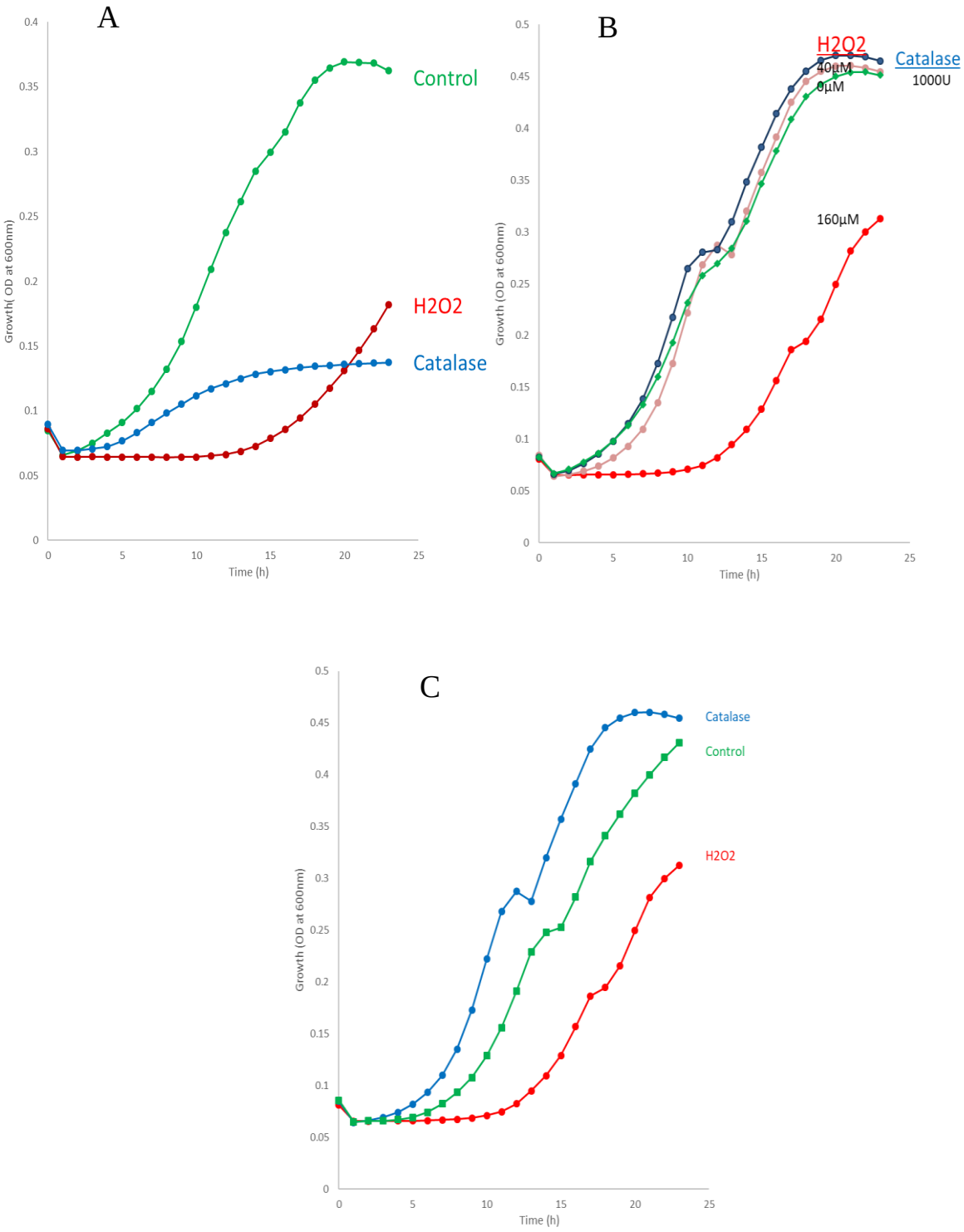

Figure 5.16. Effect of H_2O_2 and catalase on growth of *E. coli* JC32 transformed with pBADara at (A) pH 6, (B) pH 7 and (C) pH 8. All details as above Fig. 5.15 except for use of pBADara. Data represent the mean OD values of triplicates. H_2O_2 addition, 200 µM; catalase addition, 1000 U.

5.8. Effect for reductant (ascorbate)

The impact of the reductant, ascorbate, on the low-iron growth enhancement achieved by EfeUOB and FeoABC was tested. It was expected that the activity of both Efe and Feo in JC32 would be supported by ascorbate since both systems are considered to be specific (or display preference for) ferrous iron, and ascorbate would be expected to convert any ferric iron in the medium to the ferrous form. The growth experiments were performed in M9 medium with 1 μM DTPA, 0.4% glucose, 100 mM MES buffer at pH 6, no Mn^{2+}, with or without 2 mM ascorbate (Fig. 5.17).

The results showed that the vector-control JC32-strain failed to grow under the low-iron conditions employed, either with or without reductant. However, the wildtype grew well under both conditions with better growth observed when ascorbate was included (by ~0.1 OD units at 15 h; Fig. 5.17). This finding suggests that ascorbate supports low-iron growth of the wildtype, possibly by provision of ferrous iron.

The *efeUOB*-complemented JC32 strain showed enhanced growth (with respect to the vector control) in the absence of ascorbate, which was slightly improved by addition of ascorbate (by ~0.1 OD unit at 24 h). This is consistent with the reported preference of EfeUOB for ferrous over ferric iron (Cao *et al*., 2007). The *feoABC*-complemented JC32 strain showed no growth in the absence of ascorbate. This may result from low ferrous-iron availability or to the impact of the oxidising conditions (due to lack of reductant and availability of oxygen) on FeoABC function (possibly caused by FeoC-regulated FeoB degradation). However, when ascorbate was provided FeoABC enabled a growth advantage that was superior to that of EfeUOB. Thus, the capacity of FeoABC to support low-iron growth (under the conditions employed) appears to be heavily dependent on the presence of reductant. This effect might be due to ascorbate-mediated ferric reduction, resulting was raised ferrous iron availability (as suggested above). However, as the effect of ascorbate seen was greater for FeoABC than EfeUOB then it could

be argued that ascorbate influences FeoABC activity via a mechanism that does not apply to EfeUOB (such as stabilisation of FeoB against degradation under oxic conditions). In addition, the enhanced growth of the wildtype with ascorbate might arise as a result of FeoABC-enhanced activity (*efeUOB* in W3110 is cryptic so cannot be responsible to the observed ascorbate enhanced low-iron growth). The effect of ascorbate on aerobic FeoABC activity is explored in more detail below (Chapter 7).

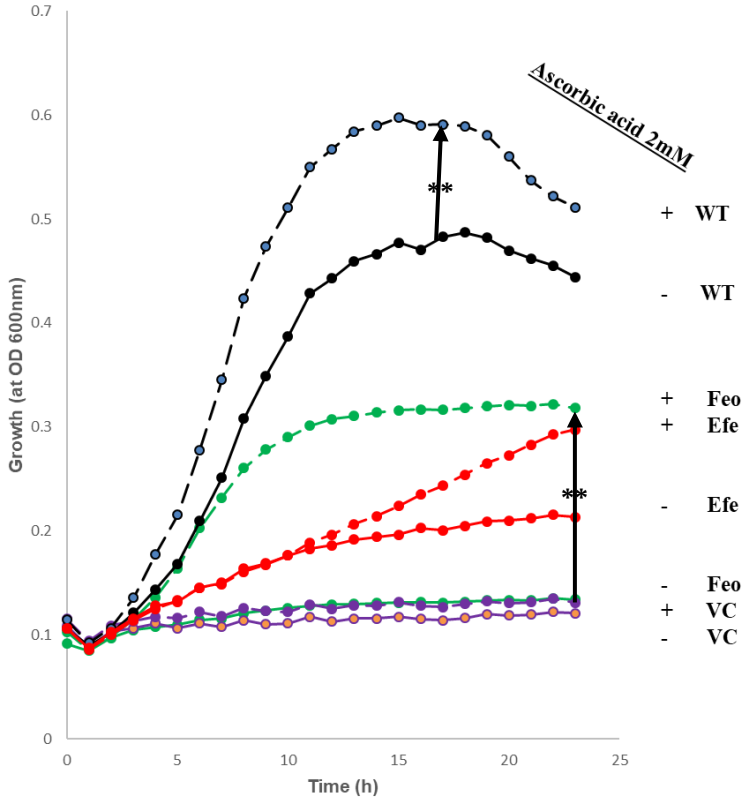

Figure 5.17: Effect of ascorbate on *feoABC*- and *efeUOB*-enhanced low-iron aerobic growth at pH 6. Strains were JC32 carrying either pBADrha-*efeUOB*^{O157}, pBADrha-*feoABC* or pBADrha; or W3110 (wildtype). Growth was in a Bioscreen C using M9 medium with 0.4% glucose, 1 µM DTPA, 100 mM MES (pH 6). Antibiotic and inducer were included as required. Ascorbate was added at 2 mM, as required. Statistically significant differences ($P<0.01$) are indicated at 24 h.

5.9. Effect of anaerobiosis on *feoABC*- and *efeUOB*-dependent low-iron growth with H_2O_2

Since the activity of FeoABC appears to be H_2O_2 inhibited (catalase-enhanced) whereas that of EfeUOB is supported by H_2O_2, the possibility that the FeoABC system may not function anaerobically if peroxide is provided, and that EfeUOB-dependent growth would be improved anaerobically with peroxide, was investigated. The transformants employed were JC32 with pBADara or pHSG576 (controls), and pBADara-*efeUOB,* pBADara-*feoABC* and pHSG-*feoABC* or pHSG-*efeUOB*^{O157}. Growths were performed anaerobically in M9 medium with 0.4% glucose, 100 mM MES (pH 6), 20 μM DTPA and 16 μM $MnCl_2$ (Figure 5.18). Interestingly, under iron-restriction, with and without H_2O_2, the growths of the transformants containing *feoABC* or *efeUOB*^{O157} were far higher than the vector controls, with little impact seen when H_2O_2 was added (Figure 5.18-.19). The results show a clear growth advantage provided for both FeoABC and EfeUOB under the anaerobic conditions employed. However, addition of peroxide had no or relatively little impact. It is surprising that the EfeUOB system was able to promote low-iron growth under conditions where no peroxide would be expected to be produced. In addition, it is a surprise that FeoABC activity was not much affected by the presence of the peroxide. Ideally, these experiments should be repeated in the presence of catalase (and absence of Mn^{2+}) in order to further explore the need for H_2O_2 for EfeUOB activity anaerobically and to ensure that exogenous Mn^{2+} does not cause decomposition of the added H_2O_2 or interfere with FeoABC and EfeUOB activity in any other way.

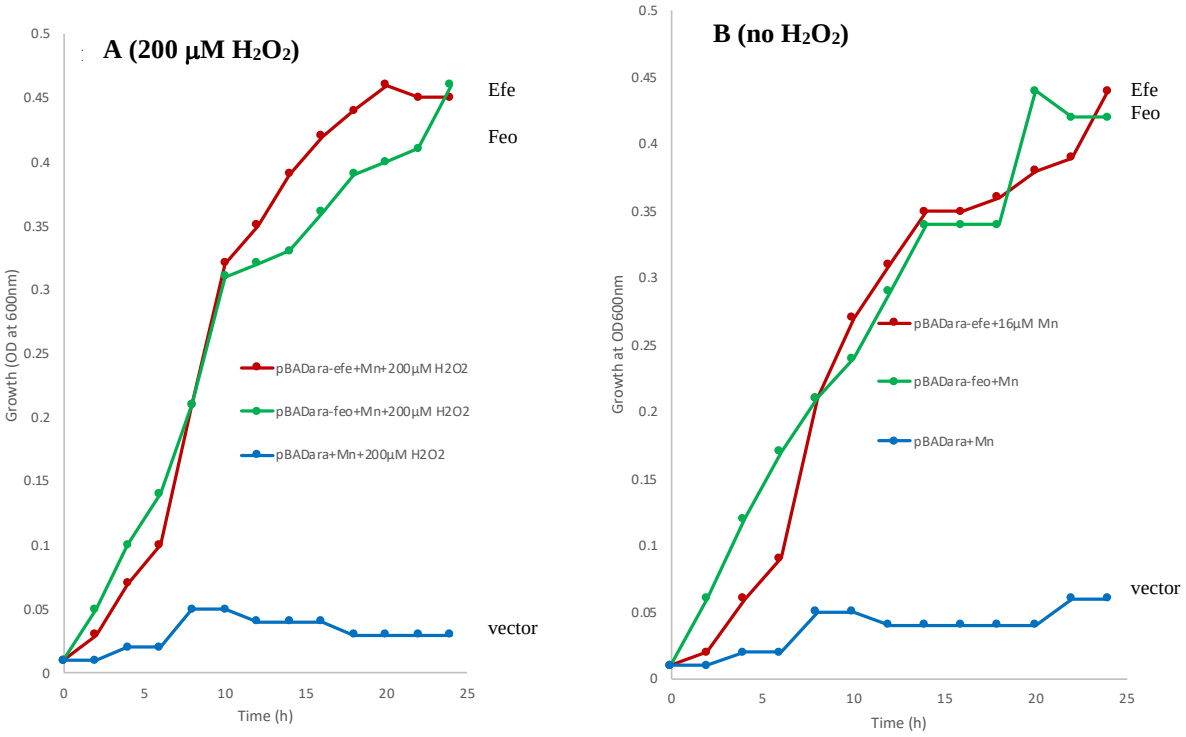

Figure 5.18. Effect of H_2O_2 on growth of *E. coli* JC32 transformed with pBADara-*efeUOB*, pBADara-*feoABC* and vector control under anaerobic conditions. Strains were grown anaerobically in 50 ml syringes containing M9 medium with 100 mM MES (pH 6), 0.4% glucose with 16 µM $MnCl_2$, 20 µM DTPA and with (**A**) **(200 µM H_2O_2)** or without (**B**) **(no H_2O_2)**. Data represent the mean OD values of triplicates.

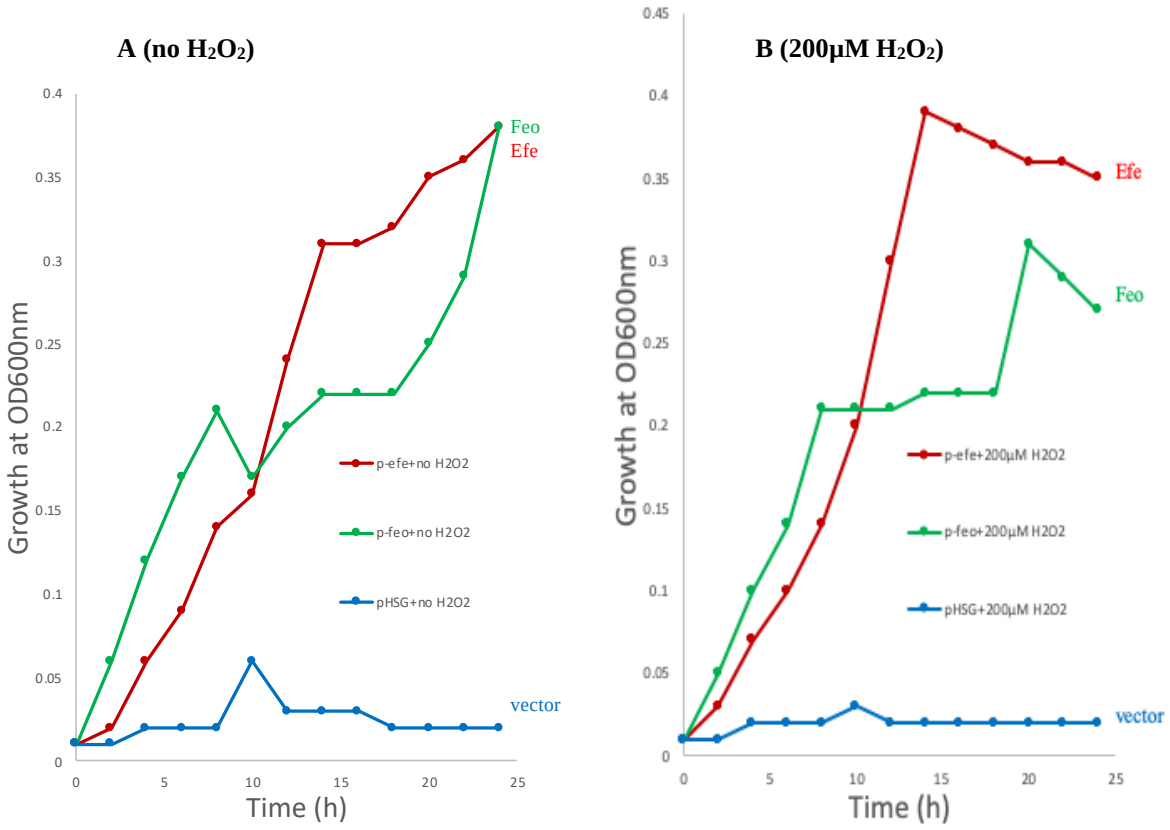

Figure 5.19. Effect of H_2O_2 on growth of *E. coli* JC32 transformed with pHSG-*efeUOB*, pHSG-*feoABC* or vector control under anaerobic conditions. Details are as for Fig. 5.18 except for the use of pHSG vectors and inducer.

5.11. Summary and Discussion

The above work shows a clear effect of catalase and peroxide on the growth advantages conferred by *efeUOB* and *feoABC* under low-iron, aerobic growth conditions. Catalase promoted low-iron growth for *feoABC* transformants, whereas for *efeUOB* transformants and the vector control, growth was inhibited. This effect was unrelated to transcriptional control since the pBADrha/ara-*feoABC* plasmids also showed an enhanced growth with catalase. The results are fully consistent with inhibition of Feo activity by endogenously produced peroxide, and could also arise from enhanced FtsH-mediated turnover of FeoB as regulated by FeoC (to be tested in subsequent chapters).

For the *efeUOB* transformants, a very different effect was observed. When peroxide was provided, an enhanced growth benefit was achieved under low-iron aerobic conditions, whereas for the *feoABC* transformants and vector control, there was a major growth impairment. This result is fully consistent with the proposed peroxide-dependence of the Efe system arising from EfeB activity. Again, the effect of peroxide is not considered to be related to transcriptional control of *efe* since the effect of peroxide was also seen for the pBAD-*efe* plasmids. It is suggested that the distinct responses of Feo and Efe to peroxide provides an explanation for the presence of two such different ferrous transporters – one functioning when peroxide is absent and the other acting to replace the peroxide-sensitive Feo system when peroxide is present. H_2O_2 is generated by *E. coli* under aerobic conditions at levels of 10^{-7} to 10^{-6} M (Seaver and Imlay 2001). Thus, H_2O_2 would be expected to be readily available for EfeUOB utilisation and FeoABC inhibition, aerobically.

The impact of ascorbate during aerobic growth was also tested and was expected to favour ferrous iron over ferric iron accumulation in the medium, enabling both the FeoABC and EfeUOB systems to operate more effectively. In addition, ascorbate might favour Efe activity through its ability to reduce oxygen to H_2O_2, although ascorbate could also scavenge H_2O_2 in

the medium, which would be expected to disfavour EfeUOB activity (Kramarenko *et al*., 2006). However, ascorbate was found to cause only a modest increase in EfeUOB-dependent low-iron growth whereas it enabled a major increase in FeoABC-dependent low-iron growth. This effect could be partly related to increased ferrous-iron availability, but could also be caused by stabilisation of FeoB against FtsH-dependent degradation, which is triggered by oxic conditions (Kim *et al*., 2013). A further potential mechanism is stabilisation of the conserved Cys residues in the Gate motifs of the FeoB permease domain against oxidation under aerobic conditions (as suggested earlier).

Anaerobic iron-limited growth conditions gave unexpected results, with both FeoABC and EfeUOB supporting JC32 growth similarly and to a high degree with respect to the vector control, in both pBAD and pHSG576 formats. In addition, provision of peroxide had little impact. However, the medium employed included 16 μM $MnCl_2$ which might act as a confounding factor. Thus, such experiments should be repeated in the absence of Mn^{2+} and presence of catalases, in order to further explore the impact of H_2O_2 on FeoABC and EfeUOB dependent low-iron growth anaerobically. Indeed, the growth test results of Chapter 4 indicate that Feo is the major iron transporter for *E .coli* anaerobically, not EfeUOB, in absence of Mn^{2+}. EfeUOB of *E. coli* was previously show to be able to provide a low-iron growth advantage in an iron-uptake-diminished strain, both anaerobically and aerobically (Cao *et al*., 2007), consistent with results reported herein.

EfeB of *E. coli* has been shown to exhibit improved peroxidase activity under acid conditions (Sturm *et al*., 2006) and the *efeU* homologue (part of an *efeUOB*-like system) of *N. meningitides* is reported to be induced by H_2O_2-mediated redox stress (Grifantini *et al*., 2004). These finding are suggestive of a role for EfeUOB during redox-stress. However, Miethke *et al.* (2013) could find no role for the *efeUOB* systems of *B. subtilis* in redox-stress resistance and so far the evidence for EfeUOB function is heavily weighted in favour of iron uptake.

The peroxidase-like nature of EfeB and the H_2O_2-mediated growth advantage provided by Efe under iron restriction, as identified above for both the *E. coli* K-12 and O157 EfeUOB systems, correlate well with the proposed model for H_2O_2-dependent EfeUOB iron uptake (Rajasekaran *et al*., 2010). Thus, this supports the view that the EfeUOB system utilises hydrogen peroxide as a ferrous-iron oxidant to drive iron uptake. This mechanism resembles that of the related Ftr1p-Fet3p system of yeast which utilises oxygen (rather than H_2O_2) to oxidise ferrous iron prior to translocation across the inner membrane. The strong growth suppression seen for the vector control with either catalase or peroxide is not understood.

Having now shown contrasting effects of peroxide on ferrous-iron uptake systems using the parameter of growth, the next approach used to support the above work involves Feo- and Efe-dependent radioactive iron uptake studies (Chapter 6).

Chapter 6: ^{55}Fe uptake by FeoABC and EfeUOB

6.1. Introduction

The previous chapters showed that both FeoABC and EfeUOB support low-iron growth of *E. coli* strains otherwise lacking iron-uptake capacity. FeoABC was shown to provide a greater growth advantage anaerobically, whilst EfeUOB gave a greater advantage aerobically. In addition, FeoABC activity appeared to be diminished by H_2O_2 whereas EfeUOB activity was enhanced by H_2O_2. Such effects appeared unrelated to transcriptional control. In order to further explore the iron-uptake properties of the Feo and Efe systems, their iron uptake activities were examined by using ^{55}Fe transport assays of *E. coli* strains expressing the corresponding transporter. Such assays allow investigation of ferrous/ferric iron preference and response to factors such as reductant, H_2O_2 and catalase, and could thus provide evidence corroborating the growth phenotype data obtained above. The strain employed (unless otherwise indicated) was *E. coli* JC32 strain (W3110 lacking all the major iron transporters) complemented with the low-copy-number plasmid (pHSG576 or pBADara) carrying *feoABC* or *efeUOB* from *E. coli* O157:H7 (or vector control).

6.2. Use of ^{55}Fe for iron import investigation and methodology

6.2.1 ^{55}Fe

Radioactive iron (^{55}Fe) is an isotope of iron and has a half-life of 2.7 years. The nucleus of ^{55}Fe contains 29 neutrons and 26 protons (compared to the stable ^{56}Fe atom which contains 30 neutrons and 26 protons) and decays by electron capture to stable ^{55}Mn (30 neutrons and 25 protons), emitting X-rays and Auger electrons. Decay through electron capture (k-electron capture) is a process by which a proton-rich nucleus of an electrically neutral atom absorbs an

electron from the k-electron shell. This process changes the nuclear proton to a neutron as well as emitting an electron neutrino.

The decay energy of the transition of ^{55}Fe to ^{55}Mn is 2.31 keV (kilo-electronvolts), produced by both X-rays and Auger electrons, and is detected by liquid scintillation counting (LSC). The collected samples containing the radioactive isotope are suspended in a scintillation 'cocktail' (Ultima Gold XR – Perkin Elmer) containing a solvent, surfactant and scintillator, within a translucent plastic scintillation vial. Emitted energy during the radioactive decay is transferred to the aromatic ring of the solvent; the energized solvent molecules transfer the captured energy to other solvent molecules, until the energy is transferred to the primary scintillator. The primary scintillator emits photons, following the absorption of the transferred energy, which are detected by two photo-multiplier tubes allowing the measurement of the radioactive decay in counts per minute (CPM). Analysis of a sample of ^{55}Fe via liquid scintillation counting shows the decay energy of 2.31 KeV (Figure 6.1), this allows adjustment of the Beckman LS-6500 multi-purpose scintillation counter to observe photon emissions within defined channels (Figure 6.1).

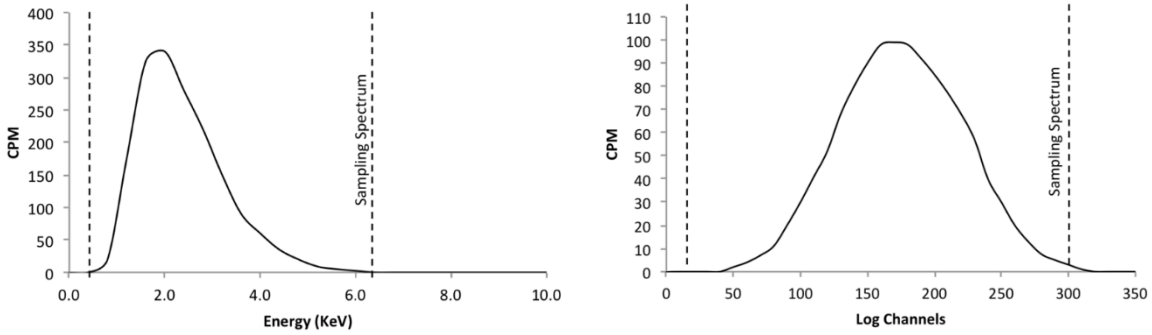

Figure 6.1: Energy emission (left) and channel range of energy emission (right) of ^{55}Fe decay. Measurement of ^{55}Fe energy emission through liquid scintillation counting as determined by counts per minute (CPM). Horizontal dashed lines represent the predefined high and low limits of detection. Beckman LS-6500 multi-purpose scintillation counter.

6.2.2. Optimisation and testing of the ^{55}Fe uptake protocol

JC32 (Table 2.12) transformants with pBADara, pBADara-*feoABC,* pBADara-*efeU*OB*$^{K-12}$, pBADara-*efeUOB*^{O157}, pHSG576, pHSG*feoABC,* pHSG*efeU*OB*$^{K-12}$ or pHSG*efeUOB*^{O157} were used for the iron uptake assays. Initially, the best type of filter paper for use in isolating ^{55}Fe-incorporated cells by filtration was investigated. In addition, the methodology was tested to determine whether uptake could be measured effectively. Strains were grown aerobically and anaerobically in 0.4% glucose M9 medium, buffered at pH 6 or pH 8, with 0.25-0.5 μM DTPA, and uptake assays were performed using harvested (0.1-0.15 OD) cells in Transport Buffer (TB; see Methods 2.35). ^{55}Fe was added to 3 ml of TB, plus cells, to initiate uptake, and at various time points 250 μl samples were filtered through filter discs and then washed with 10 ml of ice cold citrate wash buffer. However, variable data were obtained from this experiment (data not shown) when 0.2 μm glass microfiber (Whatman) filters were used, suggesting high non-specific binding of ^{55}Fe. Thus, a cell-free experiment was performed to test two different filter papers (glass microfiber and nitro cellulose filter) using the protocol above, but without including cells, and this gave results that matched with those previously reported (Cao *et al*., 2007). The results showed that the 0.2 μm nitrocellulose membrane presented with the lowest level filter iron-binding, and so these conditions were therefore used in the subsequent ^{55}Fe uptake assays.

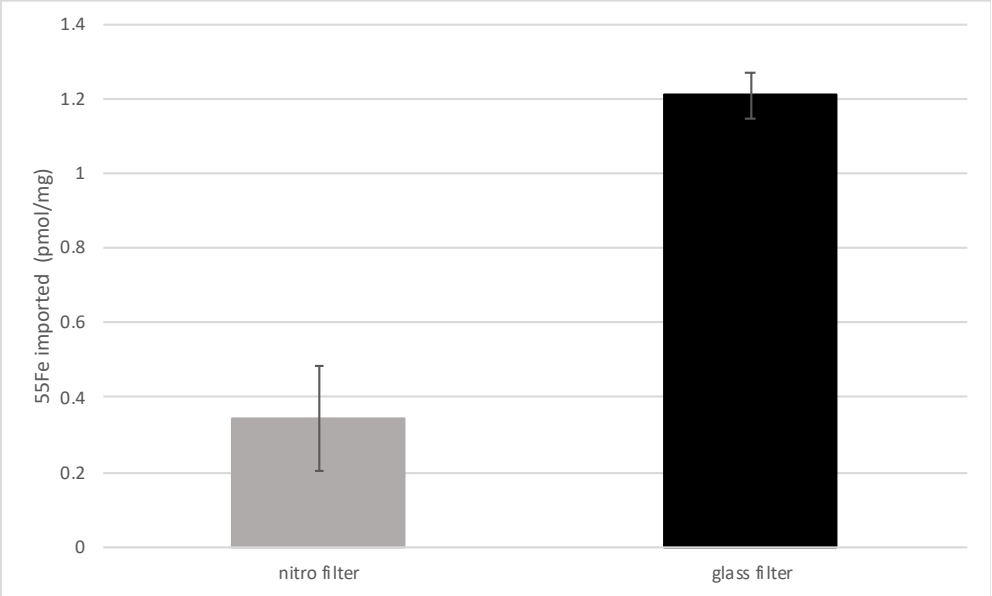

Figure 6.2 Comparison of ^{55}Fe-binding for different filters. Cell-free samples were prepared by adding 4 µCi ^{55}Fe to 6 ml of minimal medium containing 0.4% glucose, 100 mM MES (pH 6), 2 mM ascorbate, and 0.25 µM DTPA. 500 µl of sample was either filtered through a filter paper followed by washing with 10 ml of ice cold citrate wash buffer (Wyckoff *et al*., 2006) The filters used were: 0.2 µm glass microfibre disc (Whatman; 'glass'), 0.2 µm nitrocellulose membrane (Whatman; '0.2 µm nitro'), error bars indicate the standard deviations.

6.3. Effect of complementation of JC32 with pHSG-*efeUOB* and pHSG-*feoABC* on ^{55}Fe uptake at pH 6 and with reductant

The uptake experiments were performed in triplicate. First of all, the uptake assays were performed at pH 6 under aerobic conditions (overnight cultures were also grown aerobically in 0.4% glucose, M9 medium at pH 6). The pHSG-*efeUOB*^{O157} and pHSG-*efeU*OB*$^{K-12}$ transformants showed a far higher ^{55}Fe uptake (0.42-0.58 pmol/min) than the pHSG-*feoABC*^{O157} or pHS576 strains (~0 pmol/min) over the 5-15 min stage (Fig. 6.3), with ~fivefold more ^{55}Fe accumulated at 20 min. This result matches that of Cao *et al*. (2007) who showed an 13-fold greater iron-uptake activity for a strain (JC28) otherwise lacking iron uptake systems when complemented with functional *efeUOB*.

Since ascorbic acid was included at high concentration, the form of iron taken up is expected to be Fe^{2+}.

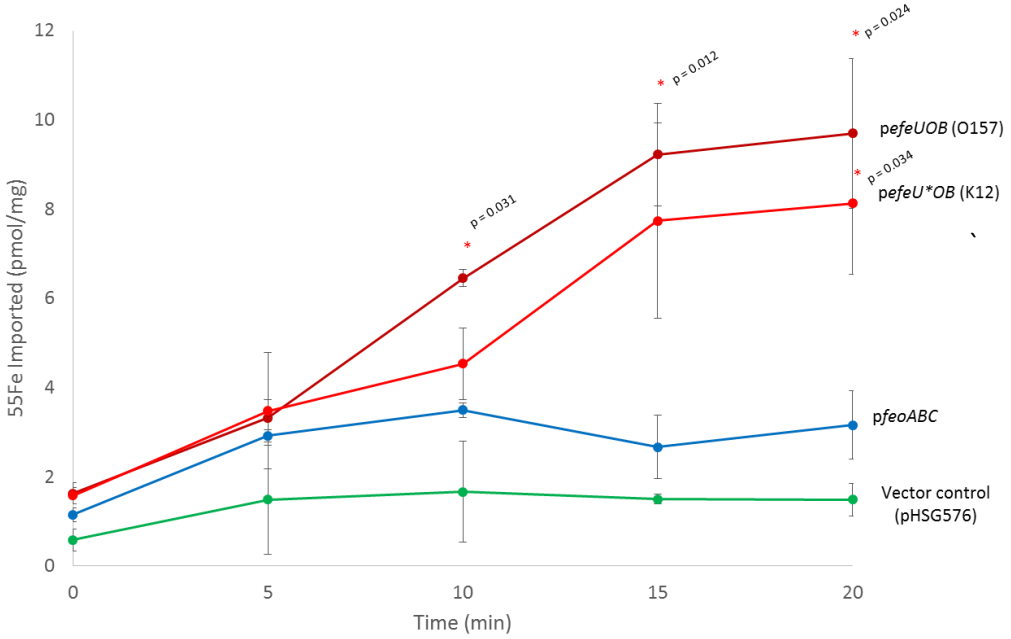

Figure 6.3. ^{55}Fe import by Efe and Feo under aerobic, reducing conditions at pH 6. JC32 with either pHSG576, pHSG-*efeUOB* or pHSG-*feoABC* was grown aerobically to mid-log phase in M9 medium containing 0.4% glucose, 100 mM MES (pH 6), and 1 µM DTPA. ^{55}Fe uptake was induced using ferrous iron (with 2 mM ascorbate) at 2 µM final concentration (4 µCi ^{55}Fe). The data are the mean and standard deviations from three replicates, the asterisk (*) denotes a statistically significant difference (indicated in the Fig.) between the data obtained with respect to the vector control and *efeUOB*^{O157} strain (Student *t*-test).

6.4. The effect of H_2O_2 and catalase on EfeUOB and FeoABC mediated ^{55}Fe uptake under aerobic conditions at pH 6 with reductant

The above work shows that EfeUOB functions well under the aerobic conditions tested as an iron (ferrous) import system, and that in contrast, the FeoABC system appears to be largely inactive under these conditions. These results are consistent with the growth data showing that EfeUOB is more effective aerobically than FeoABC. The growth studies of Chapter 5 suggest that EfeUOB and FeoABC respond oppositely to the presence of H_2O_2 indicating that the poor activity of FeoABC aerobically could be due to its inhibition by peroxide, whereas EfeUOB

activity may be enhanced by peroxide. Therefore, the effect of peroxide on Efe and Feo driven ^{55}Fe import was examined.

JC32 carrying pHSG-*efeUOB*^{O157} gave a ~twofold ($P < 0.001$) increase in ^{55}Fe import with addition of exogenous H_2O_2 (Fig. 6.4), while addition of catalase reduced EfeUOB-mediated import by ~fourfold ($P<001$) (Fig. 6.4). This result supports the view that ferrous-iron uptake by EfeUOB^{O157} is H_2O_2 dependent. In contrast, complementation by *feoABC*^{O157} resulted in weak iron uptake (as above) that was ~fourfold lower ($P < 0.001$) than seen for EfeUOB. H_2O_2 slightly reduced FeoABC-mediated ^{55}Fe import whereas addition of catalase increased import by ~six fold ($P<0001$) (Fig. 6.4). The difference in iron uptake driven by FeoABC with catalase or with H_2O_2 is ~11.4 ($P<0.001$). Thus, these iron uptake data are fully consistent with the hypothesis that Feo is H_2O_2 inhibited whereas Efe activity is enhanced by H_2O_2.

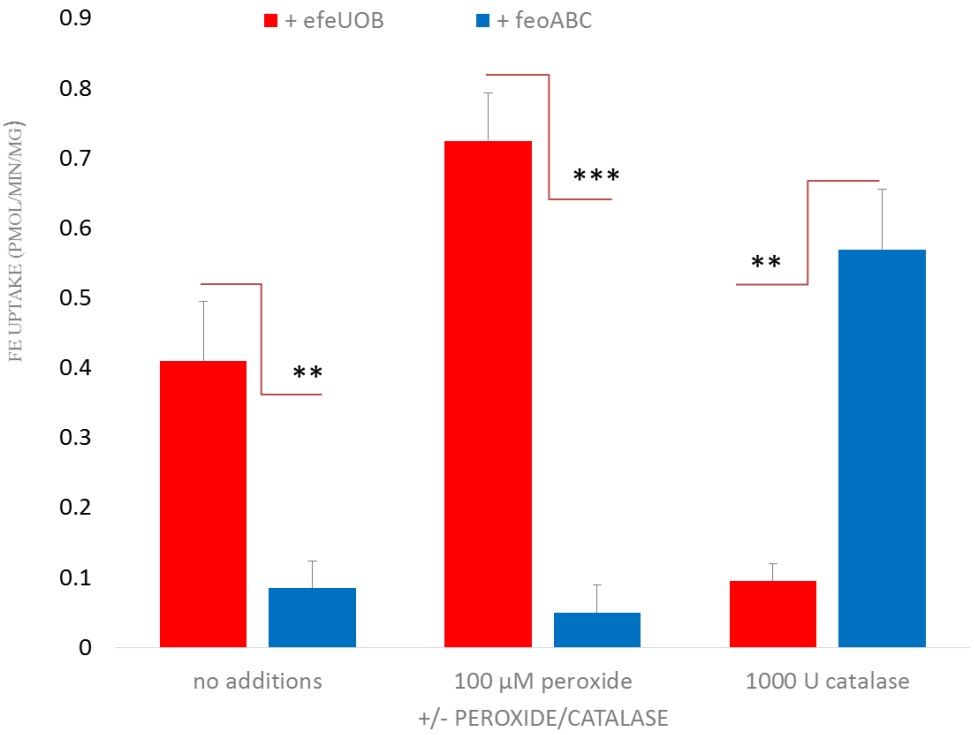

Figure 6.4: Effect of H_2O_2 and catalase on Efe- and Feo-dependent ^{55}Fe import. Iron uptake was performed as in Fig. 6.1, except for the inclusion or exclusion of 100 µM H_2O_2 or 1000 U catalase in the ^{55}Fe-uptake medium. Data is that recorded over 20 min, only data for '*efeUOB*^{O157}' is included here, and the vector control data has been subtracted from all values. The data is the average of three sets of data achieved on three separate occasions, giving a triplicate data set.

6.5. Effect of expressing *efeUOB* and *feoABC* from inducible promoters on ^{55}Fe uptake activity

To investigate ^{55}Fe uptake activity for JC32 carrying *efe* and *feo* in inducible format (to ensure that the effects on iron uptake are related to biochemical activity rather than changes in expression), pBADara-*feoABC*^{O157} and pBADara-*efeUOB*^{O157} were employed. The ^{55}Fe-uptake results showed that both FeoABC^{O157} and EfeUOB^{O157} raise iron-uptake capacity of JC32 with respect to vector control (~15-fold for FeoABC and ~30-fold for EfeUOB; P<0.0001; Fig. 6.5). The impact of catalase on Efe- and Feo-mediated ^{55}Fe-uptake activity was stark: catalase eliminated Efe-mediated iron uptake but stimulated that of Feo by ~497-fold (P<0.0001);

whereas in contrast, H_2O_2 raised Efe-dependent uptake by ~36% ($P<0.001$) and entirely inhibited Feo-mediated iron uptake (Fig. 6.5). These results thus support those obtained above (Fig. 6.2) showing similar responses to peroxide and catalase. This indicates that the results obtained above are not related to environmental effects on promoter activity for *feo* or *efe* expression. However, the relatively high FeoABC-mediated iron-uptake activity observed with pBADara-*feoABC* cf. pHSG*feoABC* indicates that the weak level seen in Fig. 6.2 is likely due to weak *feoABC* expression from its natural FNR-regulated promoter. It should be noted that the vector control, showed weak uptake activity with or without peroxide or catalase.

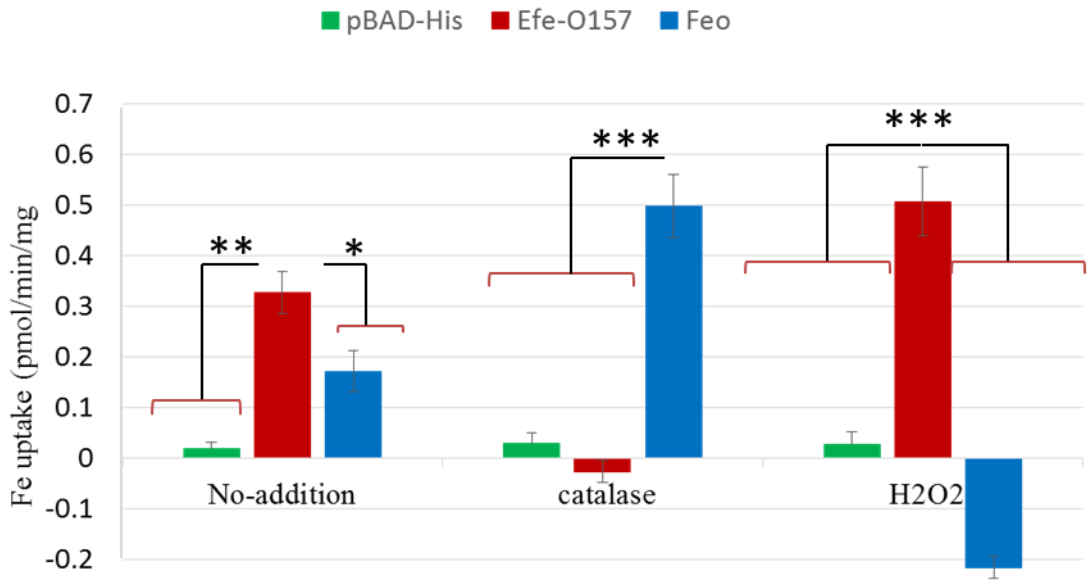

Figure 6.5: Effect of H_2O_2 and catalase on Efe- and Feo-dependent ^{55}Fe import cloning pBADara-*efeUOB*^{O157} or pBADara-*feoABC*^{O157} into pBADara vector. Iron uptake was performed as in Fig. 6.4, except for the inclusion of arabinose as inducer and use of pBADara-derived plasmids.

6.7. ^{55}Fe uptake by FeoABC and EfeUOB under anaerobic conditions

For *Escherichia coli* under aerobic iron-limitation conditions, siderophore-mediated Fe^{3+} transport is thought to dominate (Köster, 2001). However, under anaerobiosis the Fe^{2+} uptake system, FeoABC, plays the major iron uptake role (Kammler *et al*., 1993; Lau *et al*., 2016). Under aerobic, low-pH conditions with a competing metal, it appears that EfeUOB is the key iron transporter (Cao *et al*., 2007). The results in earlier chapters show that FeoABC provides a strong advantage during anaerobic, low-iron growth, but can also provide a strong advantage aerobically in the presence of reductants. The anaerobic requirement for FeoABC to strongly promote low-iron growth was not caused by the FNR-dependence of its expression, since *feoABC* under control of P*araBAD* showed a similar anaerobic preference. In order to confirm that FeoABC function requires anaerobiosis, the iron uptake experiments performed above were repeated under anaerobic conditions.

6.7.1 pBADara-*feoABC* and pBADara-*efeUOB*^{O157} in JC32

Transformants were grown overnight in 5 ml 0.4% glucose M9 medium, from which 1 ml was used to inoculate 50 ml of fresh medium with 1 μM DTPA (with antibiotic) which was then drawn into a 50 ml syringe to maintain anaerobiosis during growth. At (0.1-0.15 OD) (6-8h), cells were induced with 0.2% arabinose. Induced cells were harvested by centrifugation (5000 x g 4 °C, 10 min) and used for ^{55}Fe-uptake experiments (Methods 2.35). Anaerobic conditions were maintained by washing cells with degassed (with N_2) transport buffer and by performing the uptake experiment in a reaction cell sealed with an o-ringed plunger. The results show that JC32 carrying pBADara-*feoABC* gave a relatively high level of ^{55}Fe import activity anaerobically (Fig. 6.9), while the pBADara-*efeUOB* strain showed no substantive iron uptake activity (Fig. 6.9), as was the case for the vector control. This result supports the view that ferrous-iron uptake by FeoABC is dependent on the absence (or near absence) of oxygen,

whereas in contrast, EfeUOB-dependent iron uptake is weak under anaerobic conditions. These findings correlate well with those in the previous chapters showing anaerobic and aerobic preferences for FeoABC and EfeUOB, respectively, low-iron growth stimulation. The results anaerobically contrast with those obtained aerobically where FeoABC iron-uptake activity was weak and EfeUOB activity was strong.

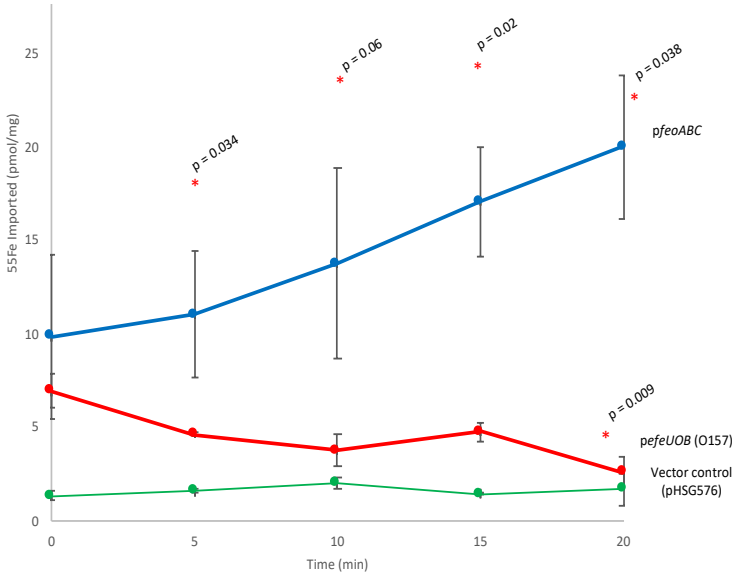

Figure 6.6. ^{55}Fe import by Efe and Feo under anaerobic, reducing conditions at pH 6. JC32 with either pBADara, pBADara-*efeUOB*^{O157} or pBADara-*feoABC* was grown aerobically to mid-log phase in M9 medium containing 0.4% glucose, 100 mM MES (pH 6), and 1 µM DTPA. ^{55}Fe uptake was induced using ferrous iron (with 2 mM ascorbate) at 2 µM final concentration (4 µCi ^{55}Fe). The data are the mean and standard deviations from three replicates, the asterisk (*) denotes a statistically significant difference (indicated in the Fig.) between the data obtained with respect to the vector control (Student *t*-test).

6.7.2 pHSG-*feoABC* and pHSG-*efeUOB*^{O157} in JC32

Similar results were obtained when the pHSG-*feoABC* and –*efeUOB* plasmids were employed (Fig. 6.7), thus confirming the poor iron-uptake activity of EfeUOB anaerobically with respect to FeoABC. Note that since the strains were propagated anaerobically under low iron, low pH conditions it is expected that both *efeUOB* and *feoABC* would be induced.

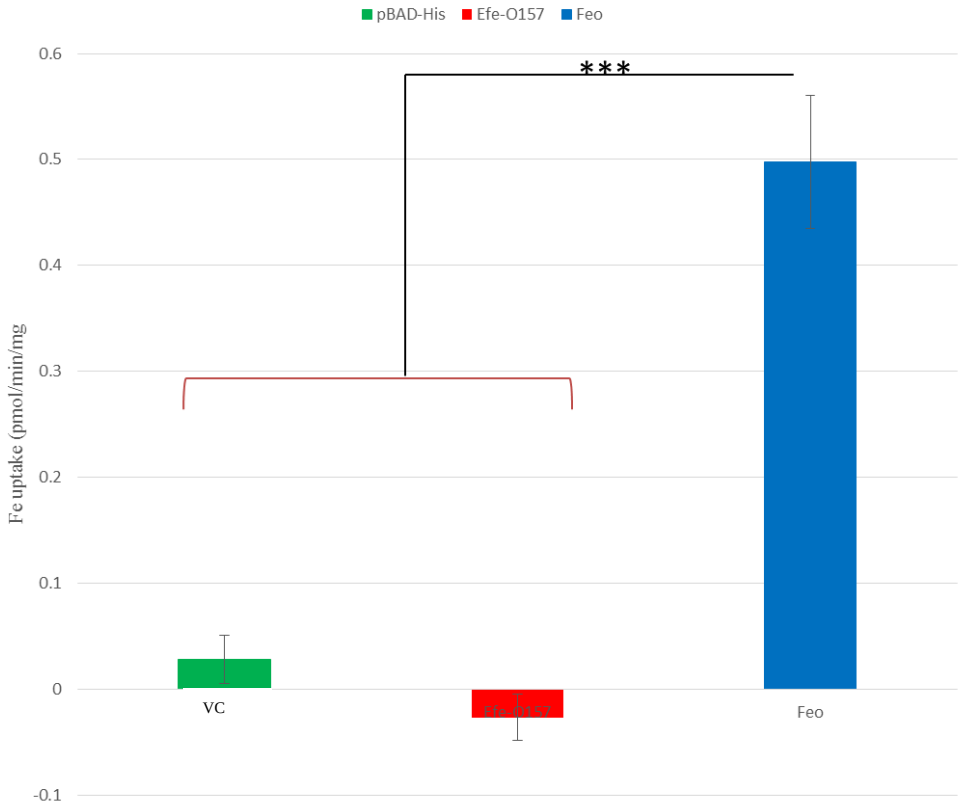

Figure 6.7. ^{55}Fe import by Efe and Feo under anaerobic, reducing conditions at pH 6. JC32 with either pHSG576, pHSG-*efeUOB* or pHSG-*feoABC* was grown aerobically to mid-log phase in M9 medium containing 0.4% glucose, 100 mM MES (pH 6), and 1 µM DTPA. ^{55}Fe uptake was induced using ferrous iron (with 2 mM ascorbate) at 2 µM final concentration (4 µCi ^{55}Fe). The data are the mean and standard deviations from three replicates, the statistically significant difference ($p<0.0001$) (indicated in the Fig.) between the data obtained with respect to the vector control (Student *t*-test).

6.7.3 Effect of hydrogen peroxide and catalase on anaerobic FeoABC- and EfeUOB-dependent ^{55}Fe uptake

To determine whether the contrasting impact of peroxide on FeoABC and EfeUOB-dependent iron uptake observed above also occur under anaerobic conditions, the anaerobic iron-uptake experiments were repeated with and without 200 µM H_2O_2 in the transport buffer.

To explore ^{55}Fe uptake activity for JC32 carrying *feoABC* in inducible format (to ensure that the effects on iron uptake are related to biochemical activity rather than changes in expression)

under anaerobic conditions and the effect of H_2O_2 on iron uptake activity, pBADara-*feoABC*^{O157} and pBADara-*efeUOB*^{O157} were employed. The ^{55}Fe-uptake results showed that both FeoABC^{O157} and EfeUOB^{O157} raise iron-uptake capacity of JC32 with respect to vector control (~228-fold for FeoABC and ~74-fold for EfeUOB; P<0.001; Fig. 6.8) might be the oxygen levels was not restricted. The impact of peroxidase on Efe- and Feo-mediated ^{55}Fe-uptake activity was stark: H_2O_2 eliminated Feo-mediated iron uptake but stimulated that of Efe by ~2-fold (P<0.001); whereas in contrast, H_2O_2 diminished Feo-dependent uptake by ~35% (P<0.001) and entirely inhibited Feo-mediated iron uptake (Fig. 6.4). These results thus support those obtained above (Fig. 6.5) showing similar responses to peroxide. This indicates that the results obtained above are not related to environmental effects on promoter activity for *feo* or *efe* expression.

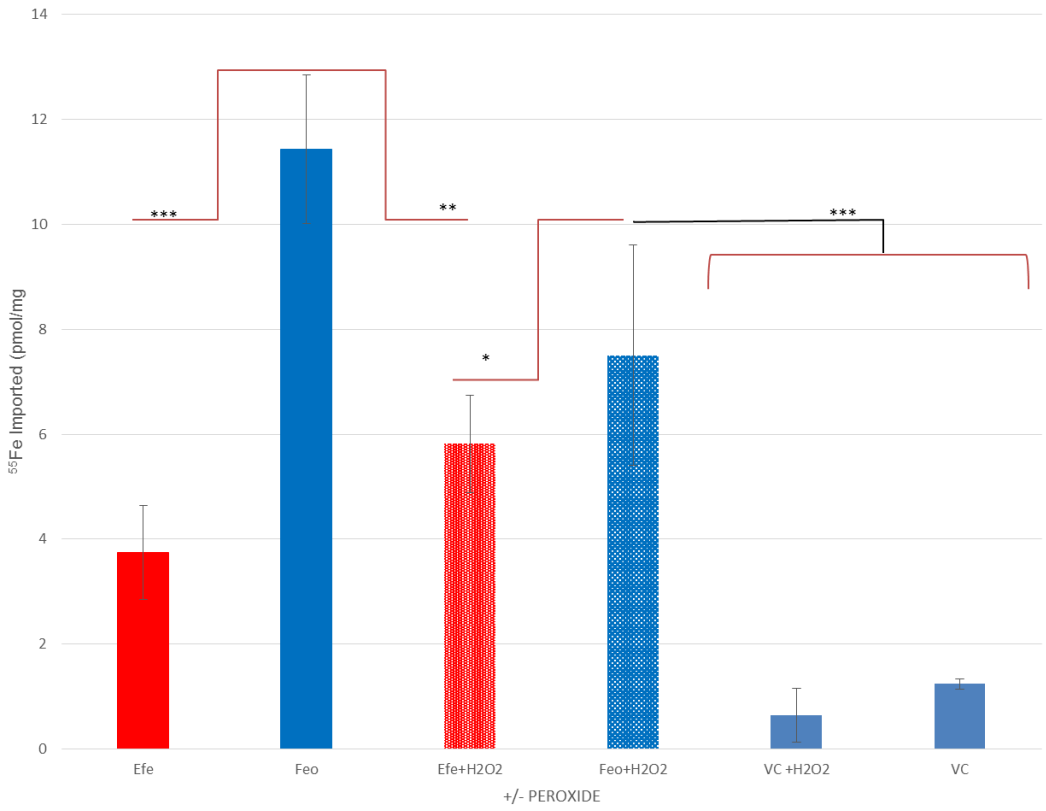

Figure 6.8. ^{55}Fe import by Efe and Feo under anaerobic, reducing conditions at pH 6. JC32 transformants with either pBADara, pBADara-*efeUOB* or pBADara-*feoABC* were grown as in Fig. 6.6. Iron uptake was also measured as in Fig. 6.6, except for the inclusion of 200 µM H_2O_2 as indicated.

In order with examination conducted for the Para-*feoABC* and Para-*efeUOB* constructs transformed into JC32, investigation of the impact of H_2O_2 upon iron import rate at pH8 (Figure 6.9). Adding 200 µM H_2O_2 at T_0 resulted in a significant increase in ^{55}Fe import by 12 pmol mg-1 (~2.4 fold) at T_{10} for *efe* complement, compared to no hydrogen peroxide addition anearobically, while diminution 1.7 fold of ^{55}Fe import though Feo complementation, it may due to the concentration does not engh to reduce the import activity of 200 µM H_2O_2, to furether study will increase the concentration and adding in each time point.wheare as, no bighest effect for catalase under anearbosis condition (Figure 6.10)

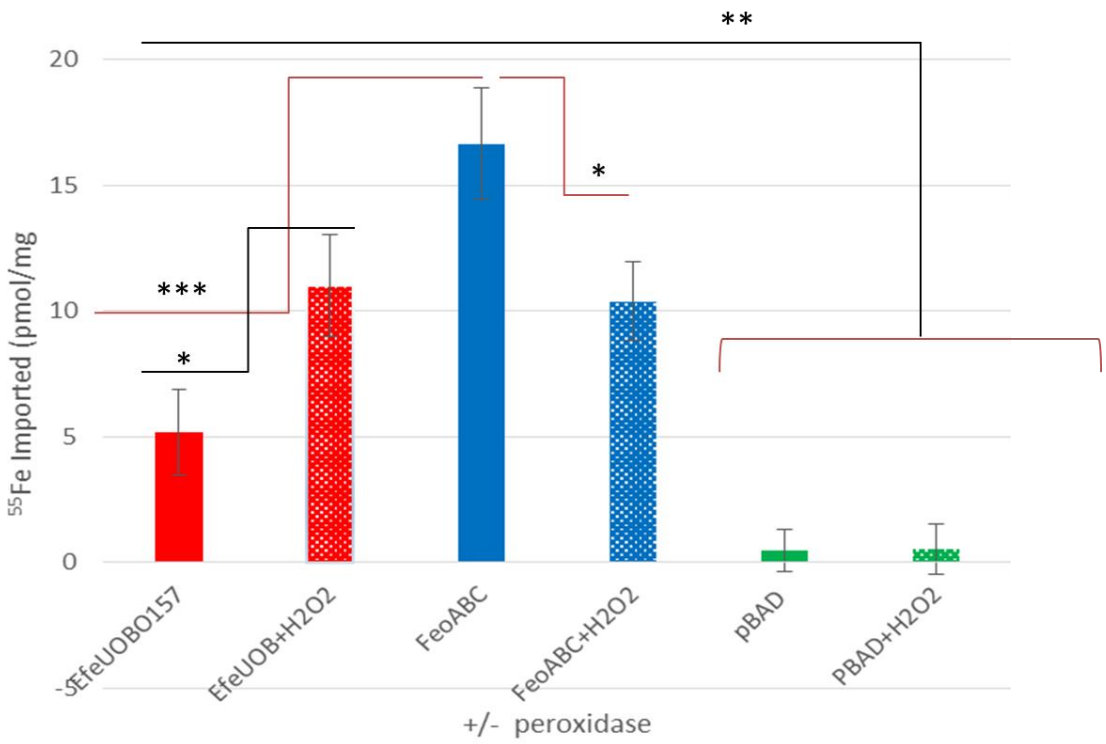

Figure 6.9. ^{55}Fe import by Efe and Feo under anaerobic, reducing conditions at pH 8. JC32 with either pBADara, Para-*efeUOB* or Para-*feoABC* was grown aerobically to mid-log phase in M9 medium containing 0.4% glucose, 100 mM TAPS (pH 8), and 1 µM DTPA. ^{55}Fe uptake was induced using ferrous iron (with 2 mM ascorbate) at 2 µM final concentration (4 µCi ^{55}Fe). The data are the mean and standard deviations from three replicates, the asterisk (*) denotes a statistically significant difference (indicated in the Fig.) between the data obtained with respect to the vector control (Student *t*-test).

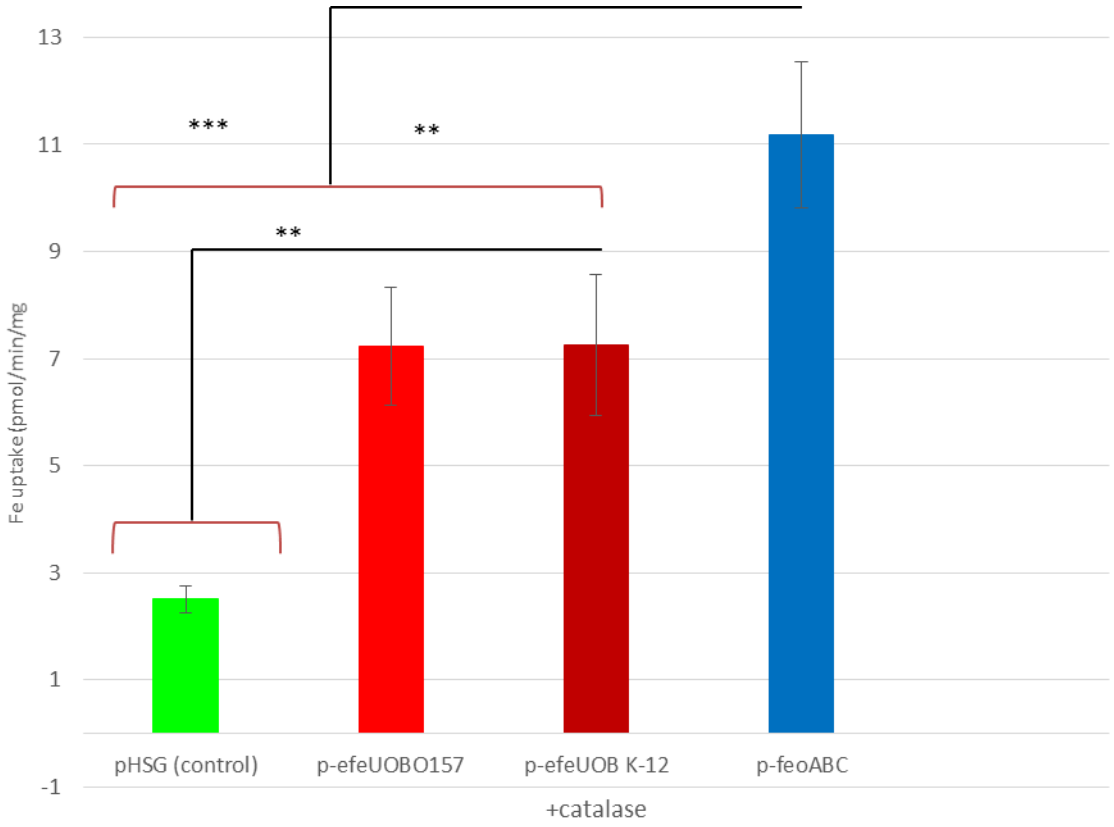

Figure 6.10. ^{55}Fe import by Efe and Feo under anaerobic, reducing conditions at pH 8. JC32 with either pBADara, Para-*efeUOB* or Para-*feoABC* was grown aerobically to mid-log phase in M9 medium containing 0.4% glucose, 100 mM TAPS (pH 8), and 1 µM DTPA. ^{55}Fe uptake was induced using ferrous iron (with 2 mM ascorbate) at 2 µM final concentration (4 µCi ^{55}Fe). The data are the mean and standard deviations from three replicates, the asterisk (*) denotes a statistically significant difference (indicated in the Fig.) between the data obtained with respect to the vector control (Student *t*-test).

T_o increase iron export under depleted oxygen conditions 200 µM hydrogen peroxide was introduced via hypodermic syringe injection through the o-ringed sealed plunger at T_{15}. It is possible that during this procedure up to 4 µM O_2 will have been introduced, due to the injected hydrogen peroxide solution not being de-gassed. It is unlikely however, that this small addition of O_2 will have yielded the observed increase in imported iron. (T_o avoid this, hydrogen peroxide solutions should also be de-gassed as described above). Additions of hydrogen peroxide, catalase (*Micrococcus lysodeikticus*) were made immediately prior to addition of cells to the reaction chamber.

6.8. EfeUOB and degradation of peroxide

Since iron uptake by EfeUOB appears to be driven by H_2O_2 and it is proposed that H_2O_2 acts as a ferrous-iron oxidant to drive iron uptake through EfeU, and previous work has demonstrated peroxidase activity for EfeB (Cao *et al*.,2007; Wang *et al*.,2018), the ability of EfeUOB to elicit degradation of H_2O_2 was investigated. This was enabled by employing the Amplex Red (10-acetyl-3,7-dihydroxyphenoxazine) H_2O_2 assay kit (ThermoFisher). *E. coli* JC32 transformants were inoculated into 5 ml 0.4% glucose in M9 medium (starting OD of 0.05), with 0.2% arabinose inducer for 2-3 h once the OD reached 0.5, washed once with 10 ml cold WB then twice with TB and diluted to 1 OD unit ml^{-1} and then hydrogen peroxide was assayed as in Methods 2.36.

To account for spontaneous degradation of H_2O_2, a control observation of 15 μM hydrogen peroxide in 1 ml transport buffer solution was included. The absorbance at 560 nm of Amplex Red remained stable over the 10 min assay period, enabling experimentation to progress without the need to correct for spontaneous degradation. The addition of 1 OD unit of *E. coli* LC106 (lacking catalases and alkyl hydroperoxidase – the primary H_2O_2 scavengers in *E. coli*; (Seaver and Imlay 2004) to 15 μM H_2O_2 resulted in no significant reduction in H_2O_2 concentration, whereas, addition of the parental wild type *E. coli* W3110 resulted in rapid degradation of H_2O_2 at a relatively high rate up to the 4 min time point; there-after levels were low but continued to drop slightly reaching a steady, low level (Figure 6.11). Thus, LC106 (unlike W3110) was unable to cause significant depletion of H_2O_2 during the course of the experiment indicating that the activity observed in W3110 arises from catalase/alkyl-hydroperoxidase activity.

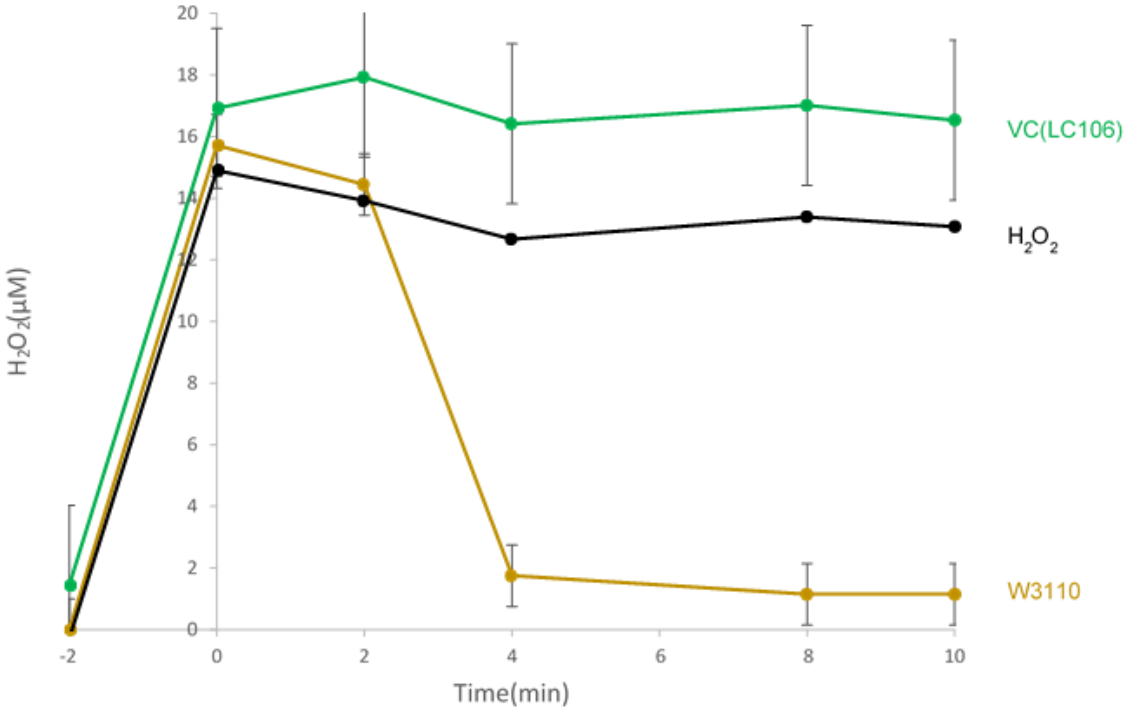

Figure 6.11: Degradation of hydrogen peroxide by *E. coli*. Quantitation of the disproportionation of 15 μM H_2O_2 by *E. coli* LC106 transformed with pBADara (vector control, VC) and *E. coli* W3110. Data shown are the means ± standard deviation of three independent experiments conducted in triplicate.

Addition of *E. coli* LC106 pBADara-*efeUOB* to the H_2O_2 consumption assay resulted in a major decline in peroxide levels over 10 min (50% loss at 10 min; Fig. 6.12). However, LC106 pBADara-*feoABC* and the vector control failed to have any notable impact on H_2O_2 degradation. This observation clearly shows that the Efe system is able to mediate the degradation of H_2O_2 when present in *E. coli*, further supporting a role for H_2O_2 consumption by EfeB in assisting Efe-mediated iron uptake

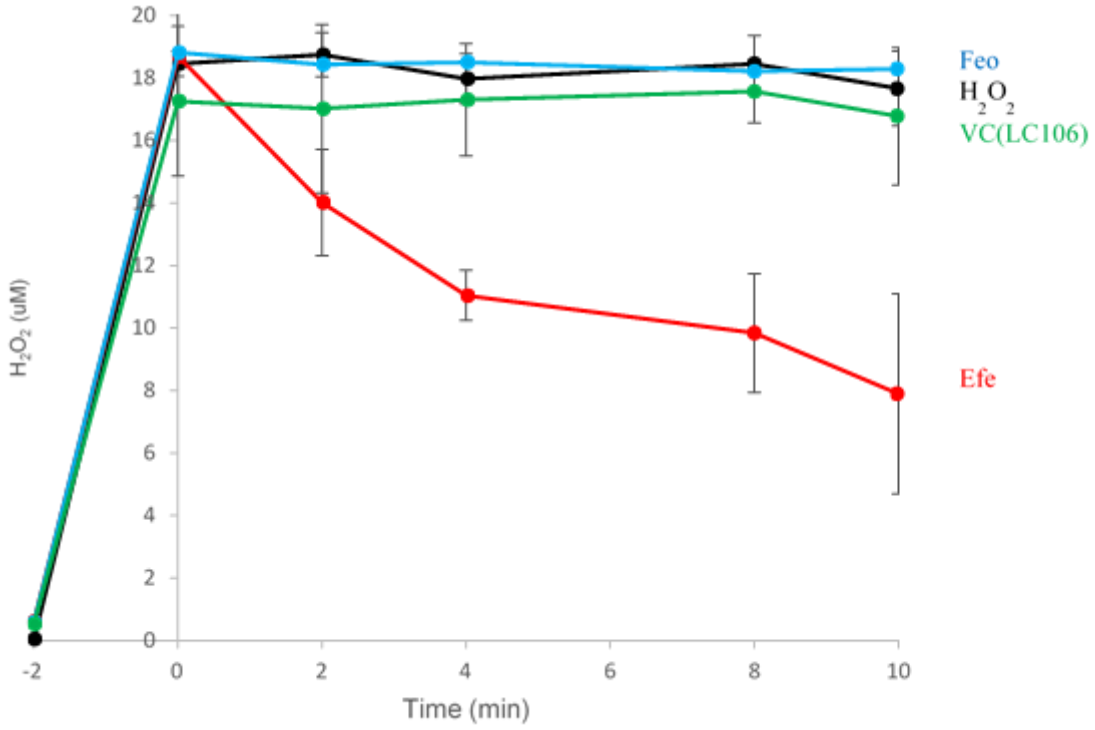

Figure 6.12: Degradation of hydrogen peroxide by Efe. As above, except to the use of *E. coli* LC106 transformed with pBADara (vector control, VC), pBAD*ara-efeUOB* or pBADara-*feoABC*. Inducer was included in the cultures. 'H_2O_2' indicates no bacteria.

6.9. Discussion

In this study, ^{55}Fe uptake assays were performed to further test the functions of EfeUOB and FeoABC as distinct ferrous iron transporters performing identical uptake roles (in terms of the substrate utilised) under discrete environmental conditions. Both Feo and Efe were shown to enhance iron uptake of JC32, and generally this effect was not much influenced by the plasmid employed to carry the corresponding operons under control of either a surrogate inducible promoter or the corresponding natural promoters. Efe was shown to give a greater uptake activity than Feo under the aerobic conditions employed, for both vector types. However, the pBADara borne *feoABC* system gave a higher transport rate than the pHSG576 carried operon under standard aerobic conditions (0.17 cf. 0.1 pmol/min/mg), which suggests that the ability to induce *feo* from the Para promoter in pBADara enhances Feo activity through increasing expression. In future work, this should be tested by comparing iron uptake rates with and without inducer, and by including the pBADrha plasmids to confirm the effect of induction on iron uptake activity.

The results suggest that peroxide is required for EfeUOB iron uptake since catalase greatly diminished or eliminated the Efe activity, whereas H_2O_2 caused an increase (Fig 6.4 & 6.5). In contrast, FeoABC iron uptake was increased by catalase but lessened by H_2O_2. (Fig. 6.4 & 6.5). This finding might be explained, in part, by previous work showing degradation of FeoB under oxidising conditions (Kim *et al*., 2015). The effect of peroxide and catalase on Feo-dependent iron uptake might thus be related to loss of the 4Fe-4S cluster from FeoC causing increased proteolytic degradation by FtsH of FeoB. To test this possibility, further work is required using *ftsH* mutants (and *lon* mutants, since Lon degrades FeoC) or by monitoring FeoB levels in the cell (by Western blotting) in response to peroxide/catalase. The observed effects of peroxide/catalase on ^{55}Fe uptake are unlikely to be related to transcription control, since uptake was measured over a short time period and nutrients were not included (other than glucose)

such that growth was not possible. Further, the use of pBAD vectors to allow controlled induction of *efe* and *feo* eliminated this possibility. However, the suggestion that H_2O_2 could act directly to inhibit Feo activity by oxidation of conserved Cys residues associated with the Gate motifs remains a possibility that requires exploration.

The above work provides a more complete rationale for these two distinct types of ferrous iron transporters in *E. coli* (and other bacteria), which appears to be related to peroxide: Feo is sensitive to H_2O_2 and so cannot function well aerobically; in contrast EfeUOB is dependent on H_2O_2 for its activity and so would be expected to require aerobic/oxidative conditions for function. Thus, EfeUOB appears to have evolved to function under conditions that are unsuited to FeoABC, and vice-versa.

A low pH-enhanced peroxidase activity was previously reported for EfeB of *E. coli* (Sturm *et al*., 2006) and the *efeU/ycdN* gene (part of an EfeUOB system) of *N. meningitidis* is induced by H_2O_2-mediated redox stress (Grifantini *et al*., 2004). These finding are suggestive of a role for EfeB in peroxide consumption. In addition, the results described in this thesis indicate that the EfeUOB system is dependent on H_2O_2 for its activity and thus may use hydrogen peroxide as an oxidant to drive iron uptake and ferrous-iron oxidation, in a manner resembling that of the Ftr1p-Fet3p system. However, it should be pointed out that Miethke *et al.* (2013) found no role for the EfeUOB systems of *B. subtilis* in peroxide resistance indicating no significant ability to consume peroxide over and above that offered by endogenous catalases and peroxidases. In this chapter, the ability of EfeUOB to consume H_2O_2 was tested in an H_2O_2-consumption assay. This clearly showed that, in a mutant strain lacking alternative peroxide degradation capacity, the EfeUOB system supports a major degradation of H_2O_2 (Fig. 6.12). This finding is consistent with the suggestion that consumption of H_2O_2 and import of iron by EfeUOB are coupled. Thus, this observation supports the view that the EfeUOB system utilises hydrogen peroxide as a ferrous-iron oxidant to drive iron uptake and that it thus engages in an iron-uptake mechanism

resembling that of the related Ftr1p-Fet3p system of yeast which utilises oxygen (rather than H_2O_2) to oxidise ferrous iron prior to translocation across the inner membrane.

It is unclear why the EfeUOB system has evolved to employ H_2O_2 to drive ferrous iron uptake. One possibility is that this would ensure that EfeUOB only functions well when FeoABC is unable to (if FeoABC is indeed subject to H_2O_2 inhibition, as here suggested); this could avoid any complications associated with the concurrent engagement of multiple routes of iron import and the need to avoid any consequent iron toxicity. In addition, the consumption of peroxide by EfeUOB to drive iron uptake might offer an energy efficient uptake pathway for iron as well as serve as a mechanism to supress redox stress through peroxide consumption

Chapter 7. The role of the three Feo components in FeoABC-dependent iron uptake in E. coli

7.1. Bacterial iron homeostasis and Feo

Soluble ferrous iron (Fe^{2+}) transport is mediated by the Feo system in *E. coli* K-12 (Kammler *et al*., 1993*)*. Operating under low-oxygen conditions, the Feo system consists of three proteins: FeoA, FeoB, and FeoC, all encoded by the *feoABC* operon (Carton *et al*., 2006). FeoB is a transmembrane transporter; its N-terminal domain is a G-protein regulating Fe^{2+} uptake (Marlovits *et al*., 2002). FeoA directly binds to FeoB thus controlling its activity, and this interaction is necessary for Fe^{2+} transport (Kim *et al*., 2012). FeoC also directly interacts with FeoB to protect it against FtsH protease-mediated degradation, thus promoting a higher concentration of cellular FeoB under low oxygen and iron levels. Under such conditions, *feoB* and *feoC* transcription is mediated by Fnr activation and Fur depression (Hantke ,1987; Sarah *et al*.,2006; Cartron *et al*.,2006; Kim *et al*., 2013) (Figure 7.1). *feo* operons have been identified in a range of bacteria. FeoB is common to all Feo systems and functions as the iron permease. The purposes of *feoA* and *feoC* are not so clear, and these genes are not present in all *feo* operons (Lau *et al*., 2016). Thus, an increased understanding of Feo function might be provided by further study of FeoA and FeoC.

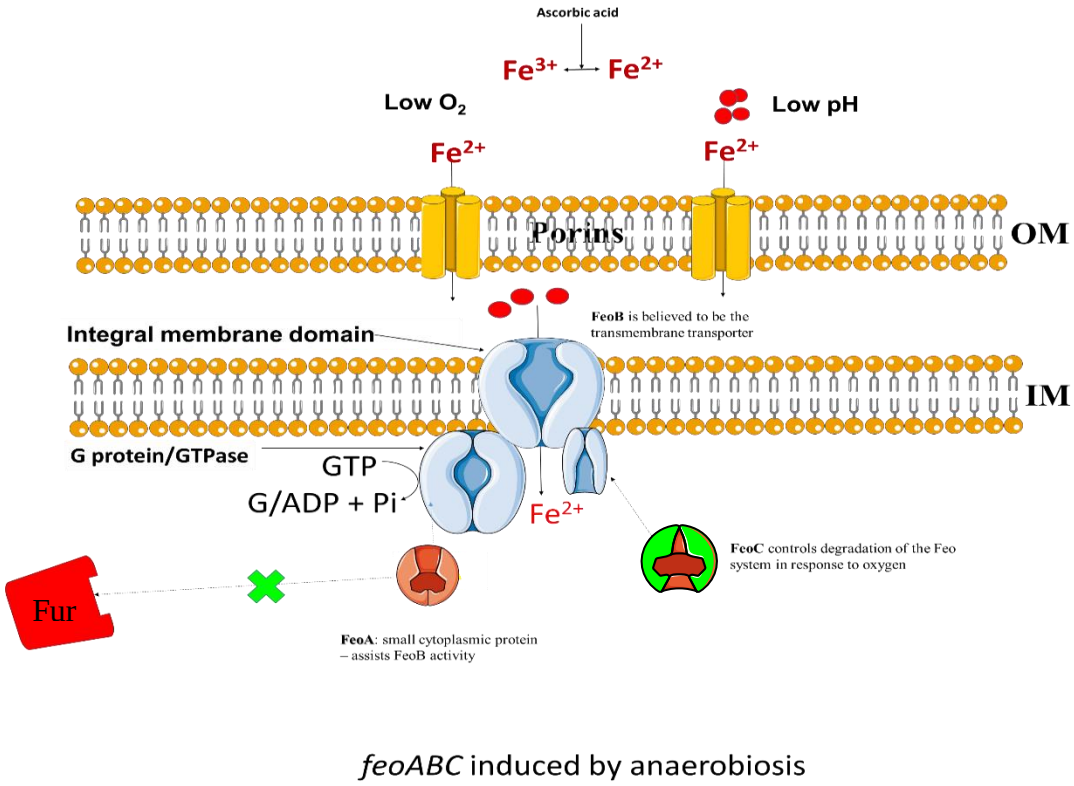

Figure 7.1: Schematic of bacterial Fe^{2+} transport by the Feo system under iron-restricted conditions and low O_2. The Feo system of *E. coli* K-12 is composed of three proteins: FeoA, small cytoplasmic protein; FeoC, small protein controlling degradation of FeoB in response to oxygen; and FeoB, integral membrane protein. FeoA and FeoB are highly conserved. In many bacteria, the *feo* genes are downstream of operators for FNR and Fur. FeoB (pale blue) permits ferrous iron across the membrane into the cystol. The G domain could regulate the open and closing of transport channel. FeoA (orange) may trigger FeoB activity under low iron conditions, and is suggested here to bind to the ferrous-Fur complex (red) under high iron. FeoC (green) protects FeoB from degradation under anaerobic conditions.

The cytoplasmic FeoA protein is necessary for Feo function, since its deletion results in defective iron transport. It is suggested that *feoA* deletion reduces the level of *feoB* mRNA (Krewulak and Vogel, 2008). FeoA was thought to function as a GTPase-activating protein acting on the FeoB N-terminal domain (NFeoB) (Raymond and Dertz, 2004), but it was recently proposed to instead cooperate with the conserved core region of FeoB (Yue *et al*., 2003). FeoA has a β-barrel, two α-helices and interconnecting loops, with the overall fold resembling an SH3 domain. It is this SH3 domain which suggests that FeoA may be involved in activating GTPases

or G-protein interaction (De Serrano, 2016; Larsen *et al*.,1999). SH3 domains typically bind G-proteins via proline-rich sequences (PXXP), and the PXXP recognition site in FeoB is hidden in the protein core (Yue *et al*., 2003). In 89% of bacterial Feo systems, FeoA and FeoB were found to exist together in a single operon, suggesting their close proximal functioning with entwined roles (Yue *et al*.,2003; Haemig *et al* 2010).

The N-terminus of FeoC (NFeoC) has a helix-turn-helix motif with a β-pleated hairpin between the second and third helices (Fig. 7.2) (Raymond and Dertz, 2004). Such motifs traditionally act as transcriptional repressors, with the third helix intercalating into the major groove of DNA to regulate transcription. FeoC also has a 'wing' region – a region with four cysteine residues which may be involved in forming the 4Fe-4S cluster of FeoC (Li, 2005; Rosen *et al*., 1992).

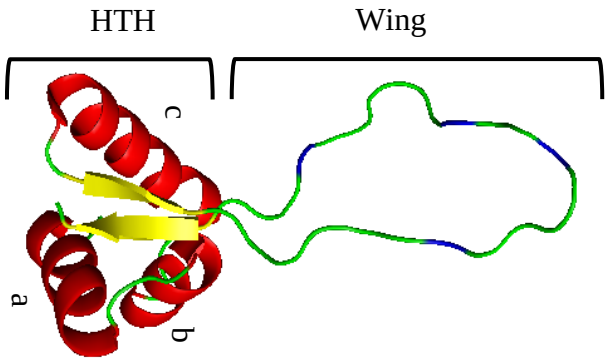

Figure 7.2: *E. coli* FeoC protein structure, displaying a helix-turn-helix motif. Three α-helices in red (labelled a,b,c), β-pleated hairpin in yellow a helix-turn-helix (HTH), cysteine residues on 'wing' in blue, wing structure are believed responsible for O_2-dependent FeoC control through binding an Fe-S cluster. Image generated in PyMOL using PDB code 1XN7, shown in cartoon view.

7.2. Aim of this chapter

The aim is to confirm the roles of FeoA and FeoC in FeoB-dependent iron uptake. This will involve the growth of *E. coli* under conditions were growth is dependent on a plasmid-borne FeoABC system such that the impact of absence of FeoA and FeoC can be tested. Thus, growth under iron restriction will used as the indicator of FeoABC activity.

7.3. Can *E. coli* JC32, complemented with *feo*, grow under iron-limitation conditions aerobically?

7.3.1. General experimental approach

The Ara and Rha inducible *feo* plasmids generated above provide the opportunity to test the ability of the FeoABC system to function aerobically. For this purpose, multiple growth measurements of *E. coli* JC32 with a range of *feo*-carrying plasmids were performed using a Bioscreen C apparatus aerobically, with or without iron, and with or without chelator (DTPA). Single and double transformations were performed using a range of plasmids from the following set: $pBAD_{Rha}$-FeoA, $pBAD_{ara}$-FeoBC, $pBAD_{ara}$-FeoA, $pBAD_{Rha}$-FeoBC, $pBAD_{Rha}$-FeoC, $pBAD_{ara}$-FeoAB, $pBAD_{ara}$-FeoC, $pBAD_{Rha}$-FeoAB, $pBAD_{Rha}$-FeoC, $pBAD_{ara}$-FeoB, $pBAD_{ara}$-FeoC, $pBAD_{Rha}$-FeoB, $pBAD_{Rha}$-FeoA, $pBAD_{ara}$-FeoB, $pBAD_{ara}$-FeoA and $pBAD_{Rha}$-FeoB, and $pBAD_{ara}$ and $pBAD_{Rha}$ (vectors only, acting as control).

Overnight cultures for all double and single transformants were grown in M9 broth with 10 μM ferric citrate and the appropriate antibiotic(s). The overnights were 'washed' twice to remove iron. Starting OD_{600} for all growth experiments was 0.01. Culture volumes of 300 μl were dispensed in each well of a 200-well plate. Growths were performed in a Bioscreen apparatus

C aerobically or a FLUOstar Omega system under low oxygen regime. Measurements were taken hourly, over 24 h, with the plates set to continuous shaking.

7.3.2 Plasmid construction

7.3.2.1 Propagation of pBAD$_{ara}$ and pBAD$_{Rha}$ vectors with *feo* genes

To prepare the cloning vectors, pBAD$_{ara}$ and pBAD$_{Rha}$ were transformed into competent cells. The plasmids were then extracted from single colonies using a ThermoScientific™ GeneJET™ Plasmid Miniprep Kit. The concentrations of extracted plasmid were measured using a NanoDrop Spectrophotometer and the plasmids were subsequently digested with *Hin*dIII and *Bam*HI, respectively. Uncut plasmids are in their circular form; therefore, they travel further down the gel as they have less points of contact with the gel matrix and a smaller surface area than linear DNA.

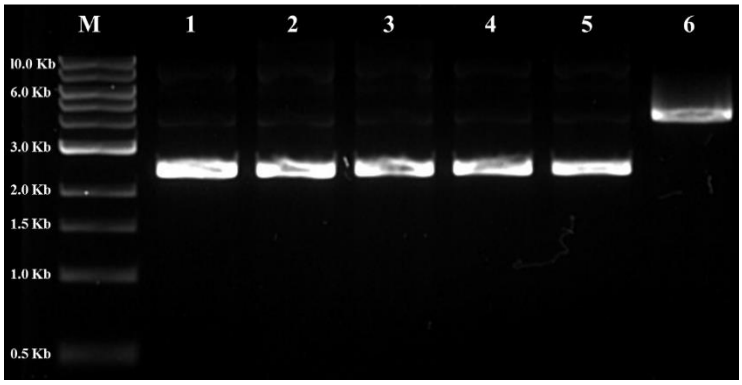

Figure 7.3: Confirmation of pBAD$_{ara}$ plasmids by restriction digestion. M: Quick-Load® 1 kb DNA Ladder; Lanes 1-5: Uncut plasmid; Lane 6: Plasmid cut with *Hin*dIII.

Figure 7.3 shows the expected bands of uncut pBAD$_{ara}$, with band size ~2.5 kb in lanes 1-5. The single digest in lane 6 shows the expected band size of 4.1 kb (Figure 7.3).

Figure 7.4 shows the expected bands of uncut pBAD$_{Rha}$, with mobility of 4 kb in lanes 1-5. The single digest in lane 6 shows the expected band size of 6.1 kb (Figure 7.4).

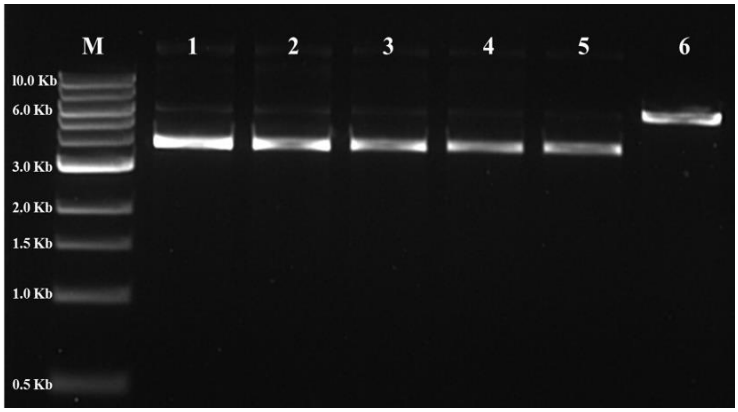

Figure 7.4: Confirmation of $pBAD_{Rha}$ plasmids by restriction digestion. M: Quick-Load® 1 kb DNA Ladder; Lanes 1-5: Uncut plasmid; Lane 6: Plasmid cut with *Bam*HI.

7.3.2.2 Double digestion of $pBAD_{ara}$ and $pBAD_{Rha}$ vectors and their extraction from the gel

Double digestion of $pBAD_{ara}$ and $pBAD_{Rha}$ was performed so that the required genes can be introduced for controlled expression. $pBAD_{ara}$ was double digested with *Nco*I and *Hin*dIII, and $pBAD_{Rha}$ was double digested with *Nde*I and *Sal*I. The samples were analysed by 0.6% agarose gel electrophoresis, using a thin gel. Once the gel electrophoresis had reach completion, the vectors were extracted from the gel using the ThermoScientific™ GeneJET™ Gel Extraction Kit (Method 2.13.3). The concentrations of isolated DNA was determined by NanoDrop to determine appropriate volume for use in subsequent cloning. The samples were stored at -20 °C for future use.

7.3.2.3. Amplification and Purification of *feoA, feoB, feoC, feoAB, feoBC* and *feoABC* PCR products

Amplification of *feo* inserts was as in Methods (2.15) and purification was done using the ThermoScientific™ GeneJET™ PCR Purification Kit (Methods 2.13.3). The purified PCR samples were analysed by gel electrophoresis (Figures 7.5, 7.6 & 7.7), and the expected sizes were achieved in all cases.

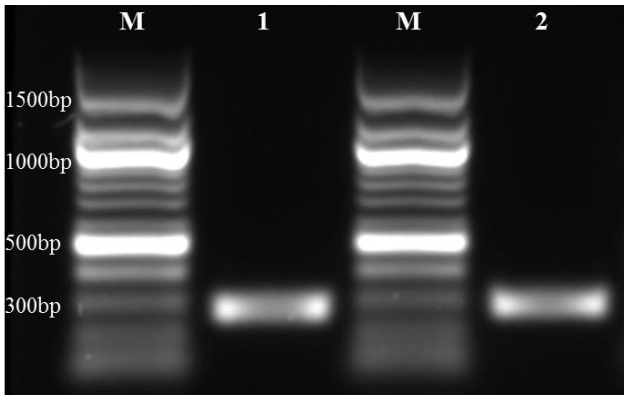

Figure 7.5: *feoA* and *feoC* PCR products. Lane M: 100bp molecular marker; Lane 1: *feoA*; lane 2: holds *feoC*.

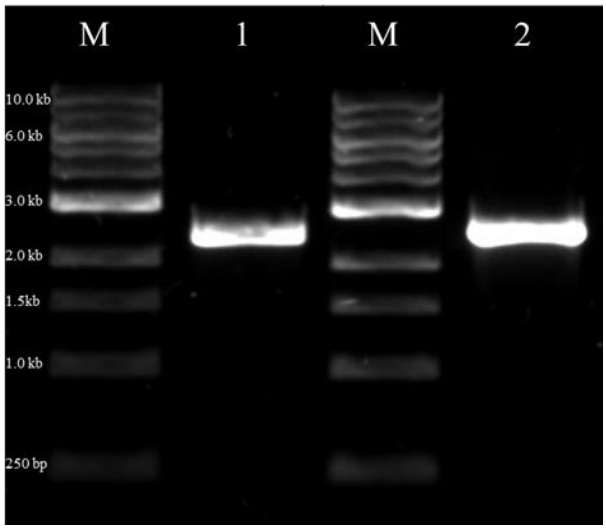

Figure 7.6: *feoB* and *feoAB* PCR products. Lane M: 1 Kb molecular marker; lane 1: feoB; lane 2: *feoAB*.

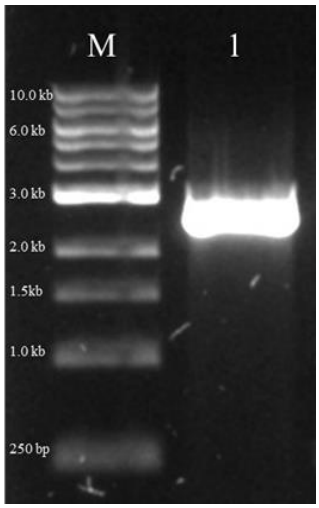

Figure 7.7: *feoBC* PCR products. Lane M: 1 Kb molecular markers; lane 1: *feoBC*.

The expected bands of *feoA* at ~228 bp and *feoC* at ~237 bp can be seen, with the *feoC* bands appearing ever so slightly higher than the *feoA* bands (Figure 7.5). The expected bands of *feoB* at ~2322 bp and *feoAB* at ~2550 bp can also be seen, with the *feoAB* bands appearing slightly higher than the *feoB* band (Figure 7.6). The expected bands of *feoBC* at ~2559 bp can also be seen (Figure 7.7). Therefore, PCR was successful, and the inserts can be inserted into the pBAD vectors.

7.3.2.4. Cloning of *feoA, feoB, feoC, feoAB, feoBC* and *feoABC* genes into pBAD vectors

The total size of the *feoABC* gene set is 2787 bp, with *feoA* being 228 bp, *feoB* being 2322 bp, *feoC* being 237 bp, *feoAB* being 2550 bp and *feoBC* being 2559 bp in size. Therefore, successful cloning should release these fragment sizes with agarose gel electrophoresis.

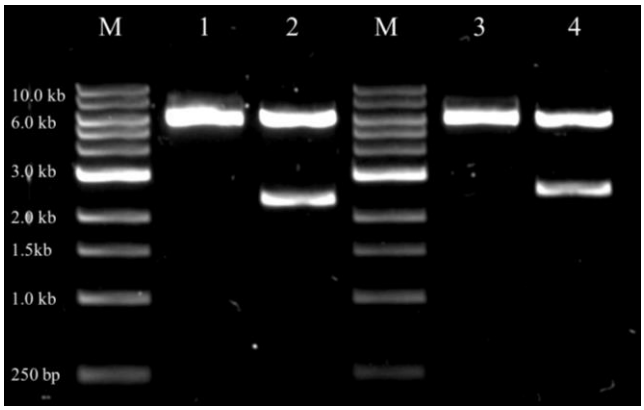

Figure 7.8: Restriction analysis of pBAD$_{Rha}$-*feoB* and –*feoAB* isolates Digestion was with *Nde*I and *Hind*III. M: 1 Kb Quick-Load purple ladder, lane 1 and 2: pBAD$_{Rha}$-*feoB* uncut and cut, 3 and 4: pBAD$_{Rha}$-*feoAB* uncut and cut.

The expected band size were observed (Figure 7.9): 6.1 and 2.3 kb for pBAD$_{Rha}$-*feoB*, and 6.1 and 2.5 kb for pBAD$_{Rha}$-*feoAB*.

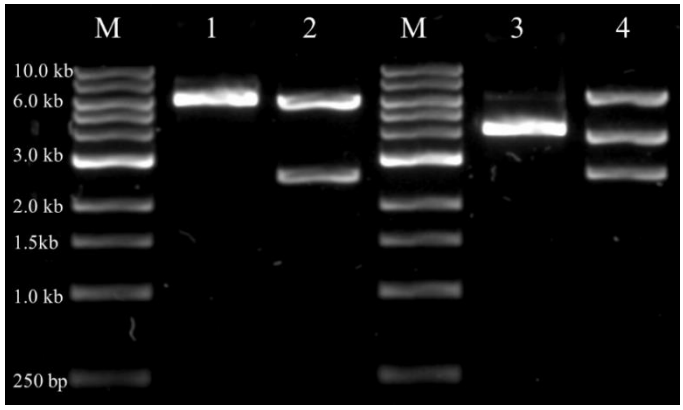

Figure 7.9: Restriction analysis of pBAD$_{rha}$-*feoBC* and pBAD$_{ara}$-*feoBC* isolates. Digestion was with *Nde*I and *Hin*dIII. M: 1 Kb Quick-Load purple ladder, lane 1 and 2: pBAD$_{rha}$-*feoBC* uncut and cut, 3 and 4: pBAD$_{ara}$-feoBC uncut and cut.

The expected bands for both plasmids were observed (Figure 7.10): 6.1 and ~2.5 kb for pBAD$_{Rha}$-*feoBC*, 4.1 and ~2.5 kb (and ~6.6 kb) for pBAD$_{ara}$-*feoBC* (the ~6.6 kb fragment is considered to represent single cut plasmid DNA).

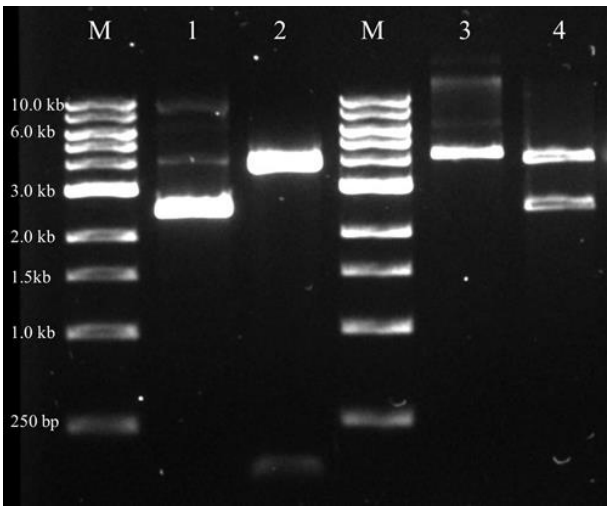

Figure 7.10: Restriction analysis of pBAD$_{ara}$-*feoA* and pBAD$_{ara}$-*feoB* isolates Digestion was with *Bam*HI and *Hin*dIII. M: 1 Kb Quick-Load purple ladder, lane 1 and 2: pBAD$_{ara}$-*feoA* uncut and cut, 3 and 4: pBAD$_{ara}$-*feoB* uncut and cut.

The expected bands for both plasmids was obtained (Figure 7.11). 4.1 kb and 228 bp for pBAD$_{ara}$-*feoA*, and 4.1 and ~2.3 kb for pBADara-*feoB*.

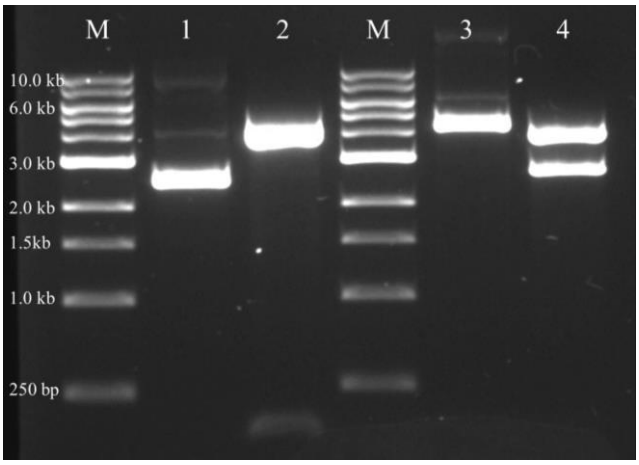

Figure 7.11: Restriction analysis of pBAD$_{ara}$-*feoC* and pBAD$_{ara}$-*feoAB* isolates. Digestion was with *BamH*I and *Hin*dIII. M: 1 Kb Quick-Load purple ladder, lane 1 and 2: pBAD$_{ara}$-*feoC* uncut and cut, 3 and 4: pBAD$_{ara}$-*feoAB* uncut and cut.

The expected bands for both plasmids were obtained (Figure 7.12): 4.1 kb and 237 bp for pBADara-*feoC*, and 4.1 and ~2.5 kb for pBADara-*feoAB*.

Once cloning of the inserts had been confirmed to be successful, the samples were all sent to Eurofins Genomics for sequencing.

7.3.4. *E. coli feoA* and *feoB* are required for Feo-mediated iron uptake, and *feoC* is required for optimal uptake

7.3.4.1 Introduction

Functional studies on Feo-mediated ferrous iron uptake systems have been mainly limited to the G protein domain of FeoB (Weaver *et al*., 2013). Previous work has shown that the *feoABC* of *E. coli* can restore iron transport capacity to *E. coli* and *S. flexneri* iron transport mutants

(Janecky *et al*., 2003; Lau *et al*., 2015). Iron transport by *E. coli* with only FeoAB available was vulnerable to O_2. This indicates a role for FeoC in oxygen-related control of FeoAB activity through a proteolytic digestion pathway (Kim *et al*., 2013; 2015). In order to confirm which Feo components are required for Feo activity in *E. coli* under a range of conditions, a set of inducible and complementary *feo* plasmids was generated (above) that can be used to complement *E. coli* strains defective in iron transport (JC32 and JC28). In this way, *feoA* and *feoB* can be expressed as a single operon, or as two independent cistrons, as is the case for *feoAB* and *feoC*. This will allow the specific roles of FeoA and FeoC to be investigated under low and high O_2 conditions.

7.3.4.2. FeoA and FeoC are required for full Feo activity under aerobic conditions at pH 6

Here the aim was to test the hypothesis that FeoA and FeoC are required for Feo function under aerobic growth conditions. Thus, JC32 (Table 2.2.5) transformants carrying a range of inducible *feo* constructs in pBADara or pBADrha were tested for their growth under high and low iron availability. Growths were in 0.4% glucose M9 medium, with inducer, using a Bioscreen C system.

With added iron (Fig. 7.13) at pH 6, all transformants (including vector control) achieved high OD levels with similar maximum OD values obtained (0.95-1.1). The greatest maximum OD (1.1) was achieved by the wildtype and the lowest was that of the JC32 vector controls (Fig. 7.12). However, these differences are relatively minor. At pH 8 the findings were similar (Fig. 7.13), with little differences between strains again observed, although average growth was slightly higher at this pH. Thus, the various *feo* constructs appear to provide no marked growth advantage to the JC32 strains under iron sufficiency, as expected.

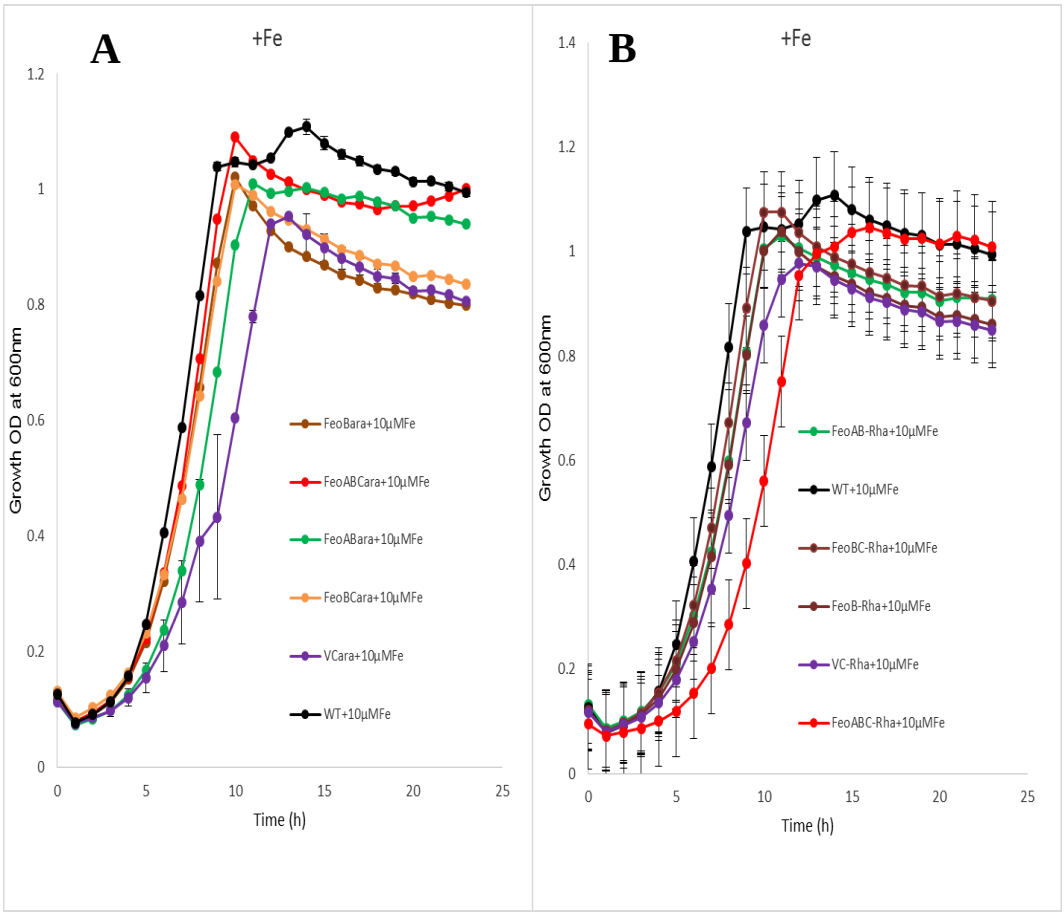

Figure 7.12. Growth of *E. coli* iron-transport mutant (JC32) under high iron complemented with *feoB, feoAB, feoABC* or *feoBC*, at pH 6. **A**. JC32 with pBADara-*feoABC*, -*feoAB*, -*feoBC*, and -*feoB*, or pBADara, and the wildtype (W3110). **B.** As 'A', except for use of pBADrha constructs. Growth was in 0.4% glucose in M9 medium pH 6 (plus 50 µg/ml chloramphenicol or 100 µg/ml ampicillin), with 10 µM ferric citrate, at 37 ˚C in a Bioscreen apparatus system (300 µl volumes) with constant shaking at 250 rpm. Values are averages of data from three biological replicates, error bars are standard deviation. Pre-cultures were growth overnight in 0.4% glucose M9 medium (37 ˚C, 250 rpm) with 10 µM ferric citrate and were washed in iron-free M9 medium before use. Starting cell density of all Bioscreen cultures was adjusted to OD_{600} (0.01). arabinose or rhamnose were included throughout at 0.02%.

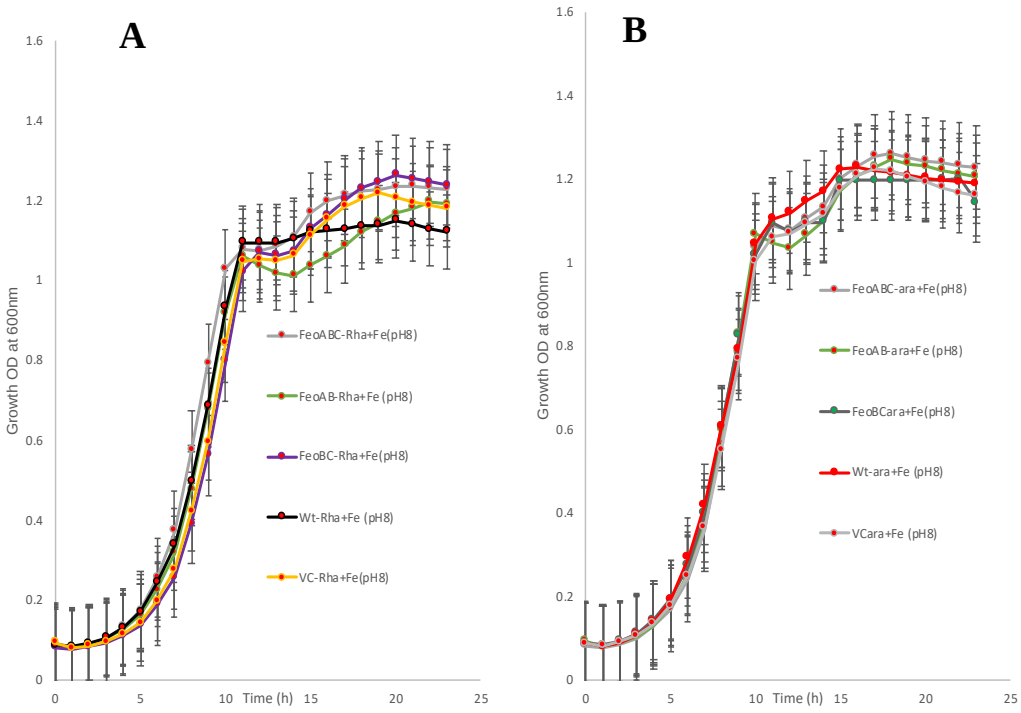

Figure 7.13. Growth of *E. coli* iron-transport mutant (JC32) under high iron complemented with *feoAB, feoABC* or *feoBC,* at pH 8. All details are as above except that pH was 8 (not 6) with 100 mM TAPS buffer, *feoB* complementation is not included, and details of A and B are switched.

Under iron deficiency (M9 medium without iron), the JC32 vector control grew very poorly showing a total growth increase over 24 h of just 0.02 OD units (Fig. 7.14A), whereas the wildtype grew well (max OD of 0.6) with an overall greater growth (cf. the JC32 vector control) of 30-fold. The JC32 strain complemented with *feoABC* showed high growth, reaching a maximum OD of 0.43 and achieving a 22-fold greater overall growth than the vector control (Fig. 7.14A). Thus, as expected, the *rha*-inducible *feoABC* construct provided effective complementation of low-iron growth of JC32 aerobically at pH 6. The *feoB*-complemented strain grew very weakly, similar to the vector control, indicating that FeoB does not provide iron-uptake activity in absence of the other Feo components. However, the *feoAB* complemented strain showed a clear growth advantage of the vector control (Fig. 7.14A), showing an OD increase over 24 h of 0.1 OD units (fivefold greater than the vector control). Thus, when FeoA and FeoB are provided together a moderate iron uptake activity is achieved.

However, the growth increase seen was considerably less than that of the *feoABC*-complemented strains (5- versus 22-fold, respectively), thus FeoC is required under the conditions used to for maximal Feo activity. The *feoBC*-complemented strain showed a very weak growth increase with respect to the vector control of 0.03 OD units over 24 h (cf. 0.02 for the control) (Fig. 7.14A), which indicates little or no iron transport activity was provided by the FeoB-FeoC combination. When DTPA was included in the medium, a similar growth pattern was observed (Fig. 7.14B), although overall growth was weaker. The *feoBC*-complemented strain gave a slightly better growth than the vector control, and in this case the *feoB*-complemented strain also gave slightly better growth than the vector control – although growth was still very weak. Thus, the results suggest that FeoB and FeoBC may gave a very weak iron uptake activity. However, it is clear that lack of FeoC reduced Feo activity considerably, reducing growth in M9 medium by more than fourfold, whereas lack of FeoA results in very little or no apparent activity such that growth is little different from that of the vector control.

Provision of DTPA increased the growth difference between the wildtype and the *feoABC*-complemented strain from 1.4 to 2.7 fold, indicating that FeoABC does not compete well with DTPA (a ferric iron chelator) for iron.

In summary, the result above indicate that the minimal requirement for Feo activity is FeoA and FeoB, and that addition of FeoC maximises that activity exhibited by FeoAB.

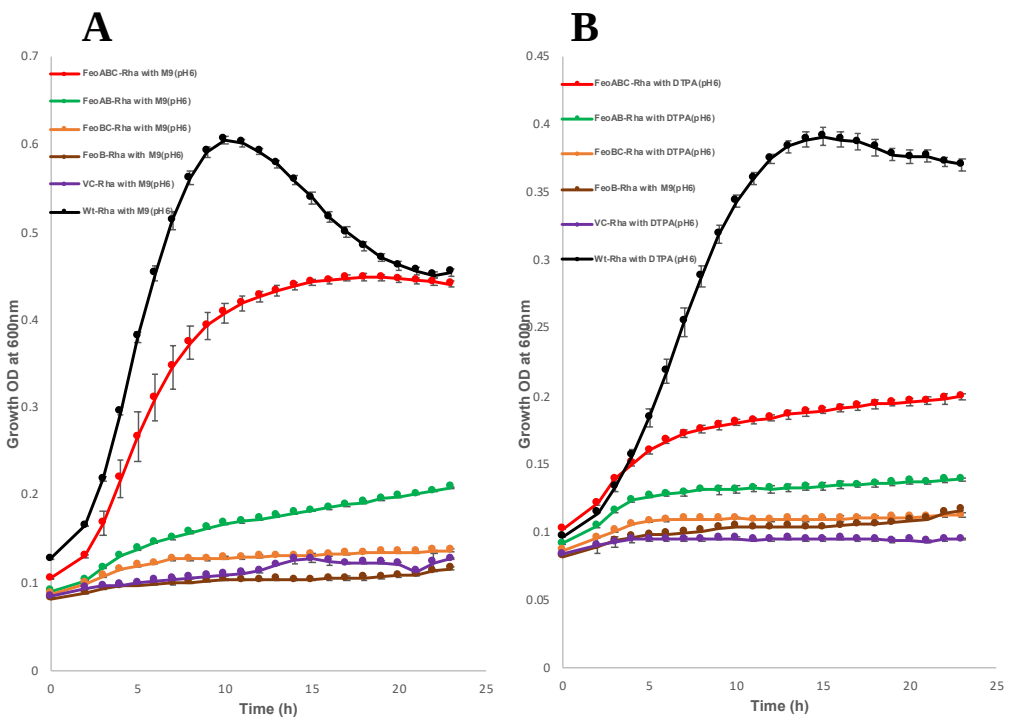

Figure 7.14. Growth of *E. coli* iron-transport mutant (JC32) under low iron complemented with *rha*-inducible *feoAB, feoABC, feoB* or *feoBC,* at pH 6. The details as in Fig 7.13 except only pBADrha constructs are included (with 0.02% rhamnose), and ferric citrate was not used in the growths above; instead, either no addition (**A**) was applied or 1 μM DTPA (**B**) (pH was 6).

Results obtained with the pBADara constructs under low-iron conditions (Fig. 7.15) reflect those obtained with the pBADrha constructs above (Fig. 7.14). *feoABC* complementation gave a substantial growth advantage in iron-restricted M9 medium with respect to the vector control (growth increase over 24 h of 0.52 OD units compared to no apparent growth increase for the vector control Fig. 7.15A). As before, *feoAB* complementation resulted in a modest growth increase of 0.09 OD units. However, *feoB* and *feoBC* complementation showed little impact on growth. When DTPA was included in the growth medium, the growth advantage afforded by *feoABC* was reduced substantially to ~3 fold, such that the difference in advantage provided by *feoABC* and *feoAB* was less stark (from 6.5- to 2.5-fold difference). Thus, the results obtained with the pBADara complementations support the conclusions made above from the pBADrha complementation data.

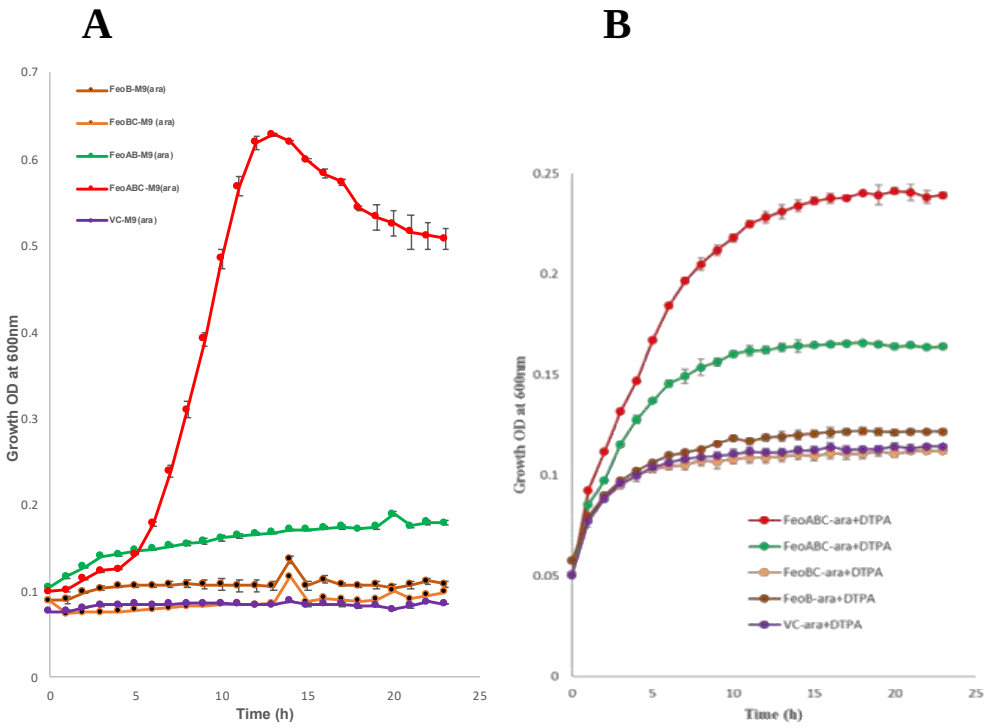

Figure 7.15. Growth of *E. coli* iron-transport mutant (JC32) under <u>low iron,</u> complemented with <u>*ara*</u>-inducible *feoAB, feoABC, feoB* or *feoBC*, at pH 6. The details as in Fig 7.13 except only pBADara constructs are included (with 0.02% arabinose), and ferric citrate was <u>not</u> used in the growths above (just in the overnight cultures); instead, either no addition (**A**) was applied or 1 μM DTPA (**B**) (pH was 6).

7.3.4.3. FeoA and FeoC are required for full Feo activity under aerobic conditions at pH 8

The experiments described above were repeated at pH 8, in order to determine whether Feo might be pH sensitive, possibly as a result of lower stability of ferrous iron to oxidation at low pH.

In low-iron M9 medium, with the pBADrha palsmids, the *feoABC* and *feoAB* complemented strains showed a slightly better growth than the vector control and other complemented strains, and results were similar for the pBADara and pBADrha complmentations (Fig. 7.16). *feoABC*-complementation gave a slightly better growth than *feoBC* complementation, particularly for the pBADara complementations (Fig. 7.16B). The difference seen in result at pH 6 and 8

largely relates to the superior growth of the vector control at the higher pH, which might reflect higher iron availability. This would limit the potential for *feo*-mediated complementation.

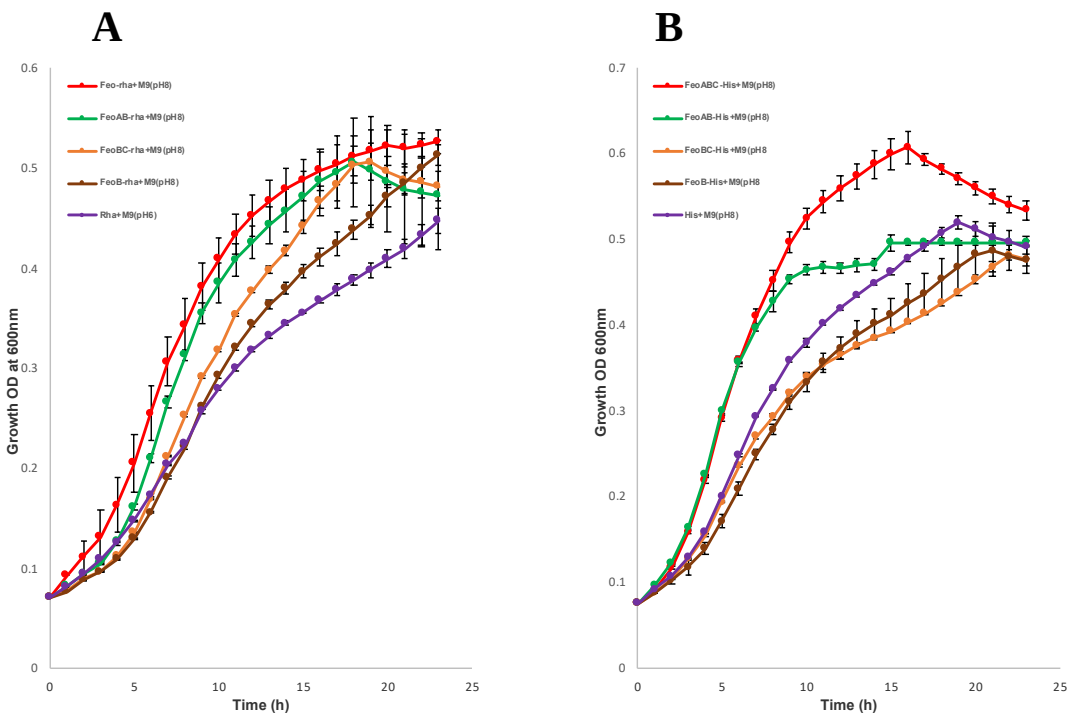

Figure 7.16. Growth of *E. coli* iron-transport mutant (JC32) under <u>low iron with/without DTPA,</u> complemented with <u>*rha*</u>-inducible *feoAB, feoABC, feoB* or *feoBC*, at pH 8. The details as in Fig 7.13 except only pBADrha constructs are included (with 0.02% rhamnose), and ferric citrate was <u>not</u> used in the growths above (just in the overnight cultures); instead, either no addition (**A**) was applied or 1 μM DTPA (**B**) (pH was 8).

For the pBADara plasmid constructs, there was a clearer growth enhancement for the *feoABC* and *feoAB* complemented mutant with respect to the vector control (Fig. 7.17). This likely reflects differences in adventitious iron content of the media at the time of growth. The overall growths achieved both with and without DTPA were very weak (maximum OD of 0.16), suggesting extreme iron limitation. In absence of DTPA, the *feoABC*-strain showed superior growth to that of the *feoAB*-complemented strain, but with DTPA the two strains showed similar growth (Fig. 7.17B). This suggests that under extreme iron limitation aerobically, at pH 8, the FeoC proteins offers little advantage for Feo activity.

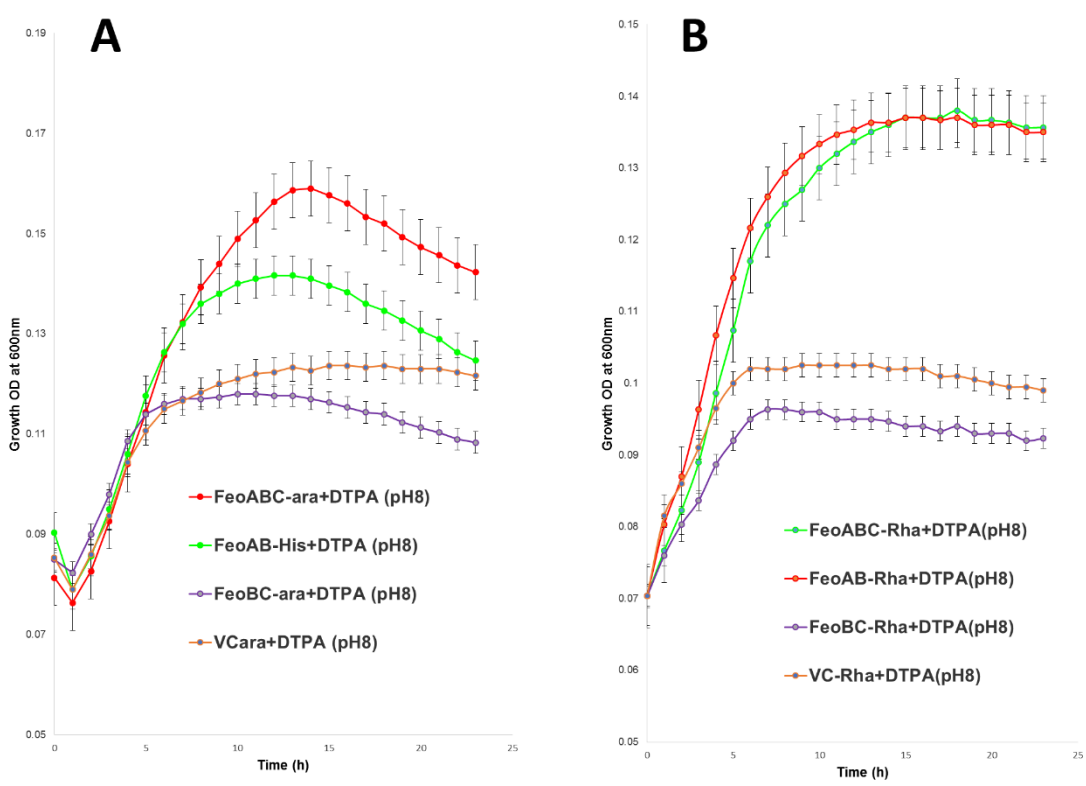

Figure 7.17. Growth of *E. coli* iron-transport mutant (JC32) under low iron with/without DTPA, complemented with *ara*-inducible *feoAB, feoABC* or *feoBC*, at pH 8. The details as in Fig 7.17 except only pBADara constructs are included (with 0.02% arabinose), and ferric citrate was not used in the growths above (just in the overnight cultures); instead, either no addition (**A**) was applied or 1 μM DTPA (**B**) (pH was 8), twice time repeat and similar result was obtain.

7.3.5. Combination of *feo* genes in-trans results in complementation of aerobic, low-iron growth deficiency

The above results indicate that FeoB requires FeoA for Feo activity under aerobic conditions, and that FeoC is required for maximal activity. In order to confirm these findings and eliminate any possible artefact arising from the organisation of the *feo* genes within a co-transcribed operon, the genes had been cloned in single or pairwise format into the pBAD vectors to allow their co-induction within double transformants (see above). Thus, a series of double

transformants were made in JC32 and the impact of provision of *feoB* with *feoC* or *feoA* in trans, or in cis, was investigated.

The results show (Fig. 7.18) that combining *feoAB* with *feoC* in trans results in enhanced JC32 growth (with respect to the vector control) under iron restriction by threefold ($P<0.01$; without and with DTPA, respectively). Similar growth enhancement was seen for the two plasmid combinations (*ara-feoAB* with *rha-feoC*, and *rha-feoAB* with *ara-feoC*) (Fig.7.18). However, when *feoBC* was combined with *feoA*, although a growth enhancement was seen, it was less than that obtained with the *feoAB/feoC* combination (2 and 1.2 fold, without and with DTPA respectively cf. the vector control; $P<0.01$). The reason for this difference is unclear but could relate to a negative polarity effect on *feoC* expression when positioned downstream of *feoB*.

At pH 8, the results obtained were generally similar with the *feoAB/feoC* combinations resulting in enhanced growth of JC32, with respect to the vector control, that was greater than seen for any other combination (Fig. 7.19). The *feoA/feoBC* combination again gave a growth enhancement that was weaker than that of the *feoAB/feoC* combinations, but with DTPA the difference was minimal (28% at 24 h). Although the *feoB/feoC* combination gave weak growth enhancement with DTPA, with growth similar to that of the vector control, in absence of DTPA a moderate growth enhancement was seen (1.5 fold at 10 h cf. the vector control; Fig. 7.19A) which was similar to that obtained by the *feoA/feoBC* combination. These observations suggest that the impact of the different *feo* expression formats on iron-limited growth might be dependent on the details of the growth conditions employed (i.e. pH and degree of iron availability).

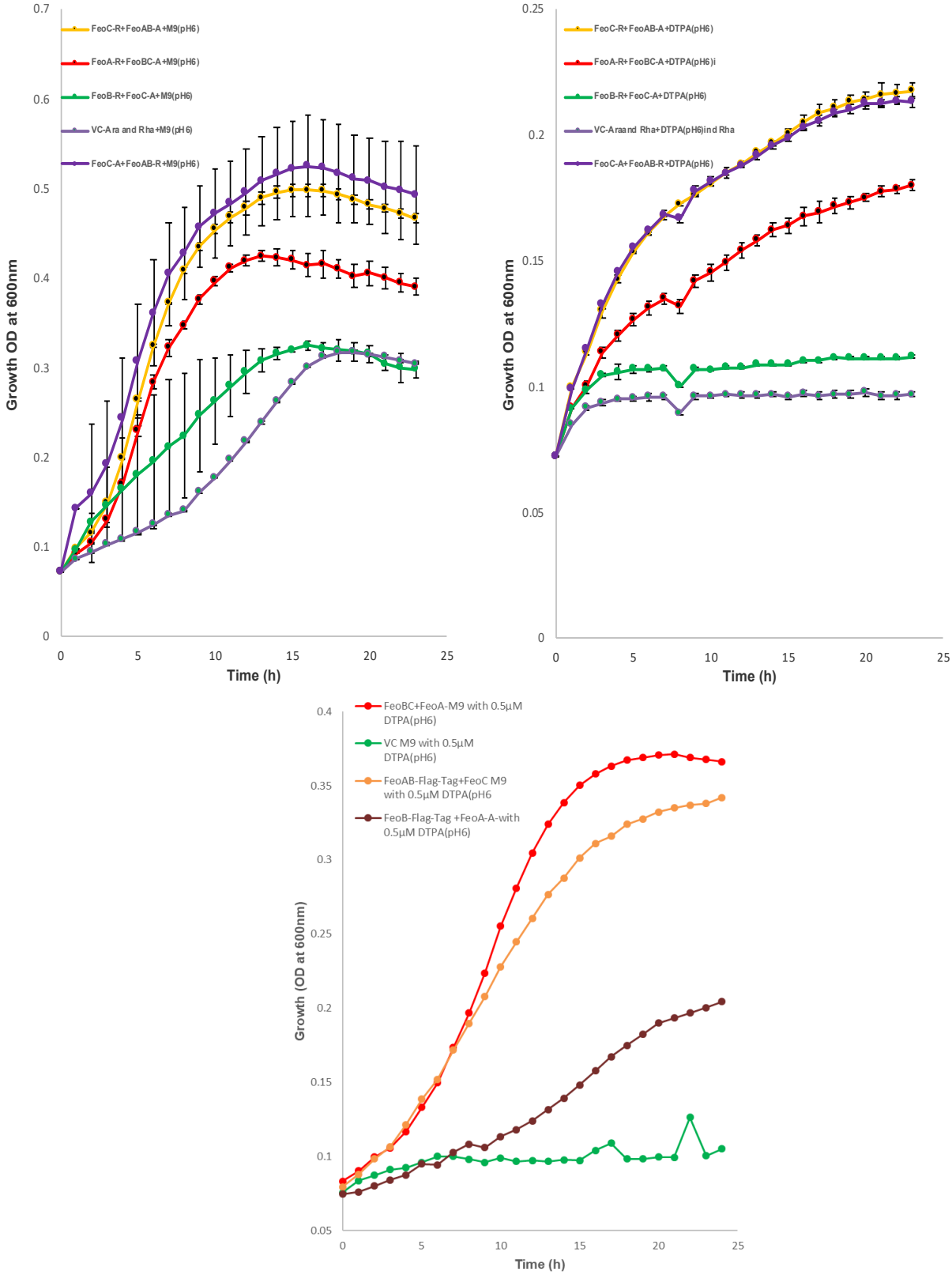

Figure 7.18. Growth of *E. coli* iron-transport mutant (JC32) under low iron +/-DTPA, complemented with *ara*-inducible *feoA*, *feoAB* or *feoBC* with rha-inducible *feoA*, *feoAB*, *feoB* or *feoC* at pH 6. Growth was in M9 medium and aerobic. The details as in Fig 7.18 except JC32 carried two plasmids, a pBADara (A) and a pBADrha (R) construct, as indicated. **A.** No addition. **B.** 1 µM DTPA. **C**. 0.5 µM DTPA. pH was 6. Data shown are the means of three independent growths. This experiment was conducted in triplicate and similar result obtained. Arabinose and rhamnose were included at 0.02% and 0.002%, respectively.

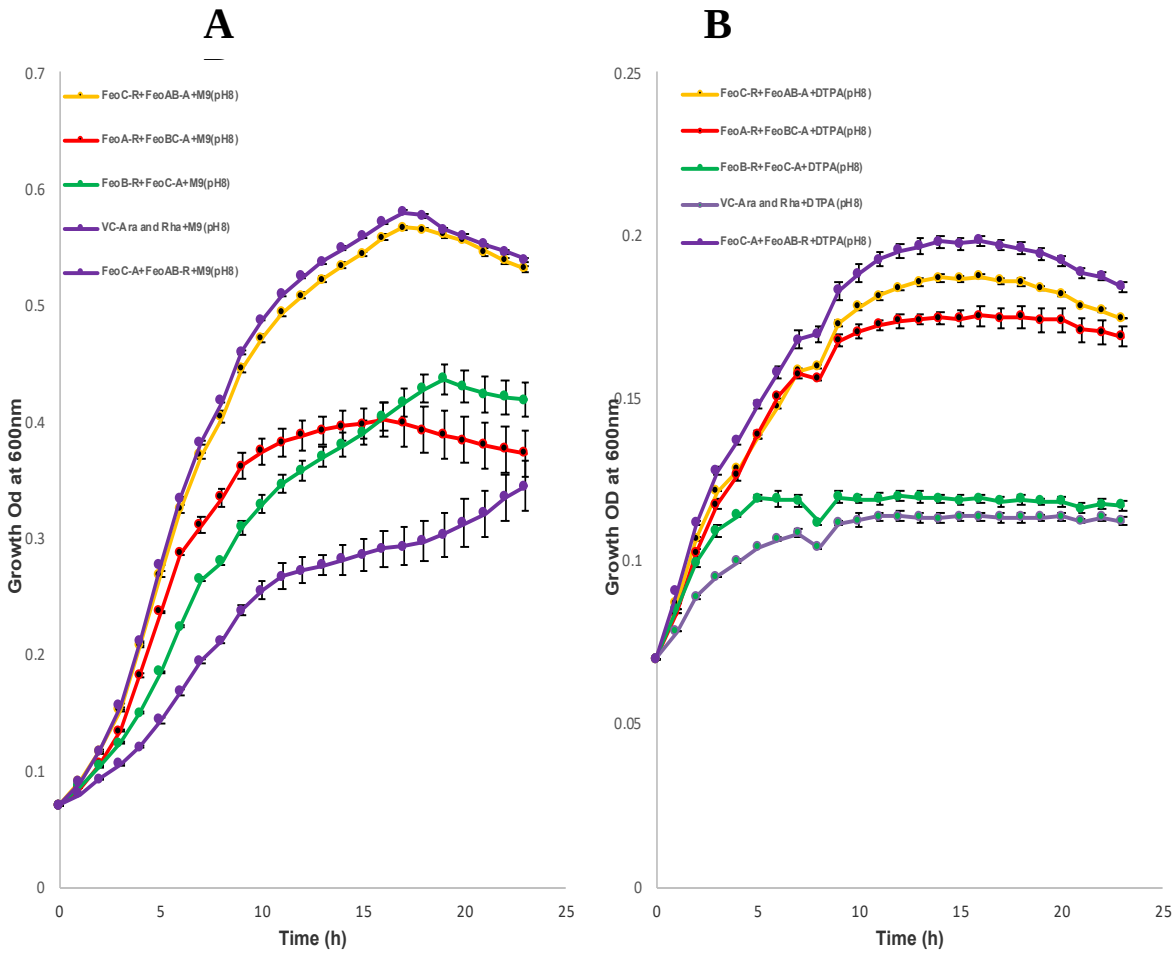

Figure 7.19. Growth of *E. coli* iron-transport mutant (JC32) under low iron +/-DTPA, complemented with *ara*-inducible *feoA*, *feoBC* or *feoAB* with rha-inducible *feoAB*, *feoA*, *feoB* or *feoC* <u>at pH 8</u>. As in Fig. 7.19, except at pH 8.

7.4. Impact of ascorbic acid on Feo-enhanced low-iron growth

7.4.1. Effect of ascorbate on growth of W3110 and JC32 under low-iron conditions

The above work shows that FeoABC and FeoAB can support bacterial growth under aerobic, iron limited conditions. Since FeoABC is considered to be an anaerobic/microaerobic iron transporter and is reported to be subject to degradation in the presence of oxygen, it is possible that presence of a reducing agent would improve FeoABC activity under aerobic conditions, by provision of ferrous iron and by acting as an antioxidant that would preserve the integrity of the FeoC 4Fe-4S cluster, as well as maintain the reduced status of the conserved Cys residues (Giustarini *et al*., 2008) within the Gate motifs of the FeoB permease domain. Indeed, ascorbic acid is a well-known dietary inducer of iron absorption as it converts Fe^{3+} to Fe^{2+} (White, 1970). However, it can also act as a pro-oxidant in the presence of metals.

The experimental approach used here was as described above (and in Section 2.3.6), with *E. coli* JC32 transformants (and W3110 wildtype) grown aerobically using a Lab System Bioscreen apparatus at 37 ºC (250 rpm) in 0.4% glucose M9 medium with/without 2 mM ascorbate, and 0.5 or 1 µM DTPA.

Initially, the effect of the presence of the ascorbic acid on growth in M9 medium with DTPA was tested, to ensure that growth was not unduly effected by 2 mM levels of ascorbate. The results obtained (Fig. 7.20) show that the wildtype grew well with ascorbate under low-iron conditions, whereas the JC32 strain grew poorly. Indeed, 2 mM ascorbate caused a major increase (~sixfold) in growth (at pH 8; Fig. 7.20A) for the wildtype suggesting that its presence supports delivery of iron.

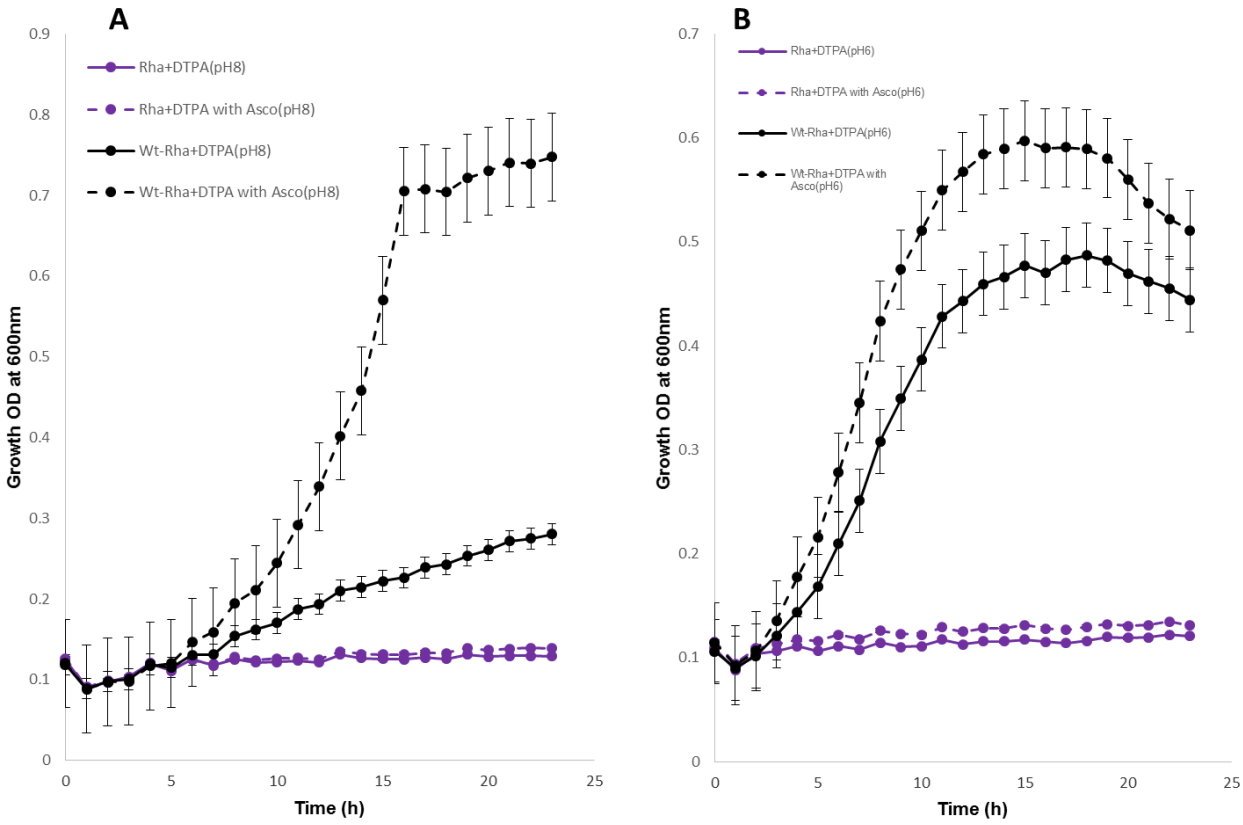

Figure 7.20. Growth of wildtype and iron-transport mutant (JC32) under low iron with/without ascorbate. Strains used were W3110 (pBADrha) (black) and JC32(pBADrha) (purple). Medium was 0.4% glucose in M9 medium at pH 8 (**A**) or 6 (**B**), with appropriate antibiotic, and with 1 µM DTPA and either with/without 2 mM ascorbate. Growth was aerobic at 37 ˚C in a Bioscreen system (300 µl volumes) with constant shaking at 250 rpm. Values are averages from three biological replicates, with standard error shown. Pre-cultures were growth overnight in 0.4% glucose M9 medium (37 ˚C, 250 rpm) with 10 µM ferric citrate and were washed in iron-free M9 medium before use. Starting cell density of all Bioscreen cultures was adjusted to OD_{600} (0.01).

7.4.2. Effect of ascorbic acid on low-iron growth of *E. coli* JC32 complemented with *feo* genes

When the JC32 strain was complemented with pBADara-*feoABC*, ascorbate enabled an ~twofold increase in growth under low-iron conditions win respect to growth without ascorbate (at pH 6), resulting in a major growth increase with respect to the vector control (5.2 fold, Fig. 7.21A). The pBADara-*feoAB* plasmid also allowed an increased growth with ascorbate with respect to that without ascorbate (1.75-fold increase; Fig. 7.21A), but the overall growth was much less (~five time less) than that achieved with *feoABC*. The other *feo* gene combinations tested did not support low iron growth with or without ascorbate. At pH 8, a similar effect was seen but the enhancement in growth caused by ascorbate was greater than at pH 6 (Fig. 7.21B), and the growth enhancement caused by *feoABC* without ascorbate was much less than seen at pH 6. In summary, these results indicate that the presence of the FeoC greatly enhances aerobic Feo activity both with and without ascorbic acid.

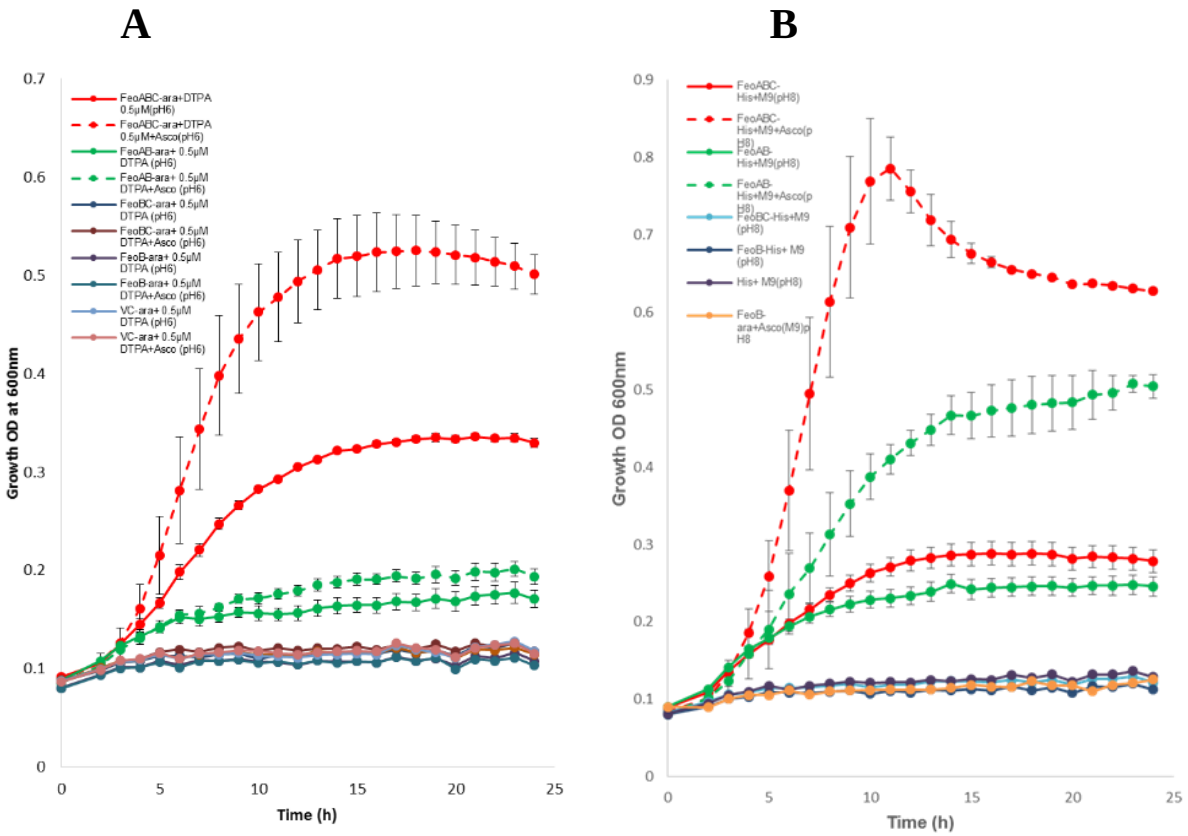

Figure 7.21: Effect of ascorbic acid on low-iron growth of *E. coli* JC32 transformed with pBADara-*feoB*, -*feoBC*, -*feoAB* or -*feoABC*. The indicated JC32 transformants were grown aerobically using a Bioscreen apparatus lab system C in M9 medium with 100 mM MES (pH 6) (**A**) or TAPS (pH 8) (**B**), 0.4% glucose, 0.02% arabinose, antibiotic and 0.5 μM DTPA, with/without and 2 mM ascorbic acid. Data represent the mean (and standard error) OD values of triplicates. All other details are as above. 'VC', vector control (JC32 with pBADara).

When the above experiments were repeated with DTPA (to enhance iron-restriction still further), it was found that the *feoABC* and *feoAB* complemented strains failed to grow in the absence of ascorbate (Fig. 7.22). Indeed, growth of the *feoAB* complemented strain was entirely inhibited both with and without ascorbate when DTPA was applied. However, growth in the presence of DTPA was restored for the *feoABC*-complemented strain when ascorbate was provided (Fig. 7.22). As can be observed, the wildtype was little affected by the inclusion of DTPA (compare with data in Fig. 7.21). These results thus indicate that FeoC provides the Feo system with the capacity to acquire iron under aerobic, reducing conditions when iron limitation is enhanced by presence of a ferric chelator.

It is suggested that ascorbate has two effects relevant to the growth phenotypes observed, it acts as an antioxidant and also assists in mobilization/solubilisation of iron. However, with addition of DTPA it is likely that the iron-mobilization activity of ascorbate would be negated as DTPA would likely sequester iron more favourably than ascorbate. Thus, when both ascorbate and DTPA are present, iron availability is likely to be more greatly restricted but conditions would remain reducing.

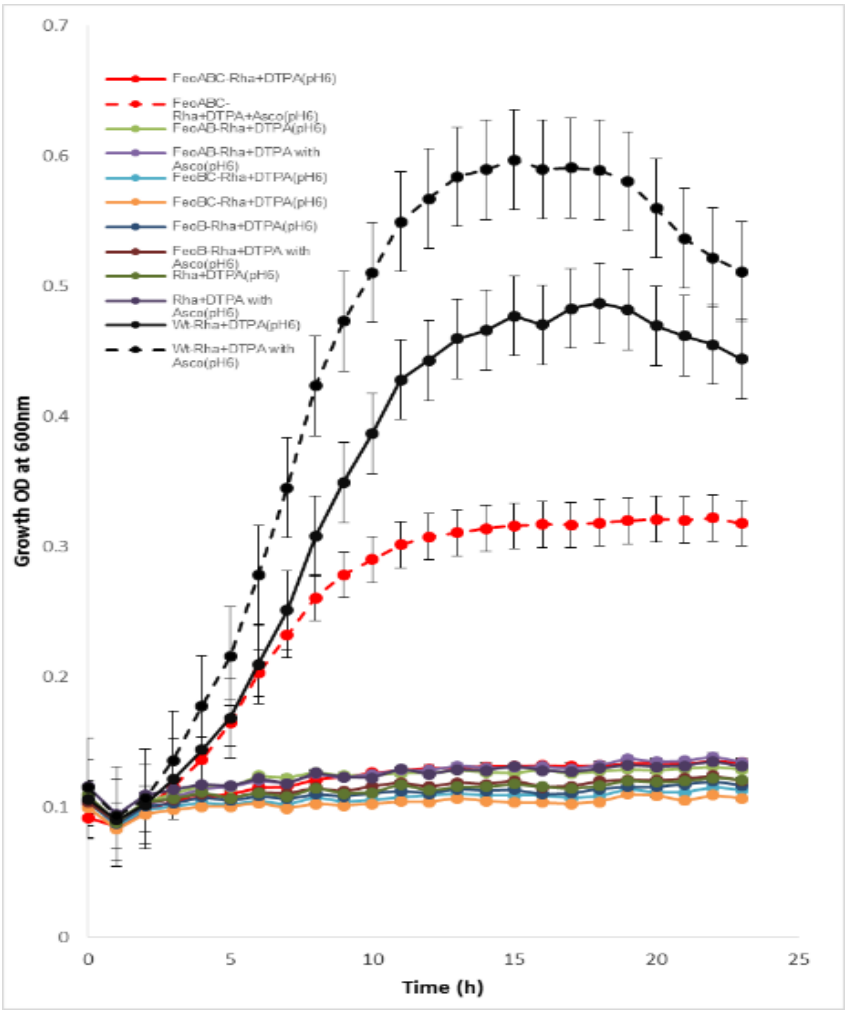

Figure 7.22: Effect of ascorbic acid on low-iron growth of *E. coli* JC32 transformed with pBADrha-*feoB*, -*feoBC*, -*feoAB* or -*feoABC* in presence of 0.5 µM DTPA, at pH 6. Details are as above except that pBADrha plasmids were used and 0.5 µM DTPA was included.

Similar results to those seen above were obtained at pH 8, with DTPA combined with ascorbate (Fig. 7.24). With 0.5 or 1 µM DTPA, the growth of the *feoABC*-complemented strain was the same as that of the *feoAB*-complemented strain (Fig. 7.23). However, when ascorbate was added, there was a major increase in growth of the *feoABC*-complemented strain (4.5- or two-fold, Fig. 7.23A and B, respectively), but not for the *feoAB* strain (or any of the other *feo* constructs used). Thus, as seen above, when DTPA is present, ascorbate only supports the growth of the *feoABC*-complemented JC32 strain.

The results confirm the observation above that FeoC provides FeoAB with the capacity to act as an iron transporter under DTPA-dependent iron limitation, in the presence of ascorbate. This effect could arise from the protection of FeoB degradation by the 4Fe-4S-form of FeoC under aerobic, reducing conditions, but not under aerobic non-reducing conditions (Lau et al., 2016; Sestok *et al*., 2018).

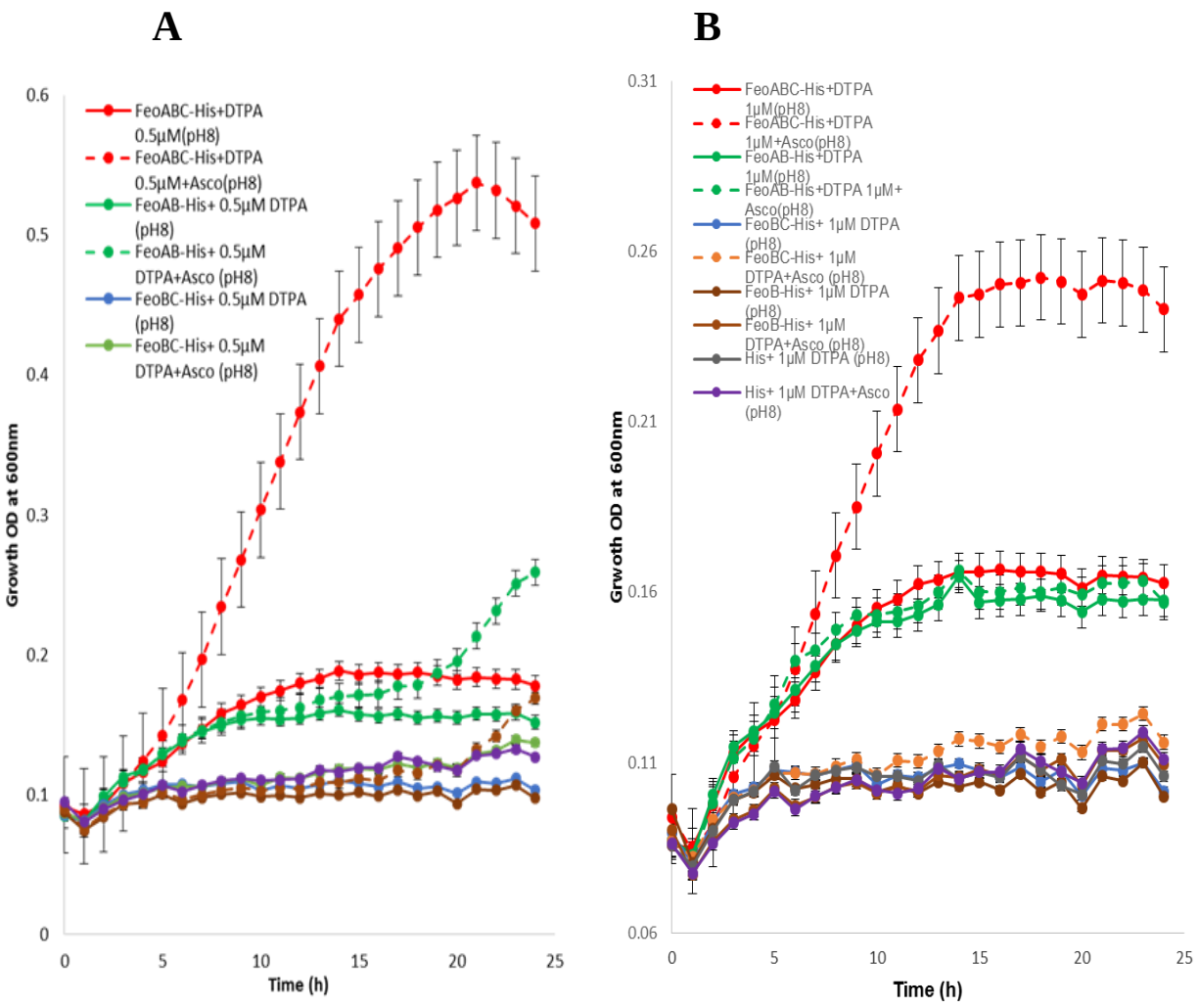

Figure 7.23: Effect of ascorbic acid on low-iron growth of *E. coli* JC32 transformed with pBADara-*feoB*, -*feoBC*, -*feoAB* or -*feoABC* in presence of DTPA, at pH 8. Details are as above except that pBADara plasmids were used at pH 8 (100 mM TAPS) with 0.5 (**A**) or 1 µM (**B**) DTPA. Growth was in A Bioscreen C system.

7.5. Effect of catalase on aerobic Feo-activity in presence of DTPA

The effect observed for ascorbate on FeoABC activity in the presence of DTPA, could be related to the anti-oxidant properties of ascorbate which might assist in inhibiting the FtsH-mediated (and FeoC-inhibited) degradation of FeoB in presence of oxygen. If this effect is indeed caused by anti-oxidant activity, then it is possible that provision of catalase could have a similar effect by preventing the accumulation of H_2O_2. To test this possibility, catalase was included in growth experiments (as above).

When catalase was included at pH 6, the growth of the *feoABC*-complemented strain with DTPA was considerably greater (<twofold) than that of the *feoAB*-complemented strain, which showed a modest growth with respect to the vector control (1.5 fold greater at 16 h) (Fig. 7.24). Since the *feoABC*- and *feoAB*-complemented strains gave similar growth with DTPA when catalases was absent (Fig. 7.23), this indicates that absence of H_2O_2 supports enhanced iron uptake by FeoAB when FeoC is also present. This would be consistent with the role of FeoC in protecting FeoB from degradation by FtsH under aerobic conditions, but suggests that FeoC responds to peroxide rather than O_2.

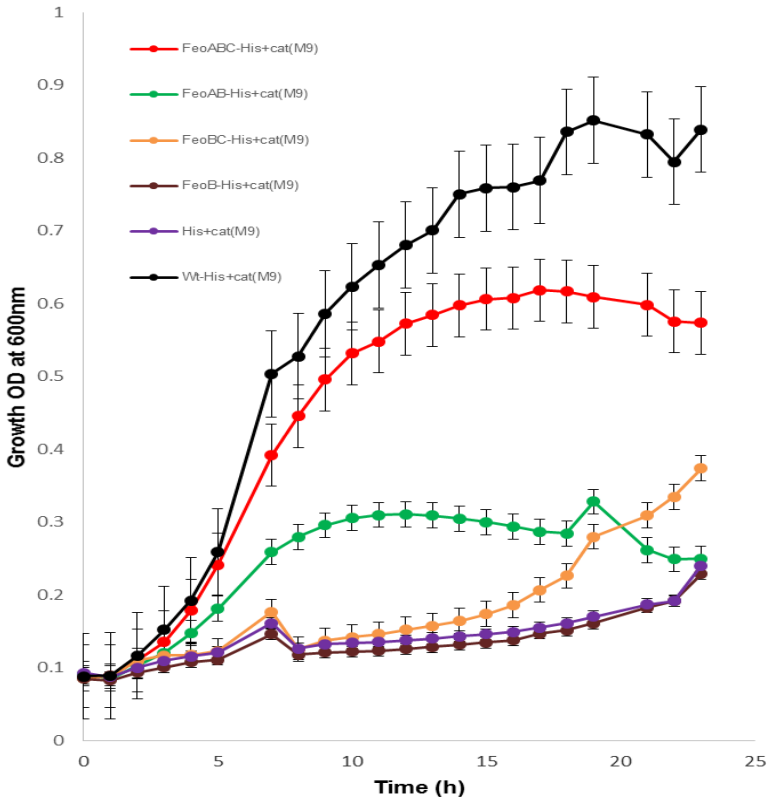

Figure 7.24. Effect of catalase on iron-limited growth of *feo*-complemented JC32 in the presence of 0.5 µM DTPA. Strains were grown aerobically in M9 medium with 100 mM MES (pH 6), 0.4% glucose with 0.5 µM DTPA and 1000-unit catalase. Data represent the mean OD values of triplicates. Strains were W3110 (W) and JC32 with pBADara-*feoABC*, -*feoAB*, -*feoBC* and -*feoB*, and pBADara. All other details are as above.

Comparison of the effect of ascorbate and catalase indicated that similar growth effects are generated by these two agents in the presence of DTPA (Fig. 7.25). Thus, iron-restricted growth of JC32 with FeoABC was greatly supported (~twofold) by either catalase or ascorbate when DTPA was present. Catalase or ascorbate caused an increase in growth for the *feoABC*-complemented strain of 0.28-0.29 OD units (cf. growth without these additions), whereas for the *feoAB*-complemented strain the increase seen was 0.05 and 0.02 OD units, respectively, which suggests that catalase provides a greater benefit than ascorbate for the FeoAB system (Fig. 7.25). Ideally, these effects would be more thoroughly explored using a range of chelators and reductants, as well as catalase, at various concentrations in order to gain a more detailed understanding to the relationship between FeoC and FeoAB activity.

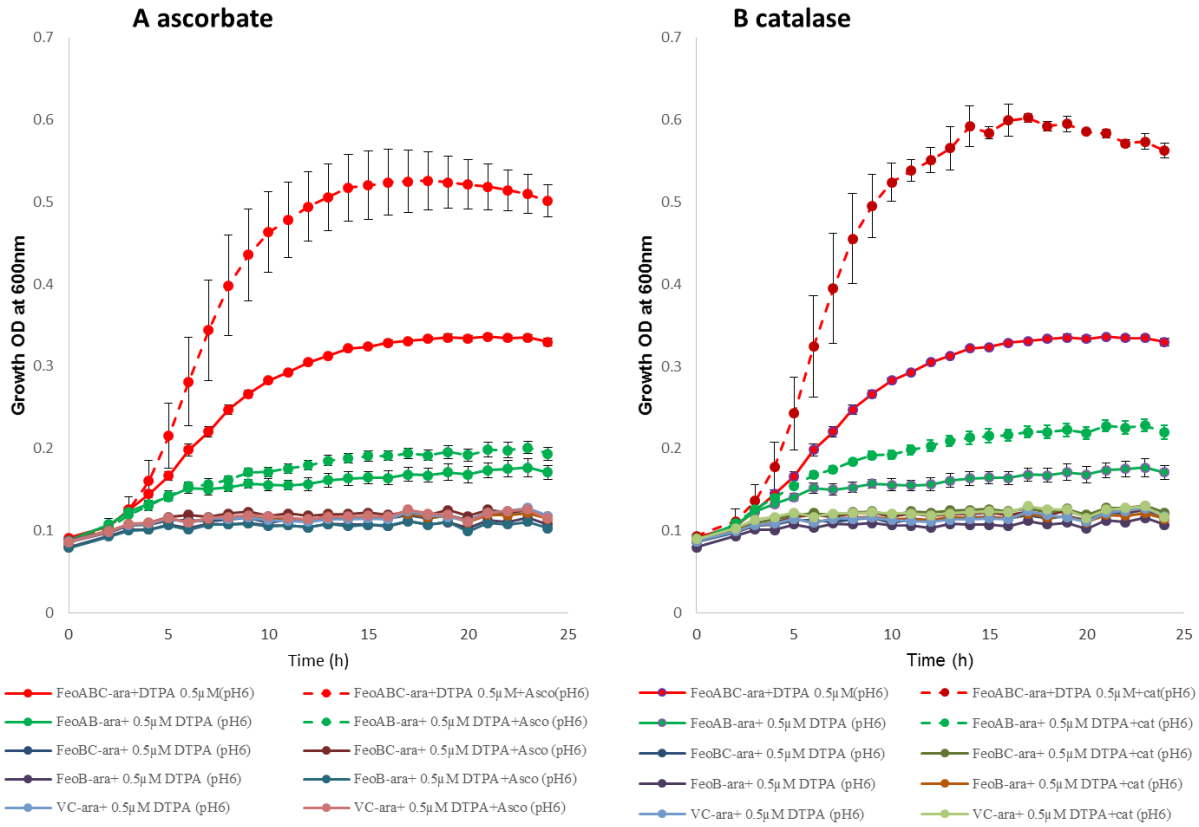

Figure 7.25: Comparison of the effects of ascorbic acid or catalase on Feo-dependent growth of *E. coli* JC32 under low-iron conditions with 0.5 µM DTPA. All details were as above except that medium included either 2 mM ascorbate (**A**) or 1000U catalase (**B**), or no additions. the pH was 6 and 0.5 µM DTPA was included in all cases. Data represent the mean OD values of triplicates. All

7.6. Comparison of the effect of catalase on *feoABC*- and *feoAB*-mediated low-iron growth of JC32 without DTPA

The studies in Chapter 5 showed that the FeoABC-supported low-iron growth under aerobic conditions is enhanced when catalase is provided. In addition, FeoABC-mediated iron uptake was shown to be dependent on the absence of H_2O_2. In this section, the impact of catalase on the low-iron growth of the *feoAB*- and *feoABC*-complemented JC32 strains was tested, in the absence of DTPA (i.e. as in Chapter 5), to determine whether FeoAB-dependent iron uptake is also subject to H_2O_2-dependent inhibition. Such a finding would be significant, since any

FeoAB response to peroxide cannot be moderated by FeoC, and thus any such effect observed would suggest the existence of a FeoC-independent mechanism for control of Feo activity by peroxide, such as via oxidation of key Cys residues in FeoB.

Growth conditions were as used generally throughout this chapter, and both the pBADara and pBADrha constructs (single complementation format) were used for transformation of JC32 (Fig. 7.26). The results again show the major growth advantage of the *feoABC*-complemented strain under aerobic iron restriction, and the moderate growth advantage of the *feoAB*-complemented strain. Catalase caused a small increase in growth of the *feoABC*-complemented strain, but a major increase was seen for the *feoAB*-complementations (Fig. 7.26) of up to threefold. This clearly indicates that the FeoAB system is subject to post-transcription control by H_2O_2 in a FeoC-independent fashion, and thus evidence for a second mechanism by which Feo activity is regulated post-transcriptionally by O_2 and/or H_2O_2.

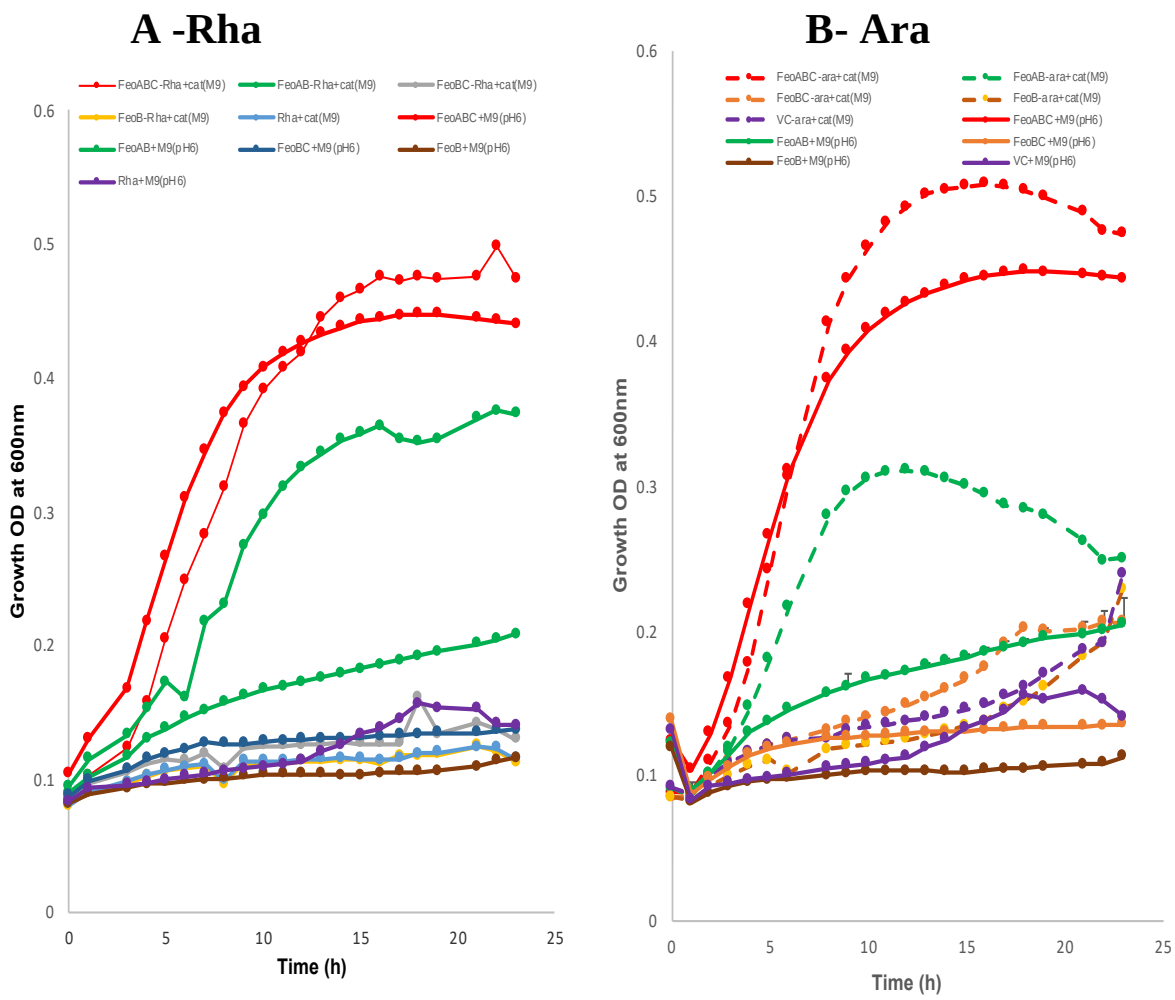

Figure 7.26: Effect of catalase on growth of *E. coli* JC32 transformed with pBAD-Feo. Strains were grown aerobically in a Bioscreen system using M9 medium with 100 mM MES (pH 6), 0.4% glucose with 1000U catalase. Data represent the mean OD values of triplicates. All other details were as above.

7.7. Are FeoC and FeoA necessary for the Feo-mediated import of ferrous iron uptake under anaerobiosis?

The results in this chapter suggest that FeoC may provide the Feo system with a higher iron uptake activity under conditions where O_2 and/or H_2O_2 are abundant. In order to further test this possibility, and determine whether FeoC (and FeoA) is required for anaerobic Feo activity, the growth experiments with complemented JC32 were repeated under anaerobic conditions.

Initial results indicated that the *feoABC*-complemented mutant achieves similar growth under anaerobic, low-iron conditions as that of the wildtype (Fig. 7.27A), and that a greater growth difference is obtained with respect to the vector control when DTPA is included (Fig. 7.27B) since the JC32(pBADara) strain failed to grow under such conditions. This suggests that much of the anaerobic iron-uptake activity of the wildtype is FeoABC dependent, particularly when DTPA is present. Interestingly, the degree of growth enhancement achieved with *feoAB* complementation under anaerobic conditions (with DTPA) was close to that seen for *feoABC* (maximum ODs of 0.16 and 0.19, respectively; P=0.299) complementation which suggests that absence of FeoC have only a minor impact on Feo activity under the conditions employed (Fig. 7.27C).

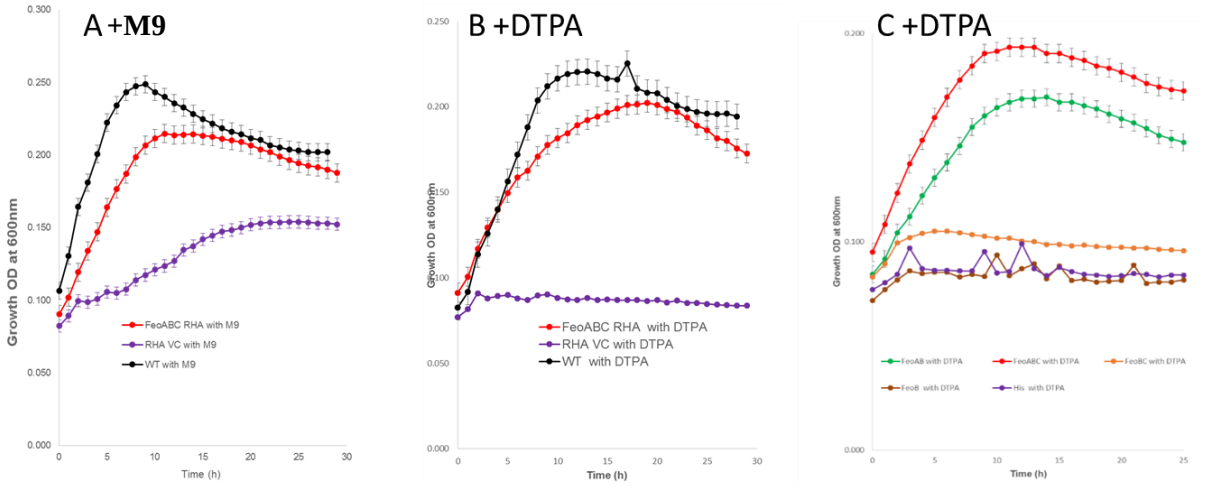

Figure 7.27: <u>Anaerobic growth</u> of *E. coli* JC32 transformed with pBADara-*feoB, feoAB, feoBC* or -*feoABC* M9 medium with/without <u>0.5 µM DTPA</u>. 'His' or 'VC' represents the vector control, and 'WT' indicates W3110 (wildtype). Data represent the mean values of duplicate with standard error shown; growth was at 37 ˚C in a FLUOstar plate reader. **A**, wildtype compared to *feoABC*-complemented and vector-complemented JC32. **B**, as A, but with 0.5 µM DTPA. **C**, as B but with comparison of different *feo* complementations of JC32.

The relatively high growth under anaerobic, low-iron conditions supported by *feoAB*-complementation of JC32 is further illustrated when the impact of the pBADara and pBADrha constructs is compared (Fig. 7.28). Both pBADara-*feoAB* and pBADrha-*feoAB* enhanced growth of JC32 to levels very similar to those achieved with the corresponding *feoABC* complementations (Fig. 7.28A) – maximum OD values of 0.25/0.27 and 0.24/0.25, respectively (P= 0.311). A similar effect was seen with 1 and 2 µM DTPA (Fig. 7.28BC) – although again vector control and other *feo* combinations showed very little growth with DTPA and so the difference in growth with respect to that achieved by the *feoAB/feoABC* complementations was greater than that seen without DTPA. This result further highlights a lack of requirement for FeoC for Feo activity under anaerobic conditions. It also confirms the need for FeoA along with FeoB under anaerobiosis, since the *feoB* and *feoBC* complementations provided no notable growth advantage (Fig. 7.28).

The poor anaerobic, low-iron growth of the JC32 transformants lacking *feoAB/feoABC* was reversed when iron was added to the growth medium, such that growth levels for all JC32 transformants were very similar to that of the wildtype (Fig. 7.29A). Thus, the growth effects observed in the absence of added-iron are clearly related to differences in capacity to cope with iron-restricted conditions applied, and can be presumed to correlate with differences in iron uptake activity.

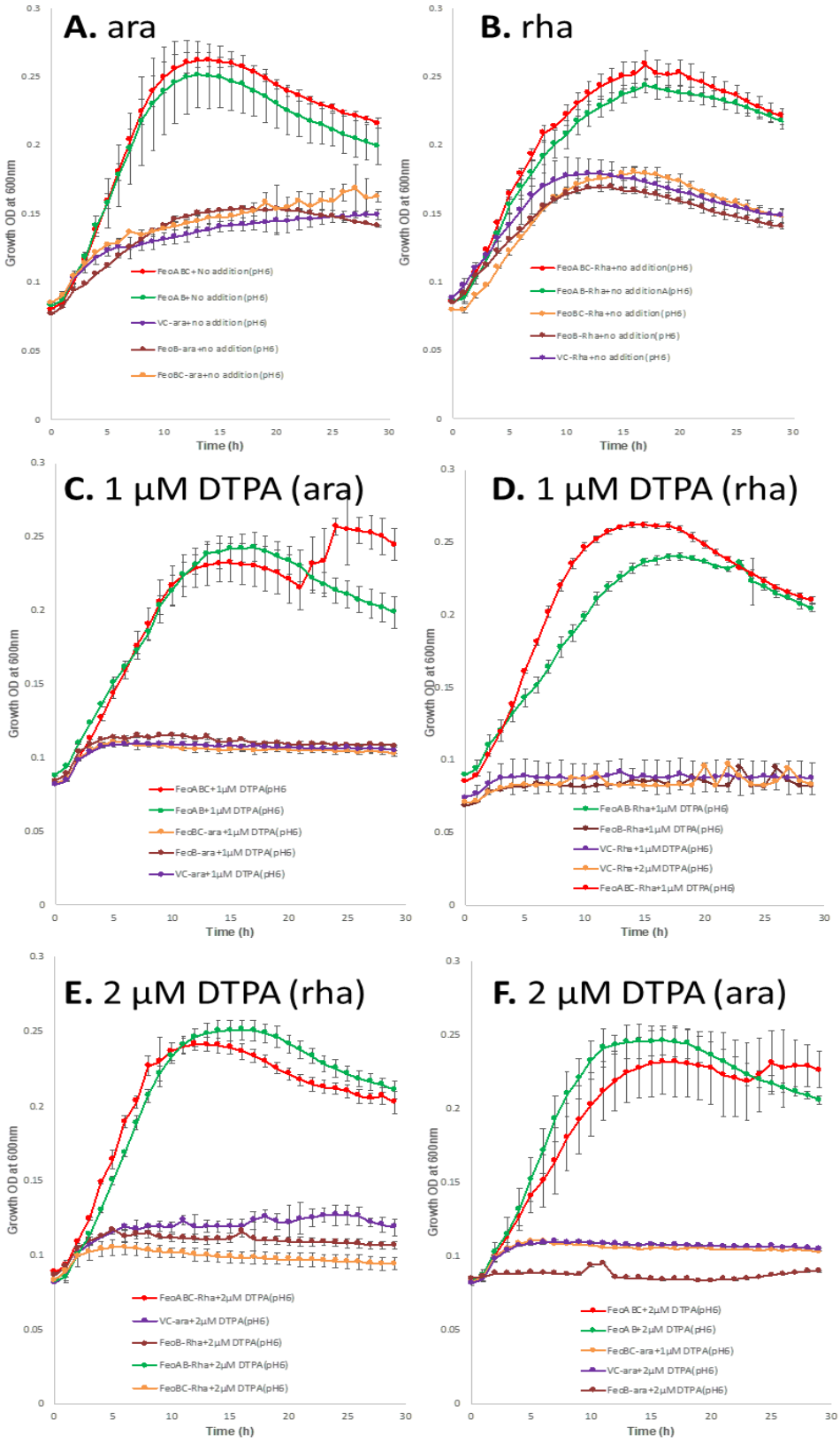

Figure 7.28: Anaerobic growth of *E. coli* JC32 transformed with pBADara/rha-*feoB, feoAB, feoBC* or -*feoABC* in M9 medium with/without DTPA. 'VC' represents the vector control. Conditions are as in the Fig. above except for DTPA levels (as indicated). In this case, both pBADara and pBADrha constructs were employed in JC32.

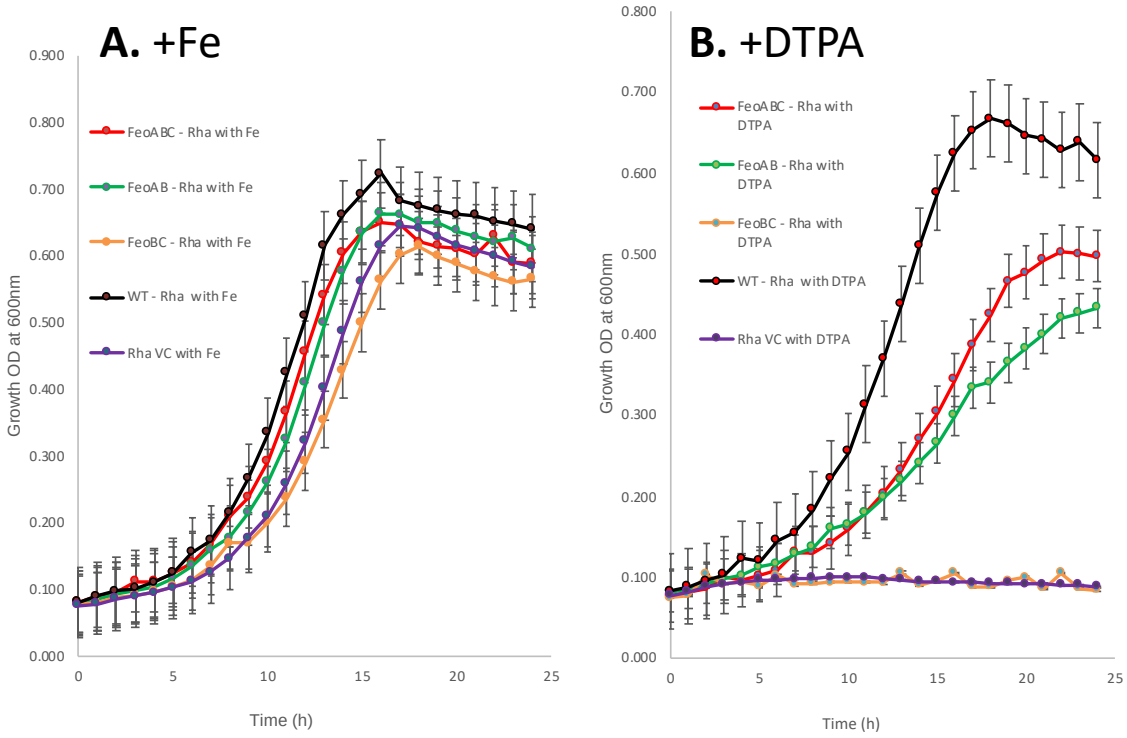

Figure 7.29: Anaerobic growth of *E. coli* JC32 transformed with pBADrha-*feoAB, feoBC* or -*feoABC* in M9 medium with <u>added iron</u>. 'VC' represents the vector control. 'WT' indicates wildtype (W3110). Conditions are as in the Fig. above except for inclusion of 10 µM ferric citrate (**A**) or 1/2 µM DTPA (**B**). Only pBADrha constructs were employed in JC32. Data represent the mean values of duplicate; growth was at 37 ˚C in anaerobic conditions in a FLUOstar.

7.8. DISCUSSION

Fe^{2+} uptake by Feo is considered the most common, iron-specific bacterial ferrous-iron uptake pathway, and this system has been linked to bacterial colonisation and survival in various hosts, and pathogenic virulence (Carton *et al*., 2006; Nalikare *et al*., 2006; Perry *et al*., 2007; Lau *et al*., 2015; Caharles *et al*., 2013; Perez *et al*., 2016; Sestok *et al*., 2018). The more soluble, ferrous form of iron is likely to predominate under conditions where oxygen is scarce, and since brackish water, sediments and the human intestinal tract are all likely to be low in oxygen, ferrous iron may be the predominant form of iron available to *E. coli* and other bacteria in many such ecological niches. The *feo* operon of the Enterobacteriaceae encodes three proteins: FeoA, the small cytoplasmic protein that has an unclear purpose in enabling FeoB activity; FeoB, the major protein in the Feo system which consists of a cytoplasmic G-protein domain capable hydrolysing GTP coupled to a ferrous-iron transporting, nucleoside-transporter-like permease domain; and FeoC, a small cytoplasmic winged-helix 4Fe-4S protein reported to protect FeoB from degradation anaerobically (Boulette *et al*., 2007; Hsueh *et al*., 2013; Kim et al., 2013). Much remains to be learned concerning the specific purposes of these three components, their mechanisms of action and their interactions.

In order to assess whether the Feo proteins of *E. coli* are functional when divorced from their natural promoters and then expressed to similar levels under aerobic conditions, and to test the requirement for all three Feo components under conditions where transcription and translation are under control of a surrogate expression system, the plasmids $pBAD_{ara}$ and $pBAD_{rha}$ were used as complementary inducible vector systems. This enabled the controlled expression of the Feo proteins from the inducible *ara* and *rha* promoters in a mutant (JC32) that was otherwise devoid of any apparent iron transport route that would apply within the minimal medium growth conditions employed. An experiment to assess JC32 growth when complemented with the

pBADrha-*feo* constructs under aerobic conditions showed that *feoABC* supports low-iron growth to a high degree, providing growth levels similar to those of the wildtype. However, when DTPA was included in the medium, the induced *feoABC* system was ~threefold less effective in supporting growth (with respect to that seen by the wildtype), indicating that FeoABC functions weakly aerobically under extreme iron restriction (Fig. 7.15). FeoAB was also found to support aerobic, low-iron growth of JC32, but this was up to fivefold lower than that achieved by FeoABC, indicating an important role for FeoC in aerobic Feo function. FeoB and FeoBC failed to support low-iron growth and thus it is clear that the minimal requirement of Feo function is the combination of FeoA and FeoB. The results obtained with the *rha*-inducible constructs were reflected with those obtained with the *ara*-inducible format (Fig. 7.16). At pH 8 under aerobic conditions, the difference in low-iron growth enhancement between the *feoABC* and *feoAB* complemented JC32 was greatly reduced with respect that seen at pH 6, largely due to a poorer apparent Feo activity provided by the FeoABC system (Fig. 7.17). This effect may be caused by lower ferrous iron availability resulting from the higher pH.

Expression of the Feo components from complementary plasmids was used in order to avoid any complications arising from polarity effects when expressed in co-transcript format. This work confirmed that the presence of all three Feo components is required for high Feo activity aerobically (Fig. 7.19-20). It also showed that FeoAB with FeoC gives a better Feo activity than FeoA with FeoBC, suggesting that there may be a polarity effect of *feoC* expression when it is located downstream of *feoB*. The combination of FeoA and FeoB was shown to provide moderate Feo activity, as found when the corresponding genes were expressed as a *feoAB* co-transcript.

The possibility that FeoABC performance would be enhanced by provision of a reductant due to either increased ferrous iron availability or to an anti-oxidant effect on FeoB stability was

tested. It was found that ascorbate increased both FeoABC- and FeoAB-dependent Feo activity, aerobically (Fig. 7.22). However, when DTPA was also provided, the presence of ascorbate had little impact on FeoAB-dependent Feo activity, but ascorbate continued to increase the activity exhibited by FeoABC in the presence of DTPA (Fig. 7.23-24). This suggests that FeoC strongly supports aerobic FeoAB function under high-iron restriction conditions in the presence (but not absence) of reductant, and this effect may occur through protection of aerobic FeoB degradation by FeoC (Kim *et al*., 2012). Catalase was found to generate a similar low-iron growth enhancement for the *feoABC* and *feoAB* complemented JC32 strain, as was seen for ascorbate (Fig. 7.26), suggesting that a major cause of the higher low-iron growth observed for the *feoABC*- and *feoAB*-complemented strains with ascorbate is due to the resulting anti-oxidant effect. Indeed, when the growth experiments were performed anaerobically, the *feoABC*-complementation resulted in low-iron growth (with or without DTPA) that was very similar to that of the wildtype (Fig. 7.28) indicating the major role played by Feo in anaerobic iron acquisition by *E. coli*. Surprisingly, the *feoAB*-complemented JC32 strain gave very similar low-iron growth to that seen for *feoABC*-complementation (Fig. 7.28-30) suggesting that FeoC has little importance anaerobically. This is a surprise because FeoC is reported to protect FeoB from degradation under reducing (anaerobic) conditions in *S. enterica* and is essential for Feo activity in *Vibrio cholerae* (Kim *et al*., 2012; Hung *et al*., 2012; Weaver *et al*., 2013; Stevenson *et al*., 2016). Thus, it is anticipated that lack of FeoC would result in poorer anaerobic low-iron growth with FeoAB than seen with FeoABC. This discrepancy may arise because the role of FeoC in FeoB protection was determined in *S. enterica*, whereas the work here is in *E. coli*. However, these two organisms are very similar (in terms of their FeoABC and FtsH proteins) and so such a difference would be unexpected. Another reason for the lack of any role for FeoC anaerobically as observed here could be related to copy number and expression levels, since raised FeoB levels with respect to those of the wildtype might result in poor FtsH degradation

due to excess FeoB substrate saturating FtsH degradation capacity. The pBADara vector has a pACYC183 (p15A) *oriC* giving ~15 copies per cell so there is considerable potential for such an effect. However, it should be pointed out that a role for FeoC was observed aerobically indicating that FeoC functionality has been maintained under the experimental conditions employed in this thesis.

In *V. cholerae*, both *feoA* and *feoC* were found to be required for Feo activity. These conclusions were based on in-frame knockout experiments. The potential for reduced *feoAB* expression in absence of *feoC* was considered by measurement of *feoAB* transcription which showed that lack of *feoC* does not markedly impact *feoAB* transcription (Weaver *et al*., 2013). However, in this work the *V. cholerae feo* genes were studied in a surrogate host (*Shigella flexneri*) which provides potential for artefactual findings.

Although the roles of the FeoA and FeoC proteins in Feo function remain to be clarified, it is clear from this thesis and from past research that FeoA is required for FeoB function (Kammler *et al*., 1993; Weaver *et al*., 2013). In addition, there is good evidence to indicate interaction between FeoB and, both FeoA and FeoC, such that a FeoABC complex is formed (Stevenson *et al.*, 2016). Indeed, mutation of the G-protein domain residues of the *V. cholerae* FeoB is reported to prevent such interaction indicating the both FeoA and FeoC interact with FeoB at the N-terminal domain (Stevensen *et al.*, 2016). No evidence for FeoC function as a transcription factor has been provided (Weaver *et al*., 2013; Kim *et al*., 2013) and indeed BACTH assays support a role for FeoC in binding to the N-terminal domain of FeoB (Weaver *et al*., 2013; Kim *et al*., 2013), and FeoA binding to FeoB (Kim *et al*., 2012). The FeoC interaction with FeoB is further supported by the co-crystallisation structure of *K. pneumoniae* FeoC and the N-terminal domain of FeoB in a 1:1 ratio (Hung *et al*., 2013).

The most significant finding in this chapter is the confirmation that FeoA is required for FeoB activity, and the unique observation that FeoC is not required. It appears that under anaerobic conditions, the Feo system of *E. coli* has little (if any) requirement for FeoC. However, under conditions where oxygen is available then FeoC promotes FeoAB activity considerably. This suggest that the role of FeoC is to support the activity of FeoAB under oxidative conditions. This effect appears largely unrelated to any expression control and so likely orrelates to either a direct stimulus of FeoB uptake activity or to a role in preserving FeoB from degradative turnover. The effect of FeoC on FeoB levels is explored in the following chapter.

Chapter 8: Effect of oxygen and FeoC-status on FeoB protein levels as determined using Flag-tag fusions and semi-quantitative Western blotting

8.1. Introduction

Enteric pathogens or commensal microorganisms, such as *E. coli* K-12, are primarily found in the gastrointestinal tract (GIT) (Russell *et al*., 2000). In the small intestine, iron is rapidly absorbed from the lumen into the epithelial cells of the villi; excess iron is stored in these cells as a ferritin (Rzymski *et al*., 2018), and the remainder passes into the bloodstream where it is incorporated into transferrin (Ganz *et al*., 2018; Zughaier *et al*., 2018). Consequently, while in the intestine, bacteria experience conditions of both anaerobiosis and iron depletion (Reigstad *et al*., 2007; Merrell *et al*., 2002). Thus, their ability to acquire iron under such conditions is an important aspect of their colonisation potential.

The Feo system is the major ferrous iron transporter used by *E. coli* anaerobically. It remains unclear why this system is only functional anaerobically/microaerobically, but the results relayed earlier in this thesis show that Feo can function aerobically when expressed from promoters that are not subject to aerobic repression. Further, the physiological purposes of FeoA and FeoC remain to be fully defined. Here, it is suggested that FeoA provides FeoB with iron-dependent control (through Fe-Fur interaction). In addition, the evidence above indicates that FeoC enhances Feo activity under oxidative conditions, thus suggesting that the role of FeoC is to enable FeoAB to continue to uptake iron well under oxic conditions. However, previous work indicates that FeoC is essential for FeoB function anaerobically (in contrast to the finding here) and is involved in protection of FeoB from degradation under reducing conditions (Kim *et al*., 2013; Weaver *et al*., 2013). The results provided herein do not support these suggestions, but could be consistent with a role for FeoC in protecting FeoB from

degradation aerobically, such that FeoC would support aerobic Feo activity by preventing loss of FeoB resulting from enhanced turnover in the presence of oxygen. It is clear that FeoC is not required in those organisms that possess a functional Feo transporter but lack any apparent FeoC equivalent, such as is the case for *Campylobacter jejuni* and *S. aureus* (Lua *et al*., 2015). However, it may be that in such organisms the role of FeoC is filled by an unrelated protein. It should be pointed out that Perry *et al*. (2007) report that whilst FeoA and FeoB are essential for Feo activity, but FeoC is not (in contrast to the report by Weaver *et al*., 2013). Thus, the results of Perry *et al.* (2007) reflect those reported in the previous chapter concerning the non-essential nature of FeoC.

In this chapter, the mechanism by which FeoC influences Feo activity is explored. This was achieved by generating tagged versions of FeoB such that the levels of FeoB can be monitored by Western blotting in response to key factors such as oxygen and FeoC status.

8.2. The aim and experimental approach of this study

The hypothesis presented here is that the level of the FeoB protein is controlled by oxygen and FeoC in a post-transcriptional fashion, and that such control influences Feo activity. Thus, the highest FeoB levels are expected during anaerobiosis but would lower under aerobic conditions. Here, any transcriptional control by FNR or Fur that would normally affect FeoB levels is eliminated as a result of expression from the pBAD vectors. Levels of FeoB in *E. coli* where strictly dependent on the pBAD vector since no chromosomally-encoded version was present in the host strain (JC32) employed. Western blotting was used to determine the level of functional-versions of FeoB and FeoA proteins (as Flag-tag or His-tags) expressed under each given condition of interest.

8.3. Generation of FeoB-Flag-tag and FeoB-His-tag fusions

8.3.1 Overview

In order to allow investigation of the levels of the FeoB protein, both FeoB- and FeoA-FLAG-tag and -His-tag fusions were generated using the inducible pBADara vector for the His-tags and pBADrha for the Flag-tags, to give both C- and -N-terminal epitope-tagged versions. First, DNA fragments encoding the corresponding tag (encompassing 18 bp for the His_6 tag, and 24 bp for the FLAG tag: DYKDDDDK), fused to FeoA or FeoB (N- or C-terminally), were generated by PCR amplification with the tags incorporated as part of the primer design. The selected regions were PCR-amplified and cloned into linearised vector ($pBAD_{rha}$ or $pBAD_{ara}$) to give the following 14 constructs:

pBADara-HisTAG-*feoA*^{O157}

pBADara-*feoA*^{O157}-HisTAG

pBADara-*feoB*^{O157}-HisTAG

pBADara-HisTAG-*feoB*^{O157}

pBADara-*feoAB*^{O157}-HisTAG

pBADara-HisTAG-*feoAB*^{O157}

pBADara-HisTAG-*feoBC*^{O157}

pBADrha-FlagTAG-*feoA*^{O157}

pBADrha-*feoA*^{O157}-FlagTAG

pBADrha-*feoB*^{O157}-FlagTAG

pBADrha-FlagTAG-*feoB*^{O157}

pBADrha-*feoAB*^{O157}-FlagTAG

pBADrha-FlagTAG-*feoAB*^{O157}

The construction of the above is described in detail below.

8.3.2. Cloning of *feo* genes to generate Flag-tag or His-Tag fusions in the Prha and Para inducible vectors

8.3.2.1. PCR amplification of *feo* genes with Flag-Tag fusions

Genomic DNA of *E. coli* O157 was used as template for generation of all *feoA* and *feoB* Flag-tag fusions (PCR products: *feoAB*-Flag-Tag, *feoB*-Flag-Tag, Flag-Tag-*feoBC, feoA*-Flag-Tag and Flag-Tag-*feoAB*). PCR was in a thermocycle Bio-Rad machine (Section 2.10.2) using specific primers (FWD and Rev; Table 2.4). These primers were designed for use in In-Fusion cloning (Section 2.14.3.1 and 2.14.3.2). The Amp HiFi PCR premix DNA polymerase (Clontech) was used as it provides accurate and efficient DNA amplification and is recommended for In-Fusion PCR cloning. The amplified fragments were analysed by agarose gel electrophoresis and the sizes expected were observed (Fig. 8.1).

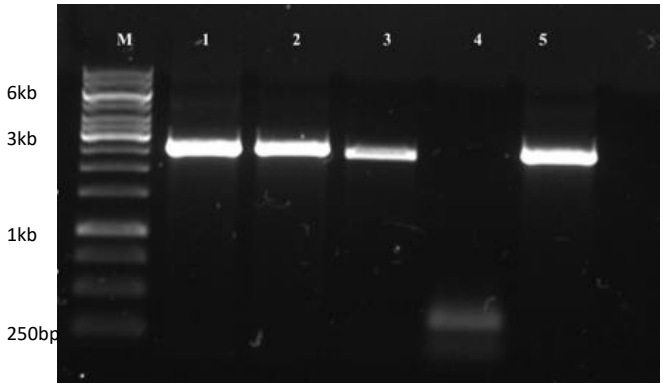

Figure 8.1 Gel electrophoresis of purified PCR products of *feo* Flag-Tag fusions. 1, purified PCR product of *feoAB*-Flag-tag (~2900 bp). 2, purified PCR product of Flag-tag-*feoAB* (~2900 bp). 3, purified PCR product of *feoB*-Flag-tag (~2700 bp). 4, purified PCR product of *feoA*-Flag-tag (~300 bp). 5, purified PCR product of Flag-tag-*feoBC* (~2900 bp). M, marker, 1 kb GeneRuler (Fermentas).

8.3.2.2. Gene amplification *feo* genes with His-Tag fusion

PCR products of the *feoAB*-His-Tag, *feoB*-His-Tag, His-Tag-*feoBC*, His-Tag-*feoAB* and *feoA*-His-Tag fusions were generated as above. Figs. 8.2-8.3 show the PCR products after PCR purification and all had the expected sizes.

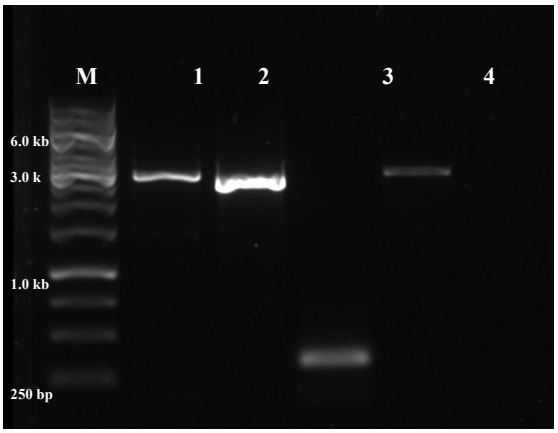

Figure 8.2 Gel electrophoretic analysis of the purified PCR products of *feo* His-tag fusions. 1, purified PCR product of *feoAB*-His-tag (~2900 bp). 2, purified PCR product of His-tag-*feoAB* (~2900 bp). 3, purified PCR product of *feoA*-His-tag (~288 bp). 4, purified PCR product of *feoB*-His-tag (~2700 bp). M, marker, 1 kb GeneRuler (Fermentas).

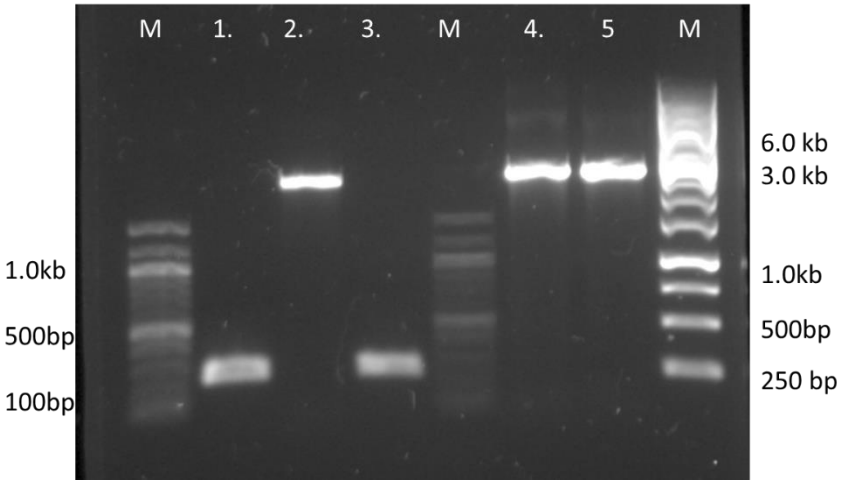

Figure 8.3 Gel electrophoretic analysis of the purified PCR products of *feo* epitope-tagged fusions. 1, purified PCR product of His-tag-*feoA*-His-tag (~300 bp). 2, purified PCR product of His-tag-*feoB* (~2700 bp). 3, purified PCR product of Flag-tag-*feoA*-Flag-tag (~288 bp). 4, purified PCR product of His-tag-*feoBC* (~2900 bp). 5, purified PCR product of *feoAB*-Flag-tag (~2700 bp). M, marker, 1 kb GeneRuler (Fermentas).

8.3.2.3. Cloning of the *feoB* and *feoA* Flag-Tag and -His-Tag fusions into inducible vectors

The PCR products generated above were cloned into the $pBAD_{ara}$ and $pBAD_{rha}$ vectors, to allow controlled expression in response to arabinose or rhamnose inducer. The plasmid $pBAD_{rha}$ and $pBAD_{ara}$ were obtained from laboratory stocks. $pBAD_{ara}$ and $pBAD_{rha}$ transformants were then generated, and plasmid DNA was isolated from four samples using (Section 2.14.7). The isolated plasmids were screened by electrophoretic analysis and the presence of plasmid DNA of high mass corresponding to the expected size (4.1, 6.1 kb; Fig. 8.4) was confirmed.

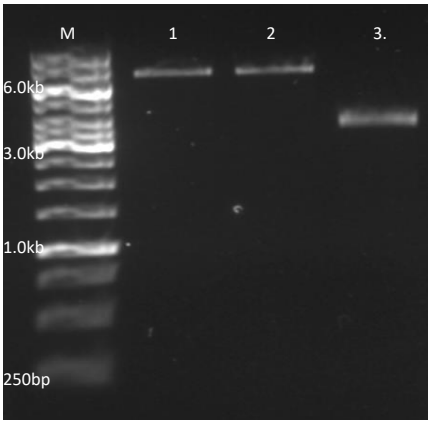

Figure 8.4 Agarose gel (0.7%) electrophoretic analysis of digested $pBAD_{rha}$ and $pBAD_{ara}$. M, Marker 1 kb Generuler (Fermentas); lane 1-2, pBADrha (6.1 kb); lane 3, pBADara (4.1 kb).

The PCR products were cloned into $pBAD_{ara}$ or $pBAD_{rha}$, at the *Nco*I and *Hin*dIII, and *Nde*I and *Bam*HI sites, respectively, using Gibson cloning methodology (Section 2.15.2.3.). The resulting reaction products were used to transform chemically competent *E. coli* Top10 (section 2.15.2.4). Resulting Ap^R/Cm^R colonies were selected for plasmid 'miniprep' isolation using (Section 2.12.7). These plasmids were then further analysed by restriction digestion (Section 2.12.4; Figs. 8.5-8.6) to release the insert from the vector. Following analysis by agarose gel electrophoresis, all of the isolated plasmids were shown to carry an insert of the expected size (~2900, ~2700 or ~300 bp) or to be of the expected size following single digestion (Figs. 8.7-8.9). Two of each of the type of plasmid construct were subjected to nucleotide sequencing by

Source Bioscience using $pBAD_{ara}$-F and $pBAD_{ara}$-R or $pBAD_{rha}$-F and $pBAD_{rha}$-R primers (Table 2.4). The sequences obtained were compared with the sequence database using BLAST which confirmed that the inserts have the correct sequence correctly located at the desired cloning sites (Appendix 12). These plasmids were employed in future studies, as described below.

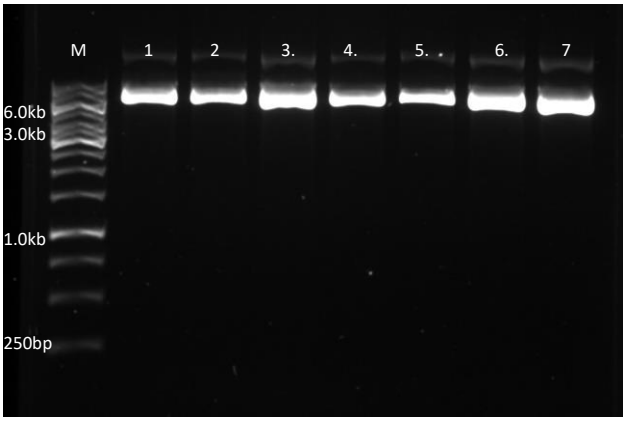

Figure 8.5. Agarose gel (0.7%) electrophoretic analysis of undigested pBADrha with tagged-*feo* genes. M, Marker 1 kb Generuler (Fermentas); lane 1-2, pBADrha-*feoAB*-Flag-tag; lane 3-4, pBADrha-*feoB*-Flag-tag; lane 5-6, pBADrha-Flag-tag-*feoBC*; lane 7, pBADrha-*feoA*-Flag-tag.

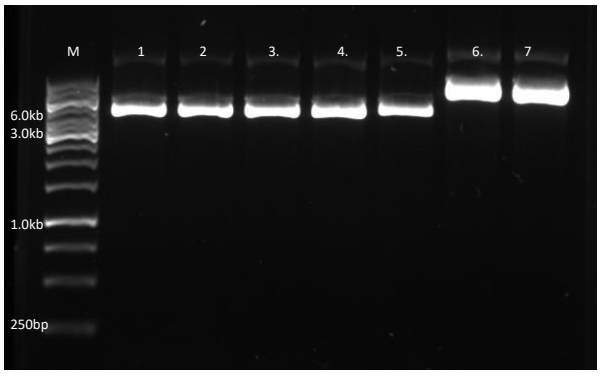

Figure 8.6 Agarose gel (0.7%) electrophoretic analysis of undigested pBADara containing tagged-*feo* genes. M, Marker 1 kb Generuler (Fermentas); lane 1-2, pBADara-*feoAB*-His-tag; lane 3-4, pBADara-*feoB*-His-tag; lane 5-6, pBADara-His-tag-*feoBC*; lane 7, pBADara-*feoA*-His-tag (some mobilities not as expected probably dues to concatemer foramtion.

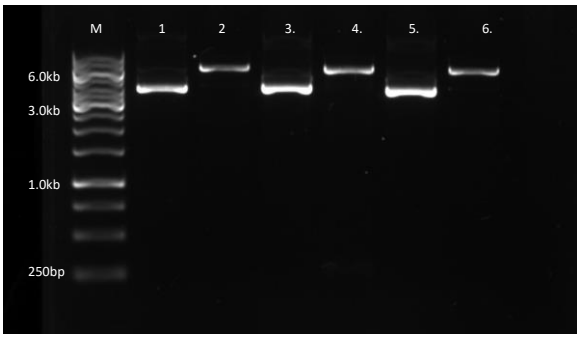

Figure 8.7: Agarose gel (0.6%) electrophoretic analysis of pBADara-*feo*-tagged plasmids following linaerisation with *Hin*dIII. M, 1 kb ladder (Fermentas). Lane 1, pBADara-*feoB*-His-tag undigested; 2, pBADara-*feoAB*-His-tag single digested (7 kb); 3, pBADara-*feoAB*-His-tag undigested; 4, pBADara-*feoAB*-His-tag single digested (7 kb); 5, pBADara-His-tag-*feoBC* undigested; 6, pBADara-His-tag-*feoBC* single digested (7 kb).

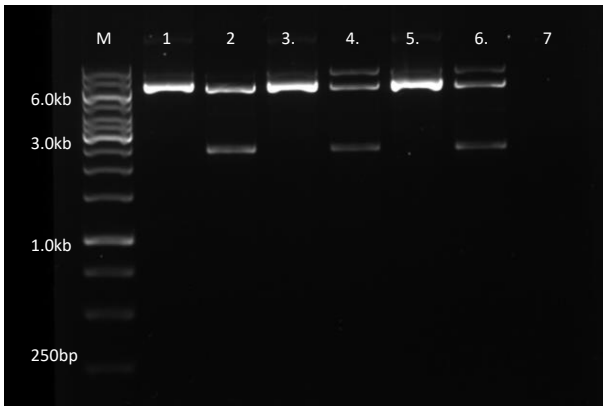

Figure 8.8: Agarose gel (0.6%) electrophoretic analysis of pBADrha-*feo-tag* plasmids following restriction digestion with *Bam*HI and *Nde*I. M, 1 kb ladder (Fermentas). Lane 1, pBADrha-*feoB*-Flag-tag undigested; 2, pBADrha-*feoB*-Flag-Tag double digested; 3, pBADrha-*feoAB*-Flag-Tag undigested; 4, pBADrha-*feoAB*-Flag-tag double digested; 5, pBADrha-Flag-tag-*feoBC* undigested; 6, pBADrha-Flag-tag -*feoBC* double digested.

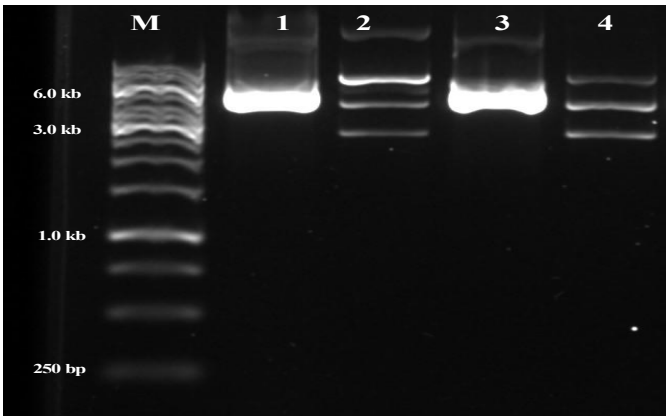

Figure 8.9: Agarose gel (0.6%) electrophoretic analysis of pBADrha-*feo-tagged* constructs following restriction digestion with *BamH*I and *Nde*I. M, 1 kb ladder (Fermentas). Lane 1, pBADrha-Flag-tag-*feoAB* undigested; 2, pBADrha-Flag-tag-*feoAB* double digested; 3, pBADrha-*feoAB*-Flag-Tag undigested; 4, pBADrha-*feoAB*-Flag-tag double digested.

8.3.2.4. Confirmation by PCR

All plasmids generated above were further analysed by PCR and all gave bands of the expected size (Fig. 8.10): *feoB* insert 2.7 kb, *feoAB* insert 2.9 kb, *feoBC* ~insert 2.9 kb and *feoA* insert 288 bp (primers were those used for the original amplifications of the inserts; Section 2.4.6).

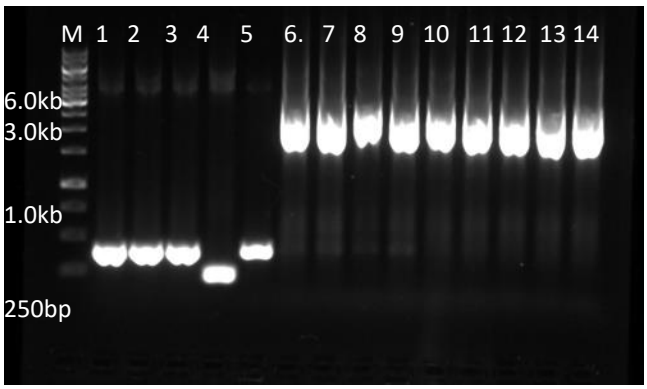

Figures 8.10: Gel electrophoresis analysis of PCR products confirming the tagged *feo* constructs. *feoA-Flag, Flag-feoA, feoA-His, His-feoA, feoC* (1, 2, 3, 4 and 5, respectively); *feoB-flag, flag-feoAB, feoAB-flag, flag-feoBC* (6, 7, 8, 9, respectively); *feoB-His, feoAB-His, His-feoAB, His-feoBC, feoABC* (10, 11, 12, 13, 14, respectively). Bands of ~300 bp were observed and expected for *feoA* or *feoC*; 2700-2900 bp for *feoB* with/without *feoA* or *feoC*.

8.4. Does Flag-Tag or His-Tag fusion impair Feo system function?

To ensure that there is no effect of the fusions on *feo* functionality, the various fusions created above were used to complement the JC32 mutant during iron-restricted growth, such that either *feoA* and *feoB*, or *feoA, feoB* and *feoC* were provided. Conditions were as described in Chapter 7 (section 2.10.2): precultures were grown overnight in M9-medium (0.4% glucose) with 100 mM MES (pH 6) with 10 µM ferric citrate. Next day, the strains were tested in the same medium, with our ferric citrate but with/without 0.5 µM DTPA, and with/without ascorbic acid with a starting OD_{600} of 0.01. Growth was at 37 ˚C with constant shaking, either in a Bioscreen C apparatus aerobically or a FLUOstar plate reader under microaerobic/anaerobic conditions.

All growths were performed in triplicate and were performed three times with similar results obtained, and representative results displayed.

Aerobic growths in M9 medium with 0.5 µM DTPA, with/without 2 mM ascorbate, showed that the *feoAB*-Flag-tag fusion complemented the JC32 strain as effectively as non-tagged *feoAB* under low-iron growth, both with and without ascorbate, when combined with *feoC* (Fig. 8.11). However, in the absence of *feoC*, the *feoAB*-Flag-tag complemented strain performed less well than the *feoAB*-complemented strain. This effect was only seen in the presence of ascorbate as in the absence of ascorbate no effective complementation was achieved for *feoAB* without *feoC* (Fig. 8.11). The growth difference was ~0.23-0.11 OD units (~twofold) and was significant ($P<0.01$). Thus, there appears to be a limited impact of the C-terminal Flag-tag on FeoB function, that only applies in the absence of FeoC.

In general, the results obtained reflect those in Chapter 7 showing that FeoABC provides superior aerobic Feo activity than FeoAB when DTPA is present, and that ascorbate promotes Feo activity. Note that the N-terminal FeoB Flag-tag protein (Flag-tag-*feoB* and -*feoBC*) failed to provide a growth advantage (data not shown).

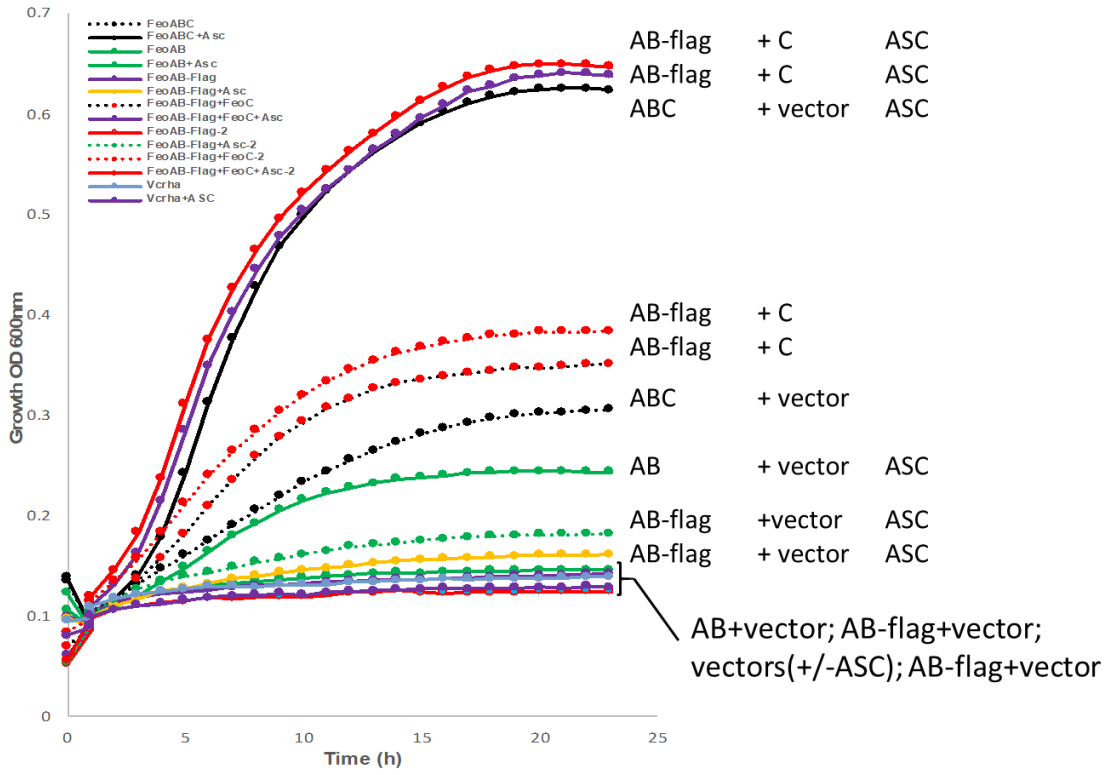

Figure 8.11: Aerobic growth of JC32 carrying *feoAB*-Flag-Tag fusions under low iron conditions (with DTPA and with/without 2 mM ascorbic acid). Strains used were JC32 with both a pBADara and pBADrha plasmids: *feoAB*-Flag-Tag, +/- *feoC* or vector; *feoABC* + vector; *feoAB* + *feoC* or vector; or vectors only. Medium was 0.4% glucose in M9 medium (plus 50 µg/ml chloramphenicol and 100 µg/ml ampicillin), 0.5 µM DTPA, with/without ascorbate (ASC). Both inducers were included. Growth was at 37 ˚C in a Bioscreen (300 µl volumes) with constant shaking at 250 rpm. Pre-cultures were grown overnight in 0.4% glucose M9 medium (37 ˚C, 250 rpm) with 10 µM ferric citrate and were washed in iron-free M9 medium before use. Starting cell density of all Bioscreen cultures was adjusted to OD_{600} (0.01).

The *feoAB*-His-tag fusion also provided a high level of low-iron growth for JC32 under aerobic iron-restriction, when *feoC* was also provided (Fig. 8.12A). Low-iron growth was enhanced by ascorbate, and reduced by DTPA (Fig. 8.12A), as expected. The *feoAB*-His fusion also complemented the low-iron growth of JC32 in the absence of *feoC*, but this was relatively weak (~fivefold lower than with *feoAB*-His and *feoC*) and required the presence of ascorbate (Fig. 8.12A), but this finding is consistent with that of Chapter 7. The *feoB*-His fusion also gave a complementation effect when combined with *feoA* and ascorbate, which was similar to that

achieved by *feoAB*-His (Fig. 8.12A). These results thus indicate that the *feoAB*-His and *feoB*-His fusions are fully functional.

The His-*feoBC* fusion also allowed good low-iron growth (with ascorbate) for JC32 when combined with *feoA-flag* (0.5 OD units greater than the vector control; Fig. 8.12B), similar to that of the *feoABC*-complemented strain (not shown); although when complemented with *feoA* (non-flag-tagged) the level of growth achieved was somewhat weaker (maximum OD of 0.4 cf. 0.54; Fig. 8.12B). The His-*feoAB* complemented strain also showed strong low-iron growth with ascorbate when *feoC* was provided, although this was somewhat weaker than that seen with *feoAB*-His/*feoC* (Fig. 8.12B; 0.48 cf. 0.6 OD units maximum growth, respectively). The His-*feoAB* and *feoAB*-His constructs gave a modest complementation in the absence of *feoC*, which was as expected (Fig. 8.12B; two-eightfold lower than equivalent growths seen with *feoC*). These results thus indicate that the His-*feoAB* and His-*feoBC* fusions provide good Feo activity.

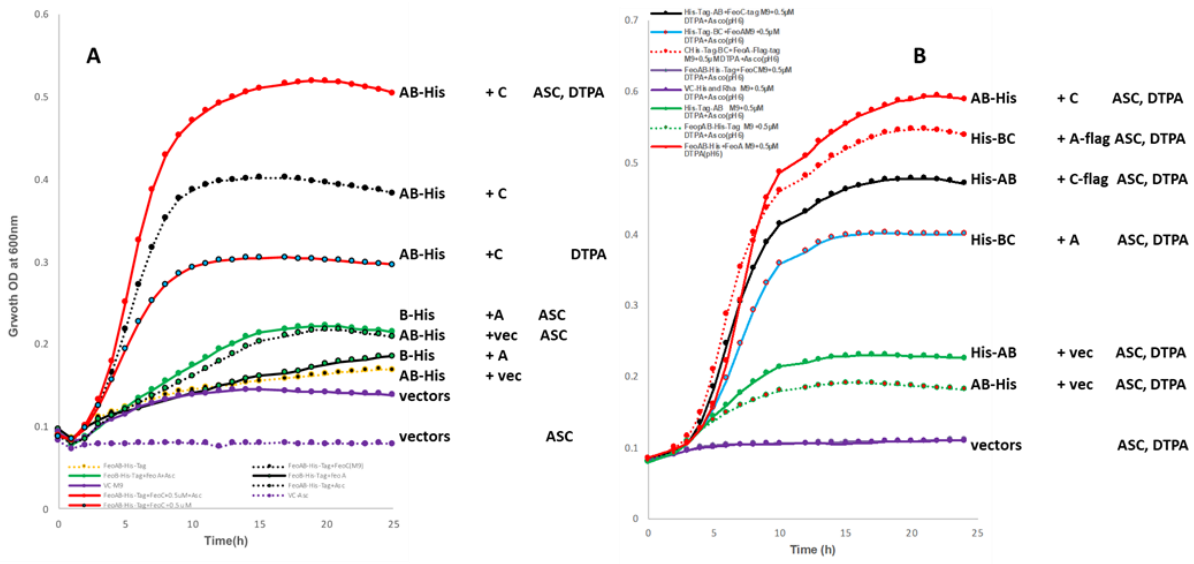

Figure 8.12: Aerobic growth of *feoAB-His-Tag* +/- *feoC* complemented iron transport mutant (JC32) under low iron, with/without 0.5 µM DTPA and +/-2 mM ascorbic acid. Strains used were JC32 complemented with a pBADara and pBADrha plasmid carrying: *feoAB*-His-Tag, *feoB*-His-Tag, His-Tag-*feoAB* or His-Tag-*feoBC*, or vector only – together with one other plasmid (as indicated). All details as above.

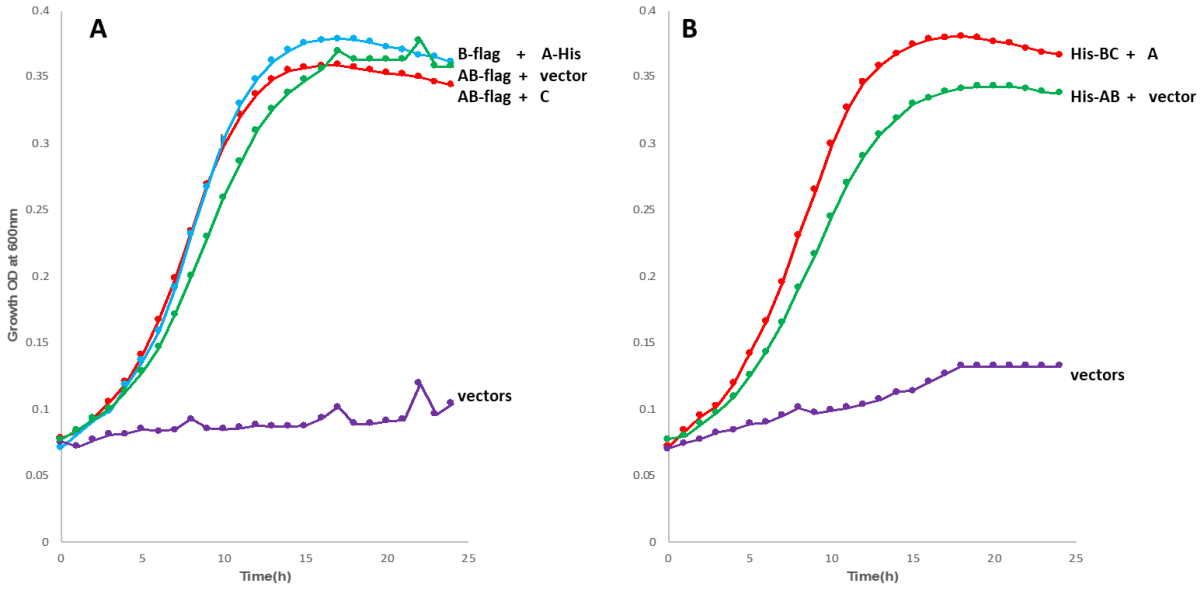

Figure 8.13: Anaerobic growth of *feo-Flag-tag* and *feo-His-tag* complemented JC32 under low iron, with chelator. **A.** Flag-tag fusions. **B.** His-tag fusions. Strain was JC32 with a pBADara and a pBADrha plasmid, as indicated**.** Growth details are as in Fig. 8.12 except for use of low O_2 growth conditions in a FLUOstar plate reader. Note that ascorbate had no impact anaerobically (data not shown).

Under low-O_2 conditions, the *feoAB*-Flag and *feoB*-Flag/*feoA* complementations provided a high level of growth under iron restriction indicating a strong degree of JC32 complementation and thus anaerobic functionality for the Flag-tag constructs (Fig. 8.13A). Addition of *feoC* had little impact (as seen before under anaerobiosis). For the His-*feoBC* (with *feoA*) and His-*feoAB* constructs, again a high degree of growth was obtained for the JC32 complementations under anaerobic, iron restriction. These observations support those above indicating that the corresponding fusions are functional.

In summary, the above data indicate that most of the fusions generated have little impact on Feo function and thus can be deployed in studies aimed at determining the role of FeoC in FeoB protein levels in the *E. coli* cell using a Western-blotting approach. However, the N-terminal Flag-tag-FeoB fusions failed to complement the growth defect of JC32 (data not shown). Only

a subset of the complementation results obtained are shown here, but a summary table is provided below for all fusions.

Only data for the Flag-tag constructs are shown below, as these provided superior blots (see an example blot for the His-tag constructs in the Appendix).

Table 8.1 Summary of fusion complementation

Fusion Plasmid	**Complementation achieved**
pBADara-HisTAG-*feoA*^{O157}	Functional
pBADara-*feoA*^{O157}-HisTAG	Functional
pBADara-*feoB*^{O157}-HisTAG	functional
pBADara-HisTAG-*feoB*^{O157}	functional
pBADara-*feoAB*^{O157}-HisTAG	Functional
pBADara-HisTAG-*feoAB*^{O157}	Functional
pBADara-HisTAG-*feoBC*^{O157}	Functional
pBADrha-FlagTAG-*feoA*^{O157}	Functional
pBADrha-*feoA*^{O157}-FlagTAG	Functional
pBADrha-*feoB*^{O157}-FlagTAG	Functional
pBADrha-FlagTAG-*feoB*^{O157}	**Non-functional**
pBADrha-*feoAB*^{O157}-FlagTAG	Functional
pBADrha-FlagTAG-*feoAB*^{O157}	Functional
pBADrha-FlagTAG-*feoBC*^{O157}	**Non-functional**

8.5. Impact of environmental factors and FeoC status on FeoA and FeoB protein levels in *E. coli* under low-iron (M9) conditions

8.5.1. Expression profiles for the FeoA-and FeoB-Flag protein in JC32 in response to O_2 and FeoC

The levels of FeoA-Flag and FeoB-Flag proteins were monitored (by western blotting) during aerobic and anaerobic growth in low-iron 0.4% glucose M9 medium (at pH 6 with 0.5 μM DTPA), since such conditions gave maximum growth advantage with Feo (see above). The impacts of O_2 and FeoC were thus examined, and proteins of the expected size (FeoA, ~11 kDa observed, expected ~13 kDa for FeoA-Flag; FeoB, ~84 kDa observed, expected ~84.4 kDa for FeoB-Flag) in the corresponding samples were detected (Fig. 8.14). The results show that FeoA-Flag protein was generated in the presence of FeoB or FeoBC under low-O_2 conditions, but levels were considerably lower under aerobic conditions (Fig. 8.14 – compare sample-lanes 1-2, with lane 3). FeoB-Flag was not detected in absence of FeoA (this was a consistent finding in other data, not shown). However, when FeoA, or FeoA and FeoC, were present then relatively high FeoB-Flag levels were observed anaerobically, but not under aerobic conditions (Fig. 8.14). The presence/absence of FeoC did not appear to affect the FeoA or FeoB levels observed (but see below). Thus, both FeoA and FeoB levels are strongly impacted by O_2 levels, but not greatly by FeoC, under the conditions employed (Fig. 8.14).

It should be noted that *feo* status has a major impact on growth such that JC32 with *feoB*-only grew very poorly; this could influence the FeoB-Flag levels subsequently observed.

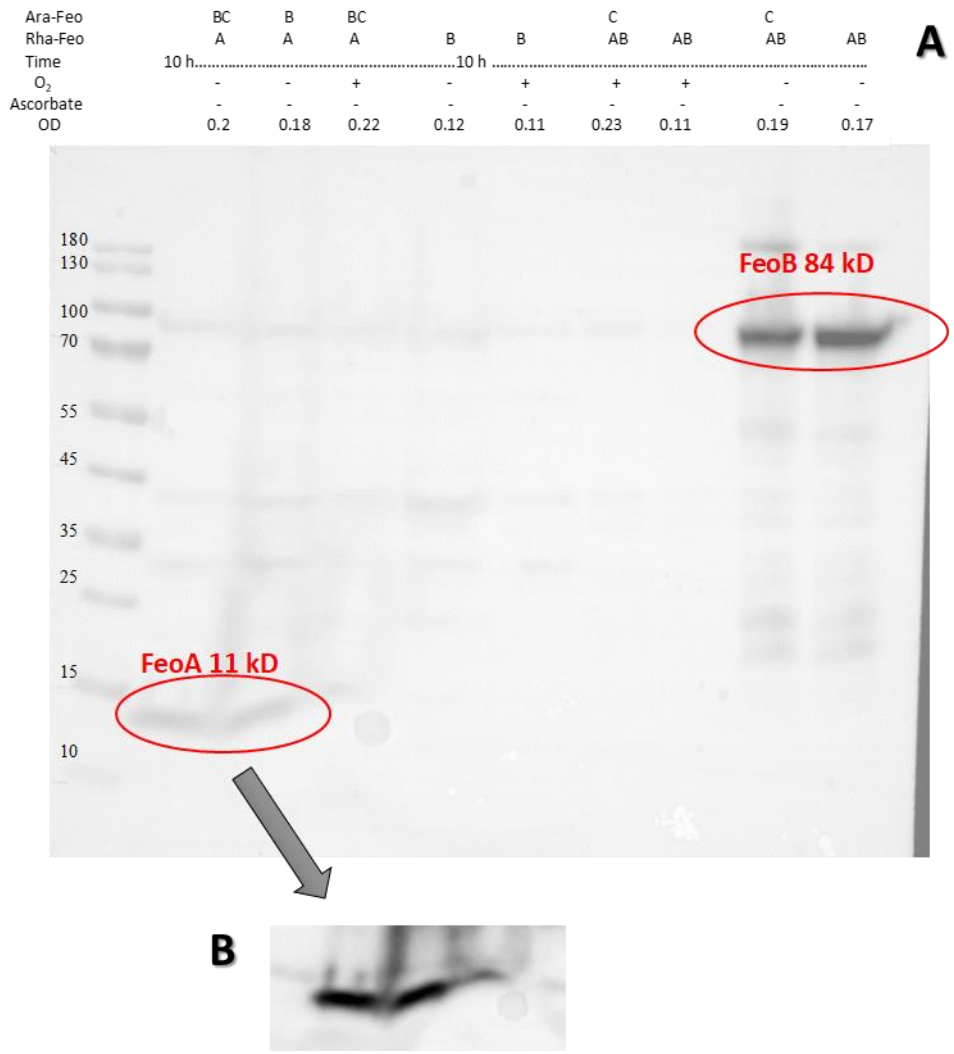

Figure 8.14: Detection of the FeoA- and FeoB-Flag Tag fusion proteins by western blotting: effect of O_2 and FeoA/FeoC (at 10 h). Strains were JC32 containing: pBADrha and pBADara (control); pBADrha-*feoAB*-Flag tag fusion with pBADara or pBADara-*feoC*; or pBADrha-*feoA*-Flag with either pBADara-*feoBC* or pBADara-*feoB*. Overnight cultures were diluted 1:100 into M9 medium with 0.5 µM DTPA and 100 mM MES (pH 6) with 0.4% glucose, and grown anaerobically in 50 ml syringes or aerobically in 250 ml acid-washed flasks to mid-log phase (times and ODs at harvesting are indicated). Equal numbers of cells were electrophoresed on a 12% SDS-polyacrylamide gel and then transferred to a nitrocellulose membrane. FeoA and FeoB-Flag Tag fusions were detected using an HRP-conjugated antibody to the Flag tag. The estimated sizes of FeoA-Flag and FeoB-Flag are approximately ~10 and 86 kDa. All of the pBADrha- plasmids used in this chapter encoded *feoA*-, *feoB*-, or *feoAB*-flag-tags; all of the pBADara plasmids used encoded non-tagged gene products. **B** shows FeoA-Flag protein visualised more clearly by extending the exposure time.

8.5.2. Expression profiles for the FeoA-and FeoB-Flag proteins in response to ascorbate

Since ascorbate had a major impact on Feo function aerobically, the effect of ascorbate on aerobic FeoA-Flag and FeoB-Flag levels was determined under conditions otherwise as used above (Fig. 8.14). The results showed that the FeoA-Flag protein can indeed be detected aerobically, but only when ascorbate is present (at 12 h) (Fig. 8.15). Thus, as shown in Fig. 8.14, FeoA is not detected aerobically (without ascorbate), but is present at relatively high level anaerobically or aerobically with ascorbate. FeoA levels appeared slightly higher under anaerobiosis than under aerobiosis with ascorbate (Fig. 8.15; see sample lanes 1-2 cf. 7-8). FeoC status had little impact on FeoA abundance (Fig. 8.15). This finding suggests that the weak performance of the Feo system aerobically (without ascorbate) is caused by lack of FeoA (and lack of FeoB; Fig. 8.14).

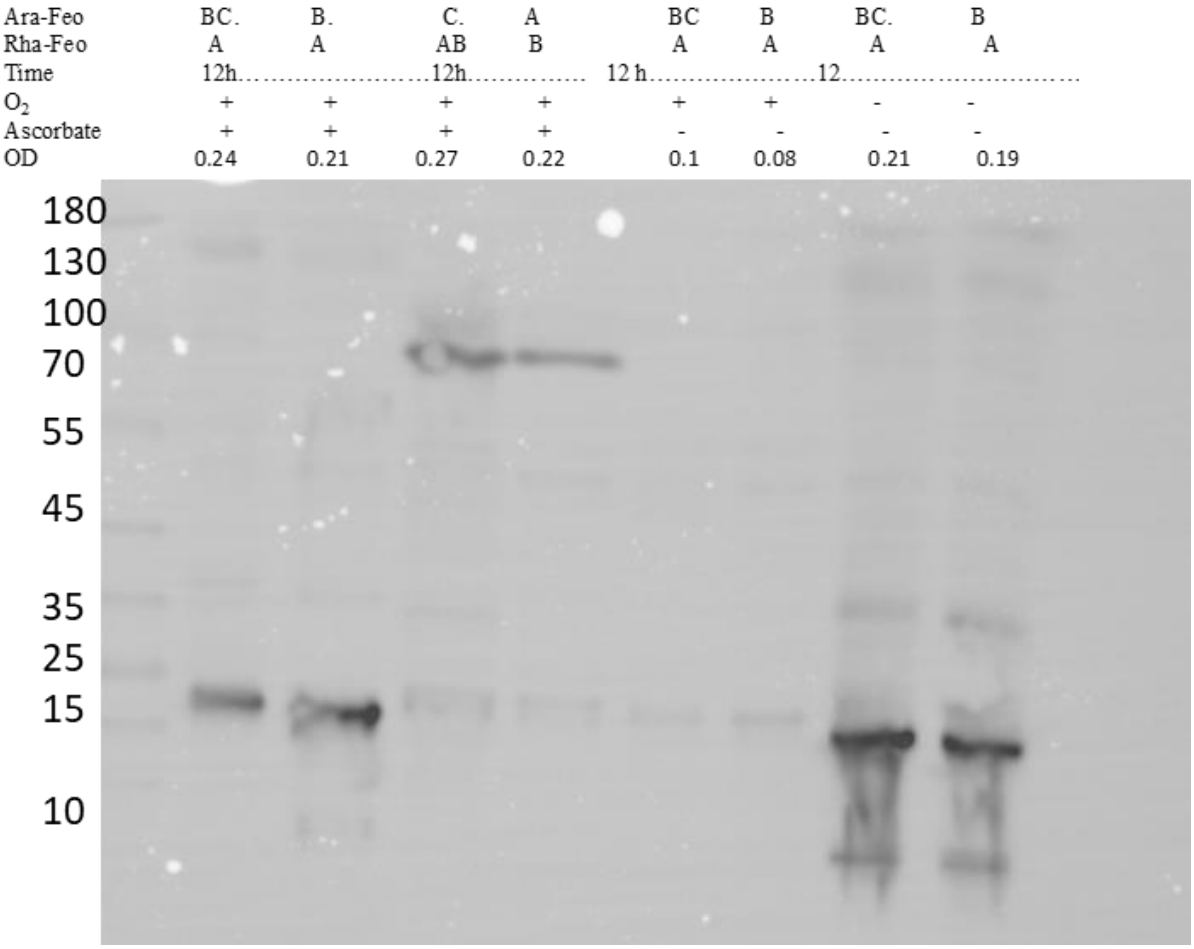

Figure 8.15: Detection of the FeoA-Flag fusion proteins by western blotting: effect of ascorbate (at 12 h). Conditions were as in Fig. 8.14 but samples were taken at 12 not 10 h, and ascorbate was included in some cases.

FeoA-Flag levels were not notably affected by FeoC status during anaerobic growth at any point in the growth curve (see Fig. 8.17 for FeoA levels +/-FeoC at 16 h). Thus, although FeoA levels appear to be very strongly impacted by the redox environment during growth, FeoC does not apparently contribute to FeoA levels post-transcriptionally.

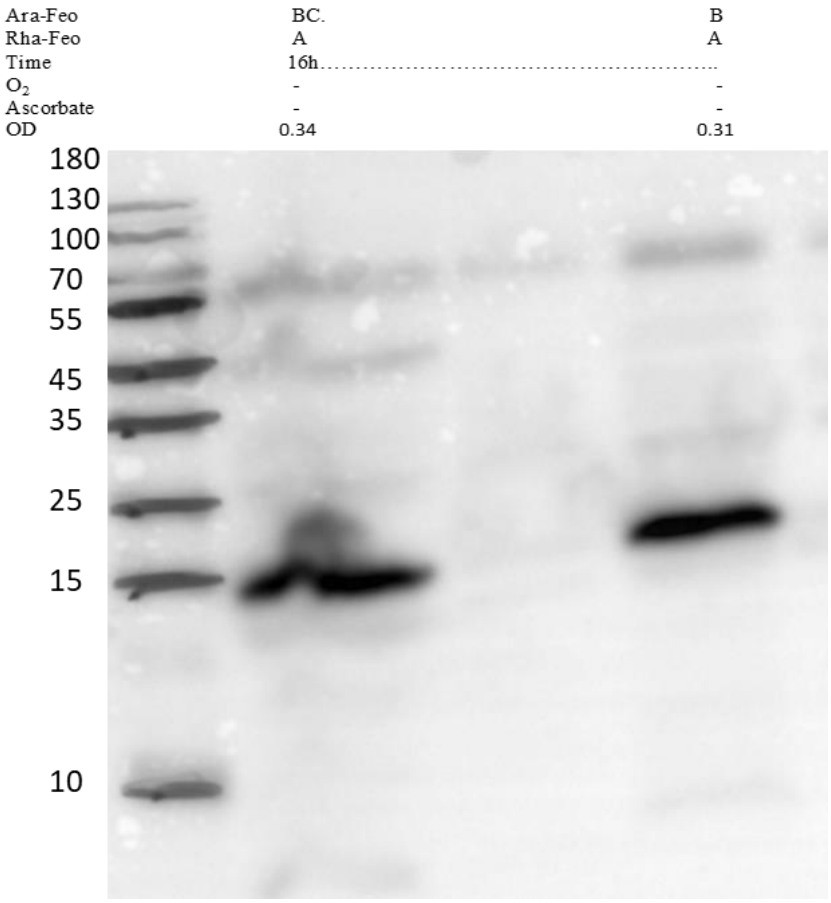

Figure 8.16: FeoA-Flag levels are not affected by FeoC status under anaerobiosis. All the details are as above except that samples were taken at the end of growth (16 h)**.**

FeoB-Flag levels were also found to be strongly affected by ascorbate aerobically (Fig. 8.17). Quantification of the band intensities obtained for FeoB-Flag (at 16 h growth) showed that ascorbate enables a four-sixfold increase in FeoB-Flag levels aerobically, and that anaerobiosis enables a six-tenfold increase (Fig. 8.17). Lack of FeoC caused a slight reduction in FeoB-Flag levels (not clearly apparent in previous blots), and this was more apparent aerobically without ascorbate (~45% reduction) than anaerobically or aerobically with reductant (~7 and ~22% reductions, respectively). Thus, FeoC appears to cause a modest increase in FeoB levels, although such effects are somewhat complicated by the influence that FeoC status has on low-iron growth, particularly under aerobiosis (see OD values provided in Fig. 8.17).

At 8 h (mid log-phase), absence of FeoA resulted in undetectable levels of FeoB both aerobically and anaerobically, which could be caused by the poor growth of *feoB*-only strains or by the need for FeoA in order to ensure FeoB stability against degradation (Fig. 8.18). The format of *feoA* expression, in trans (*feoAB*) or in cis (*feoA* and *feoB*), did not impact levels of FeoB (Fig. 8.18; sample lanes 7 & 8). FeoB levels were again strongly dependent on O_2 and weakly dependent on FeoC (10-14-fold increases anaerobically; 11-50% increase caused by presence of FeoC).

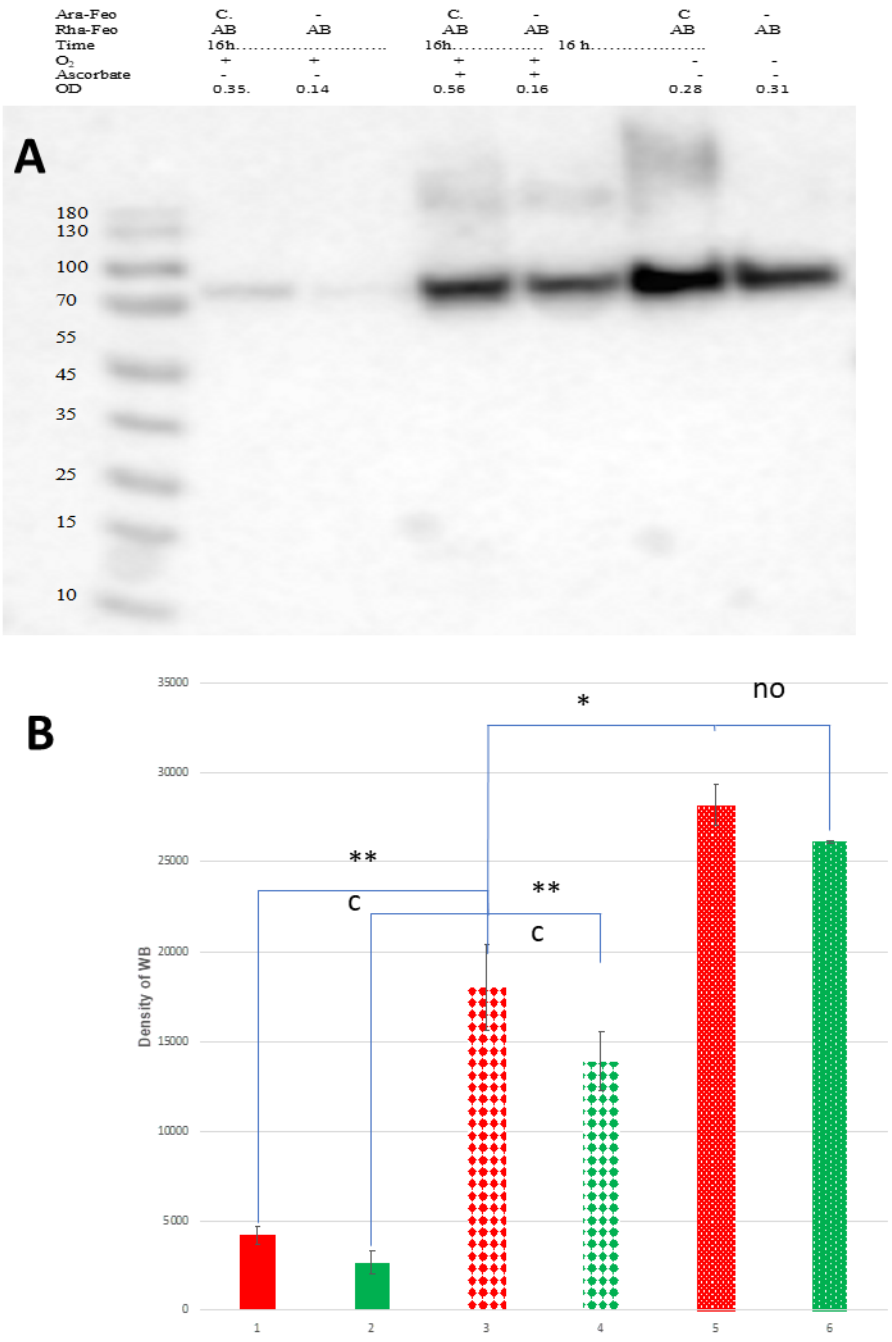

Figure 8.17: Western blot (A) and density analysis (B) of FeoB-Flag status in response to FeoC, O_2 and ascorbate at stationary phase (16 h). All details as above. Strain used was JC32 containing pBADrha-*feoAB*-Flag with pBADara-*feoC* and pBADara. Density analysis (using Gene Tools) is presented in B, with data from two blots and error bars indicating +/- values with respect to the mean. Samples collected at 16 h.

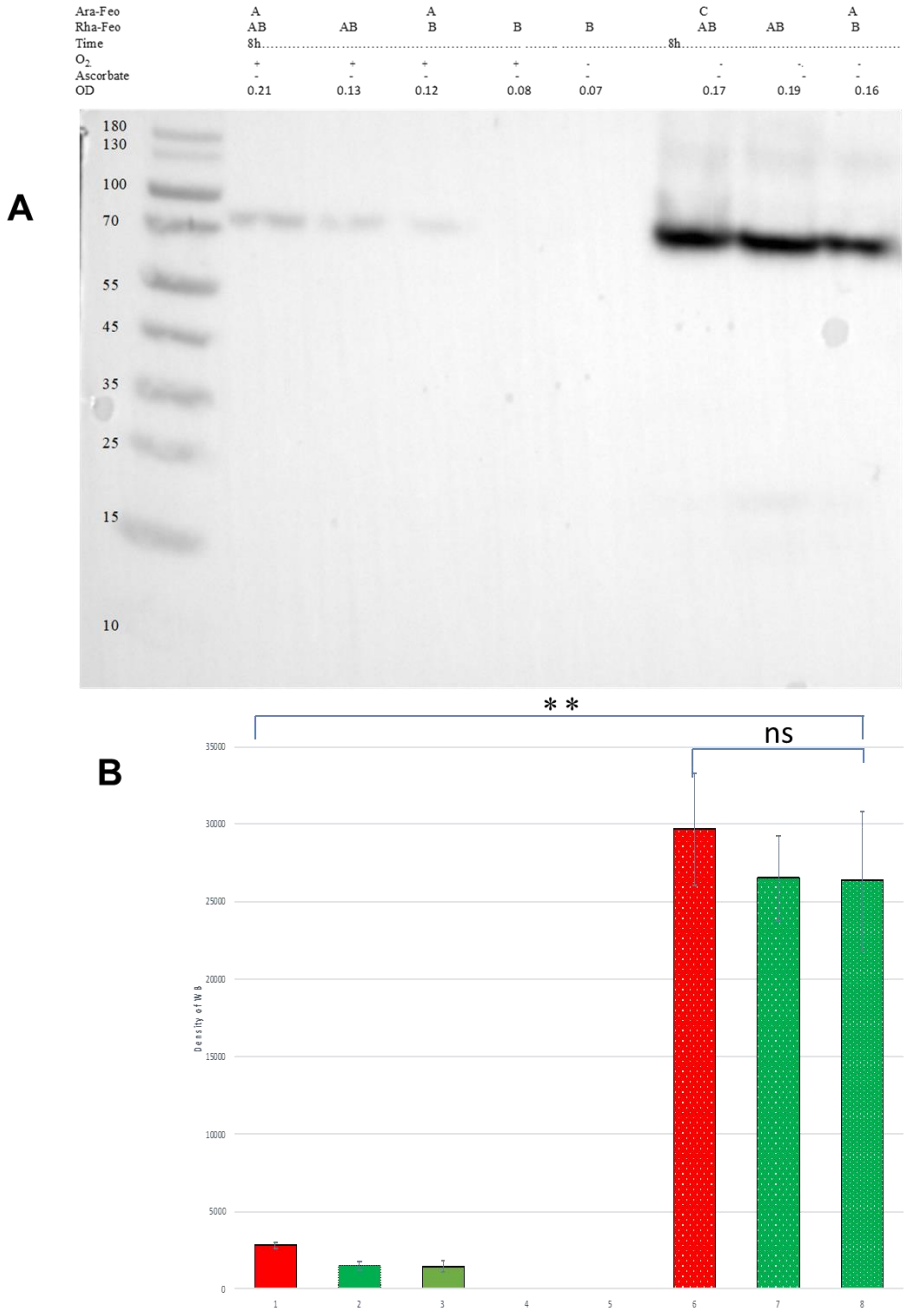

Figure 8.18: Levels of FeoB-Flag are modestly affected by FeoC under both aerobic and anaerobic conditions but are strongly affected by lack of FeoA (mid-log, 8 h). Conditions are as above but no ascorbate is included and FeoB expression without FeoA is considered. Also, cells were harvested at 8 h.

8.5.3. Impact of iron availability on FeoB-Flag levels

Since JC32 growth under the low-iron conditions employed above is strongly impacted by Feo status, there is a possibility that the expression levels of FeoB-Flag presented above are influenced by growth inhibition of strains lacking FeoA and FeoC. Thus, in an attempt to overcome this issue, experiments were also performed in rich broth (LB) with 0.4% glucose (allowing anaerobic fermentative growth) at pH 6 (100 mM MES), with 10 µM DTPA (but DTPA at this level did not influence growth) and/or 2 mM ascorbate.

Fig. 8.19A shows that the various JC32 transformants grow equally well in rich medium aerobically, with or without ascorbate, and that a similarly high OD is achieved even for the vector control lacking a functional Feo system. Anaerobically, lack of a functional form of Feo had a slight negative impact on growth (16-24% lower), but all transformants grew to a relatively high level (0.55-0.68 OD), although this was much less than observed aerobically (≥7 OD; Fig. 8.19B). Thus, any difference in FeoB-Flag levels detected under these growth conditions is unlikely to be caused by growth effects. Note that provision of DTPA at up to 10 µM had little impact on growth also (data not shown).

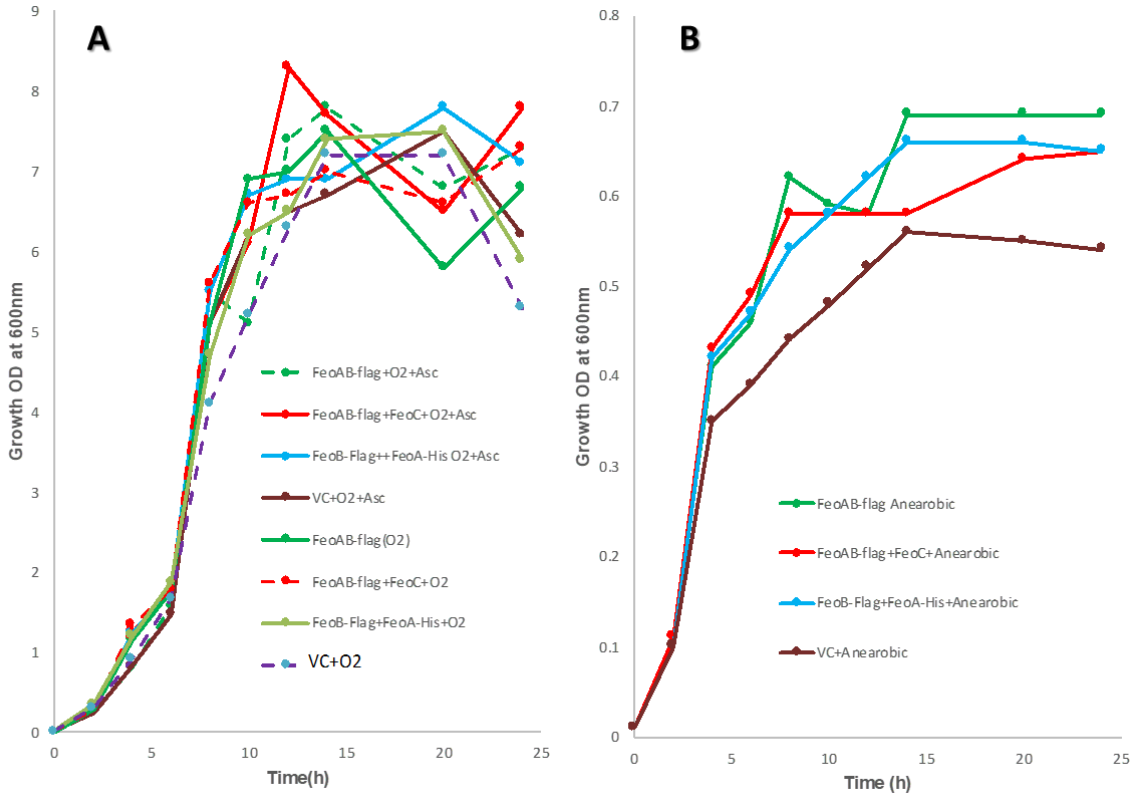

Figure 8.19: Aerobic and anaerobic growth of JC32 containing *feoAB*- or *feoB*-Flag, combined with *feoA*, *feoC* or vector control, under iron-rich conditions (LB medium). Strains used were JC32 with a pBADrha and a pBADara construct, as indicated in the keys. **A**. Aerobic with/without 2 mM ascorbate. **B**. Anaerobic. LB medium with 0.4% glucose, 100 mM MES pH 6, (plus 50 µg/ml chloramphenicol and ampicillin 100 µg/ml), 10 µM DTPA and 0.02% rhaminose and 0.002% arabinose. Bacterial growth was measured every two hours at 37 ˚C.

8.5.3.1. Comparison of FeoB-Flag levels under anaerobic and aerobic (with ascorbate conditions), under <u>iron replete</u> conditions

In LB medium, FeoB-Flag levels were lower under aerobiosis (with ascorbate) than under anaerobiosis at 4 h (Fig. 8.20) by ~sevenfold. However, at 6 h the difference was less pronounced at ~2-fold with a marked increase in FeoB-Flag seen in the presence of FeoC (~4.7-fold increase between 4 and 6 h). In most cases, lack of FeoC caused only a modest decrease in FeoB levels (12-88%), but for the aerobiosis with ascorbate at 6 h there was a

major increase (~1.4 fold) in FeoB caused by presence of FeoC (Fig. 8.20, see sample lanes 5 and 7).

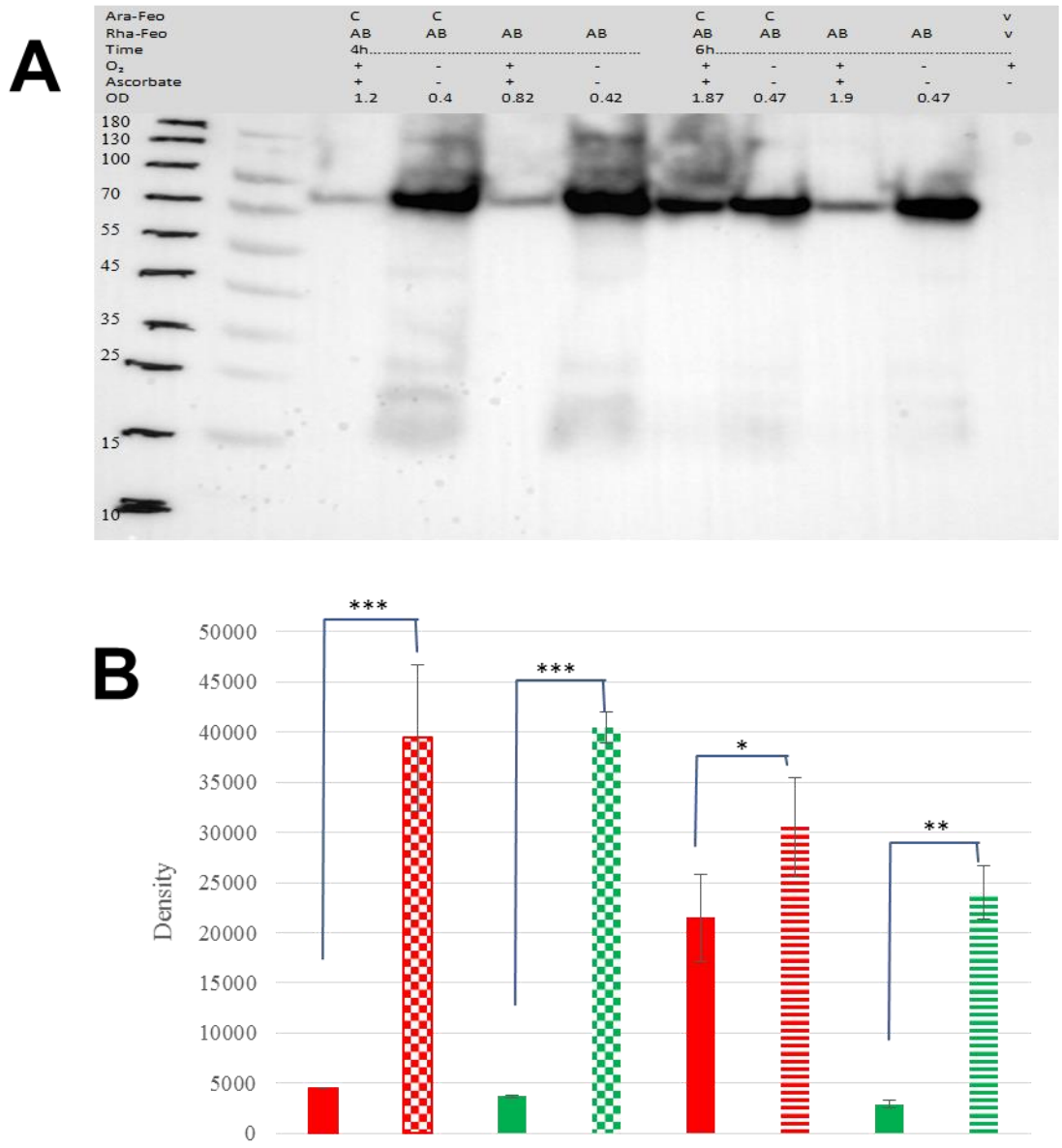

Figure 8.20: FeoB-Flag levels under iron-rich conditions: effect of aerobiosis (with ascorbate) and anaerobiosis (4-6 h). A. Anti-Flag Western blot. **B.** Densities derived from duplicate experiments**.** Growth was in LB medium with 0.4% glucose, 100 mM MES (pH 6) containing 100 µg/ml ampicillin, 50 µg/ml chloramphenicol, 0.02% rhamnose at 37 °C. Strains were JC32 with pBADrha-*feoAB-flag*^{O157} and pBADara or pBADara-*feoC*, as indicated. *, P <0.05 **, P < 0.01.

At 8-16 h, the difference in FeoB-Flag levels between the aerobic-with-ascorbate and the anaerobic growths was much reduced (Fig. 8.21) to between 1.5 and 2.0-fold. This difference is similar to that observed in low-iron M9 medium. The impact of FeoC remained relatively modest, with FeoC causing a 10-57% increase in FeoB-Flag (Fig. 8.21). Thus, the low FeoB-Flag levels aerobically at 4 h (Fig. 8.20) are likely growth-phase related (early versus mid log; see Fig. 8.19).

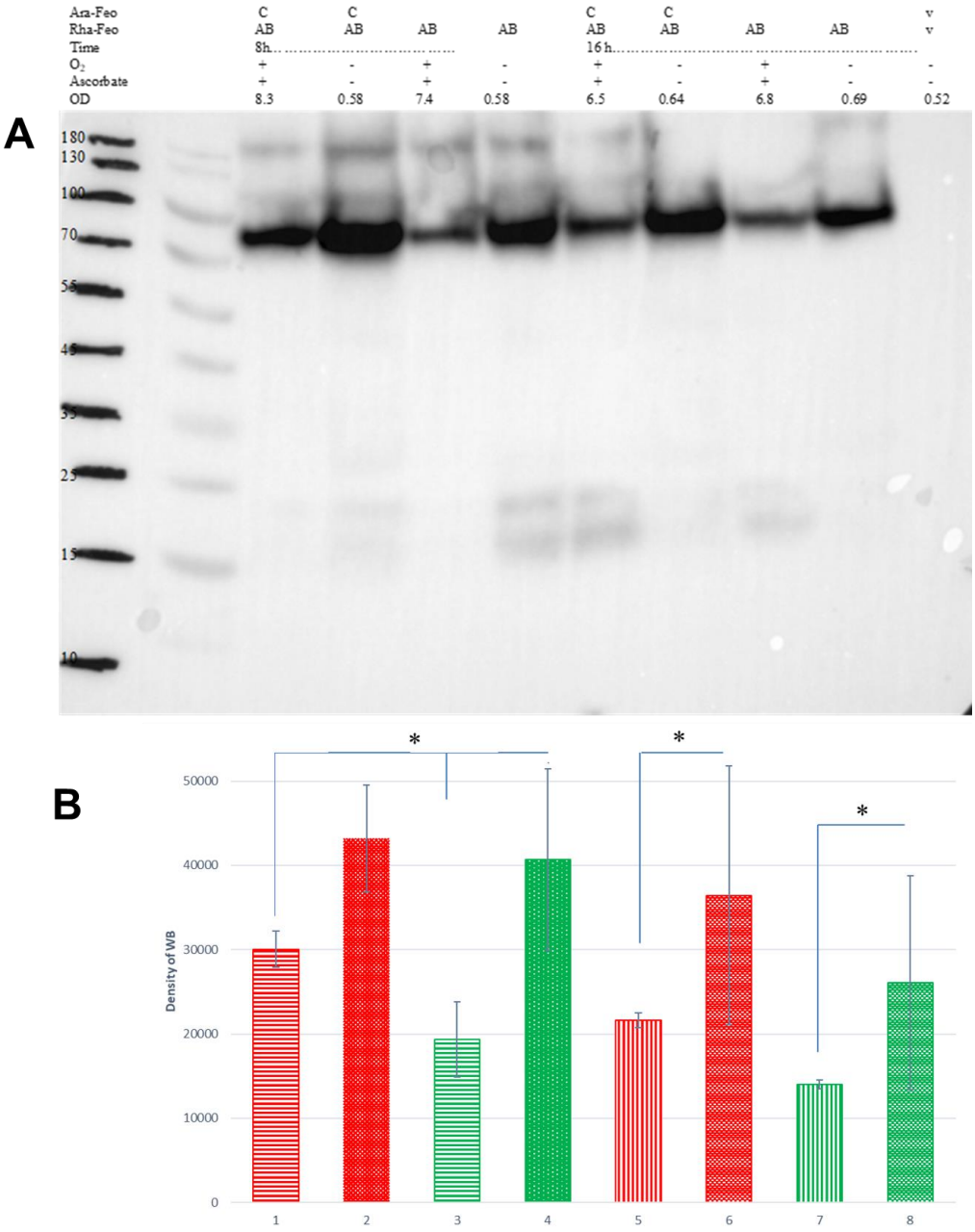

Figure 8.21: FeoB-Flag levels under iron-rich conditions: effect of aerobiosis (with ascorbate) and anaerobiosis (8-16 h). Details are as above except for harvesting times (as indicated).

In order to more directly consider the impact of time and growth phase, samples taken at 4-16 h were compared side-by-side (Fig. 8.22 & 8.23). These comparisons clearly show that, in absence of *feoC*, aerobic (minus ascorbate) FeoB levels remain much lower than those obtained anaerobically, and that time related changes in FeoB levels are relatively minor (Fig. 8.22). With FeoC present (Fig. 8.23), a similar effect is observed. Thus, under iron repletion, FeoB levels both anaerobically and aerobically (minus ascorbate) are not markedly affected by time/growth-phase, either with or without FeoC.

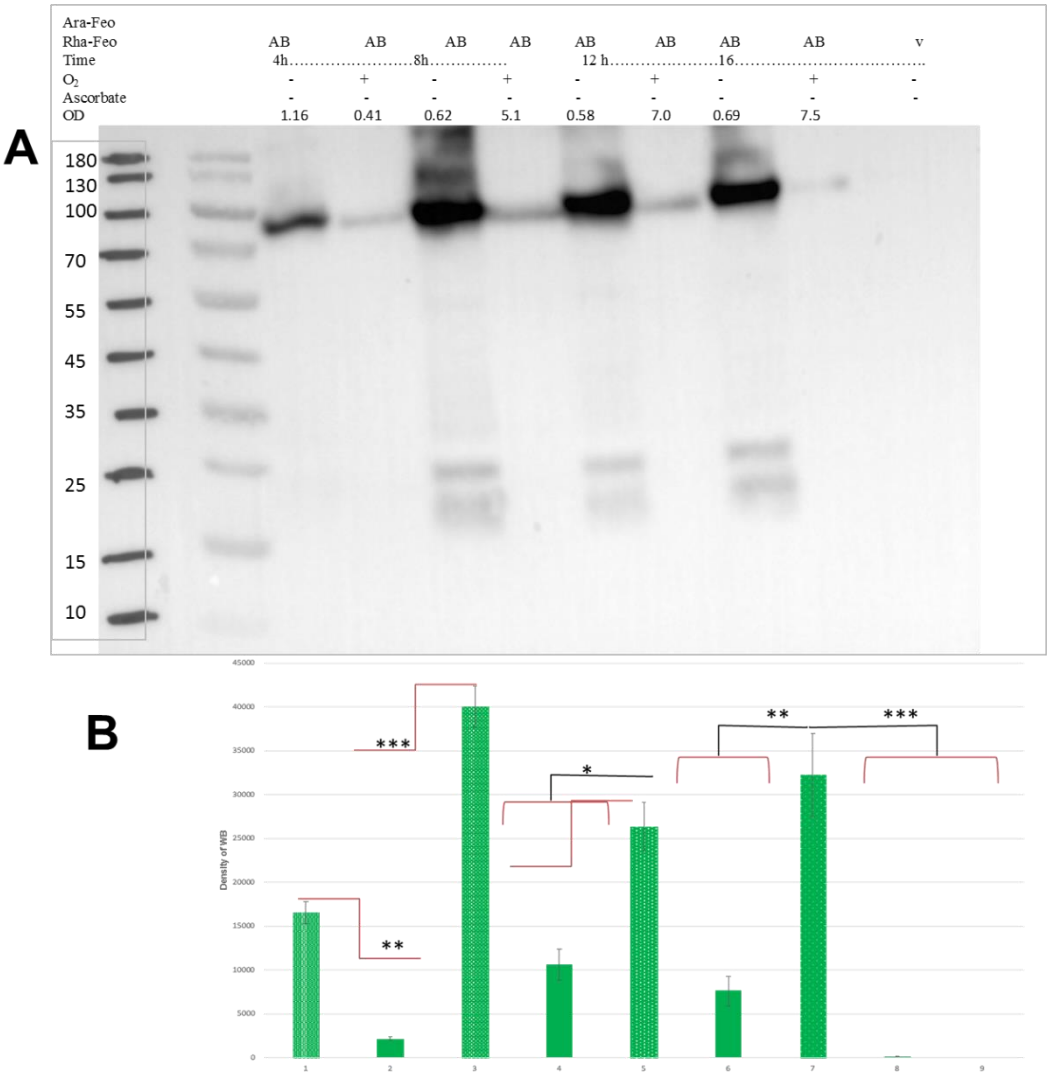

Figure 8.22: FeoB-Flag levels under iron-rich conditions under aerobic (without ascorbate) and anaerobic conditions, <u>without FeoC</u>: effect over time (4-16 h). All details were as above, except that ascorbate was excluded, four time points are considered (as indicated) and *feoC* is absent throughout.

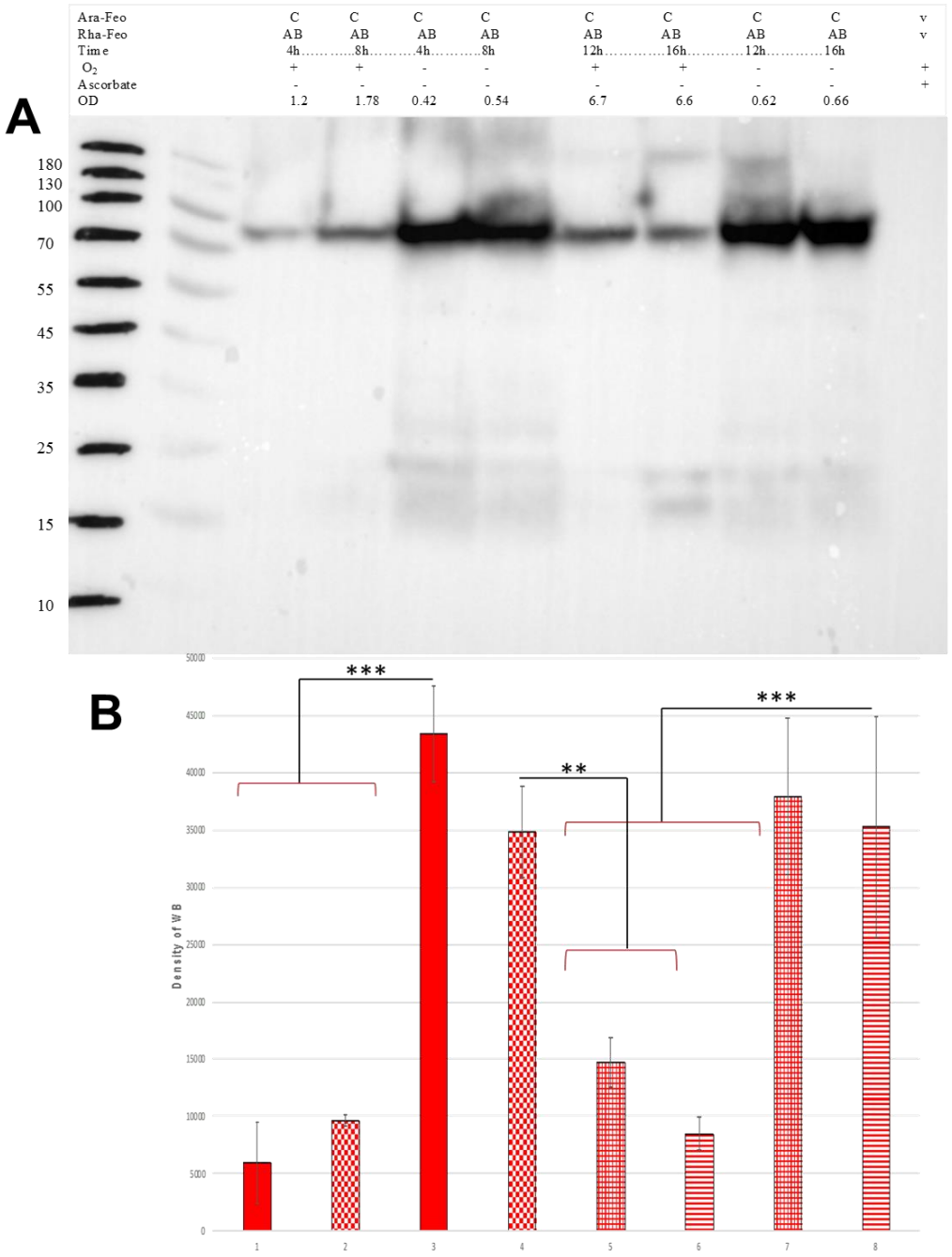

Figure 8.23: FeoB-Flag levels under iron-rich conditions under aerobic (without ascorbate) and anaerobic conditions, <u>with FeoC</u>: effect over time (4-16 h). As above, except that pBADara-*feoC* is included in place of pBADara – as indicated.

Further western blots confirming the effect of O_2, ascorbate and FeoC on FeoB-Flag levels are provided in the Appendix.

8.6. Discussion

In this chapter, the levels of cellular FeoA and FeoB were determined using Flag-tagged constructs and an inducible *feo* expression system anticipated to be divorced from oxygen (FNR) and iron (Fur) dependence. A total of 14 tagged constructs were generated (seven His and seven Flag) and these were all found to complement the JC32 strain under iron restriction, apart from the Flag-*feoB* and Flag-*feoBC* constructs, which were therefore not used in subsequent western blot analyses. Thus, twelve of the tagged constructs generated were functional and could be used to monitor Feo protein levels is response to FeoC status and oxygen in their biologically-relevant context. Unfortunately, the His-tagged constructs gave very poor western blotting patterns (see Appendix) and so were not utilised in this thesis. However, the FeoA-Flag and FeoB-Flag-tagged constructs could be detected by western blotting as immune-reactive bands of the anticipated mass (Fig. 8.15). Thus, these fusions were employed for all further western blotting work within the chapter. The western blot analyses allowed several conclusions to be made concerning post-transcriptional factors influencing Feo protein levels in *E. coli*.

1. **In the absence of FeoA, FeoB could not be detected**. Thus, FeoB appears to require FeoA for its stability. The most likely cause of such an effect would be proteolysis of FeoB in absence of FeoA-FeoB complex formation. This finding should be confirmed using a wider range of time points and using iron-sufficient conditions, since the low FeoB level could arise as a result of poor growth of JC32 in absence of functional Feo. However, if this finding is confirmed then further work on the impact of Fur status on FeoB levels should be performed to determine if absence of Fur (in presence of FeoA) enhances FeoB levels under iron sufficiency due to lack of Fur-FeoA complex formation (as hypothesised earlier) which in turn should promote FeoA-FeoB complex formation.
2. **FeoB levels are only weakly affected by FeoC**. Generally, the level of FeoB was <twofold reduced in absence of FeoC. This effect was often more apparent aerobically (without ascorbate) since FeoB levels are relatively low under such conditions. Whether this effect is of biological significance is

unclear, but it seems highly unlikely that this effect would account for much of the impact that FeoC has on Feo activity, as shown in Chapter 7. It is likely that FeoC forms a complex with FeoB (Weaver *et al.*, 2013, Lau *et al*., 2016) and it is probable that any lack of complex formation would have a negative influence on FeoB stability, but such a modest degree of impact is unlikely to account for the major effect of FeoC on Feo activity under aerobic conditions with ascorbate. Therefore, it can be concluded that the findings of Kim *et al.* (2013) on the role of FeoC in controlling FeoB proteolytic degradation in *Salmonella* by FtsH in response to oxygen, do not apply to *E. coli*. Thus, FeoC appears to promote FeoB activity via a mechanism that has yet to be discerned, but which applies to aerobic conditions only. Possibly, the role of FeoC is related to the facultative nature of the Enterobacteriaceae in that it enables FeoAB to continue to function under mildly aerobic/oxidative conditions. Such a requirement would not be of relevance to obligate anaerobes (e.g. the Clostridia and Bacteroidetes) that carry *feoAB* without *feoC*. How FeoC might support activity of FeoAB under oxidising conditions is unclear and should be the subject of future work. However, the presence of a 4Fe-4S cluster in FeoC is suggestive of a potential redox function for FeoC in supporting FeoAB activity aerobically.

3. **The effect of FeoC status on FeoB levels is particularly weak under anaerobiosis.** This finding matched that of Chapter 7 where FeoC was shown to have no/little impact on Feo activity anaerobically.
4. **FeoA and FeoB levels are dramatically influenced by O_2 (but only weakly by FeoC).** The major effect observed in this chapter was the low level of FeoB (and FeoA) under aerobic conditions. The increase in FeoB levels seen without oxygen was up to 14-fold, and this effect was consistent over time and was observed under both iron sufficiency and deficiency. This observation suggests that FeoB levels are subject to a major post-transcriptional regulatory response to O_2 that is independent of FeoC.
5. **The impact of O_2 on FeoB levels is largely reversed by ascorbate.** The addition of 2 mM ascorbate under aerobiosis largely eliminated the major reduction in FeoB levels seen aerobically with respect to those obtained anaerobically. This indicates that the response of FeoB levels to O_2 is related to a redox effect rather than O_2 per se. Future work should consider use of a range of O_2

and reductant levels in order to determine the impact of O_2 and reductant concentrations on FeoB. In addition, future work should utilise catalase aerobically, and H_2O_2 anaerobically, in order to determine whether peroxide generation is a cause of the loss of FeoB in response to O_2. The mechanism by which redox status controls FeoB levels is unclear. This could be a proteolytic effect, since FtsH has been shown to cause degradation of FeoB in response to O_2 in *Salmonella* (Kim *et al*., 2013). The impact of exposure to O_2 on FeoB degradation over time should be determined in future work to establish whether change in FeoB turnover is indeed a major mechanism by which O_2 controls FeoB. Also, the manner in which mutations in relevant proteases (e.g. FtsH) affect FeoB levels with O_2 should be determined (see Chapter 10).

6. **Iron availability has no major effect on post-transcriptional control of FeoB levels.** The response of FeoB to O_2, ascorbate and FeoC was reiterated under iron sufficiency. However, ideally, this work should be repeated in M9 medium with added iron.

Two major conclusions can thus be derived from the research in Chapter 7 and 8. Firstly, FeoC supports FeoAB activity under aerobic conditions with ascorbate, but this effect is not related to changes in FeoB-protein levels. Secondly, O_2 (in absence of reductant) has a major impact on Feo activity which is independent of FeoC but appears to be caused (in large part) by major reductions in FeoA and FeoB protein levels.

It should be noted that the above work may be subject to artefact since fusions were used that might affect Feo post-translational regulatory response to oxygen, although the fusions did not have any major effect on Feo activity. Also, the Feo components were produced from multicopy plasmids using surrogate promoters which would likely result in higher levels than normally seen for Feo components in the cell, which could also affect the results obtained. Ideally, antibodies would be raised to the various Feo proteins to enable protein-level determination in the wildtype, or the fusion constructs would be incorporated into the chromosome.

The reason for the differences in results between those observed here and those of Kim *et al*. (2015) is unclear, although could be due to the use of different members of the Enterobacteriaceae. However, both this thesis and the data of Kim *et al.* (2013; 2015) indicate that O_2 causes a major reduction in FeoB levels through a post-transcriptional mechanism. Interestingly, Kim *et al*. (2015) found that FeoC stability is also (along with FeoB) affected by O_2, with a high breakdown by Lon under aerobic conditions. FeoC stability was not considered in this thesis but fusions are available that would allow such work in future.

Chapter 9. The importance of only nine conserved residues changed and the C-terminal sub-domain in FeoB-mediated iron uptake

9.1 Introduction

FeoB is common to all Feo systems (Fig. 9.1) and is presumed to function as the iron permease (Cartron *et al*., 2006). Various issues remain to be resolve concerning its mechanism of function and its interaction with the FeoA and FeoC proteins. One approach that can assist such understanding involves the use of site-directed mutagenesis (SDM). This methodology can be used to target key residues, identified on the basis of conservation and/or predicted location, and determine their relevance in processes such as ferrous iron uptake assays as performed here or by others in studying Feo function (Kammler *et al*., 1993; Eng *et al*., 2008).

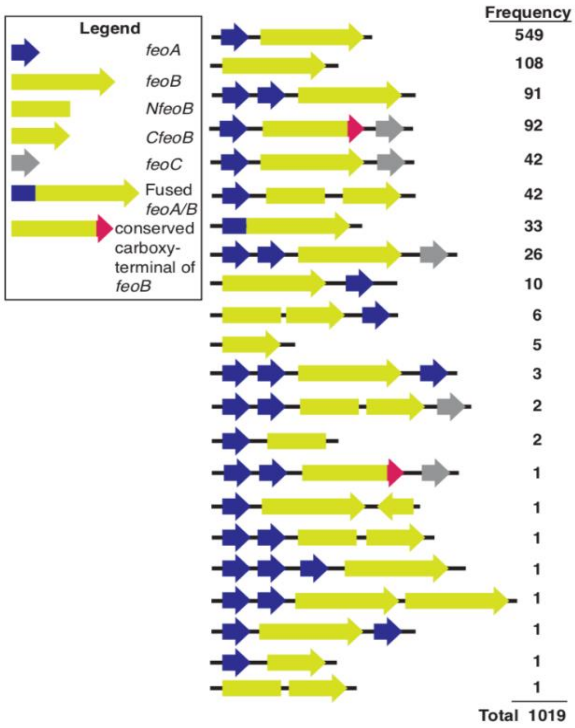

Figure 9.1: Feo system organisation in all most of bacteria in genomic sequences *feoA* and *feoB* more common (adapted from Krewulak *et al*., 2015).

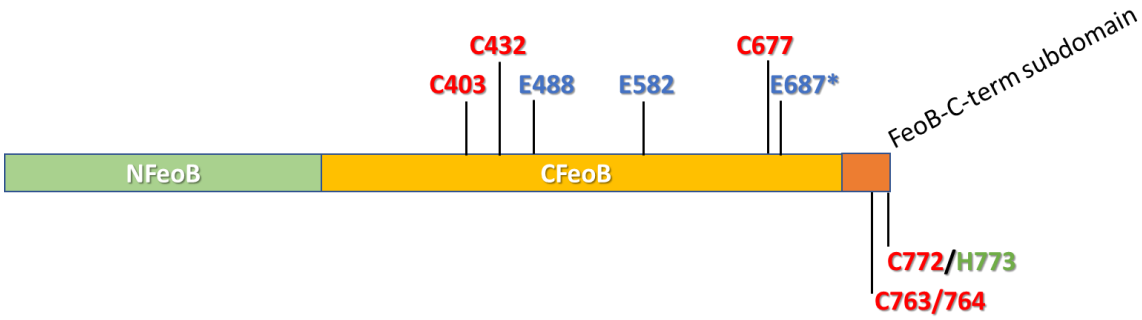

Figure 9.2: Overview of mutations in FeoB. FeoB protein consists of a G-domain (residues 1-170), a helical domain (residues 170-270) (the N domain, in green) and a membrane domain (residues 270-773; in orange), with a short C-terminal subdomain (cytosolic) in orange.

The first full structural model of FeoB was recently published, using homology modelling of sequence data derived from the *P. aeruginosa* FeoB protein (Seyedmohammad *et al*., 2016).

The model suggested that the protein forms a trimer with three C-terminal domains combiming in the membrane for form a central transport channel lined with the conserved Cys residues associated with the Gate motifs. This channel is connected to the distinct central pore formed by three G-domains, as found in the resolved crystal structure (Hung *et al*., 2012). However, the model can be considered to be invalid as the homology-modelling template (the glutamate transporter, GltPh, from *P. horikoshii*; PDB code 1XFH) used for the C-terminal domain structure does not carry Gate motifs and is not a member of the nucleoside transporter family, as has been predicted for FeoB (Cartron *et al*.,2006). Indeed, the template was selected on the basis of pairwise sequence similarity, which was low (22%). However, the suggestion that FeoB oligomerizes into a trimer is supported by previous work on the N-terminal domain of *E.coli* FeoB, which crystallised in trimeric form (Hung *et al*., 2012), although a more recent in depth study found evidence to indicate that FeoB is primarily monomeric in solution (Hagelueken *et al*., 2016).

The function of the GTPase domain has been the subject of much debate. Some would argue that FeoB is likely a GTP-gated pore, which regulates iron flow according to the energy status of the cell (Lau *et al*., 2016; Seyedmohammad *et al*., 2016). Others believe GTP activity provides energy to actively pump Fe^{2+} through the inner membrane (Ash *et al*., 2010; Smith *et al*., 2018). It has often been stated that the GTP-hydrolysis rate of the FeoB G-domain is too slow to support active transport (Seyedmohammad *et al*., 2016). The data on which this observation is based is primarily derived from *in vitro* studies monitoring the GTPase activity of the isolated N-terminal domain (Smith *et al*., 2018). Only two studies have investigated the GTPase activity of N-terminal FeoB when the C-terminal domain is attached; one of which found no evidence to suggest that GTPase activity differed significantly from the values obtained by other studies (Seyedmohammad *et al*., 2016). However, the most recent study showed that FeoB from *K. pneumoniae* can achieve a hydrolysis rate close to what would be expected if it were driving active transport (Smith *et al*., 2018). This observation was limited to FeoB particles isolated using detergents which would be expected to cause limited disruption of protein structure. Although this isolated study on FeoB derived from one species does not provide definitive evidence that FeoB transporters from all species are capable of hydrolysis at such a rate, it does suggest that this could be the case in general. Indeed, it raises questions as to the reliability and accuracy of previous estimates of basal GTPase activity using the isolated N-terminal domain, thus casting doubt on the argument that FeoB cannot be an active transporter because it is incapable of rapid GTP hydrolysis (Smith *et al*., 2018).

FeoA is a β-barrel formed from 5-6 β sheets located at the centre of the protein, with 2-4 α- or 310-helices are also present (Lau *et al*., 2013). The conservation of FeoA varies between organisms (Figure 9.1), but work reported here shows it is absolutely required for Feo function in *E. coli* and it is also required in *V. cholerae* (Perry *et al*., 2006; Weaver *et al*., 2013; Lau *et al*.,2013; Stevenson *et al*., 2016). A role for FeoA as a prokaryotic GAP has been proposed,

based on structural similarities to eukaryotic GAPs and the idea that the apparent abnormally slow rate of FeoB GTP hydrolysis may require stimulation to a higher rate (Su *et al*., 2010). However, as discussed above, the observed rate of GTP hydrolysis may be negatively affected by sample preparation methods. Moreover, purified *E. coli* FeoA does not appear to affect the hydrolysis rate of purified N-terminal FeoB, although the study from which these conclusions are reached has limitations in that it does not consider GTPase activity of full length FeoB (Lau *et al*., 2013). Additionally, the detergents used may have interfered with GTPase activity (Smith *et al*., 2018). The role of FeoA therefore remains open to debate.

FeoC is found in γ-Proteobacteria, and in *E. coli* it enhances FeoB activity in absence of O_2 (see above). It was first proposed to be an iron-responsive transcription factor, as it contains a winged helix fold common to several DNA binding proteins and four conserved cysteine residues which provide a potential binding site for Fe-S clusters (Cartron *et al*., 2006). Formation of Fe-S clusters at the proposed binding site has been confirmed in *K. pneumoniae* and these may be degraded in the presence of oxidising agents, changing FeoC conformation and thus activity (Hsueh *et al*., 2013). It therefore appears likely that FeoC regulates FeoB activity in response to the oxygen/redox status of the cell. However, it has been shown that FeoC does not regulate transcription of the *feo* operon in *Y. pestis* or *V. choerae* (Weaver *et al*., 2013; Fetherston *et al.*, 2012), and no DNA binding activity has been detected to date (Hsueh *et al*., 2013). There are currently two models for FeoC-mediated regulation at the post-translational level; FeoC may act as a G-protein regulator or as a protease inhibitor (Hsueh *et al*., 2013). The protease inhibitor model is based on the observation that the protease, FtsH, degrades FeoB in the absence of FeoC, and that FeoC is itself subject to Lon-dependent degradation aerobically (Kim *et al*., 2013). Binding of FeoC to the N-terminal domain of FeoB has been observed, and it is suggested that this interaction may prevent FeoB degradation (Kim *et al*., 2013). Thus, there is strong evidence published to support the protease inhibitor model

(in *Salmonella*), although results in the preceding chapter cast serious doubt on the validity of this evidence (at least for *E. coli*).

Although several studies have investigated the ability of various conserved N- terminal domain FeoB residues or motifs to facilitate GTPase activity, only one has focused on residues within the C-terminal domain (Seyedmohammad *et al*., 2016). This is likely due to a lack of structural models for this region. The study examined the roles of the highly conserved Cys^{429} and Cys^{675} residues in Fe^{2+} transport in *P. aeruginosa* (Seyedmohammad *et al*., 2016). The authors predicted that Cys^{429}, as found in the Gate 1 motif, lines the central pore or the predicted trimer, whereas Cys^{675}, as found in Gate 2, faces the lipid bilayer; although the homology model used to generate these predictions was seriously flawed (see above). Mutation of Cys^{429} to Ser had no impact on the Fe-induced stimulation of GTPase activity; intriguingly, however, mutation of Cys^{675} to Ser caused a substantial reduction in activity. These results led the authors to propose a model in which Cys^{675} acts as a sensor, enabling GTP cleavage and opening of the FeoB pore when Fe^{2+} is present. Cys^{429} would interact with Fe^{2+} and aid translocation through the pore. These results are interesting, although it is possible that the methods used for isolation of FeoB interfered with GTPase activity, affecting the results (Smith *et al*., 2018). These two residues are also thought to occupy identical positions in the Gate motifs and therefore are expected to share a common, conserved function in interacting with Fe^{2+} and guiding it through the channel (Cartron *et al*., 2006). It is suggested in this thesis that oxidation of their thiol groups to sulfonic acid could block the iron-uptake function of the pore. The cysteine residues might therefore act as a biochemical switch which prevents iron uptake under aerobic conditions, thereby limiting oxidative stress caused by free iron.

A further interesting observation is that FeoB from γ-Proteobacteria has an additional C-terminal sub-domain with one conserved His and three conserved Cys residues (Cartron *et al*.,

2006). The function of this region is currently unknown; however, given that another unique feature of Gammaproteobacterial Feo systems is the presence of FeoC, it is plausible that this region might act as a site of interaction with FeoC.

9.2. Aims of this chapter

In this chapter, nine highly-conserved residues in the FeoB C-terminal domain (six Cys, two Glu acid and one His) will be altered by SDM and the impact on FeoB function determined. Moreover, the effect of removing the FeoB C-terminal sub-domain region will be assessed. Cys residues will be substituted for Ser residues, which differ by exchange of an SH for and OH. Glu and Gln also have similar properties (COOH in place of $CONH_2$), so Glu will be exchanged for Gln. In addition, a C-terminal truncation will be generated. Mutants generated will be tested for their ability to support low-iron growth of JC32. The roles of Cys^{432} and Cys^{677} in *E. coli* FeoB (the equivalents of Cys^{429} and Cys^{675} in *P. aeruginosa*) in Feo-mediated iron uptake will be considered. Three other highly conserved residues in the region of the FeoB Gate motifs will also be investigated (Cys^{403}, Glu^{488} and Glu^{582}). Of these, Cys^{403} had previously been shown to display a high level of conservation (Cartron *et al*., 2006). Four other highly conserved residues in the tail of the FeoB protein will also be investigated (Cys^{763}, Cys^{764}, Cys^{772} and His^{773}).

9.3. Identification of FeoB-residues of interest

It has previously been demonstrated that Cys^{432} and Cys^{677} might facilitate iron uptake (Cartron *et al*., 2006; Seyedmohammad *et al*., 2016). Cys^{403} is also known to be highly conserved and may be of interest because Cys residues can interact with Fe^{2+} (Cartron *et al*., 2006). An alignment of FeoB amino acid sequences was performed; this confirmed that each of these residues displays a high level of conservation, and therefore are appropriate candidates for site

directed mutagenesis (Figure 9.3). A topology model of *E. coli* FeoB was generated to better enable visualisation of the locations of the well-conserved residues or interest (Figure 9.4). Cys^{432} and Cys^{677} appear to be located in transmembrane helices of the Gate 1 and 2 motifs, respectively. Cys^{403} forms part of a cytoplasmic loop attached to the transmembrane helix containing Cys^{432}.

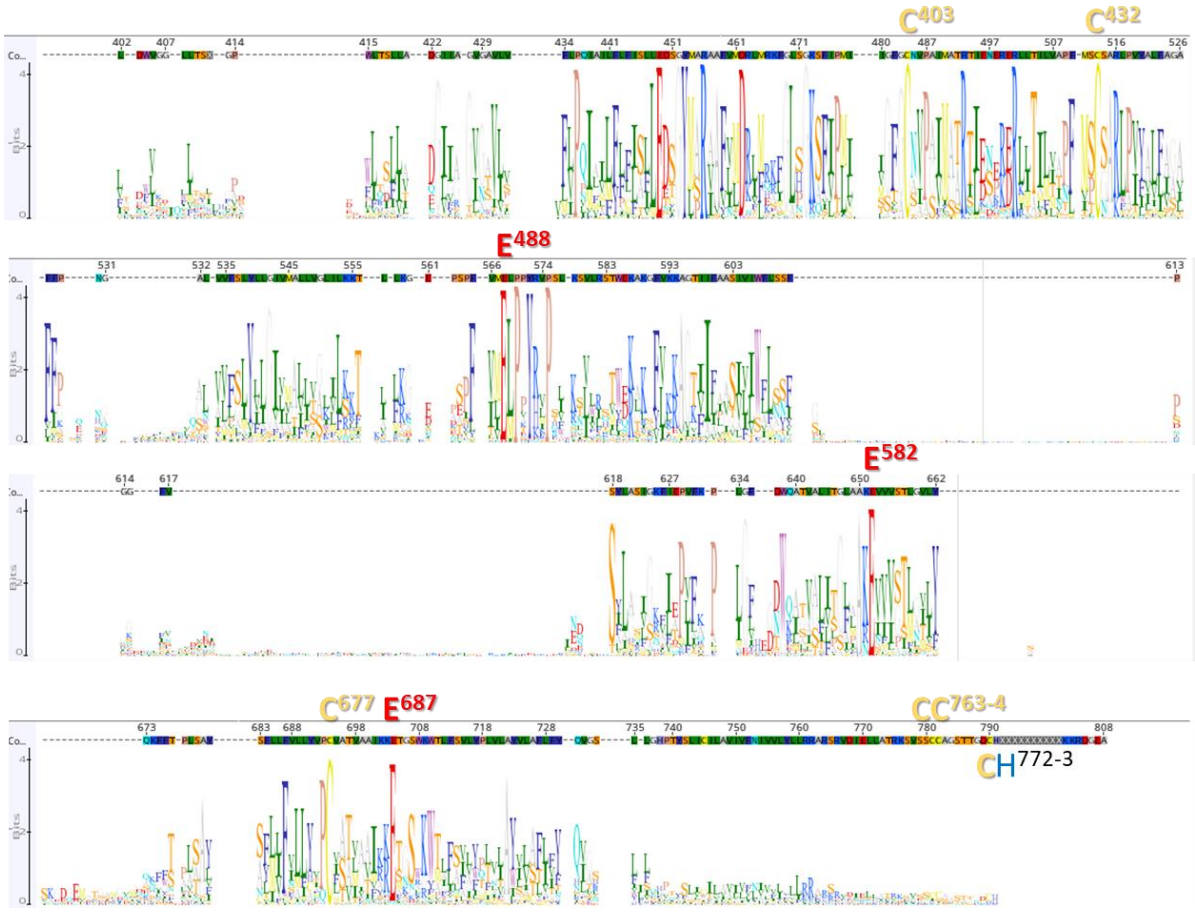

Figure 9.3: Multiples amino acid sequence alignment showing the level of conservation of FeoB residues. Approximately 600 sequences were used to generate this alignment, which was used to select residues for mutation. The residues investigated in this are indicated. Only the C-terminal domain of FeoB is considered here.

A well-conserved motif (Cys-Cys…Cys-His) is located in the C-terminal sub-domain of FeoB (Fig. 9.3). This is predicted to be located in the cytoplasm (Fig. 9.4). Here, it is suggested that

it may bind iron, respond to the redox and/or interact with FeoC. The purpose of this motif will be tested by mutation of the Cys residues to Ser, and the His residue to Gln.

The alignment (Fig. 9.3) was used in conjunction with structural predictions to inform selection of two additional residues for investigation. The two Glu residues (488 and 582) were chosen because such residues are commonly involved in iron binding in other proteins. The residues are in Gate 1 a or 2 motifs (Figure 9.4). Glu^{687} was mutated to a stop codon in these experiments. Ideally, this residue should be changes to a Gln.

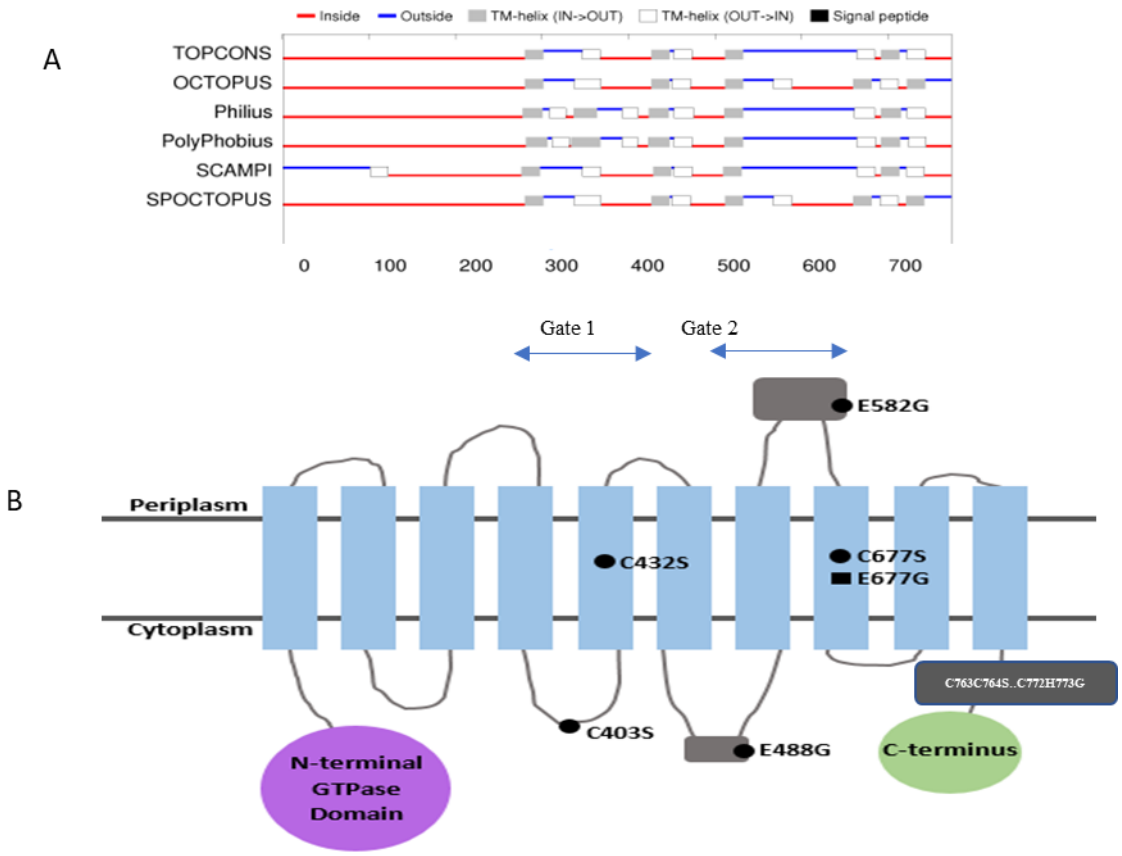

Figure 9.4: The estimated locations of the ten FeoB residues subjected to site directed mutagenesis. **A** shows topology prediction for *E. coli* FeoB obtained from TOPCONS. Predictions from a variety of servers are shown. There are some discrepancies with regards to the number of helices and consequently the locations of some of the loops. **B** shows a membrane topology model of *E. coli*-derived FeoB, based on the topological features most commonly observed across all predictions from TOPCONS and UniProtKB. The estimated locations of the residues which were mutated are shown. The residues substituted for amino acids with similar properties are represented by circle. The square indicates the Glu^{687} where a stop codon was inserted.

A convincing homology model was generated (Dr Liam McGuffin, University of Reading) using a nucleoside transporter protein with two Gate motifs as the template (Fig. 9.5). This shows that three of the residues selected for SDM are closely-located at a potential metal-binding site in the predicted pore region of the FeoB permease.

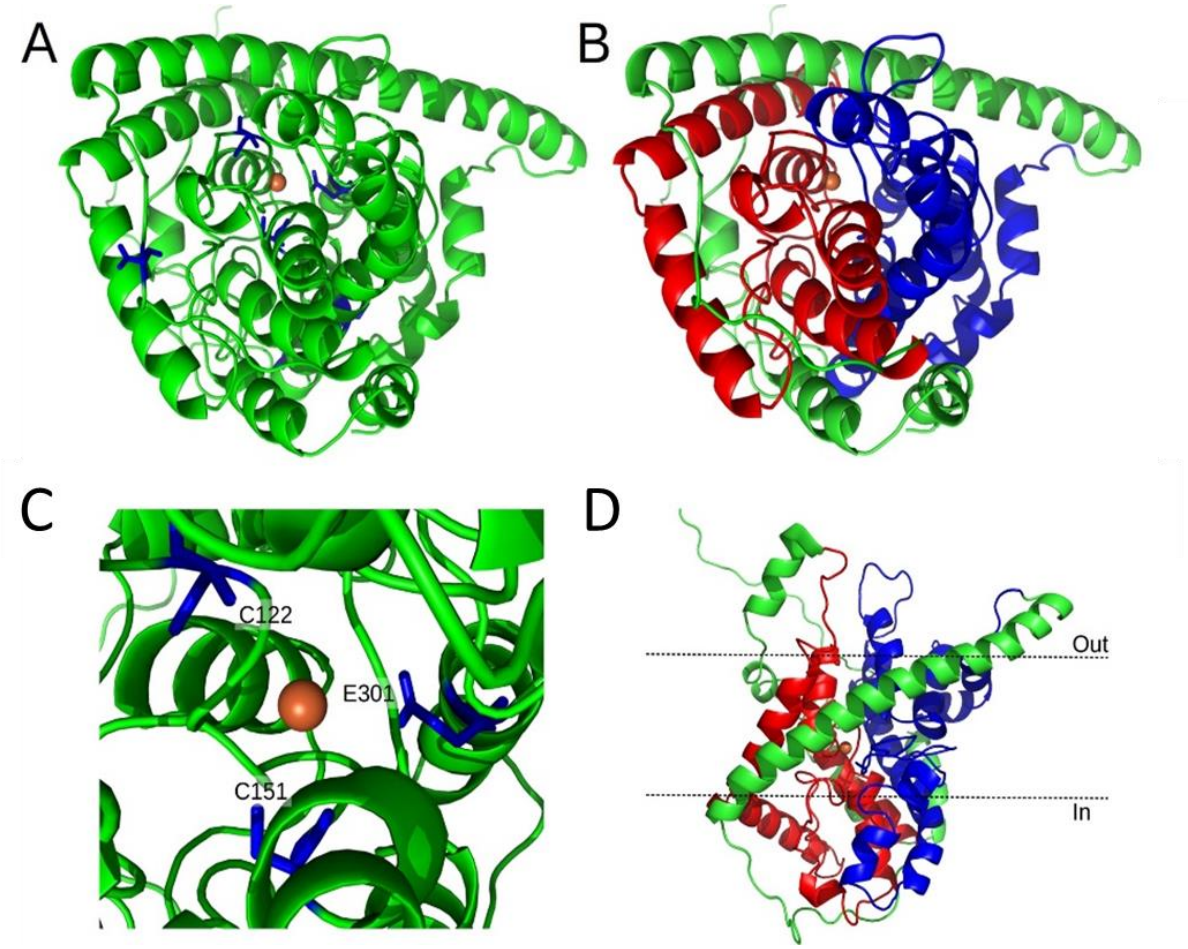

Figure 9.5: Predicted structure of the FeoB C-terminal domain of *E. coli*. The structure of the C-terminal domain of FeoB has yet to be solved experimentally. The template used for modelling was of 5L24 from *Neisseria wadsworthii* 9715 (Hirschi *et al*., 2017) and modelling was performed by Dr Liam McGuffin with the IntFOLD Integrated Protein Structure and Function Prediction Server program (https://www.reading.ac.uk/bioinf/IntFOLD/). It indicates two homologous motifs, oppositely orientated in the membrane for the FeoB protein - highlighted in red and blue (95-220 Gate 1; 290-415 Gate 2 (**B**). **A.** Key FeoB residues highlighted are: Cys 403 (122 in the model), Cys 432 (151), Cys 677 (395), Glu 488 (206), Glu 582 (301), Glu 687 (405). The possible presence of a binding site for ferrous iron (orange sphere) is indicated in **C**, along with nearby residues of interest (Cys 403 & 432, Glu 582). **D** shows the orientation in the membrane with the channel between the two Gate motifs where iron might bind. Images were edited using Pymol.

9.4. Primer design and generation of mutant plasmids

Primers were designed using Agilent software. The melting temperatures were determined using the equation: Tm=81.5+0.41(GC%)-(675/N)-%mismatch (where N is the length of the primer expressed in base pairs). Glu^{687} was converted to a stop signal, and other changes were conservative to minimise potential disruption to the protein structure. Codons were changed to the most frequently used codon in *E. coli* for the desired amino acid.

The mutated codon was located in the middle of the primer (Table 2.8) and the Tm was equal to or above 78 ˚C, as is stipulated in the mutagenesis protocol used. In addition, melting temperatures of all primers used were approximately equal to allow all PCR reactions to be completed together. SDM was performed on the pBAD-*feoAB* plasmids (with and without the Flag tag) generated above using the Aglient QuikChange II XL Site -Directed Mutagenesis kit (Methods 2.27). All mutants thus generated were confirmed by nucleotide sequencing.

The mutation work performed here was in collaboration with a final year project student (Emma Bartram) who was under my supervision.

9.4.1. Construction of pBAD-*feoAB* site-directed mutants

For SDM of the Cys, His and Glu residues, the procedure was as described in Methods 2.2.25 As can be seen in Figure 9.6, following the SDM procedure, plasmid DNA of the expected size was recovered from transformants in all cases (~6.7 kb). A single restriction digest using *Hin*dIII confirmed identity of the plasmids (Fig. 9.7). Two plasmids for each mutagenesis were submitted for nucleotide sequencing. The results show that all but one of the samples (the first C677S mutant, not shown) had the expect mutation (Fig. 9.8). The paired reads from the sequencing data were assembled with the original template sequence in CLC Genomics Workbench to check for any additional mutations within the sequenced region. The only

deviations from the template sequence which appeared on both strands were the mutations induced by the primer. All plasmids containing the mutated *feoB* genes were used for phenotype testing. The use of plasmids derived from two colonies for each mutation increased the reliability of the final results. PCR is low-fidelity process; additional mutations may have been introduced with an impact on FeoB folding or function. However, it is unlikely that two plasmids will have obtained such mutations.

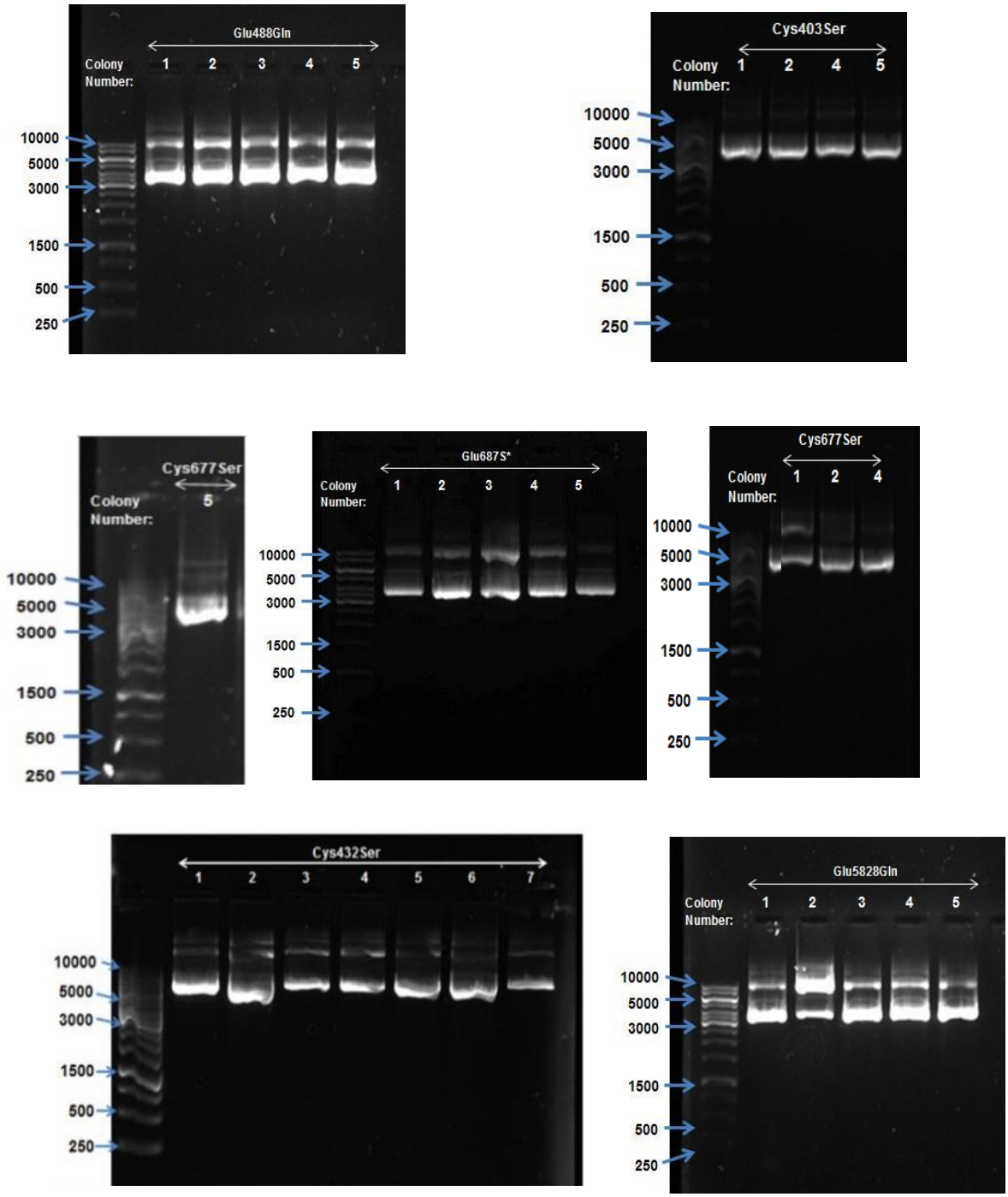

Figure 9.6: Gels showing pBAD-*feoAB* plasmids recovered after SDM. The gels show that the plasmid minipreps successfully isolated plasmid DNA from each culture. Plasmid products of each of the six mutagenesis reaction (C432S, C403S, C677S, E488N, E582N and E687*) are shown.

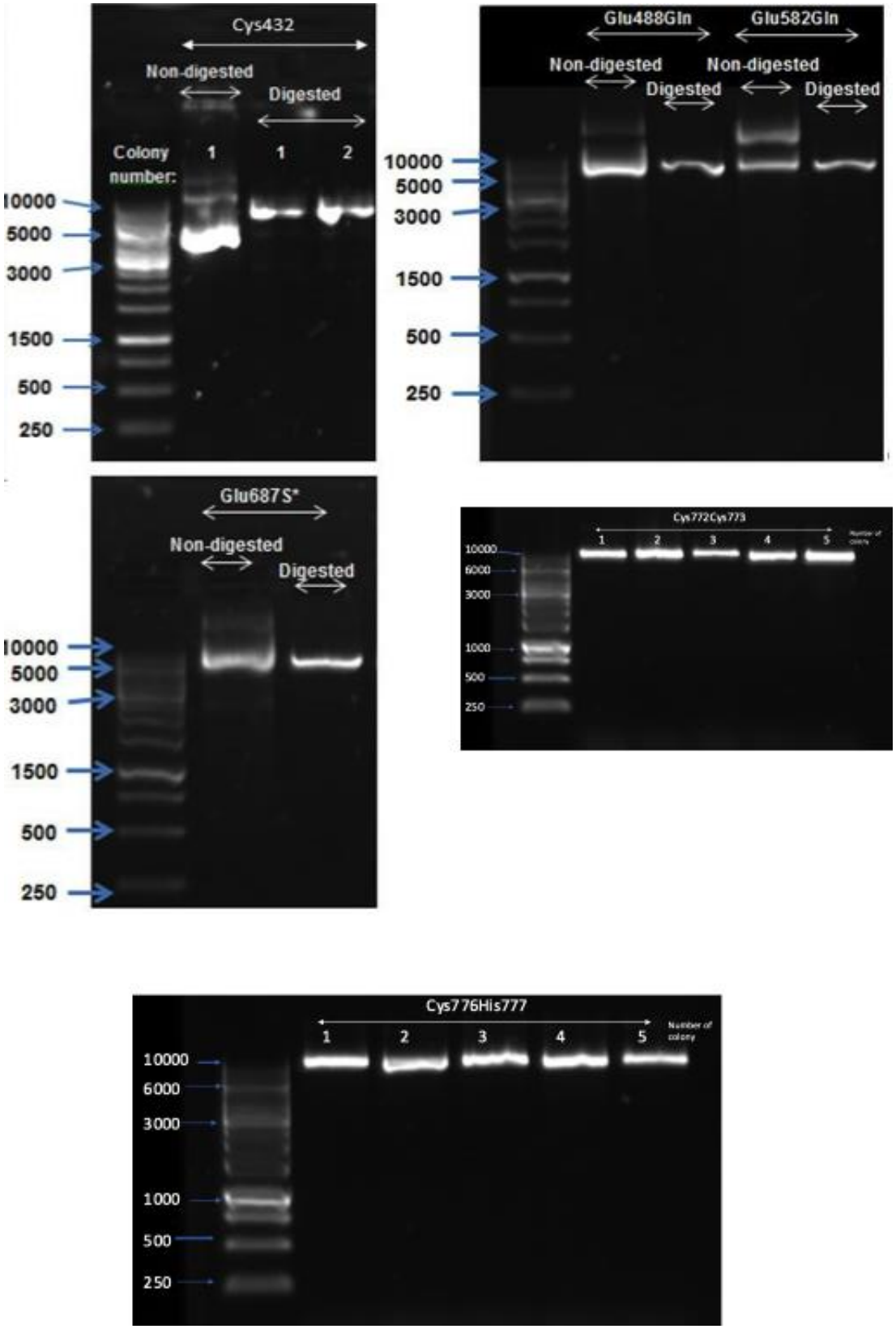

Figure 9.7: Gels showing the isolated plasmid DNA post-SDM after digestion with *Hin*dIII.The bands generated by non-digested samples are shown for comparison. The restriction digest eliminated the presence of additional bands on the gel, indicating that these bands were caused by concatermerization.

Cys403Ser:
For: CTGATCGTCGGTTTCGGTTCTAACGTACCGTCGGTAATG

Cys432Ser:
For: ATGGCACCGTTTATGTCCTCTGGCGCGCGTCTGGCTATC

Cys677Ser:
For: GTCCTGCTGTATGTACCATCTATCTCGGTGATGGGAGCC

Glu488Gln:
For: GCGACGCCGTTTGTCATGCAGCTGCCGGTCTACCATGTA

Glu582Gln:
For: ACGGGTGCAATGGCGAAACAGGTGGTGGTGGGTACGCT

Glu687Stop*:
For: ATGGGAGCCATCGCCCGTTAATCAAGCCGTGGCTGGATG

Cys763SerCys764Ser:
For: ACCCGCAAGTCGGTAAGTAGTAGCAGCGCAGCCAGCACC

Cys772Ser, His773Glu:
For: GCAGCCAGCACCACCGGTGATAGCCAGGATTATAAAGATG

Figure 9.8: Nucleotide sequence of the relevant part of the selected mutated plasmids. Successfully mutated codons are highlighted in red.

9.5. Phenotypic analysis of iron-transport depleted *E. coli* JC32 carrying mutations in the Gate-motif regions of *feoB*

The *E. coli* JC32 was used for transformation with plasmids carrying the mutated and wildtype versions of *feoB*. Some cells were co-transformed with plasmid containing mutated pBADara-*feoAB* and pBADrha-*feoC*.

9.5.1. Can the mutant forms of *feoB* support growth JC32 under iron-depletion conditions aerobically?

Growth tests were as described in previous chapters (Methods 2.25.1.1) using a Bioscreen apparatus and 0.4% glucose in M9 minimal media at pH 6 (100 mM MES), containing the

required antibiotics and inducers. Precultures were always grown with 10 μM ferric citrate iron, and 0.5 μM DTPA and/or 2 mM ascorbic acid were added as indicated during growth comparisons. Growths with 0.5 μM DTPA showed that five of the six substitutions (C403S, C432S, C677S, E582N and E687*) resulted in complete loss of Feo activity, both with and without FeoC, under aerobic conditions (Fig. 9.9). Interestingly, the E488N mutation had no impact when FeoC was present, but caused a moderate diminution of growth in the absence of FeoC, with respect to that seen for the wildtype *feoB* control. This suggests that E488 is important for FeoB activity when FeoC is absent, but not when it is present, under aerobic iron restriction.

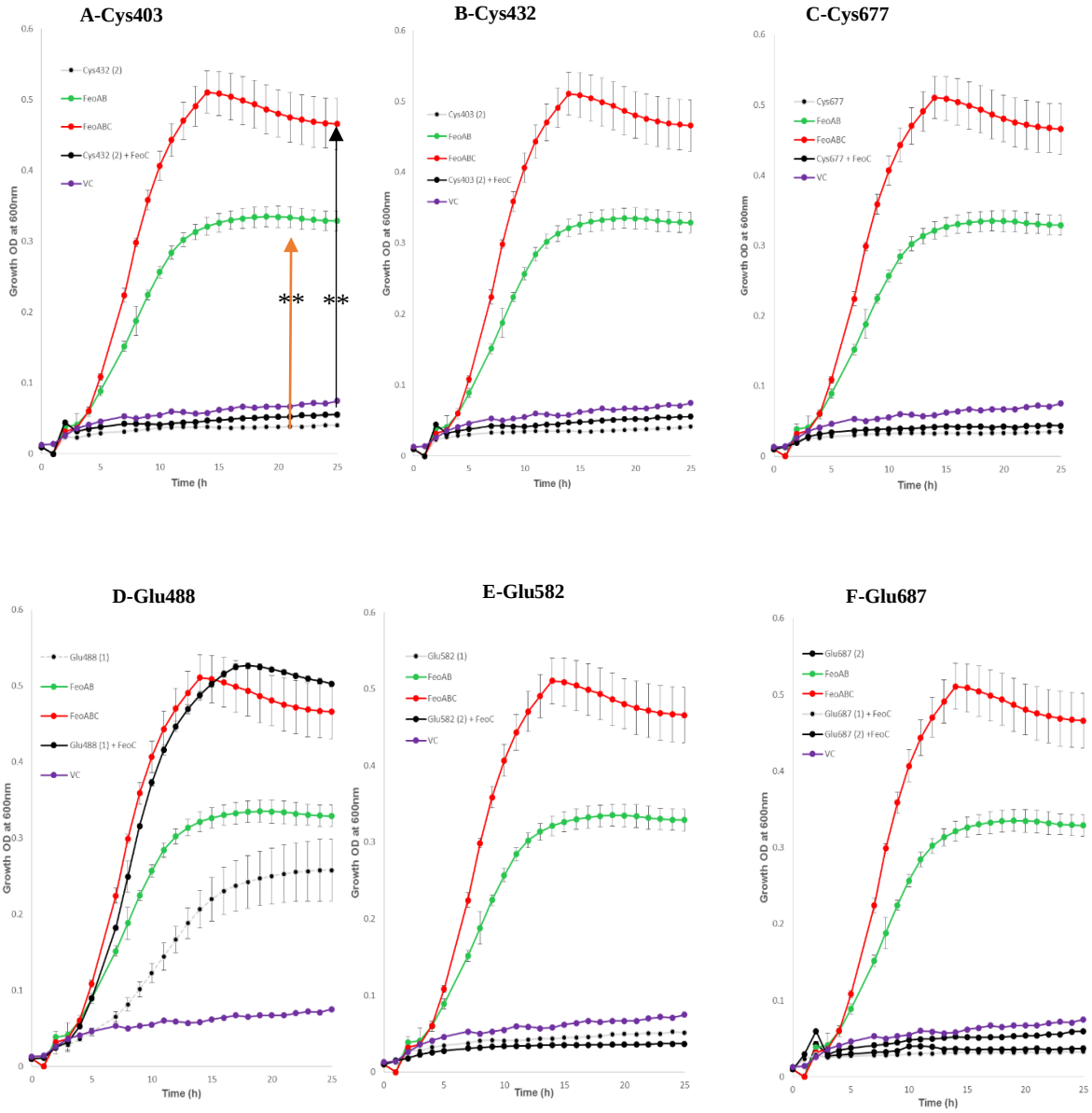

Figure 9.9: Aerobic growth of *E. coli* JC32 containing mutated *feoB* in M9 minimal medium. JC32 with pBADara-*feoAB* (with wildtype or mutated *feoB*, as indicated) with either pBADrha-*feoC* or pBADrha. **A**. C432S. **B**. C403S. **C**. C677S. **D**. E488N. **E**. E582N. **F**. E687*. Each point is the average of 3 parallel cultures with standard deviations shown. The M9 medium (pH 6) induced 0.5 µM DTPA. Two different isolates were considered, and similar results were obtained (not shown). An ANOVA ($p<0.01$) was carried out on the data derived from the 24 h time point; indicted on the graph by the ** symbol.

9.5.2. Effect of *feoB* Gate motif mutations on JC32 growth under anaerobic iron deficient conditions

Anaerobic growth was completed using 10 ml of M9 medium with 0.4% glucose and 100 mM KNO_3 (as anaerobic respiratory acceptor) in 10-ml syringes. The medium was deprived of oxygen by being subjected to bubbling with N_2 gas for 30 min. Another method was employed for anaerobic/microaerobic growth analysis using FlUOstar machine, where growth was measured with no shaking and with 85% N_2 and 15% CO_2 (Methods 2.23.2).

The results obtained anaerobically were largely the same as those obtained aerobically (Fig. 9.10). The difference in growth between the strains with and without *feoC* was much less than that seen aerobically, reduced from ~50% greater growth with *feoC* to ~10%. The five substitutions (C403S, C432S, C677S, E582N and E687*) that resulted in no apparent Feo activity aerobically, gave the same effect anaerobically (Fig. 9.10). The E488N mutation resulted in a slightly enhanced growth for in the presence of *feoC*, and caused no notable difference in the absence of FeoC (Fig. 9.10E). The good growth with *feoC* anaerobically for the E488N mutant reflects that seen aerobically. However, it is interesting that the diminished growth seen aerobically in absence of *feoC* is not observed anaerobically. This suggests that FeoB-E488N has raised sensitivity to aerobic conditions in absence of FeoC.

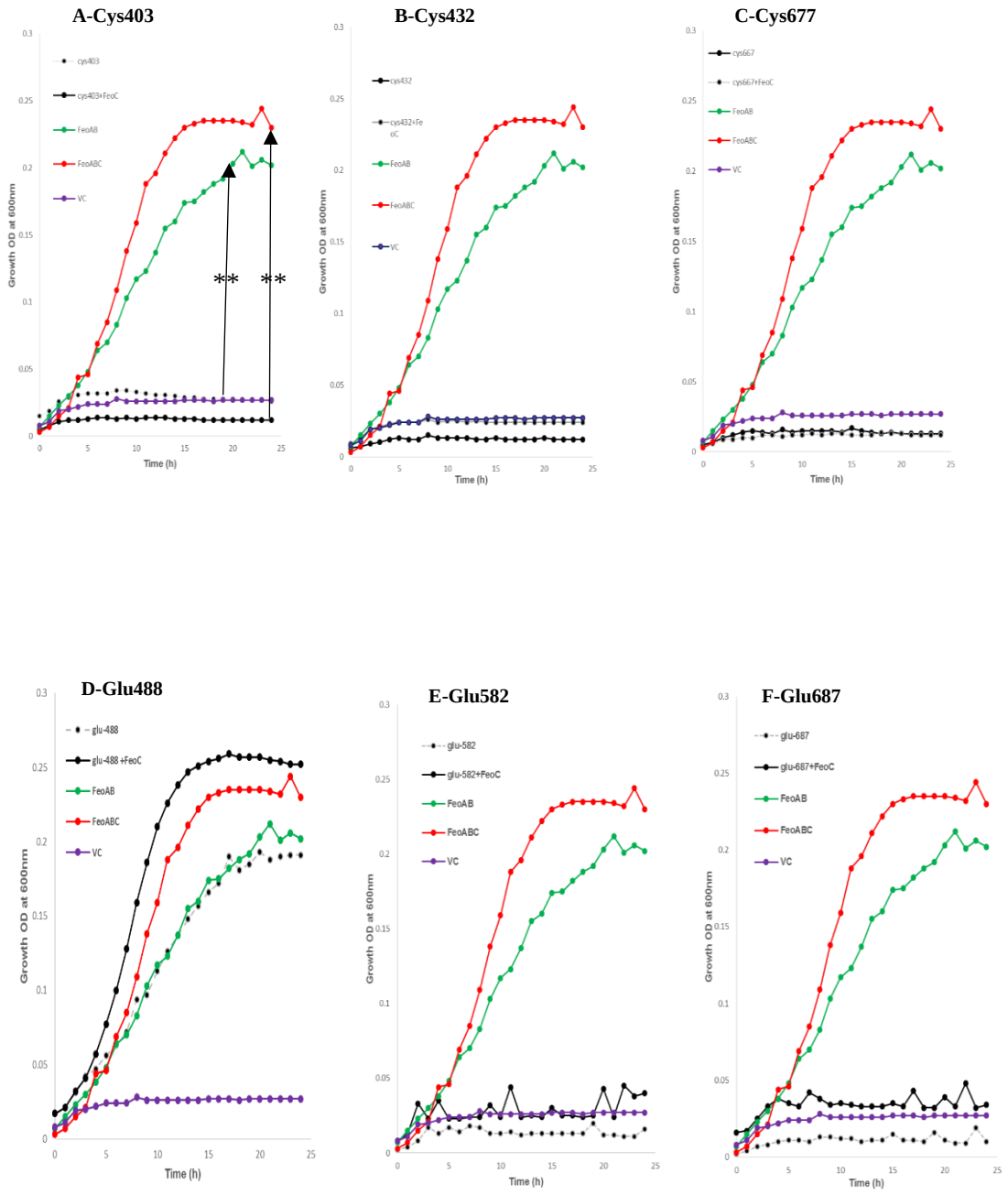

Figure 9.10: Anaerobic growth of *E. coli* JC32 containing mutated *feoB* in M9 minimal medium. Details are as in Fig. 9.9 except for use of the FLUOstar for growth under O_2 free conditions, and the presence of 100 mMKNO_3. An ANOVA ($p>0.01$, n=3; **) was carried out on the data derived from the 24 hour time point; this was accompanied by a Dunnett analysis to identify bacteria which exhibited a significant difference in growth comparative to bacteria completely lacking a Feo system (empty plasmid).

9.5.3. Effect of *feoB* Gate motif mutations on JC32 growth under aerobic iron deficient conditions with ascorbate

Growth experiments were performed as above under aerobic conditions with 1 µM DTPA with or without 2 mM ascorbate, using a Bioscreen apparatus. The mutation in FeoB (C432S, C403S, C677S, E582N and E687*) that prevent growth previously, had the same affect with ascorbate under aerobiosis (Fig. 9.11). For wildtype FeoB, the presence of ascorbate increased FeoABC and FeoAB dependent growth of JC32 by ~twofold, but growth with FeoC was much greater than that without (as seen previously under these conditions). The E488N mutation had only slight effects under these conditions, causing slightly reduced growth with ascorbate (the presence of FeoC did not influence this effect), slightly enhanced growth with FeoC in absence of ascorbate and no effect in absence of both ascorbate and FeoC. However, one of the positive controls (FeoABC without ascorbate) grew unusually weakly in Fig. 9.11D, and so the E488N may have caused a decreased growth without FeoC, both with and without FeoC. If so, this resembles the data of Fig. 9.9 showing slightly reduced aerobic caused by the FeoB-E488N mutation.

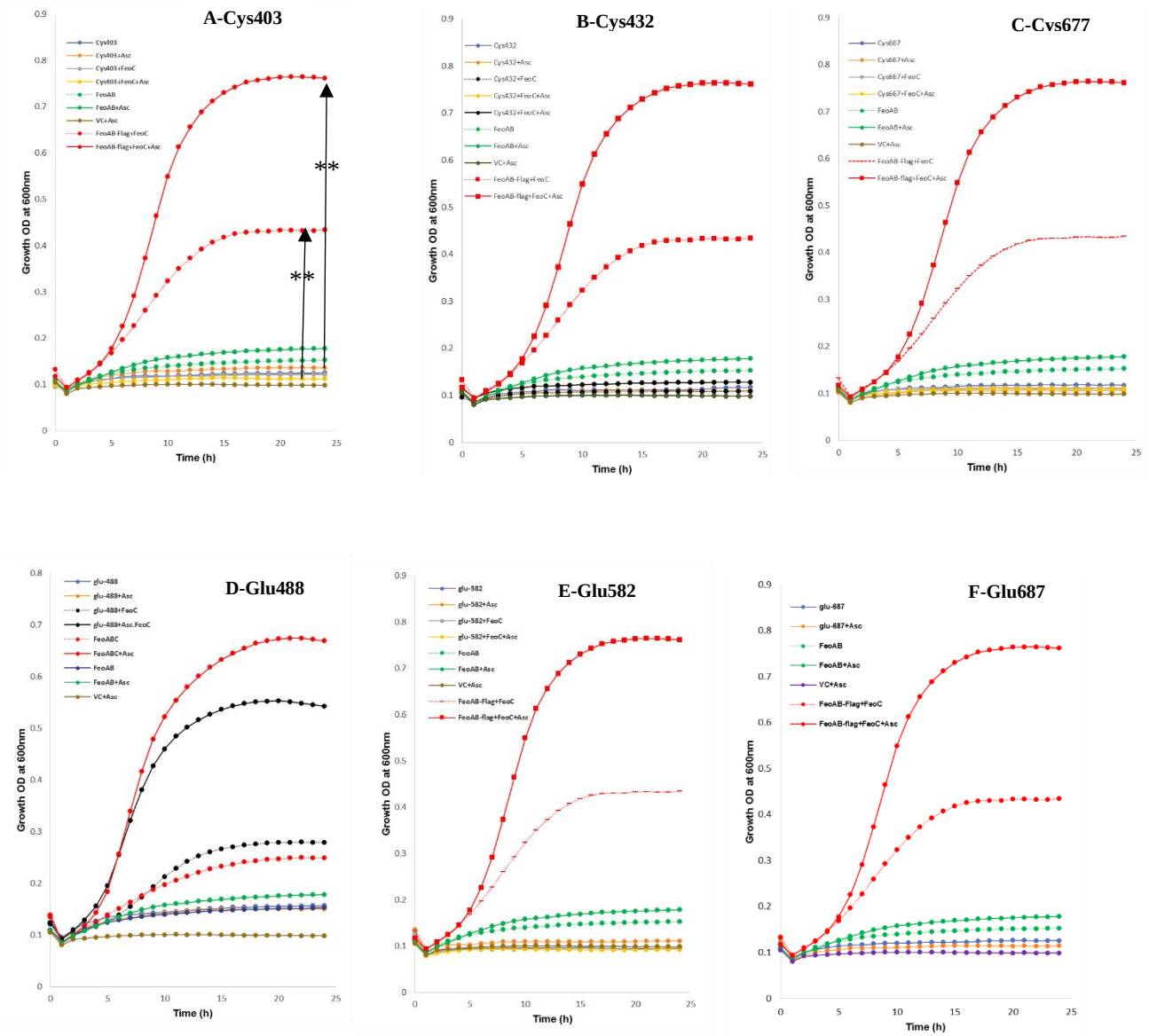

Figure 9.11: Aerobic growth of *E. coli* JC32 containing mutated *feoB* in M9 minimal medium 0.5 µM DTPA and 2 mM ascorbic acid. Details are as in Fig. 9.9, except for inclusion of 2 mM ascorbate, as indicated, the *feoAB*-flag encoding plasmids (as indicated). An ANOVA ($p>0.05$, $n=3$; * *) was carried out on the data derived from the 24 h time point; this was accompanied by a Dunnett analysis to identify bacteria which exhibited a significant difference in growth comparative to bacteria completely lacking a Feo system (empty plasmid).

9.6. pBAD$_{rha}$-*feoAB*-flag-tag plasmids containing Cys and His mutations in the C-terminal sub-domain of FeoB

9.6.1 Mutant generation

SDM of pBADrha-*feoAB*-Flag was performed as described previously (see Methods 2.27) for pBADara-*feoAB*. Here, the aim was to introduce mutations of the conserved Cys and His residues in the C-terminal sub-domain of FeoB-Flag, such that the impact of these mutations on FeoB cellular levels and iron-uptake activity could be determined. Following mutagenic PCR and transformation, the resulting plasmid DNA was analysed by electrophoresis; all samples gave a single plasmid band migrating at ~9 kb, as expected (Fig. 9.12 & 9.13).

The plasmid DNA was then digested with *Nde*I and *Hin*dIII, to release the insert. Electrophoresis revealed bands matching the sizes expected for the insert (2676 bp), vector (6101 bp) and singly cut plasmid (8.9 kb; Fig 9.14). The inserts carried by the plasmids were sequenced (by Source Bioscience) with primers pBAD-F and pBAD-R, and the sequence was found to contain the expected changes, and no other alteration. One plasmid of each type was thus designated pBADrha-*feoAB*(C763S/C764S)-Flag and pBADrha-*feoAB*(C772S/H773G)-Flag, and these were used in further experiments.

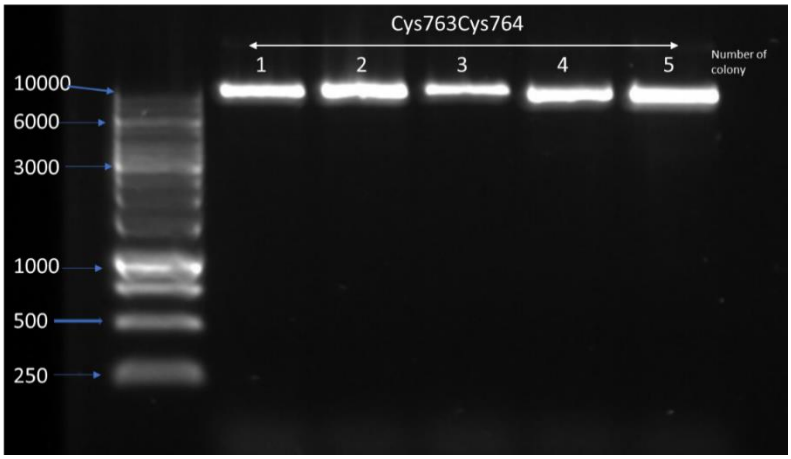

Figure 9.12: Gel electrophoretic analysis of pBADrha-*feoAB*-Flag Cys763-Cys764 mutant. Isolated plasmid DNA was not digested. Electrophoresis was performed using a 0.6% agarose TBE gel. L is GeneRuler® 1 kb ladder (far right). Sample 1 (far left) was used for further work.

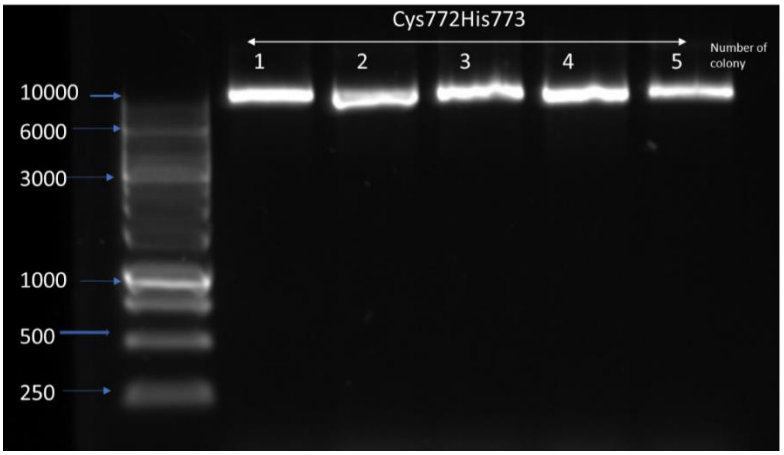

Figure 9.13: Gel electrophoretic analysis of pBADrha-*feoAB*-Flag Cys772-His773 mutants. Details are as above.

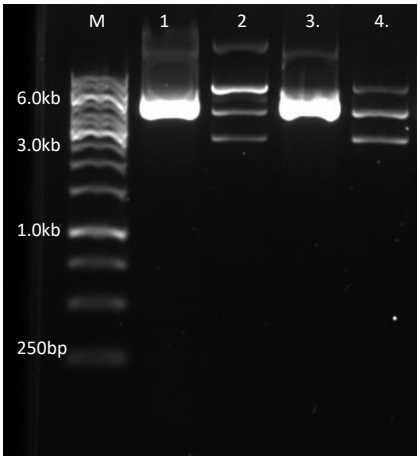

Figure 9.14: Gel electrophoretic analysis of pBADrha-*feoAB*-Flag C763/764 and C772-H773 mutants following restriction digestion. Details are as above. Samples were digested with *Nde*I and *Hin*dIII. M is GeneRuler® 1 kb. Sample 1 and 2, non-digested and digested Cys763/Cys764 mutant; sample 3 and 4, non-digested and digested Cys772/His773 mutant.

9.6.2. Impact of FeoB C-terminal sub-domain on FeoB activity

Under aerobic iron-limited growth conditions, the C763S/C764S and C772S/H763G mutations both caused an ~40% increase in growth of JC32 with *feoABC* (Fig. 9.15). In contrast, there was little effect for JC32 with *feoAB* (Fig. 9.15). This suggests the C-terminal subdomain caused reduced aerobic Feo activity, but only when FeoC is present.

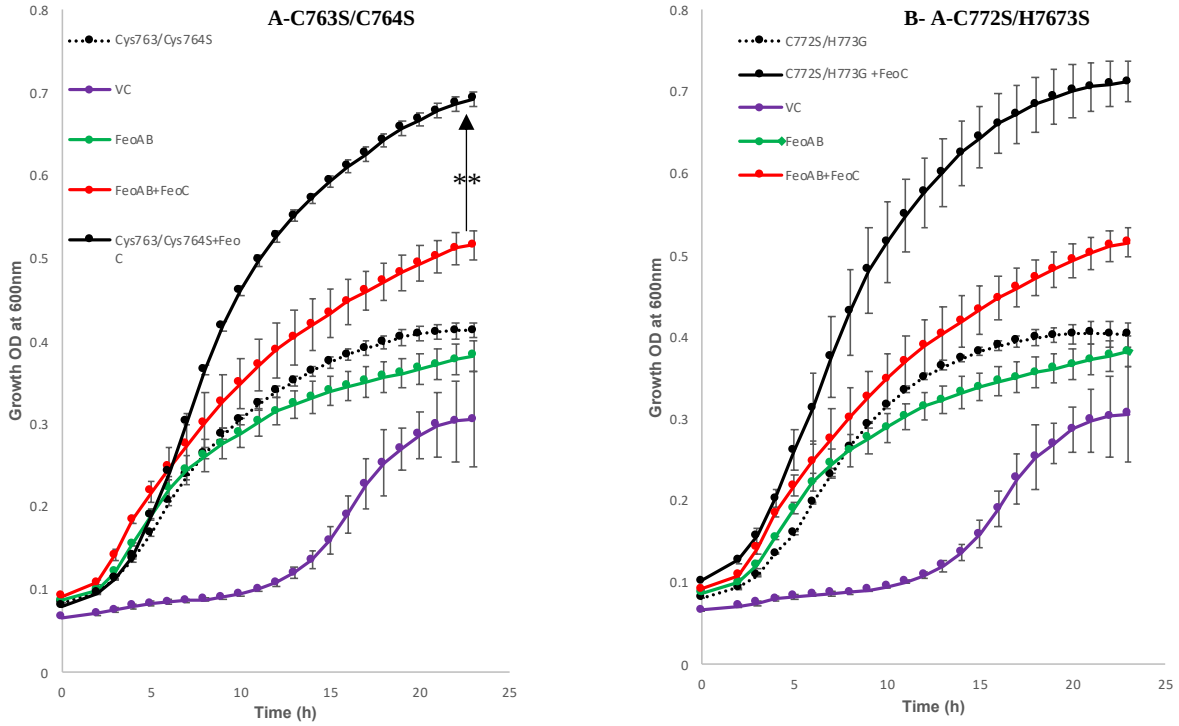

Figure 9.15: Impact of mutations in the C-terminal sub-domain of FeoB on growth of *E. coli* JC32 in M9 medium, under <u>aerobic conditions without DTPA</u>. Growth of JC32 transformed with pBADrha-*feoAB* or *feoABC*, with or without the indicated mutations. A vector control (pBADrha) is also included. Growth was aerobic in M9 medium with 0.4% glucose, at pH 6, with no DTPA. An ANOVA ($p>0.01$, $n=3$; **) was carried out on the data derived from the 24 h time point; this was accompanied by a Dunnett analysis to identify bacteria which exhibited a significant difference in growth comparative to bacteria completely lacking a Feo system (empty plasmid).

Under anaerobic conditions, results were similar, with both mutant-forms again providing greater growth for the *feoABC* complemented strain (Fig. 9.16). However, for the *feoAB*-complemented strains, the two types of mutation gave different results. C763S/C764S *feoAB* gave a weaker growth with respect to the non-mutant control whereas C772S/H763G *feoAB* gave a stronger growth (same as for the C772S/H763G *feoABC* complemented strain). Previous results (Chapter 7) show that FeoC provides little added advantage during low-iron growth mediated by Feo, anaerobically. Thus, the result in Fig. 9.16A for the C763S/C764S mutant is somewhat unexpected (but is it reproducible??), whereas the finding with the C772S/H763G mutant (no effect of FeoC anaerobically) is consistent with earlier data. The key finding from

the results in Fig. 9.16 A & 9.16B is that the mutations in the C-terminal sub-domain have little or no negative impact on Feo function.

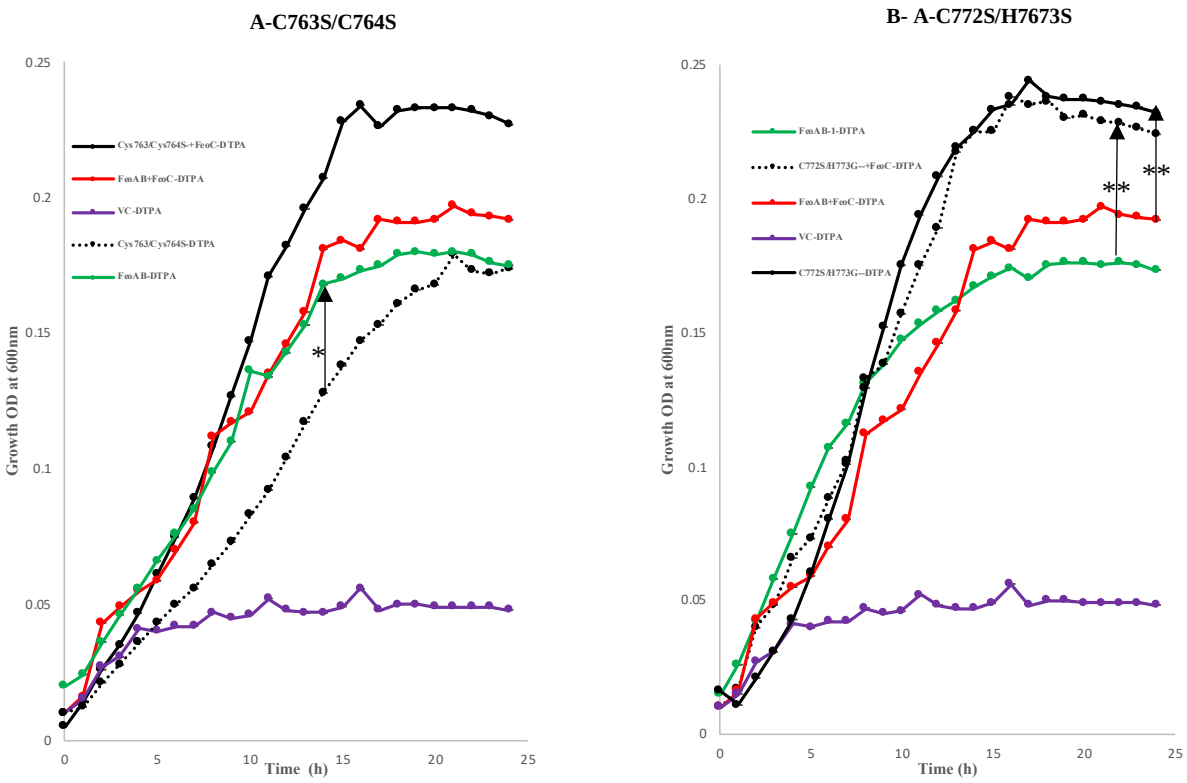

Figure 9.16: Impact of mutations in the C-terminal sub-domain of FeoB on growth of *E. coli* JC32 in M9 medium, under <u>anaerobic conditions with 0.5 µM DTPA.</u>.. All details as above except for use on anaerobic conditions with DTPA. An ANOVA ($p>0.01$, $n=3$; **) was carried out on the data derived from the 24 h time point.

When the anaerobic growths were performed without DTPA, both mutations were found to provide a modest (~10%) increased growth for the *feoABC*-complemented strain with respect to that seen for the non-mutant *feoABC* complemented strain (Fig. 9.17). This effect is therefore similar to that seen with DTPA (Fig. 9.16), but is weaker (presumably due to the greater availability of iron and therefore reduced Feo dependence).

The results presented so far thus suggest that the sub-domain mutations result in enhanced Feo function anaerobically (with/without FeoC) and aerobically (with FeoC).

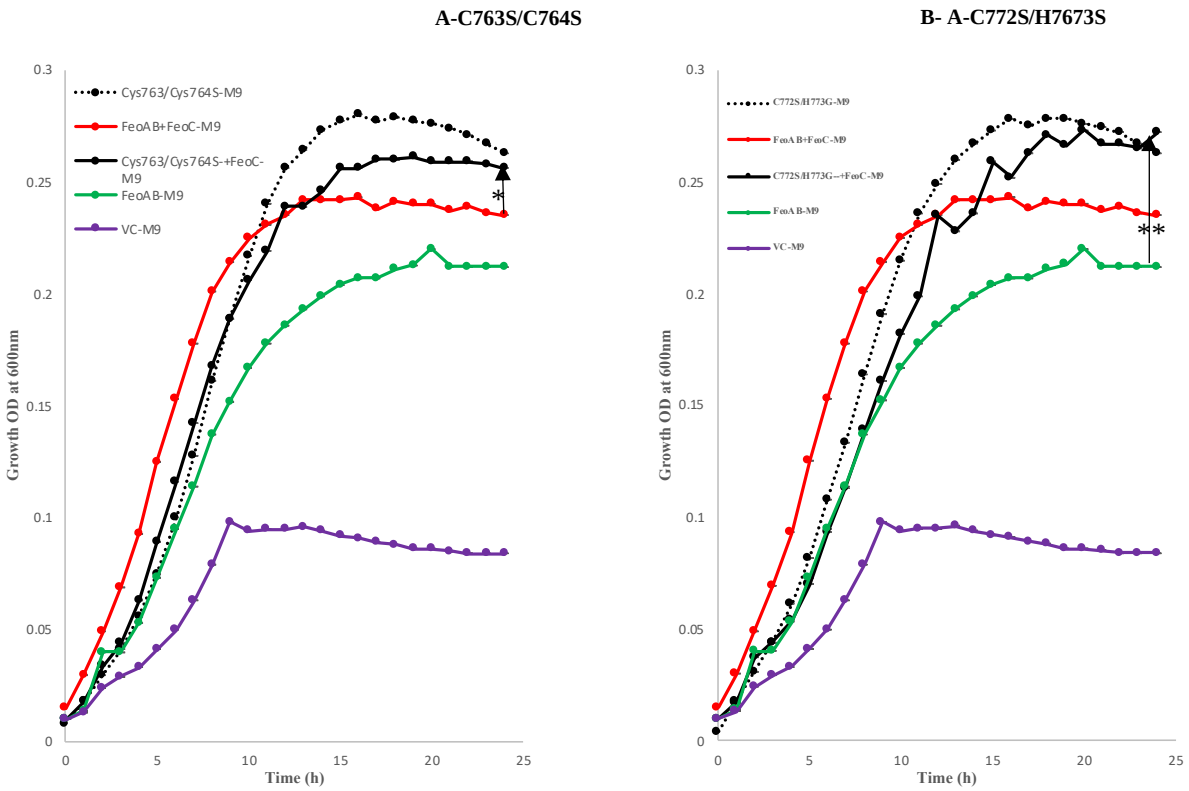

Figure 9.17: Impact of mutations in the C-terminal sub-domain of FeoB on growth of *E. coli* JC32 in M9 medium, under anaerobic conditions without DTPA. All details are as above except for the absence of DTPA.

In the presence of ascorbate and DTPA, aerobically, the mutations again resulted in improved growth for the *feoABC* complemented JC32 strain (Fig. 9.18). However, in the absence of ascorbate any growth advantage provided was less apparent (Fig. 9.18). Aerobically, a good growth advantage was conferred by the mutations upon *feoABC* complementation when DTPA was absent (Fig. 9.15). Thus, when DTPA is supplied alone the aerobic growth advantage of the mutant forms of *feoABC* is no longer observed. The experiment in Fig. 9.18 was repeated and similar result were obtained (Fig. 9.19).

Aerobically with DTPA, complementation with *feoAB*-only gave only a slight growth advantage, as seen in Chapter 7.

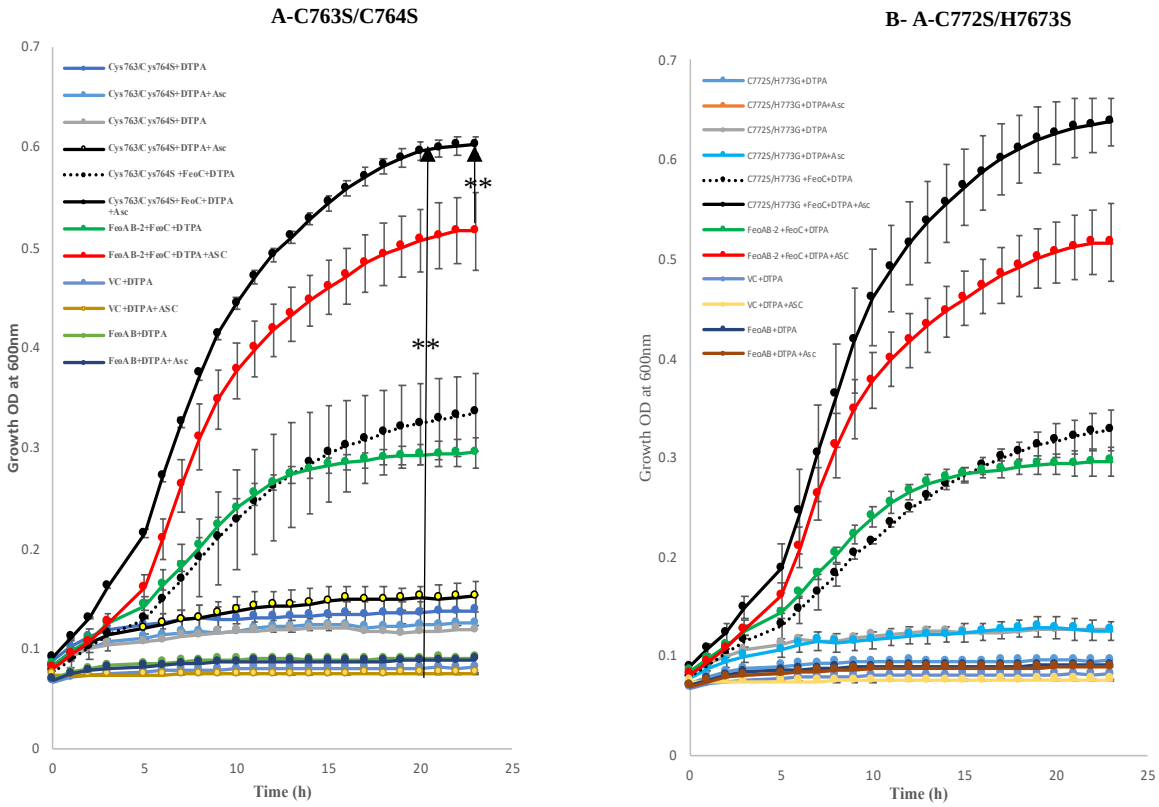

Figure 9.18: Impact of mutations in the C-terminal sub-domain of FeoB on growth of *E. coli* JC32 in M9 medium, under aerobic conditions with 2 mM ascorbate and/or 0.5 µM DTPA (I). .All details as in Fig. 9.15 except for the use of ascorbate as indicated.

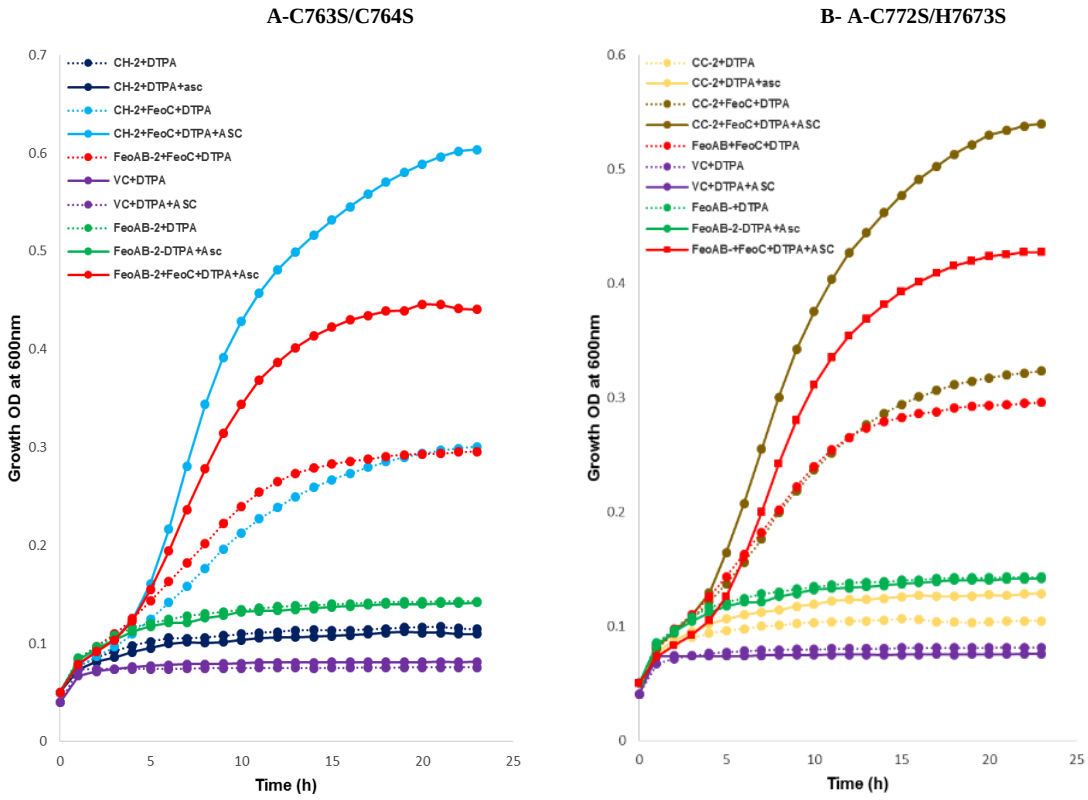

Figure 9.19: Impact of mutations in the C-terminal sub-domain of FeoB on growth of *E. coli* JC32 in M9 medium, under aerobic conditions with 2 mM ascorbate and/or 0.5 µM DTPA (II). All details as in Fig. 9.18; this represents a repeat experiment showing effects of the *feoAB* complementations more clearly.

In summary, the results with the C763S/C764S and C772S/H763G *feoB* mutations indicate that this domain causes a reduction in Feo activity that is clearly observed in the presence of FeoC aerobically (without DTPA or with DTPA is ascorbate is also present), and in the presence or absence of FeoC anaerobically. The lack of any apparent dependence on FeoC for this phenotype anaerobically correlates well with the generally-observed lack of function for FeoC anaerobically. The results do not thus support a purpose for the C-terminal subdomain in mediation of FeoC function, since FeoC still enables the mutant forms of FeoAB to provide a major low-iron growth advantage under aerobic conditions (particularly with ascorbate).

9.7. Western blot analysis of the effect of the FeoB C-terminal sub-domain mutations on FeoB levels

The above results indicate that mutation of the FeoB C-terminal sub-domain increases Feo activity. There is a possibility that this effect is caused by an increase in FeoB cellular levels, particularly as data in Chapter 8 showed that FeoB levels are subject to substantial post-transcriptional control. To test this possibility, the impact of the C763S/C764S and C772S/H773G *feoB* mutations on cellular levels of FeoB was investigated using a *feoAB*-Flag fusion carrying the mutations of interest. JC32 transformants were grown as above in 0.4% glucose M9 medium at pH 6 containing 0.5 μM DTPA (as indicated), with/without 2 mM ascorbic acid, aerobically or anaerobically.

Anti-Flag western blotting showed that there was a generally consistent, but somewhat variable, increase in FeoB levels caused by the mutations (Fig. 9.20 & 9.21) under the conditions tested. This effect was most apparent under:

aerobic conditions with ascorbate in absence of FeoC (~5- and 2.5-fold, respectively; Fig. 9.20 & 9.21);

under aerobic conditions without ascorbate/DTPA in presence of FeoC (~1.5-fold effect; Fig. 9.20); and under anaerobic conditions with FeoC (1.5-fold effect; Fig. 9.22).

The latter two effects are consistent with the findings above concerning the effect of the sub-domain mutations on Feo activity under the corresponding growth conditions. Thus, the enhanced Feo activity caused by the C763S/C764S and C772S/H773G mutations might be the result of increased FeoB stability.

However, the data presented below are only preliminary since no repeats were performed to confirm observations made, and only one time point was considered. So, further experiments are required to provide more convincing evidence of an effect on FeoB levels that correlates

well with the associated increases in activity. Note that the effects of ascorbate, O_2 and *feoC* status on FeoB levels, as observed in Chapter 8, are reiterated in the blots below for both the mutated and non-mutated versions of FeoB which further indicates that the mutations have no dramatic impact on Feo function.

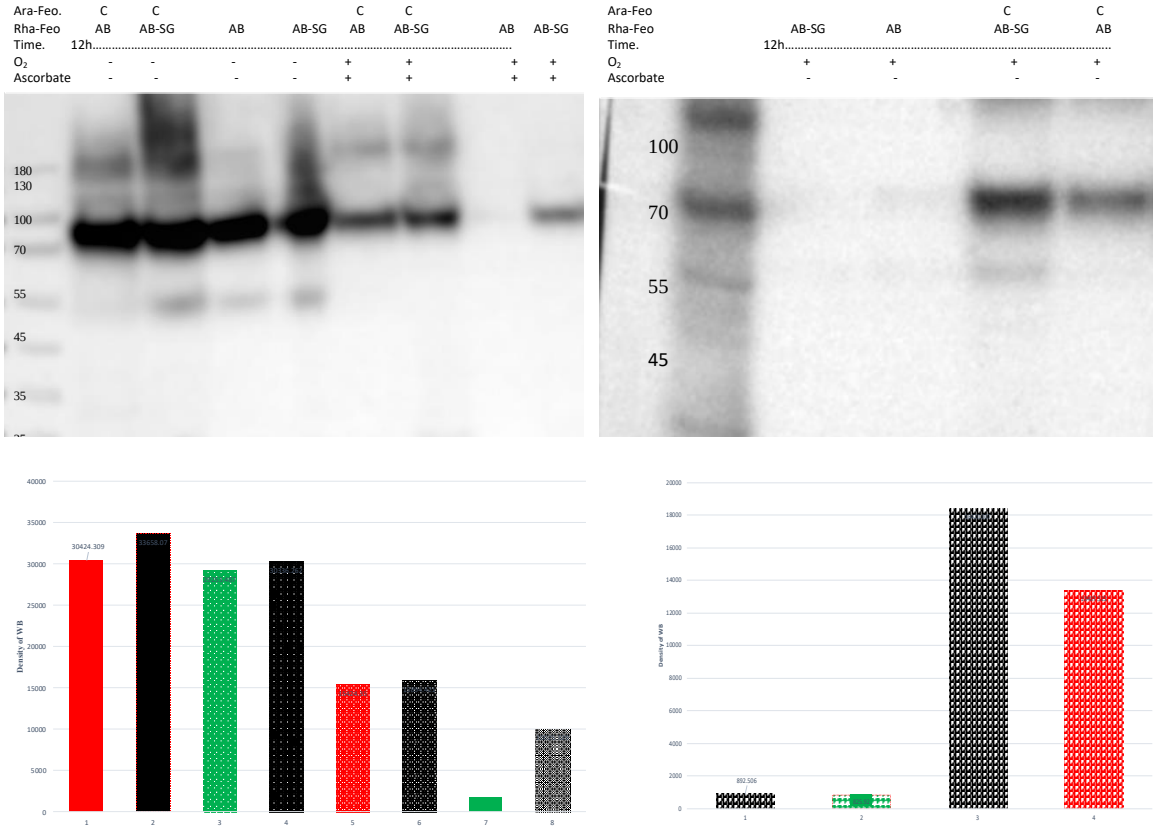

Figure 9.20: Western blot analysis of the effect of Cys763S/Cys764S mutation of FeoB on FeoB-Flag levels. Strain was JC32 with pBADrha-*feoAB*-Flag together with pBADara-*feoC* or pBADara. Growth was in M9 medium, aerobically with/without 2 mM ascorbate, or anaerobically with 0.5 µM DTPA.

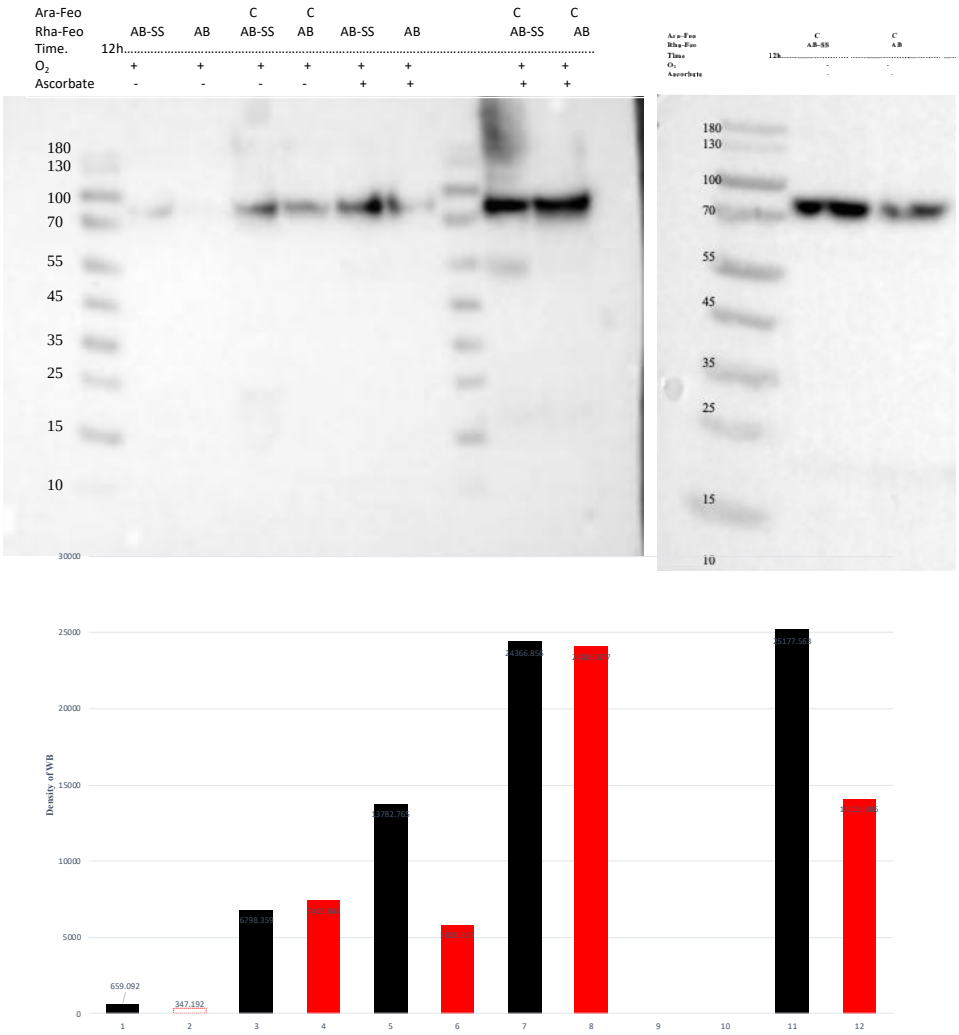

Figure 9.21: Western blot analysis of the effect of C772S/H773G mutation of FeoB on FeoB-Flag levels. Details are as for the above Fig. except for use on the C772S/H773G mutant**.**

9.8. Discussion

9.8.1 Summary

To further understand the mechanisms involved in Feo function and anaerobic iron uptake by bacteria, the major component (FeoB) of the Feo system of *E. coli* was subjected to a site-directed mutagenesis investigation of the role of conserved residues anticipated to be of importance. Four (C403, 432 & 677, and E582) of the five substitutions in the 'Gate motif' region of the permease domain resulted in a major FeoB defect that was exhibited by a failure of the mutated Feo system to support low-iron growth of the JC32 strain. This illustrates the essential nature of these residues in FeoB function. The introduction of a stop codon in place of E687 also resulted in complete apparent loss of Feo activity: this is as expected since the stop codon would cause formation of a truncated FeoB polypeptide lacking the Glu^{687} C-terminal residues, which include a portion of the predicted membrane-integral region expected to be required for transport activity. In contrast, the E488 *feoB* mutation had only a mild impact on Feo function indicating that this conserved residue does not have an essential role in FeoB activity.

In addition to the Gate motif mutations, three conserved Cys residues and one conserved His residue in the C-terminal sub-domain (restricted to γ-Proteobacteria) were also mutated, to generate two double mutations: C763/C764 and C772/H773. These double mutations caused a similar enhancement of Feo-dependent low-iron growth, suggesting that the sub-domain inhibits Feo function. Preliminary FeoB-Flag western blot analysis indicated that the C763/C764 and C772/H773 mutations caused a general, although inconsistent, increase in FeoB levels, which might explain the raised Feo activity as indicated by the iron-limited growth studies. The role of this sub-domain remains unclear, although it appears not to be required for

FeoC function. It is suggested that the impact of deletion of this sub-domain should be tested in future work, or mutation of all four of the residues targeted here in combination.

The impact of the site-directed mutations is summarised in the graph below (Fig. 9.22).

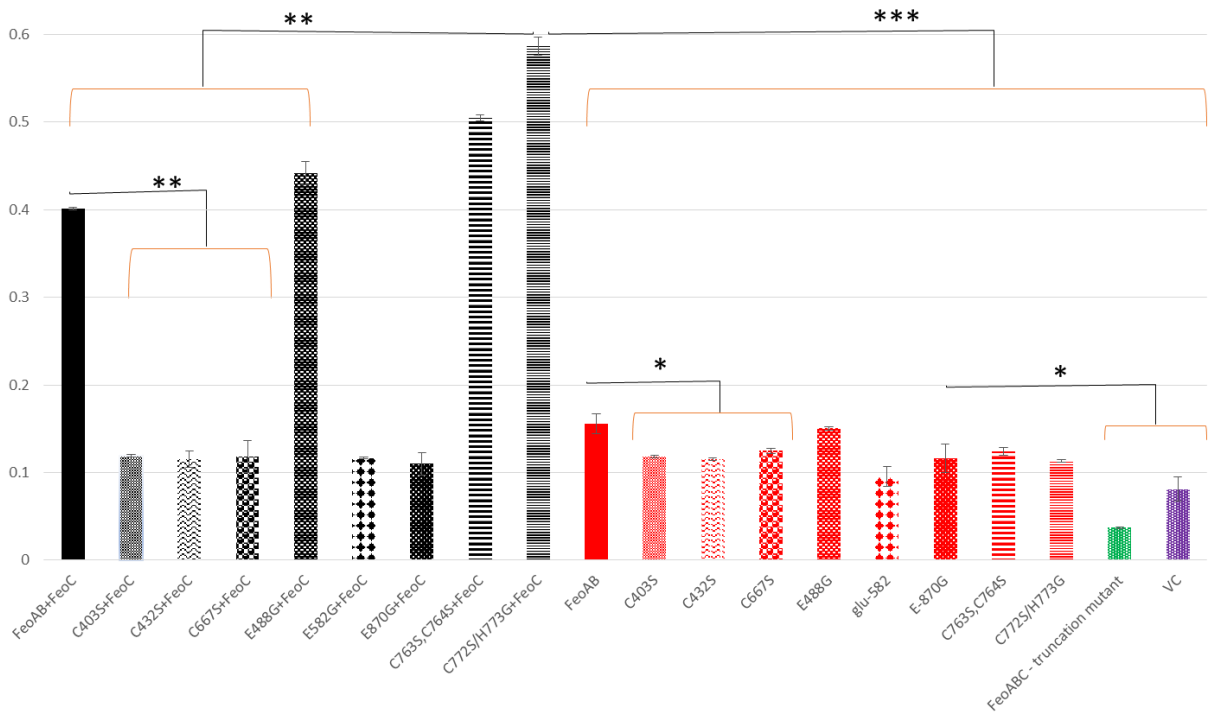

Figure 9.22: Summary of the impact of the site-directed mutations of *feoB* on aerobic growth of *E. coli* JC32 in M9 minimal medium supplemented with DTPA and ascorbic acid at 24 h. ANOVAs with Dunnett analysis were carried out on the data and ($p<0.001$)'***' ,($p<0.01$) **, $p<0.05$*where the mutations cause a significant different to growth.

9.8.2. The potential role of the conserved residues

As discussed above, the roles of Cys^{432} and Cys^{677} have previously been investigated in *P. aeruginosa* (Seyedmohammad *et al.*, 2016). These residues are predicted to occupy identical positions in Gate motifs 1 and 2, respectively (Cartron *et al.*, 2006), and thus were anticipated to possess important roles in FeoB iron uptake, potentially acting as direct Fe^{2+} ligands. Mutation of Cys^{677} reduced the 1.3-fold enhancement of GTPase activity observed in response

to 1.5 mM Fe^{2+} (but there was no effect in the absence of iron), and this residue was proposed to act as a Fe^{2+} sensor; whilst Cys^{432} had no effect on GTP hydrolysis and it was considered that it may associate with Fe^{2+} during transport (Seyedmohammad *et al*., 2016). Note that Seyedmohammad *et al*. (2016) did not consider iron uptake activity, only GTP consumption using FeoB solubilised in detergent and then incorporated into proteoliposomes. Thus, the results obtained might not be entirely reflective of the *in vivo* functions of these residues, as the procedures used to isolate FeoB may have influenced GTPase activity (Smith *et al*., 2018). Further, Fe^{2+} caused only a modest (1.3-fold) stimulation of GTPase activity, and it is unclear whether this stimulation would correlate with uptake activity and whether other cations would give a similar response; this point is particularly relevant given the extremely high iron levels used. As shown here, the absence of FeoA would be a major confounding factor for the work of Seyedmohammad *et al*. (2016) such that the results obtained are highly unlikely to be reflective of the normal functional FeoB state.

The results presented here represent the first evidence that Cys^{432} and Cys^{677} are absolutely required for iron-uptake activity, and the dramatic impact of alteration of these residues on Feo function *in vivo* is in stark contrast to the lack of (or low) impact seen by Seyedmohammad *et al*. (2016).

Others have also performed functional studies on purified whole-FeoB protein. Hagelueken *et al.* (2015) purified *E. coli* FeoB in detergent and found that the protein formed either a trimer or tetramer (the N-terminal domain also forms a trimer state; 3HYT), but they did not investigate the activity of the purified protein. Seyedmohammad *et al*. (2014) purified FeoB from *P. aeruginosa* and incorporated the protein into proteoliposomes. They were able to detect low rates of GTPase activity levels similar to those reported for the isolated N-terminal domain, suggesting that the low GTPase activity of the isolated N-terminal domain is not caused by its

separation from the C-terminal domain. Smith and Sestok (2018) also purified FeoB (from *K. pneumoniae*) and, in contrast to previous work, found that upon reconstitution FeoB provided high GTPase activity (despite the lack of FeoA). These findings highlight some of the issues associated with understanding of FeoB function using the purified protein in an unnatural context.

Ovchinnikov *et al.* (2017) have also predicted a model for the FeoB C-terminal domain of *E. coli*, although this was part of a metagenomics structural prediction project and the validity of the model is yet to be established. However, a bacterial nucleoside transporter was used as the template (as above; Fig. 9.5) and the resulting model thus resembles that presented here. These models can be used to indicate the potential roles of the residues targeted here. Four of the five Gate residues mutated here are predicted to be closely located within the core of the protein within the membrane. They line the predicted channel and thus could directly associate with ferrous iron during uptake (Fig. 9.23).

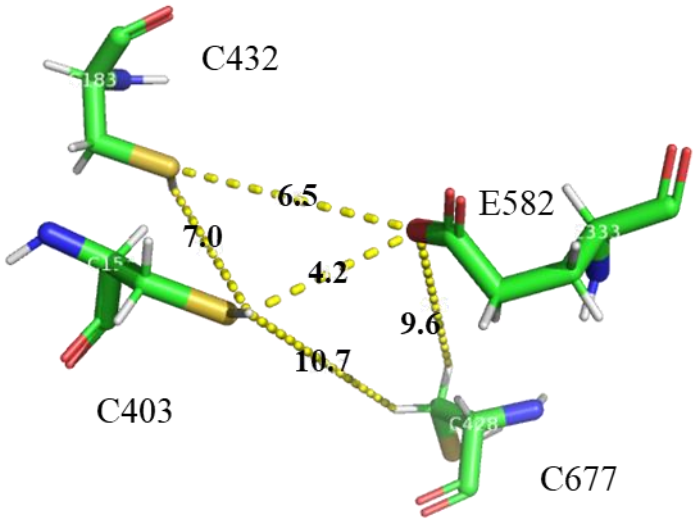

Figure 9.23. Model of FeoB showing juxtapositions of four conserved residues subject to mutation in this chapter, that line the predicted pore region and form a potential Fe^{2+}-binding site. Model obtained from Ovchinnikov *et al.* (2017) and image generated in PyMol. Distances (Å) between atoms is indicated by yellow dashed lined. Atoms are colour coded: H, white; C, yellow; O, red; N, blue, C, green.

The essential C432 and C677 residues are both included, along with C403 (also essential) and E582 (also found to be essential for Feo activity). E582 was altered to a Q residue, which is a conservative change that could allow partial function. However, no partial function was observed which further emphasises the critical nature of this residue.

The observation that all three conserved Cys residues targeted are essential supports the proposal that these residues could be subject to H_2O_2 oxidation during aerobic growth (in absence of reductant) which could then cause the observed inactivation of FeoB iron-uptake capacity. Indeed, although all three Cys residues are within the membrane-embedded part of the FeoB N-terminal domain, the model suggests that they would be exposed to the central transport channel and thus potentially accessible to H_2O_2. Future work should involve recovery of FeoB-Flag by immunoprecipitation following exposure to membrane-non-permeable Cys-specific labelling compounds (e.g. a maleimide compound), before and after peroxide treatment, to determine whether these residues are indeed subject to oxidation, using an MS approach.

Thus, the experiments here are consistent with the notion that the thiol groups of these three Cys residues might become oxidised to sulfonic acid (and further oxidation products) when cells are incubated aerobically, in such a way that Fe^{2+} transport would be shut down by preventing binding of the Cys residues with iron. This 'biochemical switch' would enable the cell to respond rapidly to exposure to oxygen by preventing intracellular accumulation of Fe^{2+}, which promotes formation of damaging radical species under oxidative conditions. If this were the case, then it would be expected that a mechanism of 're-setting' the switch by reduction of the oxidised sulfonic acid groups would be required (Poole, 2015). It is unclear how this could be achieved for an inner-membrane protein and whether the cytoplasmic glutaredoxin/thioredoxin or periplasmic Dsb pathways might contribute to FeoB resistance to

Cys oxidation. However, there is a possibility that FeoC may contribute to this given its ability to support Feo activity aerobically and its 4Fe-4S cluster which could provide a ferredoxin-like function.

What remains unclear, however, is how the exposure to O_2 (H_2O_2) causes the observed post-transcription reduction in FeoB protein levels. The western blotting experiments should be repeated with catalase and peroxide, to confirm that H_2O_2 is the cause of this effect. In addition, a range of alkylhydroperoxides should be tested to determine if larger peroxides can mediate the same effect as H_2O_2 or whether they might be excluded from the proposed FeoB transport channel.

Glu^{488} was shown to play a role in enhancing Feo activity but is not essential for function. This residue is located in an intracellular loop between the Gate motifs and lies at the bottom of the helical bundle formed by the FeoB N-terminal domain, at a distance from the channel exit. Alteration of this residue should be repeated with a less conservative change to determine whether a stronger phenotype might be achieved. Given its cytoplasmic location, it could interact with the N-terminal G-protein domain and thus affect coupling of GTPase activity to iron uptake.

A role for this residue in promoting interaction of FeoB and FeoC is unlikely on the basis that FeoC appeared to increase the activity of the E488G-FeoB in M9 medium containing DTPA and ascorbic acid. Moreover, Glu^{488} is conserved in FeoB derived from a broad range of species and would therefore be expected to play a critical role in bacteria from outside the γ-Proteobacteria lineage. Such bacteria do not include FeoC (Lau *et al*., 2016).

Chapter 10: Exploring the role of FtsH in degradation of FeoB during aerobiosis

10.1 Introduction

10.1.1 FtsH

In all living organisms, peptidases are essential for sustaining life under ever-changing conditions. Therefore, microbes possess a basic set of shared peptidases that fulfil housekeeping functions. For *E. coli* for instance, there are several types of ATP-dependent proteases such as ClpAP, ClpXP, HslUV, Lon and FtsH. The latter is exclusive amongst the ATP-dependent proteases not only because it is essential for cell survival but also because it is the only one that is membrane-embedded (Tomoyasu *et al*., 1992). The *E. coli* FtsH protein includes a carboxy-terminal cytoplasmic domain that is homologous in all members of the AAA ATPase family (Kunau *et al*., 1993; Confalonieri and Duguet, 1995). The FtsH proteases are thus membrane-integrated ATP-dependent metalloproteases. They are members of the 'triple A' (AAA) family of proteins, which in turn consists of a distinct group within the Walker-type superfamily of ATP/GTPases (Walker *et al*., 1982; Kunau *et al*., 1993). The most distinguishable feature of the AAA family of proteins is the existence of one or two copies of a conserved sequence of 220-250 amino acids, commonly known as the 'AAA cassette' (Kunau *et al*., 1993), located towards the carboxyl terminus of the protein. FtsH is the only ATP-dependent protease of *E. coli* that is considered crucial for cell viability (Chin *et al*., 1993). The amino-terminal region of FtsH flanks a periplasmic domain of 72 amino acids and two segments of transmembrane, while the central region has sequence homology to the AAA family of ATPase; this is followed by the carboxyl-terminal region which has a Zn^{2+}-metalloprotease motif (HEXXH) and is cytoplasmically located (Clary *et al*., 1990).

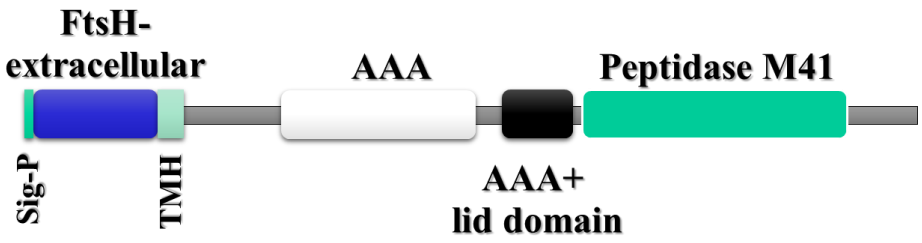

Figure 10.1: Domain organisation of FtsH of *E. coli.* Total length is 644 amino acids. Redrawn from Pfam.

FtsH is required for processive degradation (from either terminus) of both membrane and cytoplasmic proteins into small peptides (of 6-25 amino acids). It degrades membrane proteins that are misfolded, and is thus thought to have a role in quality control of membrane-embedded proteins. Mutation causes a 'filamentous temperature-sensitive' phenotype, raised lysogenisation with lambda bacteriophage and increased tolerance to colicin (Narberhaus *et al*., 2009; Langklotza *et al*., 2012)

FtsH enzymes are ubiquitous in bacteria and Eukarya, but unlike other AAA protease are not found in Archaea (Tomoyasu *et al*., 1993; Swaffield & Puruggan 1997; Langer, 2000). Their high sequence conservation and almost universal distribution is suggestive of an essential function, a hypothesis that is supported by the strong phenotypes associated with *ftsH* mutants in various organisms (Tomoyasu *et al*., 1993; Tomoyasu *et al*., 1995; Deuerling *et al*., 1997; Komenda *et al*., 2006; Mann *et al*., 2000). They are capable of digesting both transmembrane and periplasmic segments of a substrate protein, and they can combine chaperone like activities with proteolytic function. FtsH is usually activated by the Zn^{2+}, although there is *in vivo* experimental evidence for functional association of *E. coli* FtsH with Fe^{2+}, Ni^{2+}, Mn^{2+} and Co^{2+} ions (Herman *et al*., 1995).

The *ftsH* gene was discovered through three different phenotypes (Narberhaus *et al*., 2009); *tolZ* - for colicin tolerance; *hlfB* – mutants showing a high frequency of lysogenization when

infected with phage lambda; and *ftsH* - for filamentous temperature sensitive. FtsH proteases, like other ATP dependent enzymes, exist in wild type cells of *E. coli* as multimeric complexes forming hexameric ring-like structures with the catalytic sites of their subunits buried within the central cavity (Shotland *et al*., 1997; Krzywda *et al*., 2002; Niwa *et al*., 2002). Even though every subunit appears to be in the same conformational state within the hexameric ring structure, the mode of ATP hydrolysis, either synchronised or sequential is not yet clear (Niwa *et al*., 2002). Nevertheless, it is assumed that the active sites subunits are self-compartmentalized, and thus excluded from the cytoplasmic environment.

The mechanism that allows the FtsH proteases to digest both transmembrane and periplasmic regions of a substrate protein is not fully understood. It is not clear, how the hydrophobic, membrane-spanning domains of the substrate protein are subjected to proteolysis, since the hydrolysis requires availability of water. Two working models for the destruction of membrane proteins by FtsH have been suggested; the shedding model and pulling model. The first requires the presence of two FtsH complexes from both sides of the membrane. The two FtsH proteases cleave off the exposed loops or domains of the substrate protein from either side of the membrane, thereby destabilising the hydrophobic part of the protein and making it accessible for further proteolytic degradation from the membrane surface (Leonhard *et al*., 1996; Langer, 2000). In the pulling model, ATP hydrolysis promotes an active extraction of membrane embedded parts of the substrate protein and its translocation into a hydrophobic environment of the protease (Langer, 2000), followed by its degradation into small fragments. The proteolytic mechanism mediated by FtsH proteases is elaborate and seems to be regulated by many factors. In *E. coli*, hetero-oligomeric complexes composed of FtsH proteins and two homologous polypeptides HflK and HflC have been identified on the periplasmic site of the plasma membrane. Mutational studies on *hflK* and *hflC* genes have demonstrated that these two proteins modulate the proteolytic activity of FtsH (Kihara *et al*., 1996; 1997; 1998).

10.1.2 Is there a relation between FtsH and Feo?

The role of the small iron-sulphur protein, FeoC, is still unclear (as this study has demonstrated) but FeoC supports Feo-mediated ferrous uptake in *E. coli* experiencing high oxygen levels under low-iron regime with reductant. Previous work in *Salmonella enterica,* indicated that FeoB is subject to rapid degradation aerobically, and that anaerobically the FeoC protein binds directly to the FeoB transporter protecting it from degradation leading to increased cellular levels of FeoB anaerobically (Kim *et al*., 2013). In an *ftsH* mutant, lack of FtsH permitted high levels of FeoB in the absence of any protection by FeoC (Kim *et al*., 2013); it was proposed that the FeoC protein defends the FeoB protein from FtsH-mediated proteolysis.

The research reported in the previous chapters shows that FeoB is indeed subject to major post-transcriptional control in response to O_2. However, this appears to be little influenced by FeoC. FeoC enhances Feo activity in the presence of O_2 (particularly with ascorbate), but this effect seems to be largely independent of change in FeoB level. To further explore the model proposed by Kim *et al*. (2013) for FeoB control by O_2 and FeoC, the impact of *ftsH* status on Feo activity and FeoB stability is here explored using the *feo* constructs created previously.

10.2. *ftsH* gene knockout in JC32

10.2.1. Confirmation of the ftsH mutation

The *ftsH* mutation required for this study had previously been generated in *E. coli* as a Δ*ftsH*::*kan* substitution mutation (Akiyama *et al*., 1998). This mutation was to be transferred from strain AR3289 by P1 transduction into JC32 (Miller, 1992; section 2.28).

Table 10.1 Primers designed for confirmation of the *ftsH* gene mutation and loss of Kan^R cassette.

Name of primer	Sequence
FWD-FtsH	ACCGGGAGATTTCAGACGAAAGTT
Rev-FtsH	CCAGGGATAACATCATGAAA
FWD-Kan	TATAAATGGGCTCGCGATAATGTCG
Rev-Kan	TCGGGCTTCCCATACAATCGATAGATT
FWD-Del	ATGGATGGCTTCGAAGGTAACGAA
Rev-Del	TTGTGGTCGGCTTGCCAGATGTTC

A

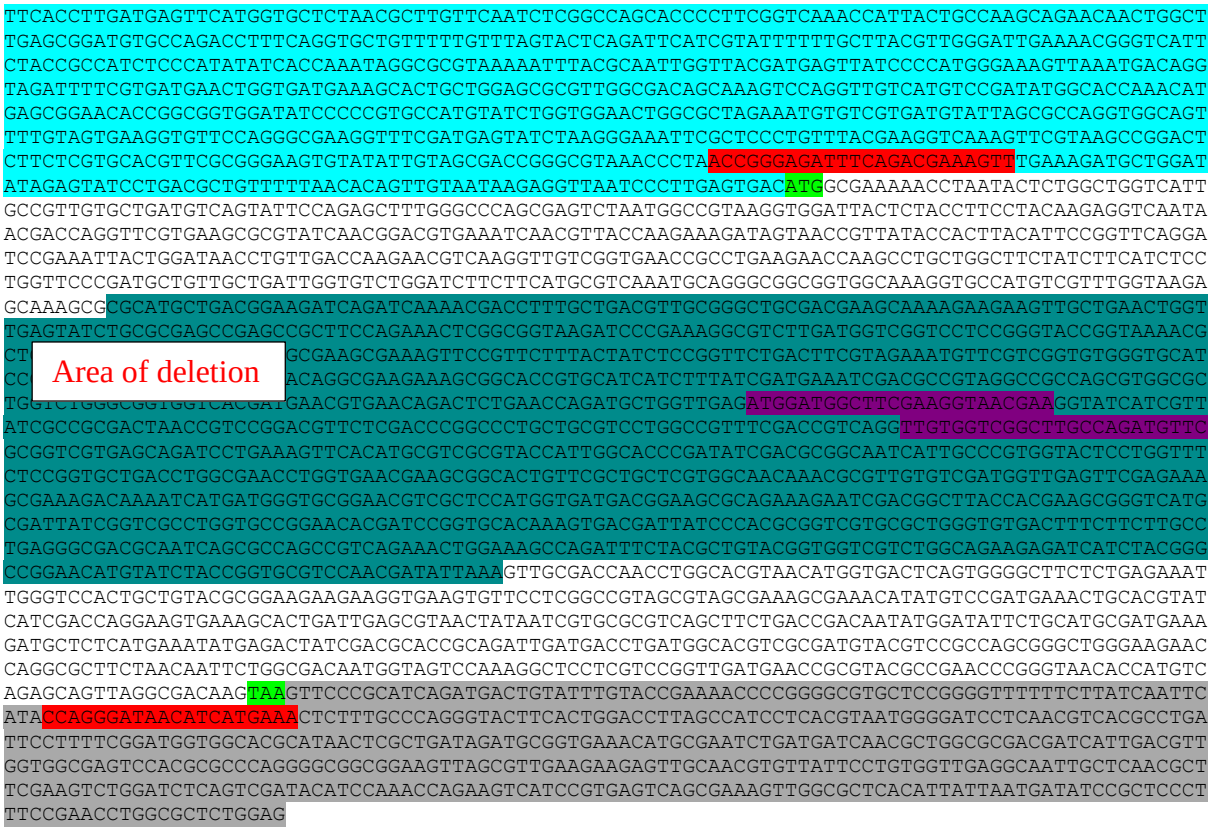

B

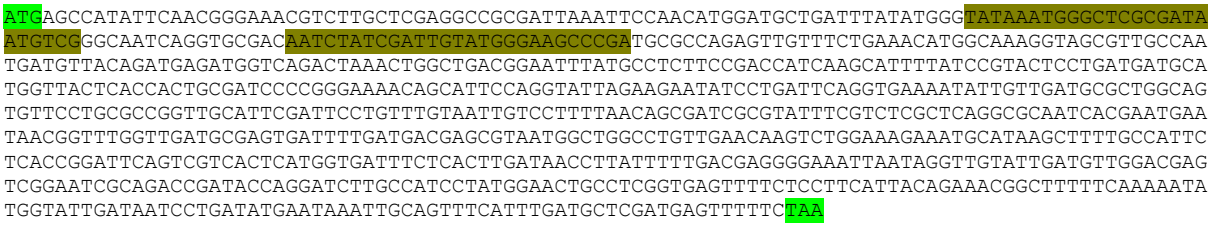

Fig. 10.2. A. Nucleotide sequence of the *ftsH* region of the *E. coli* genome, deleted region and binding sites for confirmatory PCR primers. B. Nucleotide sequence of Kan^R cassette (815 bp). Red, primer sites used to amplify *ftsH* region; purple, primer sites lost in *ftsH* mutant; olive-green, primer sites for confirmation of Kan^R cassette; green, start and stop codons for *ftsH* or *kan*.

FWD-FtsH and Rev-FtsH primers (Tables 2.7 & 10.1) were used to amplify a ~1.9 kb *ftsH* or Δ*ftsH* fragment from the *E. coli* AR3289, AR3291 (a kind gift from Dr. Teru Ogura, University of Kumadai, Japan) and JC32 strains with High Fidelity Phusion® DNA polymerase (Hot start; Thermo Fisher Scientific). The amplified fragment was of the expected size in wildtype and

JC32 (~1900 bp), but for the *ftsH* mutant the expected fragment size was also 1.9 kb, since the region deleted is the same approximate size as the Kan^R cassette inserted (Fig 10.3).

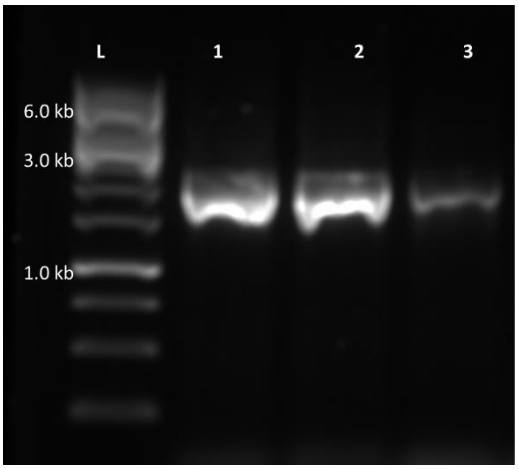

Figure 10.3. Electrophoretic analysis of *ftsH*-amplification products of Δ*ftsH*::*kan* mutants. Strains were: 1, AR3291 (Δ*ftsH*::*kan*); 2, AR3289 (wildtype); 3, JC32 recipient. L, I Kb ladder. Primers used FWD-FtsH and Rev-FtsH. L, Ladder; 1, ~1900 bp,2, ~1900 bp, 3, , all these band shown same size, to confirm the deletion *ftsH* send the PCR product to sequence.

To further test the *ftsH* mutant strain, primers amplifying the Kan^R cassette and *ftsH* flanking regions were used in PCR reactions (Table 10.1; Fig. 10.2). For each reaction, one primer was designed to anneal inside the Kan^R cassette and another within the *ftsH* flanking region. The expected amplification product sizes were 1.4 and 0.9 kb for AR3291 (Δ*ftsH*::*kan*), but no band was expected in the wildtype AR3289 or JC32 recipient strain. Figure 10.4 shows that the expected PCR products were generated for the mutant strain but there was no band the recipient (and none in the wildtype, not shown).

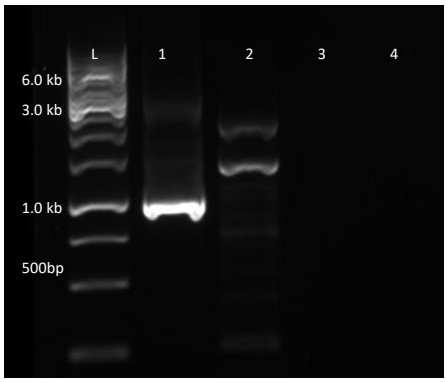

Figure 10.4 Electrophoretic analysis of *ftsH*-amplification products of Δ*ftsH*:: *kan* mutant (AR3291) with FWD-ftsH and Rev-Kan and FWD-Kan and Rev-ftsH. L, I kb ladder; 1 & 2 donor strain AR3291 (Δ*ftsH*::*kan*); Lane 3 & 4, JC32 receipent strain. FWD-FtsH and Rev-Kan (2 and 4, 1.4 kb expected); REV-FtsH & FWD-Kan (1 and 3, 0.9 kb expected).

10.2.2 P1 transduction of the *ftsH* mutation into *E. coli* JC32

Transduction is the transfer of genetic material from a donor cell to a recipient cell via a bacteriophage vector. Some phages, such as P1, have the capacity to transfer any kind of gene from a donor to a recipient strain. Such mobilised DNA can be stably incorporated into the recipients chromosome by homologous recombination to generate a recombinant genotype. The methodology employed for transduction is indicated in the Methods (Section 2.28).

P1 transduction was used to attempt to transfer the mutations of interest from *E. coli* AR3291 (W3110 Δ*ftsH*::*kan)* into *E. coli* JC32 (W3110, Δ*fecABCDE*, Δ*zupT*, Δ*mntH*, Δ*entC*, Δ*feoABC* Δ*efeU*,). P1 phage lysate from AR3291 was used to produce Kn^R JC32 transductant. These were confirmed for their Δ*ftsH*::*kan* status by colony PCR. The amplification product sizes for the transductants were the same as for the donor when using the *ftsH* specific primers (not shown). The Δ*ftsH*::*kan* status of the transductants was confirmed (Fig. 10.5 & 10.6) by colony PCR using primers amplifying the region between the deleted *ftsH* gene and the inserted Kn^R cassette. The PCR gave the expected band sizes whereas no PCR products were obtained in the wildtype or recipient. This confirmed the identity of the transductants.

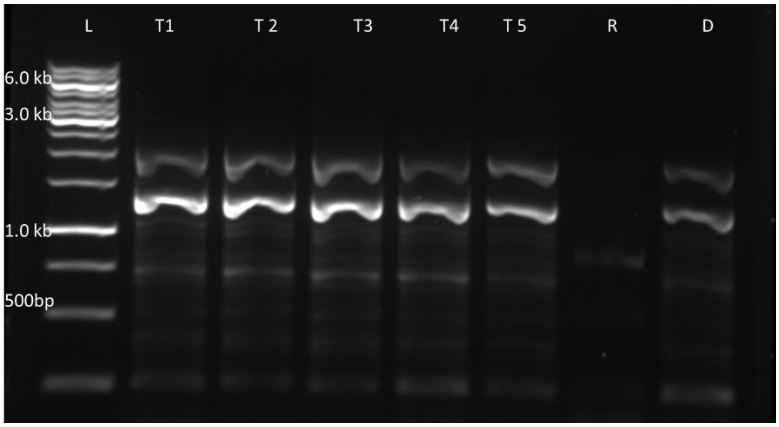

Figure 10.5. Electrophoretic analysis of *ftsH*-amplification products of potential Δ*ftsH*::*kan* transductants using *ftsH*- and *kan*-specific primers. Ladder I Kb; Lane 5 ,6, 7, 8 & 10 - Kn^R transductants (T1, T2, T3, T4 and T5*)*; lane R, receipeint; Lane D, donor AR3291 (Δ*ftsH*:: *kan*). Expected band size was 1.4 kB. Rev-FtsH and Fwd-Kan primers were used.

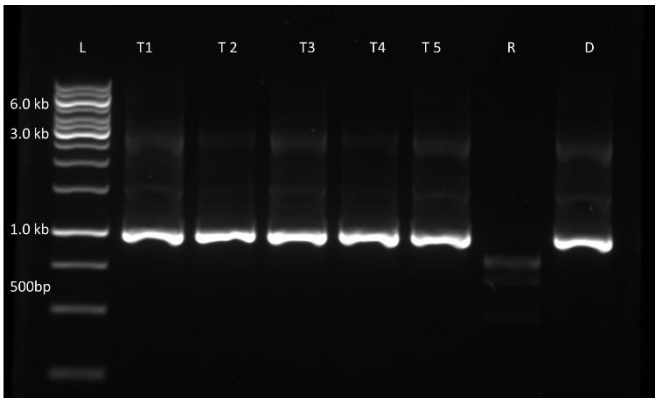

Figure 10.6. Electrophoretic analysis of *ftsH*-amplification products of potential Δ*ftsH*::*kan* transductants using *kan*- and *ftsH*-specific primers. Ladder I Kb; Lane 5 ,6, 7, 8 & 10 - Kn^R transductants (T1, T2, T3, T4 and T5*)*; lane R, receipeint; Lane D, donor AR3291 (Δ*ftsH*:: *kan*). Expected band size was 0.9 kB. FWD-FtsH and Rev-Kan primers were used.

Genomic DNA was isolated from one candidate transductant (T1) and the *ftsH* deletion status reconfirmed by PCR, as above (Fig. 10.7).

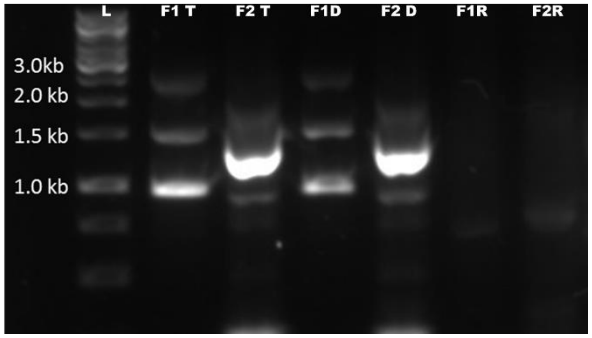

Figure 10.7. Electrophoretic analysis of *ftsH*-amplification products of a candidate Δ*ftsH*::*kan* transductant using *kan*- and *ftsH*-specific primers. T, transductant; D, donor; R, recepient. F1, ~900 bp PCR product with FWD-ftsH and Rev-Kan; F2 ~1400 bp PCR product with *FWD-Kan and Rev-ftsH*. Ladder I Kb. Chromosomal DNA was used as template.

To confirm that the transductant was indeed derived from the recipient, and had not arisen due to contamination with the donor strain, the mutations carried by the JC32 recipient were confirmed in the transductant by PCR. Primers for all mutant genes in JC32 (Table 2.7) were employed in PCR reactions. These were analysed by electrophoresis and PCR products were of the expected sizes and were a match in the two strains, except for *ftsH*, as expected (Fig. 10.8), confirming the identity of the transductant.

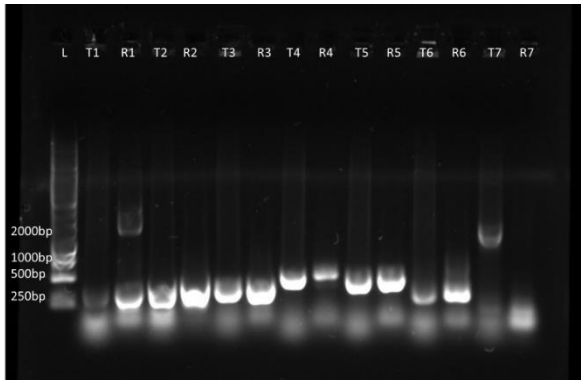

Figure 10.8. Electrophoretic analysis of PCR products for mutated loci in JC32 and JC32Δ*ftsH*. This figure demonstrates that all genes was deleted from strain JC32. Strains: T, transductant; R, recipient. PCR products: 1, Δ*zupT*; 2, Δ*entC*; 3, Δ*efeU*; 4, Δ*fec*; 5, Δ*feo*; 6, Δ*mntH*; 7, Δ*ftsH* (1.4 kb product). L, Ladder.

10.3 Scanning electron microscope (SEM) analysis of the *ftsH* mutant

SEM (see Methods 2.41) was used to show that the *ftsH* mutation caused an altered the cell morphology (size/shape). *E. coli* W3110, *E. coli* AR3291 (Δ*ftsH*; donor strain), *E. coli* JC32 (recipient strain) and JC32Δ*ftsH* (transductant strain) were compared, following overnight growth in M9 medium. Figs 10.9 & 10.10 below show the different SEM morphological features of the *ftsH* mutant as compared to the wildtype control. Controls, *E. coli* W3110 and *E. coli* JC32 (Figs 10.9/10A) in each figure showed the rod shaped morphology typical of *E. coli*. However, the donor strain (*E. coli* AR3291) and transductant strain (*E. coli* JC32Δ*ftsH*) show filamentous shape (Figs 10.9/10B) demonstrating that the JC32Δ*ftsH* bacterial cells possess the expected filamentous phenotype (Zellmeier *et al*., 2002). The $ftsH^+$ strains had cell lengths of under 2 µm, but the $ftsH^-$ cells had lengths of up to 7 µm (Figs. 10.9 & 10.10).

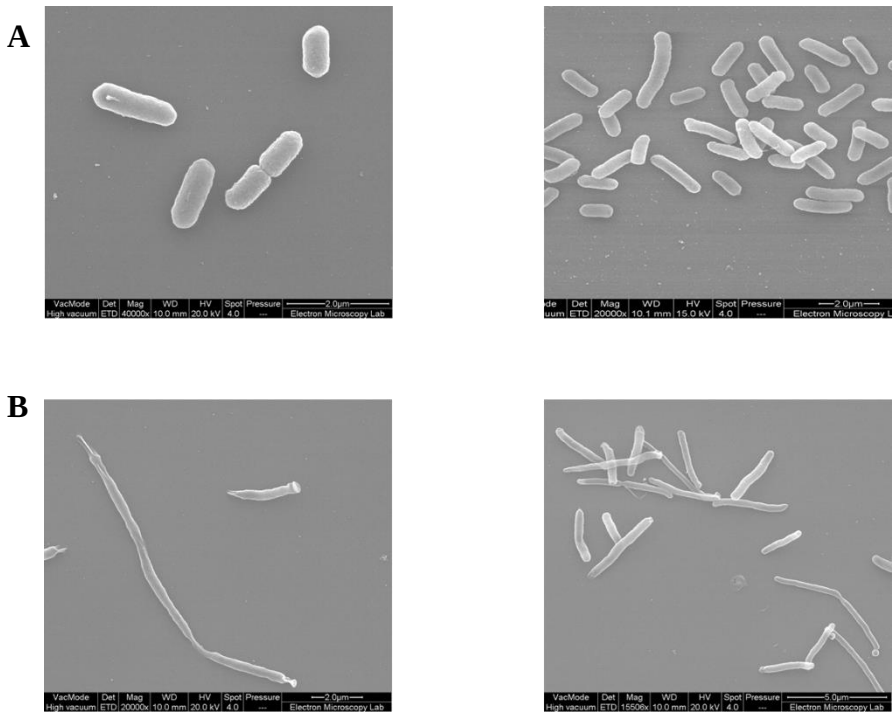

Figure 10.9. SEM image of *E. coli* A3289 (W3110) wildtype (A) and *E. coli* AR3291 (Δ*ftsH*) (B).

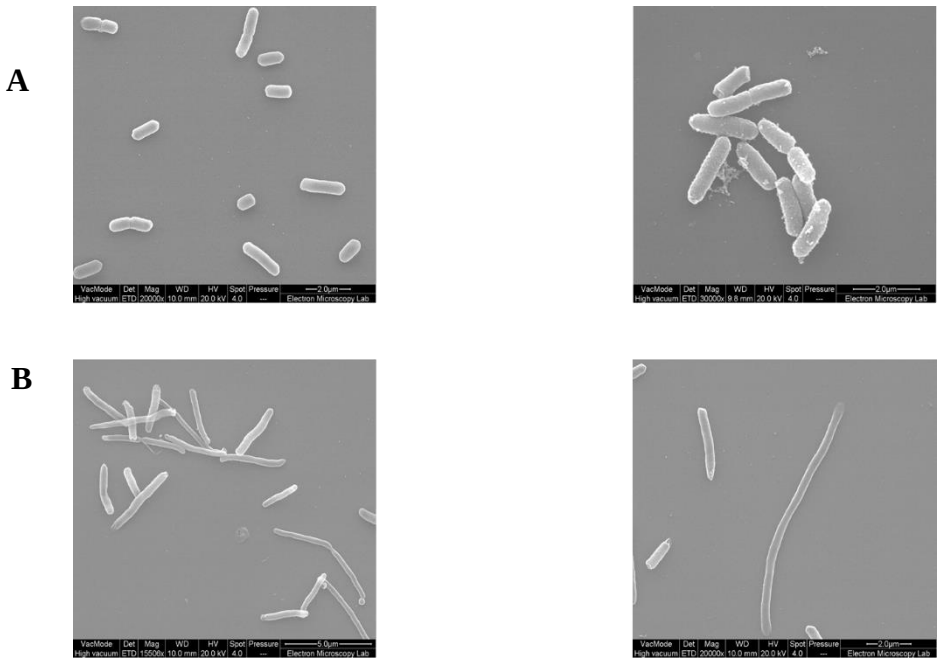

Figure 10.10. SEM image of *E. coli* JC32 (A) and *E. coli* JC32Δ*ftsH* (B).

10.4 Impact of the Δ*ftsH* mutation on Feo function

10.4.1 Introduction

Of the five AAA+ proteases in *E. coli*, only FtsH is considered important for viability (Langklotz *et al*., 2012), although mutants have been reported (Koreaki Ito and Yoshinori Akiyama, 2005), certainly used in the work reported here, indicating that the mutation of *ftsH* is not lethal. FtsH recognises membrane proteins in a sequence independent fashion by virtue of exposed N- or C-termini of ~20 or 10 (respectively) amino acid residues which are subject to progressive degradation (Chiba *et al*., 2002). Membrane proteins targeted by FtsH include subunit A of the F0 ATPase, SecY (protein secretion), FeoB (ferrous iron uptake) and YccA (a BI-1 family member of unclear function that inhibits FtsH activity) (Kihara *et al*., 1999; Uckelhoven *et al*., 2004; Kim *et al*., 2013). Cytoplasmic proteins degraded by FtsH include LpxC (lipid A biosynthesis), KdtA (WaaA; lipid A synthesis), and RpoH (heat-shock sigma factor) (Nonaka *et al*., 2006), and these appear to be recognised through internal structural

motifs. FtsH also has a function in oxidative stress regulation by degrading SoxS (the regulator that induces genes required for superoxide-stress resistance) (Griffith *et al*., 2004) and potentially through its ability to degrade the apo form (FMN-free) of flavodoxin (activity only observed in vitro) (Okuno *et al*., 2006).

After the confirmation of the identity of the transductant by colony PCR and SEM, the next step was to investigate the effect of the *ftsH* mutation on Feo function, with and without FeoC.

10.4.2 Effect of *fstH* mutation on low-iron growth of JC32 carrying *feoAB*-Flag with/without *feoC* under aerobic conditions

To investigate the effect of FtsH on Feo function, JC32 and JC32Δ*ftsH* transformants were grown aerobically in iron-limited M9 medium (Fig. 10.12 & 10.13). The results show that the vector controls for the $ftsH^+$ and $ftsH^-$ strains both grow weakly under the conditions employed, whereas the *feoAB/feoC* complemented strains grow well and similarly, indicating the strong complementation achieved by provision of FeoABC. This effect was seen using two different plasmid combinations: pBADara-*feoAB* with pBADrha-*feoC*, and pBADrha-*feoAB* with pBADara-*feoC*. However, the *feoAB*-complemented strains showed an *ftsH*-dependent growth difference (Fig. 10.12 & 10.13), with the *ftsH* mutant displaying a statistically-significant enhanced growth (30-36%) with respect to the equivalent $ftsH^+$ strain. This effect was only seen in the absence of *feoC*. This finding is consistent with the previous report of Kim *et al*. (2013) indicating that FeoC protects FeoB from degradation under aerobic conditions. No difference in growth was seen under iron sufficiency for all mutant strains (data not shown).

In summary, results show that the *ftsH* mutation, in absence of *feoC* and presence of FeoAB, produces a low-iron growth defect enhancement effect. It is probable that the enhanced iron-restricted growth of the *ftsH* mutants arises as a result of the lower degradation of FeoB. This hypothesis will be explored further below.

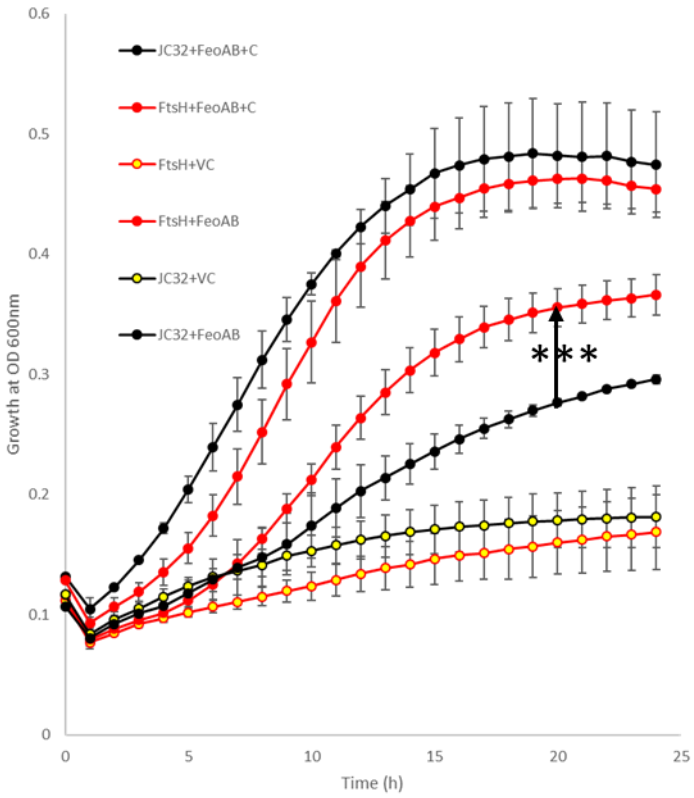

Figure 10.11: Effect of *ftsH* status on Feo activity, with and without FeoC, under aerobic iron-limited conditions. 300 µl bacterial cultures were grown aerobically with constant shaking in M9 medium with 0.4% glucose, 0.25 µM DTPA, 0.02% rhamnose and arabinose, and chloramphenicol (50 µg/ml) and ampicillin (100 µg/ml) using 100 well Bioscreen plates. The strains employed were: JC32Δ*ftsH* transformed with plasmids pBADrha or pBADrha-*feoAB*-Flag-tag, and pBADara-*feoC* or pBADara. Precultures were grown overnight in the same medium (no DTPA) with 10 µM ferric citrate, and were washed prior to use as inocula to give a starting OD of 0.01. Each growth curve is the average of three replicates and error bars indicate standard deviation. Statistically significant differences between the JC32 and JC32Δ*ftsH* strains complemented with *feoAB* is indicated (***, $p<0.001$ at 20 h).

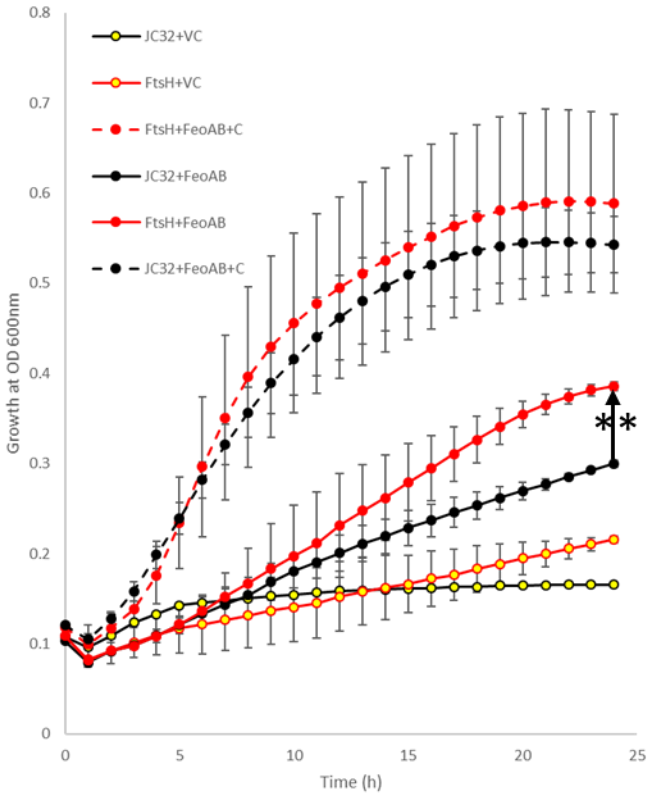

Figure 10.12: Effect of *ftsH* status on Feo activity, with and without FeoC, under aerobic iron-limited conditions. Same details Fig.10.11, but a different set of plasmids were used: pBADara-*feoAB* or pBADara, with pBADrha, or pBADrha-*feoC*. Statistical difference ($p<0.001$) at 24 h is indicated (**).

10.4.3 Effect of *fstH* mutation on low-iron growth of JC32 carrying *feoAB* with/without *feoC* under anaerobic conditions

Under anaerobic conditions (medium used was as above), the *ftsH* mutation had little impact on the low-iron growth of the *feoAB* or *feoAB/feoC* complemented strains (Fig. 10.13). The *feoAB*- and *feoABC*-complemented strains both grew well, and exhibited similar levels of growth which is consistent with findings in Chapter 7 showing that FeoC offers little advantage anaerobically. This finding is not consistent with the work of Kim et al. (2013), since they reported that lack of *feoC* results in degradation of FeoB and thus reduced Feo activity.

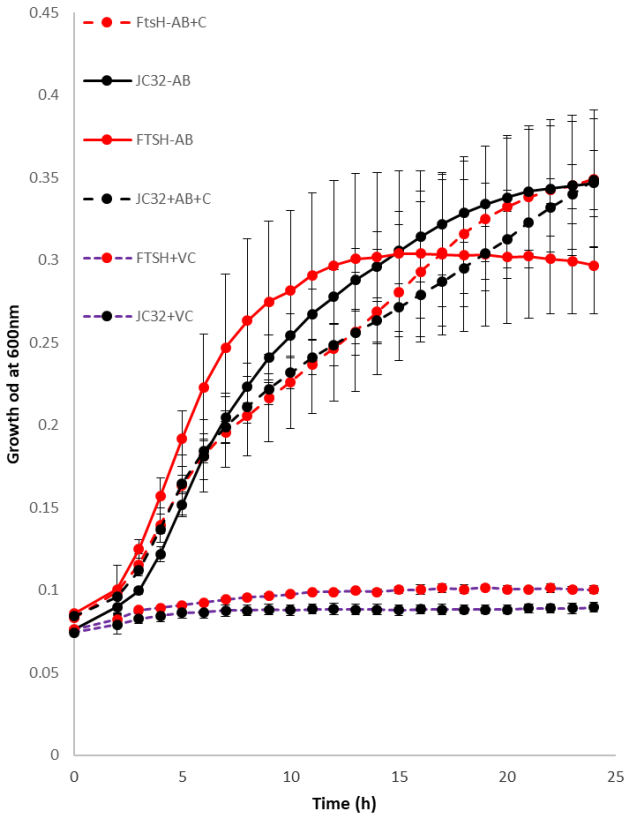

Figure 10.13. Effect of *ftsH* status on Feo activity, with and without FeoC, under microaerobic iron-limited conditions. The FLUOstar (1% O_2 15% CO_2) was used for growth and each growth curve is the average of two replicates and error bars indicate standard deviation. Strain/plasmid combinations were as in Fig. 10.11. Medium was M9 with 0.4% glucose, with antibiotics and inducers included as required. Repeated twice, with similar results obtained.

10.4.4 Effect of *fstH* mutation on low-iron growth of JC32 carrying *feoAB*-Flag with/without *feoC* under aerobic conditions with reductant

The above experiment (Section 10.4.2) was repeated with growth under aerobic conditions in the presence of ascorbate (Fig. 10.14). The results show that in the presence of ascorbate, the *ftsH* mutation does not causes a notable effect on the growth of the *feoAB*-complemented strains. However, it is noticeable that in the presence of *feoC*, ascorbate induces a weaker growth increase for the *ftsH* mutant (10%) than for the *ftsH*$^+$ strain (40%) (Fig. 10.14). This

suggests that ascorbate induces a greater enhancement of Feo activity in the presence of FtsH, than its absence, when FeoC is also present. This again is consistent with the notion that FeoC protects FeoB from FtsH degradation under oxidising conditions

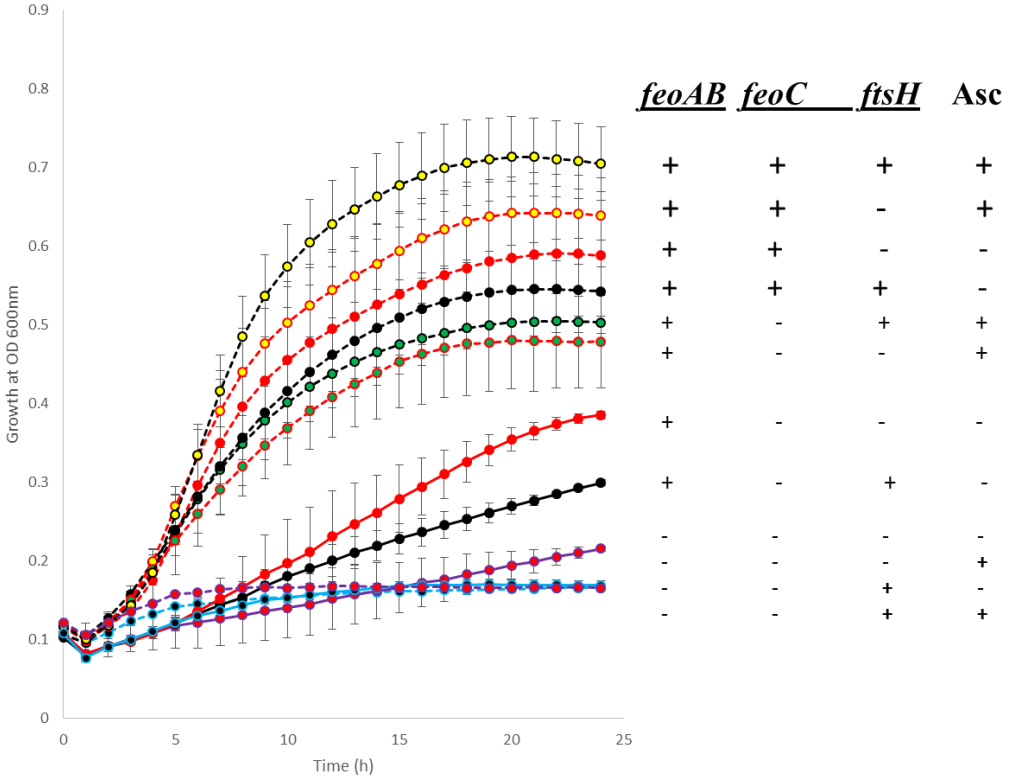

Figure 10.14 Effect of *ftsH* status on Feo activity, with and without FeoC, under aerobic iron-limited conditions, with 2 mM ascorbate. Details are as for Fig. 10.13 except for aerobic conditions and presence (as well as absence) of 2 mM ascorbate. The data in absence of ascorbate is from Fig. 10.12.

10.4.5 Effect of *ftsH* status on FeoB-Flag levels

Earlier results provided in this thesis show that FeoB levels are greatly reduced under aerobic conditions in a fashion that appears independent of transcriptional control. In addition, Kim *et al*. (2013) report that FtsH causes degradation of FeoB aerobically or in absence of *feoC*. The above experiments suggest that lack of FtsH protease modestly increases Feo activity aerobically in the absence of FeoC and ascorbate, consistent with Kim *et al*. (2013). However, the lack of FtsH had little apparent effect on Feo activity anaerobically, which is not consistent

with Kim *et al.* (2013). To determine whether FtsH has any influence on FeoB levels, western blot analyses were performed using JC32 and JC32Δ*ftsH* strain carrying *feoAB*-Flag.

Note that the data below represents preliminary findings since replicates were not performed due to lack of time. It is suggested that such repeats should be part of future work.

Under aerobic conditions, *ftsH* status mostly had little impact of FeoB-Flag levels (Fig. 10.15), although at 8 h, a ~60% higher level was seen for the *ftsH* mutant carrying *feoAB*, with respect to the equivalent *ftsH*$^+$ strain. This effect is consistent with that observed in Figs. 10.11 & 10.12, and suggests that the raised Feo activity seen for the *feoAB*-complemented JC32 strain, as caused by lack of FtsH, is a result of raised FeoB levels. However, this does not necessarily mean that this effect is caused by any direct effect on FtsH-dependent FeoB degradation since *ftsH* mutation has pleiotropic effects influencing multiple aspects of *E. coli* physiology which could in turn affect FeoB levels.

In the presence of ascorbate, there was little effect of *ftsH* status on FeoB-Flag levels in the presence of *feoC*, but lack of FtsH did result in a slight (~10%) increase in FeoB levels in the absence of *feoC* (Fig. 10.16). A similar effect (but weaker, ~10%) of lack of FtsH on FeoB levels in the *feoAB* complemented strains was again seen in the absence of ascorbate (Fig. 10.16) as was seen in Fig. 10.15.

Anaerobically, the *ftsH* mutant caused a slight increase in FeoB-Flag levels in presence and absence of FeoC (26 and 48%, respectively; Fig. 10.17). However, FtsH appeared not affect Feo activity anaerobically (see above). This difference may arise because under anaerobic conditions FeoB levels are relatively high such that the modest reduction causes by FtsH does not much affect the observed Feo-dependent growth. Interestingly, the FtsH$^+$ strains show an additional band at 55 kDa that might account form the lower level of the 84 kDa band.

In summary, *ftsH* mutation caused a modest increase in FeoB levels under both aerobic and anaerobic conditions, which in some cases reflect the effect that the mutation has on Feo-

dependent growth enhancement. However, the changes in FeoB levels seen were relatively modest and would not appear to reflect any major post-transcriptional Feo-regulatory response to O_2 levels or FeoC status, as reported by Kim *et al*. (2013). It should be noted that the Flag tag used here could influence the sensitivity of FeoB to degradation by FtsH. However, experiments in Fig. 10.12 involved use of *feoAB* lacking any Flag-tag and results obtained were extremely similar to those seen with the Flag-tag (Fig. 10.11).

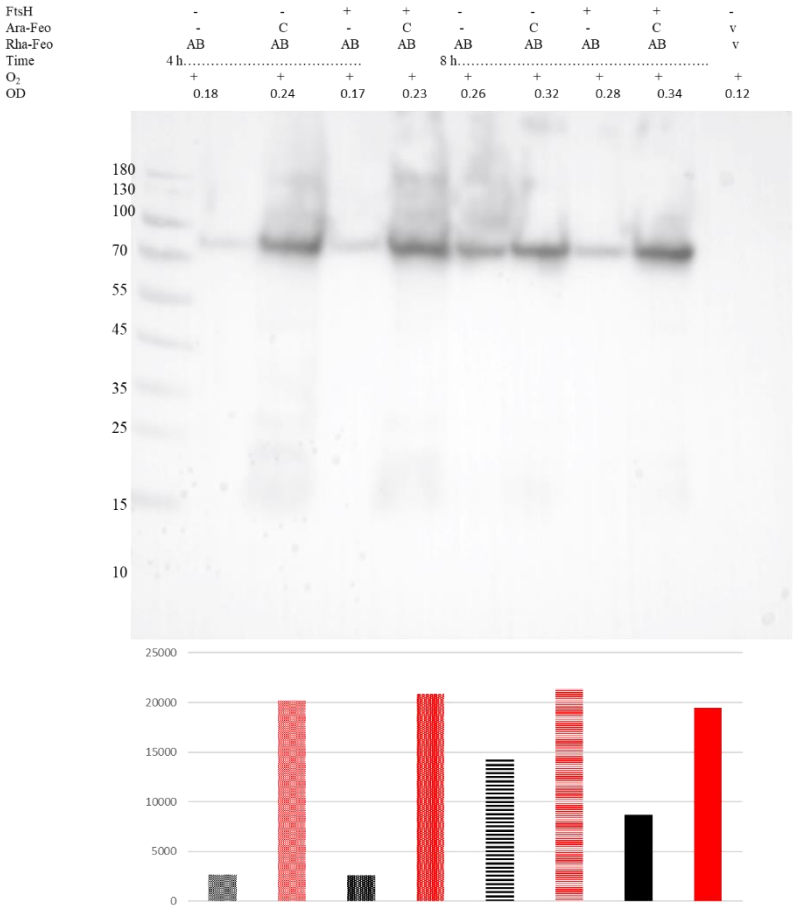

Figure 10.15: Western-blot analysis of FeoB-Flag levels in JC32Δ*ftsH* and JC32 grown <u>aerobically</u> under iron deprivation conditions. Growth was performed in M9 medium, 0.4% glucose, 100 mM MES pH 6, with 100 μg/ml ampicillin and 50 μg/ml chloramphenicol, 0.5 μM DTPA. 0.02% rhamnose and 0.002% arabinose were added. Strains carried either pBADrha-*feoAB-flag*^{O157} or pBADrha, and pBADara-*feoC*^{O157} or pBADara, as indicated. The bar chart is based on the densities of the FeoB-Flag bands in the corresponding tracks above.

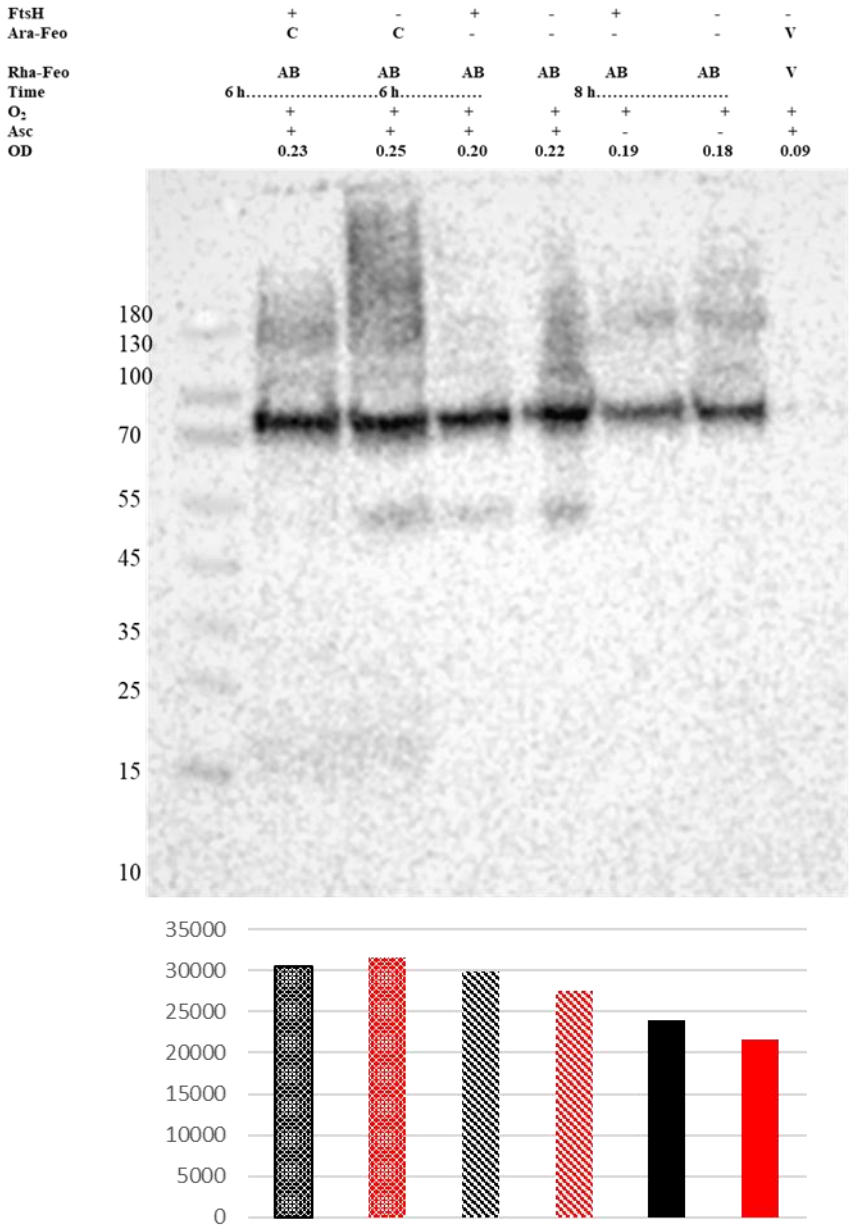

Figure 10.16: Western-blot analysis of FeoB-Flag levels in JC32Δ*ftsH* and JC32 grown <u>aerobically</u>, with and without <u>ascorbate</u>, under iron deprivation conditions. All details as in Fig.10.15, except for use of aerobic conditions and 2 mM ascorbate as indicted.

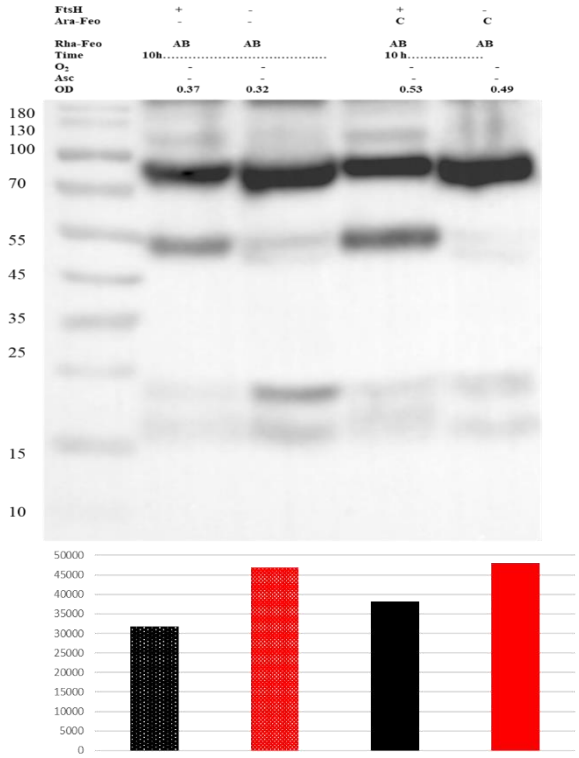

Figure 10.17: Western-blot analysis of FeoB-Flag levels in JC32Δ*ftsH* and JC32 grown <u>anaerobically</u> under iron deprivation conditions. All details as in Fig.10.15, except for use of anaerobic conditions

10.5 Conclusion

Previous research in *S. enterica* indicated that FeoB is protected by FeoC from proteolysis by FtsH under anaerobic conditions, and that aerobically this protection is bypassed such that FeoB degradation by FtsH progresses (Kim *et al*., 2013). The results above support a role (either direct or indirect) for FtsH in down-regulating FeoB levels in a manner that is independent of *feo* transcriptional or translational control. However, the effect of FtsH appears relatively modest and the absence of FtsH does not result in an increase of FeoB to levels that match those observed anaerobically. In addition, absence FtsH does not prevent enhancement of Feo activity by FeoC. These findings suggest that FeoC has a function in stimulating aerobic (in presence of reductant) Feo activity that is largely FtsH independent, and that the weak levels of FeoB seen aerobically are not a consequence of raised FtsH degradation.

Thus, the mechanism by which FeoC controls Feo activity aerobically remains unclear. Measurement of the effect of oxygen and H_2O_2 on FeoB half-life would indicate whether the differences in FeoB levels observed (aerobically and anaerobically) are caused by a change its degradation. In addition, experiments should be directed at examining the stability of the *feoABC* transcript in case this is subject to control e.g. by a small regulatory RNA. This can first be tested by considering the impact of an *hfq* mutant.

Chapter 11: Overexpression of FeoB

11.1 Introduction

The levels of membrane proteins naturally obtained in bacterial cells are generally not enough to readily allow isolation of sufficient amounts of protein for the structural and functional studies. Most membrane protein targets therefore need to be overexpressed. Expression systems have been improved to produce large amounts of soluble proteins in host cells. However, the overexpression of membrane proteins, from the nascent polypeptide chain to the membrane, is a limiting factor in membrane protein research (Drew *et al.* 2003; Dalbey and Chen 2004).

Membrane proteins expression can be enhanced in various ways, such as optimising codon bias, improving the stability and translational efficiency of mRNA or enhancing the properties of the host cell (Peti and Page 2007). However, overexpressed membrane proteins are normally toxic to the host and the degree of overexpression achieved is often limited. In overloaded host cells, overproduced nascent membrane proteins can end up forming aggregates such as inclusion bodies. While refolding of membrane proteins is possible, and has been particularly effective for the β-barrel type outer-membrane proteins, it is extremely hard or impossible for the inner-membrane proteins (Drew *et al.* 2003; Geertsma *et al.* 2008). Currently, there are no realistic rules or unique suitable conditions recognised to achieve satisfactory membrane-protein overproduction. The optimisation of factors such as host strains, medium and expression temperature are also target specific (Graslund *et al.* 2008).

Due to the huge number of variables in the parameters involved, the task of finding the best expression circumstances for a target protein is similar to other problematic multi-parameter difficulties such as protein crystallisation. The main issue is that given finite resource availability, how can the most effective expression conditions for a given target protein be best determined (Berrow *et al.* 2006). A time saving and economic way to explore protein

expressions is to work on a small-scale and, if a large number of targets or factors are under research, to employ high throughput pathways (HTP). The use of small-scale HTP expression screens for the identification of successful expression conditions for FeoB, as a membrane protein-HisTag target, is described it in this chapter.

11.2 Aim of this chapter

The soluble N-terminal domain of FeoB has been structurally defined (Petermann *et al*., 2009), but the structure of the C-terminal membrane-embedded domain remains to be determined, although models have been generated (see Chapter 9). The aim of the work described in this chapter is to optimise the expression and purification of the entire FeoB membrane protein to allow structural studies. The availability of the protein would also allow functional studies (i.e. iron uptake studies in membrane vesicles or lipoproteosomes) and generation of polyclonal antibodies (for western-blot analysis of FeoB levels e.g. in response to O_2 regime). Two different expression hosts will be employed, *E .coli* BL21 and insect cells using the Baculovirus expression system. The *feoB* gene of *E. coli* O157 will be cloned in the pTriEx1.1 vector which permits expression (and subsequent isolation) of membrane proteins in *E. coli* and insect cells. The expressed recombinant FeoB protein will be purified by Ni^{2+} chromatography and solubilised in detergents.

The baculovirus expression system could therefore provide a more suitable technique for membrane protein isolation. The baculovirus expression system was used to produce recombinant baculoviral stocks and recombinant protein in insect cells. The use of baculovirus as an expression vector relies on the high yield of recombinant proteins in insect cells due to very strong virus gene promoters and on similar post-translational modifications as found in mammalian cells (Kelly et al., 2007, Zhao et al., 2003). The expression vector used in this study, *Autographa californica* multiple nucleopolyehedorvirus (AcMNPV), is a large circular double

stranded DNA virus with a genome of 133,894 bp genome that has the major envelope protein called glycoprotein 64 (gp64) on its budded from (Kelly et al., 2007, Zhao et al., 2003). Recombinant viruses are produced with an efficiency of 100% by a genetic modification of the baculovirus genome (Grabherr et al., 2001, Pengelley et al., 2006). The pTriEx1.1 plasmid is amplified in *E. coli*, isolated and linearised for co-transfected together with viral DNA into *Sf*9 insect cells to produce recombinant viruses (Pengelley et al., 2006).

11.3 Construction of pTriEx-*feoB* His-Tag or Flag-Tag constructs

pTriEx™-1.1 is a plasmid conferring ampicillin resistance in *E. coli* and carrying an IPTG inducible T7 promoter. It is designed to allow rapid expression of target genes in multiple expression systems. The pTriEx™-1.1 vector can use to test expression in insect cells, vertebrate cells and *E. coli*. Expression in *E. coli* is tightly controlled by a T7 *lac* promoter and requires hosts expressing the T7 RNA polymerase. For expression in insect cells, pTriEx-1.1 contains flanking baculovirus sequences to allow the generation of recombinant baculoviruses using the BacVector™ System. The p10 promoter drives late expression in insect cells upon baculovirus-infection. Mammalian cell expression is enabled by virtue of the chicken actin promoter. The three promoters are tandemly arranged upstream of the multicloning site, so a single vector allows expression screening in several hosts. The insect cell system is an attractive option as high-level expression of 7TM proteins have been previously successful in the baculovirus/insect cell systems allowing crystallisation and the derivation of an atomic structure (Siu *et al*., 2013).

Maps of pTriEx1.1 with *feoB* inserted in different formats are shown in Fig 11.1. Note that the His_6- and Flag-tags indicated where incorporated using the F or R primer, and the His_8- and HSV tags of the vector were not incorporated into the *feoB* orf when cloned into pTriEx.

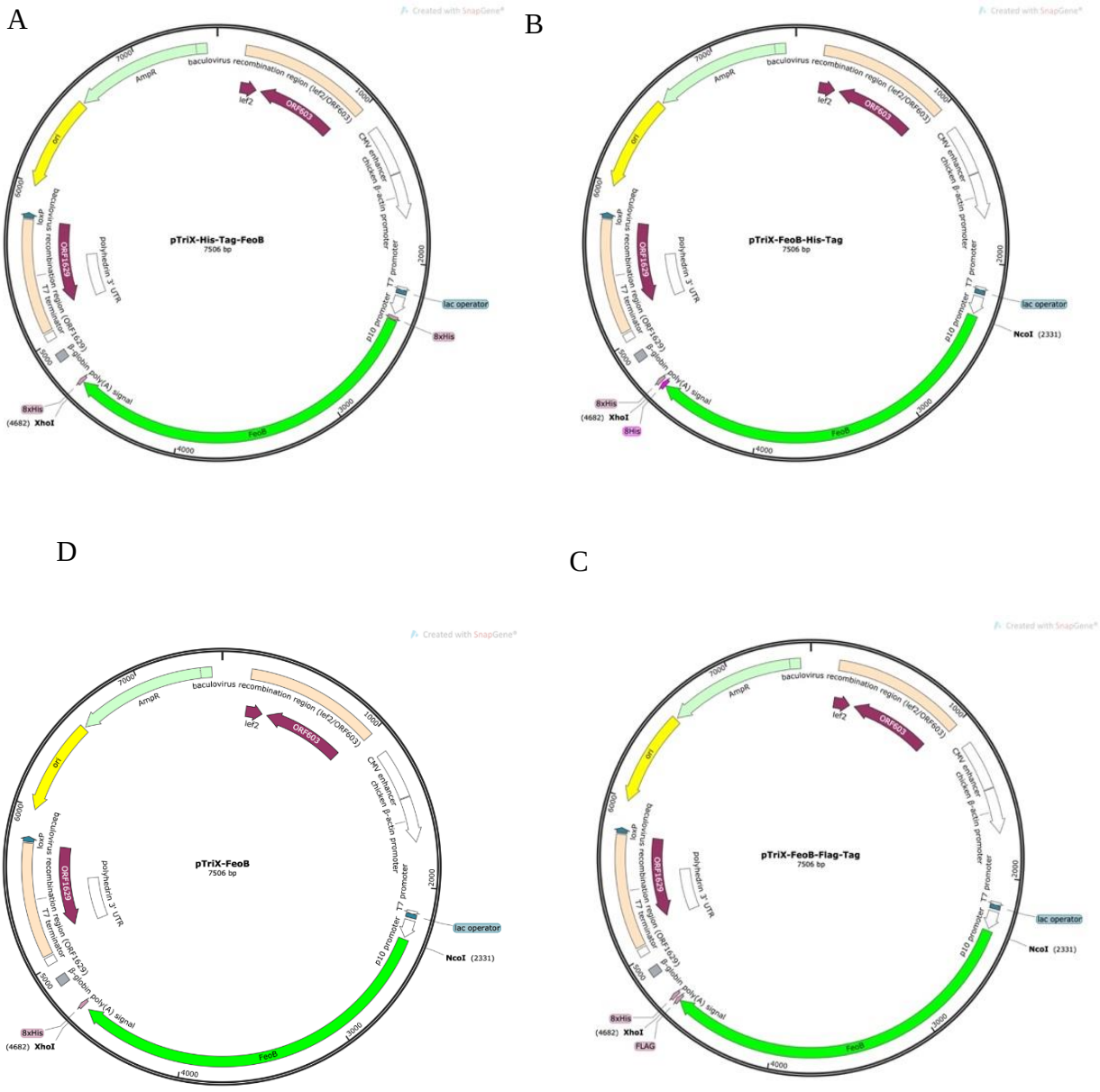

Figure 11.1: Genetic maps of the pTriEx 1.1 expression vector with *feoB* inserted. The FeoB sequence was inserted between the *Nco*I and *Xho*I sites (indicated) to give: **A**, pTriEx-HisTag-*feoB*; **B**, pTriEx-*feoB*-HisTag; or **C**, pTriEx-*feoB*-FlagTag. The pTriX1.1 vector is shown in **D**. The final recombinant vectors were confirmed by sequencing prior to its use to generate a recombinant baculovirus system. Images generated with Snapgene™.

11.3.1 PCR amplification of *feoB* with His-tag or Flag-tag

Amplification was performed using an In-Fusion® HD Cloning Kit (Clontech Laboratories). In-fusion PCR primers: pTriEx-FeoB_FWD and pTriEx-FeoB_Rev-FeoB (Table 2.9) were used to amplify *feoB* from chromosomal DNA using HIFI DNA polymerase (Methods 2.13.2). Amplified fragments were analysed by agarose gel electrophoresis to evaluate their sizes. The expect size of fragment (~2800 bp) was thus created for cloning into pTriEx 1.1.

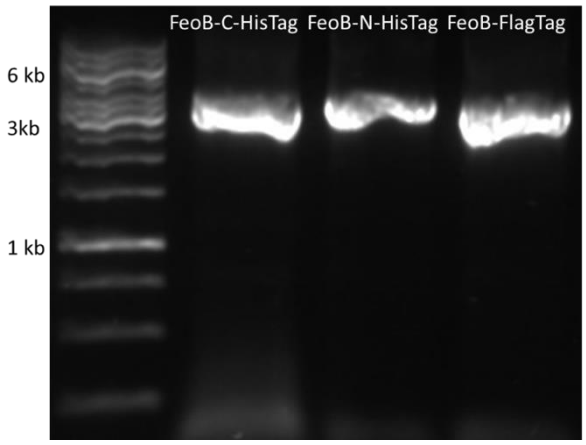

Figure 11.2: Gel electrophoretic analysis of *feoB* PCR products. Electrophoresis was performed using a 0.7% agarose TBE gel. Lane L, 1 µl GeneRuler® 1 kb ladder (Fermentas); lane 1, 2 and 3, PCR products as indicated.

11.3.2. In-Fusion transformation of pTriEx-*feoB* cloning reaction into Top10 competent cells

The In-Fusion reaction mixtures consisting of *Nco*I/*Xho*I-digested vector and PCR products (5 µl) were used to transform *E. coli* Top10. From the resultant Amp^R transformants, 10 were subjected to plasmid 'miniprep' isolation using GeneJET^{TM} Plasmid Miniprep Kit (Fermentas). Isolated plasmids were screened by agarose gel electrophoresis and many with mobilities matching that anticipated for the excepted construct (equivalent to ~7.9 kb; Fig. 11.3) were then further analysed by restriction digestion.

Two samples were digested with *Xho*I and *Nco*I to release the *feoB* fragment from the vector and to permit validation of the recombinant plasmid. The digested samples were expected to give two bands of ~2800 bp (insert) and ~5.1 kb (the vector) (Figure 11.4). Digested samples gave the expected sizes and thus were sequenced by Source Bioscience using T7F and T7R reverse primers. The sequences achieved were compared with the sequence database using BLAST. The result showed that the insert has the expected sequence with no errors. Plasmids was selected for more work and designated as: pTriEx-*feoB*, pTriEx-HisTag-*feoB*. pTriEx-*feoB*-HisTag and -pTriEx-*feoB*-FlagTag..

11.3.3 Cloning and isolation pTriEx-*feoB* plasmids

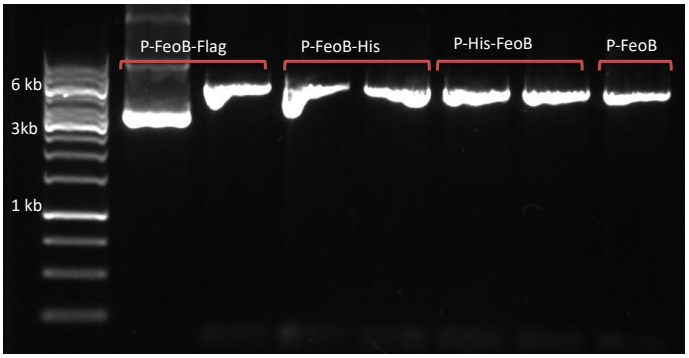

Figure 11.3: Agarose gel electrophoresis analysis of potential pTriEx-*feoB* plasmids. Transformant colonies were subjected to 0.6% agarose gel electrophoresis. L indicates the GeneRuler® unstained DNA marker (Fermentas).

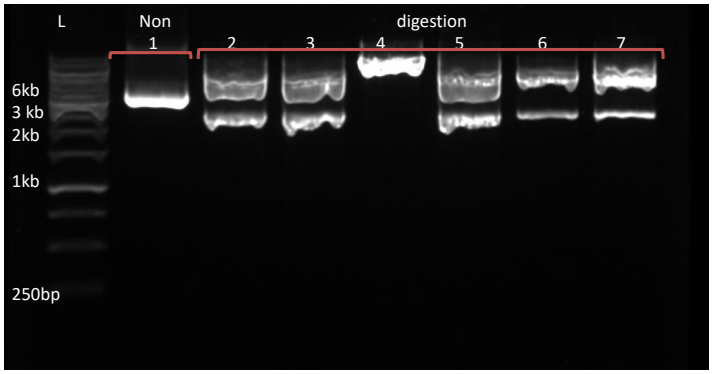

Figure 11.4: Gel electrophoretic analysis of the pTriEx1.1-*feoB* isolates by restriction digestion. Plasmids were digested with *Xho*I and *Nco*I. Lane L, GeneRuler® 1 kb ladder (Fermentas); lane 1, pTriEx-*feoB* nondigested; lanes 2 & 3, double digested pTriEx-*feoB*-HisTag; lanes 4 & 5, double digested pTriEx-HisTag-*feoB*, pTriEx-*feoB*-HisTag; and lanes 6 & 7, double digested pTriEx-*feoB*-FlagTag.

11.4. Overexpression of FeoB proteins in *E. coli* BL21

feoB encodes a membrane protein whose expression in *E. coli* BL21 may be problematic to achieve or detect. As part of the expression strategy, the complete gene was cloned into pTriEX1.1 (EMD BioSciences), as above, allowing expression in three distinct phyla: Proteobacteria, using the T7 system analogous to that used by the pET series of vectors; mammalian cells by virtue of the chicken actin promoter present on the vector; and insect cells by virtue of the p10 promoter, derived from the baculovirus *Autographa californica* multiple nucleocapsid polyhedersis virus (AcMNPV).

Due to functional-study limitations for FeoB in S*f9* insect cells, expression and purification of the integrated full length His-tagged FeoB protein was first investigated in *E. coli* using the LOBSTR™ strain. BL21/λDE3 was also used as the host strain in later experiments. The pTriEx-*feoB*-HisTag plasmid was transformed into *E. coli* LOBSTR™, which is designed to eliminate the most abundant histidine-rich *E. coli* protein contaminants **(**section 2.29.4.1**).** The transformants were grown in 50 ml LB containing 100 µg/ml ampicillin at 37 °C and induced

by the addition of 1 ml of 20 mg/ml IPTG (producing a final concentration of 400 µg/ml) at an OD_{600} of 0.5. Samples were taken at regular intervals (1-5 h). Unfortunately, no band corresponding to the ~84 kDa FeoB protein could be detected by SDS-PAGE upon induction (data not shown). Whole-cell samples were also subjected to analysis by western blotting using anti-His antibodies (Methods 2.29.3), but no immune-reactive band at ~84 kDa could be detected (data not shown).

Small-scale overexpression was also attempted in BL21/λDE3 carrying pTriEX-HisTag-*feoB* (N-terminal His-tag). However, again no expression was evident upon SDS-PAGE analysis (data not shown). Three potential reasons for this lack of success were identified: firstly, since FeoB is a membrane protein it is insoluble and potentially remains embedded within the membrane and may not be readily solubilised by SDS; secondly, by overexpressing a membrane protein it could prove toxic causing cell damage and ultimately death (unlikely given that growth was observed post IPTG induction); and thirdly, boiling membrane proteins in 1x SDS digestion buffer often causes the membrane proteins to form aggregates making analysis by SDS-PAGE difficult. In order to rectify these three issues, changes to the procedure were immediately implemented. Firstly, a new strain was used, BL21*, which display enhanced expression of recombinant proteins. This would potentially allow high levels of expression of the FeoB protein into the cell. Secondly, rather than using traditional SDS digestion buffer a modified version was utilised to include the mild detergent Triton-X-100 at a concentration of 1% to solubilise the membrane effectively improving the potential for FeoB protein for visualisation. Thirdly, instead of boiling of the cell-pellet sample in SDS digestion buffer, the sample was gently warmed at 37 °C for 1 h to prevent aggregation while enabling effective solubilisation. These changes were subsequently trialled using both the N- and C-terminal-His-Tag constructs, but again no induced protein matching the mobility anticipated for FeoB could be observed by SDS-PAGE (data not shown).

Despite this lack of success, a large-scale over-expression (using 5 L LB broth, 1 h IPTG induction) was performed in an attempt to obtain FeoB through concentration by purification. Following induction (1 h), harvested cells (LOBSTR with pTriEX-*feoB*-HisTag) were ruptured by sonication in 50 mM phosphate buffer pH 7.5, 500 mM NaCl, 1% NP-40 (Methods 2.29.4.2.2). The membrane protein was isolated by centrifugation and detergents (NP-40) were used to screen for optimisation of protein extraction and solubilisation. Triton-X-100 and Tween 20 were used for the large-scale isolation as they gave the highest yields of soluble protein obtained (data not shown). However, no band corresponding to FeoB was obtained following HisTrap affinity chromatography (data not shown).

Large-scale overexpression was repeated as above but with BL21/DE3 as the host and a 4 h induction, and rupture by French press (in 50 mM phosphate buffer pH 7.5, 500 mM NaCl, 1 mM DDT, 1% NP-40, protein inhibitor, $MgCl_2$; Methods 2.2.29.4.2). Once the membrane had been isolated (Methods 2.2.29.4.2.2), it was solubilised in NP-40, and subsequently applied to an equilibrated 5 ml HisTrap affinity column (Methods 2.29.5.1). However, again no FeoB band could be detected by SDS-PAGE.

One potential issue with the expression system use here is the aerobic conditions employed and absence of FeoA which could lead to poor FeoB stability (see Chapter 8).

11.5. Overexpression and isolation of FeoB protein from insect cells

Since FeoB could not be overexpressed from pTriEx in BL21, expression was attempted in insect cells.

11.5.1. Expression in *Sf*9 cell line culture

Sf9 insect cells originate from *Spodoptera frugiperda* pupal tissue and are used to express recombinant fusion proteins. The methodology involved is described in Methods 2.30.4. Recombinant baculovirus was generated by mixing pTriEx-*feoB* DNA with linear baculovirus DNA, followed by transfection into *Sf*9 cells (Figure 11.5). The vector includes adequate baculovirus DNA to permit recombination with the viral DNA resulting in the insertion of the transcription unit into the virus genome. The recombinant virus, 'Bac-*feoB'*, harbouring *feoB* under control of the strong p10 promoter, was raised over a period of 6-7 days and was collected from the supernatant of the transfected cells. This virus stock was stored or amplified as needed to generate sufficient volume and titre for subsequent expression analyses. A control transfection was carried out using pTriEx-eGFP to test for expression and transfection (Figure 11.6). Results showed that eGFP was produced successfully indicating that the expression system was functional and therefore suitable for introduction of Bac-*feoB*.

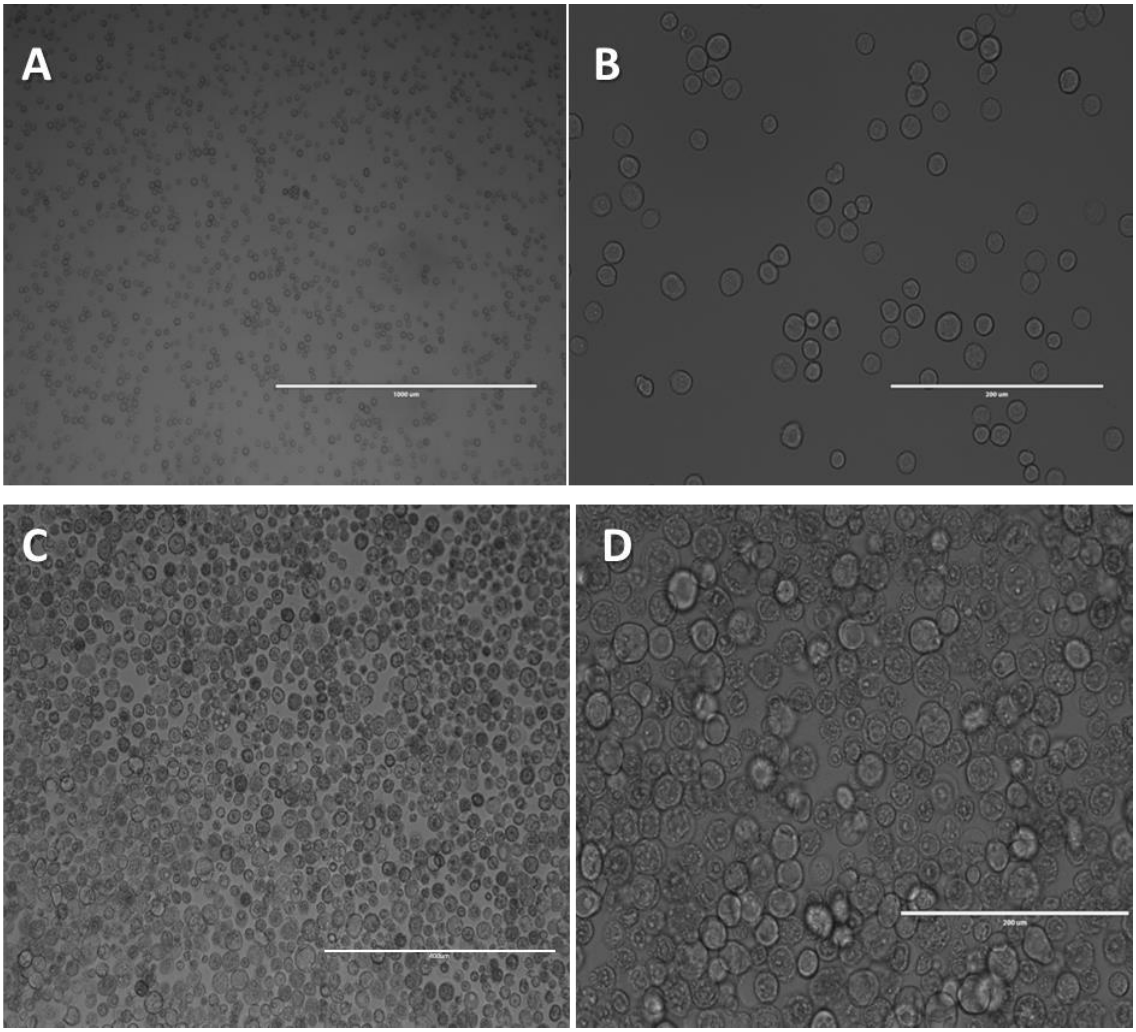

Figure 11.5: *Sf9* insect cells following co-transfection with baculovirus/pTriEx-*feoB*. A/B, non-transfected controls. **C/D,** transfected cells. The transfection is indicted by enlarged cells and expanded nucleus (passage one) with respect to the non-transfected controls.

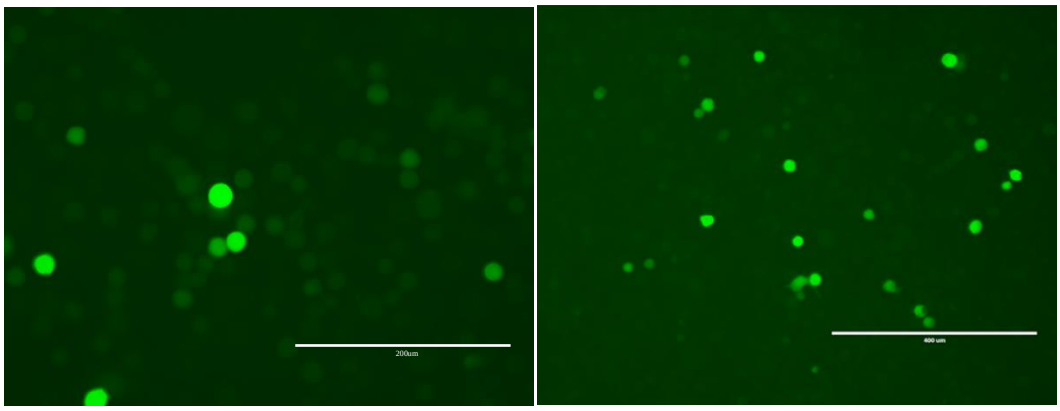

Figure 11.6: Positive control for virus-infected *Sf9* cells using a control plasmid (pTriEx-eGFP). eGFP was visualised for green fluorescence using the green channel of an EVOS digital microscope (passage one).

11.5.2. Detection of FeoB production by western blotting

To evaluate the potential of the insect cell system for *feoB* expression, four single wells each including ~10^6 *Sf*9 cells, were infected with Bac-*feoB* (pTriEx-*feoB*-HisTag) and the cells were collected at three days after infection. Due to the His_6 tag present at the C-terminus of the FeoB protein as expressed from the pTriEX vector, anti-His-tag Western blotting was used to identify the presence of FeoB within whole-cell extracts (Fig. 11.7).

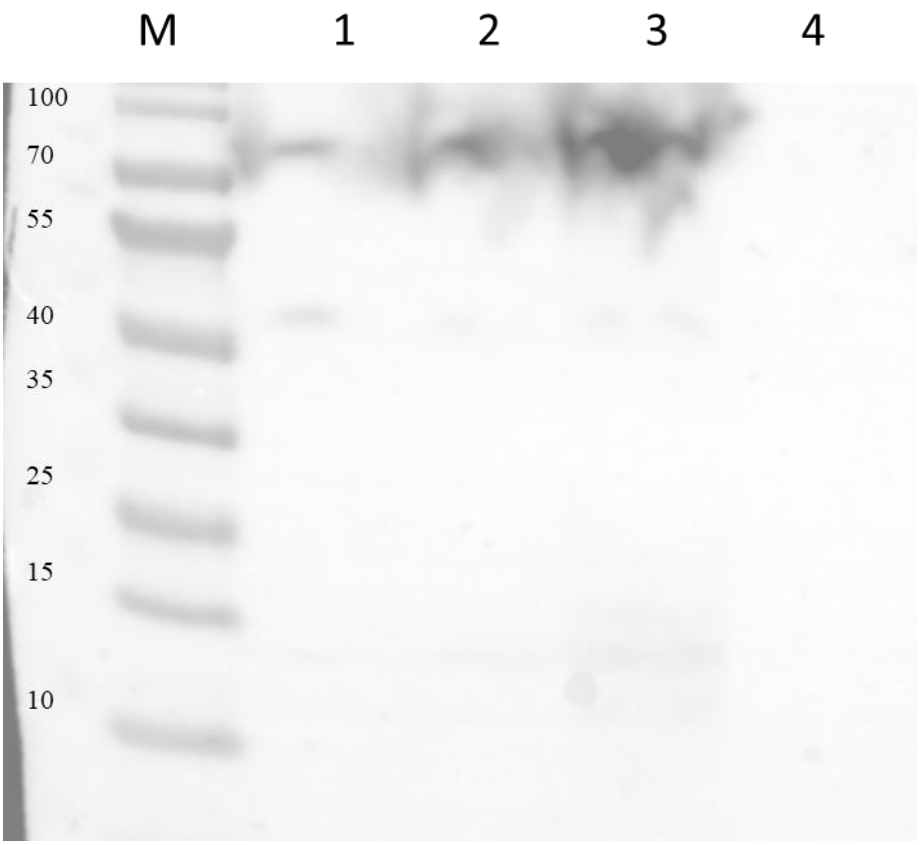

Figure 11.7: Western blot analysis of FeoB-HisTag expression upon Bac-*feoB* transfection of *Sf*9 insect cells. Lane M, protein molecular weight markers (kDa); lane 1-3, passage 1-3 lysates of infected insect cells; lane 4, untreated lysate. Whole-cell extracts were obtaining by digestion in SDS-digestion buffer (with β-mercaptoethanol) for 1 h at 37 C.

In all cases infection of Bac_*feoB* infection, a single His-tagged species with an apparent molecular weight of ~84 kDa consistent with the expression of full length FeoB protein was detected.

11.5.3. Purification of FeoB from *Sf*9 insect cells by Ni^{2+}-affinity chromatography

The above experiment showed successful FeoB production and so the next step was to increase the scale of the insect cultures (to 1 litre) to enable purification by Ni^{2+}-affinity

chromatography. Thus, four 1 l cultures were prepared, corresponding to the four different pTriEx-*feoB* constructs. To confirm successful infection of the recombinant baculovirus carrying the *feoB* constructs, a western blot analysis of the infected insect cells (and culture supernatants) was performed at three days post infection, using antibodies specific for the baculovirus protein gbsd64 (Fig. 11.8). The results clearly showed good gp64 production in all four cases (Fig. 11.8) indicating successful infection had been achieved.

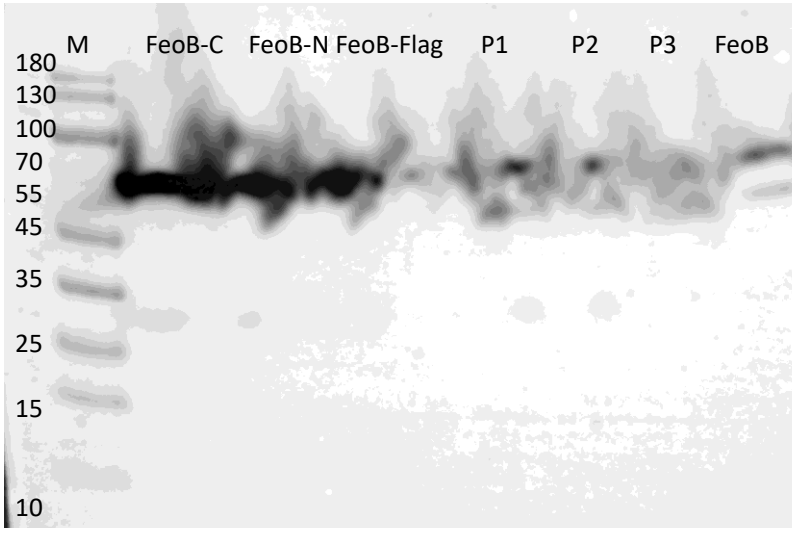

Figure 11.8: **Western blot analysis of gp64 in insect cells infected with Bac-*feoB*.** Lane M, molecular weight markers (kDa); FeoB-C, FeoB-HisTag; FeoB-N, HisTag-FeoB; FeoB-Flag, FeoB-FlagTag; P1-P3, FeoB-HisTag at passages 1-3, respectively; FeoB, FeoB without tags. The location and size of gb64 is indicated.

The corresponding anti-His and anti-Flag western blots showed good production of the corresponding FeoB protein also, with a mobility at ~70-80 kDa (Fig. 11.9).

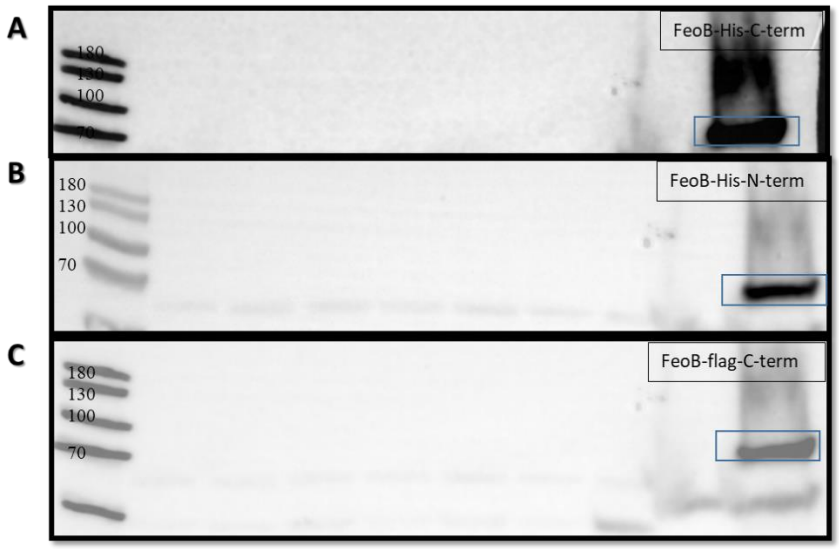

Figure 11.9: Western blot analysis of Bac-*feoB* transfected *Sf*9 insect cells expressing FeoB. A, FeoB-HisTag (anti-His immunodetection); B, HisTag-FeoB (anti-His immunodetection); C, FeoB-FlagTag (anti-Flag immunodetection). Left, MW markers; right, FeoB sample.

The HisTag-FeoB and FeoB-HisTag 1 l cultures were subject to protein purification. This involved whole cell lysis in 1% NP-40 detergent using a French press (Method 2.2.30.5), followed by soluble supernatant isolation by high-speed centrifugation. Purification of the His-tagged FeoB protein was achieved using nickel-based metal-affinity chromatography. This purification method depends on the reversible binding of the His-tag residues in the protein to the affinity ligand (Ni^{2+}) linked to the chromatographic matrix. A standard protocol of equilibrating the column with binding buffer (500 mM NaCl 20 mM imidazole, 20 mM PBS, and 0.1% Tween 20 pH 7.4) and eluting the protein with an imidazole gradient (0.015-1 M) was employed. Fractions corresponding to a broad peak were analysed by SDS-PAGE (Fig. 11.10A & 11A), together with the flow through. The chromatograph demonstrated that the single narrow peaks obtained with the imidazole gradient contained a single major protein corresponding to FeoB (~80 kDa) in size (Figs 11.10B & 11.11B). Fractions carrying high levels of pure FeoB-HisTag or HisTag-FeoB were pooled together into two pools (20 and 25 ml, respectively), which were subsequently concentrated (see below).

Part of each pool was dialysed against a buffer (10 mM ammonium acetate pH 7, 0.81 μM Tween 20) to allow ESI-MS (CAF, University of Reading) analysis. Unfortunately, no protein was detected by MS, even when the FeoB protein was provided in alternative solutions (HPLC H_2O or 50 mM phosphate buffer, pH 7.4, 1% NP-40, 500 mM NaCl). Upon concentration by ultrafiltration in elution buffer, ESI-MS still failed to detect any protein corresponding to FeoB (data not shown). MS is notoriously difficult for membrane proteins due to their poor solubility and tendency to aggregate (Isabel Moraes, personal communication).

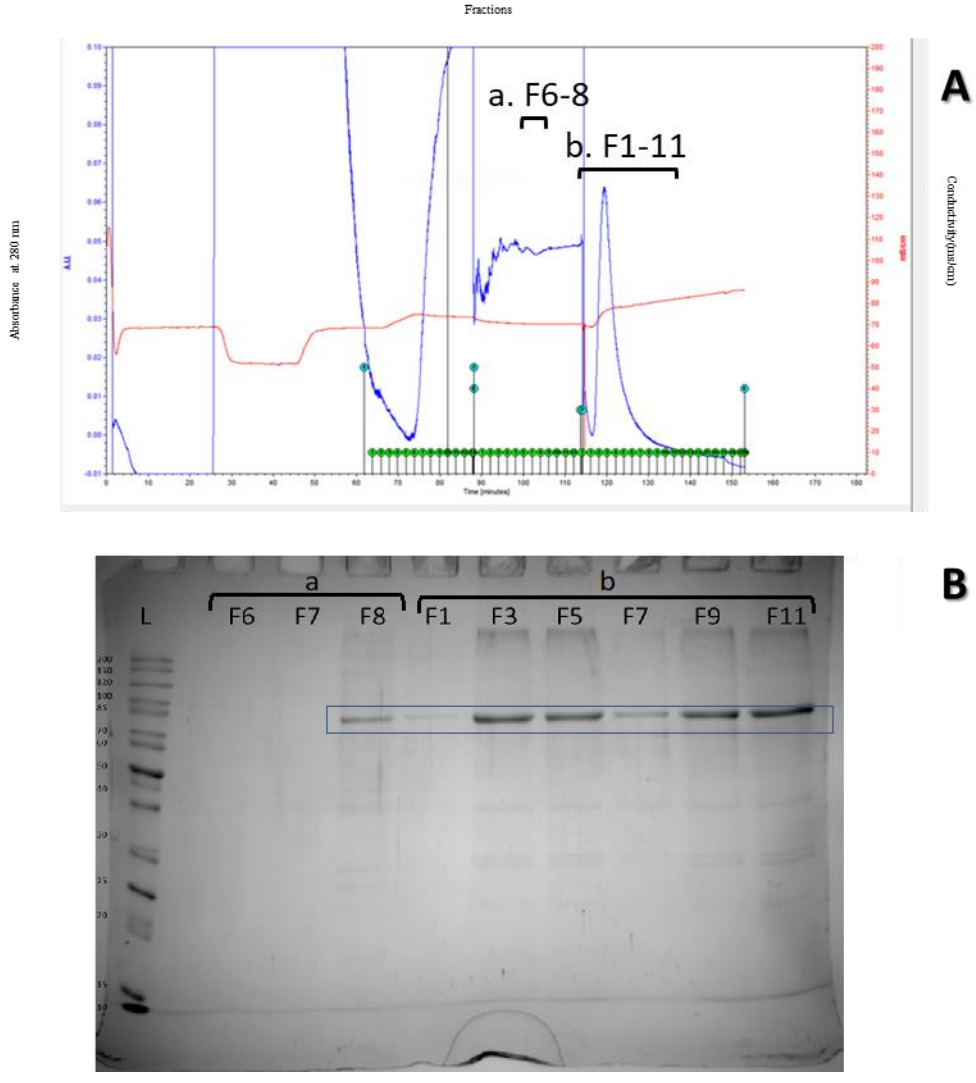

Figure 11.10: Purification of HisTag-FeoB by Ni^{2+}-Sepharose™ immobilised-metal-affinity chromatography. (A) Elution profile from the nickel Sepharose™ column with fractions analysed by

SDS-PAGE indicated. (B) SDS-PAGE (12% acrylamide) analysis of fractions (10 µl) collected during chromatography. Blue box indicates bands corresponding to the size of FeoB protein.

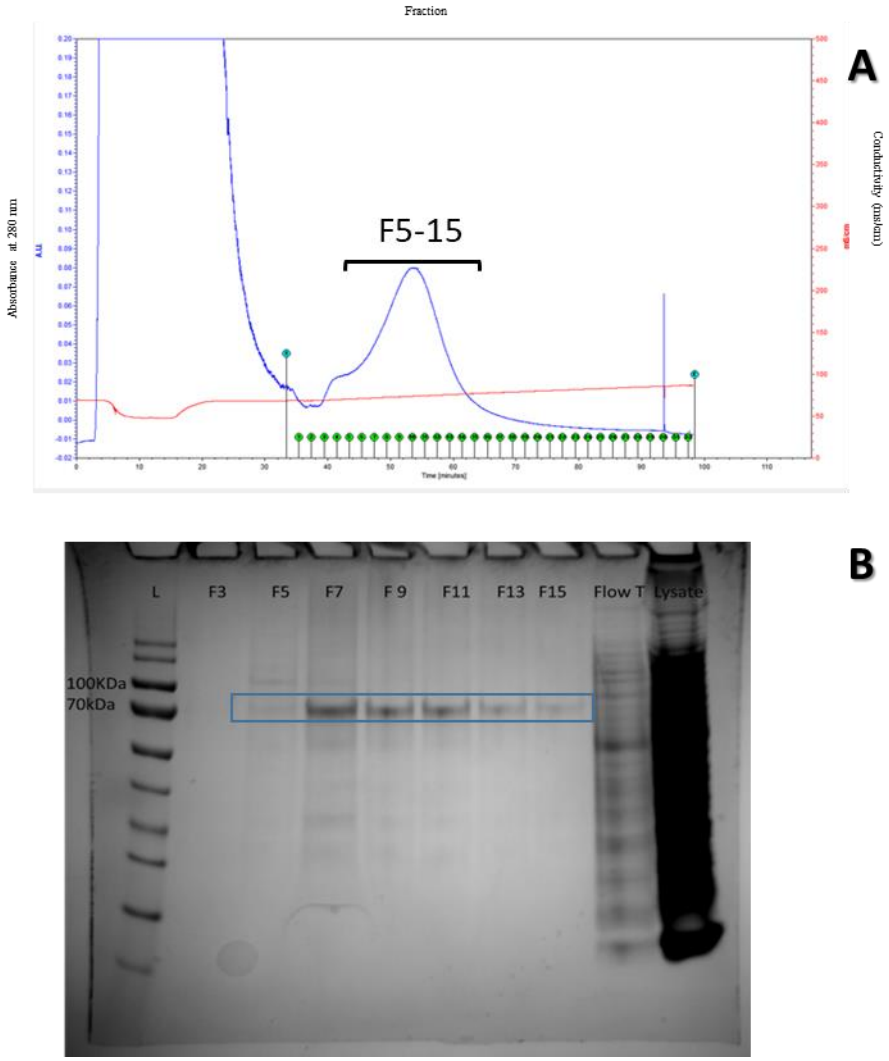

Figure 11.11: Purification of FeoB-HisTag by Ni^{2+}-Sepharose™ immobilised-metal-affinity chromatography. (A) Elution profile from the nickel Sepharose™ column with fractions analysed by SDS-PAGE indicated. (B) SDS-PAGE (12% acrylamide) analysis of fractions (10 µl) collected during chromatography. Blue box indicates bands corresponding to the size of FeoB protein. Flow through and lysate samples are shown.

.

The C-terminal fusion provided better yields than the N-terminal fusion (see below, Fig. 11.12) and so a second FeoB-HisTag preparation was made (Figure 11.13).

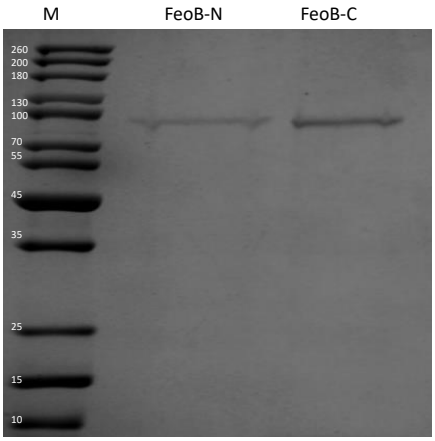

Figure 11.12: SDS-PAGE analysis of purified HisTag-FeoB and FeoB-HisTag after concertation and dialysis.

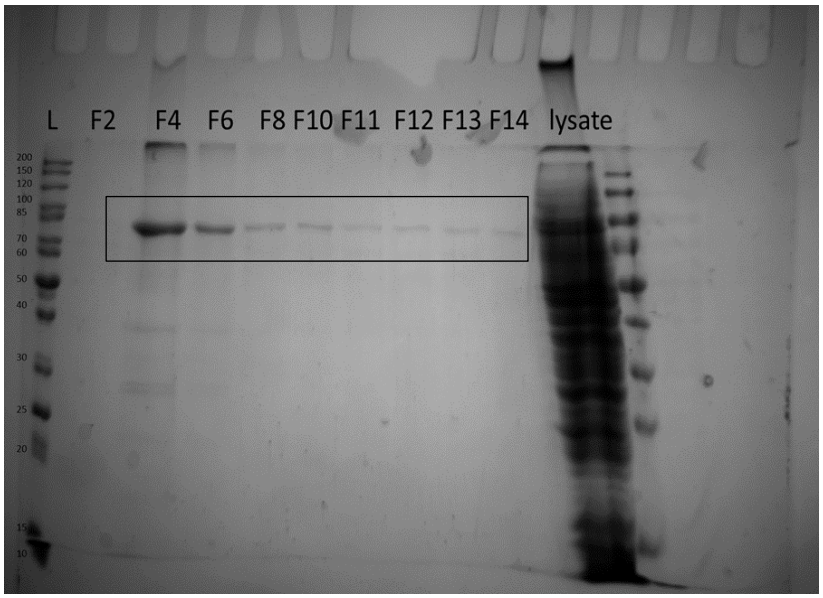

Figure 11.13: Second purification of FeoB-HisTag by Ni^{2+}-Sepharose™ affinity chromatography. Only the SDS-PAGE analysis of fractions is shown. Black box indicates bands corresponding to the size of FeoB protein.

Fractions obtained were also analysed by anti-His-tag Western blotting (Figure 11.14), which showed that the isolated ~80 kDa protein is reactive towards the anti-His antibodies, but also indicated the presence of a significant immunoreactive protein at a higher mass, which might correspond to aggregated protein. Note that the higher MW anti-His reactive protein was less apparent upon SDS-PAGE analysis (Fig. 11.10).

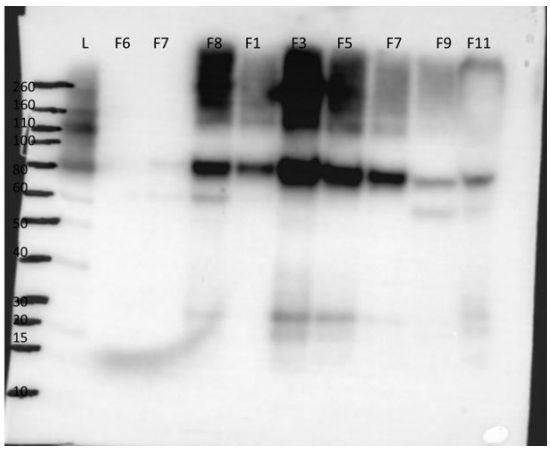

Figure 11.14: Anti-HisTag western blot analysis of purified HisTag-FeoB. Samples were from Fig. 11.10.

Fractions 4-14 and 3-13 from the first and second HisTag-FeoB purifications were pooled in preparation for concentration and further purification by gel filtration chromatography (Superdex 75 HR 16/60) in chromatography buffer (50 mM phosphate, 200 mM NaCl, 0.1% NP-40, pH 7.5).

11.5.4 Further purification of FeoB using gel filtration chromatography

In order to further purify the FeoB-HisTag protein from the large-scale overexpression described above, the pooled fractions (kept at -80 ˚C or on dry ice) were transferred to the

laboratory of Isabel Moraes (Harwell). FeoB-HisTag, solubilised in a buffer containing NP-40 detergent and concentrated by ultrafiltration (Vivaspin 20, 50000 MWCO, Sartorius Stedim Biotech), was loaded onto a fully equilibrated Superdex 75 HR 16/60 column in SEC buffer A (50 mM Tris, 200 mM NaCl, 1 mM DDT, pH 7.5). The column was washed after use with column equilibration, SEC buffer B (50mM PBS, 0.1% NP-40, 1mM DDT,150 mM NaCl) to remove unbound protein (see Methods 2.31.8 for details).

Purification by SEC gave one large, early elution peak at 7.5 ml and a few smaller peaks at later elution points. There was also a major peak in conductivity at 22-23 ml, representing the salt peak. The peak at 7.5 ml was assumed to contain aggregated FeoB and so the corresponding fractions were not further considered. However, fractions (200 μl) corresponding to the other peaks were analysed by 12% SDS-PAGE. Fractions for peaks at 14.3 and 15.7 ml contained a band, as seen previously, at ~70 kDa (Figure 11.23). The early elution of the major peak (7.5 ml) suggests that the protein is largely in an aggregated form, with only a relatively small fraction in a form that may not be aggregated. Indeed, the peak at 15.7 ml carrying FeoB is the peak most likely to contain FeoB in a non-aggregated state as it eluted with the highest volume. The scale of the SEC column was insufficient for generating FeoB protein for further analysis, and the apparently aggregated nature of the eluted protein indicates that further work is required to determine and control its aggregation state.

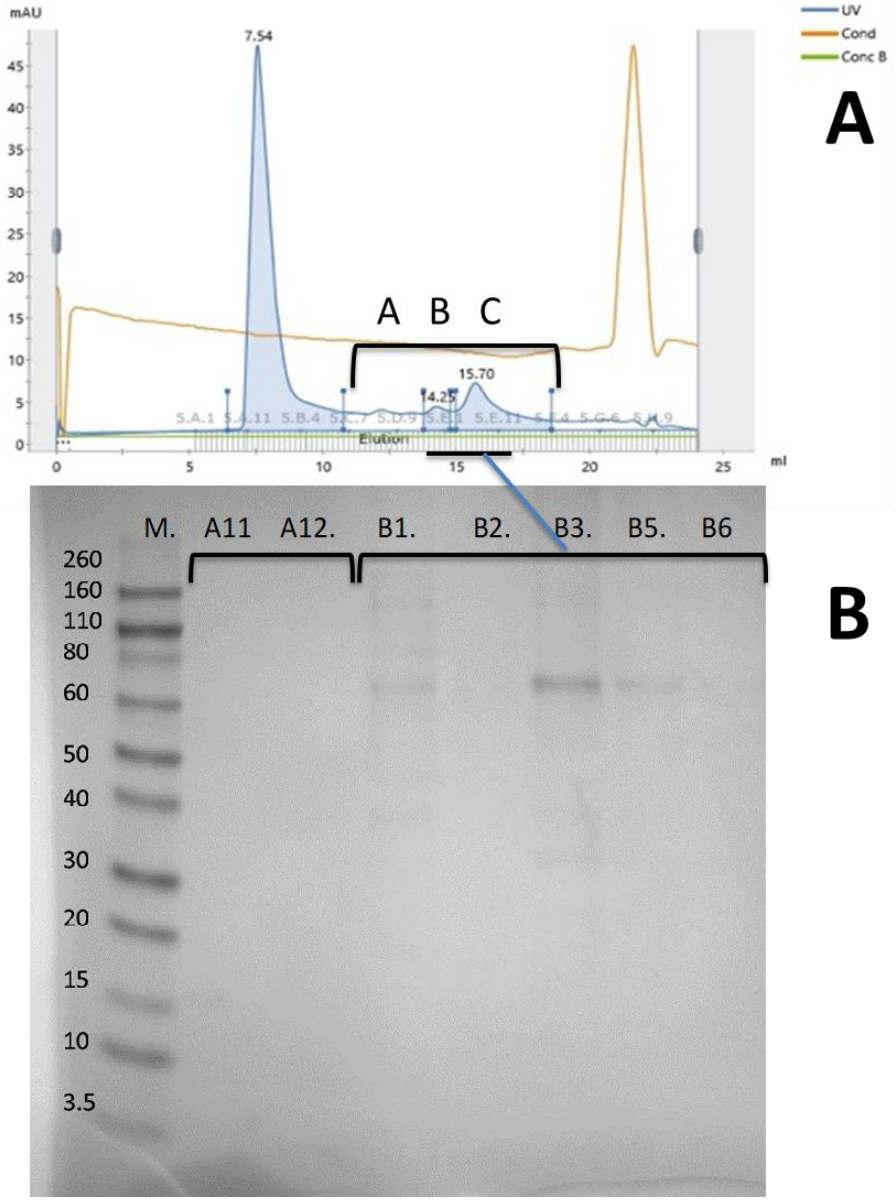

Figure 11.15: SEC purification of FeoB-HisTag by size exclusive chromatography. (A) Elution profile obtained for FeoB protein on a Superdex 75 HR 16/60. UV, absorbance at 280 nm; Cond, conductivity; Conc B, gradient (none applied). 250 µl of a 1.7 mg/ml sample were loaded. (B) SDS-PAGE (12% acrylamide) analysis of fractions (10 µl) collected during chromatography. Mass of protein markers is indicated in kDa. Black arch indicates bands corresponding to the size of FeoB protein with mobility at ~70 kDa.

11.6. Analysis of His-tagged FeoB aggregation state by Dynamic Light Scattering (DLS)

DLS, also known as a photo-correlation spectroscopy or quasi-elastic light scattering, is used for measuring and characterising particles in solutions. It correlates the Brownian movement of particles with their sizes. Brownian motion is simply the random movement of particles, the bigger the particles, the slower the Brownian movement and vice versa. Brownian motion also depends on the temperature and medium viscosity. However, when in solution macromolecules do not always have "spherical" shapes and are constantly solvated. So, when calculating the diameter from a DLS instrument this is be referred to as the "hydrodynamic diameter". This is the diameter of a 'model sphere', which can also be called a hard sphere, which includes associated molecules such as water. In the case here, the membrane-protein/detergent complex would be considered. During DLS, particles in solution are illuminated by a monochromatic laser while a detector records the fraction of light scattered by the particles. The intensity of the scattered light fluctuates over time due to the movement of the particles (Brownian motion) which causes constructive or destructive interference of scattered light generating information on particle motion which correlates with size.

The results from the DLS measurements for HisTag-FeoB and FeoB-HisTag after Ni^{2+}-affinity purification and concentration (Fig. 11.16) show that there is a major HisTag-FeoB protein/NP-40 complex with a hydrodynamic radius (Rh) of around 9 nm, which is suggestive of a non-aggregated form that would be suitable for crystallisation trials. However, there are also major complexes at ~50 nm and >1 μm suggestive of considerable aggregation in NP-40 for both forms of FeoB; this would explain the SEC elution peak at 7.5 ml (Fig. 11.15). Thus, DLS indicated that the purified FeoB in NP-40 is largely in an aggregated form that would not be

suitable for crystallisation trials. Thus, an alternative detergent should be sought to solubilise the protein in a form where the non-aggregated from is the major species (see next chapter).

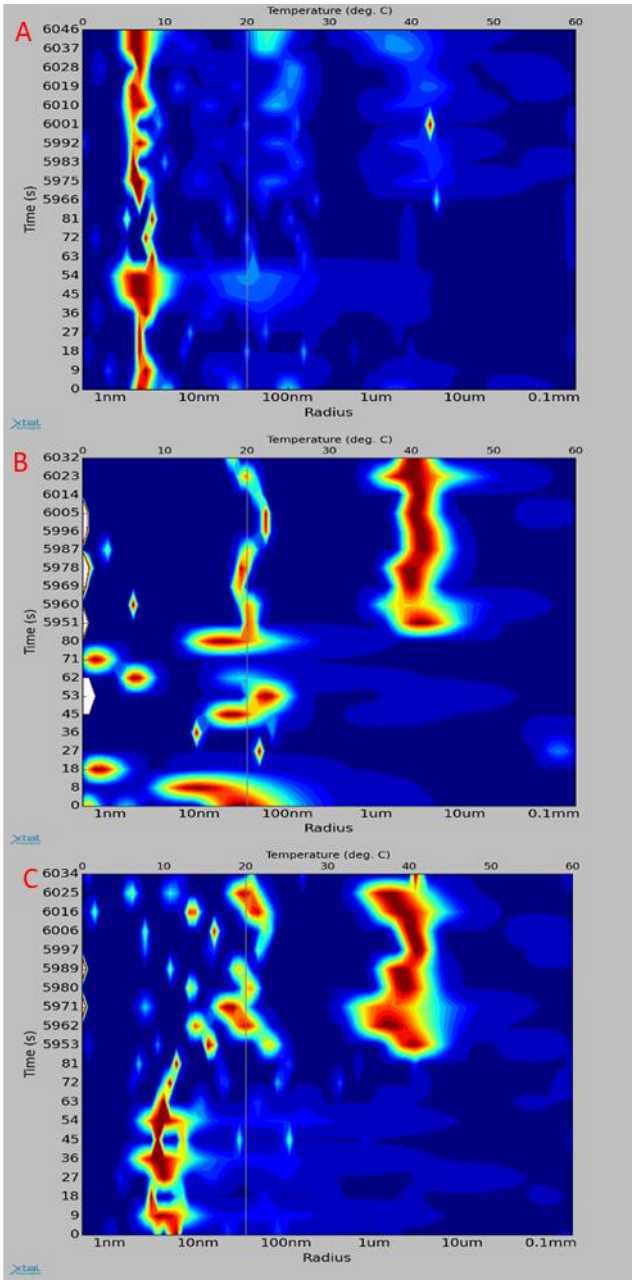

Figure 11.16. DLS analysis of FeoB-detergent complex formation. (A) Buffer detergent control without protein. (B) FeoB-HisTag protein. (C) HisTag-FeoB protein. The same detergent mixture was used in the presence and absence of FeoB protein. FeoB was solubilised in 0.01% NP-40. (20mM Tris pH 7.5, 150mM Nacl, 0.05% DDM). A SpectroLight 610 (XtalConcepts GmbH, in Hamburg, Germany) instrument was used for in situ DLS at 293 K. Sample volume was 2 µl in a 72-well Terasaki plate (Hamburg, Germany), and samples were shielded with paraffin oil. The radius distribution plots are presented as signal heat maps (blue, low particle concentration; red, high particle concentration). Samples were centrifuged just before DLS analysis.

11.7 Discussion

In order to allow functional and structural studies, the FeoB protein was overexpressed, using the pTriEx vector, in various forms: with a C-terminal His_6-tag; with an N-terminal His_6-tag; with a Flag-tag; and without any tags. Overexpression was achieved in insect cell culture, but no expression was obtained in *E. coli*. Upon expression of recombinant FeoB in insect cells, maximum production of protein occurred 3-4 days after transfection. SDS-PAGE analysis of the recovered lysates revealed a band (70-80 kDa) corresponding in size to FeoB for all four recombinant forms of FeoB. Anti-His western blot analysis confirmed FeoB expression for the His-tagged forms. FeoB was produced in sufficient quantity to allow purification of the two His-tagged forms to proceed. Two steps have so far been utilised to achieve purification of the two His-tagged forms, nickel-based metal-affinity chromatography and analytical SEC. A concentration of ~0.39 (HisTag-FeoB) and ~0.32 mg/ml (FeoB-HisTag) of FeoB was obtained (Bradford assay) giving 7.8 and 8 mg of total FeoB protein, respectively, after Ni^{2+}-affinity chromatography. After concentration, ~1.7 mg/ml of HisTag-FeoB and 2.3 mg/ml of FeoB-HisTag protein were obtained. The detergents Tween 20 and NP-40 was used to solubilise the FeoB proteins, but further work is needed to examine solubility and aggregation characteristics in other detergents (e.g. MNG, DM or DDM), to permit high concentrations to be achieved and improve purification of the non-aggregated forms for crystallisation trials

SEC and DLS analysis indicated that the NP-40 solubilised FeoB proteins are largely present in aggregated form, and thus not suitable for crystallisation trials. However, SDS-PAGE analysis revealed one major band at ~70 kDa for the isolated FeoB His-tagged protein that appeared to be relatively pure (no other major bands apparent). The apparently low MW (~70 kDa rather than the expected ~83 kDa) as determined by SDS-PAGE likely reflects the higher electrophoretic mobility of integral-membrane proteins (Rath et al., 2009).

Chapter 11: Overexpression of FeoB

In the next chapter, purification of FeoB-HisTag is optimised and a suitable detergent identified to enable sufficient protein isolation in non-aggregated form for crystallisation.

Chapter 12: Expression, Purification and Crystallisation of FeoB

12.1 Introduction

The linking points between the cell and the outside are provided by membranes which can be considered to have a key role in an extraordinary number of cellular processes, including the contact of the cells with other cells or adhesion surfaces, the transport of ions and small molecules, energy transduction, catalysis signalling and intra-and extracellular enzymes. Up to a third of genes generate membrane proteins but in most cases their protein structures remain undetermined. High-resolution structures are poorly represented for membrane proteins compared to soluble proteins (approximately a 1:100 ratio) (Berman *et al*., 2003). This is because membrane proteins are normally considered to be much more difficult to produce than their soluble counterparts resulting in a severe imbalance in structure solution (Bill *et al*., 2011). A huge effort in the field of membrane protein structures is focussed on different genetic constructs and conditions in order to produce higher expression levels and more stable, pure and properly folded proteins (Rawlings, 2016). Because of this, membrane protein structure projects are considered expensive and very time-consuming to follow, especially for small laboratories. The detergent choice is crucial for the preparation of membrane proteins. Several detergents are suitable for membrane protein solubilisation, allowing for the determination of the best detergent for keeping a protein monodispersed and stable or to permit the protein to form crystals (Loll, 2014). A medium- or large-scale protein preparation to screen for the right detergent for a particular protein is normally made one detergent at a time (Tulumello and Deber, 2012). The protein is then run within a test to assess its stability, homogeneity and multimeric state using size exclusion chromatography (SEC) and polyacrylamide gel electrophoresis before starting to subject it to crystallisation trials or for cryo-EM preparation

or for biochemical studies (Moraes *et al*., 2014). The detergent can be exchanged if the protein does not crystallise in the solubilisation detergent, and this is frequently done for one with a smaller micellar size which raises the chance of forming a crystal contact (Ai and Caffrey, 2000). The detergent used for crystallisation is less important for lepidic cubic phase (LCP) crystallisation (Moraes *et al*., 2014), as throughout the meso-crystallisation trials, the protein is stripped of most of its detergents upon entering the cubic phase. However, some of the more common detergents have been demonstrated to negatively impact LCP, triggering swelling in the phase structure and in the formation of the lepidic sponge phase. Screening for detergents that solubilise a protein well and that can still be kept at a low concentration with only slight adverse effects on the LPC itself are, therefore, of utmost significance in meso crystallisation. With the introduction of the direct electron detector and the "resolution revolution", cryo-electron microscopy is currently gaining popularity for solving the structures of proteins and protein complexes at a high resolution (Caffrey, 2015). The choice of detergent plays a vital function in gaining a homogenous sample that is suitable for data collection. Furthermore, the capacity to quickly screen for suitable expression and purification conditions for membrane protein complexes or a membrane protein significantly raises the chances of success. To increase the rapidity of the tedious, iterative procedure of obtaining a reliable protocol for the preparation of a particular target protein, several strategies have been actively used to monitor the quality of membrane proteins (Hahn *et al*., 2016; Fiedorczuk *et al*., 2016).

In one study, a modified GFP molecule, folding reporter GFP, was C-terminally joined to a set of globular proteins to allow for the monitoring of protein folding. The amount of GFP fluorescence was demonstrated to be roughly related to whether or not the N-terminally attached protein was suitably folded or not. In addition, the GFP moiety was only be fluorescent when the fusion protein was suitably inserted into the plasma membrane (Waldo *et al*., 1999). Another study illustrated that a membrane protein that showed a GFP fusion as a single

symmetric peak in a fluorescence-detection size exclusion chromatography (FSEC) trace is likely to perform satisfactorily in subsequent crystallisation experiments. The FSEC analysis of the protein can be accomplished on detergent-solubilised membranes without the extensive purification that is required for the other types of detection. Folding reporter GFP has since been used to screen many membrane proteins targets to move them onto crystallisation trails, as well as to determine the dimensional topologies for *E. coli* membrane proteins (Kawate and Gouaux, 2006).

The screening protocols used here allowed a number of conditions to be tested simultaneously and rapidly, and for optimisation of the purification of the target protein is suitable form. Thus, guided by the screening data, large-scale purification was accomplished of a high-quality protein sample suitable for crystallography trials.

12.1.1. Membrane proteins

Although, membrane proteins constitute an important part of cellular membranes, more significantly they play a crucial role in numerous physiological processes such as energy transduction in respiration, photosynthetic systems and transport. They construct up to 30% of the total proteome of most organisms (Heijne, 2006) and they are of significant theoretical interest, comprising in excess of 60% of known drug targets (Yildirim *et al*., 2006; Anderson *et al*., 2011).

Membranes proteins form a permeability barrier, regulating the passage of substances across the membrane. They are permeable for gases such as oxygen (Al-Awaqati, 1999). Membrane proteins are essential for cell function by not only controlling the transportation of nutrients and metabolites but also by maintaining the ionic balance in the cells and thus the electric potential, thereby controlling the pH (Pohorille *et al*.,2005).

Membrane protein expression and purification mostly requires solubilisation in detergents (Helenius and Simons, 1975; Aronld and linke, 2008). Detergents are water-soluble amphiphilic surfactants with a polar or ionic headgroup and a non-polar tail that self-associate into spherical assemblies in aqueous solutions above a threshold concentration. This is referred to as the critical micellar concentration (CMC). They can be (1) non-ionic, (2) ionic, meaning that they have a charged head-group or (3) zwitterionic (Seddon *et al*., 2004; Prive, 2007). Non-ionic detergents, such as Triton X-100 and DDM, are typically milder (less-denaturing) than ionic detergents such as SDS. Zwitterionic detergents, such as CHAPS and LDAO, combine the properties of ionic and non-ionic detergents, and can thus be beneficial in the initial membrane solubilisation steps (Table 12.1). Short-chain detergents (e.g. OG, n-octyl-β-D-maltoside) are typically more denaturing than their longer-chain counterparts (e.g. DDM). DDM and Triton X-100 are most widely used in membrane protein research because of their relative mildness, allowing for the retention of biological function. They are often used in combination with lipid or cholesterol-like additives (e.g. cholesteryl hemisuccinate, CHS) in mixed detergent-lipid micelles (Seddon *et al*., 2004; Thompson *et al*., 2011). Detergents can be removed through a variety of methods such as gel filtration, dialysis and adsorption, and even through polystyrene beads (e.g. Bio-Beads) (Arnold and Linke, 2008; Rigaud and Levy, 2003). The first two methods work best for high CMC detergents, while the last is more generally applicable. One of the best fundamental physical characteristics of a detergent is the critical micelle concentration (CMC) (Helenius *et al*., 1979; Rosen, 2004). The critical micelle concentration provides the minimum amount of detergent monomers needed to form a micelle in the buffer (Helenius *et al*., 1979). The amphipathic character of the detergent monomer limits its solubility and the formation of micelles is driven by the hydrophobic effect at concentrations above the CMC (Neugebauer, 1990; Privè, 2007). The micelle detergent concentration can be detected as the total detergent concentration minus the CMC (Anatrace, 2008). The CMC is

powerfully influenced by the length of the alkyl tail group. The CMC is, for most detergents, inversely proportional to the temperature, increasing with a decrease in temperature (Anatrace, 2008). A variety of techniques can be used to measure the CMC of a detergent, such as light scattering or even by the measurement of surface tension (Mittal, 1972).

Table 12.1: Detergents used in this research (Stetsenko and Guskov, 2017)

Type	Detergent	Aggregation Number	Micelle size [kDa]	CMC [%]	Mw (Da)
Ionic	SDS	50-80	18	0.075	288
Non ionic	DDM	78–149	70	0.075	510.6
Zwitter ionic	LDAO	70	17–21	0.023	229.4
Zwitter ionic	Fos-Choline12	108	47	0.005	-
Zwitter ionic	MNG	-	-	0.001	1005.19
Zwitter ionic	DM	69	40	0.087/1.8	482.6
Zwitter ionic	UDM	71	50	0.029/0.59	496.6

Zwitter ionic	OG	30–100	25	0.53/20	292.4
Zwitter ionic	CHAPSO	11	7	0.5/8–10	630.9
Zwitter ionic	CYMOL	91	32	0.028/0.56	508.6
Zwitter ionic	C12 E8	90–120	66	0.005/0.09	538.7
Nonionic	NP-40	149	-	0.29	617
Nonionic	TRITON	60–90	75-165	0.01/0.2	624.8

12.1.2 Structural biology of membrane proteins

Protein function mechanism can be investigated through a knowledge of its three-dimensional structure. Achieving a detailed picture of a protein at an atomic level is possible via the analysis of diffraction images from X-rays passing through identical protein molecules within a crystal matrix. X-ray crystallography is considered today to be the most successful method for the structural determination of proteins. Nevertheless, the amphipathic nature of membrane proteins renders such proteins as the most difficult class of protein structures to solve. The first major success for a structure of a membrane protein was that of Deisenhofer and colleagues upon publication of the structure of the photosynthetic reaction centre (Deisenhofer *et al.*, 1985). Subsequently, a more than 200 unique membrane protein structures were obtained from their research (White, 2008; McLuskey *et al.*, 2009). X-ray crystallography relies on the

availability of well-ordered protein crystals and this is now possible with smaller amounts of protein via the improved use of high-throughput (HTP) methods and robotics for crystallisation trials, which means that current difficulties with membrane proteins generally arise through expression and purification. Generally, structural studies demand milligram amounts of pure and monodispersed membrane proteins (Carpenter *et al*., 2008). Considerable problems are encountered in the expression and purification of large amounts of stable membrane proteins; the difficulties in relation to membrane protein structure determination, from their expression and purification through to crystallisation, are indicated in the previous chapter and in the results below.

12.1.3 Classification of membrane proteins and their function

Membrane proteins can be classified as peripheral or integral membrane proteins, depending on their location within the membrane. Integral membrane proteins are amphipathic. They involve at least one hydrophobic membrane spanning segment and they can extend out of the membrane. They also involve hydrophilic parts within the polypeptide chain. Integral membrane proteins are linked with the membrane via hydrophobic interactions with the fatty acid tails of the lipids (Heijne, 2007). Peripheral membrane proteins do not extend into the hydrophobic bilayer and they are associated with the membrane mostly via non-covalent interactions with other membrane proteins or lipid head groups. They can be separated from the membrane using gentle extraction procedures, such as changes in the ionic strength of the solute or changes in the pH (Alberts *et al.,* 1983).

12.2 Aims of this chapter

In the previous chapter, FeoB was successfully overexpressed from insect cells and isolated via Ni^{2+}-affinity chromatography, although the protein appeared to be largely in an aggregated, non-monodisperse state. The aim now is to identify detergents that provide sufficient amounts of FeoB in a monodisperse state that is suitable for crystallography, and then to generate diffracting crystals for structure solution.

12.3 Results

12.3.1 Construction and use of a FeoB-GFP fusion to assist determination of purification conditions

12.3.1.1 Introduction

In order to more easily explore the optimal conditions for solubilisation of FeoB, a FeoB-GFP-HisTag fusion was generated (12.3.2). The fusion was used, as described by others (McLuskey *et al*., 2009), to more readily monitor the monodispersed nature of FeoB in a range of detergents, using a fluorescent-detection size-exclusion chromatography (FSEC) approach (Sjostrand *et al*., 2017).

12.3.1.2 PCR amplification of *feoB*-eGFP-HisTag

Cloning was performed using the In-Fusion® HD Cloning Kit (Clontech Laboratories) and PCR was with High-Fidelity HIFI DNA polymerase. Primers FWD-FeoB and Rev-Histag-FeoB (with *E. coli* chromosomal DNA as template), and FWD-eGFP and Rev-eGFP (with

pTriEx-eGFP as template) (Table 2.6), were used to generate *feoB* and eGFP fragments of 2.8 and 0.7 kb, respectively (Fig. 12.1). These were then combined together and used as templated for 'overlap' PCR with pTriEx-FeoB_FWD and pTriEx-FeoB_Rev-eGFP-FeoB primers (Table 2.6) to generate a *feoB*-eGFP product of 3.5 kb (Fig. 12.2) suitable for cloning into pTriEx 1.1

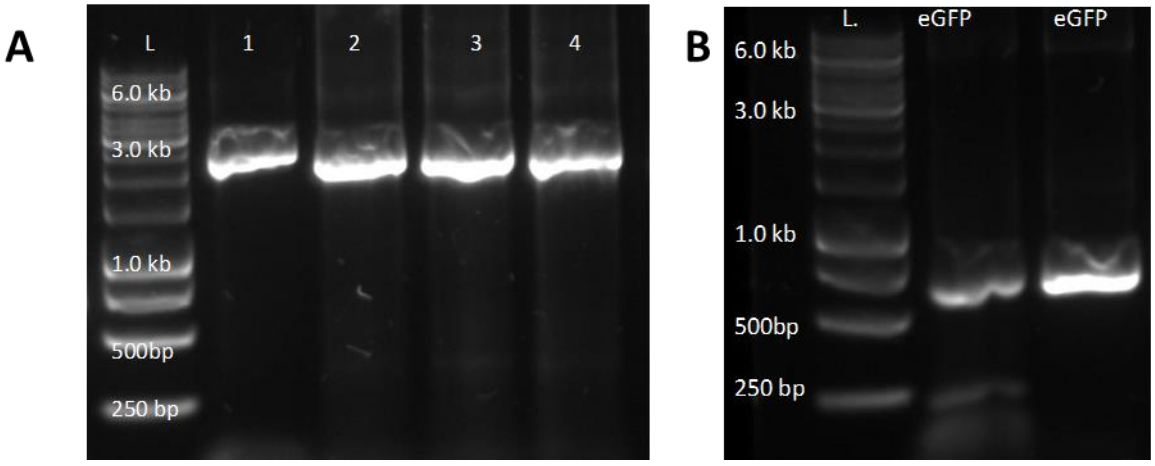

Figure 12.1: Gel electrophoretic analysis of *feoB* (A) and *eGFP* (B) PCR products. Electrophoresis was performed using a 0.7% agarose TBE gel. Lane L involved 1 µl GeneRuler® 1 kb ladder (Fermentas). **A**. Lanes 1-4, *feoB* PCR products. **B**. eGFP lanes are indicated.

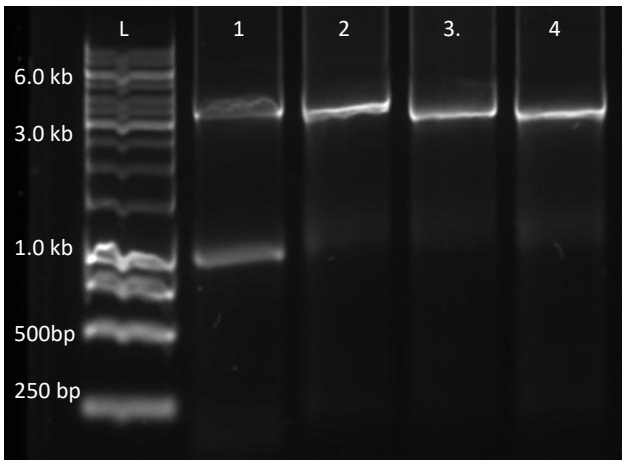

Figure 12.2: Gel electrophoretic analysis of the *feoB*-eGFP-HisTag fusion PCR product. Electrophoresis was performed using a 0.7% agarose TBE gel. Lane L involved a 1 µl GeneRuler® 1 kb ladder (Fermentas). Lanes 1, 2, 3 and 4 were the PCR products.

12.3.3 Cloning of *feoB-eGFP-HisTag* into pTriEx 1.1

The two PCR products were combined with of *Nco*I/*Xho*I-digested pTriEx 1.1 in an In-Fusion reaction. From the resultant Amp^R transformants in TOP10, 10 were subjected to plasmid 'miniprep' isolation Methods 2.21). The isolated plasmids were screened using agarose gel electrophoresis and five with mobilities matching that anticipated for the desired construct (equivalent to ~8.9 kb) were then analysed through restriction digestion with *Xho*I and *Nco*I to release any FeoB-eGFP-HisTag fragments from the vector. The digested samples were expected to give two bands of ~3.5 kb (insert) and ~5.3 kb (the vector), as was observed (Figure 12.3). The digested samples gave the expected sizes and thus they were sequenced by Eurofins using T7F and pTriEx reverse primers(Ian Lab). The sequences achieved were compared with the sequence database using BLAST. The results showed that the insert had the expected sequence with no errors. The plasmids were selected for further work and designed as pTriEx-*feoB*-eGFP-HisTag Fig. 12.4).

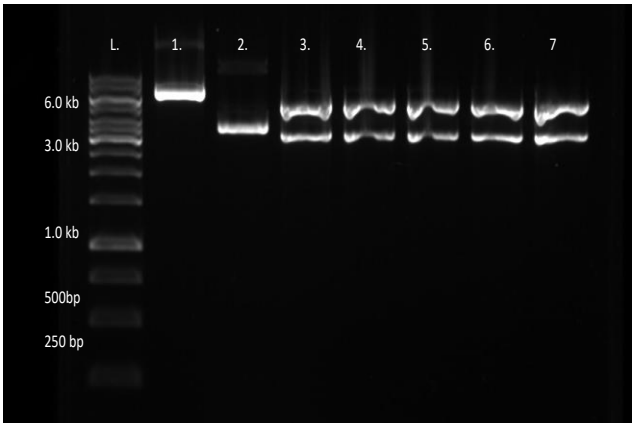

Figure 12.3: Restriction analysis of the pTriEx-*feoB*-eGFP-HisTag isolates. Plasmids were digested with *Xho*I and *Nco*I. Lane L was the GeneRuller® 1 kb ladder (Fermentas); lane 1 was pTriEx-*feoB*-eGFP-HisTag single digest, lane 2 was was pTriEx-*feoB*-eGFP-HisTag nondigested and lanes 3, 4, 5, 6 and 7 were double digested pTriEx-*feoB*-eGFP-HisTag (isolates 1-5).

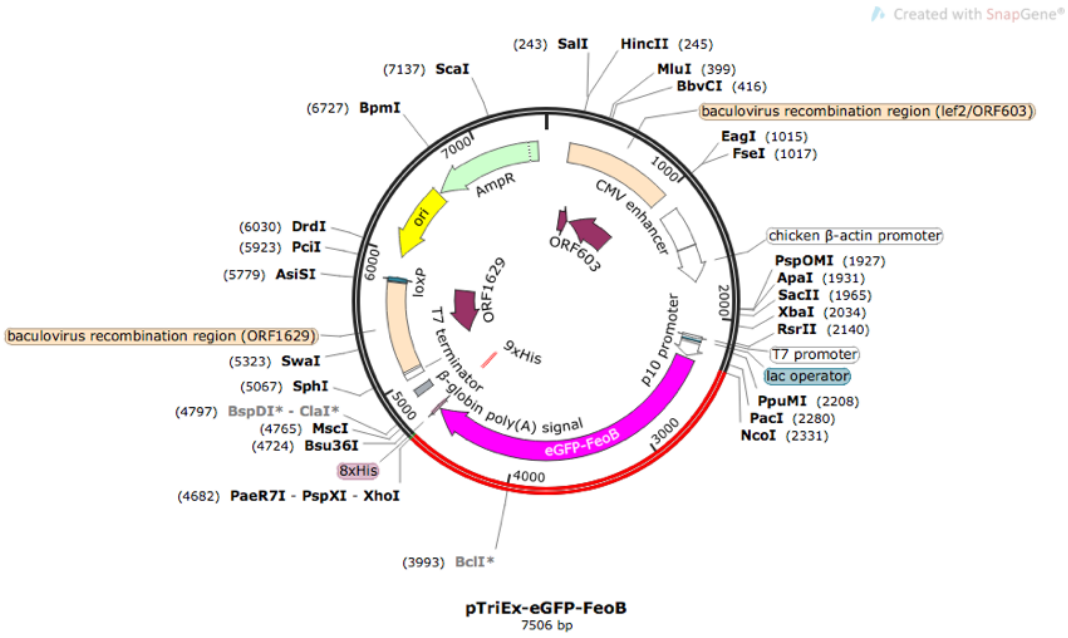

Figure 12.4: Map of pTriEx-FeoB-eGFP-HisTag. The FeoB-eGFP-HisTag sequence was inserted between the *Nco*I and *Xho*I sites (indicated) of pTriEx 1.1 to generate pTriEx-FeoB-eGFP-HisTag. Image generated using SnapGene.

12.3.4 Expression of FeoB-eGFP fluorescence in *E. coli* BL21/DE3

To confirm that a functional GFP fusion had been generated, the pTriEx-FeoB-eGFP-HisTag plasmid was introduced into the *E. coli* BL21/DE3 to allow eGFP fusion expression. The transformants were examined using confocal microscopy (Figure 12.5).

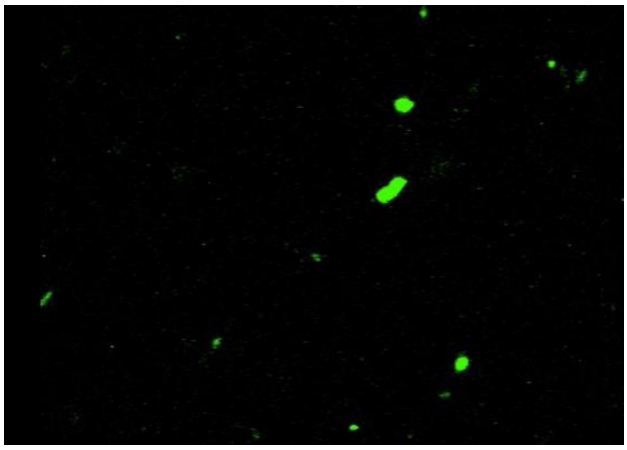

Figure 12.5: Confirmation of expression of fluorescence from pTriEx-*feoB*-eGFP-HisTag in *E. coli* BL21/DE3. Confocal microscopy was at 100 magnification using 515 nm excitation and 405-488 nm emission detection.

12.4 Generation of recombinant baculovirus

The above pTriEx-*feoB*-eGFP-HisTag was mixed with linear baculovirus DNA and transfected into *Sf9* cells (Figure 12.6A). The recombinant Bac/*feoB*-eGFP virus was amplified over a period of 6-7 days and collected from the supernatant of the transfected cells. This virus stock was stored or amplified as necessary to create a volume and titre sufficient for subsequent expression analyses. The cytopathic effect of Bacmid infection can be observed when infected insect cells are compared to those that are non-infected (Fig. 12.6).

12.4.1. Expression confirmation

To evaluate the potential of the insect cell system for FeoB-eGFP-HisTag expression, *Sf9* cells (~10^6) were infected with Bac/*feoB*-eGFP-HisTag. The cells were collected three days after infection. The cell pellet was harvested and examined using anti-His-tag Western blotting, which showed an immune-reactive protein of the expected size (Fig. 12.7).

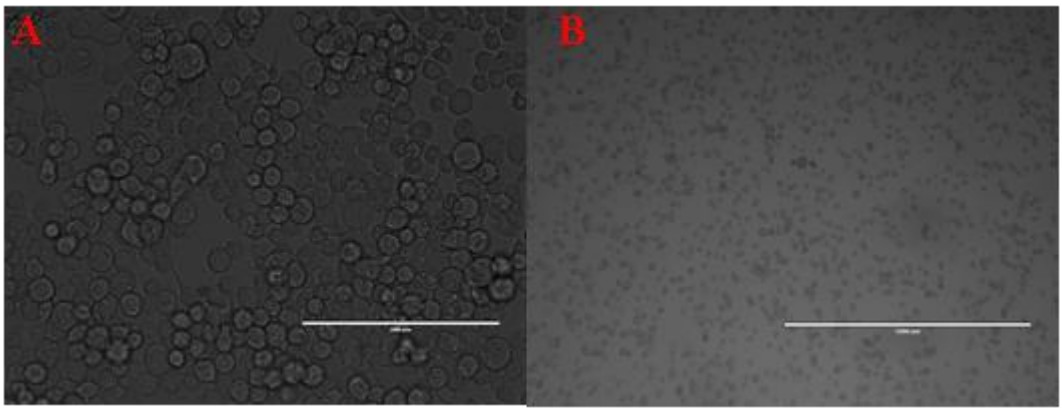

Figure 12.6: A: *Sf*9 Bac/*feoB*-eGFP-HisTag infected cell B: *Sf9* insect cells non-transfected cell controls. White bars indicate 400 and 1000 nm scales, respectively.

12.4.2 Detection of FeoB-eGFP-HisTag expression in transfected insect cells

Western blotting with anti-His antibody was used to identify the presence of the FeoB-eGFP-HisTag within the infected insect cells. The infected insects were subjected to small-scale overexpression followed by western blotting, which showed an immunoreactive band of the expected size, confirming that expression had been achieved (Fig. 12.7).

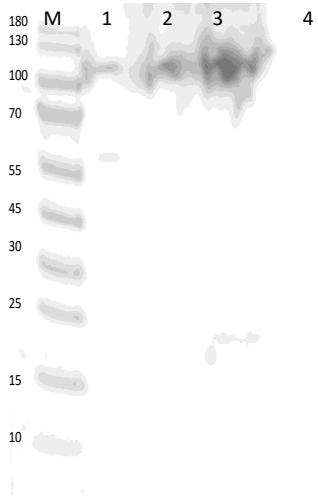

Figure 12.7: Western blotting confirms the expression passage (1, 2 and 3) of the BAC-MED virus fusion *feoB*-eGFP-Histag transfected into S*f9* cells. Western blotting analysis was conducted focused

on the insect cells infected with a Bac/*feoB*-eGFP-HisTag. Lane M, protein molecular weight markers (kDa). Lane 1-3, passage 1-3 lysates from the infected insect cells. Lane 4, the non-infected cells.

Figure 12.8 shows the different passage transfection results for the *Sf9* cells carrying Bac/*feoB*-eGFP-HisTag that were used to prepare virus stocks for the next step of infection. The images shown the expression of the eGFP fusion at all three stages (passage 1 to 3).

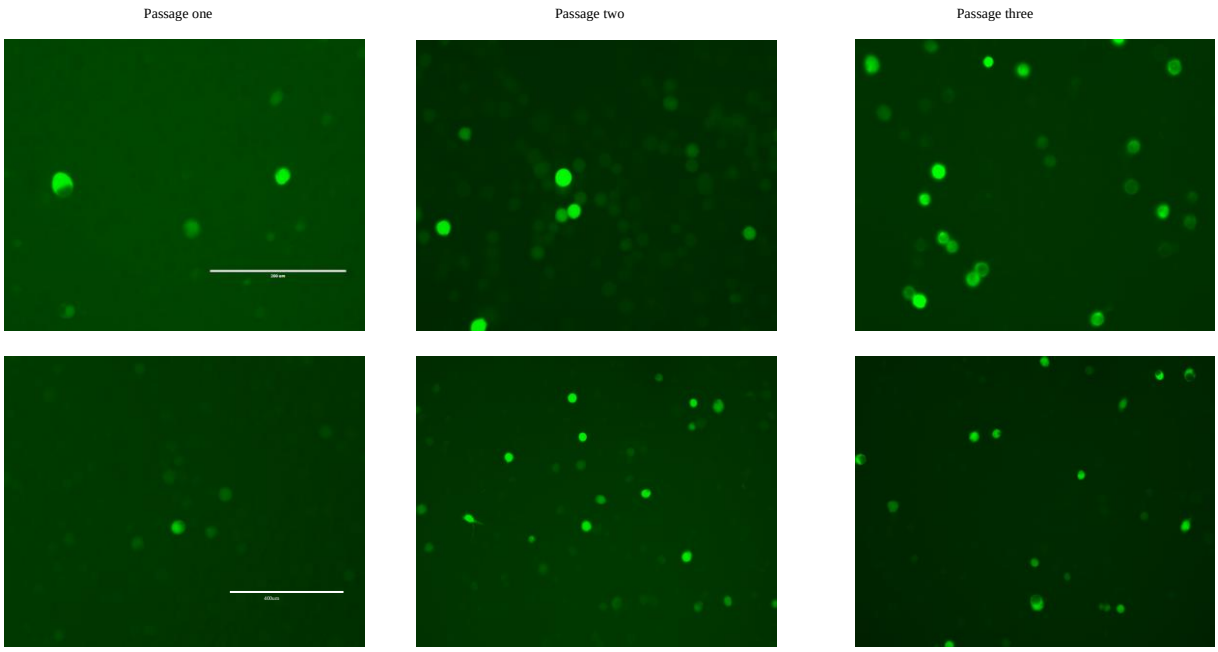

Figure 12.8: Sf9 cells following co-transfection with baculovirus/pTriEx-*feoB*-eGFP-HisTag. The transfection is indicted by the green fluorescence of the insect cells. An inverted wide-field epifluorescence microscope (Olympus IX81) was used equipped with a 488 nm laser for the excitation of the GFP and a 561 nm laser for the excitation of the mCherry.

12.5. Comparison of the expression of eGFP-*feoB*-HisTag in *Ao*38 and S*f*9

Two well-known cell lines, *Ao*38 and *Sf*9, were tested for their relative capacity to expressed *feoB*-eGFP-HisTag. *Ao*38 cells were originally isolated from eggs of the black witch moth (*Ascalapha odorata*) and are highly effective protein expression hosts (*Ao*38, a new cell line

from eggs of the black witch moth, *A. odorata* (Lepidoptera: Noctuidae), is permissive for AcMNPV infection and produces high levels of recombinant proteins (Hashimoto *et al*., 2010).

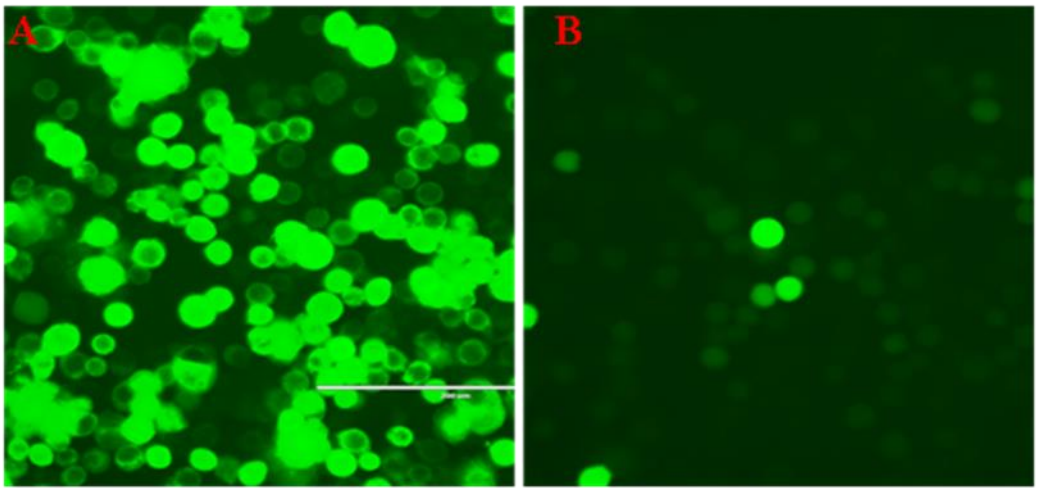

Figure 12.9: Expression of eGFP-FeoB in insect cells line at 72 h post infection. Cells are infected with Bac/pTriEx-eGFP-*feoB* (10% virus infection at a ratio 1/10 inocula/culture). **A**. *Ao*38. **B**. *Sf*9 cells.

Figure 12.9 & 12.10 illustrate the comparison of expression in the two different cells line as visualised by florescent microscopy. The eGFP signal was considerably stronger in the *Ao*38 cells compared with the *Sf9* cells. This indicates a considerably greater *feoB* expression and suggests that *Ao*38 cells should be used in future work for small-scale expression and large-scale expression.

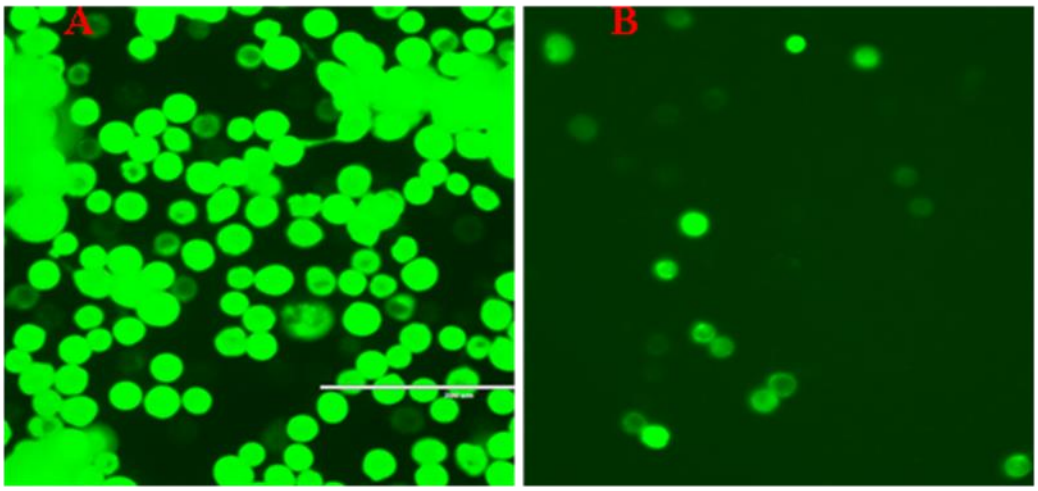

Figure 12.10: Expression of eGFP-FeoB in insect cells line at 72 h post infection with a 5% virus infection. A. *Ao*38; **B**. *Sf*9. Other details are as above.

Western blot analysis of baculovirus infection and expression in infected *Ao*38 and *Sf*9 cells using anti-gp64 anti body confirmed the presence of the 64 kDa protein and thus demonstrated virus infection in both cells lines at similar levels (Fig. 12.11).

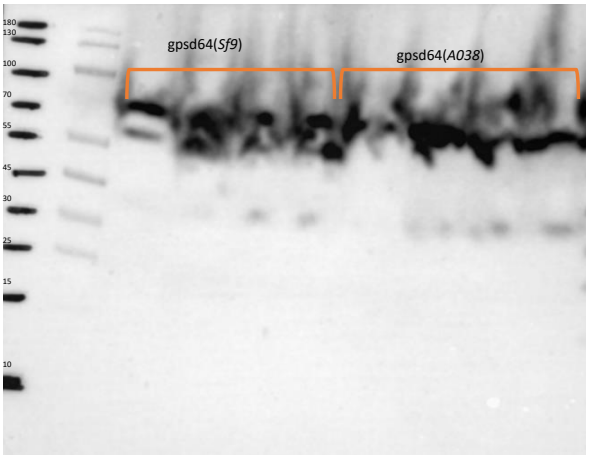

Figure 12.11: **Confirmation of infection with a recombinant baculovirus through anti-gp64 western blot analysis of insect cells.** Lane M, protein molecular weight markers (kDa). Other lanes contain lysates of insect cells (*Sf*9 or *Ao*38) infected by the Bacmid(pTriEx-*feoB*-eGFP-HisTag).

Figure 12.12 shows the comparison of the expression of FeoB-eGFP-HisTag in the two cell lines - *Ao*38 and *Sf*9 – through anti-His western blotting. A band of the expected mass is observed clearly in the *Ao*38 extracts that shows far greater intensity than that obtained for *Sf*9 cells. This confirms the fluorescence microscopy data above indicating that *Ao*38 gives far higher FeoB-eGFP-HisTag expression levels than *Sf*9 cells.

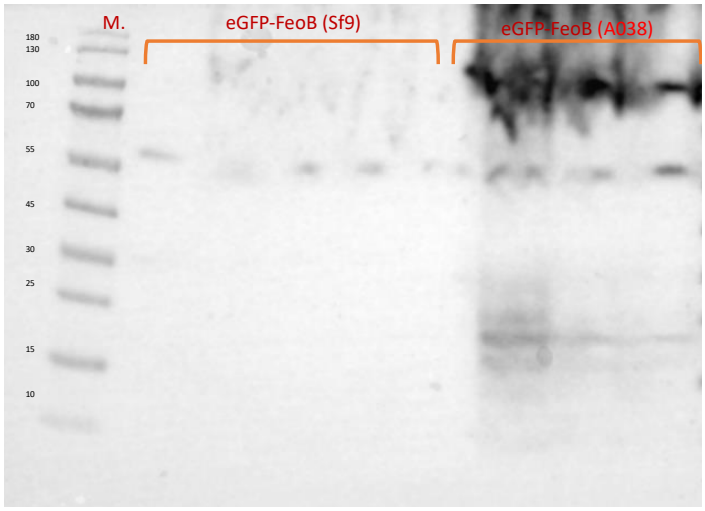

Figure 12.12: **Compression of *feoB*-eGFP-HisTag expression in *Ao*38 and *Sf*9 cells through anti-His western blotting.** Lane M, protein molecular weight markers (kDa). Other lanes contain lysates of insect cells (*Sf*9 or *Ao*38) infected by Bacmid(pTriEx-*feoB*-eGFP-HisTag). The location of FeoB-eGFP-His tag is at around 100 kDa.

12.6. Small-scale high-throughput detergent solubilisation screen

The main parameters involved in expression are the employed construct, host cells, media and temperature. The FeoB membrane protein target has been cloned and strong overexpression in *Ao*38 cells established. This leaves the latter two parameters to be tested.

12.6.1. The detergents used for the solubilisation of FeoB

To purify a membrane protein, it has to be isolated from its native membrane. Membrane proteins can be solubilised with the help of detergents (Helenius *et al.*, 1979). The solubilisation process incorporates a critical solubilisation concentration (CSC) that dictates the minimal amount of detergent needed to disrupt the membrane assembly into a state that it is dominated by the existence of micelle-protein complexes (Privè, 2007). The CSC depends on the parameters of the solubilisation, particularly the lipid content.

The CSC is reliant on temperature and reduces with a higher temperature. However, the instability of membrane proteins requires work at lower temperatures, normally 4 °C (Seddon *et al*., 2004). In cases where the CSC is reached, a change in the turbidity of the solution can be seen. Once the membrane protein is solubilised, a typical rule of thumb is to work with detergent concentrations of at least twice the CMC in solution (Anatrace, 2008). However, the solubilisation of the membrane protein may need far higher detergent specific concentrations. A detergent to lipid ratio of at least ten to one is recommended (Anatrace, 2008). The non-ionic detergent DDM is a mild detergent with a long alkyl chain and a CMC of 0.009%, but it needs to be added to a final concentration of 1.5 % to be effective (Privè, 2007). DDM is a good initial starter for solubilisation and purification of membrane proteins as it has been used in many successful crystallisation trials yielding membrane protein crystals (Privè, 2007).

Zwitterionic detergents are normally intermediate between the ionic and the non-ionic detergents in terms of mildness. Both positive and negative charges are present in their head-groups such that they are electrically neutral. For example, lauryldimethyl amine oxide (LDAO) was used effectively in the structural characterisation of the photosynthetic reaction centre (Deisenhofer *et al*., 1985) and the external membrane complex BtuB: TonB (Shultis *et al*.,

2006). Dodecylphosphocholine (Fos-Choline 12) is also a zwitterionic detergent that has been used successfully in membrane protein structure determination (Hwang *et al*., 2002; Oxenoid and Chou, 2005).

The physical properties of all detergents of relevance are presented in Table 1.1. The different options of detergent for membrane protein purification is often a compromise between solubilisation efficiency and protein stability (Seddon *et al*., 2004). By ensuing the solubilisation of the target, purification can then commence.

The purification of the FeoB membrane proteins can employ the same established techniques as those developed for soluble proteins, such as ion exchange, affinity and size exclusion chromatography. However, the detergent often influences the effectiveness of these methods by, for example, interfering in the binding of the protein purification tags to columns or by changing their elution patterns. Instability leading to precipitation is often encountered, making a change of purification techniques necessary. As indicated in the previous chapter, the monodispersity of a membrane protein sample, which can be estimated through analytical gel filtration or dynamic light scattering, is crucial when it comes to allowing the formation of well-ordered single crystals that are necessary for protein crystallography.

12.6.2. Fluorescent-detection Size-Exclusion Chromatography (FSEC)

FSEC was used for rapid microscale solubilisation and affinity purification in order to be able to rapidly assess whether the FeoB membrane protein is in a suitable form for use in structural studies. Twelve detergents from three family groups were used, with varying sizes and head chemistry groups, for comparative purposes table above (Table 12.1).

For the screening trials, the FeoB-eGFP-HisTag protein was expressed from pTriEx1.1 in *Ao*38 cells.

The aim of the FSEC analysis was to discover protein-detergent combinations that render strong, sharp fluorescence peaks, without the presence of large molecular weight aggregation products. The samples should maintain such properties after the IMAC purification process.

FSEC analysis (Shimadzu and conditions used e.g. vols, flow rates, sample size) was implemented on cell lysates solubilised in a range of detergents (Figure 12.13) and shows that nine detergents solubilised the protein to give an apparently mono-disperse form, with only one detergent failing to generate solubilised and non-aggregated FeoB-eGFP-HisTag (OG, Fig. 12.13 & 12.14). The FeoB-eGFP-HisTag protein showed good elution characteristics with UDM, DM, DDM and MNG – which relatively high levels of mono-disperse protein observed and low levels of aggregated protein. Generally, DDM and MNG gave particularly favourable profiles (Fig. 12.13). In addition, these two detergents gave good solubilisation yields by western blot and SDS-PAGE analyses (Fig. 12.14). The protein solubilised in the longer-chain versions (DDM/MNG) exhibited sharper and higher peaks with less evidence of free eGFP and aggregate and so these two detergents were selected for further work.

It has been noticed previously that the GFP moiety may be cleaved during the protein purification process (Kawate and Gouaux, 2006; Tarry *et al*., 2012), as observed here in most cases, and particularly strongly with LDAO (Fig. 12.13).

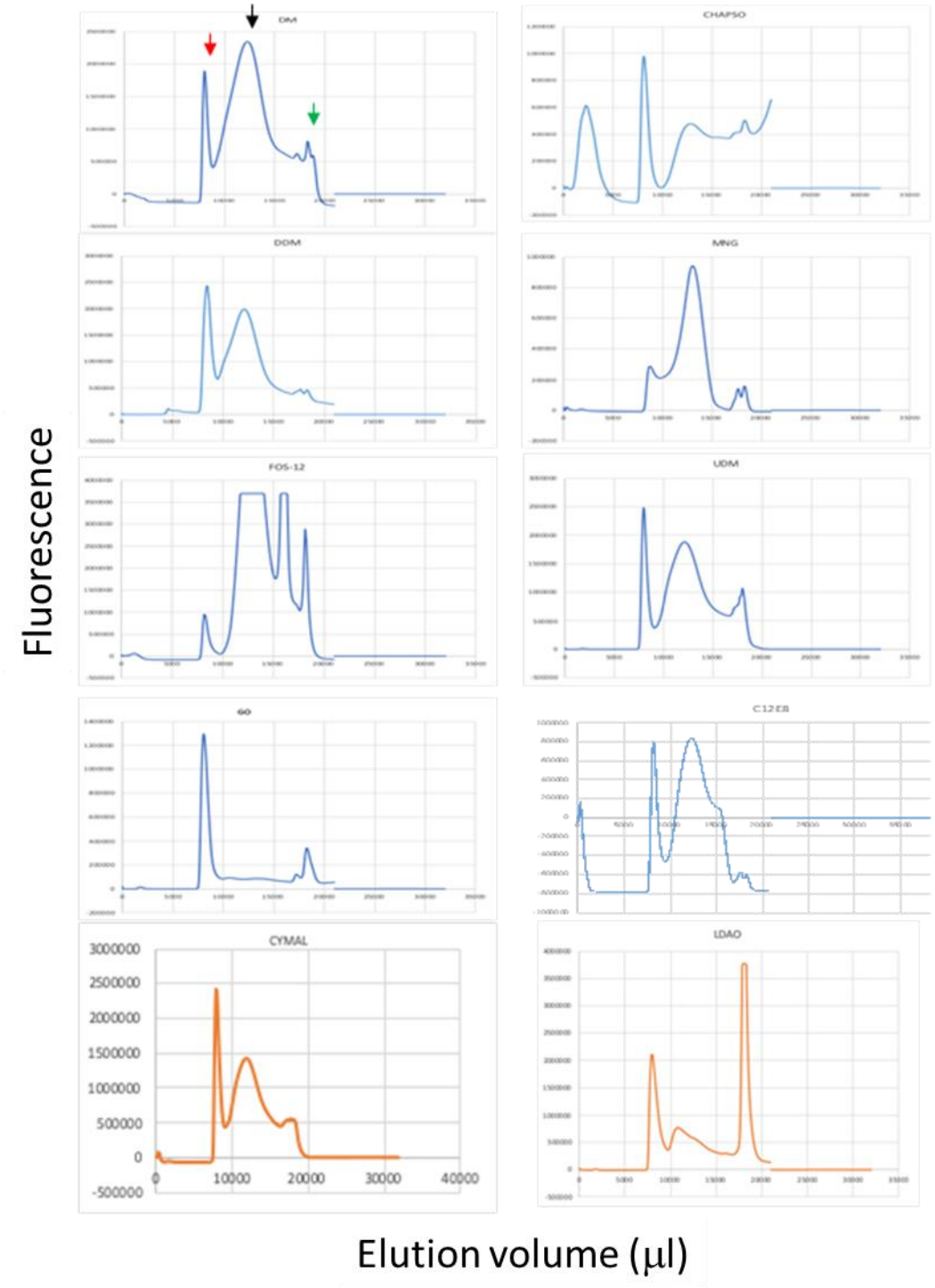

Figure 12.13: FSEC analysis of FeoB-eGFP-HisTag from crude lysates in a range of detergents. Each graph shows the FeoB protein in one family of detergents. The red arrow indicates an aggregation product at <10,000 µl, the black arrow shows the non-aggregated FeoB-eGFP-HisTag protein at 10,000-15,000 µl and the green arrow shows the free GFP at 15,000-20,000 µl. The Y-axis shows the fluorescence intensity. The profiles with NP-40 and Triton-X-100 are shown in Fig. 12.17. The buffer used was: 1x PBS, protein inhibitor, 2 mM DNase, 2 mM $MgCl_2$, with the indicated detergent. Samples were incubated in detergent for 2 h prior to FSEC.

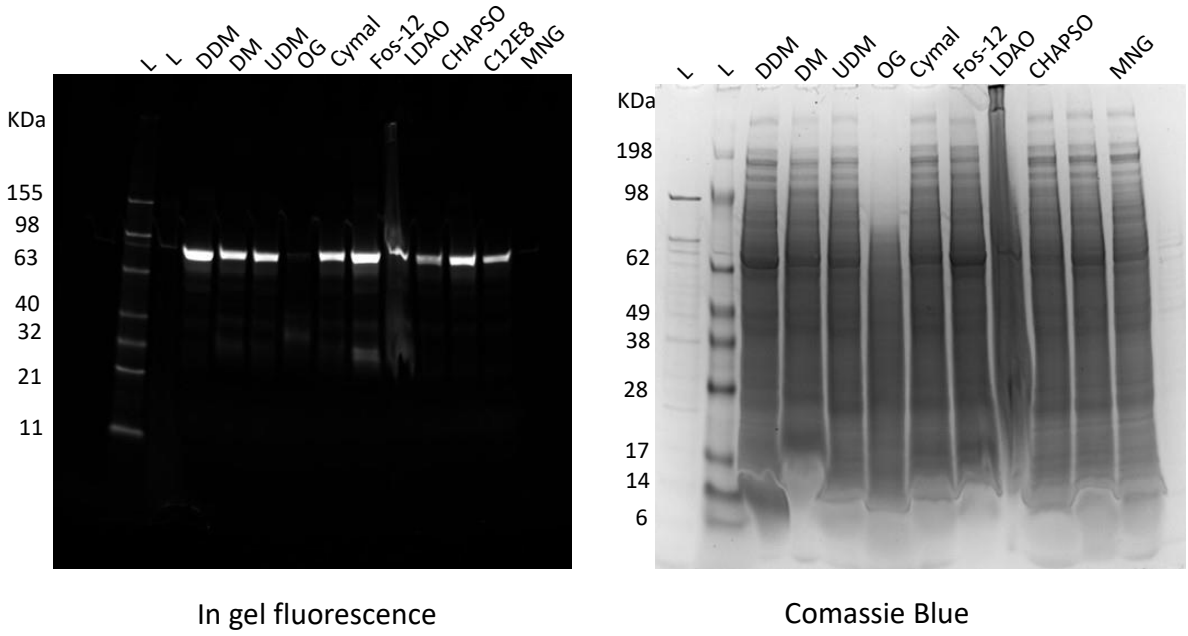

Figure 12.14: SDS-PAGE analysis of FeoB-eGFP-HisTag solublisation in a range of detergents. Samples were from the solubilized proteins analysed by FSEC in Fig. 12.12. Screening of Integral Membrane Proteins (eGFP-FeoB) using the detergents indicated.

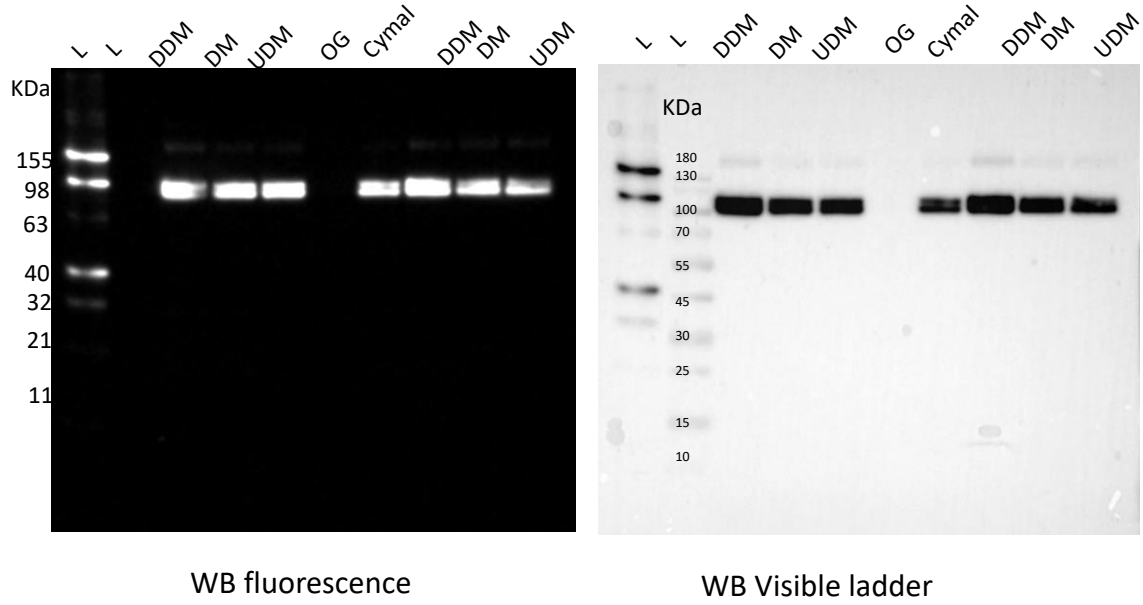

Figure 12.15: Western blotting analysis of FeoB-eGFP-HisTag solubilized in detergents. Samples were from the solubilized proteins analysed by FSEC in Fig. 12.12.

12.7 Effect of incubation time on detergent solubilisation

In order to determine the effect of detergent-solubilisation incubation time, the FSEC analysis was repeated following insect-cell sample incubation for 2, 4 or 16 h in running buffer (1x PBS with 0.03% DDM) (Figures 12.16 & .18-19). The results show that incubation time has relatively little impact on the elution profiles and that 2 and 4 h are suitable times for solubilisation for both detergents, since little improvement is seen upon overnight incubation.

The cheaper detergents, as used in the first trial expression in Chapter 11 (NP-40 and Triton X-100), were also tested as these could be useful for the initial solubilisation as a cost-saving option (Figs 12.17-19).

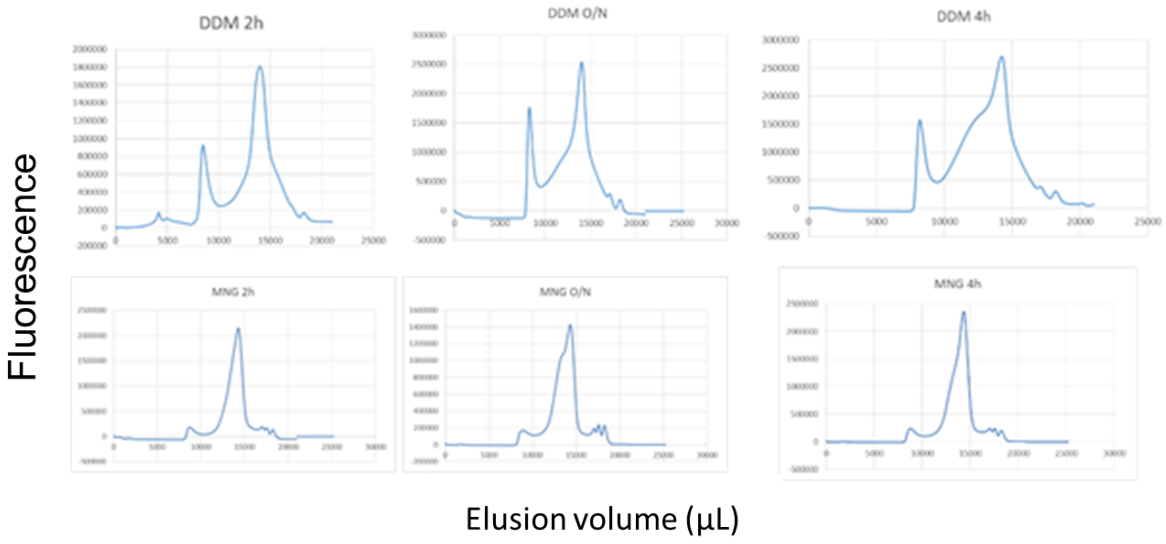

Figure 12.16. FSEC chromatograms for FeoB-eGFP-HisTag solubilised in MNG and DDM for different incubation times. The effect of time of incubation on the aggregation state of FeoB-eGFP-HisTag is shown after 2, 4 and 16 h incubation.

The results show that both detergents are effective at generating FeoB-eGFP-HisTag in a form where there is a substantial fraction of protein soluble and in non-aggregated form. Thus, either detergent could be used for initial purification provided that the purified protein is subsequently transferred to a detergent more suitable for crystallisation.

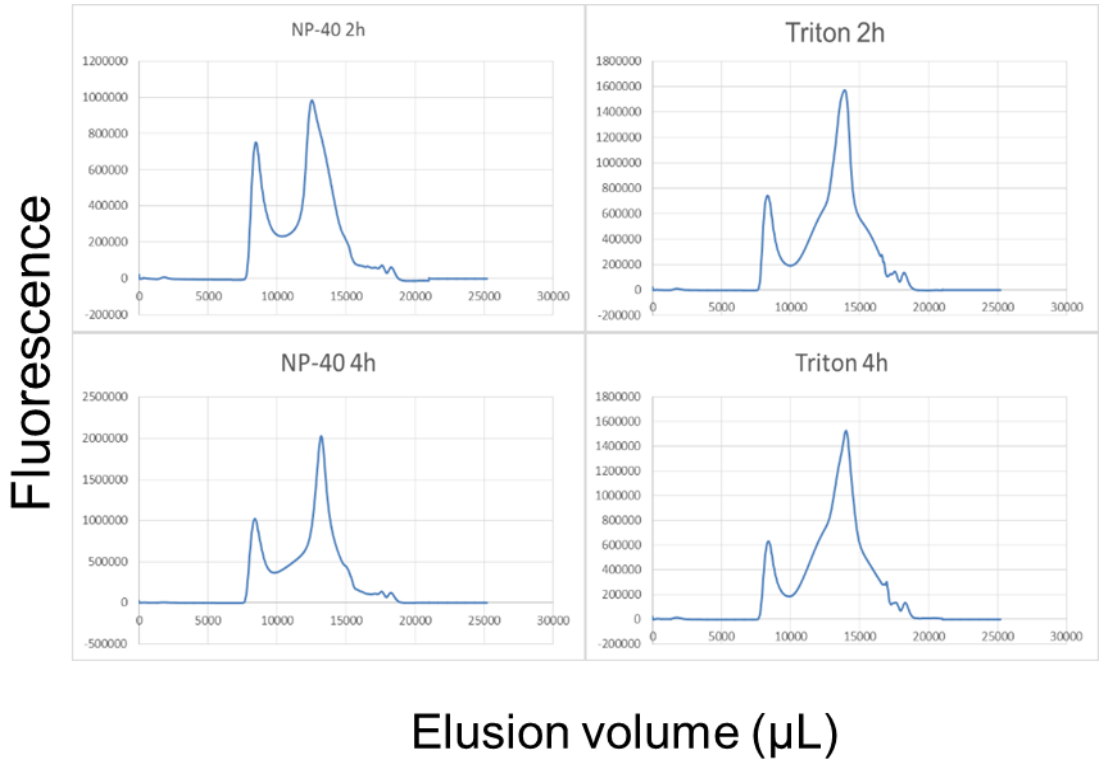

Figure 12.17: FSEC chromatograms for FeoB-eGFP-HisTag solubilised in ND-40 and Triton X-100 for different incubation times. The effect of time of incubation on the aggregation state of FeoB-eGFP-HisTag is shown after 2 and 4 h incubation.

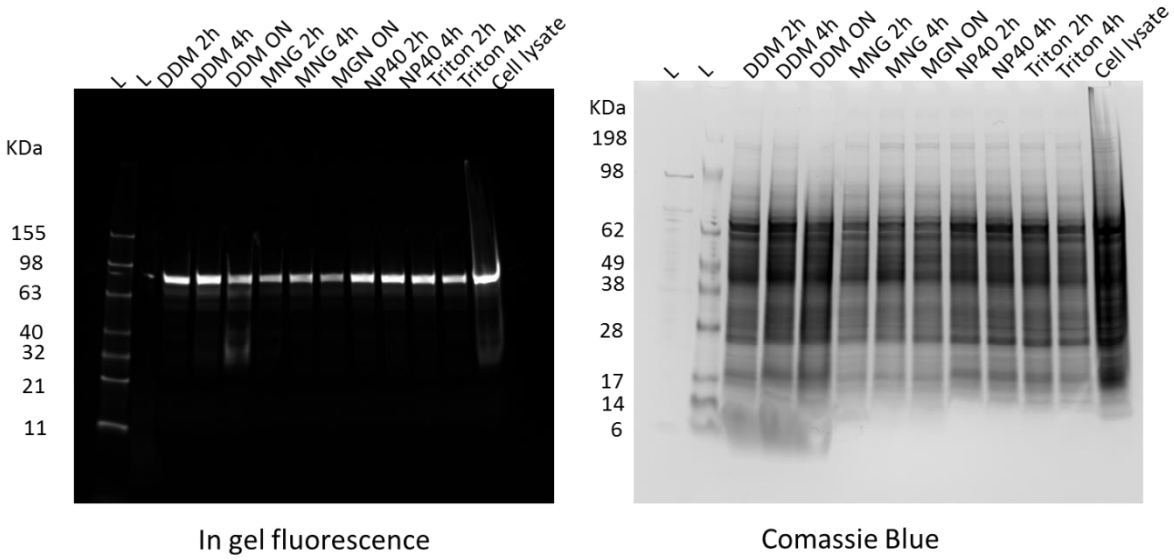

Figure 12.18: SDS-PAGE analysis of FeoB-eGFP-HisTag detergent solubilisation at different time points.

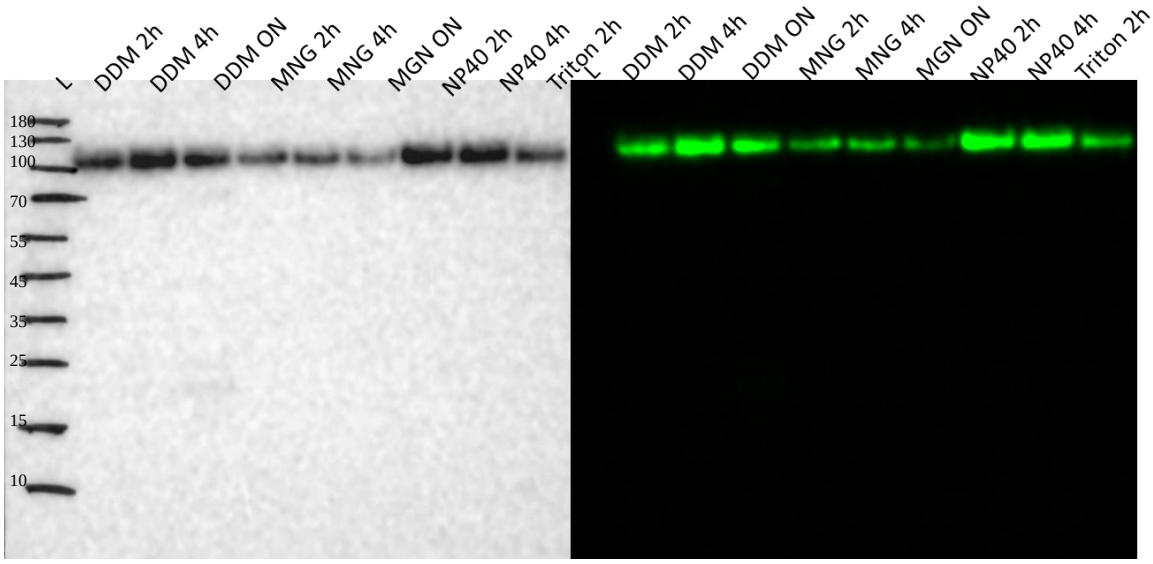

Figure 12.19: Anti-HisTag western blotting analysis of FeoB-eGFP-HisTag detergent-solubilisation at different time points.

12.8 Small-scale purification of FeoB-HisTag from *Ao*38 cells

12.8.1 Purification in DDM by IMAC

The screens above determined the optimal expression and solubilisation conditions for the FeoB-eGFP-HisTag protein in *Ao*38, which were subsequently used for the FeoB-HisTag protein, as generates from 1000 ml *Ao*38 cultures. The infected *Ao*38 cells were lysed in 1% DDM (50 mM Tris pH 7.5, 150 mM NaCl, 1 mM $MgCl_2$, 1% DDM**)** and the soluble supernatant prepared by centrifugation at 100,000 g for 1 h, at 4 °C (Methods 2.31.10). The supernatant (~100 ml) was filtered (0.2 µm pore) and applied to a Ni^{2+}-NTA-column (5 ml) (Methods 2.31.11). The column was rinsed in two steps using rinse buffer 1 (50 mM Tris pH 7.5, 150 mM NaCl, 30 mM imidazole, 0.03% DDM) followed by rinse buffer 2 (50 mM Tris pH 7.5, 500 mM NaCl, 20 mM imidazole, 0.03% DDM) to remove non-binding proteins. Then a 0.3 M imidazole was applied (elution buffer: 50mM Tris pH 7.5, 150 mM NaCl, 300 mM imidazole, 0.03% DDM) to elute the FeoB-HisTag protein (Fig. 12.20). The peak fractions (F2-7; total volume of 30 ml) were combined. The purified protein showed a major band of the expected size (~80 kDa) but also a second major band at similar intensity and higher mobility (~50 kDa), which likely corresponds to a breakdown product.

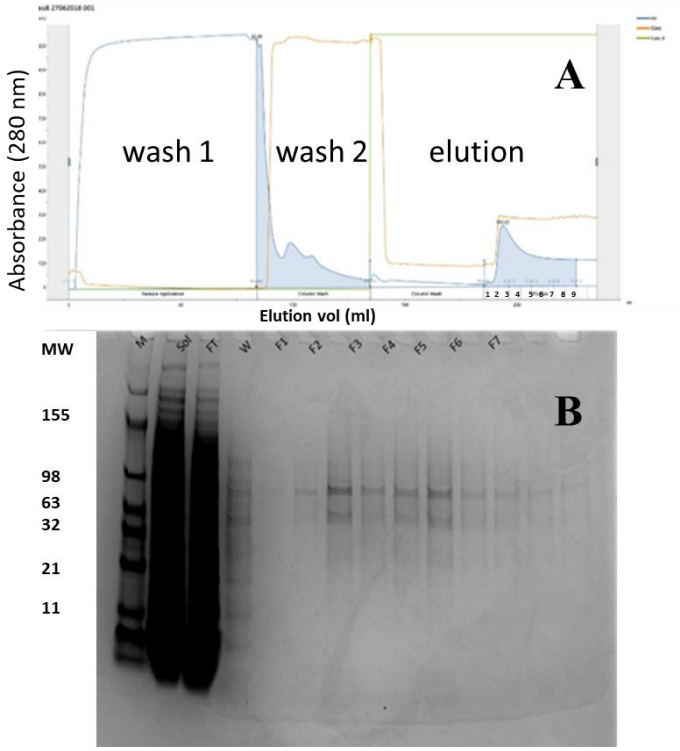

Figure 12.20: FeoB-HisTag protein purification from *Ao*38 cells. A: IMAC chromatography on an AKTA Pure, showing the three steps (two wash steps and one elution step). **B**: SDS-PAGE analysis of fractions from A (M, marker; Sol, soluble supernatant; FT, flow-through; F1-7, fractions.

12.8.2 Second-step purification in DDM by SEC

The fractions pooled (30 ml; 0.32 mg protein/ml) from the above IMAC step were concentrated using an Akta pure system (100 kDa cut off) to give a volume of 1 ml (4.7 mg protein/ml) and the concentrated FeoB-HisTag protein was then applied to a SEC column (Section 2.31.8; Fig. 12.21).

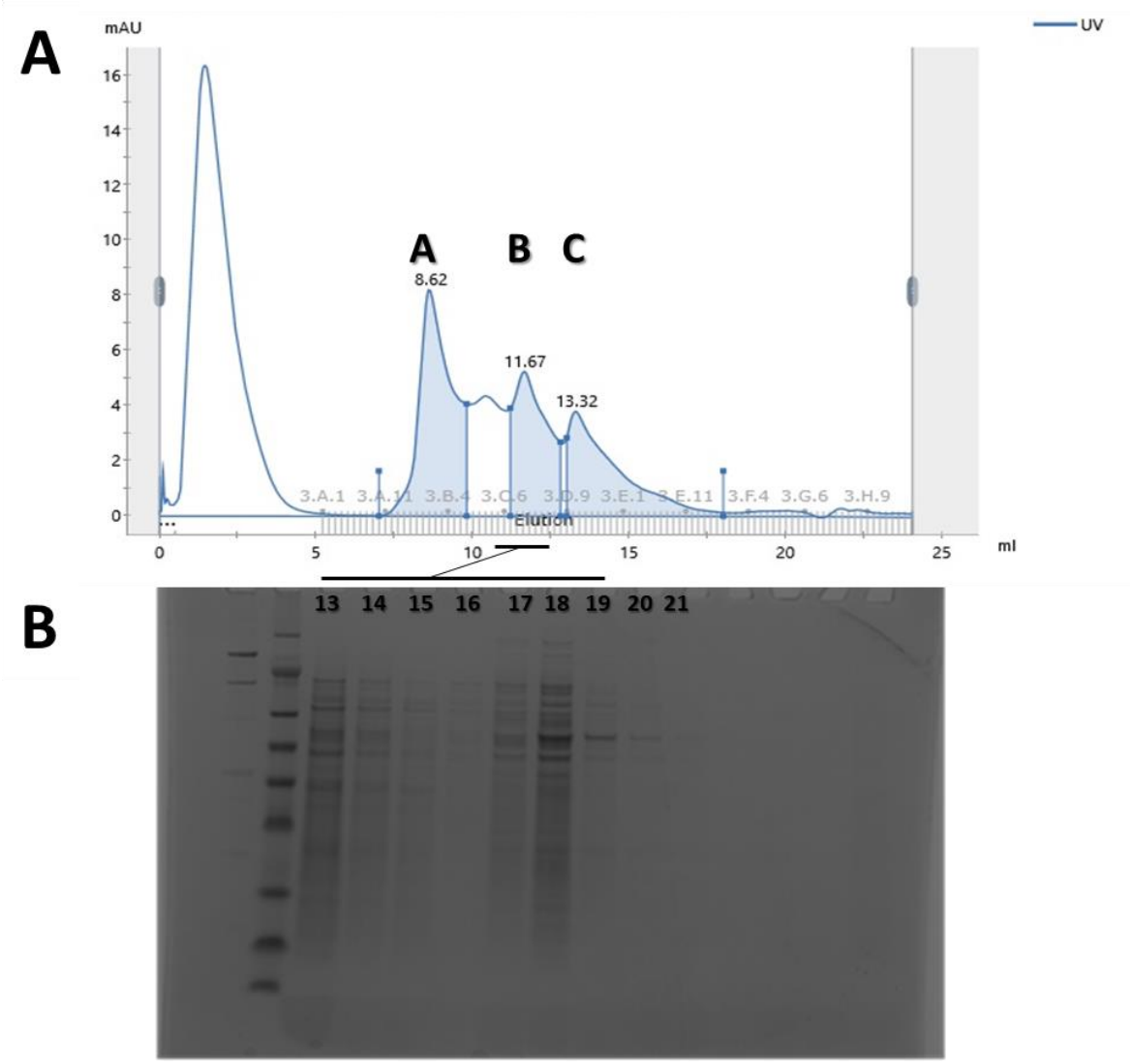

Figure 12.21: SEC of FeoB-HisTag after IMAC purification. A. SEC**.** Details are as described in Methods 2.31.8. The column used was a 'Superdex 200 increase 10/300 GL' column and the buffer employed was: 50 mM Tris, 150 mM NaCl, 1 mM TCEP, 20 mM mannitol, 0.05% DDM) at a flow rate of 0.5 ml/min. The three major peaks of interest are labelled A-C. **B**. SDS-PAGE analysis of fraction eluting in the volume corresponding to monodisperse protein.

Fractions 14-20 of Peak B (~250 µl each) were pooled and concentrated as above to a final volume of 500 µl (5.4 mg/ml).

The samples from the SEC purification (Peak B fractions and fraction eluting at 13.3 ml) were then analysed DLS (Fig. 12.22) to test for the aggregation status of the FeoB-HisTag protein.

There was clear difference in the signal obtained with respect to the buffer/detergent control, with micelles of ~4 nm observed in the control, and apparently monodisperse PDCs of ~10 nm seen for the FeoB-HisTag samples. However, the DLS indicates that the SEC step has not yielded FeoB protein suitable for crystallisation trials since the signal at 10 nm is restricted to a narrow time window indicating instability of the PDC over time. A signal similar to that seen in the buffer control (in terms of response to time) is required for crystallisation. In addition, the SDS-PAGE analysis indicated a lack of purity (Fig. 12.21).

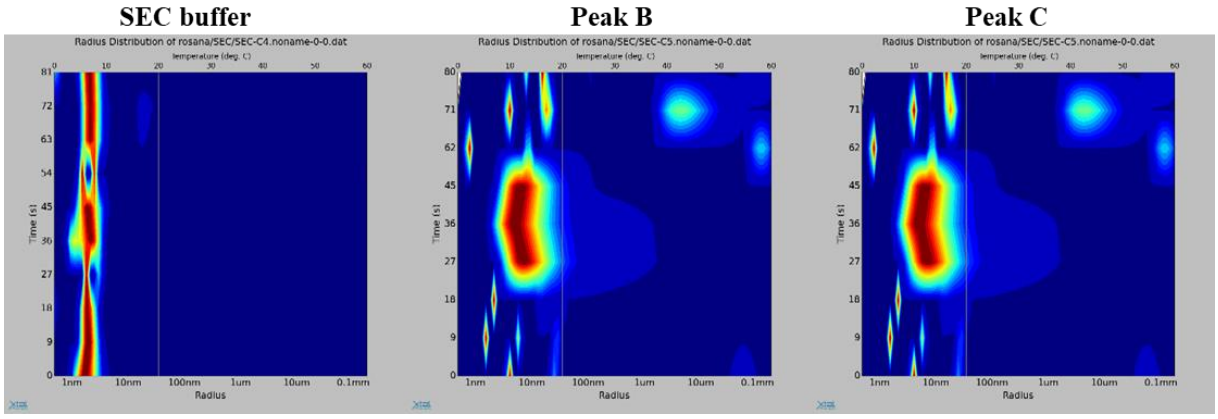

Figure 12.22: DLS analysis of FeoB-HisTag/detergent (0.03% DDM) complexes isolated by SEC. Analyses of the detergent-containing buffer and peaks B and C from Fig. 12.21 are shown. Results from the dynamic light scattering (DLS) measurements show that hydrodynamic radius (Rh) of the pure DDM micelles are around 4.5 nm while the PDC micelle in peaks B and C are around 10 nm, indicating a monodisperse complex. The in situ DLS experiments were carried out at 293 K using a SpectroLight 610 (XtalConcepts GmbH, Hamburg, Germany) instrument and 2 µl of each sample.

12.8.3 FeoB-HisTag solublisation and IMAC in MNG detergent

In the first purification trial in DDM, the protein precipitated at the 3-4 mg/ml stage during concentration, suggesting aggregation at the high concentrations (>10 mg/ml) required for

crystallisation. However, in MNG, a high concentration (up to 12 mg/ml) for FeoB-HisTag was achieved without precipitation. Therefore, the purification was repeated using the detergent MNG (at 0.05%) for solubilisation and IMAC, but DDM was used for SEC (as MNG is not as suitable for crystallisation due to its higher CMC). Other than for the change of detergent, all steps were as described for the first purification except that 0.006% CHS (cholesteryl hemisuccinate, a membrane-protein stabilising detergent) was included throughout.

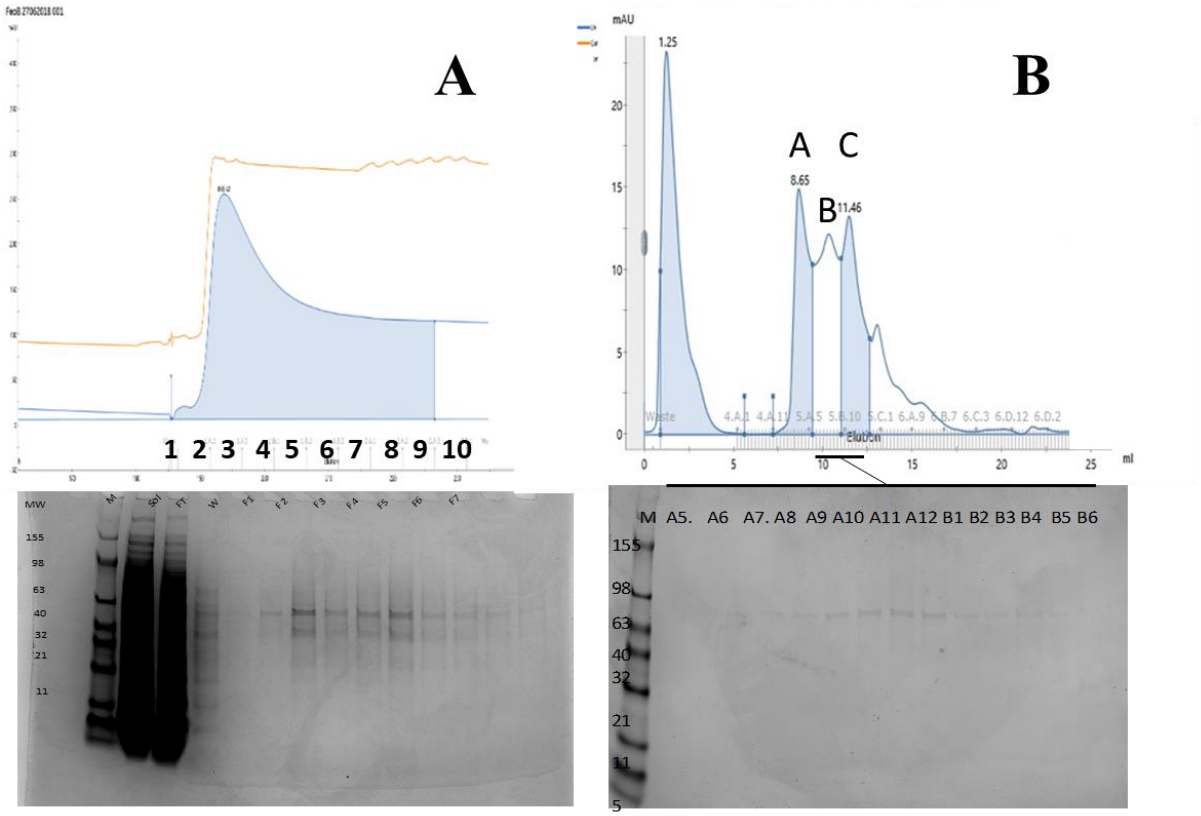

Figure 12.23: Purification of FeoB-HisTag in 0.05% MNG from *Ao*38 cells. A: IMAC purification on an AKTA Pure with SDS-PAGE analysis of fractions. **B**: SEC purification of pooled and concentrated FeoB-hisTag fractions (F2-7) from A. A5-12 correspond to the 8.65 ml peak; B1-6 correspond to the 11.46 ml peak.

The purification was similar to that achieved with DDM except that for the SEC purification SDS-PAGE showed that the isolated FeoB-HisTag was in a purer state, with one major band of

70-80 kDa observed and a low level of other bands. However, DLS (Fig. 12.24) indicated a lack of stability with time for the PDC and aggregation for 'Peak C'.

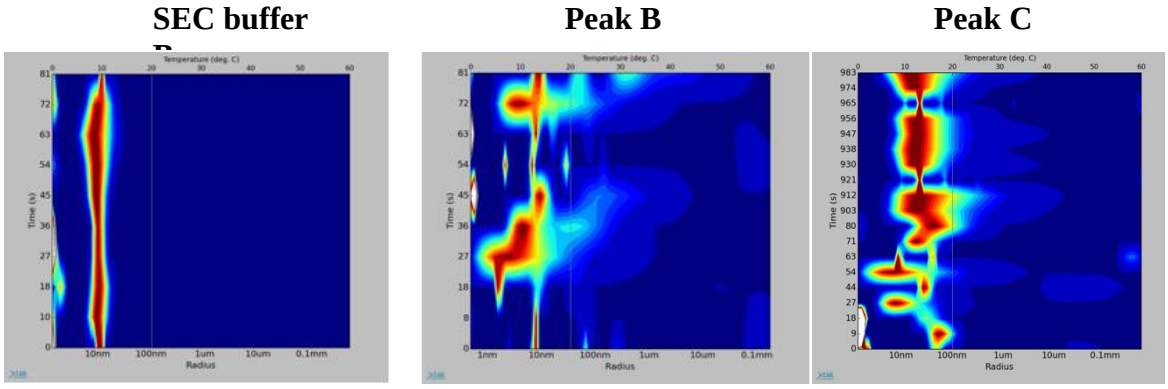

Figure 12.24: DLS analysis of FeoB-HisTag isolated by IMAC in MNG, and then by SEC in DDM. All details as above Fig. 12.22 except that the protein was isolated in MNG in the first two steps and CHS was present.

12.8.4 Third purification of FeoB-HisTag – using a modified buffer

In order to attempt to further improve the purification and aggregation characteristics of FeoB-HisTag, the purification was repeated as above except that reductant and free-radical scavenger (1 mM TCEP and 20 mM mannitol) were added. These were included since FeoB carries highly-conserved Cys residues that may be subject to oxidation and disulphide bridge formation. In addition, FeoB may bind iron which could promote free radical generation.

Purification was similar as achieved previously with a predominant 60-70 kDa band present but an also a considerable level of contaminating polypeptides visible at higher and lower mass (Fig. 12.25-26).

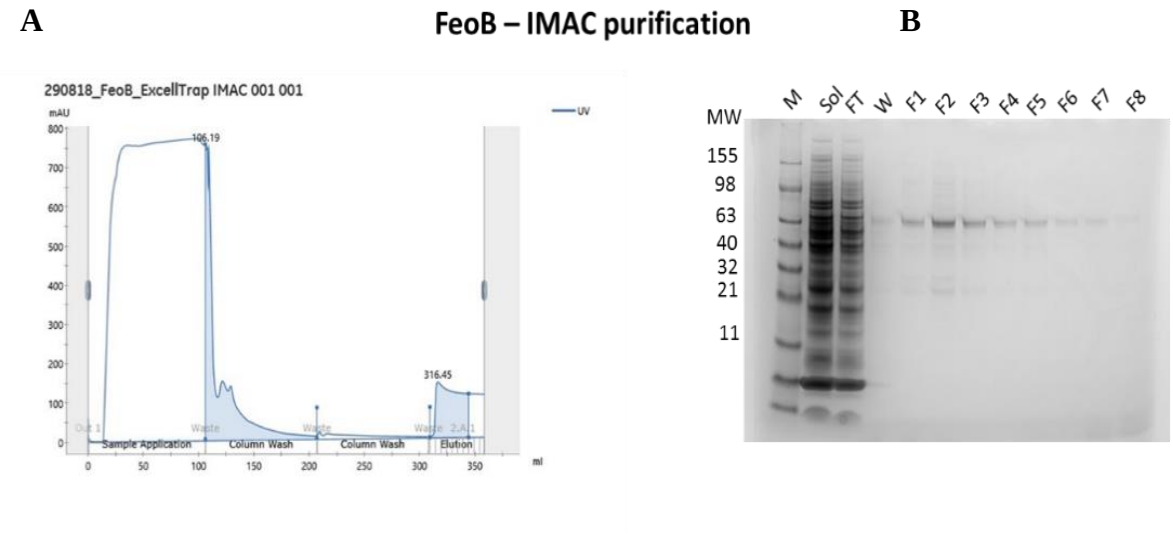

Figure 12.25: FeoB-HisTag protein purification with mannitol and TCEP. A: IMAC elution profile. **B**: SDS-PAGE analysis of fractions eluted with: 50 mM Tris, pH 7.5; 150 mM NaCl; 300 mM imidazole; 20 mM mannitol; 1 mM TCEP; 0.05% MNG, 0.006% CHS).

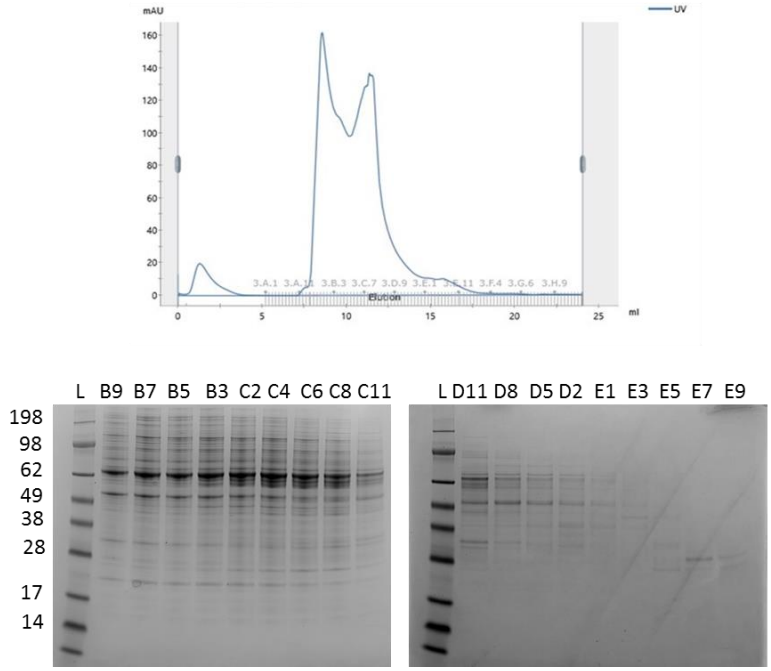

Figure 12.26: FeoB-HisTag 2nd-step purification by SEC. A: SEC elution curve. **B**: SDS-PAGE analysis of fractions.

DLS showed that the pooled peak C fractions were monodisperse (~10 nm) and had a high degree of stability over time (Fig. 12.27), indicating that the FeoB-HisTag might be in a form suitable for crystallisation.

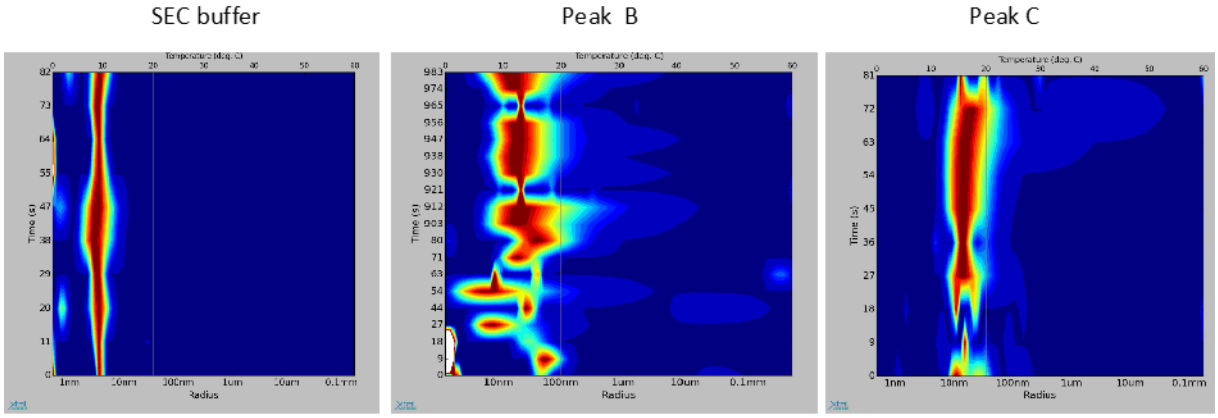

Figure 12.27: DLS analysis of FeoB-HisTag from Fig. 12.26.

To confirm that FeoB-HisTag is stable in the detergent/buffer combination selected, FeoB stability was tested using the DSF approach, with a dye (the thiol-specific fluorochrome N-[4-(7-diethylamino-4-methyl-3-coumarinyl) phenyl] maleimide; CPM) that is specific for Cys residues (Fig. 12.28). The binding of the dye is limited when the protein in properly folded and embedded in detergent micelles, but is increases as the protein becomes more fully exposed to solvent due to loss of detergent or due to unfolding, exposing Cys residues that would normally be buried in the interior of the protein (Niesen et al., 2007). The DSF analysis shows that FeoB is stable (low fluorescent binding) in the presence of DDM and MNG at 35-45 ˚C. However, at higher temperatures the degree of fluorescent binding is increased which indicates temperature-induced destabilisation. This pattern is typical for stable PDCs suitable for crystallisation. Note that in the absence of mannitol and TCEP, the curve generated showed little response to temperature (data not shown) indicating that these agent support PDC stability.

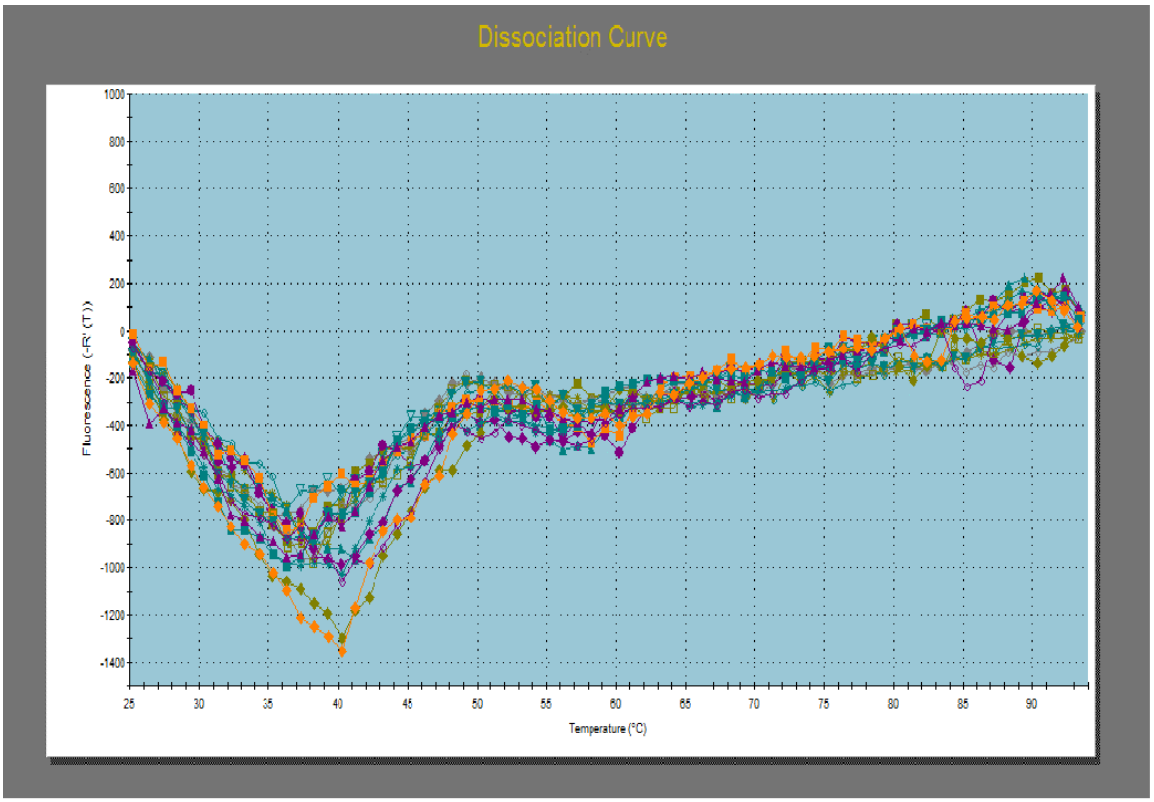

Figure 12.28. Differential scanning fluorimetry (DSF) analysis of the effect of MNG and DDM onFeoB-HisTag stability. Pure FeoB-HisTag, as isolated above, was exchanged into 0.05% MNG using an ultrafiltration system, using the buffer employed for purification. The DSF analysis was then performed on the 0.05% MNG and 0.03% DDM solubilised proteins at concentrations of 0.5, 1, 1.5 and 2 mg protein/ml. The DSF incubation conditions included the thiol-specific fluorochrome N-[4-(7-diethylamino-4-methyl-3-coumarinyl) phenyl] maleimide (CPM) dye (1% v/v).

12.9 Upscaling FeoB-HisTag overexpression and isolation

Having generated FeoB-HisTag in a semi-pure and stably-monodisperse form, the next step was to perform a large-scale preparation of the protein. The key adaptions made that supported the successful purification were: the use of *Ao*38 cells (30-50 fold increase expression cf. *Sf*9 cells); inclusion of mannitol and TCEP (increased PDC stability); use on MNG for solubilisation and purification; and inclusion of a second SEC step (raising PDC stability).

For large-scale FeoB-HisTag expression, the infected *Ao38* cells were propagated for 3 days in multiple 300 ml batches yielding a total of 5 litres of cell culture. The cell pellet was collected and stored at -80 ˚C. 12% SDS-PAGE and Western blotting confirmed good expression (data not shown). A small-scale propagation was performed in parallel with cells infected with Bac-FeoB-eGFP-HisTag to allow easy analysis of expression by fluorescent microscopy confirming high level expression (data not shown).

Solubilisation and purification were as described above (12.8.4) with solubilisation of he membrane protein with the detergent MNG. Following the re-suspension of the insect cell pellet in Lysis Buffer (50 mM Tris pH 7.5, 150 mM NaCl, 1 mM $MgCl_2$, 20 mM mannitol, 20 mg/ml DNase I (from bovine pancreas, Sigma), 1 mM TCEP, 0.006% CHS and protease inhibitors (1 tablet per 100 ml –c0mplete Mini, EDTA free, protein inhibitor cocktail tablets), the protein content was estimated by A_{280} measurement. The membrane suspension was then diluted to a protein concentration of 39 mg/ml to give a total volume of ~200 ml. The solubilisation levels with different amounts of MNG detergent were then determined using SDS-PAGE (not shown). It was found that solubilisation with 0.5% MNG was sufficient to solubilise the membrane proteins. Thus, membrane proteins were solubilised with 0.5% MNG in Lysis Buffer for 2 h at 4 ˚C with mixing. The remaining non-solubilised membranes were removed by ultracentrifugation for 1 h at 100,000 g at 4 °C to give a membrane suspension with a protein concentration of 12 mg/ml. The target protein, now solubilised as a PDC in 0.5% MNG, remained in the supernatant (as indicated by SDS-PAGE, not shown), which was filtered and subjected to the first purification step (Ni^{2+}-affinity) (Fig. 12.37). This involved incubating the supernatant (~200 ml) with Ni^{2+}-NTA beads (what type, 5 ml of slurry) overnight at 4 ˚C with gentle mixing. The next day, the beads were packed into a column and washed with 100 mL of high salt buffer (50 mM Tris pH 7.5, 500 mM NaCl, 20 mM imidazole, 20 mM mannitol, 1 mM TCEP, 0.05% MNG, 0.006 CHS) followed by 100mL of low salt buffer (50 mM Tris pH

7.5, 150 mM NaCl, 30 mM imidazole, 20 mM mannitol, 1 mM TCEP, 0.05% MNG). The protein was eluted in Elution Buffer (50 mM Tris, pH 7.5; 150 mM NaCl; 300 mM imidazole; 20 mM mannitol; 1 mM TCEP; 0.05% MNG). Fractions of 4 ml were collected during elution (Fig. 12.38), and fractions 1-5 containing a predominant band of >60 kDa, were pooled for further purification.

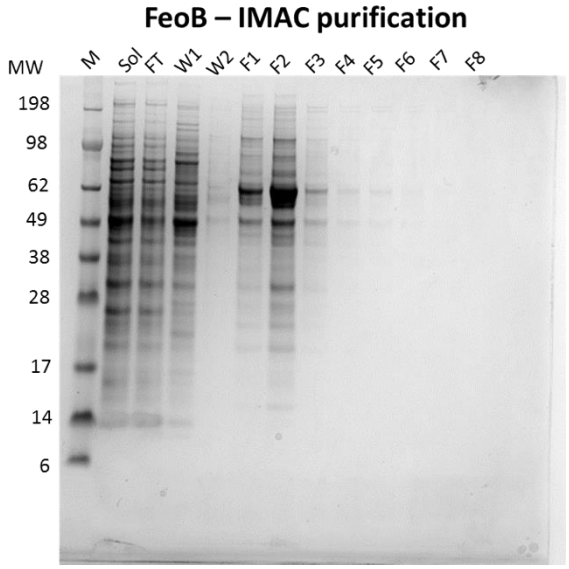

Figure 12.29. SDS-PAGE analysis of FeoB-HisTag isolation from 5 l of cells by Ni^{2+}-NTA affinity chromatography. M, marker; Sol, soluble supernatant applied to the resin; W1-2, Washes 1 and 2. Elution curve not shown.

The pooled fractions from the Ni^{2+}-affinity step were concentrated to 80 ml and 23 mg/ml, before being applied to a SEC column for further purification (Fig. 12.39). Again, a prominent band at >60 kDa considred to correspond to FeoB-HisTag. All fractions containing FeoB-HisTag protein were pooled, concentrated (30 ml, 0.89 mg/ml) and reapplied to the column for further purification (Fig. 12.30).

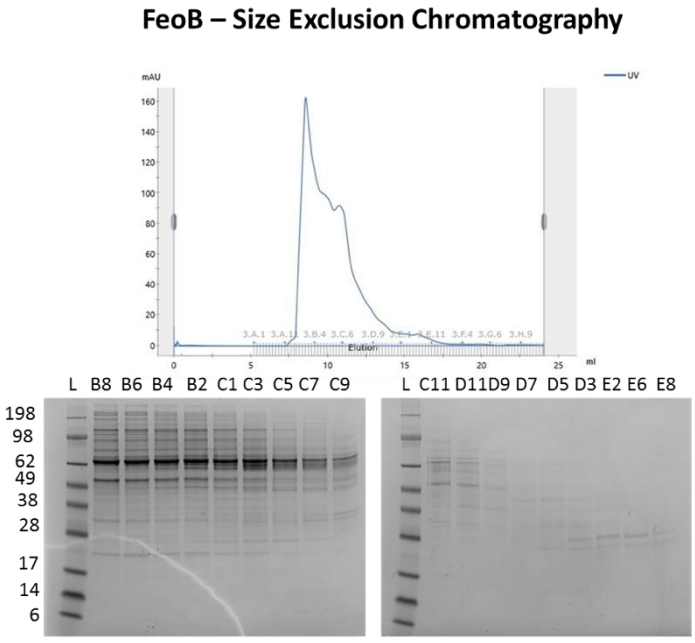

Figure 12.30. SEC purification of FeoB-Histag using a SuperdexTm 10/300 GL column. A. SEC elution curve (in 50 mM Tris, pH 7.5; 150 mM NaCl; 20 mM mannitol; 1 mM TCEP; 0.03% DDM). Flow rate: 0.45 m/min. **B**. SDS-PAGE analysis of fractions (5 ml) showing absorbance.

In the second SEC purification step, four peaks were observed (Fig. 12.30) and these were all found to contain FeoB-HisTag protein in a relatively pure state. The fractions corresponding to these four peaks (A-D) were combined into four pools for further analysis by DLS (Fig. 12.31).

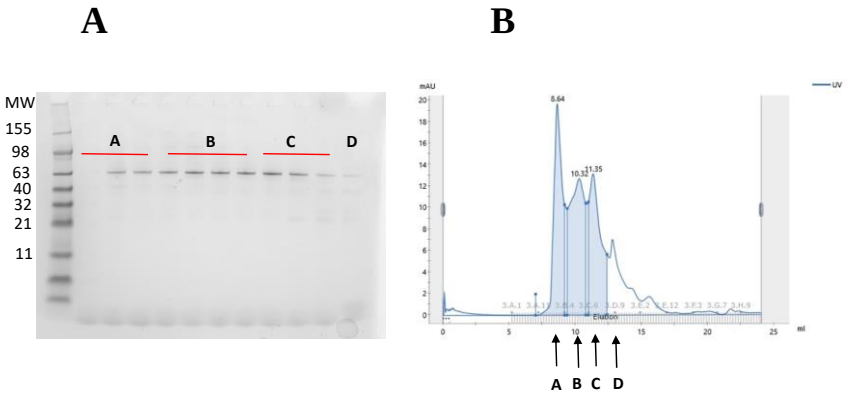

Figure 12.31: Second-step SEC purification. B. Chromatography. Buffer used: 50 mM Tris, pH 7.5, 150 mM NaCl, 20 mM mannitol, 1 mM TCEP, 0.03% DDM. Flow rate: 0.3 mL/min. Samples from the peaks were indicated were collected and checked by SDS-PAGE **A**.

The peak B and C samples were concentrated (100 kDa cut-off Vivaspin concentrator, section 2.29.5.3), as above, to give 3.8 and 12 mg/ml, and 0.5 and 0.7 ml total volume, respectively. DLS analysis of the concentrated samples indicated that the FeoB-HisTag protein in peak C, eluting at ~11.3 ml, is monodisperse (~10 nm micelles), sufficiently concentrated and in a form that is highly stable over time, and thus would be a good option for crystallisation trials. In addition, SDS-PAGE indicated a good level of purity and confirmed the high concentration (Fig. 12.32)

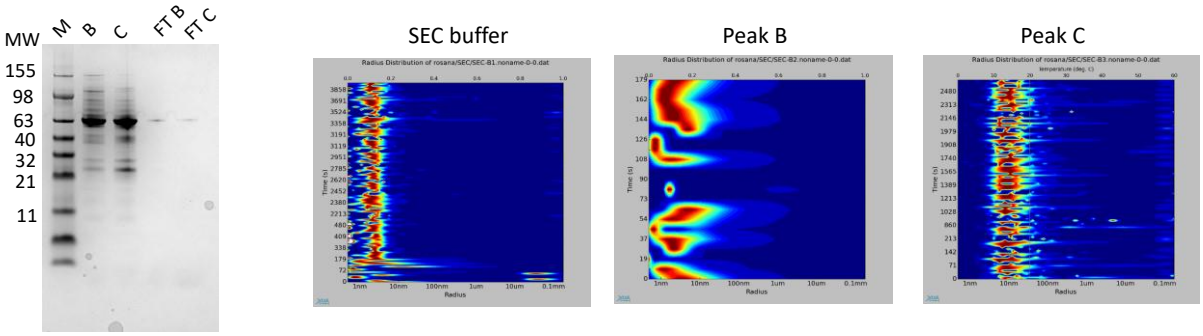

Figure 12.32: DLS analysis of FeoB-HisTag following purification by SEC. Left: SDS-PAGE analysis of FeoB-HisTag protein in the concentrated peak B and C samples (Fig. 12.39). **Right:** DLS analysis of the protein from peak B and C before/after concentration.

12.10 Crystallography

12.10.1 Introduction

The membrane protein used for the crystallisation screening was prepared using the concentrated eluate (peak C) containing the recombinant FeoB-HisTag protein, as isolated in section 12.9. Initially, to ensure that the concentration was optimal, a pre-crystallisation test (Membrane Protein Lab, Harwell Complex Research, Oxford) was carried out as per the manufacturer's guidelines. Thus, concentrated protein was used to set up the crystal screen

trays using both sitting drop and lipid cubic phase (LCP) methods. A variety of commercial screens were used throughout this work for initial screening: MemStart/MemGold™ MD1-39, MemGold2^{TM} HT-96 MD1-64, MemMeso™ FX-96 MD1-87-FX, MemMeso™ FX-96 MD1-87-FX and MemMeso^{TM}. The first three '96-condition crystallization screens' are for use with the sitting drop method and the last three are specifically designed for use with mesophases (LCP compatible). The screens were performed in the 'Membrane Protein Lab' (Harwell Complex Research, Oxford) of Dr I. Mores and T. Kwan. The screens used are listed in Table 2.13. In all cases, the plates were checked regularly, and care was taken to avoid crystal degradation through excessive plate handling.

Crystallography begins with the production of protein crystals whereby protein molecules align in repeating units in an ordered orientation to form crystalline structures. This is achieved by treating the purified protein with buffers to control pH, a precipitating agent (commonly polyethylene glycol), salts or organic alcohols, detergents and cofactors to trigger crystal formation. Commonly used crystallisation kits provide a wide variety of different buffers, precipitating agents, detergents or co-factors for crystallisation experiments to determine the optimum conditions for crystal formation.

12.10.1.1 Crystallisation trials

The targets FeoB-HisTag protein showed enough purity after the SEC step for crystallisation trial. The protein sample was concentrated for the setup of 96-well screens usually in triplicate (MemStart/Sys, MemGold, MemGold2 and MemMeso). An initial protein concentration of ~12 mg/mL was used. This concentration has been recommended as a good starting point (Iwata, 2003). All targets were initially solubilised with DDM..

12.10.2 Sitting drop method

The protein was subjected to initial crystallisation screening by means of the sitting drop vapour diffusion method in 96 well plates, in triplicate. The three 96 well crystallisation screening kits used were MemGold BN149-1-41 (design based on conditions used successfully for 121 α-helical membrane proteins), MemSys BNO81-1-33 (designed for systematic screening of crystallization parameters for membrane proteins via vapour diffusion) and MemMeso BNO29-1-87 (a screen for membrane protein crystals with lipidic meso phases). The reaction mixtures were loaded onto 96 well hanging drop vapour diffusion plates using a Hydra robotics system. Each reaction mixture was carefully drawn up into 96 needles, the screening kit was subsequently removed and the 96 well hanging drop vapour diffusion plate set in its place. The robot then dispensed the reaction mixtures into the reservoir at the bottom of each of the 96 wells of the plate. Once all plates had been dispensed, they were carefully covered with a plastic plate to ensure no evaporation during the remainder of the experiment. The filled plates were then loaded into the Cartesian robot for the generation of the hanging drop for crystallisation. The robot was set to generate hanging drops using 100 nl of protein and 100 nl of the reservoir reaction mixture. From each reservoir, 100 nl were pipetted by the robot onto the elevated platform of the wells, once this was complete for each well the tips were washed in isopropanol and water. Once the tips were cleaned the protein was loaded into just one of the Cartesian needles, this subsequently dispensed 100 nl of protein onto each of the 100 nl drops of reaction mixture on the elevated platforms to form the final sitting drop for vapour diffusion. This was repeated for each plate and the duplicates and the plates were then loaded into the Formulatrix robot for storage and imaging to monitor crystal formation. Each plate was sealed with sealing tape to ensure all wells were airtight to prevent evaporation. One plate for each screening kit was placed in the Formulatrix at 23 °C and the remaining plate was placed in the Formulatrix

at 4 °C. Images of all reactions were taken on a daily basis for the first two weeks and then weekly for the remainder of the time to monitor crystal formation.

Once conditions had yielded potential protein crystals, the respective conditions were selected to set up crystallisation optimisations. Often variations in the selected condition were established across both dimension of a 96 well crystallisation plate. For example, across the horizontal dimension precipitating agent concentration may be varied whilst across the vertical dimension pH may be altered. This allows for the identification of the best condition to generate the most suitable crystals for x-ray diffraction analysis. The conditions were dispensed, and protein dispensed as previously using the Hydra and Cartesian robotics systems. All optimisations were incubated at 23 or 4 °C in the Formulatrix robot storage and images taken at regular weekly intervals.

The protein concentrations employed were in the range where 50% of the drops remained clear after one week. In the case of FeoB sufficient protein sample was left, after setting up trials with MemGold and MemStart/Sys, so a third MemGold2 screen was also tested. Four conditions gave large numbers of crystals (Fig. 12.33; Table 12.2), all mostly oblong or needle

shaped. The identified conditions should be further explored in future work and the crystals tested by x-ray diffraction.

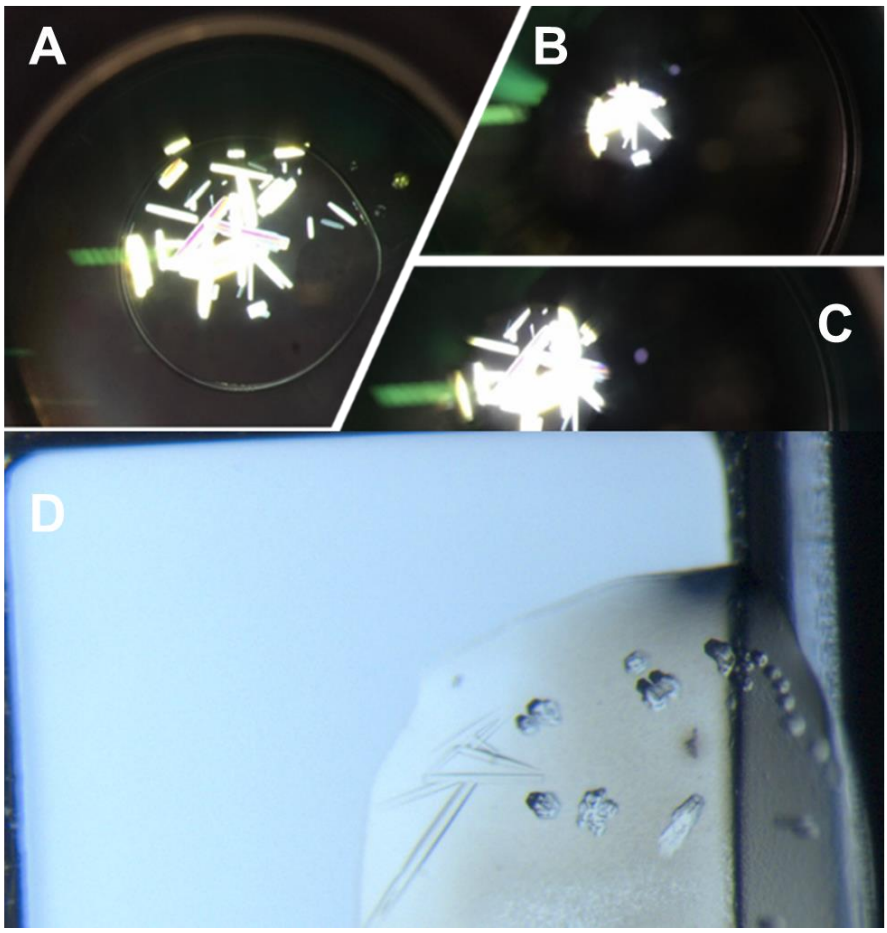

Figure 12.33: FeoB-HisTag membrane-protein crystals. Crystals were generated in four conditions (A-D; Table 12.2) using the sitting drop method with 2 µl (1:1 ratio protein sample reservoir) drops. All formed at 8-9 days at 23 ˚C.

Table 12.2 Condition in which large numbers of crystals were found using the sitting drop method.

Type of kit	Fig.	Well	Conc (M)	Salt	Conc (M)	buffer	pH	Conc	Precipitant
MemStart/Sys	A	C1	0.1	Ammonium sulphate	0.1	HEPES	7.5	30%	PEG 400
MemGold	B	C8	0.1	Sodium chloride	0.02	Tris	7.5	11%	PEG 1500
MemGold2	C	C12	0.1	Potassium chloride	0.1	MES	6.0	32%	PEG 400
MemGold	D	2-41	0.1	Sodium chloride	0.1	Tris	7.5	11 %	PEG 4000

12.10.3 Lipid cubic phase (LCP) crystallisation

LCP is a novel concept for the crystallisation of membrane proteins. LCP is a crystallisation method where the bi-continuous cubic phases consist of monopalmitolein (1-monopalmitoleyl-rac-glycerol, C16:1c9, or MP, Sigma) or monoolein (1-monooleoyl-rac-glycerol, C18:1c9, or MO, Sigma) and an aqueous phase (buffers). The micellar type cubic phases contained palmitoyl-lysophosphatidylcholine (Avanti Polar Lipids) and an aqueous phase (buffer). The preparations at 20 °C in the dark throughout the crystallisation. Crystallisation by Lipid cubic phase (LCP) is more difficult than the more traditional approaches due to the increased number of variables associated with the crystallisation parameters. This necessitates a larger number of screens in order to identify suitable crystallisation conditions. This problem can be addressed

by performing pre-crystallisation screens that help to identify conditions that are amenable, and thus reduce the number of conditions used for crystallisation. However, due to time constraints no such screens have as yet been performed for FeoB-HisTag.

Three crystallisation screening kits were used (each in triplicate) for LCP crystallisation, and the kits were the same as those used for the sitting drop vapour diffusion crystallisation. Monoolein lipid was used to generate the lipid phase by mixing a 3:2 monoolein lipid:protein(21.9 mg/ml: 14.1 mg/ml respectively) with an equal volume of the FeoB-HisTag using a syringe-mixing system. Then, 100 nl of the lipid/FeoB-HisTag mix were combined with 100 nl of crystallisation solution automatically on the surface of a glass plate, which was subsequently sealed with a plastic cover. Plates were incubated and monitored at 23 ˚C as described above.

Crystals were generated under two conditions (Fig. 12.34; Table 12.3) and were a mixture of fine needles and larger oblong-shaped crystals. As above, these crystals and the conditions should be further investigated in future.

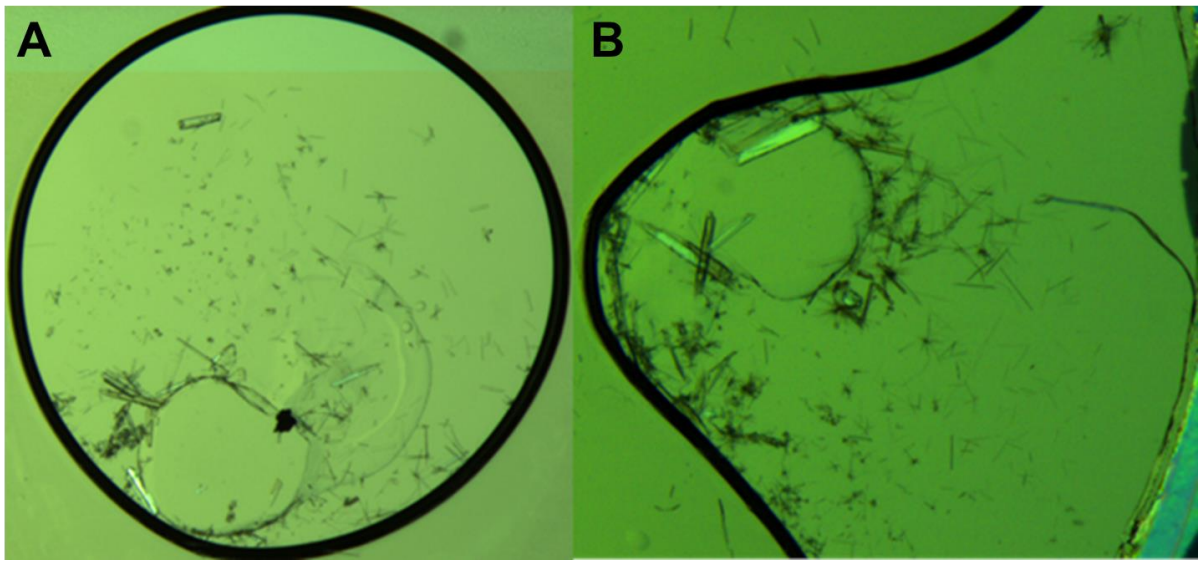

Figure 12.34: Example of FeoB-HisTag membrane-protein crystals found in MemMeso screens. (A) 0.1 M HEPES pH 7, 0.1 M NaCl, 30% PEG 300; (B) 0.1 M MES pH 6, 0.1 M Zinc acetate 30%, 30% PEG 300 at 8-9 days, 23 ˚C.

Table 12.3 Conditions in which crystals were found by the LCP method

Type of kit	Fig.	Well	Conc	Salt	Conc	buffer	pH	Conc	Precipitant
MemMeso™ MD1-86	A	1-26	0.1 M	Sodium chloride	0.1 M	HEPES	7	30%	PEG 300
MemMeso™ FX-96 MD1-87-FX	B	B12	0.1 M	Zinc acetate dihydrate	0.1 M	MES	6	30%	PEG 300

12.12. Discussion

It is more challenging to work with membrane proteins than their globular counterparts, and there are limited high-resolution structures available as a consequence. Much effort is generally spent on gaining a pure and stable protein in the preparation stage in any membrane protein structure project. This process often includes the expression of many homologues and constructs, followed by extraction via different detergents. This process is generally time consuming and highly iterative because limited conditions can be examined at a time. In this study, FeoB-HisTag in monodisperse form was isolated in sufficient quantity, purity and stability for crystallisation trials to proceed. This can be considered a major success. The key factors in FeoB-HisTag isolation were the use of *Ao*38 cells in place of *Sf*9 cells, improving expression levels by ~40x; the selection of the most effective detergents for solubilisation, stability and non-aggregation (DDM and MNG); the inclusion of agents to limit oxidation and free-radical damage, which appeared to improve stability; and the use of three chromatography steps to achieve purification. The final form isolated was relatively pure and could be

concentrated to ~12 mg/ml. In addition, it showed good stability by FSEC and by DSF, and appeared to be monodisperse.

Two methods for crystallisation were utilised, sitting drop vapour diffusion and LCP with monolemum. Three different crystallisation screening kits were used, and each condition was triplicated. Thus, ~1800 crystallisation reactions were attempted and monitored automatically, using a high throughput approach. Several of the conditions utilised gave crystals (see Table 12.2 and 12.3). These conditions should be further explored in future by repetition and by variation of key parameters utilised (e.g. pH). In addition, none of the crystals so far generated have been analysed for their protein content or diffraction characteristics, which should be pursued in future work.

The LCP approach for membrane-protein crystallisation is considered more complex than traditional crystallisation methods due to the additional parameter of the lipid phase. Indeed, membrane proteins are more difficult structural targets than soluble proteins. For this reason, pre-crystallisation screening approaches are often utilised in order to select conditions likely to be successful, and eliminate those that appear unpromising (Martin Caffrey, 2014). Such screens indicate the stability of the protein under the conditions considered for utilisation. Here, a number of screening tests were performed including use of a GFP fusion to test for expression and detergent compatibility. Also, the use of the DLS, FSEC and DSF techniques to determine stability in detergent. However, other screens should also be considered to identify appropriate conditions for LCP crystallisation, such as LCP-FRAP (LCP-fluorescence recovery after photobleaching) as this technique would establish the diffusion characteristics of FeoB in different lipid bilayers used for LCP, which is considered a critical factor for crystallisation (Landau and Rosenbusch, 1996; Aherne et al.,2012).

In future work, the FeoB-HisTag construct should be modified to introduce a cleavage site to enable removal of the His-tag after the Ni^{2+}-affinity step, since this tag might interfere with crystallisation. Further, the use of a construct lacking the soluble N-terminal domain might improve crystallisation potential,but would yield a structure that would not indicate the relationship between the G-protein and permease domains, and so would give limited insight to FeoB function. It would be very exciting to attempt to combine FeoB with FeoA (and potentially FeoC) for co-crystallisation. Indeed, there are examples of FeoA-FeoB fusions in the databases (e.g. as in *Bacteroides fragilis*) which might be excellent targets for exploring FeoA-FeoB interaction structurally. Thus, FeoA should be purified for co-crystallisation work. In LCP crystallisation, a wide range of lipids should be explored using approaches such as LCP-FRAP. In addition, the functionality of the isolated FeoB protein could be tested in proteoliposomes (in the presence/absence of FeoA), as performed previously for FeoB from *K. pneumoniae* (Smith and Sestok, 2018) and *P. aeruginosa* (Seyedmohammad *et al.*, 2016), to determine the relationship between iron uptake, GTPase activity and FeoA association.

Chapter 13. General discussion and Future work

13.1 Introduction

Iron is a significant factor for microorganism growth and many metabolic functions. In biology, iron is found in two main states, the ferric and ferrous forms. In aerobic circumstances (at or above pH 7), iron is commonly present in the oxidized and relatively insoluble ferric form, whereas ferrous iron persists anaerobically or at low pH. Bacterial Fe^{2+} acquisition systems are considered to be important for competing for restricted iron resources in anaerobic sites within the host (e.g. the gut). Indeed, it is well established that the ability of pathogenic bacteria to acquire iron is vital for successful infection and colonisation of the human host (Andrews *et al*., 2003). Although iron is essential, it is also a dangerous metal because it has the ability to catalyse production of reactive oxygen species (ROS) through the Fenton reaction (Cornelis *et al*., 2011). Such iron toxicity is largely a problem associated with aerobic conditions.

The aim of this work was to explore ferrous iron transport in *E. coli* and to determine the distinct purposes of the FeoABC and EfeUOB systems. The specific roles of the FeoA and FeoC components in FeoB-mediated transport were also explored, as well as further details of FeoB function. A key focus was to determine the distinct physiological conditions under which the FeoABC and EfeUOB systems may provide advantage, or disadvantage, to *E. coli.*

13.2. EfeUOB and FeoABC both permit *E. coli* growth under iron-restricted conditions, with aerobic and anaerobic preference, respectively

To confirm the roles of EfeUOB and FeoABC, Fe-restricted growth experiments were conducted with *E. coli* JC32 (Δ*fecABCDE* Δ*zupT* Δ*mntH* Δ*entC* Δ*feoABC* Δ*efeU*), which is devoid of iron-transport systems, complemented with *efeUOB* or *feoABC* in an inducible

expression vector (pBADara and pBADrha) or under control of their natural promoters (in pHSG576). EfeUOB restored growth during iron restriction and had only a modest effect during iron supplementation. FeoABC also restored growth during iron restriction (despite the aerobic conditions) with respect to the vector control, and again only a slight increase over the vector control was seen with iron supplementation (Fig. 4.21 & 4.22). Thus, both EfeUOB and FeoABC complement the iron-uptake mutant, JC32.

13.3. H_2O_2 inhibits FeoABC and activates EfeUOB

A key finding made here was that H_2O_2 acts conversely, in enhancing EfeUOB and inhibiting FeoABC function. The results provided here, on the impact of H_2O_2 or catalase on EfeUOB-dependent iron-restricted growth, are consistent with the view that the EfeUOB utilizes H_2O_2 to oxidise ferrous iron prior to translocation across the inner membrane (Figs. 5.2 & 5.3). Thus, EfeUOB iron-uptake activity appears to be driven by H_2O_2. This was indicated by the finding that the good growth provided by *efeUOB*^{O157} complementation under low iron, acidic conditions is dependent on the presence of hydrogen peroxide - added H_2O_2 improved the iron-restricted growth of *E. coli* JC28/32 strains complemented *efeUOB*^{O157}. However, H_2O_2 caused reduction in growth of strains complemented with *feoABC*^{O157} (as well as the vector control) (Chapter 5). Catalase led to an enhanced growth of JC32 transformants with the FeoABC^{O157} system but inhibited growth with transformants possessing the EfeUOB^{O157} system (Fig 5.4 and 5.6 respectively). The catalase enhancement of Feo-dependent growth contrasted with results obtained for the vector control and support the role of peroxide in inhibiting Feo function.

The effect on the EfeUOB^{O157} system was opposite, with added catalase causing a decrease in growth for the EfeUOB^{O157} complemented (as for the vector control, which was unexpected).

Although the Feo system enhanced growth of JC28 and JC32 under anaerobic conditions, the Efe system impaired growth under these condition was less pronounced. The results thus suggest that Feo is more functional anaerobically than aerobically, whereas the Efe system prefers aerobic condition, particularly when H_2O_2 is available. The model presented for EfeUOB function, as proposed by Rajshekaran *et al.* (2010), is thus supported by the results obtained for EfeUOB iron-transport. In this model, the DyP-like peroxidase, EfeB, uses H_2O_2 as an electron acceptor for oxidation of ferrous iron prior to uptake of the resulting ferric iron by EfeU. The results further suggest a clear rationale for the presence of two dedicated ferrous iron uptake systems in *E. coli* and other bacteria, with EfeUOB operational when peroxide is available (i.e. aerobically) at low pH (favouring ferrous iron stability) and FeoABC operational under low oxygen conditions when peroxide is not likely to be generated (again favouring ferrous iron stability).

13.3 EfeUOB permits ^{55}Fe uptake under aerobic conditions in the absence of catalase, whereas FeoABC does not

An ^{55}Fe transport assay was performed to study Efe and Feo driven iron import. Complementation of JC32 by *efeUOB* gave a 6.5-fold increase in ^{55}Fe import with respect to the vector control (Fig 6.3). Addition of exogenous H_2O_2 increased ^{55}Fe import by ~twofold (Fig 6.4 and 6.5), while addition of catalase reduced import by ~2-fold (Fig 6.4 and 6.5). This result supports the view that ferrous-iron uptake by EfeUOB is H_2O_2 dependent. In contrast, complementation by *feoABC* resulted in only a slight (~2-fold) increase in import of ^{55}Fe relative to the control (Fig 6.3). Addition of exogenous H_2O_2 had little impact on aerobic ^{55}Fe import by Feo whereas addition of catalase increased import by ~7-fold (Fig 6.4 and 6.5)

The effects of peroxide/catalase on ^{55}Fe uptake are unlikely to be related to expression control, since uptake was measured over a short time period and nutrients were not included (other than

glucose) such that growth was not possible. In addition, use of inducible promoters eliminated any transcription regulation effects. The findings match the predicted role of EfeUOB as a haem-peroxidase-dependent ferrous-iron transporter and suggests that Feo activity is subject to peroxide inhibition, possibly to limit iron uptake during redox stress. Thus, Feo and Efe provide alternative routes for ferrous-iron transport in response to H_2O_2 availability, Feo being shut down by peroxide and Efe being activated. It would be interesting to pre-treat the FeoABC strain with peroxide and then remove the peroxide followed by treatment with catalase and/or reductant to determine whether iron uptake could be restored. This should indicate whether H_2O_2 inhibition of FeoB is reversible.

Previous work on ^{55}Fe uptake with high-copy number *efeU* from *E. coli* strain Nissle 1917 showed activity that was just two-fold higher than vector control (GroBe *et al*., 2006), presumably due to absence of EfeB and EfeO. The results obtained from the iron uptake experiment resemble those of Cao *et al.* (2007) and Kammler *et al*. (1993) showing a strong aerobic and anaerobic activities for EfeUOB and Feo, respectively. A colourimetric Amplex Red hydrogen peroxide assay was used to monitor the consumption of H_2O_2 by *E. coli* LC106 (catalase and alkyl-hydroperoxidase deficient strain) expressing EfeUOB. This showed that EfeUOB mediates H_2O_2 degradation, which lends support to the notion that Efe consumes H_2O_2 in order to drive iron uptake.

13.4. The role of FeoA and FeoC in Feo-dependent iron uptake

Even though the Feo system is a common system in bacteria, its structure and the mechanism by which ferrous iron is transported are still not understood. In this study, a characterisation of the roles of the FeoA and FeoC components in *E. coli* was performed.

FeoA is a small, cytoplasmic SH3 protein that is considered essential for Feo activity; FeoB, is the ferrous permease consisting of an N-terminal, cytoplasmic G-protein domain and a C-terminal polytopic permease domain composed of two 'Gate' motif domains; and FeoC is a small Fe-S-containing HTH protein thought to control FeoB stability against FtsH degradation in response to oxygen (Cartron *et al*., 2006; Kim *et al*., 2013). The results generated here show that FeoA is indeed absolutely necessary for Feo function in *E. coli*.

The FeoC component is largely restricted to Feo systems of the γ-Proteobacteria (Cartron *et al*., 2006) indicating that it is not essential for Feo function and has a specialised purpose that is largely restricted to a specific taxonomic group of bacteria. The roles of FeoA and FeoC are unknown; in cases where they have been studied they mostly enhance FeoB activity but may not be essential (Lau *et al*., 2016). It was suggested that the FeoB C-terminal sub-domain, restricted to the γ-Proteobacteria, may enable interaction of FeoC and FeoB (Cartron *et al*., 2006), however results provided here show that this is unlikely to be the case.

In order to establish phenotypes that are independent of any polarity effect and promoter specific control, the *feo* genes where cloned into two different inducible plasmids, pBADara and pBADrha, in a range of formats, and used to complement in JC32 to give double transformants expressing various Feo subunit complements with and without epitope tags. In total, 26 such constructs were generated and used to further understand the roles of the various Feo components.

Growth experiments confirmed that FeoA is absolutely required for Feo function, and that Feo activity is weak aerobically compared to that observed anaerobically. This indicates that weak Feo aerobic activity is dependent on post-translational factors. FeoC was found to promote Feo activity aerobically, particularly in the presence of ascorbate. Interestingly, FeoC had little impact on Feo activity anaerobically.

The effect of aerobiosis and FeoC on FeoB-Flag levels was determined. Aerobiosis caused a major reduction in FeoB levels that was largely independent of FeoC, and FeoB levels remained high anaerobically in the absence of FeoC. Thus, FeoC had only minor impact on FeoB levels in response to oxygen. This finding supports the post-translational regulation of FeoB levels by O_2 as reporter by Kim *et al*. (2012; 2013) in *Salmonella*, but does not support any major role for FeoC in this process. Thus, FeoC appears to enhance Feo activity by an as yet undiscovered mechanism.

FeoC caused a modest increase in FeoB-FLAG levels, but only under aerobic conditions with ascorbate (Fig. 8.20). In the absence of ascorbate, the FeoC effect on FeoB-FLAG levels was much diminished. Thus, it appears that FeoC enhances FeoAB activity aerobically (with ascorbate) at least partly through increasing FeoB protein levels apparently via a post-transcriptional process. The result by western blot analysis of the effect of FeoC, ascorbate and oxygen on FeoB-Flag status, in minimal medium, were reiterated iron-rich LB (Figure 8.21) indicating that iron status and growth levels did not influence the FeoB levels markedly.

Previous to this work, several lines of evidence suggest that the Feo components interact. An interaction between FeoC and FeoB was observed in a BACTH assay for both the *V. cholerae* (Weaver *et al*., 2013) and *S. enterica* (Kim *et al*., 2013) proteins. Similarly, the *K. pneumoniae* FeoB and FeoC were found to co-crystallize (Hung *et al*., 2012). In *S. enterica*, FeoA was shown to interact with FeoB in a BACTH assay (Kim *et al*., 2012). The present study evidenced a role of FeoA and FeoC in FeoB activity, which is consistent with their association.

13.5 The importance of nine conserved residues and the C-terminal sub-domain in Feo-mediated iron uptake

To further understand the mechanism of FeoB iron uptake, nine highly-conserved FeoB residues within the permease domain were altered by SDM. The FeoB-C403S, -C432S, -C677S and -E582G variants failed to exhibit FeoAB-enhanced growth under iron restriction indicating

an essential role for these residues. In contrast, FeoB-E488G showed approximately normal FeoAB activity. The FeoB-C772S/H773G and -C763S/C764S (residues in the C-terminal cytoplasmic sub-domain of FeoB) variants showed enhanced Feo activity in the presence of FeoC aerobically; this indicates that FeoC may interact with the C-terminal sub-domain of FeoB or that this subdomain might inhibit FeoC-mediated enhancement of Feo activity.

It is suggested that the thiol groups of these three essential Cys residues might become oxidised to sulfonic acid when cells are incubated aerobically. This could shut off Fe^{2+} transport by preventing association of the Cys residues with iron, blocking iron access to the permease binding site. This 'biochemical switch' would enable the cell to respond rapidly to exposure to oxygen by preventing intracellular accumulation of Fe^{2+}, which promotes formation of damaging radical species under oxidative conditions. The finding that substitution of these three residues for Ser eliminates the activity of FeoB, supports this hypothesis and suggests structural changes to these residues induced through oxidation would prevent iron uptake activity. The structural prediction indicating that the three essential Cys residues (and one essential Glu residue) occupy locations suitable with a roles as direct Fe^{2+} ligands is consistent with their essential roles and the suggested Cys-oxidation-by-peroxide effect under aerobic conditions.

Further, three conserved Cys residues and one conserved His residue in the C-terminal sub-domain were also mutated, to generate two double mutations: C763/C764 and C772/H773. These double mutations caused a similar enhancement of Feo-dependent low-iron growth, suggesting that the sub-domain inhibits Feo function in the presence of FeoC. Preliminary FeoB-Flag western blot analysis indicated that the C763/C764 and C772/H773 mutations caused a general, although inconsistent, increase in FeoB levels, which might explain the raised Feo activity as indicated by the iron-limited growth studies. The role of this sub-domain remains unclear, although it appears not to be required for FeoC function.

The roles of Cys^{432} and Cys^{677} had previously been investigated in *P. aeruginosa* (Syedmahmood *et al*., 2016) using FeoB reconstituted into liposomes. Cys^{677} was found to play a modest role in enhancing GTPase activity in response to iron, and was proposed to act as a Fe^{2+} sensor; whilst Cys^{432} had no effect on GTP hydrolysis but was suggested to associate with Fe^{2+} during transport (Syedmahmood *et al*., 2016). However, these results are not likely reflective of the *in vivo* functions of these residues, as no FeoA was included in the assays and thus the system employed would be expected to be inactive for iron uptake.

13.6. Role of FtsH in control of FeoB levels

In order to test the reported role of FtsH in degradation of FeoB under aerobic conditions, the *ftsH* mutation was introduced into JC32 and the impact on Feo activity determined. Only a slight effect of *ftsH* mutation was observed with an increase in Feo activity indicated. However, FeoC enhancement of Feo activity was retained in the *ftsH* mutant, indicating that the role of FeoC in promoting Feo activity is not dependent on regulation of FeoB sensitivity to FtsH. The results suggest that although FeoC has a function in stimulating Feo activity under aerobic conditions with reductant, this occurs largely independently of FtsH. In addition, the weak aerobic levels of FeoB do not appear to be caused by an increased rate of FeoB degradation by FtsH. Thus, the mechanism by which FeoC stimulates Feo activity remains to be determined.

13.7. Model of post-translational control of Feo activity in *E. coli*

The model below summarises the major findings as they relate to the post-translational control of the FeoABC system of *E. coli*. The evidence suggests that oxygen (or H_2O_2) causes a major reduction in FeoB levels and activity. However, the mechanism involved remains unclear. Although oxidation of the three key Cys residues is a possible mechanism for loss of activity,

this does not explain the observed reduction in FeoB levels. Potentially, oxidation of these residues could allow formation of a disulphide bond triggering a conformation change leading to rapid turnover. Key residues in the C-terminal subdomain appear to reduce Feo activity when FeoC is present, which suggests an interaction between the subdomain and FeoC may influence Feo activity.

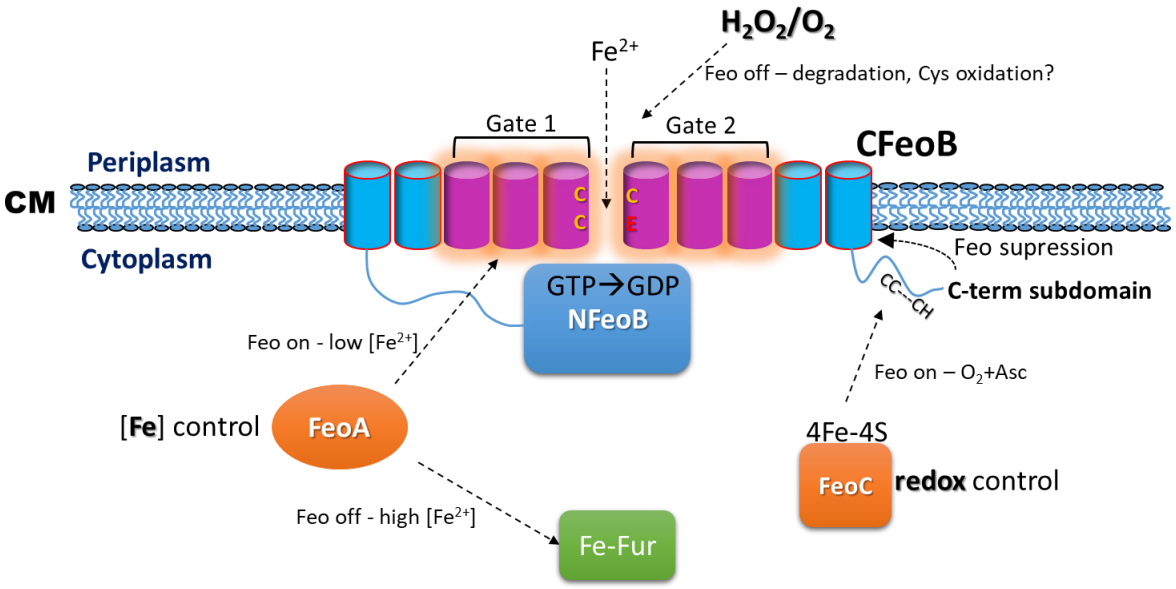

Figure 13.1. Model of Feo post-translational control by O_2/H_2O_2 and Fe in *E. coli*
Little evidence for FeoC control of FeoB degradation was obtained. However, FeoC enhances FeoB activity aerobically with ascorbate. In addition, Feo activity and FeoB levels are strongly reduced aerobically in a post-translational fashion, but it is unclear how this is achieved. It is proposed that FeoA interacts with the ferrous-Fur complex to control Feo activity in response to cytoplasmic iron levels. In addition, this might have an effect of O_2/H_2O_2-dependent Feo activity since Fur levels are OxyR and SoxRS controlled. Potentially, FeoA might stabilise FeoB against degradation. The four essential residues identified here are indicated in CFeoB. FeoC enhancement of Feo activity is increased when the indicated conserved residues in the C-terminal subdomain are mutated.

Little role for FtsH- and FeoC-regulated degradation of FeoB was indicated by the results in this thesis, and so this process is not included in the model above.

13.8. Future outlook

13.8.1. EfeUOB

The effect alternative peroxides should be tested, and the ability of exogenous EfeB to interfere with EfeUOB function should be explored. Different catalase species should also be tested, including Mn-catalase, to further confirm the impact of peroxide on Efe function. Ideally, the amount of H_2O_2 consumed by Efe should be correlated with the amount of iron taken up to determine if any relationship exists. Further, iron-uptake experiments should be performed under a range of iron concentrations in order to provide an estimate of affinity of Efe for iron as a transport substrate. The impact of various inhibitors (e.g. pmf dissipaters and competing metals) should also be tested to further understand the Efe transport mechanism. A challenge will be to ensure that added iron does not catalyse peroxide consumption – this should be controlled by chelation.

13.8.2 Regulation of FeoB activity by hydrogen peroxide, FtsH and FeoC

The structural model for NFeoB suggests that the three well-conserved Cys residues are located at the junction between the two Gate motifs and are within the ‘channel’ or ‘pore’ that provides a route for ferrous iron to translocate into the cell across the inner membrane. In this thesis it is shown that Feo Fe uptake function in is lost when cells are exposed to peroxide. However, in previous work by Kim *et al.* (2012; 2013) suggests that Feo is activity is inhibited by oxygen and that this involves proteolysis of FeoB by FtsH such that FeoB is degraded aerobically and so cannot take up iron. However, the results provided here do not support this hypothesis. Instead, it is proposed that Feo activity is inhibited by exposure to aerobiosis, and that this is achieved through H_2O_2-mediated oxidation of the conserved Cys residues in the FeoB channel. This suggestion should be tested by use of soluble Cys-labelling reagents applied to whole cells

– before and after peroxide treatment – using cells expressing FeoAB-Flag/His (with/without FeoC). The FeoB-Flag/His protein should then be isolated by pull down and then subjected to tryptic digestion and MS analysis to determine whether those peptides carrying the conserved Cys residues have been successfully labelled before peroxide treatment, but not before after peroxide treatment. In addition, the effect of blocking FeoB activity with competing metals, by excluding FeoA or by mutation of the G-protein domain would be interesting to explore since competing metals (or lack of activity) might protect the key Cys residues from oxidation which would thus support their suggested role as Fe^{2+} ligands.

13.8.3. Role of FeoA: interaction with the ferrous-Fur complex

FeoA is absolutely required for FeoB transport activity, but is it not clear what FeoA does – how it mediates FeoB activity. FeoA is an SH3 domain protein – such proteins interact with other proteins. The hypothesis suggested here is that FeoA controls FeoB activity in response to iron availability – such that FeoA switches on the uptake activity of FeoB when there is little iron in the cytoplasm. However, FeoA does not contain any obvious Fe binding site (structure is known). So, it is suggested that FeoA indirectly responds to iron levels by interacting with the cellular iron regulator, Fur. Thus, the hypothesis is that FeoA interacts with the Fe^{2+}-Fur complex and that this prevents FeoA binding with FeoB such that FeoB become inactive. At the same time, the binding of FeoA and Fe^{2+}-Fur is expected to result in deregulation of the Fur regulon (but only anaerobically, as *feoABC* is only expressed anaerobically). Indeed, research shows that FeoABC deregulates the Fur regulon anaerobically (Beauchene *et al.*, 2015). Further, there are examples in the genome databases of genes specifying Fur-FeoA fusions associated with *feo* operons. Also, the global iron regulator of high G+C Gram-positive bacteria (DtxR) carried a FeoA-like SH3 domain of unclear purpose that might perform a

similar role (biochemical coordination of iron uptake and iron regulation) to that suggested here for FeoA.

Further work should involve purification of Fur and FeoA, and examination of their potential to form a complex in the presence and absence of Mn^{2+}. In addition, the effect the FeoA has on Fe^{2+}-Fur-dependent gene regulation and DNA binding should be explored, both *in vivo* and *in vitro*. Whether the aerobic production of FeoA can deregulate the Fur regulon should also be tested. In addition, the possibility that over production of Fur can prevent Feo activity by titration of FeoA should also be tested.

13.8.4. Characterisation and structural study

No structure of an intact FeoB has been so far published, which represents a major gap in understanding of the FeoABC system. Getting structural information on an intact, membrane embedded FeoB, will be important for deciphering the mechanism of ferrous iron transport and for discerning the potential regulation of this process by FeoA and FeoC. As yet, there is no agreement of the parts played by FeoA and FeoC in their interaction with the FeoB polypeptide; the sites of these interactions must be identified to elucidate how these proteins may contribute to ferrous iron transport control.

To continue this study for EfeUOB, overproduction, purification and crystallisation trials should be performed for EfeU. Subsequent incorporation of EfeU into liposomes should also be conducted and metal transport analysis performed using previously purified EfeO and EfeB, monitoring transport of iron using chromogenic chelating agents, fluorescence or radiation. This would enable the iron to be traced, identifying if it is successfully transported into liposomes, helping to confirm the proposed action of the system in vitro. This would also enable

identification of the iron species transported (Fe^{2+} or Fe^{3+} using chromogenic chelating agents) and determination of whether the proposed oxidation involving EfeO and EfeB drives uptake.

Chapter 14. Appendix

14. Vectors Map

14.1. Vector NTI® software (Thermo Fisher Scientific™) was used to generate vector maps of most the generated constructs below unless otherwise indicated. Ampicillin resistance cassettes (AmpR), chloramphenicol resistance cassettes (CamR), promoters, restriction sites, regulatory control genes, and origins of replication are also depicted.

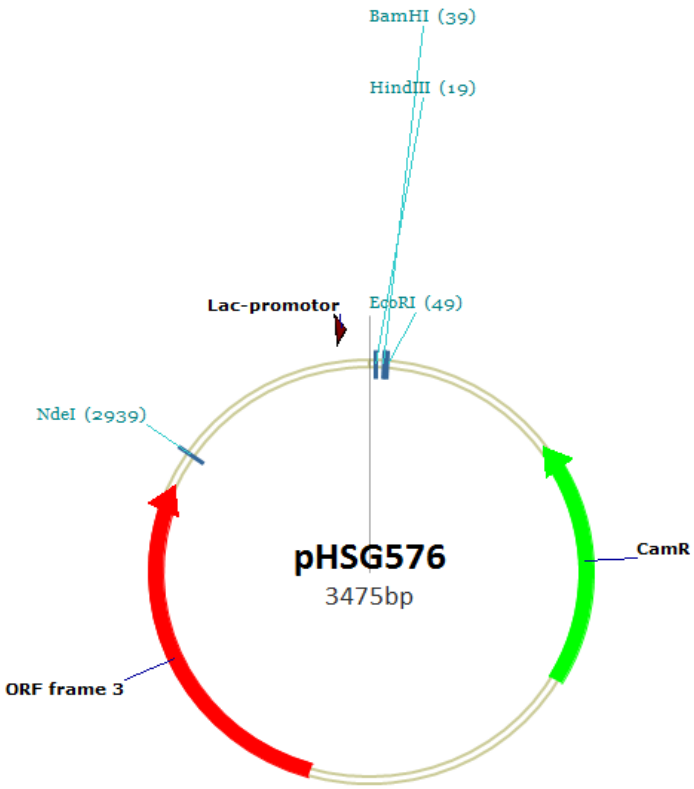

Figure 14.1. Restriction map of pHSG576. Map illustrating the multiple cloning site, Cam^R and *lacZ* promoter.

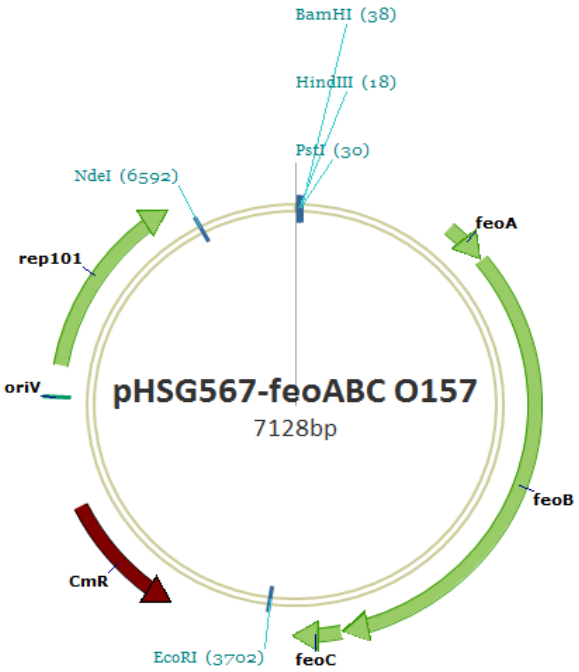

Figure 14.2. Map of pHSG576-*feoABC*. The DNA fragment containing *feoABC* from *E. coli* O157 was cloned between the *Bam*HI and *Eco*RI sites.

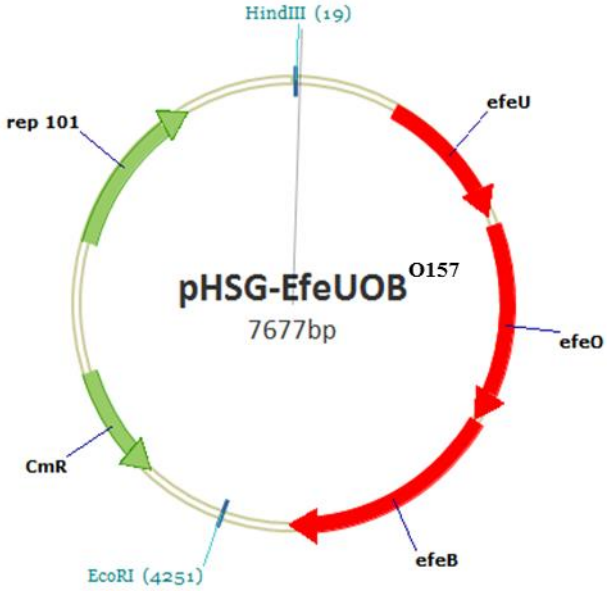

Figure 14.3. Map of pHSG576-*efeUOB*^{O157}. The DNA fragment containing e*feUOB*^{O157} was cloned between the *Hin*dIII and *Eco*RI sites.

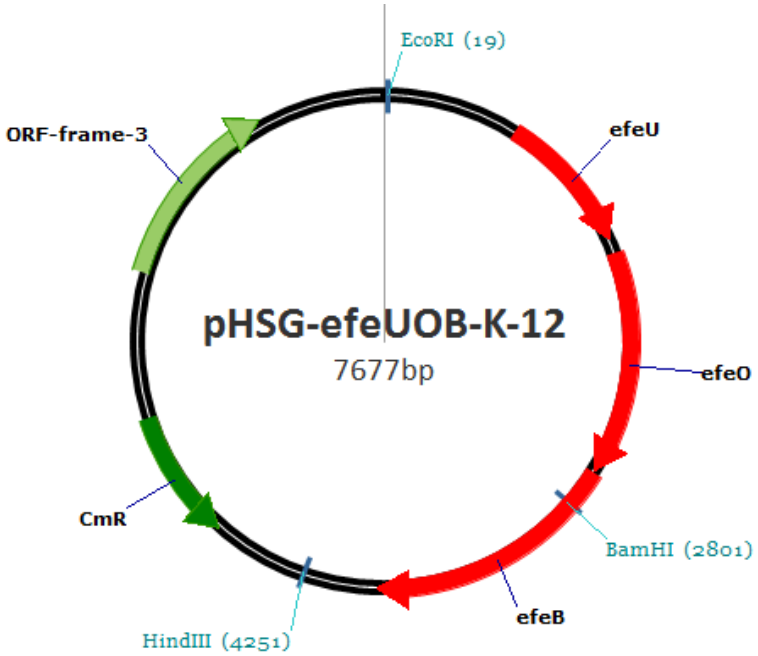

Figure 14.4. Map of pHSG576-*efeU*OB*$^{K-12}$. The DNA fragment containing e*feU*OB* was cloned between the *Hin*dIII and *Eco*RI sites.

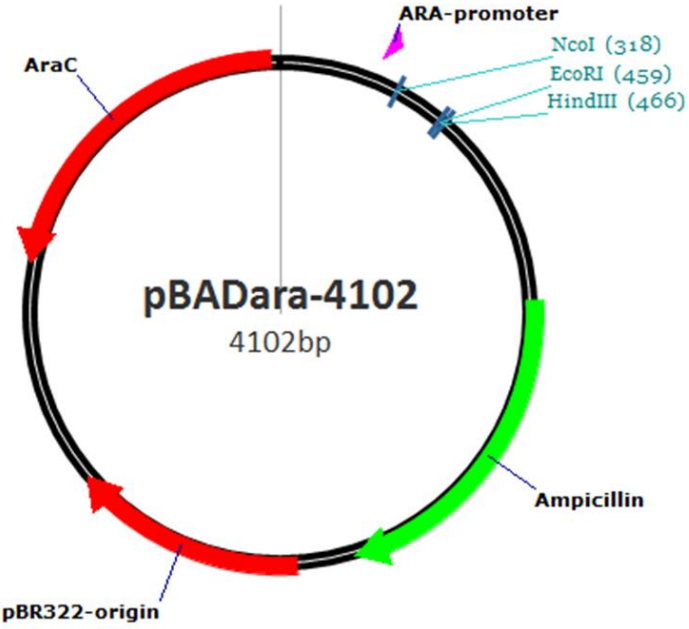

Figure 14.5. Restriction map of pBADara. Map illustrating the multiple cloning site, Amp^{R} and *araC* gene.

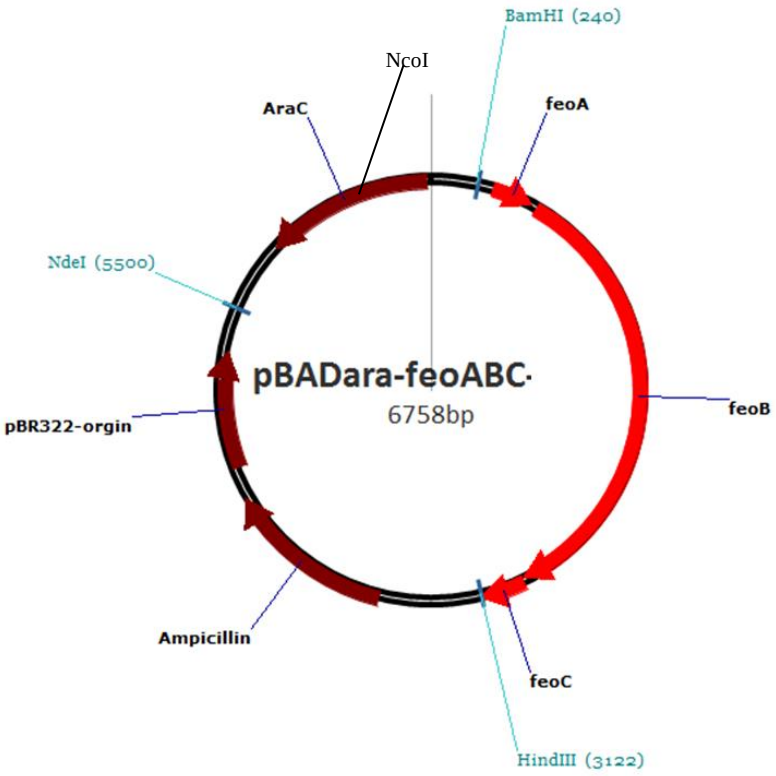

Figure 14.6. Map of pBADara-*feoABC*. The DNA fragment containing *feoABC* was cloned between the *Hin*dIII and *Nco*I sites.

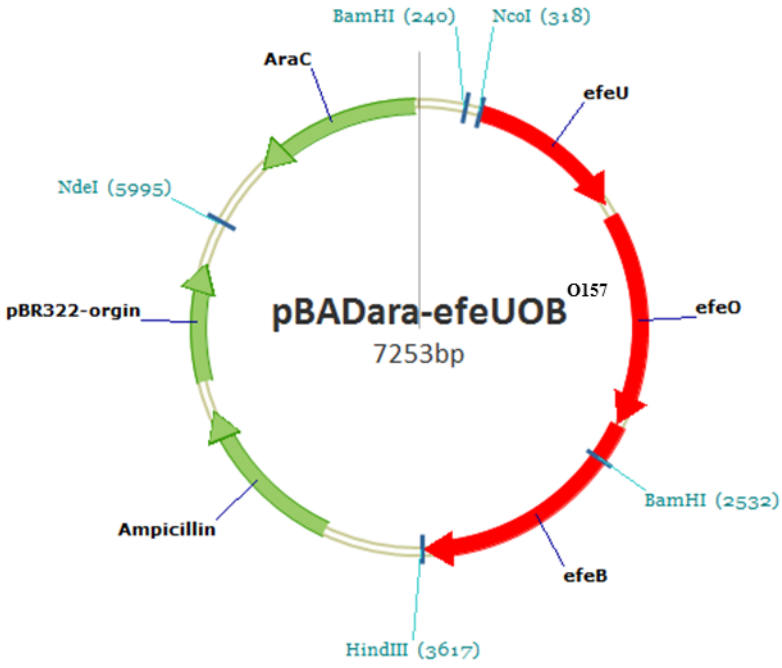

Figure 14.7. Map of pBADara-*efeUOB*^{O157}. The DNA fragment containing e*feUOB* was cloned between the *Hin*dIII and *Nco*I sites.

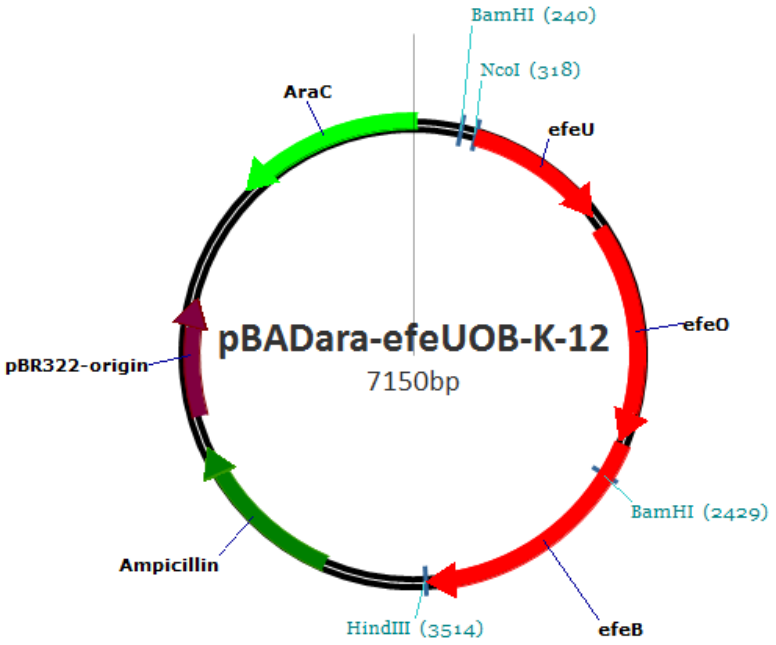

Figure 14.8. Map of pBADara-*efeU*OB*-K-12. The DNA fragment containing e*feUOB* was cloned between the *Hin*dIII and *Nco*I sites.

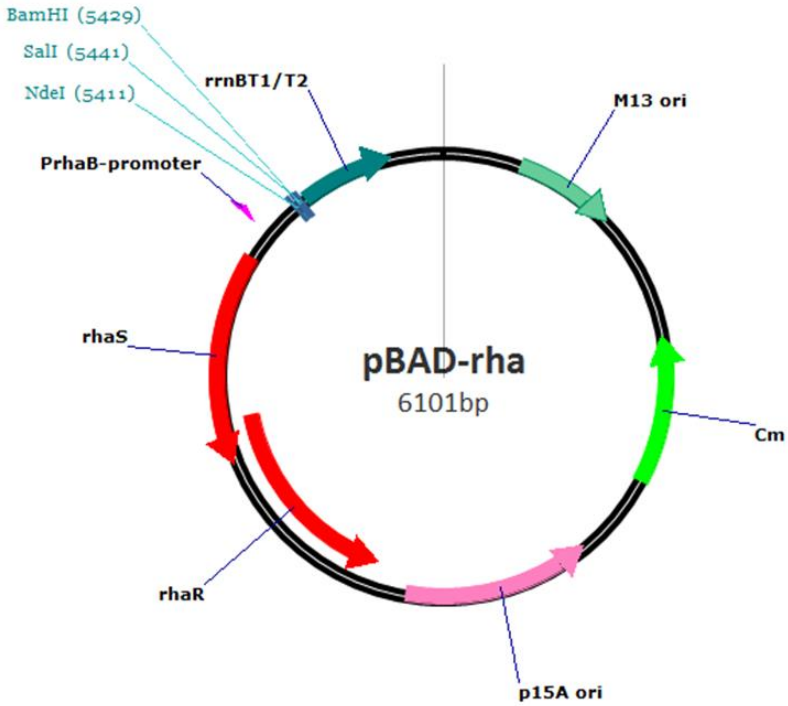

Figure 14.9. Restriction map of pBADrha. Map illustrating the multiple cloning site, Cm^R and *rhaS*, *rhaR* gene.

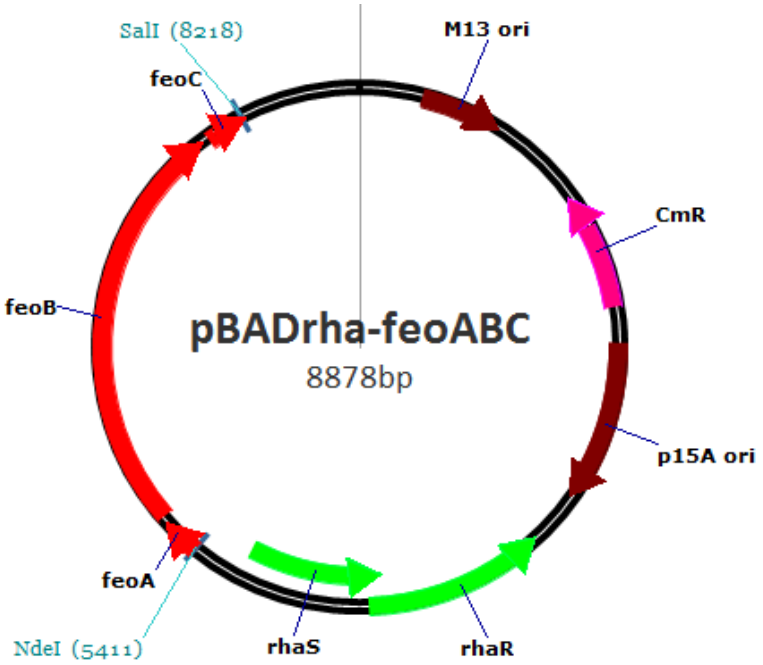

Figure 14.10. Map of pBADrha-*feoABC*. The DNA fragment containing *feoABC* was cloned between the *Nde*I and *Sal*I sites.

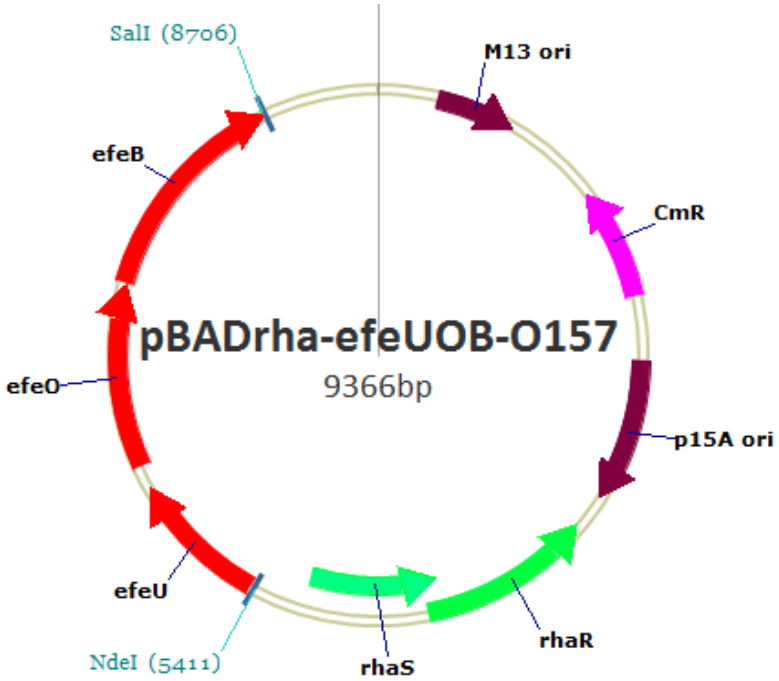

Figure 14.11. Map of pBADrha-*efeUOB*^{O157}. The DNA fragment containing e*feUOB* was cloned between the *Nde*I and *Sal*I sites.

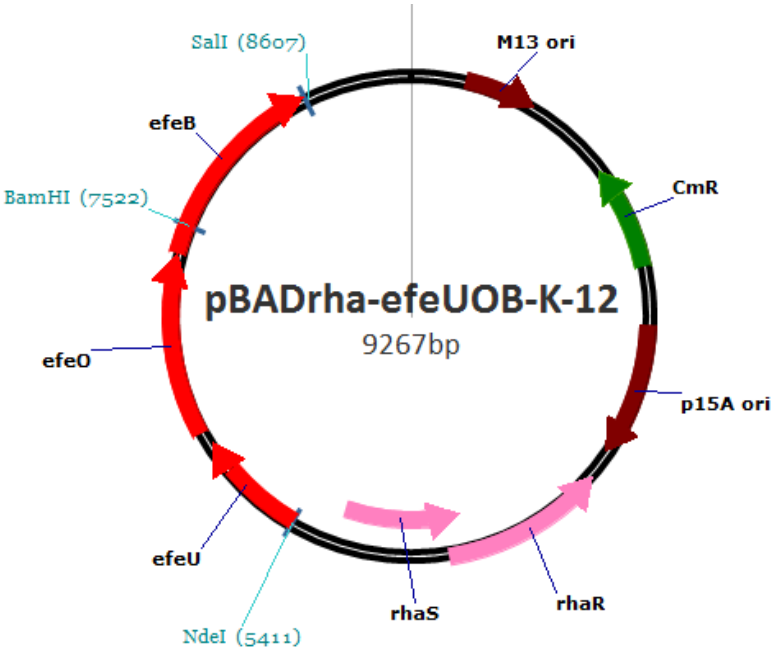

Figure 14.12. Map of pBADrha-*efeU*OB*-K-12. The DNA fragment containing e*feU*OB* was cloned between the *Nde*I and *Sal*I sites.

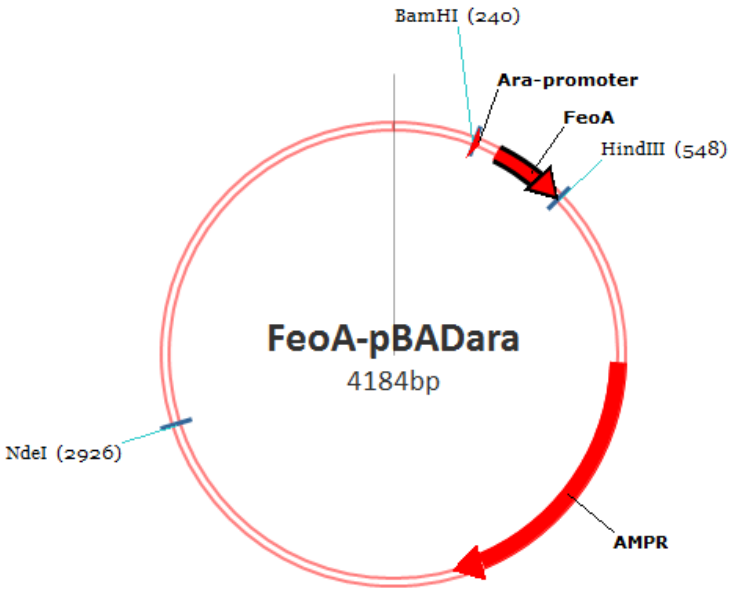

Figure 14.13: Map of FeoA in pBADAra, cloned between *Bam*HI and *Hin*dIII sites.

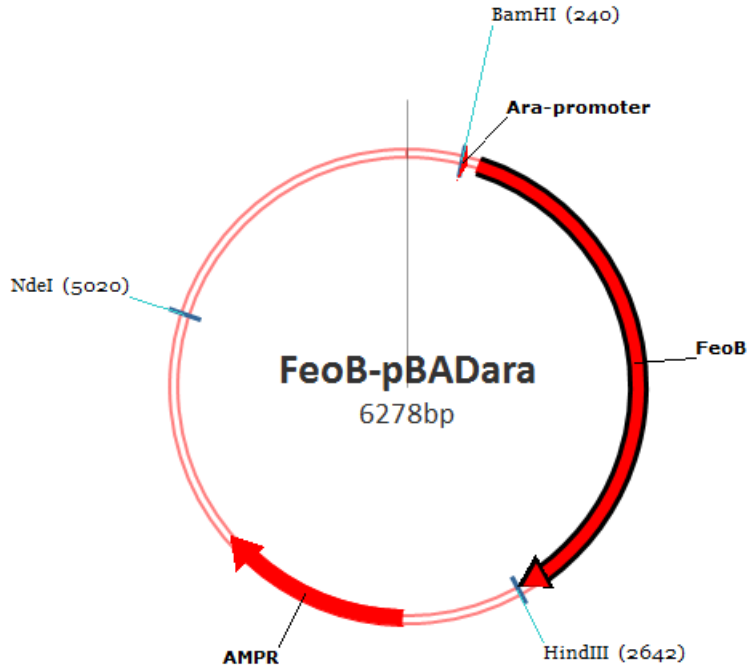

Figure 14.14: Map of FeoB in pBADAra, cloned between *Bam*HI and *Hin*dIII sites.

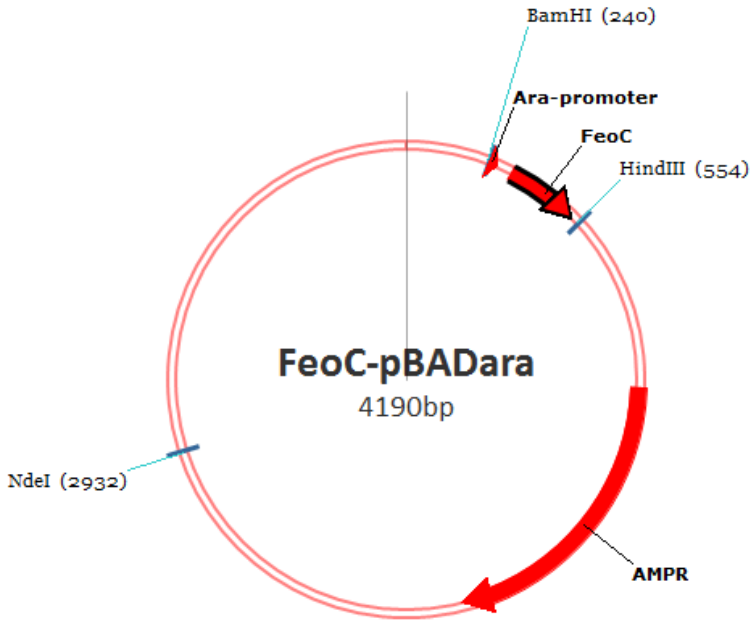

Figure 14.15: Map of FeoC in pBADAra, cloned between *Bam*HI and *Hin*dIII sites.

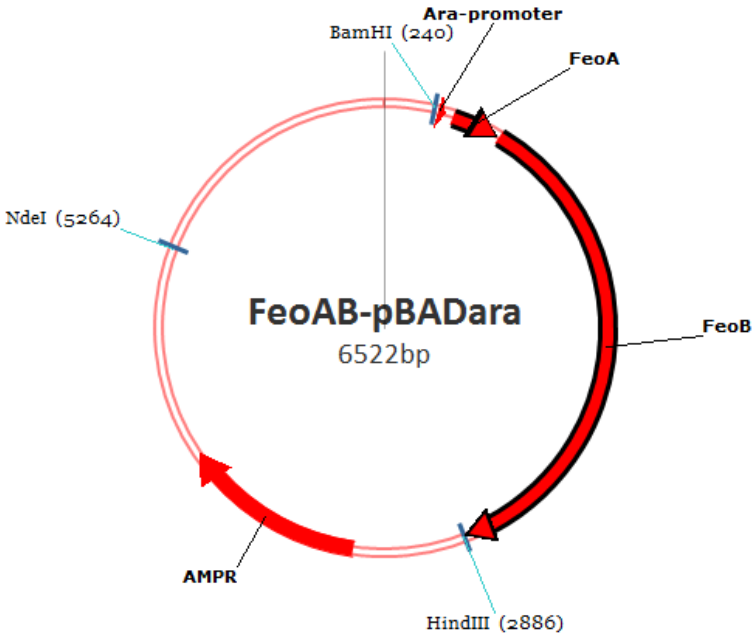

Figure 14.16: Map of FeoAB in pBADAra, cloned between *Bam*HI and *Hin*dIII sites.

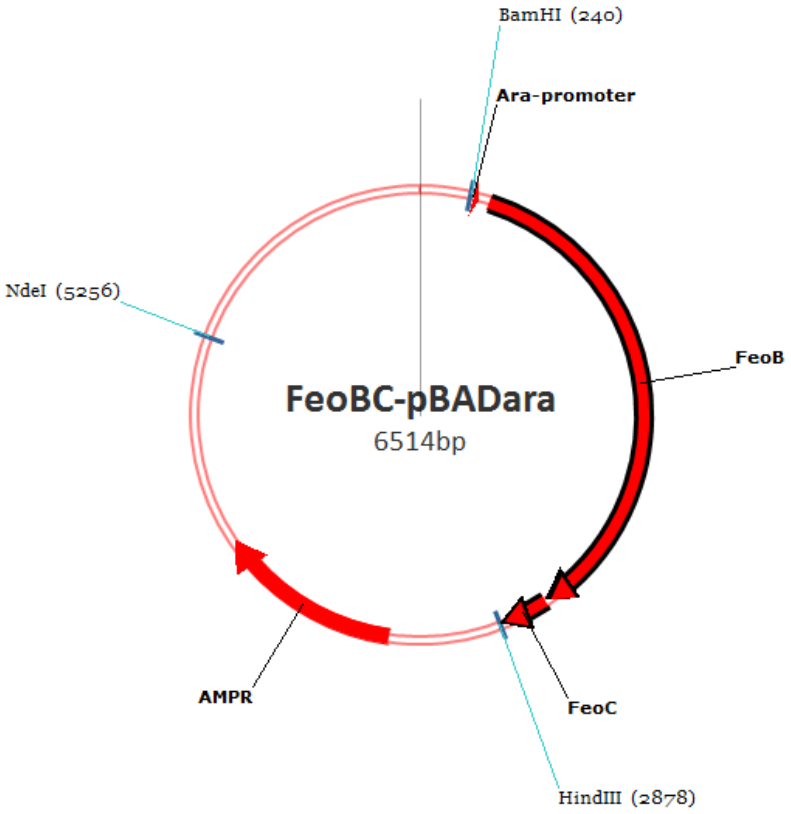

Figure 14.17: Map of FeoBC in pBADara, cloned between *Bam*HI and *Hin*dIII sites.

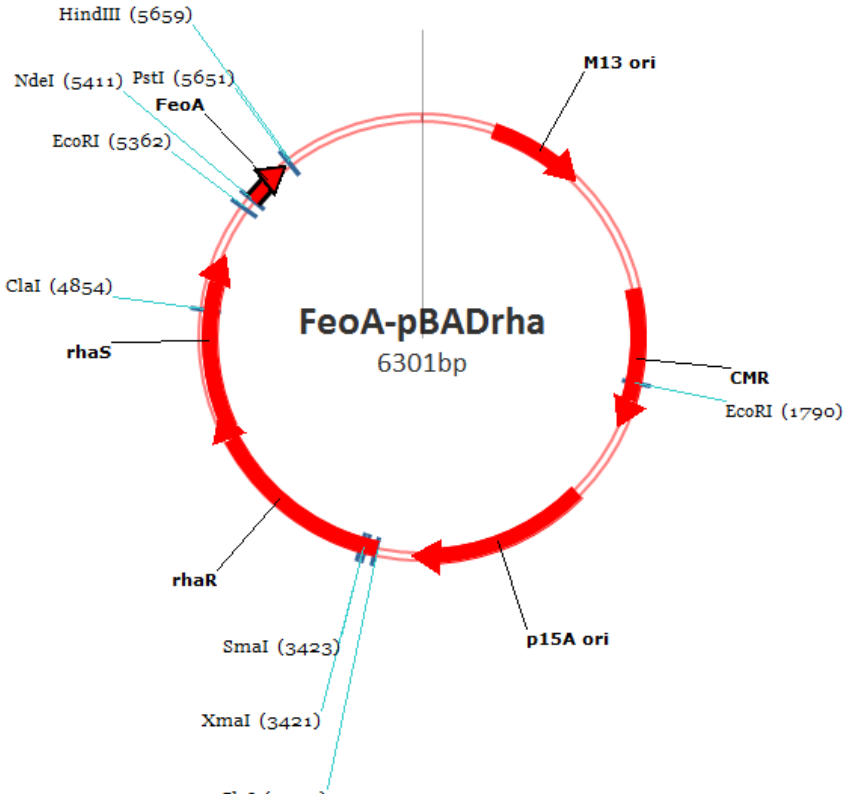

Figure 14.18: Map of FeoA in pBADRha, cloned between *Nde*I and *Hin*dIII sites.

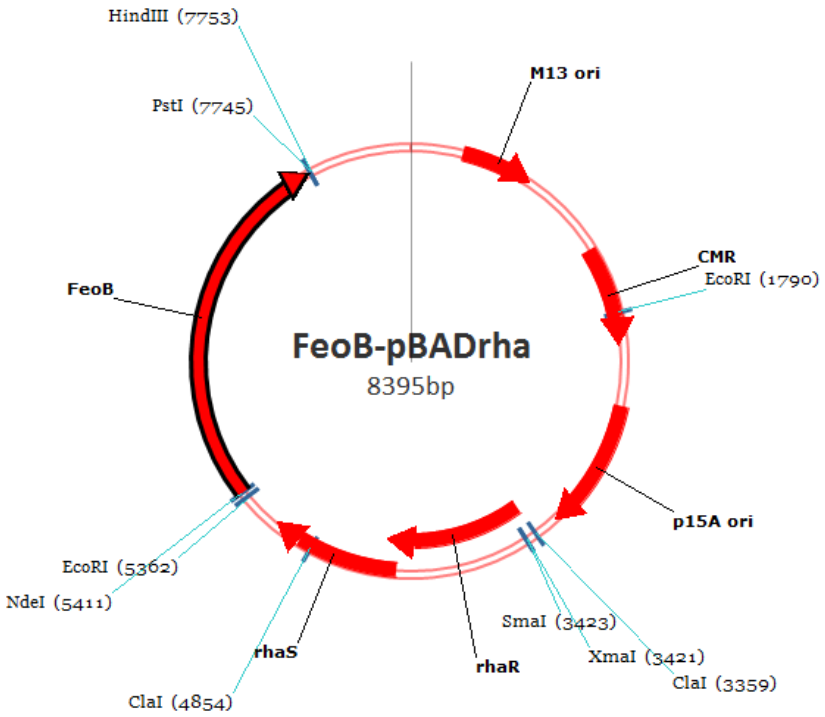

Figure 14.19: Map of FeoB in pBADRha, cloned between *Nde*I and *Hin*dIII sites.

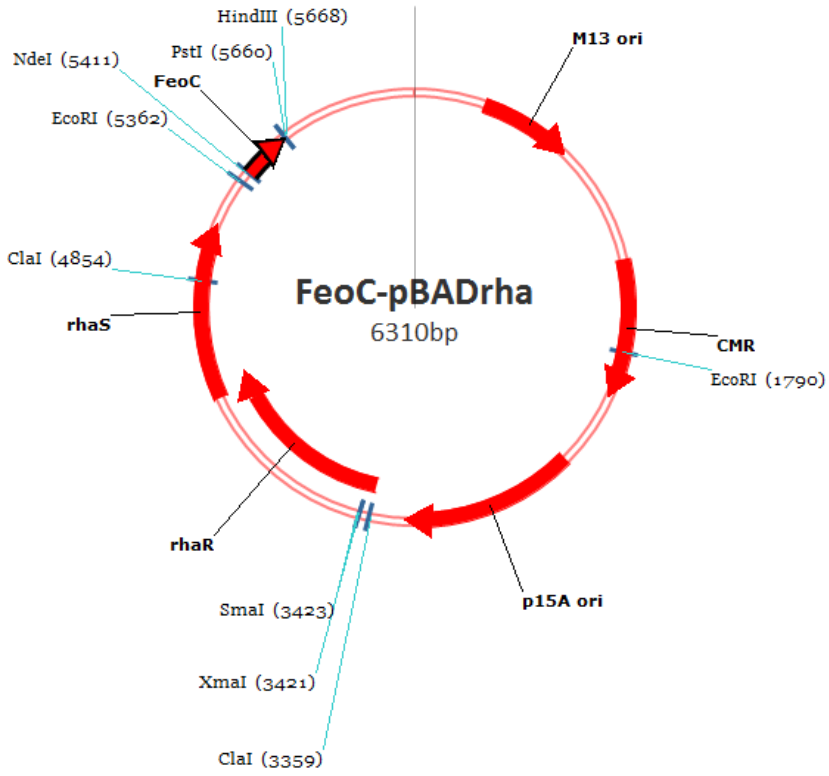

Figure 14.20: Map of FeoC in pBADRha, cloned between *Nde*I and *Hin*dIII sites.

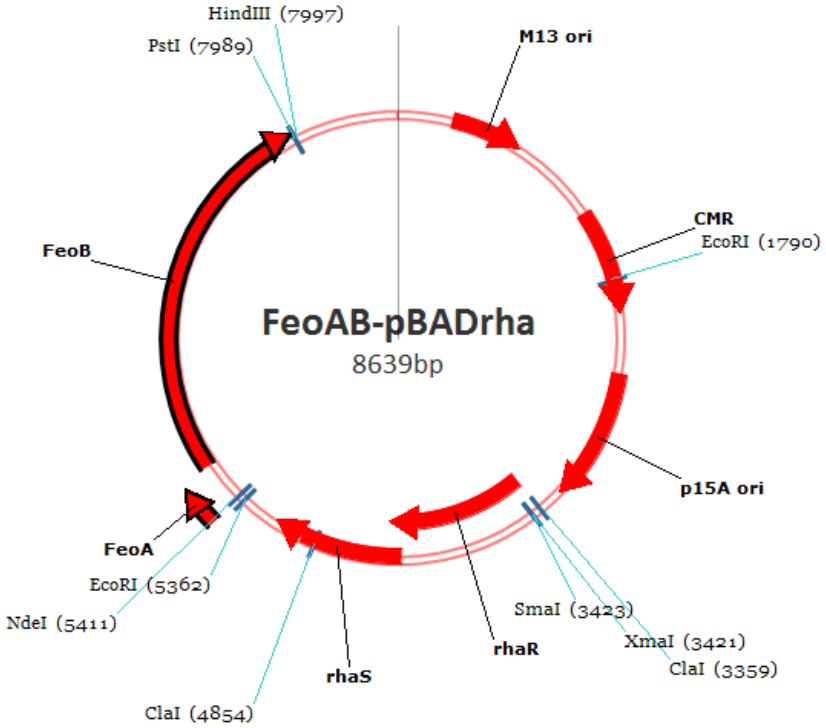

Figure 14.21: Map of FeoAB in pBADRha, cloned between *Nde*I and *Hin*dIII sites.

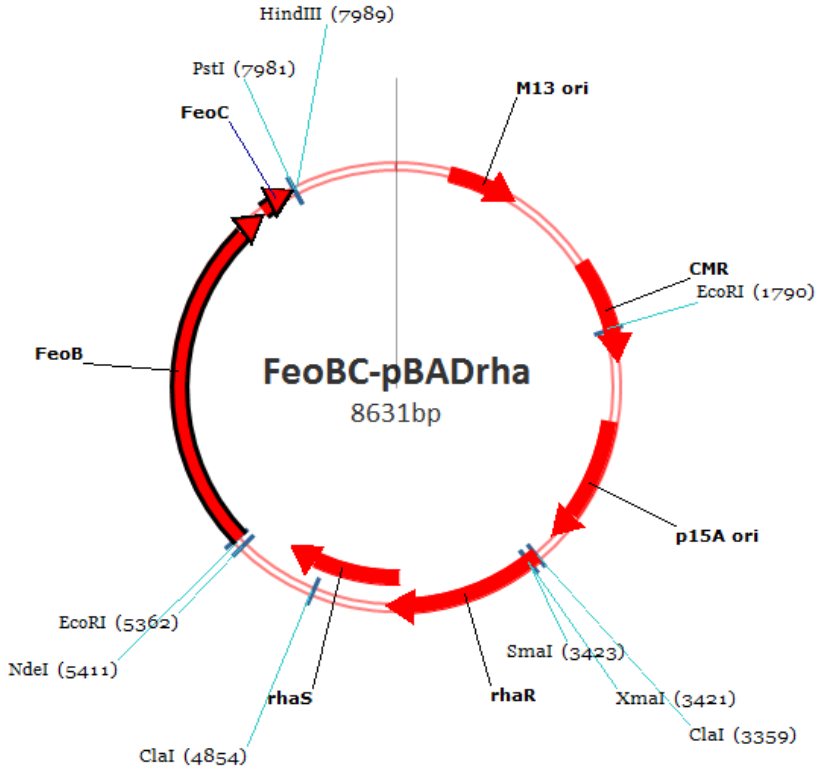

Figure 14.22: Map of FeoBC in pBADRha, cloned between *Nde*I and *Hin*dIII sites.

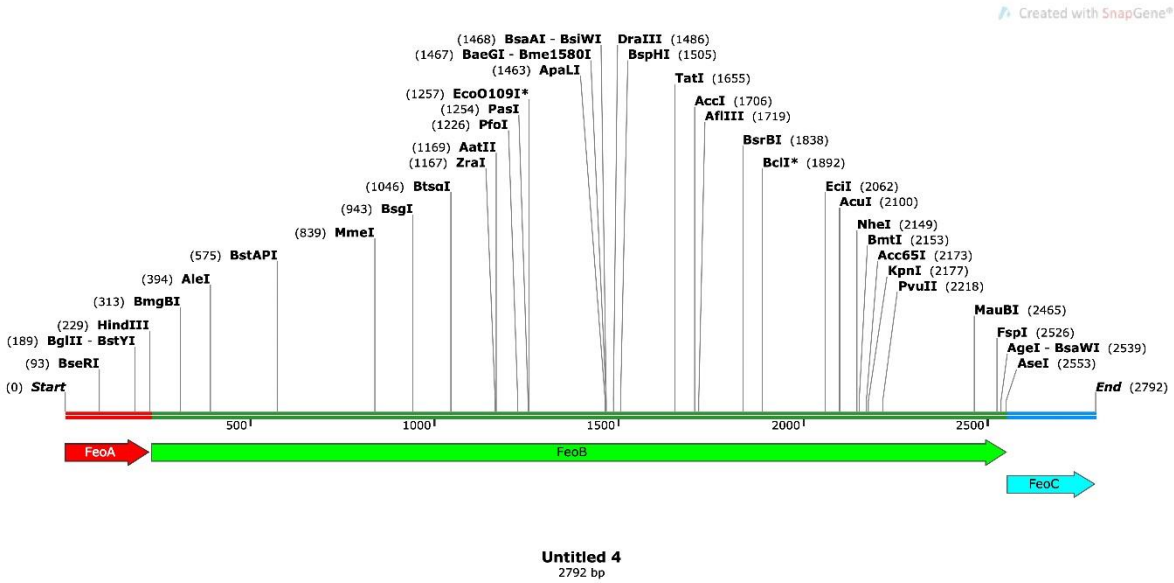

Figure 14.23: Map of *feoABC* operon.

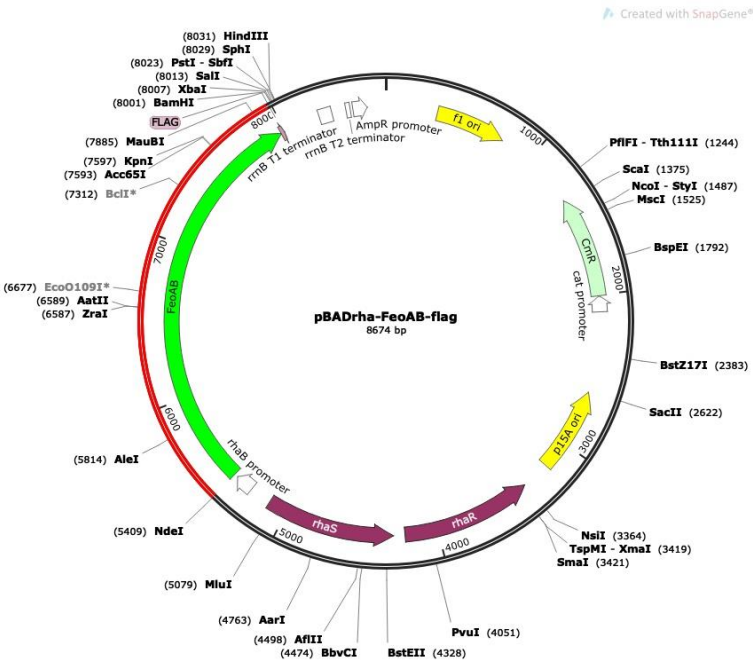

Figure 14.24: Map of FeoAB in pBADRha, cloned between *Nde*I and *Hin*dIII sites.

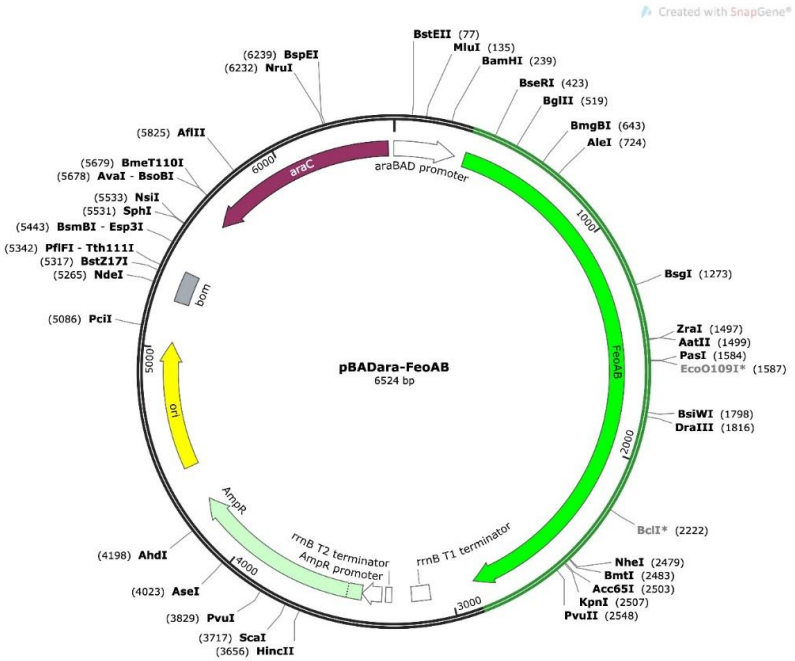

Figure 14.25: Map of FeoAB in pBADara, cloned between *Nco*I and *Hin*dIII sites.

14.2. Figures generated by Snapgene TM visualisation of the pTriEx 1.1 expression vector (EMD Millipore) with the salient features of the vector marked. Sequence was inserted between the *Nco*I and *Xho*I. The final recombinant vector was confirmed by DNA sequencing prior to its use to generate a recombinant baculovirus system.

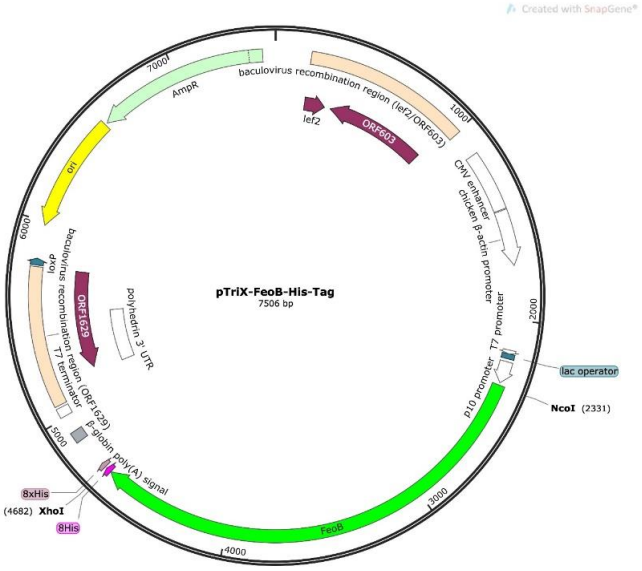

Figure 14.26: Map of FeoB-His-tag in pTriEx1.1, cloned between *Nco*I and *Xba*l sites.

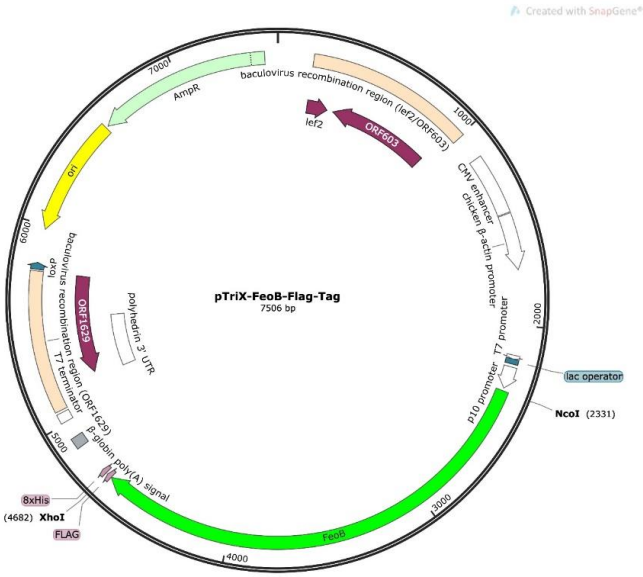

Figure 14.27: Map of FeoB-Flag-tag in pTriEx1.1, cloned between *Nco*I and *Xba*l sites.

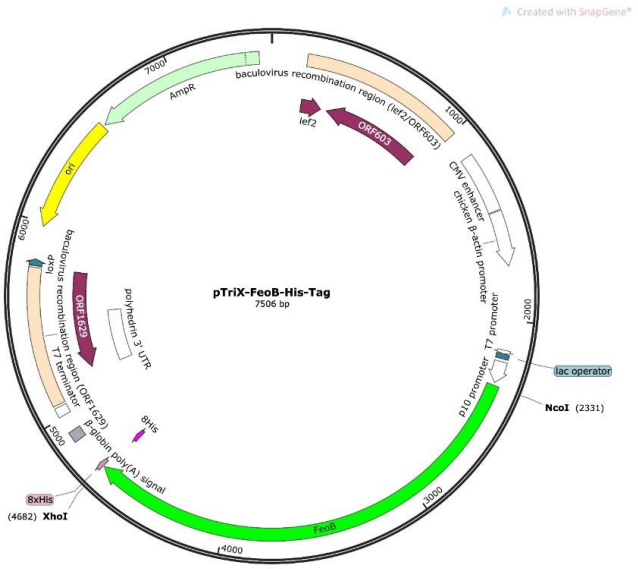

Figure 14.28A: Map of FeoB-His-tag in pTriEx1.1, cloned between *Nco*I and *Xba*l sites.

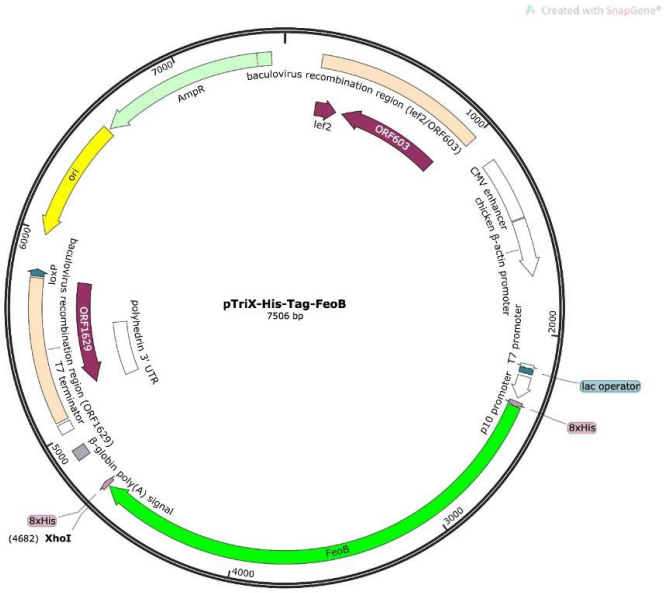

Figure 14.28B: Map of His-tag-FeoB in pTriEx1.1, cloned between *Nco*I and *Xba*l sites.

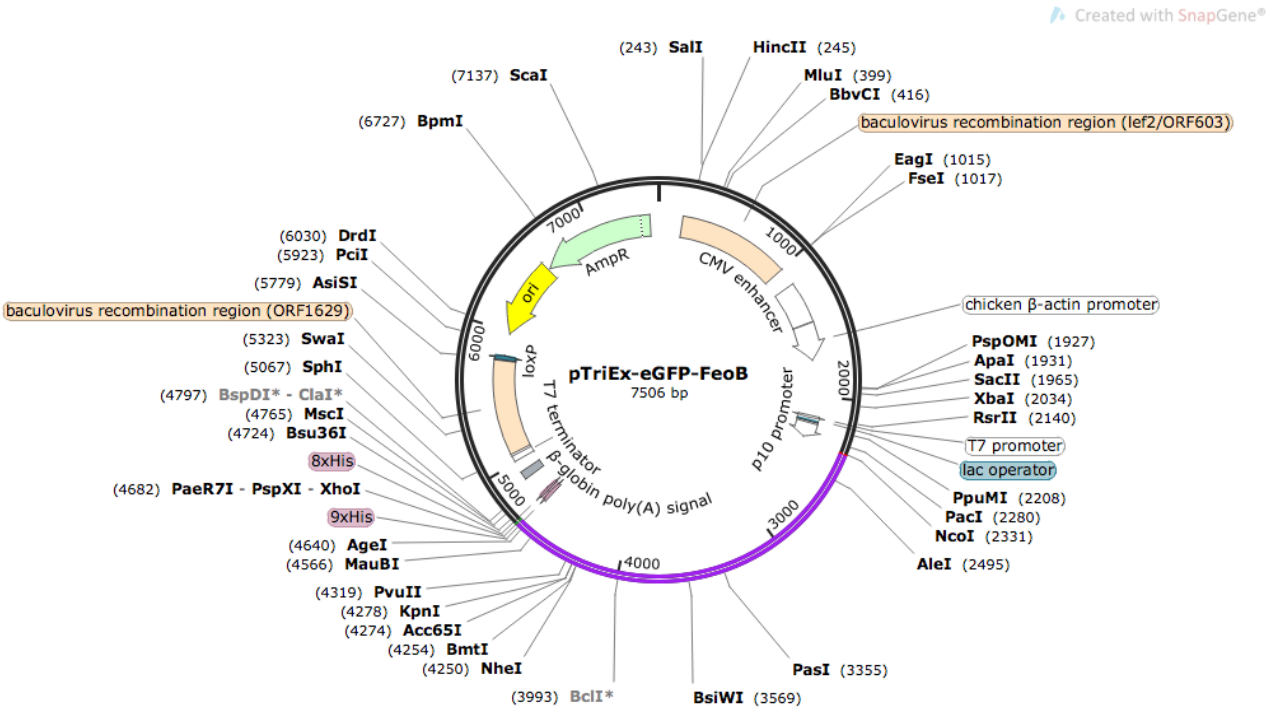

Figure 14.29: Map of -eGFP in pTriEx1.1, cloned between *Nco*I and *Xba*I sites.

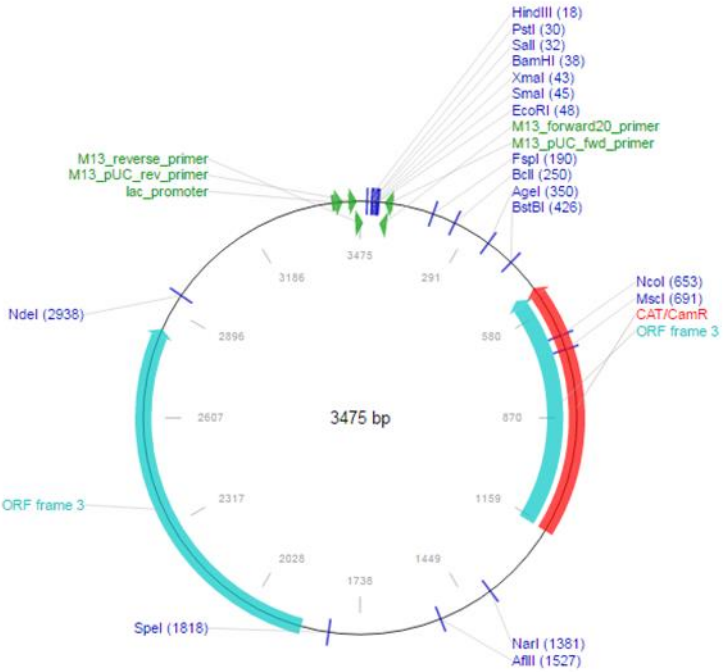

Figure 14.30. Map of pHSG576 (source Addgene)

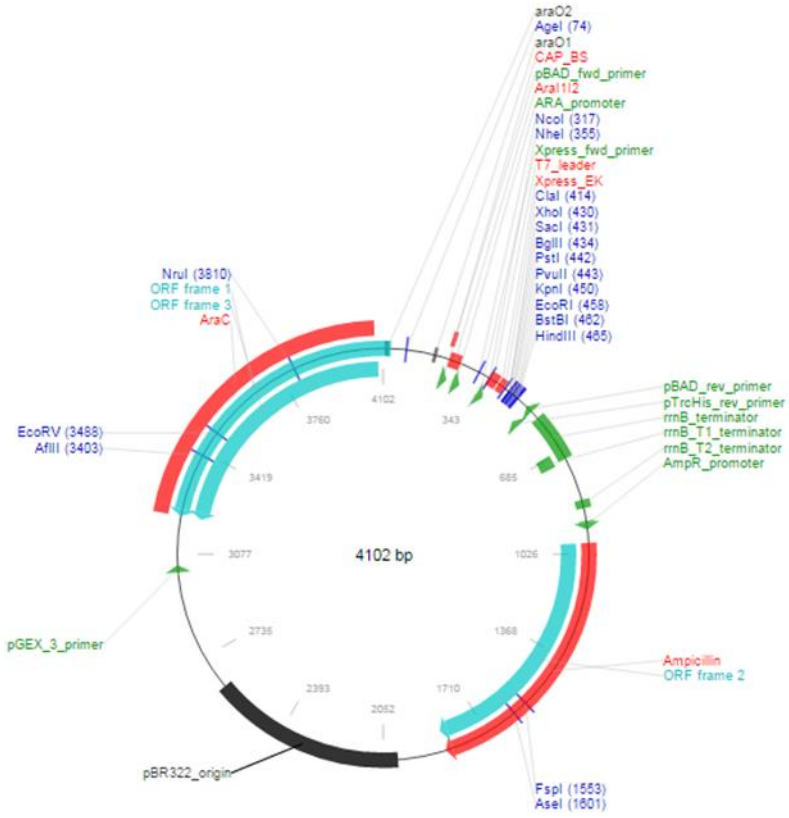

Figure 14.31. Map of pBADara (source Vetrogene)

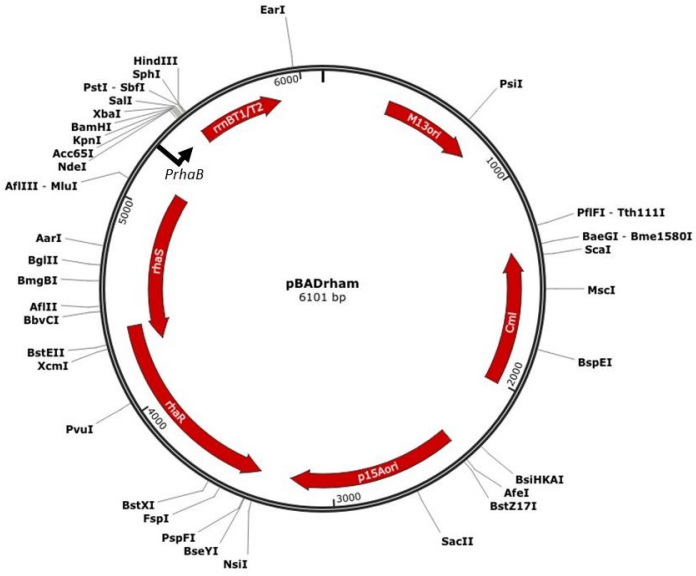

Figure 14.32. Map of pBADrha (source Genbank)

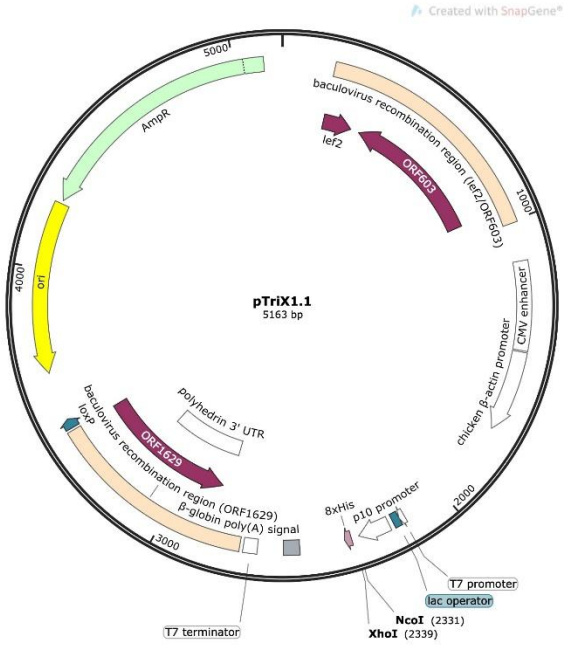

Figure 14.33: Map of pTriEx1.1.

14.3. Mutagenesis map

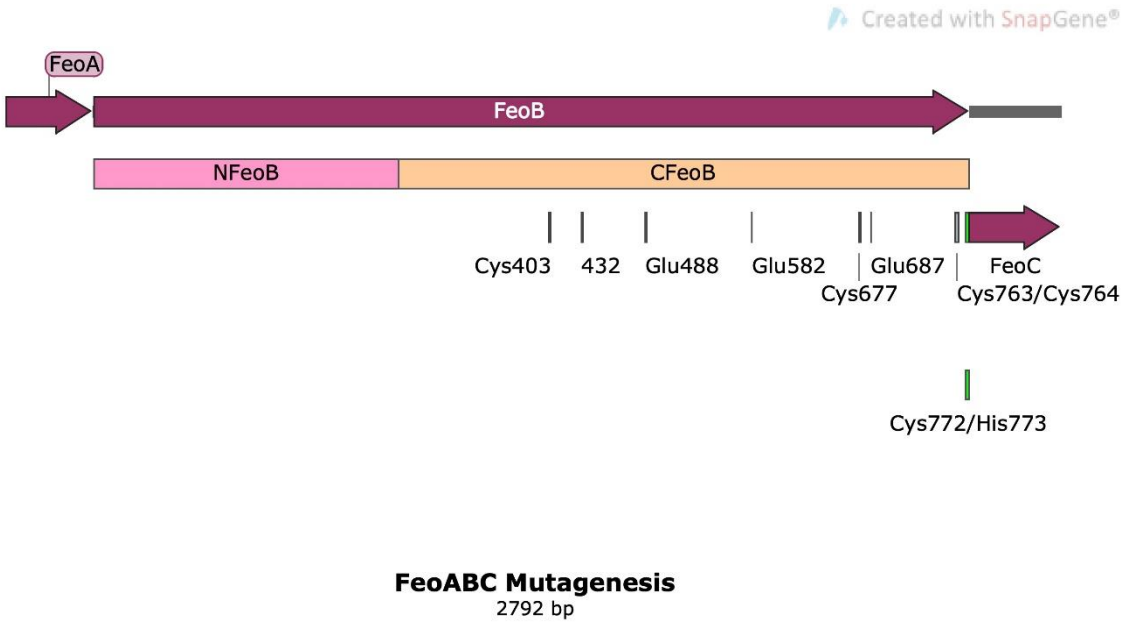

Figure 14.34: Map of Mutagenesis.

14.4. Seguencing map used Dstar softwere

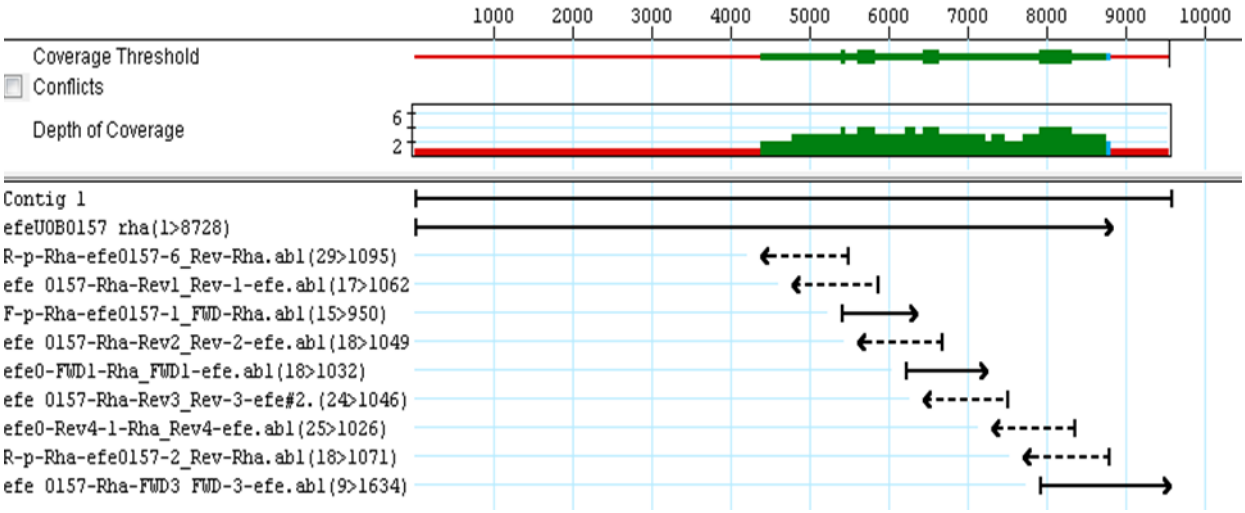

Figure 14.35. Alignment of sequence of *efeUOB* operon in pBADrha at restriction sites *Nde*I and *Sal*I. Sequences assembled by DNAStar program (*efeUOB* region only).

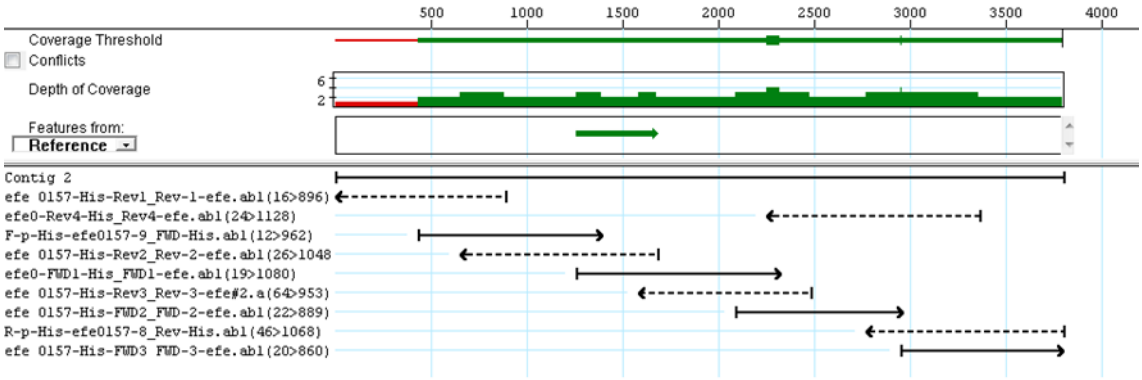

Fig. 14.36. Alignment of sequence of *efeUOB* operon which was cloned into pBADara at restriction sites *Nco*I and *Hin*dIII.

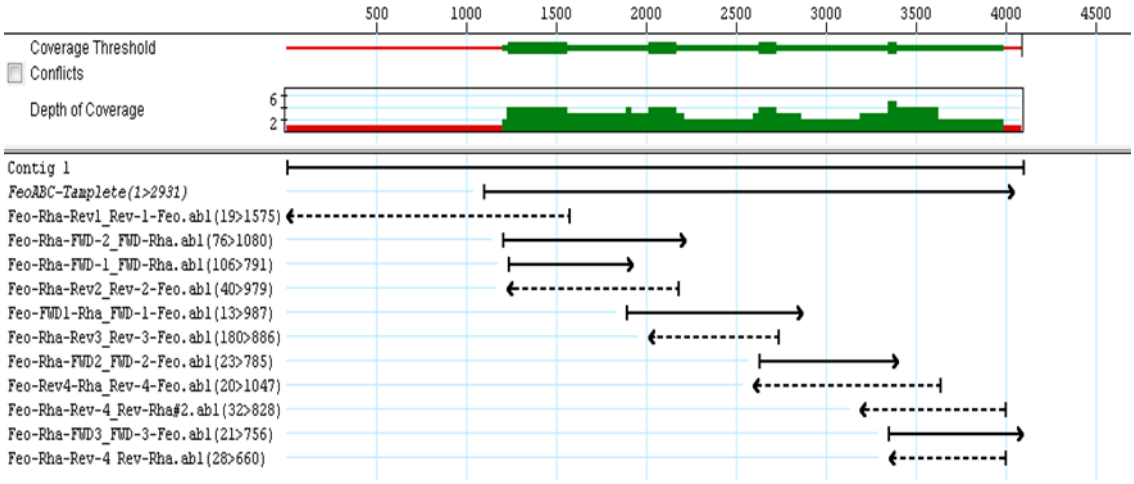

Figure 14.37. Alignment of sequence of *feoABC* operon cloned into pBADrha at restriction sites *Nde*I and *Sal*I.

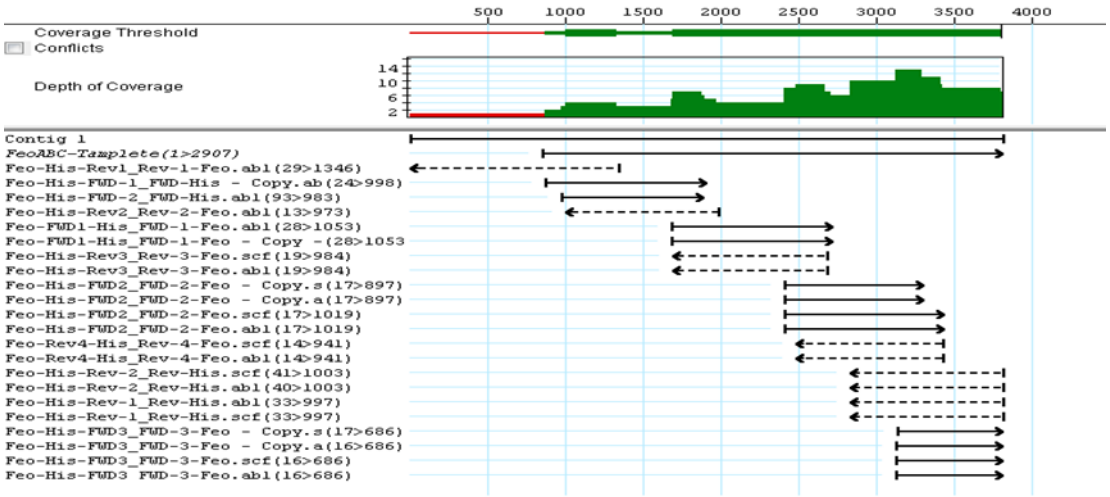

Figure 14.38. Alignment of sequence of *feoABC* operon which was cloned into pBADara at restriction sites *Nco*I and *Hin*dIII.

14.5. Sequence Alignment

NCBI Blast showed 100% identity for multiple sequence alignment of all *feoABC* clones.

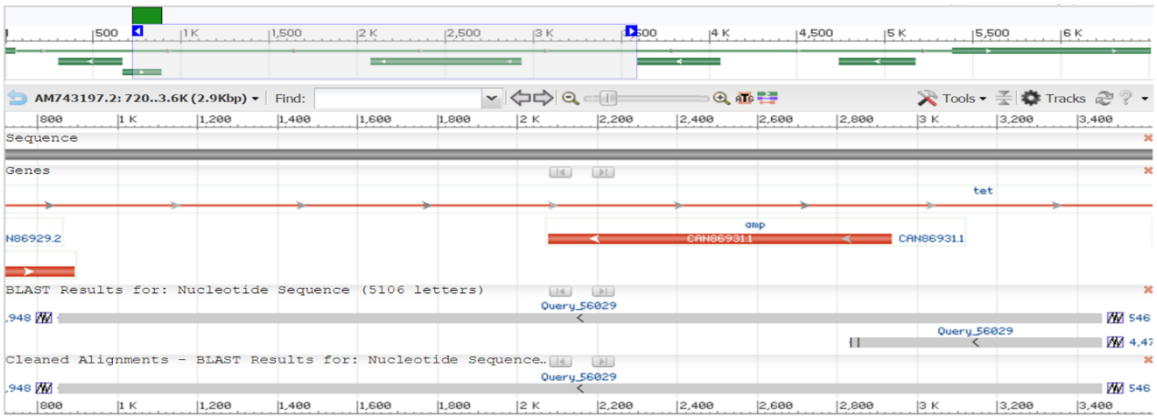

Figure 14.39: Alignment of *feoA* cloned into pBADara.

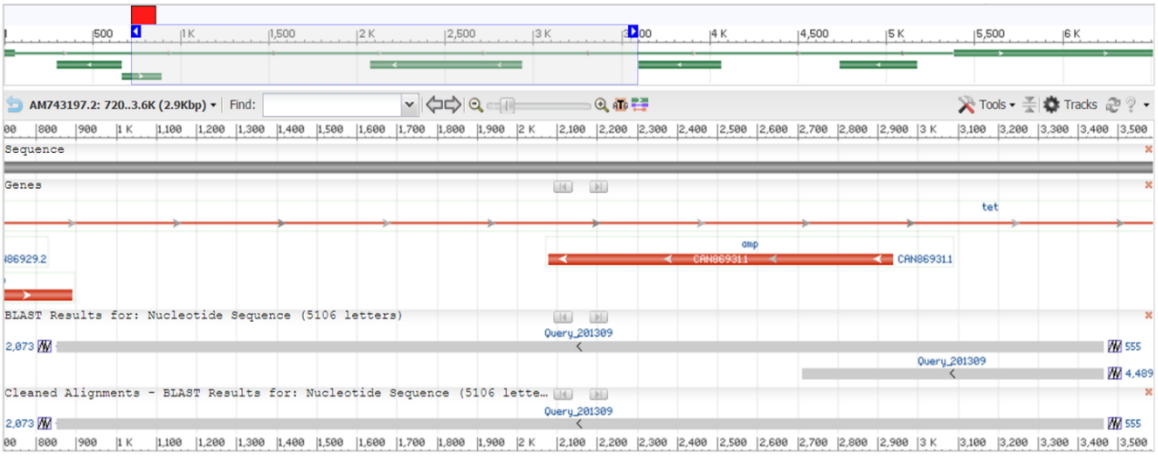

Figure 14.40: Alignment of *feoC* cloned into pBADara.

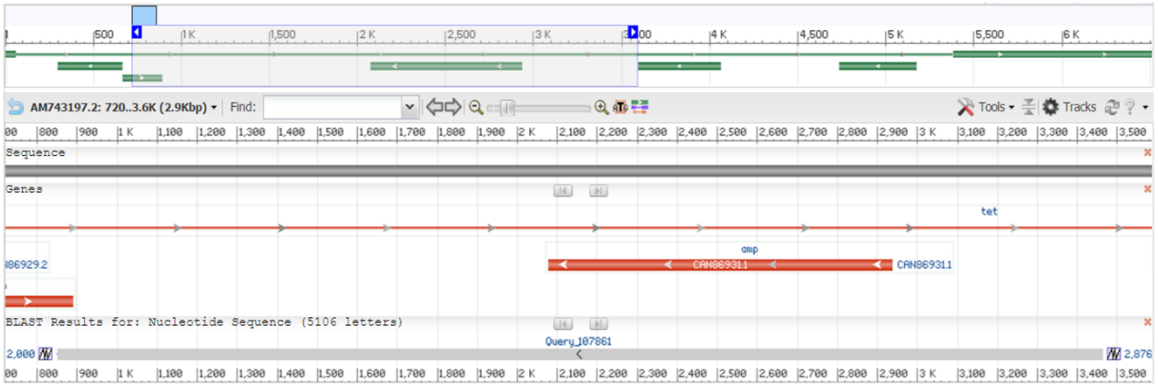

Figur 14.41: Alignment of *feoBC* cloned intoBADara.

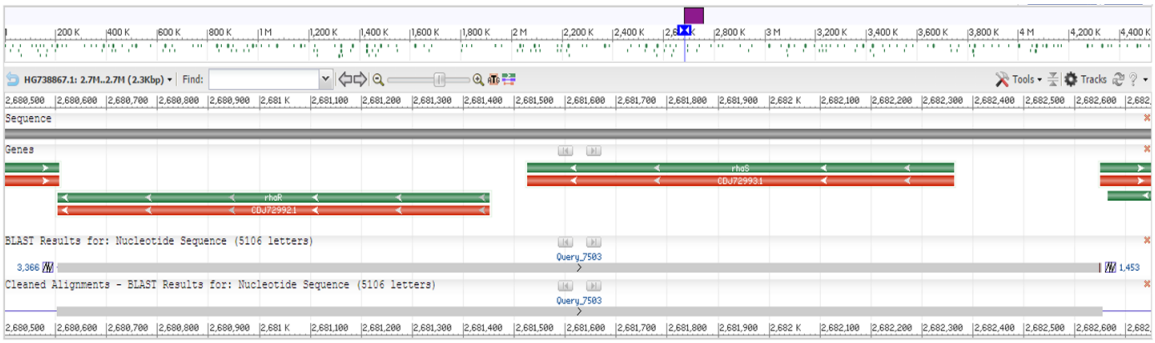

Figure 14.42: Alignment of *feoA* cloned into pBADRha.

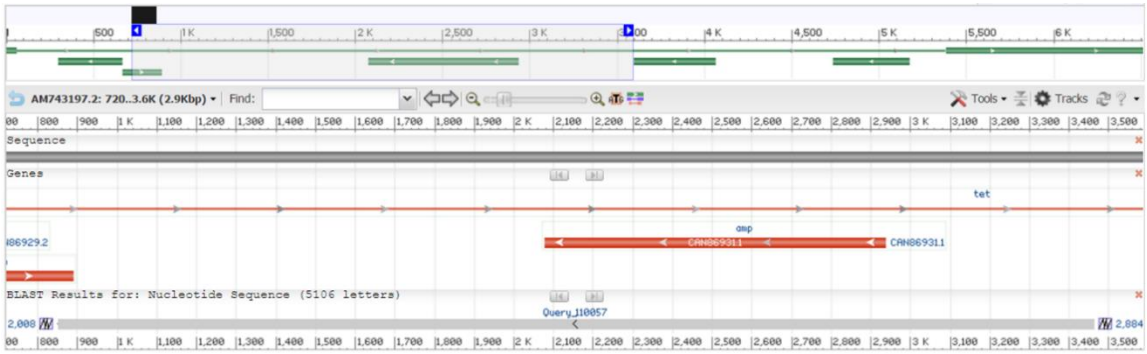

Figure 14.43: Alignment of *feoAB* cloned into pBADara.

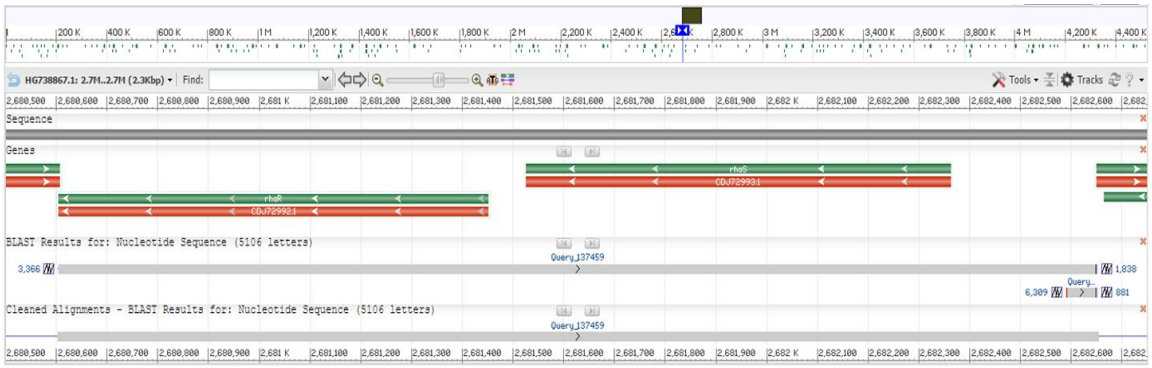

Figure 14.44: Alignment of *feoC* cloned into pBADRha.

Figure 14.45: Alignment of *feoB* cloned into pBADRha.

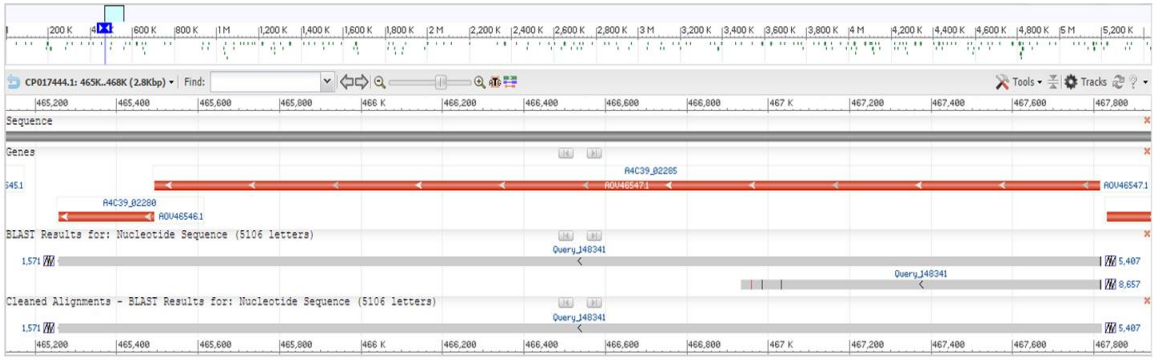

Figure 14.46: Alignment of *feoBC* cloned into pBADRha.

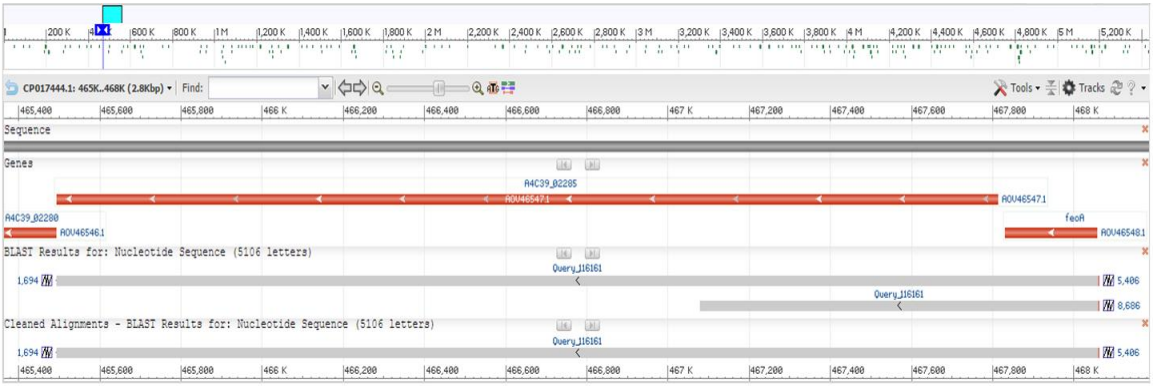

Figure 14.47: Alignment of *feoAB* cloned into pBADRha.

14.6. Western blotting extra results

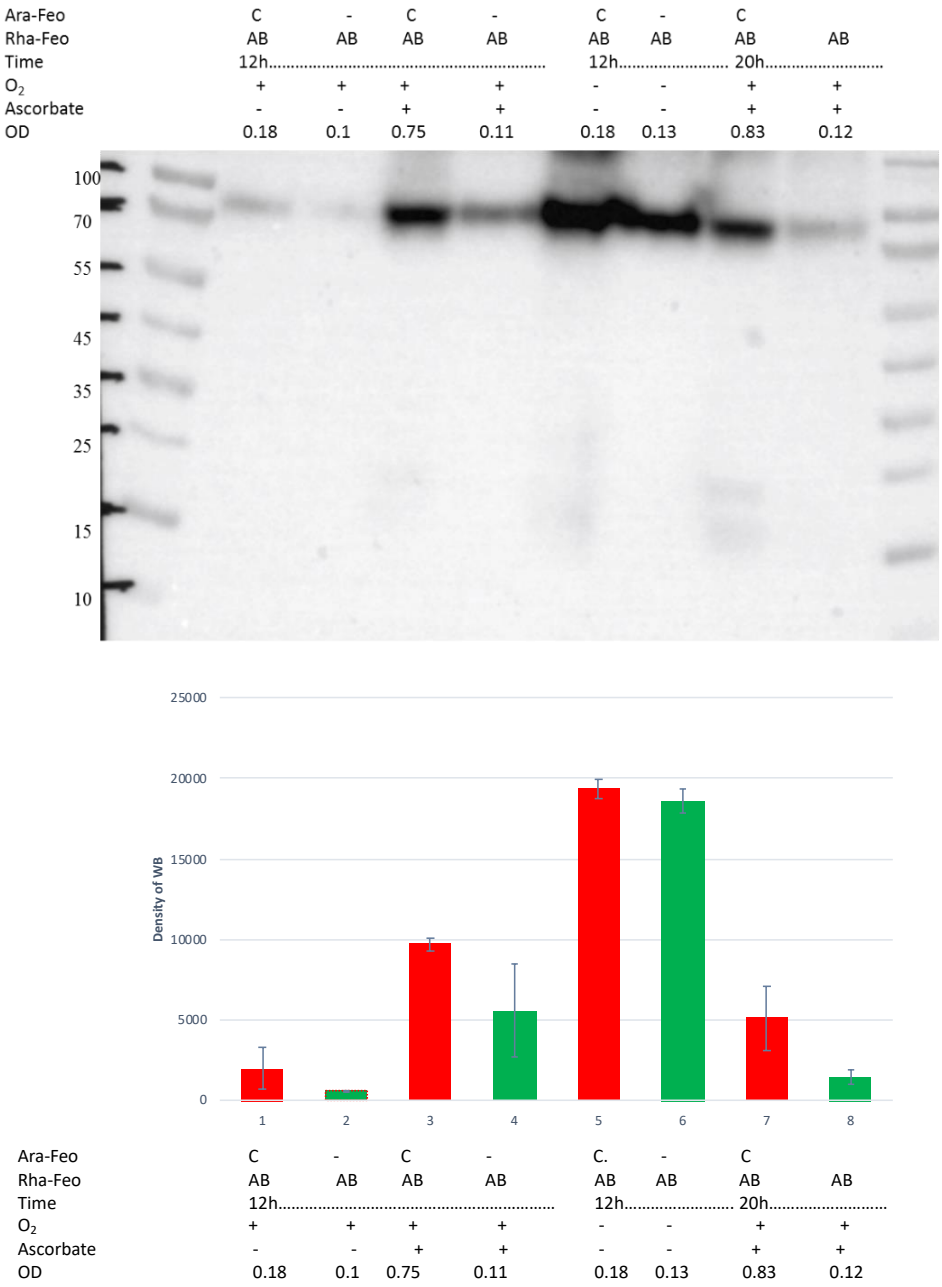

Figure 14.48 A1: Western blot analysis of FeoB-Flag levels in response to O_2, ascorbate and FeoC status (at 12 h). JC32 was grown in M9 medium with 0.5 µM DTPA, under aerobic or anaerobic conditions, with/without 2 mM ascorbate (as indicated) and carried pBADrha-*feoAB*-Flag together with the indicated pBADara plasmid.

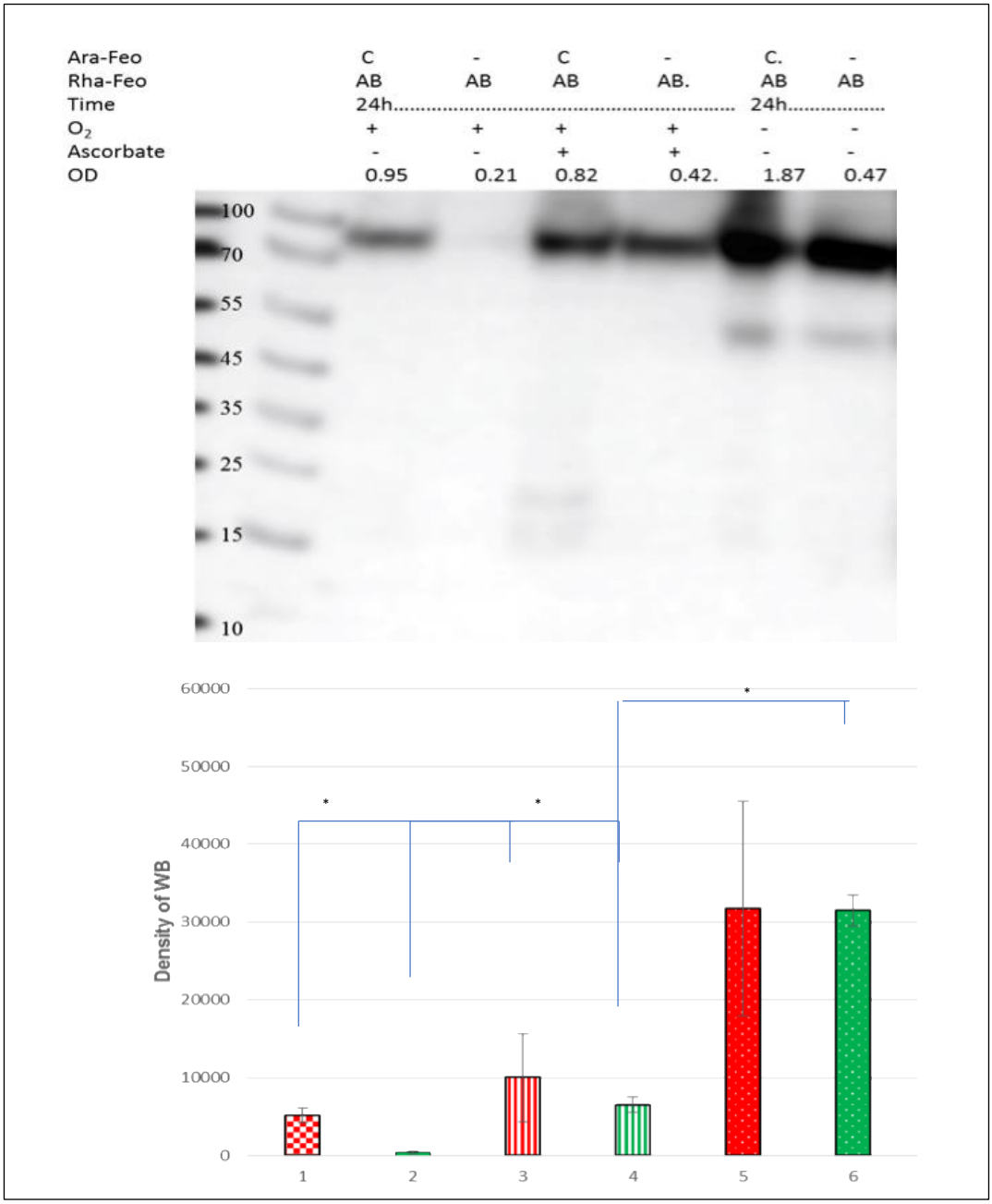

Figure 14.49 A2: Western blot analysis of FeoB-Flag levels in response to O_2, ascorbate and FeoC status (at 20 h). Conditions were as in Fig. A2 except that samples are taken at 20 h.

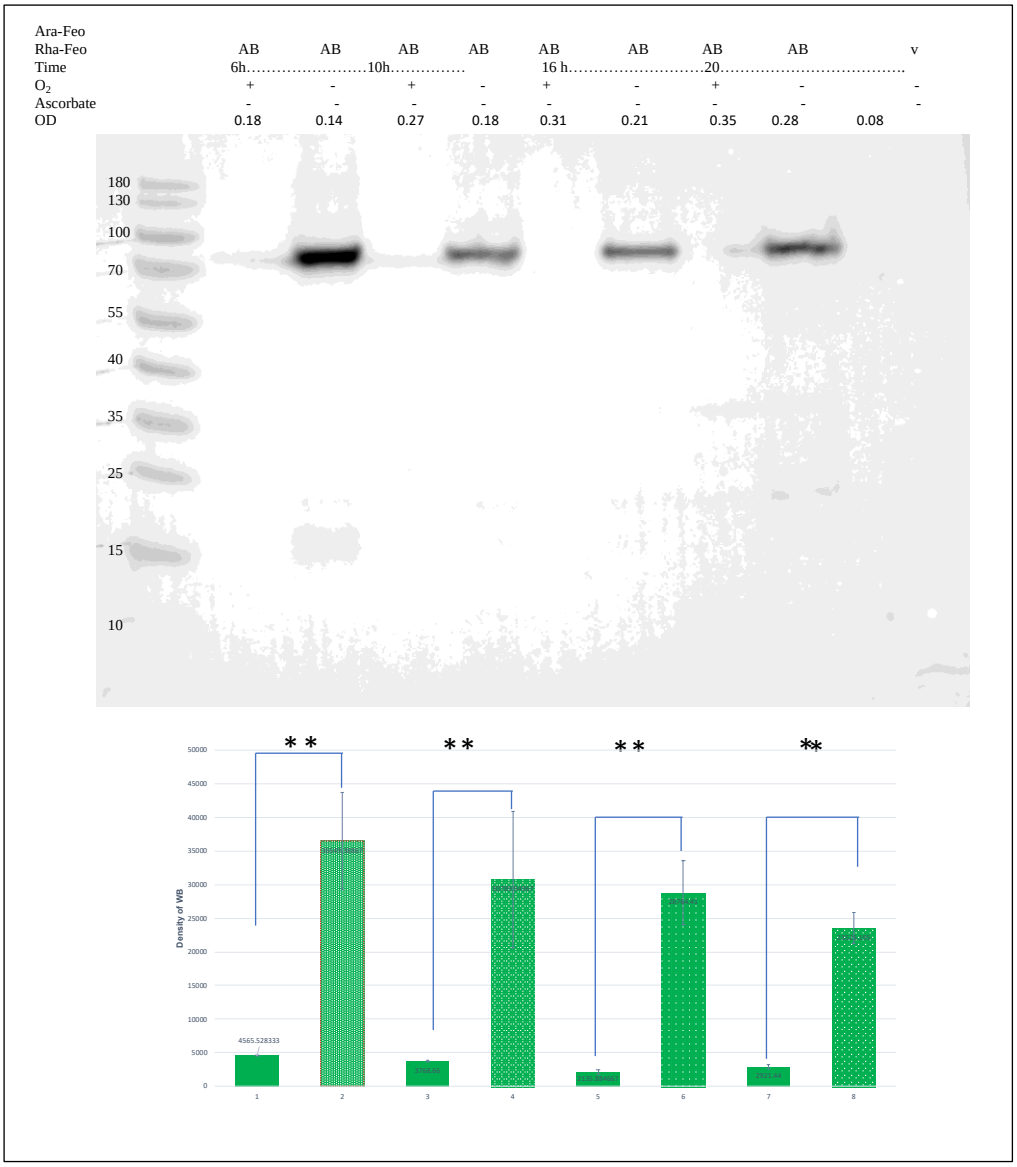

Figure 14.50 A3: Western blot analysis of FeoAB-Flag levels in absence of FeoC under aerobic (without ascorbate) or anaerobic conditions, over time (6-20 h). Conditions were as in Fig. A1, except for absence of ascorbate throughout, the times of sampling, and the absence of *feoC*.

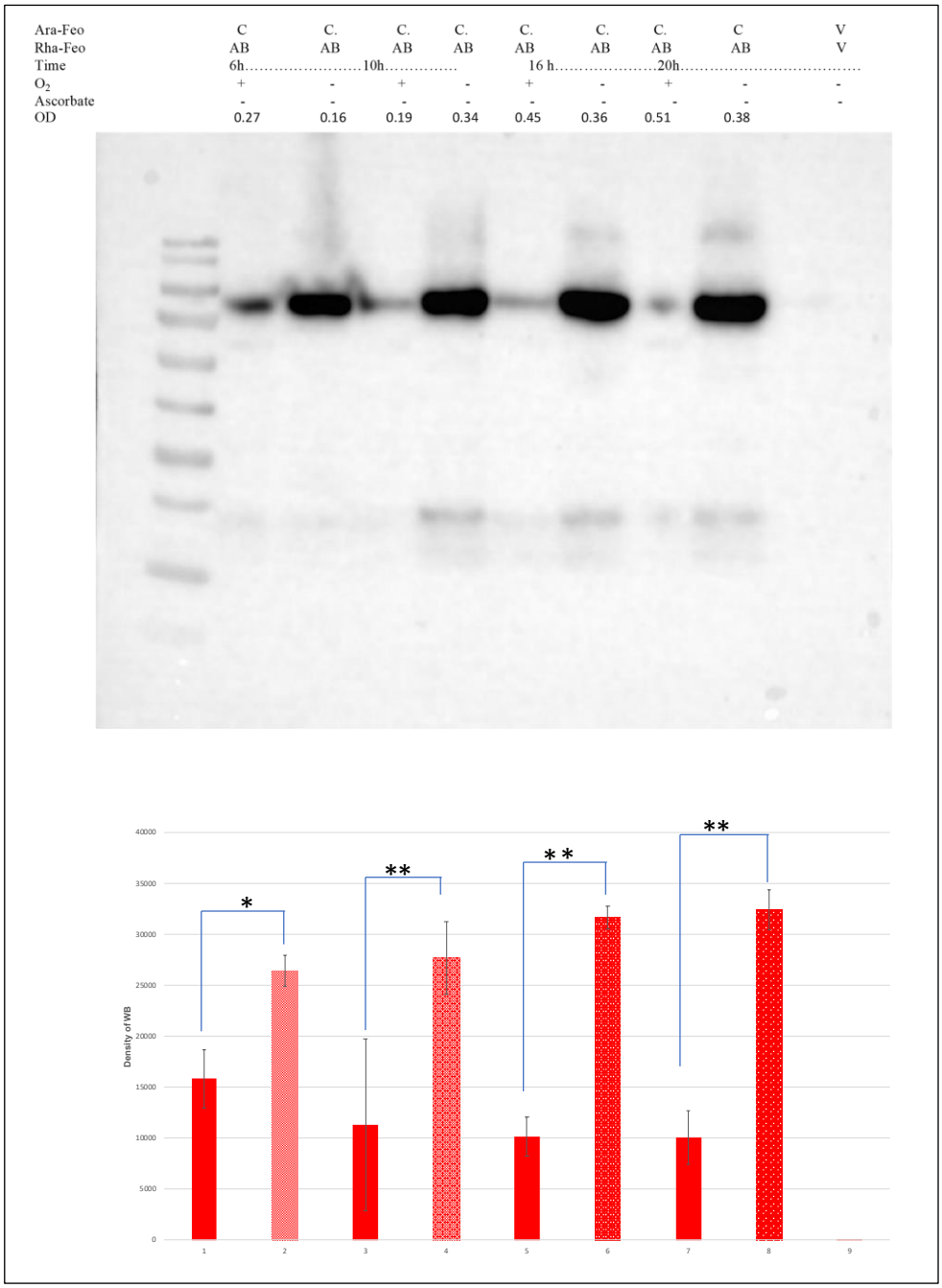

Figure14.51 A4: Western blot analysis of FeoAB-Flag levels with FeoC under aerobic (without ascorbate) or anaerobic condition, over time (6-20 h). Details are as in Fig. A3 except for presence of *feoC* in all cases.

A

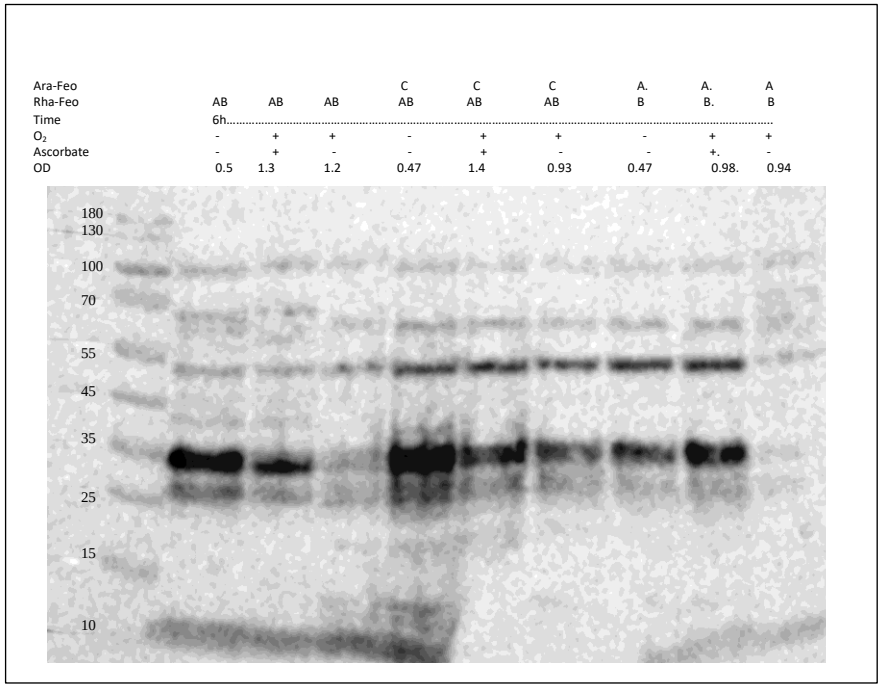

B

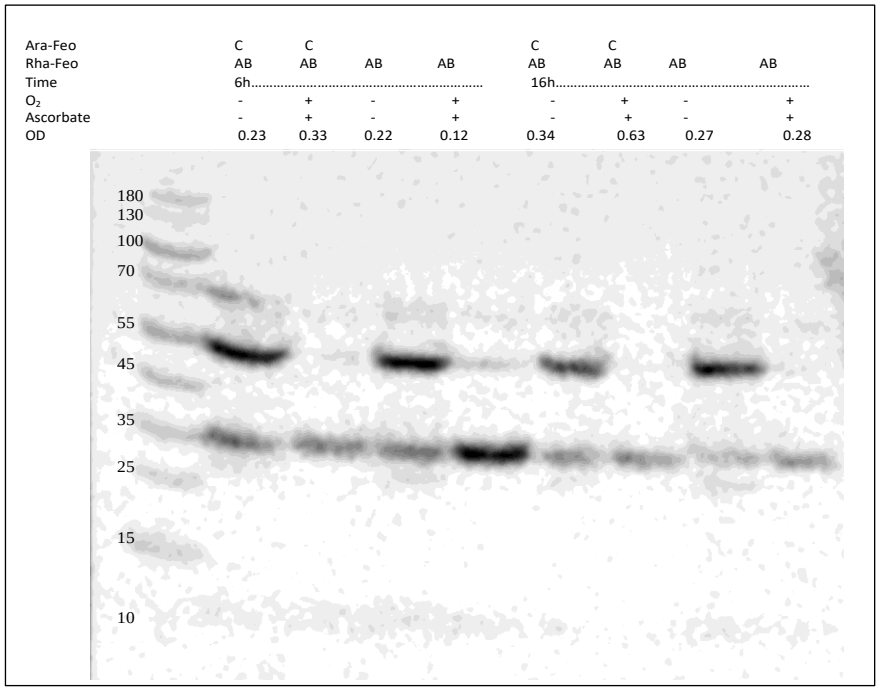

Figure 14.52 A5: Western blot analysis of FeoAB-His with/without FeoC under aerobic conditions (+/- ascorbate) and anaerobic conditions (6-16 h). A. Growth was performed in medium LB with glucose at ph 6. **B**. Growth was in M9 medium, 0.4% glucose at pH 6. 0.02% rhamnose and 0.002% arabinose were included Strains were JC32 with pBADara-*feoAB-His*^{O157} or pBADara-His-*feoB-His*^{O157} with pBADrha-*feoC*^{O157}, pBADrha-*feoA*^{O157} or pBADrha.

14.7. Bradford assay

Unknowns

Sample	Wells	OD Values	Concentration	Mean Conc.	Std.Dev.	CV%	Dilution	Adj. Conc.
Un01	C2	0.985	0.607	0.594	0.017	2.9	2.0	1.187
	D2	0.963	0.574					
	E2	0.980	0.599					
Un02	C3	0.392	0.013	0.007	0.005	66.5	10.0	0.074
	D3	0.382	0.004					
	E3	0.384	0.006					
Un03	C5	0.986	0.608	0.622	0.021	3.5	2.0	1.243
	D5	0.987	0.610					
	E5	1.009	0.647					
Un04	C6	0.588	0.167	0.067	0.086	128.3	10.0	0.672
	D6	0.394	0.015					
	E6	0.400	0.020					
Un05	C8	0.977	0.595	0.633	0.033	5.2	2.0	1.265
	D8	1.012	0.651					
	E8	1.012	0.651					
Un06	C9	0.457	0.064	0.050	0.013	26.4	10.0	0.504
	D9	0.437	0.049					
	E9	0.423	0.038					
Un07	C11	1.028	0.678	0.689	0.022	3.2	2.0	1.378
	D11	1.026	0.675					
	E11	1.049	0.714					
Un08	C12	0.420	0.036	0.043	0.014	32.7	10.0	0.432
	D12	0.418	0.034					
	E12	0.451	0.059					

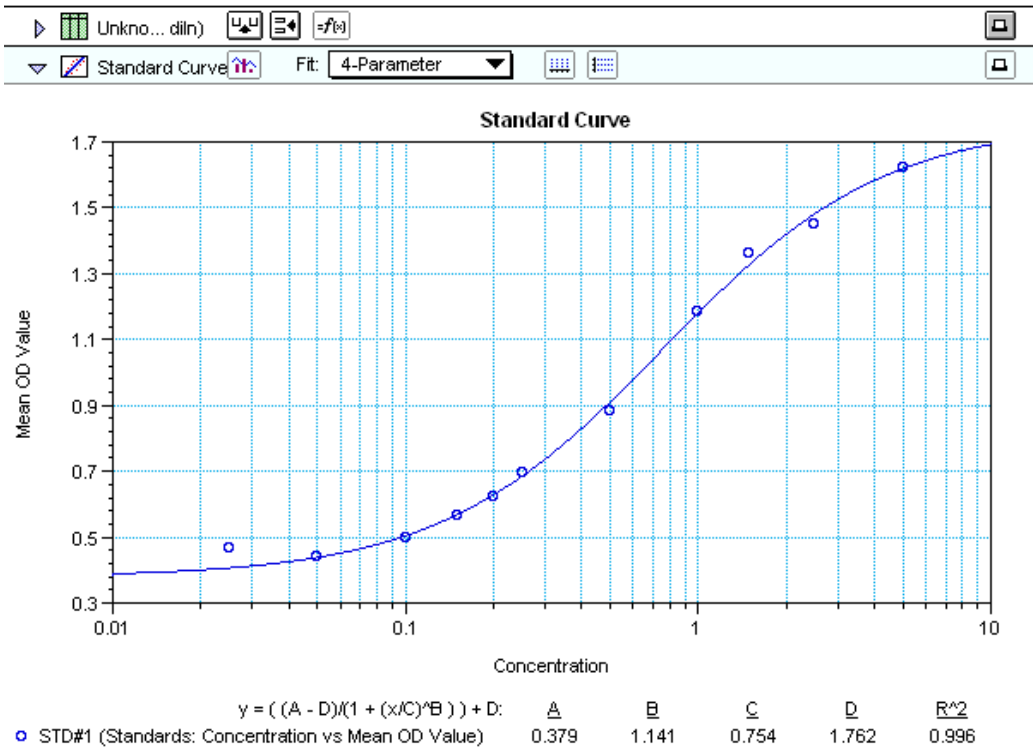

Figure 14.53: Bradford assay standard curve.

14.8. Formulations of crystillisation screens

14.8.1 MemMeso™ FX-96 MD1-87FX

Molecular Dimensions

LCP

Membrane Proteins

MemMeso™ FX-96 **MD1-87-FX**

MemMeso™ – A 96-condition crystallization screen specifically for use with mesophases (LCP compatible).

MD1-87-FX is presented as 96 x 100 µL conditions.

Features of MemMeso™:

- Optimized to work in synergy with Lipidic Cubic Phase (LCP) and the LCP crystallization method.
- Allows screening in both LCP and Sponge Phase.
- Conditions data-mined from current GPCR crystal structures.
- A semi-systematic screening kit, containing 96 conditions covering a range of pH, precipitants and salt.
- Proven successful at crystallizing the crystal structures of eight membrane proteins, including the structure of channelrhodopsin (2012, Nature).

Introduction:

Out of the successful laboratory of Prof. Osamu Nureki at University of Tokyo, Japan, this semi-systematic screen has been developed to work in synergy with the Lipidic Cubic Phase (LCP) used in membrane protein crystallization. Most commercially available crystallization screens have been optimized to work with the vapour diffusion method and are therefore not ideal to use with LCP.

Eight membrane proteins structures have already been elucidated using MemMeso™: Channelrhodopsin (2012, Nature), PfMATE (2013, Nature), NCX_Mj (2013, Science), GkPOT (2013, PNAS), and four bacterial transporters (manuscript in preparation).

Crystals grown using MemMeso™. Courtesy of H.Kato

Tips for use

Usually 800 – 1000 nL of MemMeso™ is needed for each experiment (well).

For LCP crystallization, dispense 25 – 50 nL of LCP bolus onto 96-well sandwich plate (e.g. Laminex plate), and then overlay with 800 - 1000nL of precipitant solution.

Mix the protein sample and lipid (monoolein) in a Hamilton syringe (in this process, the monoolein forms cubic phase and the protein is reconstituted in the cubic phase). Dispense the mixture (=protein in monoolein LCP) on the crystallization plate, and overlay MemMeso™ solution onto the mixture.

In some conditions, the mixtures are stable in the cubic phase, and in other conditions, the mixtures are changed to the sponge phase. It is impossible to predict whether the target protein is crystallized in the cubic phase and/or sponge phase, so MemMeso™ is ideal as it allows screening in both phases.

References:

Kato, H. *et al*, Nature. 2012 Jan 22;482(7385):369-74.
Tanaka, Y. *et al*, Nature. 2013 Apr 11;496(7444):247-51.
Doki, So. *et al*, Proc Natl Acad Sci U S A. 2013 Jul 9; 110(28):11343-8.

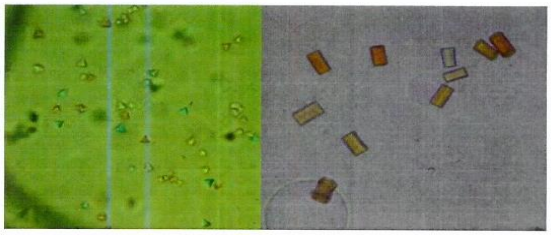

Figure 14.54 (1-1): Moecular dimension for crystilisation method MemMeso-FX 96 MD1-87-FX.

Molecular Dimensions

LCP

Membrane Proteins

Formulation Notes:

MemMeso™ reagents are formulated using ultrapure water (>18.0 MΩ) and are sterile-filtered using 0.22 µm filters. No preservatives are added.

Final pH may vary from that specified on the datasheet. Molecular Dimensions will be happy to discuss the precise formulation of individual reagents.

Individual reagents and stock solutions for optimization are available from Molecular Dimensions.

Enquiries regarding MemMeso™ formulation, interpretation of results or optimization strategies are welcome. Please e-mail, fax or phone your query to Molecular Dimensions.

Contact and product details can be found at www.moleculardimensions.com

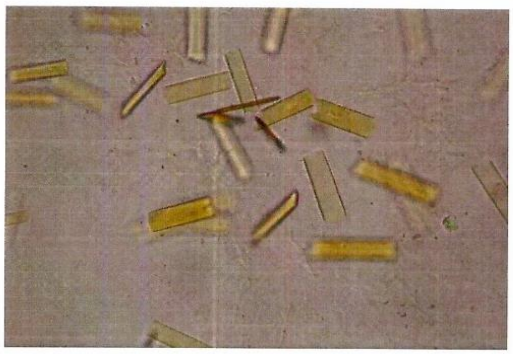

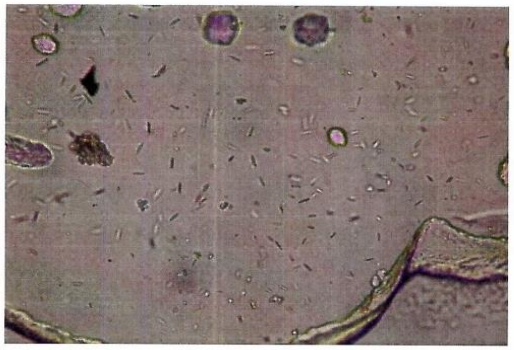

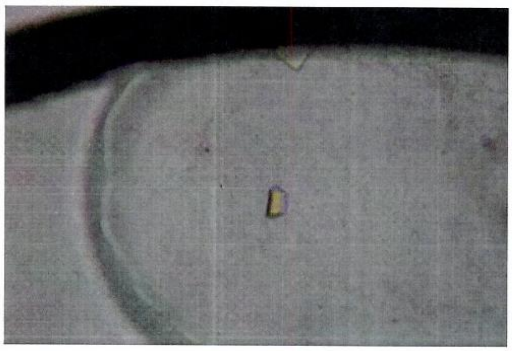

Figure 14.54 (1-2): Moecular dimension for crystilisation method MemMeso-FX 96 MD1-87-FX.

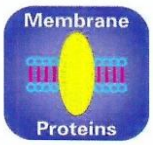

MemMeso™ FX-96 Conditions A1-D12 MD1-87-FX

Well #	Conc	Salt	Conc	Buffer	pH	Conc	Precipitate
A1	0.1 M	Magnesium chloride hexahydrate	0.1 M	Sodium citrate tribasic dihydrate	5	40 % v/v	PEG 200
A2	0.1 M	Sodium chloride	0.1 M	Sodium citrate tribasic dihydrate	5	40 % v/v	PEG 200
	0.1 M	Lithium sulfate					
A3	0.1 M	Sodium chloride	0.1 M	Sodium citrate tribasic dihydrate	5	40 % v/v	PEG 200
A4			0.1 M	Sodium citrate tribasic dihydrate	5	40 % v/v	PEG 200
A5	0.1 M	Sodium chloride	0.1 M	MES	6	40 % v/v	PEG 200
	0.1 M	Magnesium chloride hexahydrate					
A6	0.1 M	Sodium chloride	0.1 M	MES	6	40 % v/v	PEG 200
	0.1 M	Lithium sulfate					
A7	0.1 M	Sodium chloride	0.1 M	MES	6	40 % v/v	PEG 200
	0.1 M	Calcium chloride dihydrate					
A8	0.01 M	Zinc acetate dihydrate	0.1 M	MES	6	40 % v/v	PEG 200
A9	0.1 M	Sodium chloride	0.1 M	HEPES	7	40 % v/v	PEG 200
	0.1 M	Magnesium chloride hexahydrate					
A10	0.1 M	Lithium sulfate	0.1 M	HEPES	7	40 % v/v	PEG 200
A11	0.1 M	Sodium chloride	0.1 M	HEPES	7	40 % v/v	PEG 200
	0.1 M	Calcium chloride dihydrate					
A12			0.1 M	HEPES	7	40 % v/v	PEG 200
B1	0.1 M	Sodium chloride	0.1 M	Tris	8	40 % v/v	PEG 200
	0.1 M	Magnesium chloride hexahydrate					
B2	0.1 M	Sodium chloride	0.1 M	Tris	8	40 % v/v	PEG 200
	0.1 M	Lithium sulfate					
B3	0.1 M	Sodium chloride	0.1 M	Tris	8	40 % v/v	PEG 200
	0.1 M	Calcium chloride dihydrate					
B4	0.2 M	Ammonium sulfate	0.1 M	Tris	8	40 % v/v	PEG 200
B5	0.1 M	Sodium chloride	0.1 M	Sodium citrate tribasic dihydrate	5	30 % v/v	PEG 300
	0.1 M	Magnesium chloride hexahydrate					
B6	0.1 M	Sodium chloride	0.1 M	Sodium citrate tribasic dihydrate	5	30 % v/v	PEG 300
	0.1 M	Lithium sulfate					
B7	0.1 M	Sodium chloride	0.1 M	Sodium citrate tribasic dihydrate	5	30 % v/v	PEG 300
B8			0.1 M	Sodium citrate tribasic dihydrate	5	30 % v/v	PEG 300
B9	0.1 M	Sodium chloride	0.1 M	MES	6	30 % v/v	PEG 300
	0.1 M	Magnesium chloride hexahydrate					
B10	0.1 M	Sodium chloride	0.1 M	MES	6	30 % v/v	PEG 300
	0.1 M	Lithium sulfate					
B11	0.1 M	Sodium chloride	0.1 M	MES	6	30 % v/v	PEG 300
	0.1 M	Calcium chloride dihydrate					
B12	0.01 M	Zinc acetate dihydrate	0.1 M	MES	6	30 % v/v	PEG 300
C1	0.1 M	Sodium chloride	0.1 M	HEPES	7	30 % v/v	PEG 300
	0.1 M	Magnesium chloride hexahydrate					
C2	0.1 M	Sodium chloride	0.1 M	HEPES	7	30 % v/v	PEG 300
	0.1 M	Lithium sulfate					
C3	0.1 M	Sodium chloride	0.1 M	HEPES	7	30 % v/v	PEG 300
	0.1 M	Calcium chloride dihydrate					
C4			0.1 M	HEPES	7	30 % v/v	PEG 300
C5	0.1 M	Magnesium chloride hexahydrate	0.1 M	Tris	8	30 % v/v	PEG 300
C6	0.1 M	Sodium chloride	0.1 M	Tris	8	30 % v/v	PEG 300
	0.1 M	Lithium sulfate					
C7	0.1 M	Sodium chloride	0.1 M	Tris	8	30 % v/v	PEG 300
	0.1 M	Calcium chloride dihydrate					
C8	0.2 M	Ammonium sulfate	0.1 M	Tris	8	30 % v/v	PEG 300
C9	0.1 M	Sodium chloride	0.1 M	Sodium citrate tribasic dihydrate	5	30 % v/v	PEG 400
	0.1 M	Magnesium chloride hexahydrate					
C10	0.1 M	Sodium chloride	0.1 M	Sodium citrate tribasic dihydrate	5	30 % v/v	PEG 400
	0.1 M	Lithium sulfate					
C11	0.1 M	Sodium chloride	0.1 M	Sodium citrate tribasic dihydrate	5	30 % v/v	PEG 400
C12			0.1 M	Sodium citrate tribasic dihydrate	5	30 % v/v	PEG 400
D1	0.1 M	Sodium chloride	0.1 M	MES	6	30 % v/v	PEG 400
	0.1 M	Magnesium chloride hexahydrate					
D2	0.1 M	Lithium sulfate	0.1 M	MES	6	30 % v/v	PEG 400
D3	0.1 M	Sodium chloride	0.1 M	MES	6	30 % v/v	PEG 400
	0.1 M	Calcium chloride dihydrate					
D4	0.01 M	Zinc acetate dihydrate	0.1 M	MES	6	30 % v/v	PEG 400
D5	0.1 M	Sodium chloride	0.1 M	HEPES	7	30 % v/v	PEG 400
	0.1 M	Magnesium chloride hexahydrate					
D6	0.1 M	Sodium chloride	0.1 M	HEPES	7	30 % v/v	PEG 400
	0.1 M	Lithium sulfate					
D7	0.1 M	Sodium chloride	0.1 M	HEPES	7	30 % v/v	PEG 400
	0.1 M	Calcium chloride dihydrate					
D8			0.1 M	HEPES	7	30 % v/v	PEG 400
D9	0.1 M	Sodium chloride	0.1 M	Tris	8	30 % v/v	PEG 400
	0.1 M	Magnesium chloride hexahydrate					
D10	0.1 M	Sodium chloride	0.1 M	Tris	8	30 % v/v	PEG 400
	0.1 M	Lithium sulfate					
D11	0.1 M	Calcium chloride dihydrate	0.1 M	Tris	8	30 % v/v	PEG 400
D12	0.2 M	Ammonium sulfate	0.1 M	Tris	8	30 % v/v	PEG 400

Figure 14.54 (1-3): Moecular dimension for crystilisation method MemMeso-FX 96 MD1-87-FX.

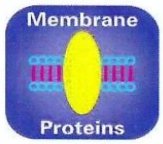

MemMeso™ FX-96 **Conditions E1-H12** **MD1-87-FX**

Well #	Conc	Salt 1	Conc	Buffer	pH	Conc	Precipitate
E1	0.1 M	Magnesium chloride hexahydrate	0.1 M	Sodium citrate tribasic dihydrate	5	30 % v/v	PEG 500 DME
E2	0.1 M	Sodium chloride	0.1 M	Sodium citrate tribasic dihydrate	5	30 % v/v	PEG 500 DME
	0.1 M	Lithium sulfate					
E3	0.1 M	Sodium chloride	0.1 M	Sodium citrate tribasic dihydrate	5	30 % v/v	PEG 500 DME
E4			0.1 M	Sodium citrate tribasic dihydrate	5	30 % v/v	PEG 500 DME
E5	0.1 M	Sodium chloride	0.1 M	MES	6	30 % v/v	PEG 500 DME
	0.1 M	Magnesium chloride hexahydrate					
E6	0.1 M	Sodium chloride	0.1 M	MES	6	30 % v/v	PEG 500 DME
	0.1 M	Lithium sulfate					
E7	0.1 M	Sodium chloride	0.1 M	MES	6	30 % v/v	PEG 500 DME
	0.1 M	Calcium chloride dihydrate					
E8	0.01 M	Zinc acetate dihydrate	0.1 M	MES	6	30 % v/v	PEG 500 DME
E9	0.1 M	Sodium chloride	0.1 M	HEPES	7	30 % v/v	PEG 500 DME
	0.1 M	Magnesium chloride hexahydrate					
E10	0.1 M	Lithium sulfate	0.1 M	HEPES	7	30 % v/v	PEG 500 DME
E11	0.1 M	Sodium chloride	0.1 M	HEPES	7	30 % v/v	PEG 500 DME
	0.1 M	Calcium chloride dihydrate					
E12			0.1 M	HEPES	7	30 % v/v	PEG 500 DME
F1	0.1 M	Sodium chloride	0.1 M	Tris	8	30 % v/v	PEG 500 DME
	0.1 M	Magnesium chloride hexahydrate					
F2	0.1 M	Sodium chloride	0.1 M	Tris	8	30 % v/v	PEG 500 DME
	0.1 M	Lithium sulfate					
F3	0.1 M	Sodium chloride	0.1 M	Tris	8	30 % v/v	PEG 500 DME
	0.1 M	Calcium chloride dihydrate					
F4	0.2 M	Ammonium sulfate	0.1 M	Tris	8	30 % v/v	PEG 500 DME
F5	0.1 M	Sodium chloride	0.1 M	Sodium citrate tribasic dihydrate	5	30 % v/v	PEG 500 MME
	0.1 M	Magnesium chloride hexahydrate					
F6	0.1 M	Sodium chloride	0.1 M	Sodium citrate tribasic dihydrate	5	30 % v/v	PEG 500 MME
	0.1 M	Lithium sulfate					
F7	0.1 M	Sodium chloride	0.1 M	Sodium citrate tribasic dihydrate	5	30 % v/v	PEG 500 MME
F8			0.1 M	Sodium citrate tribasic dihydrate	5	30 % v/v	PEG 500 MME
F9	0.1 M	Sodium chloride	0.1 M	MES	6	30 % v/v	PEG 500 MME
	0.1 M	Magnesium chloride hexahydrate					
F10	0.1 M	Sodium chloride	0.1 M	MES	6	30 % v/v	PEG 500 MME
	0.1 M	Lithium sulfate					
F11	0.1 M	Sodium chloride	0.1 M	MES	6	30 % v/v	PEG 500 MME
	0.1 M	Calcium chloride dihydrate					
F12	0.01 M	Zinc acetate dihydrate	0.1 M	MES	6	30 % v/v	PEG 500 MME
G1	0.1 M	Sodium chloride	0.1 M	HEPES	7	30 % v/v	PEG 500 MME
	0.1 M	Magnesium chloride hexahydrate					
G2	0.1 M	Sodium chloride	0.1 M	HEPES	7	30 % v/v	PEG 500 MME
	0.1 M	Lithium sulfate					
G3	0.1 M	Sodium chloride	0.1 M	HEPES	7	30 % v/v	PEG 500 MME
	0.1 M	Calcium chloride dihydrate					
G4			0.1 M	HEPES	7	30 % v/v	PEG 500 MME
G5	0.1 M	Magnesium chloride hexahydrate	0.1 M	Tris	8	30 % v/v	PEG 500 MME
G6	0.1 M	Sodium chloride	0.1 M	Tris	8	30 % v/v	PEG 500 MME
	0.1 M	Lithium sulfate					
G7	0.1 M	Sodium chloride	0.1 M	Tris	8	30 % v/v	PEG 500 MME
	0.1 M	Calcium chloride dihydrate					
G8	0.2 M	Ammonium sulfate	0.1 M	Tris	8	30 % v/v	PEG 500 MME
G9	0.1 M	Sodium chloride	0.1 M	Sodium citrate tribasic dihydrate	5	30 % v/v	PEG 600
	0.1 M	Magnesium chloride hexahydrate					
G10	0.1 M	Sodium chloride	0.1 M	Sodium citrate tribasic dihydrate	5	30 % v/v	PEG 600
	0.1 M	Lithium sulfate					
G11	0.1 M	Sodium chloride	0.1 M	Sodium citrate tribasic dihydrate	5	30 % v/v	PEG 600
G12			0.1 M	Sodium citrate tribasic dihydrate	5	30 % v/v	PEG 600
H1	0.1 M	Sodium chloride	0.1 M	MES	6	30 % v/v	PEG 600
	0.1 M	Magnesium chloride hexahydrate					
H2	0.1 M	Lithium sulfate	0.1 M	MES	6	30 % v/v	PEG 600
H3	0.1 M	Sodium chloride	0.1 M	MES	6	30 % v/v	PEG 600
	0.1 M	Calcium chloride dihydrate					
H4	0.01 M	Zinc acetate dihydrate	0.1 M	MES	6	30 % v/v	PEG 600
H5	0.1 M	Sodium chloride	0.1 M	HEPES	7	30 % v/v	PEG 600
	0.1 M	Magnesium chloride hexahydrate					
H6	0.1 M	Sodium chloride	0.1 M	HEPES	7	30 % v/v	PEG 600
	0.1 M	Lithium sulfate					
H7	0.1 M	Sodium chloride	0.1 M	HEPES	7	30 % v/v	PEG 600
	0.1 M	Calcium chloride dihydrate					
H8			0.1 M	HEPES	7	30 % v/v	PEG 600
H9	0.1 M	Sodium chloride	0.1 M	Tris	8	30 % v/v	PEG 600
	0.1 M	Magnesium chloride hexahydrate					
H10	0.1 M	Sodium chloride	0.1 M	Tris	8	30 % v/v	PEG 600
	0.1 M	Lithium sulfate					
H11	0.1 M	Calcium chloride dihydrate	0.1 M	Tris	8	30 % v/v	PEG 600
H12	0.2 M	Ammonium sulfate	0.1 M	Tris	8	30 % v/v	PEG 600

Abbreviations:

HEPES; N-(2-hydroxyethyl)-piperazine-N'-2-ethanesulfonic acid, **MES**; 2-(N-morpholino)ethanesulfonic acid, **MME**; Monomethylether, **PEG**; Polyethylene glycol, **PEG DME**; Poly(ethylene glycol) dimethyl ether, **Tris**; 2-Amino-2-(hydroxymethyl)propane-1,3-diol.

Figure 14.54 (1-4): Moecular dimension for crystilisation method MemMeso-FX 96 MD1-87-FX.

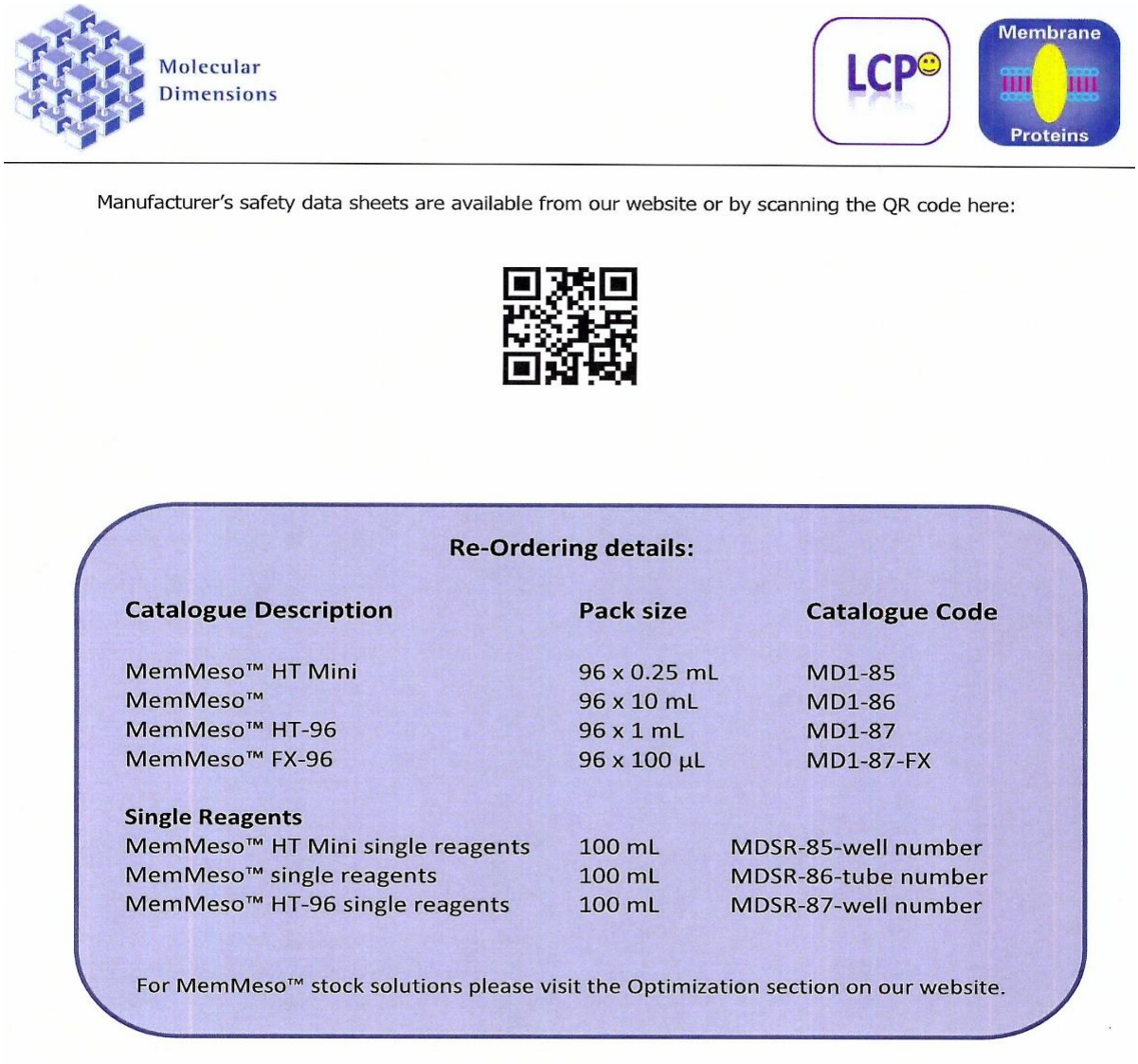

Figure 14.54 (1-5): Moecular dimension for crystilisation method MemMeso-FX 96 MD1-87-FX.

14.8.2 MemMeso™ MD1-86

Molecular Dimensions

LCP

Membrane Proteins

MemMeso™ MD1-86

MemMeso™ – A 96-condition crystallization screen specifically for use with mesophases. (LCP compatible).

MD1-86 is a targeted sparse matrix presented as a 96 x 10 mL conditions.

Features of MemMeso:

- Optimized to work in synergy with Lipidic Cubic Phase (LCP) and the LCP crystallization method.
- Allows screening in both LCP and Sponge Phase.
- Conditions data-mined from current GPCR crystal structures.
- A semi-systematic screening kit, containing 96 conditions covering a range of pH, precipitants and salt.
- Proven successful at crystallizing the crystal structures of eight membrane proteins, including the structure of channelrhodopsin (2012, Nature).

Introduction:

Out of the successful laboratory of Prof. Osamu Nureki at University of Tokyo, Japan, this semi-systematic screen has been developed to work in synergy with the Lipidic Cubic Phase (LCP) used in membrane protein crystallization. Most commercially available crystallization screens have been optimized to work with the vapour diffusion method and are therefore not ideal to use with LCP.

Eight membrane proteins structures have already been elucidated using MemMeso: Channelrhodopsin (2012, Nature), PfMATE (2013, Nature), NCX_Mj (2013, Science), GkPOT (2013, PNAS), and four bacterial transporters (manuscript in preparation).

Crystals grown using MemMeso. Courtesy of H.Kato

Tips for use

Usually 800 - 1000nL of MemMeso is needed for each experiment (well).

For LCP crystallization, dispense 25 - 50nL of LCP bolus onto 96-well sandwich plate (eg. Laminex plate), and then overlay with 800 - 1000nL of precipitant solution.

Mix the protein sample and lipid (monoolein) in a Hamilton syringe (in this process, the monoolein forms cubic phase and the protein is reconstituted in the cubic phase). Dispense the mixture (=protein in monoolein LCP) on the crystallization plate, and overlay MemMeso solution onto the mixture.

In some conditions, the mixtures are stable in the cubic phase, and in other conditions, the mixtures are changed to the sponge phase. It is impossible to predict whether the target protein is crystallized in the cubic phase and/or sponge phase, so MemMeso is ideal as it allows screening in both phases.

References:

Kato, H. *et al*, Nature. 2012 Jan 22;482(7385):369-74.
Tanaka, Y. *et al*, Nature. 2013 Apr 11;496(7444):247-51.
Doki, So. *et al*, Proc Natl Acad Sci U S A. 2013 Jul 9; 110(28):11343-8.

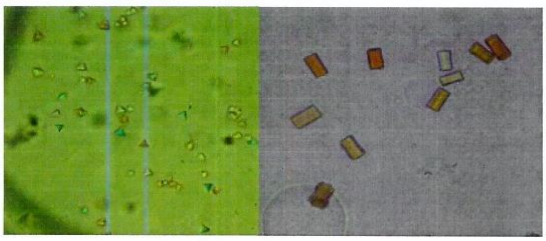

Figure 14.55 (2-1): Moecular dimension for crystilisation method MemMeso™ MD1-86.

Molecular Dimensions

LCP

Membrane Proteins

Formulation Notes:

MemMeso reagents are formulated using ultrapure water (>18.0 MΩ) and are sterile-filtered using 0.22 µm filters. No preservatives are added.

Final pH may vary from that specified on the datasheet. Molecular Dimensions will be happy to discuss the precise formulation of individual reagents.

Individual reagents and stock solutions for optimization are available from Molecular Dimensions.

Enquiries regarding MemMeso formulation, interpretation of results or optimization strategies are welcome. Please e-mail, fax or phone your query to Molecular Dimensions.

Contact and product details can be found at www.moleculardimensions.com

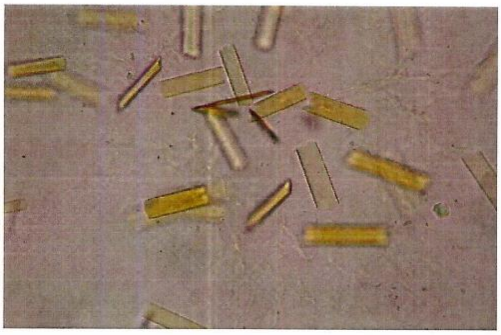

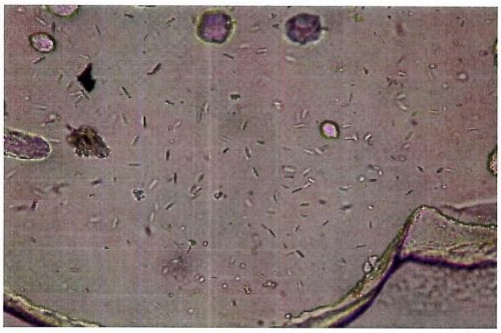

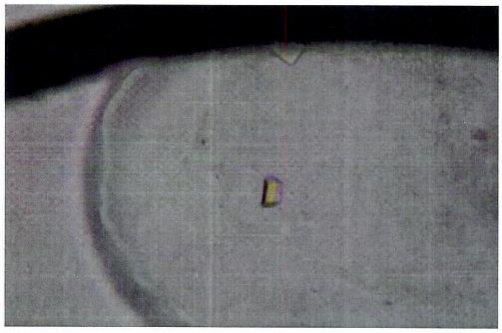

Figure 14.55 (2-2): Moecular dimension for crystilisation method MemMeso™ MD1-86

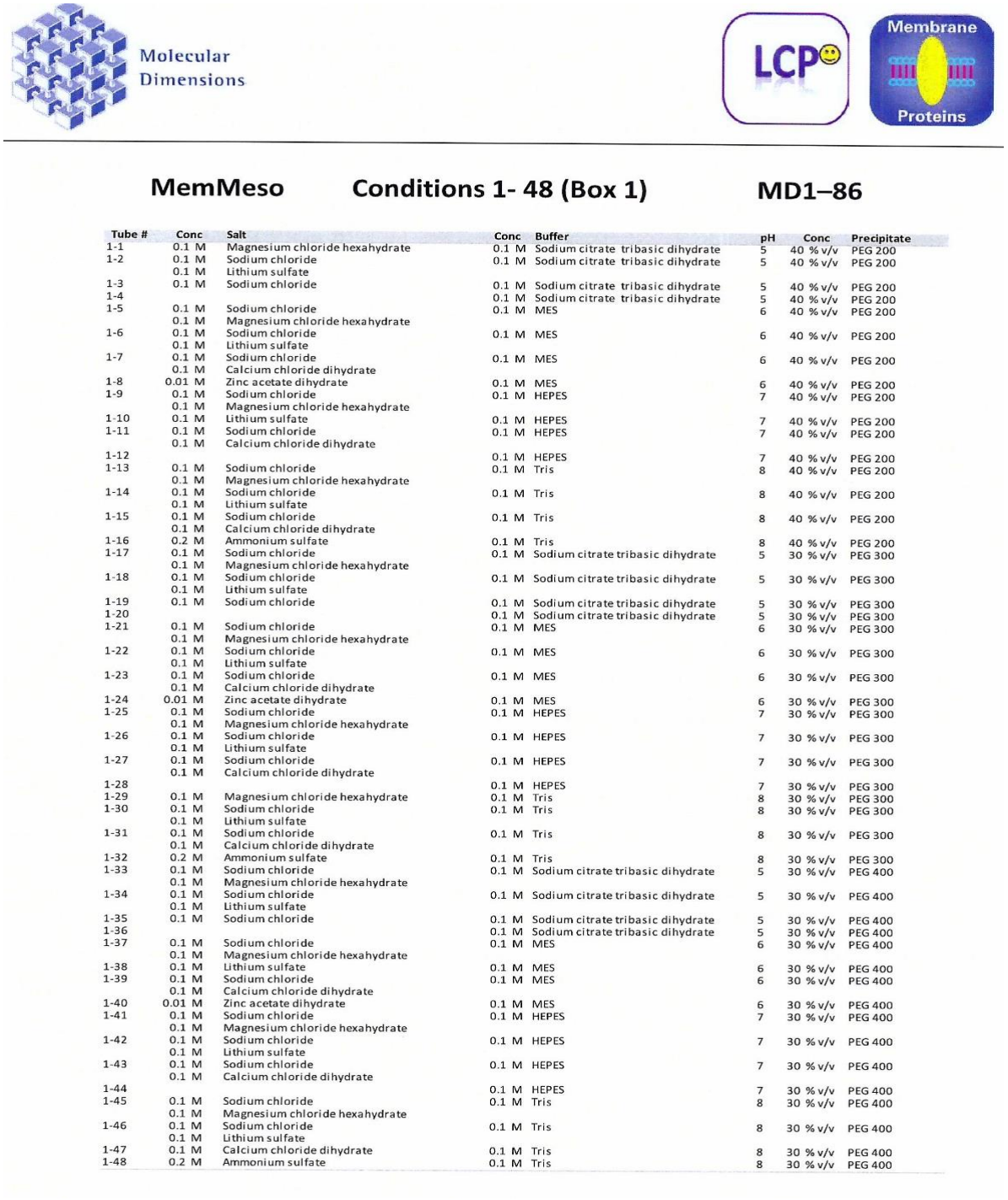

Molecular Dimensions

LCP

Membrane Proteins

MemMeso Conditions 1- 48 (Box 1) MD1–86

Tube #	Conc	Salt	Conc	Buffer	pH	Conc	Precipitate
1-1	0.1 M	Magnesium chloride hexahydrate	0.1 M	Sodium citrate tribasic dihydrate	5	40 % v/v	PEG 200
1-2	0.1 M	Sodium chloride	0.1 M	Sodium citrate tribasic dihydrate	5	40 % v/v	PEG 200
	0.1 M	Lithium sulfate					
1-3	0.1 M	Sodium chloride	0.1 M	Sodium citrate tribasic dihydrate	5	40 % v/v	PEG 200
1-4			0.1 M	Sodium citrate tribasic dihydrate	5	40 % v/v	PEG 200
1-5	0.1 M	Sodium chloride	0.1 M	MES	6	40 % v/v	PEG 200
	0.1 M	Magnesium chloride hexahydrate					
1-6	0.1 M	Sodium chloride	0.1 M	MES	6	40 % v/v	PEG 200
	0.1 M	Lithium sulfate					
1-7	0.1 M	Sodium chloride	0.1 M	MES	6	40 % v/v	PEG 200
	0.1 M	Calcium chloride dihydrate					
1-8	0.01 M	Zinc acetate dihydrate	0.1 M	MES	6	40 % v/v	PEG 200
1-9	0.1 M	Sodium chloride	0.1 M	HEPES	7	40 % v/v	PEG 200
	0.1 M	Magnesium chloride hexahydrate					
1-10	0.1 M	Lithium sulfate	0.1 M	HEPES	7	40 % v/v	PEG 200
1-11	0.1 M	Sodium chloride	0.1 M	HEPES	7	40 % v/v	PEG 200
	0.1 M	Calcium chloride dihydrate					
1-12			0.1 M	HEPES	7	40 % v/v	PEG 200
1-13	0.1 M	Sodium chloride	0.1 M	Tris	8	40 % v/v	PEG 200
	0.1 M	Magnesium chloride hexahydrate					
1-14	0.1 M	Sodium chloride	0.1 M	Tris	8	40 % v/v	PEG 200
	0.1 M	Lithium sulfate					
1-15	0.1 M	Sodium chloride	0.1 M	Tris	8	40 % v/v	PEG 200
	0.1 M	Calcium chloride dihydrate					
1-16	0.2 M	Ammonium sulfate	0.1 M	Tris	8	40 % v/v	PEG 200
1-17	0.1 M	Sodium chloride	0.1 M	Sodium citrate tribasic dihydrate	5	30 % v/v	PEG 300
	0.1 M	Magnesium chloride hexahydrate					
1-18	0.1 M	Sodium chloride	0.1 M	Sodium citrate tribasic dihydrate	5	30 % v/v	PEG 300
	0.1 M	Lithium sulfate					
1-19	0.1 M	Sodium chloride	0.1 M	Sodium citrate tribasic dihydrate	5	30 % v/v	PEG 300
1-20			0.1 M	Sodium citrate tribasic dihydrate	5	30 % v/v	PEG 300
1-21	0.1 M	Sodium chloride	0.1 M	MES	6	30 % v/v	PEG 300
	0.1 M	Magnesium chloride hexahydrate					
1-22	0.1 M	Sodium chloride	0.1 M	MES	6	30 % v/v	PEG 300
	0.1 M	Lithium sulfate					
1-23	0.1 M	Sodium chloride	0.1 M	MES	6	30 % v/v	PEG 300
	0.1 M	Calcium chloride dihydrate					
1-24	0.01 M	Zinc acetate dihydrate	0.1 M	MES	6	30 % v/v	PEG 300
1-25	0.1 M	Sodium chloride	0.1 M	HEPES	7	30 % v/v	PEG 300
	0.1 M	Magnesium chloride hexahydrate					
1-26	0.1 M	Sodium chloride	0.1 M	HEPES	7	30 % v/v	PEG 300
	0.1 M	Lithium sulfate					
1-27	0.1 M	Sodium chloride	0.1 M	HEPES	7	30 % v/v	PEG 300
	0.1 M	Calcium chloride dihydrate					
1-28			0.1 M	HEPES	7	30 % v/v	PEG 300
1-29	0.1 M	Magnesium chloride hexahydrate	0.1 M	Tris	8	30 % v/v	PEG 300
1-30	0.1 M	Sodium chloride	0.1 M	Tris	8	30 % v/v	PEG 300
	0.1 M	Lithium sulfate					
1-31	0.1 M	Sodium chloride	0.1 M	Tris	8	30 % v/v	PEG 300
	0.1 M	Calcium chloride dihydrate					
1-32	0.2 M	Ammonium sulfate	0.1 M	Tris	8	30 % v/v	PEG 300
1-33	0.1 M	Sodium chloride	0.1 M	Sodium citrate tribasic dihydrate	5	30 % v/v	PEG 400
	0.1 M	Magnesium chloride hexahydrate					
1-34	0.1 M	Sodium chloride	0.1 M	Sodium citrate tribasic dihydrate	5	30 % v/v	PEG 400
	0.1 M	Lithium sulfate					
1-35	0.1 M	Sodium chloride	0.1 M	Sodium citrate tribasic dihydrate	5	30 % v/v	PEG 400
1-36			0.1 M	Sodium citrate tribasic dihydrate	5	30 % v/v	PEG 400
1-37	0.1 M	Sodium chloride	0.1 M	MES	6	30 % v/v	PEG 400
	0.1 M	Magnesium chloride hexahydrate					
1-38	0.1 M	Lithium sulfate	0.1 M	MES	6	30 % v/v	PEG 400
1-39	0.1 M	Sodium chloride	0.1 M	MES	6	30 % v/v	PEG 400
	0.1 M	Calcium chloride dihydrate					
1-40	0.01 M	Zinc acetate dihydrate	0.1 M	MES	6	30 % v/v	PEG 400
1-41	0.1 M	Sodium chloride	0.1 M	HEPES	7	30 % v/v	PEG 400
	0.1 M	Magnesium chloride hexahydrate					
1-42	0.1 M	Sodium chloride	0.1 M	HEPES	7	30 % v/v	PEG 400
	0.1 M	Lithium sulfate					
1-43	0.1 M	Sodium chloride	0.1 M	HEPES	7	30 % v/v	PEG 400
	0.1 M	Calcium chloride dihydrate					
1-44			0.1 M	HEPES	7	30 % v/v	PEG 400
1-45	0.1 M	Sodium chloride	0.1 M	Tris	8	30 % v/v	PEG 400
	0.1 M	Magnesium chloride hexahydrate					
1-46	0.1 M	Sodium chloride	0.1 M	Tris	8	30 % v/v	PEG 400
	0.1 M	Lithium sulfate					
1-47	0.1 M	Calcium chloride dihydrate	0.1 M	Tris	8	30 % v/v	PEG 400
1-48	0.2 M	Ammonium sulfate	0.1 M	Tris	8	30 % v/v	PEG 400

Figure 14.55 (2-3): Moecular dimension for crystilisation method MemMeso™ MD1-86.

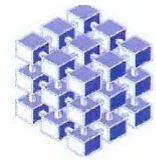

MemMeso **Conditions 1- 48 (Box 2)** **MD1–86**

Well #	Conc	Salt 1	Conc	Buffer	pH	Conc	Precipitate
2-1	0.1 M	Magnesium chloride hexahydrate	0.1 M	Sodium citrate tribasic dihydrate	5	30 % v/v	PEG 500 DME
2-2	0.1 M	Sodium chloride	0.1 M	Sodium citrate tribasic dihydrate	5	30 % v/v	PEG 500 DME
	0.1 M	Lithium sulfate					
2-3	0.1 M	Sodium chloride	0.1 M	Sodium citrate tribasic dihydrate	5	30 % v/v	PEG 500 DME
2-4			0.1 M	Sodium citrate tribasic dihydrate	5	30 % v/v	PEG 500 DME
2-5	0.1 M	Sodium chloride	0.1 M	MES	6	30 % v/v	PEG 500 DME
	0.1 M	Magnesium chloride hexahydrate					
2-6	0.1 M	Sodium chloride	0.1 M	MES	6	30 % v/v	PEG 500 DME
	0.1 M	Lithium sulfate					
2-7	0.1 M	Sodium chloride	0.1 M	MES	6	30 % v/v	PEG 500 DME
	0.1 M	Calcium chloride dihydrate					
2-8	0.01 M	Zinc acetate dihydrate	0.1 M	MES	6	30 % v/v	PEG 500 DME
2-9	0.1 M	Sodium chloride	0.1 M	HEPES	7	30 % v/v	PEG 500 DME
	0.1 M	Magnesium chloride hexahydrate					
2-10	0.1 M	Lithium sulfate	0.1 M	HEPES	7	30 % v/v	PEG 500 DME
2-11	0.1 M	Sodium chloride	0.1 M	HEPES	7	30 % v/v	PEG 500 DME
	0.1 M	Calcium chloride dihydrate					
2-12			0.1 M	HEPES	7	30 % v/v	PEG 500 DME
2-13	0.1 M	Sodium chloride	0.1 M	Tris	8	30 % v/v	PEG 500 DME
	0.1 M	Magnesium chloride hexahydrate					
2-14	0.1 M	Sodium chloride	0.1 M	Tris	8	30 % v/v	PEG 500 DME
	0.1 M	Lithium sulfate					
2-15	0.1 M	Sodium chloride	0.1 M	Tris	8	30 % v/v	PEG 500 DME
	0.1 M	Calcium chloride dihydrate					
2-16	0.2 M	Ammonium sulfate	0.1 M	Tris	8	30 % v/v	PEG 500 DME
2-17	0.1 M	Sodium chloride	0.1 M	Sodium citrate tribasic dihydrate	5	30 % v/v	PEG 500 MME
	0.1 M	Magnesium chloride hexahydrate					
2-18	0.1 M	Sodium chloride	0.1 M	Sodium citrate tribasic dihydrate	5	30 % v/v	PEG 500 MME
	0.1 M	Lithium sulfate					
2-19	0.1 M	Sodium chloride	0.1 M	Sodium citrate tribasic dihydrate	5	30 % v/v	PEG 500 MME
2-20			0.1 M	Sodium citrate tribasic dihydrate	5	30 % v/v	PEG 500 MME
2-21	0.1 M	Sodium chloride	0.1 M	MES	6	30 % v/v	PEG 500 MME
	0.1 M	Magnesium chloride hexahydrate					
2-22	0.1 M	Sodium chloride	0.1 M	MES	6	30 % v/v	PEG 500 MME
	0.1 M	Lithium sulfate					
2-23	0.1 M	Sodium chloride	0.1 M	MES	6	30 % v/v	PEG 500 MME
	0.1 M	Calcium chloride dihydrate					
2-24	0.01 M	Zinc acetate dihydrate	0.1 M	MES	6	30 % v/v	PEG 500 MME
2-25	0.1 M	Sodium chloride	0.1 M	HEPES	7	30 % v/v	PEG 500 MME
	0.1 M	Magnesium chloride hexahydrate					
2-26	0.1 M	Sodium chloride	0.1 M	HEPES	7	30 % v/v	PEG 500 MME
	0.1 M	Lithium sulfate					
2-27	0.1 M	Sodium chloride	0.1 M	HEPES	7	30 % v/v	PEG 500 MME
	0.1 M	Calcium chloride dihydrate					
2-28			0.1 M	HEPES	7	30 % v/v	PEG 500 MME
2-29	0.1 M	Magnesium chloride hexahydrate	0.1 M	Tris	8	30 % v/v	PEG 500 MME
2-30	0.1 M	Sodium chloride	0.1 M	Tris	8	30 % v/v	PEG 500 MME
	0.1 M	Lithium sulfate					
2-31	0.1 M	Sodium chloride	0.1 M	Tris	8	30 % v/v	PEG 500 MME
	0.1 M	Calcium chloride dihydrate					
2-32	0.2 M	Ammonium sulfate	0.1 M	Tris	8	30 % v/v	PEG 500 MME
2-33	0.1 M	Sodium chloride	0.1 M	Sodium citrate tribasic dihydrate	5	30 % v/v	PEG 600
	0.1 M	Magnesium chloride hexahydrate					
2-34	0.1 M	Sodium chloride	0.1 M	Sodium citrate tribasic dihydrate	5	30 % v/v	PEG 600
	0.1 M	Lithium sulfate					
2-35	0.1 M	Sodium chloride	0.1 M	Sodium citrate tribasic dihydrate	5	30 % v/v	PEG 600
2-36			0.1 M	Sodium citrate tribasic dihydrate	5	30 % v/v	PEG 600
2-37	0.1 M	Sodium chloride	0.1 M	MES	6	30 % v/v	PEG 600
	0.1 M	Magnesium chloride hexahydrate					
2-38	0.1 M	Lithium sulfate	0.1 M	MES	6	30 % v/v	PEG 600
2-39	0.1 M	Sodium chloride	0.1 M	MES	6	30 % v/v	PEG 600
	0.1 M	Calcium chloride dihydrate					
2-40	0.01 M	Zinc acetate dihydrate	0.1 M	MES	6	30 % v/v	PEG 600
2-41	0.1 M	Sodium chloride	0.1 M	HEPES	7	30 % v/v	PEG 600
	0.1 M	Magnesium chloride hexahydrate					
2-42	0.1 M	Sodium chloride	0.1 M	HEPES	7	30 % v/v	PEG 600
	0.1 M	Lithium sulfate					
2-43	0.1 M	Sodium chloride	0.1 M	HEPES	7	30 % v/v	PEG 600
	0.1 M	Calcium chloride dihydrate					
2-44			0.1 M	HEPES	7	30 % v/v	PEG 600
2-45	0.1 M	Sodium chloride	0.1 M	Tris	8	30 % v/v	PEG 600
	0.1 M	Magnesium chloride hexahydrate					
2-46	0.1 M	Sodium chloride	0.1 M	Tris	8	30 % v/v	PEG 600
	0.1 M	Lithium sulfate					
2-47	0.1 M	Calcium chloride dihydrate	0.1 M	Tris	8	30 % v/v	PEG 600
2-48	0.2 M	Ammonium sulfate	0.1 M	Tris	8	30 % v/v	PEG 600

Abbreviations:
HEPES; N-(2-hydroxyethyl)-piperazine-N'-2-ethanesulfonic acid, **MES**; 2-(N-morpholino)ethanesulfonic acid, **MME**; Monomethylether, **PEG**; Polyethylene glycol, **PEG DME**; Poly(ethylene glycol) dimethyl ether, **Tris**; 2-Amino-2-(hydroxymethyl)propane-1,3-diol.

Figure 14.55 (2-4): Moecular dimension for crystilisation method MemMeso^{TM} MD1-86.

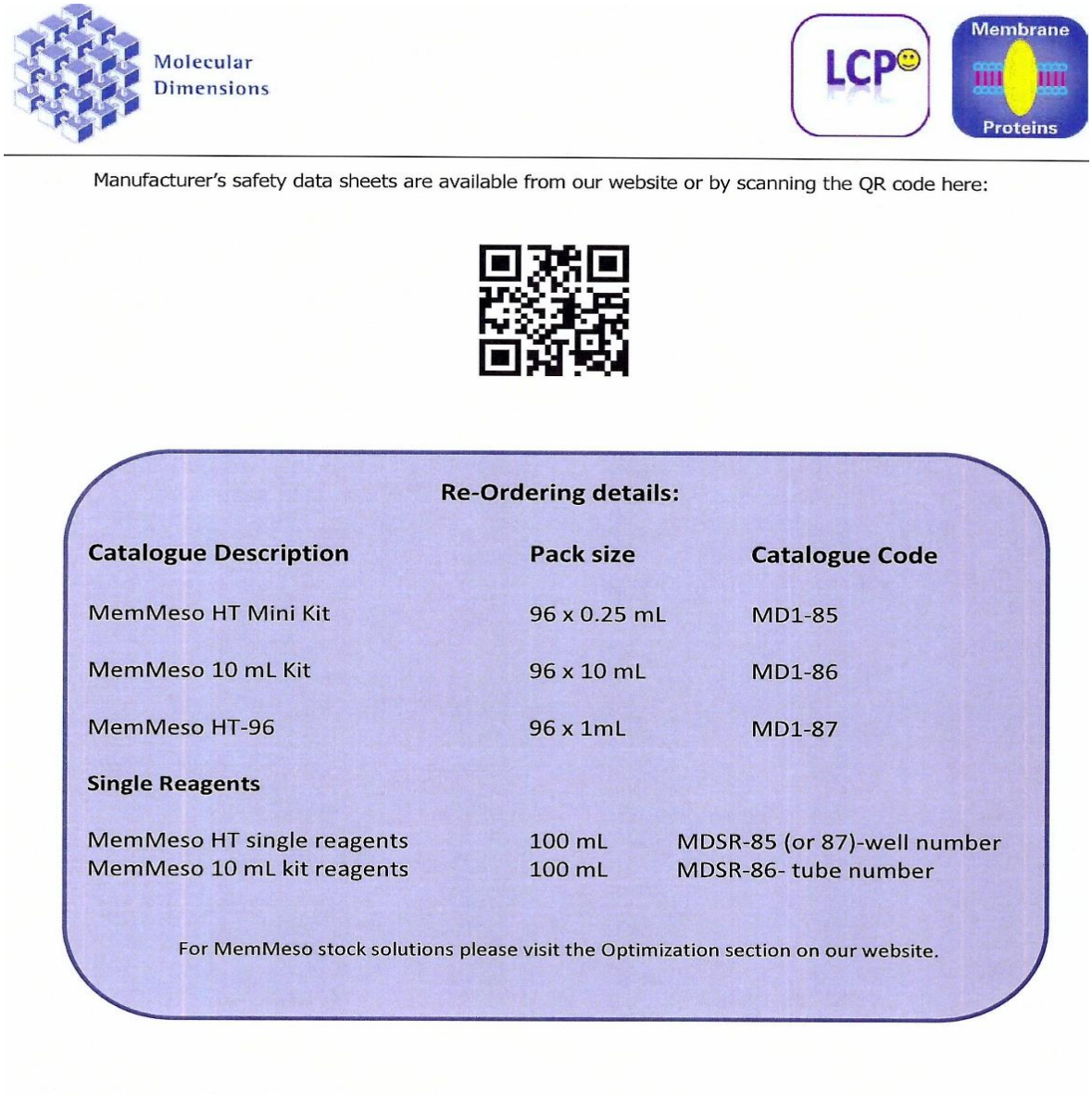

Figure 14.55 (2-5): Moecular dimension for crystilisation method MemMeso™ MD1-86.

14.8.3 MemMeso™ HT-96/FX-96 MD1-87 /MD1-87-FX

Molecular Dimensions

LCP

Membrane Proteins

MemMeso™ HT-96 / FX-96 **MD1-87 / MD1-87-FX**

MemMeso™ – A 96-condition crystallization screen specifically for use with mesophases (LCP compatible).

MD1-87 is presented as a 96 x 1 mL conditions / MD1-87-FX is presented as 96 x 100 µL conditions.

Features of MemMeso™:

- Optimized to work in synergy with Lipidic Cubic Phase (LCP) and the LCP crystallization method.
- Allows screening in both LCP and Sponge Phase.
- Conditions data-mined from current GPCR crystal structures.
- A semi-systematic screening kit, containing 96 conditions covering a range of pH, precipitants and salt.
- Proven successful at crystallizing the crystal structures of eight membrane proteins, including the structure of channelrhodopsin (2012, Nature).

Introduction:

Out of the successful laboratory of Prof. Osamu Nureki at University of Tokyo, Japan, this semi-systematic screen has been developed to work in synergy with the Lipidic Cubic Phase (LCP) used in membrane protein crystallization. Most commercially available crystallization screens have been optimized to work with the vapour diffusion method and are therefore not ideal to use with LCP.

Eight membrane proteins structures have already been elucidated using MemMeso™: Channelrhodopsin (2012, Nature), PfMATE (2013, Nature), NCX_Mj (2013, Science), GkPOT (2013, PNAS), and four bacterial transporters (manuscript in preparation).

Crystals grown using MemMeso™. Courtesy of H.Kato

Tips for use

Usually 800 – 1000 nL of MemMeso™ is needed for each experiment (well).

For LCP crystallization, dispense 25 – 50 nL of LCP bolus onto 96-well sandwich plate (e.g. Laminex plate), and then overlay with 800 - 1000nL of precipitant solution.

Mix the protein sample and lipid (monoolein) in a Hamilton syringe (in this process, the monoolein forms cubic phase and the protein is reconstituted in the cubic phase). Dispense the mixture (=protein in monoolein LCP) on the crystallization plate, and overlay MemMeso™ solution onto the mixture.

In some conditions, the mixtures are stable in the cubic phase, and in other conditions, the mixtures are changed to the sponge phase. It is impossible to predict whether the target protein is crystallized in the cubic phase and/or sponge phase, so MemMeso™ is ideal as it allows screening in both phases.

References:

Kato, H. *et al*, Nature. 2012 Jan 22;482(7385):369-74.
Tanaka, Y. *et al*, Nature. 2013 Apr 11;496(7444):247-51.
Doki, So. *et al*, Proc Natl Acad Sci U S A. 2013 Jul 9; 110(28):11343-8.

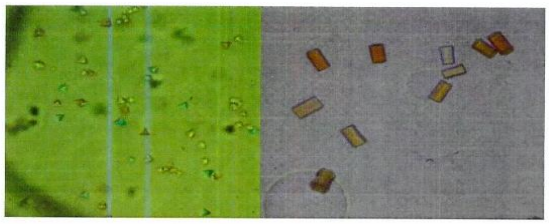

Figure 14.56 (3-1): Moecular dimension for crystilisation method MemMeso™ HT-96/FX-96 MD1-87 /MD1-87-FX

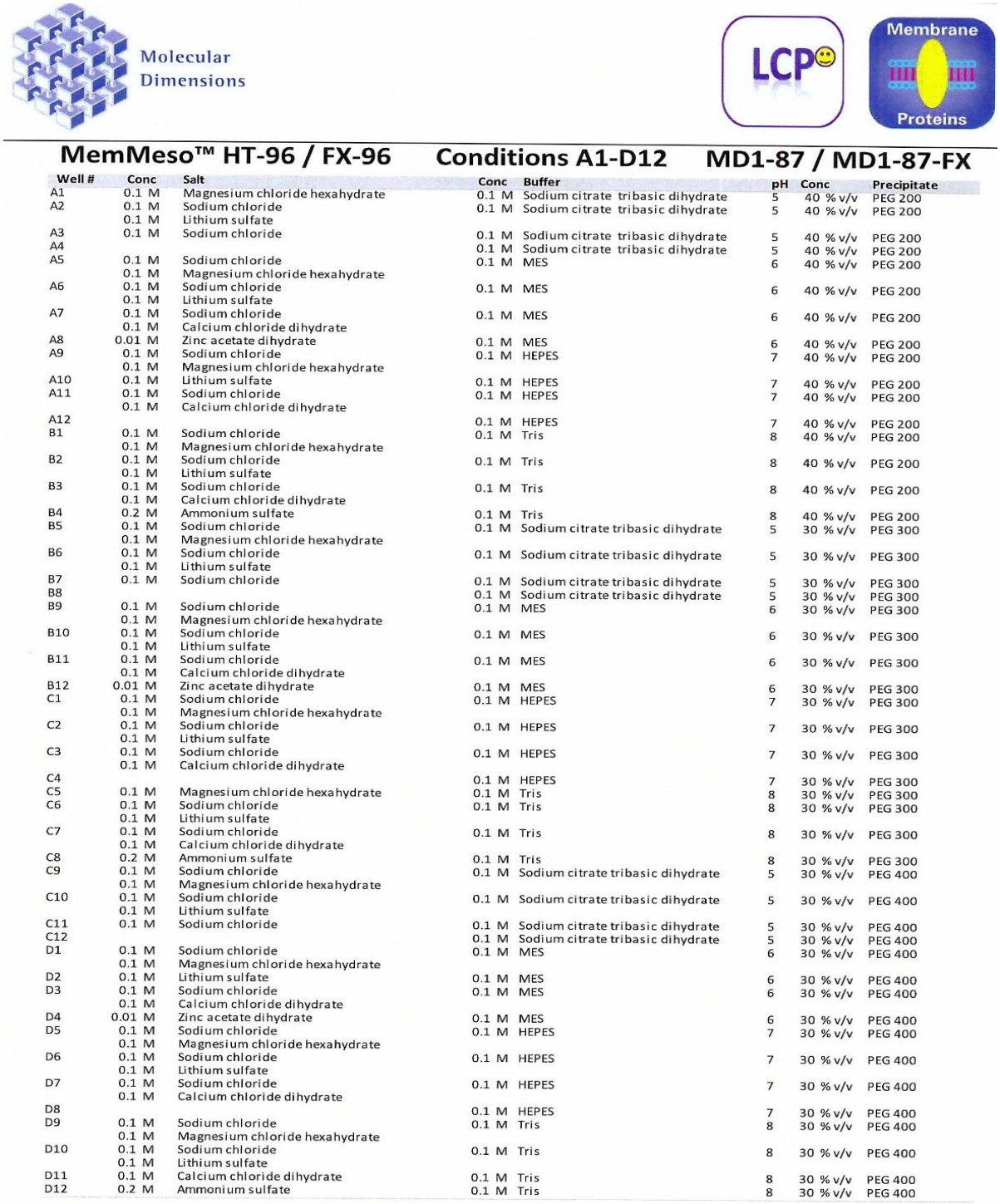

Molecular Dimensions

LCP

Membrane Proteins

MemMeso™ HT-96 / FX-96 Conditions A1-D12 MD1-87 / MD1-87-FX

Well #	Conc	Salt	Conc	Buffer	pH	Conc	Precipitate
A1	0.1 M	Magnesium chloride hexahydrate	0.1 M	Sodium citrate tribasic dihydrate	5	40 % v/v	PEG 200
A2	0.1 M	Sodium chloride	0.1 M	Sodium citrate tribasic dihydrate	5	40 % v/v	PEG 200
	0.1 M	Lithium sulfate					
A3	0.1 M	Sodium chloride	0.1 M	Sodium citrate tribasic dihydrate	5	40 % v/v	PEG 200
A4			0.1 M	Sodium citrate tribasic dihydrate	5	40 % v/v	PEG 200
A5	0.1 M	Sodium chloride	0.1 M	MES	6	40 % v/v	PEG 200
	0.1 M	Magnesium chloride hexahydrate					
A6	0.1 M	Sodium chloride	0.1 M	MES	6	40 % v/v	PEG 200
	0.1 M	Lithium sulfate					
A7	0.1 M	Sodium chloride	0.1 M	MES	6	40 % v/v	PEG 200
	0.1 M	Calcium chloride dihydrate					
A8	0.01 M	Zinc acetate dihydrate	0.1 M	MES	6	40 % v/v	PEG 200
A9	0.1 M	Sodium chloride	0.1 M	HEPES	7	40 % v/v	PEG 200
	0.1 M	Magnesium chloride hexahydrate					
A10	0.1 M	Lithium sulfate	0.1 M	HEPES	7	40 % v/v	PEG 200
A11	0.1 M	Sodium chloride	0.1 M	HEPES	7	40 % v/v	PEG 200
	0.1 M	Calcium chloride dihydrate					
A12			0.1 M	HEPES	7	40 % v/v	PEG 200
B1	0.1 M	Sodium chloride	0.1 M	Tris	8	40 % v/v	PEG 200
	0.1 M	Magnesium chloride hexahydrate					
B2	0.1 M	Sodium chloride	0.1 M	Tris	8	40 % v/v	PEG 200
	0.1 M	Lithium sulfate					
B3	0.1 M	Sodium chloride	0.1 M	Tris	8	40 % v/v	PEG 200
	0.1 M	Calcium chloride dihydrate					
B4	0.2 M	Ammonium sulfate	0.1 M	Tris	8	40 % v/v	PEG 200
B5	0.1 M	Sodium chloride	0.1 M	Sodium citrate tribasic dihydrate	5	30 % v/v	PEG 300
	0.1 M	Magnesium chloride hexahydrate					
B6	0.1 M	Sodium chloride	0.1 M	Sodium citrate tribasic dihydrate	5	30 % v/v	PEG 300
	0.1 M	Lithium sulfate					
B7	0.1 M	Sodium chloride	0.1 M	Sodium citrate tribasic dihydrate	5	30 % v/v	PEG 300
B8			0.1 M	Sodium citrate tribasic dihydrate	5	30 % v/v	PEG 300
B9	0.1 M	Sodium chloride	0.1 M	MES	6	30 % v/v	PEG 300
	0.1 M	Magnesium chloride hexahydrate					
B10	0.1 M	Sodium chloride	0.1 M	MES	6	30 % v/v	PEG 300
	0.1 M	Lithium sulfate					
B11	0.1 M	Sodium chloride	0.1 M	MES	6	30 % v/v	PEG 300
	0.1 M	Calcium chloride dihydrate					
B12	0.01 M	Zinc acetate dihydrate	0.1 M	MES	6	30 % v/v	PEG 300
C1	0.1 M	Sodium chloride	0.1 M	HEPES	7	30 % v/v	PEG 300
	0.1 M	Magnesium chloride hexahydrate					
C2	0.1 M	Sodium chloride	0.1 M	HEPES	7	30 % v/v	PEG 300
	0.1 M	Lithium sulfate					
C3	0.1 M	Sodium chloride	0.1 M	HEPES	7	30 % v/v	PEG 300
	0.1 M	Calcium chloride dihydrate					
C4			0.1 M	HEPES	7	30 % v/v	PEG 300
C5	0.1 M	Magnesium chloride hexahydrate	0.1 M	Tris	8	30 % v/v	PEG 300
C6	0.1 M	Sodium chloride	0.1 M	Tris	8	30 % v/v	PEG 300
	0.1 M	Lithium sulfate					
C7	0.1 M	Sodium chloride	0.1 M	Tris	8	30 % v/v	PEG 300
	0.1 M	Calcium chloride dihydrate					
C8	0.2 M	Ammonium sulfate	0.1 M	Tris	8	30 % v/v	PEG 300
C9	0.1 M	Sodium chloride	0.1 M	Sodium citrate tribasic dihydrate	5	30 % v/v	PEG 400
	0.1 M	Magnesium chloride hexahydrate					
C10	0.1 M	Sodium chloride	0.1 M	Sodium citrate tribasic dihydrate	5	30 % v/v	PEG 400
	0.1 M	Lithium sulfate					
C11	0.1 M	Sodium chloride	0.1 M	Sodium citrate tribasic dihydrate	5	30 % v/v	PEG 400
C12			0.1 M	Sodium citrate tribasic dihydrate	5	30 % v/v	PEG 400
D1	0.1 M	Sodium chloride	0.1 M	MES	6	30 % v/v	PEG 400
	0.1 M	Magnesium chloride hexahydrate					
D2	0.1 M	Lithium sulfate	0.1 M	MES	6	30 % v/v	PEG 400
D3	0.1 M	Sodium chloride	0.1 M	MES	6	30 % v/v	PEG 400
	0.1 M	Calcium chloride dihydrate					
D4	0.01 M	Zinc acetate dihydrate	0.1 M	MES	6	30 % v/v	PEG 400
D5	0.1 M	Sodium chloride	0.1 M	HEPES	7	30 % v/v	PEG 400
	0.1 M	Magnesium chloride hexahydrate					
D6	0.1 M	Sodium chloride	0.1 M	HEPES	7	30 % v/v	PEG 400
	0.1 M	Lithium sulfate					
D7	0.1 M	Sodium chloride	0.1 M	HEPES	7	30 % v/v	PEG 400
	0.1 M	Calcium chloride dihydrate					
D8			0.1 M	HEPES	7	30 % v/v	PEG 400
D9	0.1 M	Sodium chloride	0.1 M	Tris	8	30 % v/v	PEG 400
	0.1 M	Magnesium chloride hexahydrate					
D10	0.1 M	Sodium chloride	0.1 M	Tris	8	30 % v/v	PEG 400
	0.1 M	Lithium sulfate					
D11	0.1 M	Calcium chloride dihydrate	0.1 M	Tris	8	30 % v/v	PEG 400
D12	0.2 M	Ammonium sulfate	0.1 M	Tris	8	30 % v/v	PEG 400

Figure 14.56 (3-2): Moecular dimension for crystilisation method MemMeso™ HT-96/FX-96 MD1-87 /MD1-87-FX

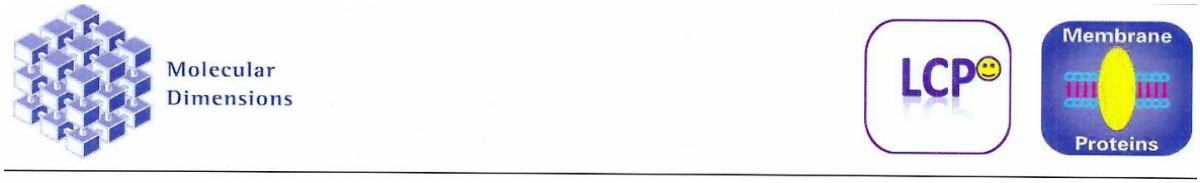

MemMeso™ HT-96 / FX-96 Conditions E1-H12 MD1-87 / MD1-87-FX

Well #	Conc	Salt 1	Conc	Buffer	pH	Conc	Precipitate
E1	0.1 M	Magnesium chloride hexahydrate	0.1 M	Sodium citrate tribasic dihydrate	5	30 % v/v	PEG 500 DME
E2	0.1 M	Sodium chloride	0.1 M	Sodium citrate tribasic dihydrate	5	30 % v/v	PEG 500 DME
	0.1 M	Lithium sulfate					
E3	0.1 M	Sodium chloride	0.1 M	Sodium citrate tribasic dihydrate	5	30 % v/v	PEG 500 DME
E4			0.1 M	Sodium citrate tribasic dihydrate	5	30 % v/v	PEG 500 DME
E5	0.1 M	Sodium chloride	0.1 M	MES	6	30 % v/v	PEG 500 DME
	0.1 M	Magnesium chloride hexahydrate					
E6	0.1 M	Sodium chloride	0.1 M	MES	6	30 % v/v	PEG 500 DME
	0.1 M	Lithium sulfate					
E7	0.1 M	Sodium chloride	0.1 M	MES	6	30 % v/v	PEG 500 DME
	0.1 M	Calcium chloride dihydrate					
E8	0.01 M	Zinc acetate dihydrate	0.1 M	MES	6	30 % v/v	PEG 500 DME
E9	0.1 M	Sodium chloride	0.1 M	HEPES	7	30 % v/v	PEG 500 DME
	0.1 M	Magnesium chloride hexahydrate					
E10	0.1 M	Lithium sulfate	0.1 M	HEPES	7	30 % v/v	PEG 500 DME
E11	0.1 M	Sodium chloride	0.1 M	HEPES	7	30 % v/v	PEG 500 DME
	0.1 M	Calcium chloride dihydrate					
E12			0.1 M	HEPES	7	30 % v/v	PEG 500 DME
F1	0.1 M	Sodium chloride	0.1 M	Tris	8	30 % v/v	PEG 500 DME
	0.1 M	Magnesium chloride hexahydrate					
F2	0.1 M	Sodium chloride	0.1 M	Tris	8	30 % v/v	PEG 500 DME
	0.1 M	Lithium sulfate					
F3	0.1 M	Sodium chloride	0.1 M	Tris	8	30 % v/v	PEG 500 DME
	0.1 M	Calcium chloride dihydrate					
F4	0.2 M	Ammonium sulfate	0.1 M	Tris	8	30 % v/v	PEG 500 DME
F5	0.1 M	Sodium chloride	0.1 M	Sodium citrate tribasic dihydrate	5	30 % v/v	PEG 500 MME
	0.1 M	Magnesium chloride hexahydrate					
F6	0.1 M	Sodium chloride	0.1 M	Sodium citrate tribasic dihydrate	5	30 % v/v	PEG 500 MME
	0.1 M	Lithium sulfate					
F7	0.1 M	Sodium chloride	0.1 M	Sodium citrate tribasic dihydrate	5	30 % v/v	PEG 500 MME
F8			0.1 M	Sodium citrate tribasic dihydrate	5	30 % v/v	PEG 500 MME
F9	0.1 M	Sodium chloride	0.1 M	MES	6	30 % v/v	PEG 500 MME
	0.1 M	Magnesium chloride hexahydrate					
F10	0.1 M	Sodium chloride	0.1 M	MES	6	30 % v/v	PEG 500 MME
	0.1 M	Lithium sulfate					
F11	0.1 M	Sodium chloride	0.1 M	MES	6	30 % v/v	PEG 500 MME
	0.1 M	Calcium chloride dihydrate					
F12	0.01 M	Zinc acetate dihydrate	0.1 M	MES	6	30 % v/v	PEG 500 MME
G1	0.1 M	Sodium chloride	0.1 M	HEPES	7	30 % v/v	PEG 500 MME
	0.1 M	Magnesium chloride hexahydrate					
G2	0.1 M	Sodium chloride	0.1 M	HEPES	7	30 % v/v	PEG 500 MME
	0.1 M	Lithium sulfate					
G3	0.1 M	Sodium chloride	0.1 M	HEPES	7	30 % v/v	PEG 500 MME
	0.1 M	Calcium chloride dihydrate					
G4			0.1 M	HEPES	7	30 % v/v	PEG 500 MME
G5	0.1 M	Magnesium chloride hexahydrate	0.1 M	Tris	8	30 % v/v	PEG 500 MME
G6	0.1 M	Sodium chloride	0.1 M	Tris	8	30 % v/v	PEG 500 MME
	0.1 M	Lithium sulfate					
G7	0.1 M	Sodium chloride	0.1 M	Tris	8	30 % v/v	PEG 500 MME
	0.1 M	Calcium chloride dihydrate					
G8	0.2 M	Ammonium sulfate	0.1 M	Tris	8	30 % v/v	PEG 500 MME
G9	0.1 M	Sodium chloride	0.1 M	Sodium citrate tribasic dihydrate	5	30 % v/v	PEG 600
	0.1 M	Magnesium chloride hexahydrate					
G10	0.1 M	Sodium chloride	0.1 M	Sodium citrate tribasic dihydrate	5	30 % v/v	PEG 600
	0.1 M	Lithium sulfate					
G11	0.1 M	Sodium chloride	0.1 M	Sodium citrate tribasic dihydrate	5	30 % v/v	PEG 600
G12			0.1 M	Sodium citrate tribasic dihydrate	5	30 % v/v	PEG 600
H1	0.1 M	Sodium chloride	0.1 M	MES	6	30 % v/v	PEG 600
	0.1 M	Magnesium chloride hexahydrate					
H2	0.1 M	Lithium sulfate	0.1 M	MES	6	30 % v/v	PEG 600
H3	0.1 M	Sodium chloride	0.1 M	MES	6	30 % v/v	PEG 600
	0.1 M	Calcium chloride dihydrate					
H4	0.01 M	Zinc acetate dihydrate	0.1 M	MES	6	30 % v/v	PEG 600
H5	0.1 M	Sodium chloride	0.1 M	HEPES	7	30 % v/v	PEG 600
	0.1 M	Magnesium chloride hexahydrate					
H6	0.1 M	Sodium chloride	0.1 M	HEPES	7	30 % v/v	PEG 600
	0.1 M	Lithium sulfate					
H7	0.1 M	Sodium chloride	0.1 M	HEPES	7	30 % v/v	PEG 600
	0.1 M	Calcium chloride dihydrate					
H8			0.1 M	HEPES	7	30 % v/v	PEG 600
H9	0.1 M	Sodium chloride	0.1 M	Tris	8	30 % v/v	PEG 600
	0.1 M	Magnesium chloride hexahydrate					
H10	0.1 M	Sodium chloride	0.1 M	Tris	8	30 % v/v	PEG 600
	0.1 M	Lithium sulfate					
H11	0.1 M	Calcium chloride dihydrate	0.1 M	Tris	8	30 % v/v	PEG 600
H12	0.2 M	Ammonium sulfate	0.1 M	Tris	8	30 % v/v	PEG 600

Abbreviations:

HEPES; N-(2-hydroxyethyl)-piperazine-N'-2-ethanesulfonic acid, **MES**; 2-(N-morpholino)ethanesulfonic acid, **MME**; Monomethylether, **PEG**; Polyethylene glycol, **PEG DME**; Poly(ethylene glycol) dimethyl ether, **Tris**; 2-Amino-2-(hydroxymethyl)propane-1,3-diol.

Figure 14.56 (3-3): Moecular dimension for crystilisation method MemMeso™ HT-96/FX-96 MD1-87 /MD1-87-FX

Molecular Dimensions

LCP

Membrane Proteins

Formulation Notes:

MemMeso™ reagents are formulated using ultrapure water (>18.0 MΩ) and are sterile-filtered using 0.22 µm filters. No preservatives are added.

Final pH may vary from that specified on the datasheet. Molecular Dimensions will be happy to discuss the precise formulation of individual reagents.

Individual reagents and stock solutions for optimization are available from Molecular Dimensions.

Enquiries regarding MemMeso™ formulation, interpretation of results or optimization strategies are welcome. Please e-mail, fax or phone your query to Molecular Dimensions.

Contact and product details can be found at www.moleculardimensions.com

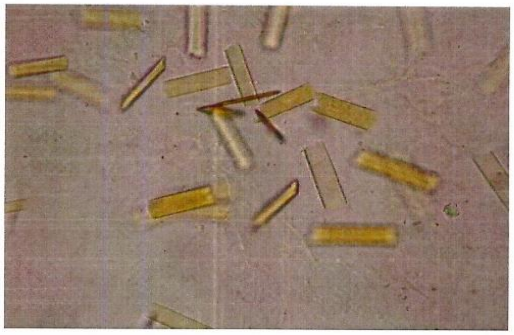

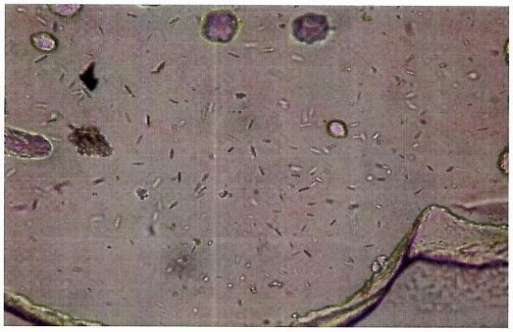

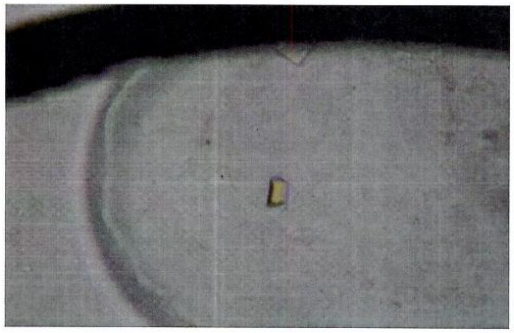

Figure 14.56 (3-4): Moecular dimension for crystilisation method MemMeso™ HT-96/FX-96 MD1-87 /MD1-87-FX

14.8.4 MemGold™ MD1-39

Molecular Dimensions

Membrane Proteins

MemGold™ MD1-39

MemGold™* is based on crystallization conditions data mined from the Protein Data Bank and is a rationalized sparse matrix screen containing 96 conditions covering a range of pH, PEGs and salt additives.

MD1-39 is presented as 96 x 10 mL conditions.

Features of MemGold™:

- Data mined from 300 crystallization conditions.
- Covers conditions for approximately 121 α-helical type membrane proteins.
- Addresses the diversity of membrane proteins studied, with many more transporters and channels and both α- and β-types.

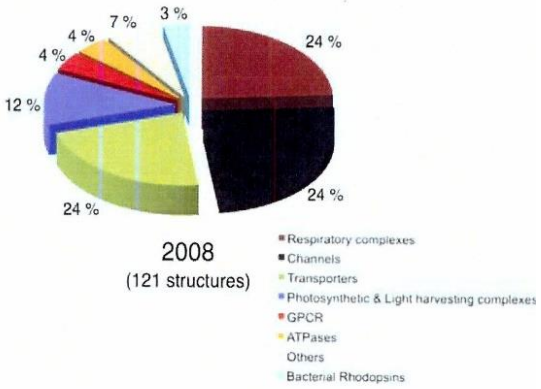

MP families. The proportion of structures belonging to each of the eight MP families in the database is shown. Bacterial rhodopsins (blue), GPCR (red), channels (black), transporters (green), photosynthetic and light harvesting complexes (purple), ATPases (orange), respiratory complexes (brown), others (DsbB-DsbA oxidase, intramembrane proteases, membrane-associated proteins in eicosanoid, and gluththione metabolism [MAPEG]) (olive).

Introduction

Recent years have seen a steady increase in the number of membrane protein structures solved and there are now (2008) approximately 130 different membrane protein structures in the PDB and over 300 crystallization conditions. The diversity of proteins has increased, with many more transporters and channels now in the database and a good number of both α- and β- types.

Work by Dr. Simon Newstead in the group of Prof. So Iwata at Imperial College, London (2004-2009), produced a new sparse matrix screen for membrane proteins, called MemGold™. MemGold™ is based on the conditions mined from the PDB and contains 96 conditions covering a range of pH, PEGs and salt additives.

Success stories: Crystals of Membrane proteins grown with MemGold™ screens

Figure 14.57 (4-1): Moecular dimension for crystilisation method MemGold™ MD1-39

Molecular Dimensions

Membrane Proteins

MemGold™ Conditions 1-48 (Box 1) MD1–39

Tube #	Conc.	Salt	Conc.	Buffer	pH	Conc.	Precipitant
1-1	2.2 M	Ammonium sulfate	0.08 M	Sodium citrate	5.2		
1-2	1.2 M	Sodium citrate tribasic dihydrate	0.01 M	Tris	8.0		
1-3			0.015 M	Tricine	8.5	24 % w/v	PEG 4000
1-4	0.36 M	Sodium chloride	0.015 M	Sodium phosphate	7.0	9.9 % w/v	PEG 4000
						0.1 % w/v	Sodium azide
1-5	0.3 M	Sodium chloride	0.01 M	Tris	8.0	27.5 % w/v	PEG 4000
1-6			0.225 M	MES/Bis-Tris	6.6	6.6 % w/v	PEG 6000
1-7	0.1 M	Ammonium sulfate	0.1 M	HEPES	7.5	12 % w/v	PEG 4000
						22 % v/v	Glycerol
1-8	0.01 M	Magnesium sulfate heptahydrate	0.02 M	MES	6.5	7.7 % w/v	PEG 1500
	0.02 M	Sodium chloride					
	0.02 M	Calcium chloride dihydrate					
1-9	2.5 M	Ammonium sulfate	0.05 M	HEPES	7.5		
1-10	1.1 M	Sodium citrate tribasic dihydrate	0.0665 M	HEPES	7.5		
1-11	3.3 M	Ammonium sulfate	0.15 M	Potassium phosphate	6.5		
1-12	0.1 M	Magnesium acetate tetrahydrate	0.1 M	Sodium citrate	5.8	14 % w/v	PEG 5000 MME
1-13	0.1 M	Soduim chloride	0.02 M	Sodium citrate	5.6	11 % w/v	PEG 3350
1-14	0.1 M	Sodium chloride	0.02 M	Sodium citrate	5.6	5.5 % w/v	PEG 3350
1-15	0.05 M	Calcium chloride dihydrate	0.1 M	Tris	8.2	32 % v/v	PEG 400
	0.05 M	Barium chloride dihydrate					
1-16	0.05 M	Sodium chloride	0.1 M	Sodium phosphate	6.2	16 % w/v	PEG 4000
1-17	0.1 M	Magnesium chloride hexahydrate	0.03 M	Tris-HCl	8.2	19 % w/v	PEG 4000
1-18	0.2 M	Sodium chloride	0.025 M	HEPES	7.5	13 % w/v	PEG 4000
1-19			0.1 M	HEPES	7.5	11 % w/v	PEG 3350
1-20	0.1 M	Sodium chloride	0.02 M	KMES	6.7	6.6 % w/v	PEG 4000
1-21	0.1 M	Potassium chloride	0.02 M	Tris	7.0	20 % w/v	PEG 4000
1-22	0.05 M	Magnesium chloride hexahydrate	0.1 M	Sodium cacodylate	6.7	6.6 % w/v	PEG 3350
						0.1 % w/v	Sodium azide
1-23	0.2 M	Potassium chloride	0.1 M	Sodium citrate	5.5	37 % v/v	Pentaerythritol propoxylate (5/4 PO/OH)
1-24			0.1 M	Tris	8.0	5.5 % w/v	PEG 4000
1-25	0.1 M	Sodium chloride	0.02 M	Tris	7.0	7.7 % w/v	PEG 4000
1-26	0.1 M	Magnesium chloride hexahydrate	0.1 M	Tris	7.5	22 % v/v	PEG 400
1-27	0.04 M	Sodium chloride	0.04 M	Tris	8.0	27 % v/v	PEG 350 MME
1-28	0.05 M	Sodium chloride	0.1 M	Sodium citrate	6.0	22 % v/v	PEG 400
	0.02 M	Magnesium chloride hexahydrate					
1-29			0.1 M	Sodium acetate	5.5	8.8 % w/v	PEG 2000 MME
1-30			0.4 M	Ammonium acetate	8.0	13 % w/v	PEG 2000 MME
1-31			0.02 M	Bis-Tris	7.0	15 % w/v	PEG 2000
1-32	0.1 M	Sodium chloride	0.02 M	Tris	7.5	11 % w/v	PEG 1500
	0.1 M	Magnesium chloride hexahydrate					
1-33	0.1 M	Sodium chloride	0.1 M	HEPES	8.0	11 % w/v	PEG 1500
	0.1 M	Magnesium chloride hexahydrate					
1-34	0.2 M	Sodium acetate trihydrate	0.1 M	HEPES	7.0	22 % w/v	PEG 3000
	0.2 M	Potassium chloride					
1-35	0.02 M	Nickel(II) sulfate hexahydrate	0.01 M	HEPES	7.0	33 % v/v	Jeffamine® M-600
1-36	0.15 M	Sodium chloride	0.1 M	Tris	8.0	13 % w/v	PEG 6000
1-37	0.2 M	Calcium chloride dihydrate	0.1 M	HEPES	7.5	53 % v/v	PEG 400
1-38	0.05 M	Magnesium acetate tetrahydrate	0.05 M	Sodium acetate	5.0	28 % v/v	PEG 400
1-39			0.05 M	HEPES	7.5	22 % w/v	PEG 4000
1-40	0.2 M	Calcium chloride dihydrate	0.1 M	Tris-HCl	8.0	44 % v/v	PEG 400
1-41	0.05 M	Magnesium acetate tetrahydrate	0.05 M	Sodium acetate	5.4	24 % v/v	PEG 400
1-42	0.2 M	Calcium chloride dihydrate	0.1 M	MES	6.5	26 % v/v	PEG 350 MME
1-43	0.1 M	Potassium chloride	0.1 M	Tris	8.5	39 % v/v	PEG 400
1-44	0.05 M	Magnesium chloride hexahydrate	0.1 M	Glycine	9.0	22 % v/v	PEG 400
1-45	0.1 M	Ammonium sulfate	0.1 M	Glycine	3.8	28 % v/v	Triethylene glycol (TEG)
1-46	0.15 M	Sodium formate	0.1 M	HEPES	7.2	18 % w/v	PEG 3350
1-47			0.2 M	Sodium acetate	6.8	8.8 % w/v	PEG 6000
1-48	0.2 M	Potassium chloride	0.1 M	MES	6.5	18 % w/v	PEG 6000

Figure 14.57 (4-2): Moecular dimension for crystilisation method MemGold™ MD1-39

Molecular Dimensions

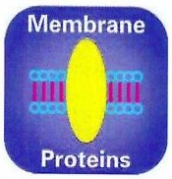

MemGold™ Conditions 1-48 (Box 2) MD1–39

Tube #	Conc.	Salt	Conc.	Buffer	pH	Conc.	Precipitant
2-1	0.22 M	Sodium citrate tribasic dihydrate	0.1 M	Tris	8.0	35 % v/v	PEG 400
2-2			0.1 M	Sodium acetate	4.5	17 % v/v	PEG 400
2-3	1.0 M	Lithium sulfate	0.02 M	Tris	8.5	1.8 % w/v	PEG 8000
2-4			0.02 M	Tris	7.5	22 % v/v	PEG 500 MME
2-5	0.05 M	Sodium chloride	0.02 M	Glycine	10.0	33 % w/v	PEG 1000
2-6	0.2 M	Magnesium chloride hexahydrate	0.1 M	Tris	8.5	25 % w/v	PEG 4000
2-7	0.2 M	Magnesium chloride hexahydrate	0.1 M	Sodium cacodylate	6.5	31 % w/v	PEG 2000
2-8			0.64 M	Sodium acetate	4.6	18 % w/v	PEG 3350
2-9	0.1 M	Sodium chloride	0.1 M	Tris-HCl	8.0	33 % v/v	PEG 400
	0.1 M	Cadmium chloride hemi(pentahydrate)					
2-10			0.1 M	BICINE	8.9	31 % w/v	PEG 2000
2-11	0.05 M	Sodium sulfate	0.05 M	Tris	8.5	35 % v/v	PEG 400
	0.05 M	Lithium sulfate					
2-12	0.1 M	Sodium chloride	0.05 M	Glycine	9.5	33 % v/v	PEG 300
2-13	0.3 M	Magnesium nitrate hexahydrate	0.1 M	Tris	8.0	23 % w/v	PEG 2000
2-14	0.12 M	Lithium sulfate	0.02 M	Tris	7.5	20 % v/v	PEG 300
			0.1 M	Sodium citrate	5.0		
2-15	0.1 M	Sodium chloride	0.12 M	Tris	9.4	20 % v/v	PEG 400
2-16	0.2 M	Sodium chloride	0.1 M	HEPES	7.0	22 % v/v	PEG 500 MME
2-17	0.1 M	Sodium chloride	0.1 M	Tris	8.0	21 % v/v	PEG 400
	0.325 M	Sodium acetate trihydrate					
2-18	0.02 M	Sodium citrate tribasic dihydrate	0.08 M	Sodium phosphate	6.2	18 % w/v	PEG 2000
2-19	0.02 M	Potassium nitrate	0.03 M	Potassium citrate	6.5	7.7 % w/v	PEG 4000
2-20	0.1 M	Sodium chloride	0.1 M	Tris	8.5	30 % w/v	PEG 2000 MME
	0.005 M	Magnesium chloride hexahydrate					
2-21	0.2 M	Calcium chloride dihydrate	0.1 M	HEPES	7.0	33 % v/v	PEG 400
2-22	0.1 M	Calcium chloride dihydrate	0.1 M	Tris	6.5	13 % w/v	PEG 2000 MME
2-23	0.2 M	Ammonium sulfate	0.02 M	Sodium acetate	4.0	33 % v/v	PEG 200
	0.02 M	Sodium chloride					
2-24	0.07 M	Sodium chloride	0.05 M	Sodium citrate	4.5	22 % v/v	PEG 400
2-25	0.2 M	Ammonium sulfate	0.1 M	Sodium acetate	4.6	28 % v/v	PEG 500 MME
2-26			0.05 M	Glycine	9.0	55 % v/v	PEG 400
2-27	0.1 M	Magnesium chloride hexahydrate	0.1 M	Tris	8.5	33 % v/v	PEG 400
	0.1 M	Sodium chloride					
2-28	0.05 M	Citric acid				19 % w/v	PEG 1000
	0.1 M	Lithium sulfate					
	0.05 M	Sodium phosphate dibasic dihydrate					
2-29	0.2 M	Magnesium chloride hexahydrate	0.025 M	Sodium citrate	4.0	33 % v/v	PEG 400
	0.1 M	Potassium chloride					
2-30	0.05 M	Zinc acetate dihydrate	0.05 M	MES	6.1	11 % w/v	PEG 8000
2-31	0.3 M	Magnesium nitrate hexahydrate	0.1 M	Tris	8.0	22 % w/v	PEG 8000
2-32	0.1 M	Sodium chloride	0.1 M	MES	6.5	33 % v/v	PEG 400
						4 % v/v	Ethylene glycol
2-33	0.05 M	Sodium chloride	0.1 M	Sodium citrate	5.5	26 % v/v	PEG 400
2-34	0.1 M	Lithium sulfate	0.1 M	Glycine	9.3	30 % v/v	PEG 400
2-35	0.15 M	Potassium citrate tribasic monohydrate				22 % w/v	PEG 6000
	0.05 M	Lithium citrate tribasic tetrahydrate					
	0.1 M	Sodium phosphate monobasic monohydrate					
2-36	0.001 M	Zinc sulfate heptahydrate	0.05 M	HEPES	7.8	28 % v/v	PEG 600
2-37	0.1 M	Sodium chloride	0.1 M	Sodium phosphate	7.0	33 % v/v	PEG 300
2-38	0.1 M	Sodium chloride	0.05 M	BICINE	9.0	33 % v/v	PEG 300
2-39	0.05 M	Zinc acetate dihydrate	0.1 M	Sodium cacodylate	6.0	6.6 % w/v	PEG 8000
						6 % v/v	Ethylene glycol
2-40	0.2 M	Lithium sulfate	0.1 M	Sodium citrate	3.5	28 % v/v	PEG 400
2-41	0.1 M	Sodium chloride	0.1 M	Tris	7.5	11 % w/v	PEG 4000
2-42	0.05 M	Lithium sulfate	0.1 M	Tricine	7.4	7 % w/v	PEG 3000
2-43	0.2 M	Calcium chloride dihydrate	0.1 M	MES	6.5	33 % v/v	PEG 400
2-44	1.0 M	Sodium chloride	0.1 M	Sodium citrate	6.0	28 % w/v	PEG 4000
2-45			0.1 M	HEPES	7.5	11 % w/v	PEG 4000
2-46	0.002 M	Zinc sulfate heptahydrate	0.08 M	HEPES	7.0	25 % v/v	Jeffamine® ED-2003
2-47	0.001 M	Cadmium chloride hemi(pentahydrate)	0.1 M	MES	6.5	30 % v/v	PEG 400
	0.03 M	Magnesium chloride hexahydrate					
2-48	3.0 M	Sodium chloride	0.1 M	Bis-Tris propane	7.0		

Figure 14.57 (4-3): Moecular dimension for crystilisation method MemGold™ MD1-39

Molecular Dimensions

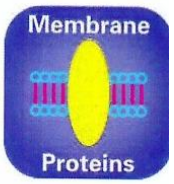

Formulation Notes:

MemGold™ reagents are formulated using ultrapure water (>18.0 MΩ) and are sterile-filtered using 0.22 µm filters. No preservatives are added.

Final pH may vary from that specified on the datasheet. Molecular Dimensions will be happy to discuss the precise formulation of individual reagents.

Individual reagents and stock solutions for optimization are available from Molecular Dimensions.

Enquiries regarding MemGold™ formulation, interpretation of results or optimization strategies are welcome. Please e-mail, fax or phone your query to Molecular Dimensions.

Contact and product details can be found at www.moleculardimensions.com

References.

Newstead, S., Ferrandon, S., Iwata, S. Protein Science 2008, 17(3)*"Rationalizing alpha-helical membrane protein crystallization"*.

*Developed by Dr. S. Newstead (So Iwata lab), 2004-2009, Imperial College, London and manufactured under licence by Molecular Dimensions Ltd.

Figure 14.57 (4-4): Moecular dimension for crystilisation method MemGold™ MD1-39

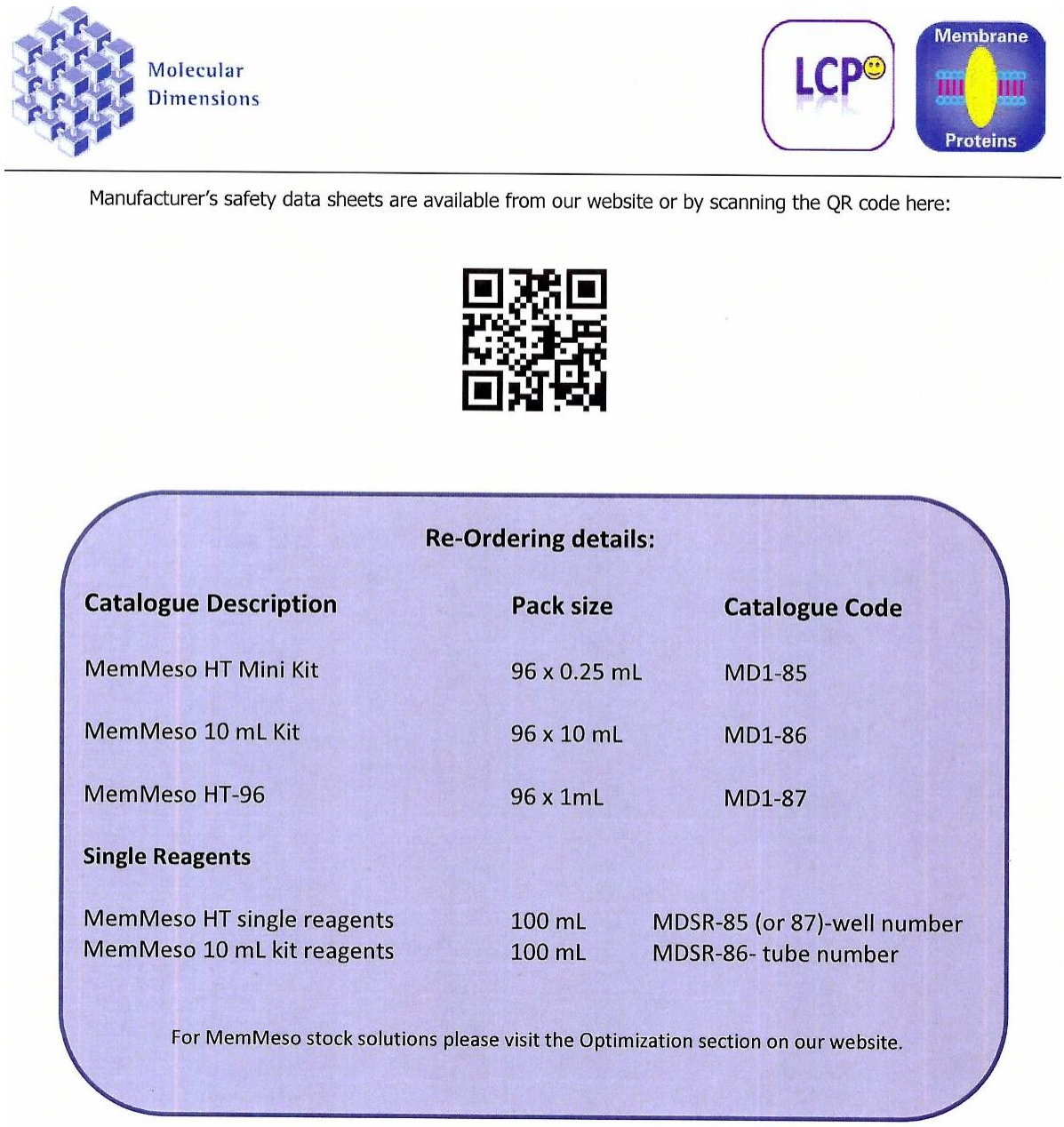

Figure 14.57 (4-5): Moecular dimension for crystilisation method MemGold™ MD1-39

Molecular Dimensions

Membrane Proteins

Abbreviations:
BICINE; N,N-Bis(2-hydroxyethyl)glycine, **HEPES**; N-(2-hydroxyethyl)-piperazine-N'-2-ethanesulfonic acid, **KMES**; 2-(N-morpholino)ethanesulfonic acid potassium salt, **MES**; 2-(N-morpholino)ethanesulfonic acid, **MME**; Monomethylether, **PEG**; Polyethylene glycol, **Tricine**; N-[Tris(hydroxymethyl)methyl]glycine, **Tris**; 2-Amino-2-(hydroxymethyl)propane-1,3-diol, **Tris HCl**; 2-Amino-2-(hydroxymethyl)propane-1,3-diol, hydrochloride.]

Manufacturer's safety data sheets are available from our website or by scanning the QR code here:

Re-Ordering details:

Catalogue Description	Pack size	Catalogue Code
MemGold™	96 x 10 mL	MD1-39
MemGold™ HT-96	96 x 1 mL	MD1-41
Eco Screens		
MemGold™ Eco Screen	96 x 10 mL	MD1-39-ECO
MemGold™ HT-96 Eco Screen	96 x 1 mL	MD1-41-ECO
Green Screens (contain fluorescent green dye - ideal for UV)		
MemGold™ Green Screen	96 x 10 mL	MD1-56
MemGold™ HT-96 Green Screen	96 x 1 mL	MD1-53
Combo Packs		
MemGold™ Combo Value Pack (MemGold™ + MemGold2™)	2 x 96 x 10 mL	MD1-74
MemGold™ HT-96 Combo Value Pack (MemGold™ + MemGold2™)	2 x 96 x 1 mL	MD1-74-HT
Single Reagents		
MemGold™ single reagents	100 mL	MDSR-39-tube number
MemGold™ HT-96 single reagents	100 mL	MDSR-41-well number

For MemGold™ stock solutions please visit the Optimization section on our website.

Figure 14.57 (4-6): Moecular dimension for crystilisation method MemGold™ MD1-39

14.8.5 MemGold2™ HT-96 MD1-64

Molecular Dimensions

Membrane Proteins

MemGold2™ HT-96 MD1-64

MemGold2™ - The latest innovation for crystallization of membrane proteins.
This screen targets all alpha helical types of Prokaryotic and Eukaryotic membrane proteins.

MD1-64 is a targeted sparse matrix presented as a 96 x 1 mL deep-well block.

Features of MemGold2:

- A brand new set of 96 of the most recent alpha-helical membrane protein crystallization conditions.
- Particularly suited for Prokaryotic and Eukaryotic alpha-helical membrane proteins.
- A great addition to any membrane protein lab.
- Works with MemGold, MemStart, MemSys & MemPlus.
- Screening over a wider range of pH's (4 - 10).
- Addition of small MW PEGs.
- Can be used in conjunction with Lipidic Sponge Phase and/or Lipidic Cubic Phases.

Formulation Notes:

MemGold2 reagents are formulated using ultrapure water (>18.0 MΩ) and are sterile-filtered using 0.22 µm filters. No preservatives are added.

Final pH may vary from that specified on the datasheet. Molecular Dimensions will be happy to discuss the precise formulation of individual reagents.
Individual reagents and stock solutions for optimization are available from Molecular Dimensions.

Enquiries regarding MemGold2 formulation, interpretation of results or optimization strategies are welcome. Please e-mail, fax or phone your query to Molecular Dimensions.

Contact and product details can be found at www.moleculardimensions.com

Introduction:

In 2008 Molecular Dimensions released MemGold[(1)] - a rationalized sparse matrix type membrane protein crystallization screen. MemGold was based on the crystallization conditions for 121 alpha helical Membrane Proteins deposited in the PDB.
Since MemGold, the number of structures has more than doubled. In response to this, MemGold2[(2)] has been developed. MemGold2 includes a further 96 crystallization conditions from unique alpha helical Membrane Protein structures including channel and transporter structures, GPCRs and ATPases.
It is suitable for both Prokaryotic and Eukaryotic alpha helical membrane proteins.

***References:**

(1) Newstead, S., Ferrandon, S., and Iwata, S. *'Rationalizing alpha-helical membrane protein crystallization'* Volume 17, Issue 3, pages 466–472, March 2008 - Protein Science, 2008 - Wiley Online Library.
(2) Parker, J. and Newstead, S. *'Current trends in alpha helical membrane protein crystallization: an update'*, Protein Science, 2012, *21(9):1358-65.*

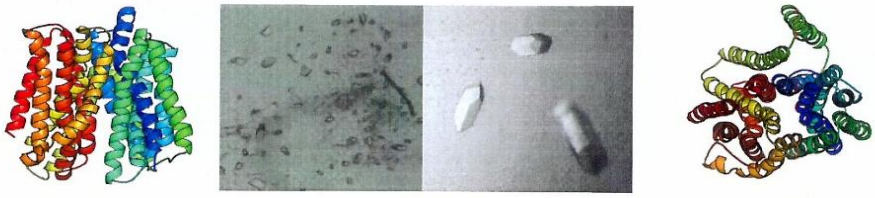

Examples of membrane protein crystals grown using MemGold2 and the structure of a membrane transport protein (previously solved using MemGold).

Figure 14.58 (5-1): Moecular dimension for crystilisation method MemGold2™ HT-96 MD1-64

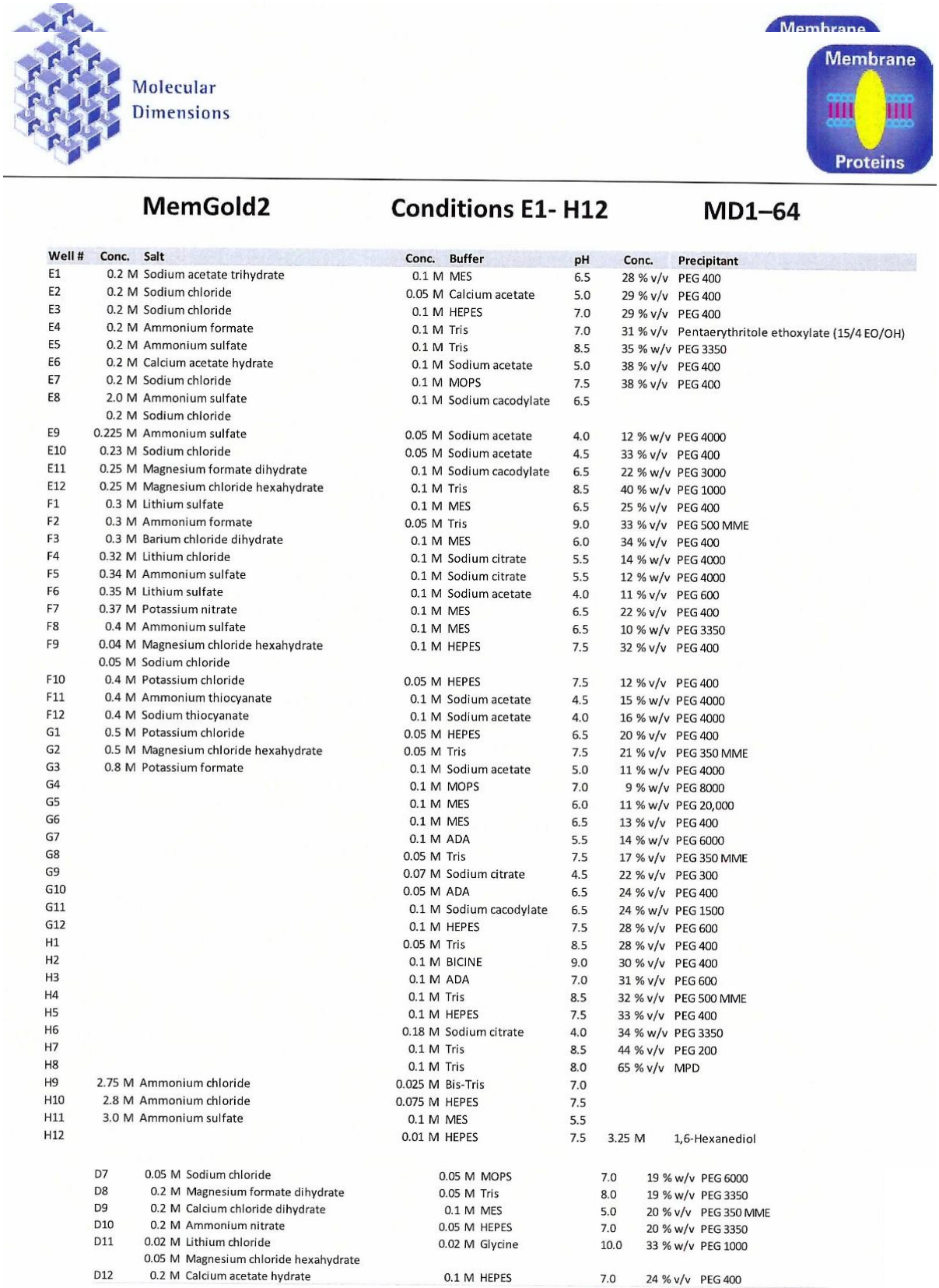

Molecular Dimensions

Membrane Proteins

MemGold2 **Conditions E1- H12** **MD1–64**

Well #	Conc.	Salt	Conc.	Buffer	pH	Conc.	Precipitant
E1	0.2 M	Sodium acetate trihydrate	0.1 M	MES	6.5	28 % v/v	PEG 400
E2	0.2 M	Sodium chloride	0.05 M	Calcium acetate	5.0	29 % v/v	PEG 400
E3	0.2 M	Sodium chloride	0.1 M	HEPES	7.0	29 % v/v	PEG 400
E4	0.2 M	Ammonium formate	0.1 M	Tris	7.0	31 % v/v	Pentaerythritole ethoxylate (15/4 EO/OH)
E5	0.2 M	Ammonium sulfate	0.1 M	Tris	8.5	35 % w/v	PEG 3350
E6	0.2 M	Calcium acetate hydrate	0.1 M	Sodium acetate	5.0	38 % v/v	PEG 400
E7	0.2 M	Sodium chloride	0.1 M	MOPS	7.5	38 % v/v	PEG 400
E8	2.0 M	Ammonium sulfate	0.1 M	Sodium cacodylate	6.5		
	0.2 M	Sodium chloride					
E9	0.225 M	Ammonium sulfate	0.05 M	Sodium acetate	4.0	12 % w/v	PEG 4000
E10	0.23 M	Sodium chloride	0.05 M	Sodium acetate	4.5	33 % v/v	PEG 400
E11	0.25 M	Magnesium formate dihydrate	0.1 M	Sodium cacodylate	6.5	22 % w/v	PEG 3000
E12	0.25 M	Magnesium chloride hexahydrate	0.1 M	Tris	8.5	40 % w/v	PEG 1000
F1	0.3 M	Lithium sulfate	0.1 M	MES	6.5	25 % v/v	PEG 400
F2	0.3 M	Ammonium formate	0.05 M	Tris	9.0	33 % v/v	PEG 500 MME
F3	0.3 M	Barium chloride dihydrate	0.1 M	MES	6.0	34 % v/v	PEG 400
F4	0.32 M	Lithium chloride	0.1 M	Sodium citrate	5.5	14 % w/v	PEG 4000
F5	0.34 M	Ammonium sulfate	0.1 M	Sodium citrate	5.5	12 % w/v	PEG 4000
F6	0.35 M	Lithium sulfate	0.1 M	Sodium acetate	4.0	11 % v/v	PEG 600
F7	0.37 M	Potassium nitrate	0.1 M	MES	6.5	22 % v/v	PEG 400
F8	0.4 M	Ammonium sulfate	0.1 M	MES	6.5	10 % w/v	PEG 3350
F9	0.04 M	Magnesium chloride hexahydrate	0.1 M	HEPES	7.5	32 % v/v	PEG 400
	0.05 M	Sodium chloride					
F10	0.4 M	Potassium chloride	0.05 M	HEPES	7.5	12 % v/v	PEG 400
F11	0.4 M	Ammonium thiocyanate	0.1 M	Sodium acetate	4.5	15 % w/v	PEG 4000
F12	0.4 M	Sodium thiocyanate	0.1 M	Sodium acetate	4.0	16 % w/v	PEG 4000
G1	0.5 M	Potassium chloride	0.05 M	HEPES	6.5	20 % v/v	PEG 400
G2	0.5 M	Magnesium chloride hexahydrate	0.05 M	Tris	7.5	21 % v/v	PEG 350 MME
G3	0.8 M	Potassium formate	0.1 M	Sodium acetate	5.0	11 % w/v	PEG 4000
G4			0.1 M	MOPS	7.0	9 % w/v	PEG 8000
G5			0.1 M	MES	6.0	11 % w/v	PEG 20,000
G6			0.1 M	MES	6.5	13 % v/v	PEG 400
G7			0.1 M	ADA	5.5	14 % w/v	PEG 6000
G8			0.05 M	Tris	7.5	17 % v/v	PEG 350 MME
G9			0.07 M	Sodium citrate	4.5	22 % v/v	PEG 300
G10			0.05 M	ADA	6.5	24 % v/v	PEG 400
G11			0.1 M	Sodium cacodylate	6.5	24 % w/v	PEG 1500
G12			0.1 M	HEPES	7.5	28 % v/v	PEG 600
H1			0.05 M	Tris	8.5	28 % v/v	PEG 400
H2			0.1 M	BICINE	9.0	30 % v/v	PEG 400
H3			0.1 M	ADA	7.0	31 % v/v	PEG 600
H4			0.1 M	Tris	8.5	32 % v/v	PEG 500 MME
H5			0.1 M	HEPES	7.5	33 % v/v	PEG 400
H6			0.18 M	Sodium citrate	4.0	34 % w/v	PEG 3350
H7			0.1 M	Tris	8.5	44 % v/v	PEG 200
H8			0.1 M	Tris	8.0	65 % v/v	MPD
H9	2.75 M	Ammonium chloride	0.025 M	Bis-Tris	7.0		
H10	2.8 M	Ammonium chloride	0.075 M	HEPES	7.5		
H11	3.0 M	Ammonium sulfate	0.1 M	MES	5.5		
H12			0.01 M	HEPES	7.5	3.25 M	1,6-Hexanediol

D7	0.05 M	Sodium chloride	0.05 M	MOPS	7.0	19 % w/v	PEG 6000
D8	0.2 M	Magnesium formate dihydrate	0.05 M	Tris	8.0	19 % w/v	PEG 3350
D9	0.2 M	Calcium chloride dihydrate	0.1 M	MES	5.0	20 % v/v	PEG 350 MME
D10	0.2 M	Ammonium nitrate	0.05 M	HEPES	7.0	20 % w/v	PEG 3350
D11	0.02 M	Lithium chloride	0.02 M	Glycine	10.0	33 % w/v	PEG 1000
	0.05 M	Magnesium chloride hexahydrate					
D12	0.2 M	Calcium acetate hydrate	0.1 M	HEPES	7.0	24 % v/v	PEG 400

Figure 14.58 (5-2): Moecular dimension for crystilisation method MemGold2™ HT-96 MD1-64

Molecular Dimensions

Membrane Proteins

Abbreviations:
BICINE; N,N-Bis(2-hydroxyethyl)glycine, **HEPES**; N-(2-hydroxyethyl)-piperazine-N'-2-ethanesulfonic acid, **KMES**; 2-(N-morpholino)ethanesulfonic acid potassium salt, **MES**; 2-(N-morpholino)ethanesulfonic acid, **MME**; Monomethylether, **PEG**; Polyethylene glycol, **Tricine**; N-[Tris(hydroxymethyl)methyl]glycine, **Tris**; 2-Amino-2-(hydroxymethyl)propane-1,3-diol, **Tris HCl**; 2-Amino-2-(hydroxymethyl)propane-1,3-diol, hydrochloride.]

Manufacturer's safety data sheets are available from our website or by scanning the QR code here:

Re-Ordering details:

Catalogue Description	Pack size	Catalogue Code
MemGold™	96 x 10 mL	MD1-39
MemGold™ HT-96	96 x 1 mL	MD1-41
Eco Screens		
MemGold™ Eco Screen	96 x 10 mL	MD1-39-ECO
MemGold™ HT-96 Eco Screen	96 x 1 mL	MD1-41-ECO
Green Screens (contain fluorescent green dye - ideal for UV)		
MemGold™ Green Screen	96 x 10 mL	MD1-56
MemGold™ HT-96 Green Screen	96 x 1 mL	MD1-53
Combo Packs		
MemGold™ Combo Value Pack (MemGold™ + MemGold2™)	2 x 96 x 10 mL	MD1-74
MemGold™ HT-96 Combo Value Pack (MemGold™ + MemGold2™)	2 x 96 x 1 mL	MD1-74-HT
Single Reagents		
MemGold™ single reagents	100 mL	MDSR-39-tube number
MemGold™ HT-96 single reagents	100 mL	MDSR-41-well number

For MemGold™ stock solutions please visit the Optimization section on our website.

Figure 14.58 (5-3): Moecular dimension for crystilisation method MemGold2^{TM} HT-96 MD1-64

Molecular Dimensions

Membrane Proteins

Abbreviations:
ADA; N-(2-Acetamido)iminodiacetic Acid, **BICINE**; N,N-Bis(2-hydroxyethyl)glycine, **Bis-Tris**; 2,2'-(Propane-1,3-diyldiimino)bis[2-(hydroxymethyl)propane-1,3-diol]. **CHES**; 2-(N-Cyclohexylamino)ethane sulfonic Acid, **HEPES**; N-(2-hydroxyethyl)-piperazine-N'-2-ethanesulfonic acid, **MES**; 2-(N-morpholino)ethanesulfonic acid, **MME**; Monomethylether, **MOPS**; 3-morpholinopropane-1-sulfonic acid, **PEG**; Polyethylene glycol, **PEG DME**; Poly(ethylene glycol) bis(carboxymethyl) ether, **Tricine**; N-[Tris(hydroxymethyl)methyl]glycine, **Tris**; 2-Amino-2-(hydroxymethyl)propane-1,3-diol.

Manufacturer's safety data sheets are available from our website or by scanning the QR code here:

Re-Ordering details:

Catalogue Description	Pack size	Catalogue Code
MemGold2	96 x 10 mL	MD1-63
MemGold2 HT-96	96 x 1 mL	MD1-64
Eco screens		
MemGold2	96 x 10 mL	MD1-63-ECO
MemGold2 HT-96	96 x 1 mL	MD1-64-ECO
Green screens (contain fluorescent green dye- ideal for UV)		
MemGold2 Green screen	96 x 10 mL	MD1-63-GREEN
MemGold2 HT-96 Green screen	96 x 1 mL	MD1-64-GREEN
Combo Packs (MemGold + MemGold2)		
MemGold Combo Value Pack	2 x 96 x 10 mL	MD1-74
MemGold HT96 Combo Value Pack	2 x 96 x 1 mL	MD1-74-HT
Single Reagents		
MemGold2 single reagents	100 mL	MDSR-63-tube number
MemGold2 HT-96 single reagents	100 mL	MDSR-64-well number

For MemGold2 stock solutions please visit the Optimization section on our website.

Figure 14.58 (5-4): Moecular dimension for crystilisation method MemGold2^{TM} HT-96 MD1-64

14.8.6 MemStart™ +MemSys™ HT-96 MD1-33

Molecular Dimensions

Membrane Proteins

MemStart™ + MemSys™ HT-96 MD1-33

A great starting point for membrane protein labs for screening and optimizing crystallization conditions for alpha - helical type transmembrane proteins.

A targeted sparse matrix of 96 x 1 mL conditions in a deep well block.

Features of MemStart™ + MemSys™ HT-96:

- Optimal starting point for screening and optimization of alpha-helical membrane proteins.
- Primarily designed for alpha type transmembrane proteins, but can be successfully applied to beta type outer membrane proteins.
- Based on the reagents typically used in the highly successful membrane protein laboratory of Prof. S. Iwata.
- Optimized to span 33 reported successful crystallization conditions for which high resolution structures of membrane proteins have been determined, including pH, type of precipitant, precipitant concentration, and salts.

Introduction

This kit is intended as a starting point for screening and optimizing crystallization conditions for alpha – helical type transmembrane proteins using vapour diffusion methods. Recently, there has been an increase in the number of membrane protein structures solved, providing a much larger database of reported conditions for successful crystallization. This kit is based on the reagents typically used in the laboratory of Prof. S. Iwata at Imperial College, London and is optimized to span the 33 reported successful crystallization conditions of membrane proteins for which high resolution structures have been determined.

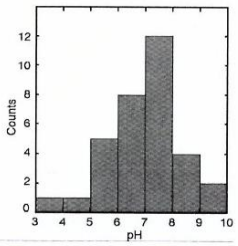

Typical pH conditions used for membrane protein crystallization.

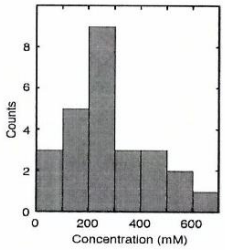

Total concentration of salts used for membrane protein crystallization.

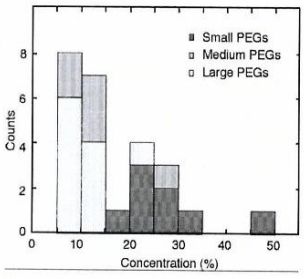

Types and concentrations of PEGs used for membrane protein crystallization.

(Small PEGs include triethylene glycol, PEG400 and PEG550 monomethylether. Medium PEGs include PEG1500, PEG2000 and PEG2000 monomethylether. Large PEGs include PEG3350, PEG4000, PEG6000 and PEG10000.)

Figure 14.59 (6-1): Moecular dimension for crystilisation method MemStart™ +MemSys™ HT-96 MD1-33

Molecular Dimensions

Membrane Proteins

Instructions for Use

MemStart™ is intended to be used in vapour diffusion crystallization methods. The protein drop is normally diluted 1:1 with the screening reagent. Detergents should also be added to this drop.

Membrane protein sample preparation

Membrane proteins often form aggregates and these will not crystallize. Electron microscopy and analytical ultracentrifugation can be more appropriate than dynamic light scattering for assessing sample homogeneity/ monodispersity of membrane protein samples prior to setting up crystallization experiments. Sample monodispersity can be improved by changing the detergent, increasing salt concentration, and ultracentrifugation.

Typical protein concentrations for crystallizing membrane proteins are in the range 40 - 80 µM. A good starting point would be 50 µM (10 mg/mL for a 200 kDa protein). Protein concentrations for crystallizing membrane proteins tend to be somewhat higher than normally recommended for soluble proteins, so if 50 µM is not successful try 100 µM (or even higher, it is often easier than changing the precipitant concentration).

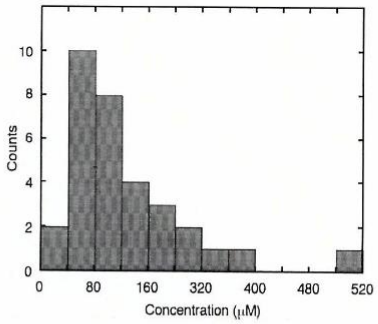

Typical protein concentrations used for membrane protein crystallization.

Detergents

Often the choices of detergent or precise concentration are critical parameters for initial screening. Good starting detergents are N-octyl β-D-Octyl glucopyranoside (OG), N-dodecyl β-D-maltoside (DDM) or N,N-dimethyldodecylamine N-oxide (LDAO). It is worth trying to crystallize with the detergent that was used during purification. Typically a concentration around 2 - 3 times the critical micelle concentration (CMC) should be used.

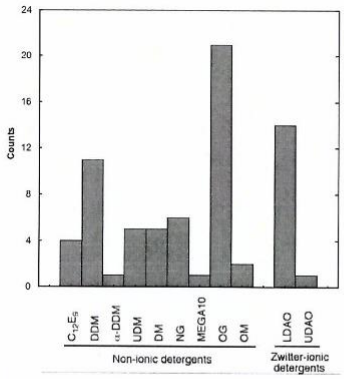

Detergents used for membrane protein crystallisation.

$C_{12}E_9$ (dodecyl nonaoxyethylene ether), DDM (N-dodecyl β-D-maltoside), α-DDM (N-dodecyl α-D-maltoside), UDM (N-undecyl β-D-maltoside), DM (N-decyl β-D-maltoside), NG (N-nonyl β-D-glucopyranoside), MEGA10 (N-decanoyl-N-methylglucamin), OG (N-octyl β-D-Octyl glucopyranoside), OM (octyl-ß-D-maltoside), LDAO (N,N-dimethyldodecylamine N-oxide), UDAO (N,N-dimethylundecylamine N-oxide).

Once a result is obtained, optimization of detergent choice and concentration is critical to obtain good quality crystals and a second detergent is often used as an additive (see below).

pH

The pH of the protein drop should not be overlooked. Most of the kit reagents are buffered and to take full advantage of this, a low concentration (20 mM) of buffer in the protein sample is desirable. Ionic strength can be increased with sodium chloride (50 – 100 mM) if protein solubility becomes a problem.

Figure 14.59 (6-2): Moecular dimension for crystilisation method MemStart™ +MemSys™ HT-96 MD1-33

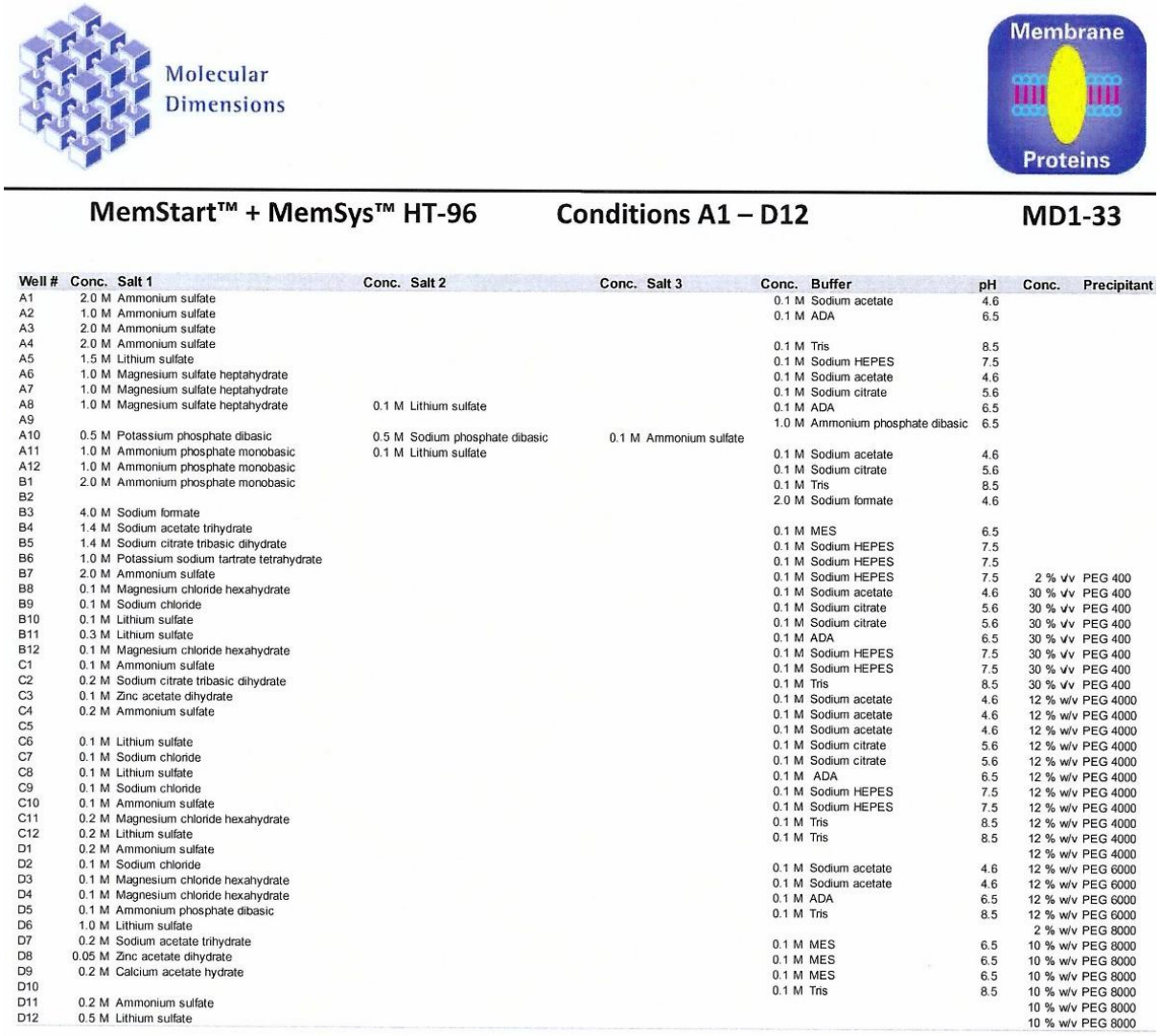

Molecular Dimensions

Membrane Proteins

MemStart™ + MemSys™ HT-96 Conditions A1 – D12 MD1-33

Well #	Conc.	Salt 1	Conc.	Salt 2	Conc.	Salt 3	Conc.	Buffer	pH	Conc.	Precipitant
A1	2.0 M	Ammonium sulfate					0.1 M	Sodium acetate	4.6		
A2	1.0 M	Ammonium sulfate					0.1 M	ADA	6.5		
A3	2.0 M	Ammonium sulfate									
A4	2.0 M	Ammonium sulfate					0.1 M	Tris	8.5		
A5	1.5 M	Lithium sulfate					0.1 M	Sodium HEPES	7.5		
A6	1.0 M	Magnesium sulfate heptahydrate					0.1 M	Sodium acetate	4.6		
A7	1.0 M	Magnesium sulfate heptahydrate					0.1 M	Sodium citrate	5.6		
A8	1.0 M	Magnesium sulfate heptahydrate	0.1 M	Lithium sulfate			0.1 M	ADA	6.5		
A9							1.0 M	Ammonium phosphate dibasic	6.5		
A10	0.5 M	Potassium phosphate dibasic	0.5 M	Sodium phosphate dibasic	0.1 M	Ammonium sulfate					
A11	1.0 M	Ammonium phosphate monobasic	0.1 M	Lithium sulfate			0.1 M	Sodium acetate	4.6		
A12	1.0 M	Ammonium phosphate monobasic					0.1 M	Sodium citrate	5.6		
B1	2.0 M	Ammonium phosphate monobasic					0.1 M	Tris	8.5		
B2							2.0 M	Sodium formate	4.6		
B3	4.0 M	Sodium formate									
B4	1.4 M	Sodium acetate trihydrate					0.1 M	MES	6.5		
B5	1.4 M	Sodium citrate tribasic dihydrate					0.1 M	Sodium HEPES	7.5		
B6	1.0 M	Potassium sodium tartrate tetrahydrate					0.1 M	Sodium HEPES	7.5		
B7	2.0 M	Ammonium sulfate					0.1 M	Sodium HEPES	7.5	2 % v/v	PEG 400
B8	0.1 M	Magnesium chloride hexahydrate					0.1 M	Sodium acetate	4.6	30 % v/v	PEG 400
B9	0.1 M	Sodium chloride					0.1 M	Sodium citrate	5.6	30 % v/v	PEG 400
B10	0.1 M	Lithium sulfate					0.1 M	Sodium citrate	5.6	30 % v/v	PEG 400
B11	0.3 M	Lithium sulfate					0.1 M	ADA	6.5	30 % v/v	PEG 400
B12	0.1 M	Magnesium chloride hexahydrate					0.1 M	Sodium HEPES	7.5	30 % v/v	PEG 400
C1	0.1 M	Ammonium sulfate					0.1 M	Sodium HEPES	7.5	30 % v/v	PEG 400
C2	0.2 M	Sodium citrate tribasic dihydrate					0.1 M	Tris	8.5	30 % v/v	PEG 400
C3	0.1 M	Zinc acetate dihydrate					0.1 M	Sodium acetate	4.6	12 % w/v	PEG 4000
C4	0.2 M	Ammonium sulfate					0.1 M	Sodium acetate	4.6	12 % w/v	PEG 4000
C5							0.1 M	Sodium acetate	4.6	12 % w/v	PEG 4000
C6	0.1 M	Lithium sulfate					0.1 M	Sodium citrate	5.6	12 % w/v	PEG 4000
C7	0.1 M	Sodium chloride					0.1 M	Sodium citrate	5.6	12 % w/v	PEG 4000
C8	0.1 M	Lithium sulfate					0.1 M	ADA	6.5	12 % w/v	PEG 4000
C9	0.1 M	Sodium chloride					0.1 M	Sodium HEPES	7.5	12 % w/v	PEG 4000
C10	0.1 M	Ammonium sulfate					0.1 M	Sodium HEPES	7.5	12 % w/v	PEG 4000
C11	0.2 M	Magnesium chloride hexahydrate					0.1 M	Tris	8.5	12 % w/v	PEG 4000
C12	0.2 M	Lithium sulfate					0.1 M	Tris	8.5	12 % w/v	PEG 4000
D1	0.2 M	Ammonium sulfate								12 % w/v	PEG 4000
D2	0.1 M	Sodium chloride					0.1 M	Sodium acetate	4.6	12 % w/v	PEG 6000
D3	0.1 M	Magnesium chloride hexahydrate					0.1 M	Sodium acetate	4.6	12 % w/v	PEG 6000
D4	0.1 M	Magnesium chloride hexahydrate					0.1 M	ADA	6.5	12 % w/v	PEG 6000
D5	0.1 M	Ammonium phosphate dibasic					0.1 M	Tris	8.5	12 % w/v	PEG 6000
D6	1.0 M	Lithium sulfate								2 % w/v	PEG 8000
D7	0.2 M	Sodium acetate trihydrate					0.1 M	MES	6.5	10 % w/v	PEG 8000
D8	0.05 M	Zinc acetate dihydrate					0.1 M	MES	6.5	10 % w/v	PEG 8000
D9	0.2 M	Calcium acetate hydrate					0.1 M	MES	6.5	10 % w/v	PEG 8000
D10							0.1 M	Tris	8.5	10 % w/v	PEG 8000
D11	0.2 M	Ammonium sulfate								10 % w/v	PEG 8000
D12	0.5 M	Lithium sulfate								10 % w/v	PEG 8000

Figure 14.59 (6-3): Moecular dimension for crystilisation method MemStart™ +MemSys™ HT-96 MD1-33

Molecular Dimensions

Membrane Proteins

MemStart™ + MemSys™ HT-96 Conditions E1 – H12 MD1-33

Well #	Conc.	Salt 1	Conc.	Salt 2	Conc.	Salt 3	Conc.	Buffer	pH	Conc.	Precipitant
E1	2.5 M	Ammonium sulfate					0.1 M	Sodium citrate	5.5		
E2	0.1 M	Sodium chloride	0.1 M	Lithium sulfate			0.1 M	Sodium citrate	3.5	30 % v/v	PEG 400
E3	0.1 M	Sodium chloride	0.1 M	Magnesium chloride hexahydrate			0.1 M	Sodium acetate	4.5	30 % v/v	PEG 400
E4	0.1 M	Sodium chloride					0.1 M	Sodium citrate	5.5	30 % v/v	PEG 400
E5	0.1 M	Sodium chloride	0.1 M	Lithium sulfate			0.1 M	Sodium citrate	5.5	30 % v/v	PEG 400
E6	0.1 M	Sodium chloride	0.1 M	Magnesium chloride hexahydrate			0.1 M	Sodium citrate	5.5	30 % v/v	PEG 400
E7	2.5 M	Ammonium sulfate					0.1 M	MES	6.5		
E8							0.1 M	MES	6.5	30 % v/v	PEG 400
E9	0.1 M	Sodium chloride					0.1 M	MES	6.5	30 % v/v	PEG 400
E10	0.1 M	Sodium chloride	0.1 M	Lithium sulfate			0.1 M	MES	6.5	30 % v/v	PEG 400
E11	0.1 M	Sodium chloride	0.1 M	Magnesium chloride hexahydrate			0.1 M	MES	6.5	30 % v/v	PEG 400
E12							0.1 M	MOPS	7.0	30 % v/v	PEG 400
F1	2.5 M	Ammonium sulfate					0.1 M	Sodium HEPES	7.5		
F2	0.1 M	Sodium chloride					0.1 M	MOPS	7.0	30 % v/v	PEG 400
F3							0.1 M	Sodium HEPES	7.5	30 % v/v	PEG 400
F4	0.1 M	Sodium chloride					0.1 M	Sodium HEPES	7.5	30 % v/v	PEG 400
F5	0.1 M	Sodium chloride	0.1 M	Lithium sulfate			0.1 M	Sodium HEPES	7.5	30 % v/v	PEG 400
F6	0.1 M	Sodium chloride	0.1 M	Magnesium chloride hexahydrate			0.1 M	Sodium HEPES	7.5	30 % v/v	PEG 400
F7	1.5 M	Lithium sulfate					0.1 M	Tris	8.5		
F8	0.1 M	Sodium chloride					0.1 M	Tris	8.5	30 % v/v	PEG 400
F9	0.1 M	Sodium chloride	0.1 M	Lithium sulfate			0.1 M	Tris	8.5	30 % v/v	PEG 400
F10	0.1 M	Sodium chloride	0.1 M	Magnesium chloride hexahydrate			0.1 M	Tris	8.5	30 % v/v	PEG 400
F11	0.1 M	Sodium chloride	0.1 M	Lithium sulfate			0.1 M	CAPSO	9.5	30 % v/v	PEG 400
F12	0.1 M	Sodium chloride	0.1 M	Magnesium chloride hexahydrate			0.1 M	CAPSO	9.5	30 % v/v	PEG 400
G1	1.5 M	Sodium phosphate monobasic monohydrate					0.1 M	Sodium citrate	5.5		
G2	0.1 M	Sodium chloride	0.1 M	Magnesium chloride hexahydrate			0.1 M	Sodium citrate	3.5	12 % w/v	PEG 4000
G3	0.1 M	Sodium chloride	0.1 M	Lithium sulfate			0.1 M	Sodium acetate	4.5	12 % w/v	PEG 4000
G4	0.1 M	Sodium chloride					0.1 M	Sodium citrate	5.5	12 % w/v	PEG 4000
G5	0.1 M	Sodium chloride	0.1 M	Lithium sulfate			0.1 M	Sodium citrate	5.5	12 % w/v	PEG 4000
G6	0.1 M	Sodium chloride	0.1 M	Magnesium chloride hexahydrate			0.1 M	Sodium citrate	5.5	12 % w/v	PEG 4000
G7	1.5 M	Sodium phosphate monobasic monohydrate					0.1 M	MES	6.5		
G8							0.1 M	MES	6.5	12 % w/v	PEG 4000
G9	0.1 M	Sodium chloride					0.1 M	MES	6.5	12 % w/v	PEG 4000
G10	0.1 M	Sodium chloride	0.1 M	Lithium sulfate			0.1 M	MES	6.5	12 % w/v	PEG 4000
G11	0.1 M	Sodium chloride	0.1 M	Magnesium chloride hexahydrate			0.1 M	MES	6.5	12 % w/v	PEG 4000
G12							0.1 M	MOPS	7.0	12 % w/v	PEG 4000
H1	1.5 M	Potassium phosphate dibasic					0.1 M	Sodium HEPES	7.5		
H2	0.1 M	Sodium chloride					0.1 M	MOPS	7.0	12 % w/v	PEG 4000
H3							0.1 M	Sodium HEPES	7.5	12 % w/v	PEG 4000
H4	0.1 M	Sodium chloride					0.1 M	Sodium HEPES	7.5	12 % w/v	PEG 4000
H5	0.1 M	Sodium chloride	0.1 M	Lithium sulfate			0.1 M	Sodium HEPES	7.5	12 % w/v	PEG 4000
H6	0.1 M	Sodium chloride	0.1 M	Magnesium chloride hexahydrate			0.1 M	Sodium HEPES	7.5	12 % w/v	PEG 4000
H7	1.5 M	Potassium phosphate dibasic					0.1 M	Tris	8.5		
H8	0.1 M	Sodium chloride					0.1 M	Tris	8.5	12 % w/v	PEG 4000
H9	0.1 M	Sodium chloride	0.1 M	Lithium sulfate			0.1 M	Tris	8.5	12 % w/v	PEG 4000
H10	0.1 M	Sodium chloride	0.1 M	Magnesium chloride hexahydrate			0.1 M	Tris	8.5	12 % w/v	PEG 4000
H11	0.1 M	Sodium chloride	0.1 M	Lithium sulfate			0.1 M	CAPSO	9.5	12 % w/v	PEG 4000
H12	0.1 M	Sodium chloride	0.1 M	Magnesium chloride hexahydrate			0.1 M	CAPSO	9.5	12 % w/v	PEG 4000

Abbreviations:

ADA; N-(2-Acetamido)iminodiacetic Acid, **CAPSO**; 3-(Cyclohexylamino)-2-hydroxy-1-propanesulfonic Acid Sodium Salt, **Sodium HEPES**; N-(2-hydroxyethyl)-piperazine-N'-2-ethanesulfonic acid, sodium salt, **MES**; 2-(N-morpholino)ethanesulfonic acid, **MOPS;** 3-(N-Morpholino)-propanesulfonic acid **PEG**; Polyethylene glycol, **Tris**; 2-Amino-2-(hydroxymethyl)propane-1,3-diol.

Figure 14.59 (6-4): Moecular dimension for crystilisation method MemStart™ +MemSys™ HT-96 MD1-33

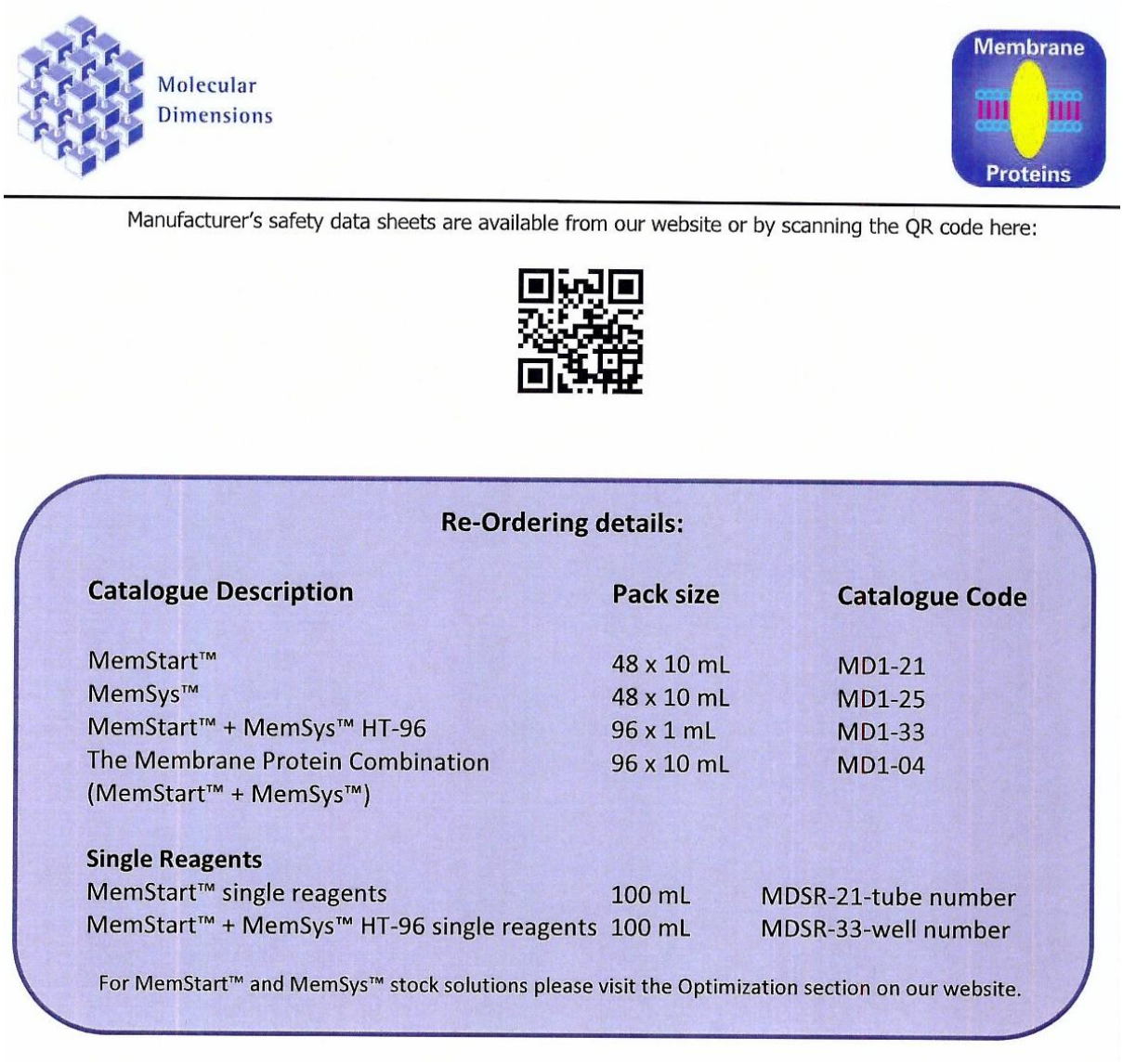

Figure 14.59 (6-5): Moecular dimension for crystilisation method MemStart-Sys-FX MD1-87-FX.

Chapter 15: References

Abbaspour, N., Hurrell, R., & Kelishadi, R. 2014. Review on iron and its importance for human health. Journal of Research in Medical Sciences: the official journal of Isfahan University of Medical Sciences, 19(2), 164.

Abdallah, F. B., & El Hage Chahine, J. M. 2000. Transferrins: iron release from lactoferrin. J Mol Biol, 303(2), 255-266. doi: 10.1006/jmbi.2000.4101

Aisen, P., Enns, C. & Wessling-Resnick, M. 2001. Chemistry and biology of eukaryotic iron metabolism. Int J Biochem Cell Biol, 33, 940-59.

Akiyama, H., Kanai, S., Hirano, M. and Miyasaka, H., 1998. Nucleotide sequence of plasmid pAQ1 of marine cyanobacterium Synechococcus sp. PCC7002. DNA Research, 5(2), pp.127-129.

Al-Awqati, Q., 1999. One hundred years of membrane permeability: does Overton still rule?. Nature Cell Biology, 1(8), p.E201.

Alexandrov, A.I., Mileni, M., Chien, E.Y., Hanson, M.A. and Stevens, R.C., 2008. Microscale fluorescent thermal stability assay for membrane proteins. Structure, 16(3), pp.351-359.

Altuvia, S., Almiron, M., Huisman, G., Kolter, R. and Storz, G., 1994. The dps promoter is activated by OxyR during growth and by IHF and σS in stationary phase. Molecular Microbiology, 13(2), pp.265-272.

Altuvia, S., Weinstein-Fischer, D., Zhang, A., Postow, L. & Storz, G. 1997. A small, stable RNA induced by oxidative stress: role as a pleiotropic regulator and antimutator. Cell, 90, 43-53.

Amabile-Cuevas, C. F. & Demple, B. 1991. Molecular characterization of the soxRS genes of Escherichia coli: two genes control a superoxide stress regulon. Nucleic Acids Res, 19, 4479-84.

Anatrace. 2008. Detergents and their uses in membrane protein science. Anatrace, Inc. Baneyx, F. 1999. Recombinant protein expression in Escherichia coli. Current Opinion. https://www.anatrace.com/Technical-Documentation/Catalogs/Anatrace-Detergents-Booklet-FINAL

Anderson BF, Norris GE, Rumball SV, Thomas DH, Baker EN. 1994. A comparison of the three-dimensional structures of human lactoferrin in its iron free and iron saturated forms. Advances in Experimental Medicine and Biology 357: 227-30.

Anderson, E. S., Paulley, J. T., Gaines, J. M., Valderas, M. W., Martin, D. W., Menscher, E., Roop, R. M. 2009. The manganese transporter MntH is a critical virulence determinant for Brucella abortus 2308 in experimentally infected mice. Infection and Immunity, 77(8), 3466–3474. https://doi.org/10.1128/IAI.00444-09.

Anderson, J. E., Sparling, P. F. & Cornelissen, C. N. 1994. Gonococcal transferrin-binding protein 2 facilitates but is not essential for transferrin utilization. J Bacteriol, 176, 3162-70.

Anderson, M.J., Crist, T.O., Chase, J.M., Vellend, M., Inouye, B.D., Freestone, A.L., Sanders, N.J., Cornell, H.V., Comita, L.S., Davies, K.F. and Harrison, S.P., 2011. Navigating the multiple meanings of β diversity: a roadmap for the practicing ecologist. Ecology Letters, 14(1), pp.19-28.

Andrews S.C. 2010. The Ferritin-like superfamily: Evolution of the biological iron storeman from a rubrerythrin-like ancestor. Biochimica et Biophysica Acta, 1800 (8): 691-705.

Andrews, N. C. 1999. Disorders of iron metabolism. New England Journal of Medicine, 341(26), 1986-1995.

Andrews, S. C. 1998. Iron storage in bacteria. Advances in Microbial Physiology (Vol. 40). https://doi.org/10.1038/279015a0.

Andrews, S. C., Robinson, A. K. & Rodriguez-Quinones, F. 2003a. Bacterial iron homeostasis. FEMS Microbiol Rev, 27, 215-37.

Andrews, S. C., Robinson, A. K. & Rodríguez-Quiñones, F. 2003b. Bacterial iron homeostasis. FEMS Microbiology Reviews, 27, 215-237.

Andrews, S. C., Robinson, A. K., & Rodríguez-Quiñones, F. 2003. Bacterial iron homeostasis. FEMS Microbiology Reviews, 27(2–3), 215–237. https://doi.org/10.1016/S0168-6445(03)00055-X.

Anjem, A., Varghese, S. & Imlay, J. A. 2009. Manganese import is a key element of the OxyR response to hydrogen peroxide in Escherichia coli. Mol Microbiol, 72, 844-58.

Aranda, J., Cortés, P., Garrido, M. E., Fittipaldi, N., Llagostera, M., Gottschalk, M., & Barbé, J. 2009. Contribution of the FeoB transporter to Streptococcus suis virulence. International Microbiology, 12(2), 137–143. https://doi.org/10.2436/20.1501.01.9.

Archibald, F.S. and Duong, M.N., 1984. Manganese acquisition by Lactobacillus plantarum. Journal of Bacteriology, 158(1), pp.1-8.

Arnold, T. and Linke, D., 2008. The use of detergents to purify membrane proteins. Current Protocols in Protein Science, 53(1), pp.4-8.

Arnoux, P., Haser, R., Izadi, N., Lecroisey, A., Delepierre, M., Wandersman, C., & Czjzek, M. (1999). The crystal structure of HasA, a hemophore secreted by Serratia marcescens. Nat Struct Biol, 6(6), 516-520. doi: 10.1038/9281.

Ash, M. R., Guilfoyle, A., Clarke, R. J., Guss, J. M., Maher, M. J. & Jormakka, M. 2010. Potassium-activated GTPase reaction in the G Protein-coupled ferrous iron transporter B. J Biol Chem, 285, 14594-602.

Askwith, C., & Kaplan, J. 1997. An oxidase-permease-based iron transport system in Schizosaccharomyces pombe and its expression in Saccharomyces cerevisiae. The Journal of Biological Chemistry, 272(1), 401–5.

Åslund, F., Zheng, M., Beckwith, J. and Storz, G., 1999. Regulation of the OxyR transcription factor by hydrogen peroxide and the cellular thiol—disulfide status. Proceedings of the National Academy of Sciences, 96(11), pp.6161-6165.

Atkinson, P. G., Blackwell, J. M. & Barton, C. H. 1997. Nramp1 locus encodes a 65 kDa interferon-gamma-inducible protein in murine macrophages. Biochem J, 325 (Pt 3), 779-86.

Ausubel, F. M., Brent, R., Kingston, R. E., Moore, D. D., Seidman, J. G., Smith, J. A., & Struhl, K. (1992). Short protocols in molecular biology. John Wiley & Sons, New York.

Bagg, a, & Neilands, J. B. (1987). Ferric uptake regulation protein acts as a repressor, employing iron (II) as a cofactor to bind the operator of an iron transport operon in Escherichia coli. Biochemistry, 26(1 970), 5471–5477. https://doi.org/10.1021/bi00391a039.

Baichoo, N., Wang, T., Ye, R., & Helmann, J. D. (2002). Global analysis of the Bacillus subtilis Fur regulon and the iron starvation stimulon. Mol Microbiol, 45(6), 1613-1629.

Bauer, S., Groh, V., Wu, J., Steinle, A., Phillips, J. H., Lanier, L. L. & Spies, T. 1999. Activation of NK cells and T cells by NKG2D, a receptor for stress-inducible MICA. Science, 285, 727-9.

Beauchene, N.A., Myers, K.S., Chung, D., Park, D.M., Weisnicht, A.M., Keleş, S. and Kiley, P.J., 2015. Impact of anaerobiosis on expression of the iron-responsive Fur and RyhB regulons. *MBio*, *6*(6), pp.e01947-15.

Beinert, H. 2000. A tribute to sulfur. Eur J Biochem, 267, 5657-64.

Benevides-Matos, N., Wandersman, C. and Biville, F. (2008) HasB, the Serratia marcescens TonB paralog, is specific to HasR. J Bacteriol . 190:21-27.

Berman, H.M., Bourne, P.E., Westbrook, J. and Zardecki, C., 2003. The protein data bank. In Protein Structure pp. 394-410. CRC Press.

Berrow, N.S., Büssow, K., Coutard, B., Diprose, J., Ekberg, M., Folkers, G.E., Lévy, N., Lieu, V., Owens, R.J., Peleg, Y. and Pinaglia, C., 2006. Recombinant protein expression and solubility screening in Escherichia coli: a comparative study. Acta Crystallographica Section D: Biological Crystallography, 62(10), pp.1218-1226.

Bill, R.M., Henderson, P.J., Iwata, S., Kunji, E.R., Michel, H., Neutze, R., Newstead, S., Poolman, B., Tate, C.G. and Vogel, H., 2011. Overcoming barriers to membrane protein structure determination. Nature Biotechnology, 29(4), p.335.

Blackwell, J. M., Searle, S., Mohamed, H. & White, J. K. 2003. Divalent cation transport and susceptibility to infectious and autoimmune disease: continuation of the Ity/Lsh/Bcg/Nramp1/Slc11a1 gene story. Immunol Lett, 85, 197-203.

Blaser, M.J., 1990. Helicobacter pylori and the pathogenesis of gastroduodenal inflammation. Journal of Infectious Diseases, 161(4), pp.626-633.

Booker, C.L., Harding, S. and Benzeval, M., 2011. A systematic review of the effect of retention methods in population-based cohort studies. BMC Public Health, 11(1), p.249.

Bou-Abdallah, F., Yang, H., Awomolo, A., Cooper, B., Woodhall, M. R., Andrews, S. C., & Chasteen, N. D. 2014. Functionality of the three-site ferroxidase center of Escherichia coli bacterial ferritin (EcFtnA). Biochemistry, 53(3), 483–495. https://doi.org/10.1021/bi401517f.

Boulette, M.L. and Payne, S.M., 2007. Anaerobic regulation of Shigella flexneri virulence: ArcA regulates Fur and iron acquisition genes. Journal of bacteriology, 189(19), pp.6957-6967.

Boyer, E., Bergevin, I., Malo, D., Gros, P., & Cellier, M. F. M. 2002. Acquisition of Mn(II) in addition to Fe(II) is required for full virulence of Salmonella enterica serovar

Typhimurium. Infection and Immunity, 70(11), 6032–6042. https://doi.org/10.1128/IAI.70.11.6032-6042.2002.

Bradley, J. M., Moore, G. R., & Le Brun, N. E. 2017. Diversity of Fe2+ entry and oxidation in ferritins. Current Opinion in Chemical Biology, 37, 122-128.

Braun, V., & Braun, M. 2002. Iron transport and signaling in Escherichia coli. FEBS Letters 529, 78-85

Braun, V., & Hantke, K. 2011. Recent insights into iron import by bacteria. Current Opinion in Chemical Biology, 15(2), 328-334.

Brock, J., Williams, P. H., Liceaqa, J., and Wooldridge, K. G. (1991). Relative availability of transferrin-bound iron and cell-derived iron to aerobactin-producing and enterochelin-producing strains of Escherichia coli and to other microorganisms. Infection and Immunity 59:3185-3190.

Brock, J.H., 1994. Iron and immunity. Journal of Nutritional Immunology, 2(3), pp.47-106.

Brown, J. S., & Holden, D. W. 2002. Iron acquisition by Gram-positive bacterial pathogens. Microbes Infect, 4(11), 1149-1156.

Brutscher, B., Brüschweiler, R. and Ernst, R.R., 1997. Backbone dynamics and structural characterization of the partially folded A state of ubiquitin by 1H, 13C, and 15N nuclear magnetic resonance spectroscopy. Biochemistry, 36(42), pp.13043-13053.

Bullen, J. J., Cushnie, G. H. & Rogers, H. J. 1967. The abolition of the protective effect of Clostridium welchii type A antiserum by ferric iron. Immunology, 12, 303-12.

Cabiscol, E., Tamarit, J., & Ros, J. 2000. Oxidative stress in bacteria and protein damage by reactive oxygen species. International Microbiology, 3(1), 3–8. https://doi.org/10.2436/im.v3i1.9235.

Cadoret, F., Ball, G., Douzi, B. and Voulhoux, R., 2014. Txc, a new type II secretion system of Pseudomonas aeruginosa strain PA7, is regulated by the TtsS/TtsR two-component system and directs specific secretion of the CbpE chitin-binding protein. Journal of Bacteriology, 196(13), pp.2376-2386.

Cadwell, R.C. and Joyce, G.F., 1992. Randomization of genes by PCR mutagenesis. Genome research, 2(1), pp.28-33.

Caffrey, M., 2015. A comprehensive review of the lipid cubic phase or in meso method for crystallizing membrane and soluble proteins and complexes. Acta Crystallographica Section F: Structural Biology Communications, 71(1), pp.3-18.

Caffrey, M., Li, D., Howe, N. and Shah, S.T., 2014. 'Hit and run'serial femtosecond crystallography of a membrane kinase in the lipid cubic phase. Philosophical Transactions of the Royal Society B: Biological Sciences, 369(1647), p.20130621.

Calderwood, S. B. & Mekalanos, J. J. 1987. Iron regulation of Shiga-like toxin expression in Escherichia coli is mediated by the fur locus. J Bacteriol, 169, 4759-64.

Campellone, K. G., Giese, A., Tipper, D. J., & Leong, J. M. (2002). A tyrosine-phosphorylated 12-amino-acid sequence of enteropathogenic Escherichia coli Tir binds the host adaptor protein Nck and is required for Nck localization to actin pedestals. Molecular Microbiology, 43(5), 1227–1241. https://doi.org/10.1046/j.1365-2958.2002.02817.x.

Camps, M., & Loeb, L. A. (2003). Use of pol I-deficient E. coli for functional complementation of DNA polymerase. Directed Enzyme Evolution: Screening and Selection Methods, 11-18.

Canonne-Hergaux, F., Gruenheid, S., Govoni, G. & Gros, P. 1999. The Nramp1 protein and its role in resistance to infection and macrophage function. Proc Assoc Am Physicians, 111, 283-9.

Cao, J., Woodhall, M. R., Alvarez, J., Cartron, M. L., & Andrews, S. C. (2007). EfeUOB (YcdNOB) is a tripartite, acid-induced and CpxAR-regulated, low-pH Fe2+ transporter that is cryptic in Escherichia coli K-12 but functional in E. coli O157:H7. Molecular Microbiology, 65(4), 857–875. https://doi.org/10.1111/j.1365-2958.2007.05802.x.

Cardona, S. T., & Valvano, M. A. (2005). An expression vector containing a rhamnose-inducible promoter provides tightly regulated gene expression in Burkholderia cenocepacia. Plasmid, 54(3), 219–228. https://doi.org/10.1016/j.plasmid.2005.03.004.

Carlioz, A. and Touati, D., 1986. Isolation of superoxide dismutase mutants in Escherichia coli: is superoxide dismutase necessary for aerobic life?. The EMBO Journal, 5(3), pp.623-630.

Carpenter, E.P., Beis, K., Cameron, A.D. and Iwata, S., 2008. Overcoming the challenges of membrane protein crystallography. Current Opinion in Structural Biology, 18(5), pp.581-586.

Carrondo M., (2003): Ferritins, iron uptake and storage from the bacterioferritin viewpoint. EMBO Journal, 22: 1959-1968.

Cartron, M. L., Maddocks, S., Gillingham, P., Craven, C. J. & Andrews, S. C. 2006. Feo--transport of ferrous iron into bacteria. Biometals, 19, 143-57.

Cartron, M. L., Mitchell, S. A., Woodhall, M. R., Andrews, S. C., & Watson, K. A. (2007). Preliminary X-ray diffraction analysis of YcdB from Escherichia coli: A novel haem-containing and Tat-secreted periplasmic protein with a potential role in iron transport. Acta Crystallographica Section F: Structural Biology and Crystallization Communications, 63(1), 37–41. https://doi.org/10.1107/S174430910604509X.

Cassat, J. E. & Skaar, E. P. 2013. Iron in infection and immunity. Cell Host Microbe, 13, 509-519.

Chakraborty, S., Patel, Y. J., Krause, J. A., & Guan, H. (2013). A Robust Nickel Catalyst for Cyanomethylation of Aldehydes: Activation of Acetonitrile under Base-Free Conditions. Angewandte Chemie International Edition,52(29), 7523-7526.

Chan, E. & Weiss, B. 1987. Endonuclease IV of Escherichia coli is induced by paraquat. Proc Natl Acad Sci U S A, 84, 3189-93.

Cherepanov, P. P., & Wackernagel, W. (1995). Gene disruption in Escherichia coli: TcR and KmR cassettes with the option of Flp-catalyzed excision of the antibiotic- resistance determinant. Gene, 158(1), 9-14.

Chiancone E., and Ceci P., (2010): The multifaceted capacity of Dps proteins to combat bacterial stress conditions: Detoxification of iron and hydrogen peroxide and DNA binding. Biochimica et Biophysica Acta (BBA) - General Subjects 1800 (8): 798–805.

Chiancone, E., Ceci, P., Ilari, A., Ribacchi, F., & Stefanini, S. (2004). Iron and proteins for iron storage and detoxification. Biometals, 17(3), 197-202.

Chiba, S., Akiyama, Y. and Ito, K., 2002. Membrane protein degradation by FtsH can be initiated from either end. Journal of Bacteriology, 184(17), pp.4775-4782.

Chin, K., Shean, C.S. and Gottesman, M.E., 1993. Resistance of lambda cI translation to antibiotics that inhibit translation initiation. Journal of Bacteriology, 175(22), pp.7471-7473.

Choi, H., Kim, S., Mukhopadhyay, P., Cho, S., Woo, J., Storz, G. & Ryu, S. E. 2001. Structural basis of the redox switch in the OxyR transcription factor. Cell, 105, 103-13.

Choi, J., & Ryu, S. (2019). Regulation of iron uptake by fine-tuning the iron-responsiveness of the iron sensor Fur. Appl. Environ. Microbiol., AEM-03026.

Christman, M. F., Storz, G. & Ames, B. N. 1989. OxyR, a positive regulator of hydrogen peroxide-inducible genes in Escherichia coli and Salmonella typhimurium, is

homologous to a family of bacterial regulatory proteins. Proc Natl Acad Sci U S A, 86, 3484-8.

Christman, M.F., Morgan, R.W., Jacobson, F.S. and Ames, B.N., 1985. Positive control of a regulon for defenses against oxidative stress and some heat-shock proteins in Salmonella typhimurium. Cell, 41(3), pp.753-762.

Chu, B. C., Garcia-Herrero, A., Johanson, T. H., Krewulak, K. D., Lau, C. K., Peacock, R. S., Slavinskaya, Z. & Vogel, H. J. 2010. Siderophore uptake in bacteria and the battle for iron with the host; a bird's eye view. Biometals, 23, 601-11.

Claiborne, A. & Fridovich, I. 1979. Chemical and enzymatic intermediates in the peroxidation of o-dianisidine by horseradish peroxidase. 2. Evidence for a substrate radical--enzyme complex and its reaction with nucleophiles. Biochemistry, 18, 2329-35.

Claiborne, A., Malinowski, D. P. & Fridovich, I. 1979. Purification and characterization of hydroperoxidase II of Escherichia coli B. J Biol Chem, 254, 11664-8.

Clary, D.O. and Rothman, J.E., 1990. Purification of three related peripheral membrane proteins needed for vesicular transport. Journal of Biological Chemistry, 265(17), pp.10109-10117.

Clément, P., Hafaiedh, I., Parra, E.J., Thamri, A., Guillot, J., Abdelghani, A. and Llobet, E., 2014. Iron oxide and oxygen plasma functionalized multi-walled carbon nanotubes for the discrimination of volatile organic compounds. Carbon, 78, pp.510-520.

Coffey, R. & Ganz, T. 2017. Iron homeostasis: An anthropocentric perspective. J Biol Chem, 292, 12727-12734.

Collet, J., Dilworth-Occhialini, C., Pacault, R., Pounds, K., Rocchia, R., Roth, E. R., & Sanford, P. (1970). Lunar occultation satellite for high resolution studies of cosmic X-ray sources. Nature, 228, 756-757.

Confalonieri, F. and Duguet, M., 1995. A 200-amino acid ATPase module in search of a basic function. Bioessays, 17(7), pp.639-650.

Cornelis, P., & Andrews, S. C. (Eds.). (2010). Iron uptake and homeostasis in microorganisms. Horizon Scientific Press.

Cornelis, P., Wei, Q., Andrews, S. C., & Vinckx, T. (2011). Iron homeostasis and management of oxidative stress response in bacteria. Metallomics: Integrated Biometal Science, 3(6), 540–9. https://doi.org/10.1039/c1mt00022e.

Cowart, L.A., Wei, S., Hsu, M.H., Johnson, E.F., Krishna, M.U., Falck, J.R. and Capdevila, J.H., 2002. The CYP4A isoforms hydroxylate epoxyeicosatrienoic acids to form high affinity peroxisome proliferator-activated receptor ligands. Journal of Biological Chemistry, 277(38), pp.35105-35112.

Cox, C.D., 1994. [24] Deferration of laboratory media and assays for ferric and ferrous ions. Methods in Enzymology Vol. 235, pp. 315-329. Academic Press.

Crichton, R.R., Wilmet, S., Legssyer, R. and Ward, R.J., 2002. Molecular and cellular mechanisms of iron homeostasis and toxicity in mammalian cells. Journal of inorganic biochemistry, 91(1), pp.9-18.

Crichton, R (2009): Inorganic Biochemistry of Iron Metabolism: From Molecular Mechanisms to Clinical Consequences. Third Edition. Chichester. John Wiley & Sons, Ltd.; West Sussex, England.

Dalbey, R.E. and Chen, M., 2004. Sec-translocase mediated membrane protein biogenesis. Biochimica et Biophysica Acta (BBA)-Molecular Cell Research, 1694(1-3), pp.37-53.

Dashper, S. G., Butler, C. A., Lissel, J. P., Paolini, R. A., Hoffmann, B., Veith, P. D., … Reynolds, E. C. (2005). A novel Porphyromonas gingivalis FeoB plays a role in manganese accumulation. Journal of Biological Chemistry, 280(30), 28095–28102. https://doi.org/10.1074/jbc.M503896200.

Datsenko, K.A. and Wanner, B.L., 2000. One-step inactivation of chromosomal genes in Escherichia coli K-12 using PCR products. Proceedings of the National Academy of Sciences, 97(12), pp.6640-6645.

Dauphas, N., & Rouxel, O. (2006). Mass spectrometry and natural variations of iron isotopes. Mass Spectrometry Reviews. https://doi.org/10.1002/mas.20078.

D'autreaux, B., Horner, O., Oddou, J. L., Jeandey, C., Gambarelli, S., Berthomieu, C., Latour, J. M. & Michaud-Soret, I. 2004. Spectroscopic description of the two nitrosyl-iron complexes responsible for fur inhibition by nitric oxide. J Am Chem Soc, 126, 6005-16.

de Castro Ferreira, I. G., Rodrigues, M. M., da Silva Neto, J. F., Mazzon, R. R., & do Valle Marques, M. (2016). Role and regulation of ferritin-like proteins in iron homeostasis and oxidative stress survival of Caulobacter crescentus. BioMetals, 29(5), 851–862. https://doi.org/10.1007/s10534-016-9956-y.

De Serrano, L.O., Camper, A.K. and Richards, A.M., 2016. An overview of siderophores for iron acquisition in microorganisms living in the extreme. Biometals, 29(4), pp.551-571.

De Silva, D.M., Askwith, C.C., Eide, D. and Kaplan, J., 1995. The FET3 gene product required for high affinity iron transport in yeast is a cell surface ferroxidase. Journal of Biological Chemistry, 270(3), pp.1098-1101.

Deisenhofer, J., Epp, O., Miki, K., Huber, R. and Michel, H., 1985. Structure of the protein subunits in the photosynthetic reaction centre of Rhodopseudomonas viridis at 3Å resolution. Nature, 318(6047), p.618.

Depuydt, M., Leonard, S. E., Vertommen, D., Denoncin, K., Morsomme, P., Wahni, K., … Collet, J.-F. (2009). A Periplasmic Reducing System Protects Single Cysteine Residues from Oxidation. Science, 326(2009), 1109–1111. https://doi.org/10.1038/nmat2382.

Deuerling, E., Mogk, A., Richter, C., Purucker, M. and Schumann, W., 1997. The ftsH gene of Bacillus subtilis is involved in major cellular processes such as sporulation, stress adaptation and secretion. Molecular Microbiology, 23(5), pp.921-933.

Ding, H. & Demple, B. 1996. Glutathione-mediated destabilization in vitro of [2Fe-2S] centers in the SoxR regulatory protein. Proc Natl Acad Sci U S A, 93, 9449-53.

Ding, H. and Demple, B., 1997. In vivo kinetics of a redox-regulated transcriptional switch. Proceedings of the National Academy of Sciences, 94(16), pp.8445-8449.

Ding, H., Hidalgo, E. & Demple, B. 1996. The redox state of the [2Fe-2S] clusters in SoxR protein regulates its activity as a transcription factor. J Biol Chem, 271, 33173-5.

Dix, D. R., Bridgham, J. T., Broderius, M. A., Byersdorfer, C. A. & Eide, D. J. 1994. The FET4 gene encodes the low affinity Fe(II) transport protein of Saccharomyces cerevisiae. J Biol Chem, 269, 26092-9.

Dominy, C.N. and Andrews, D.W., 2003. Site-directed mutagenesis by inverse PCR. In E. coli Plasmid Vectors (pp. 209-223). Humana Press.

Douglas, T., & Ripoll, D. R. (1998). Calculated electrostatic gradients in recombinant human H-chain ferritin. Protein Science : A Publication of the Protein Society, 7(5), 1083–1091. https://doi.org/10.1002/pro.5560070502.

Drechsel, H., Thieken, A., Reissbrodt, R., Jung, G., & Winkelmann, G. (1993). Alpha-keto acids are novel siderophores in the genera Proteus, Providencia, and Morganella and are produced by amino acid deaminases. J Bacteriol, 175(9), 2727-2733.

Drew, B., Phaneuf, S., Dirks, A., Selman, C., Gredilla, R., Lezza, A., Barja, G. and Leeuwenburgh, C., 2003. Effects of aging and caloric restriction on mitochondrial energy production in gastrocnemius muscle and heart. American Journal of Physiology-Regulatory, Integrative and Comparative Physiology, 284(2), pp.R474-R480.

Eakanunkul, S., Lukat-Rodgers, G. S., Sumithran, S., Ghosh, A., Rodgers, K. R., Dawson, J. H. & Wilks, A. 2005. Characterization of the periplasmic heme-binding protein shut from the heme uptake system of Shigella dysenteriae. Biochemistry, 44, 13179-91.

Edelhoch, H., 1967. Spectroscopic determination of tryptophan and tyrosine in proteins. Biochemistry, 6(7), pp.1948-1954.

Edison, E. S., Bajel, A., & Chandy, M. (2008). Iron homeostasis: new players, newer insights. Eur J Haematol, 81(6), 411-424. doi: 10.1111/j.1600-0609.2008.01143.x.

Eng, E.T., Jalilian, A.R., Spasov, K.A. and Unger, V.M., 2008. Characterization of a novel prokaryotic GDP dissociation inhibitor domain from the G protein coupled membrane protein FeoB. Journal of Molecular Biology, 375(4), pp.1086-1097.

Erhart C., (1996): In, Uptake and metabolism of iron and molybdenum, pp. 1075-1090. F.C. Neidhart, R. Curtis III, J.L. Ingraham, E.C.C. Lin, K.B. Low, B. Magasarik, W.S. Rezikoff, M. Riley, M. Schaechter, and H.E. Umbarger (ed), Escherichia coli and Salmonella; cellular and molecular biology, 2nd Ed. ASM Press, Washington DC

Escolar, L., Perez-Martin, J. & De Lorenzo, V. 1999. Opening the iron box: transcriptional metalloregulation by the Fur protein. J Bacteriol, 181, 6223-9.

Faraldo-Gomez, J. D., Smith, G. R. & Sansom, M. S. 2003. Molecular dynamics simulations of the bacterial outer membrane protein FhuA: a comparative study of the ferrichrome-free and bound states. Biophys J, 85, 1406-20.

Faraldo-Gomez, J. D.,& Sansom, M. S. (2003). Acquisition of siderophores in gram-negative bacteria. Nature Reviews Molecular Cell Biology, 4(2), 105-116.

Farr, S.B., Harvard College, 1996. Methods and diagnostic kits for determining toxicity utilizing E. coli stress promoters fused to reporter genes. U.S. Patent 5,585,232.

Fawcett, W. P. & Wolf, R. E., Jr. 1994. Purification of a MalE-SoxS fusion protein and identification of the control sites of Escherichia coli superoxide-inducible genes. Mol Microbiol, 14, 669-79.

Felice, M. R., De Domenico, I., Li, L., Ward, D. M., Bartok, B., Musci, G. & Kaplan, J. 2005. Post-transcriptional regulation of the yeast high affinity iron transport system. J Biol Chem, 280, 22181-90.

Ferreira, J.C., Icimoto, M.Y., Marcondes, M.F., Oliveira, V., Nascimento, O.R. and Nantes, I.L., 2013. Recycling of the high valence states of heme proteins by cysteine residues of Thimet-Oligopeptidase. PloS One, 8(11), p.e79102.

Ferreira, V., Koricheva, J., Duarte, S., Niyogi, D.K. and Guérold, F., 2016. Effects of anthropogenic heavy metal contamination on litter decomposition in streams–a meta-analysis. Environmental Pollution, 210, pp.261-270.

Fetherston, J. D., Mier, I., Perry, R. D., & Truszczynska, H. (2012). The yfe and feo transporters are involved in microaerobic growthand virulence of Yersinia pestis in bubonic plague. Infection and Immunity, 80(11), 3880–3891. https://doi.org/10.1128/IAI.00086-12.

Fiedorczuk, K., Letts, J.A., Degliesposti, G., Kaszuba, K., Skehel, M. and Sazanov, L.A., 2016. Atomic structure of the entire mammalian mitochondrial complex I. Nature, 538(7625), p.406.

Fillat, M. F. (2014). The fur (ferric uptake regulator) superfamily: Diversity and versatility of key transcriptional regulators. Archives of Biochemistry and Biophysics, 546, 41–52. Https://Doi.Org/10.1016/J.Abb.2014.01.029.

Fischbach, M. A., Lin, H., Zhou, L., Yu, Y., Abergel, R. J., Liu, D. R., Raymond, K. N., Wanner, B. L., Strong, R. K., Walsh, C. T., Aderem, A. & Smith, K. D. 2006. The pathogen-associated iroA gene cluster mediates bacterial evasion of lipocalin 2. Proc Natl Acad Sci U S A, 103, 16502-7.

Flo, T. H., Smith, K. D., Sato, S., Rodriguez, D. J., Holmes, M. A., Strong, R. K., . . . Aderem, A. (2004). Lipocalin 2 mediates an innate immune response to bacterial infection by sequestrating iron. Nature, 432(7019), 917-921. doi: 10.1038/nature03104.

Ford, D. C., Ireland, P. M., Bullifent, H. L., Saint, R. J., McAlister, E. V., Sarkar-Tyson, M., & Oyston, P. C. F. (2014). Construction of an inducible system for the analysis of essential genes in Yersinia pestis. Journal of Microbiological Methods, 100(1), 1–7. https://doi.org/10.1016/j.mimet.2014.01.017.

Forman, D., Newell, D.G., Fullerton, F., Yarnell, J.W., Stacey, A.R., Wald, N. and Sitas, F., 1991. Association between infection with Helicobacter pylori and risk of gastric cancer: evidence from a prospective investigation. BMJ, 302(6788), pp.1302-1305.

Foster, J. W., & Hall, H. K. (1992). Effect of Salmonella-Typhimurium Ferric Uptake Regulator (Fur) Mutations on Iron-Regulated and Ph-Regulated Protein-Synthesis. Journal of Bacteriology, 174(13), 4317–4323.

Fritsche, G., Nairz, M., Theurl, I., Mair, S., Bellmann-Weiler, R., Barton, H. C. & Weiss, G. 2007. Modulation of macrophage iron transport by Nramp1 (Slc11a1). Immunobiology, 212, 751-7.

Fuangthong, M., & Helmann, J. D. (2002). The OhrR repressor senses organic hydroperoxides by reversible formation of a cysteine-sulfenic acid derivative. Proceedings of the National Academy of Sciences of the United States of America, 99(10), 6690–6695. https://doi.org/10.1073/pnas.102483199.

Ganz, T., 2018. Iron and infection. International Journal of Hematology, 107(1), pp.7-15.

Garcia-Herrero, A., Peacock, R. S., Howard, S. P. & Vogel, H. J. 2007. The solution structure of the periplasmic domain of the TonB system ExbD protein reveals an unexpected structural homology with siderophore-binding proteins. Mol Microbiol, 66, 872-89.

Gasser, V., Baco, E., Cunrath, O., August, P. S., Perraud, Q., Zill, N., Schleberger, C., Schmidt, A., Paulen, A., Bumann, D., Mislin, G. L. & Schalk, I. J. 2016. Catechol siderophores repress the pyochelin pathway and activate the enterobactin pathway in Pseudomonas aeruginosa: an opportunity for siderophore-antibiotic conjugates development. Environ Microbiol, 18, 819-32.

Gaudu, P. and Weiss, B., 1996. SoxR, a [2Fe-2S] transcription factor, is active only in its oxidized form. Proceedings of the National Academy of Sciences, 93(19), pp.10094-10098.

Geertsma, E.R., Mahmood, N.N., Schuurman-Wolters, G.K. and Poolman, B., 2008. Membrane reconstitution of ABC transporters and assays of translocator function. Nature Protocols, 3(2), p.256.

Genco, C. A., & Dixon, D. W. (2001). Emerging strategies in microbial haem capture. Molecular Microbiology 39: 1-11.

Ghigo, J. M., Letoffe, S., & Wandersman, C. (1997). A new type of hemophore-dependent heme acquisition system of Serratia marcescens reconstituted in Escherichia coli. Journal of Bacteriology, 179(11), 3572-3579.

Giustarini, D., Rossi, R., Milzani, A. and Dalle-Donne, I., 2008. Nitrite and nitrate measurement by Griess reagent in human plasma: evaluation of interferences and standardization. Methods in Enzymology, 440, pp.361-380.

Goblirsch, B., Kurker, R. C., Streit, B. R., Wilmot, C. M. & Dubois, J. L. 2011. Chlorite dismutases, DyPs, and EfeB: 3 microbial heme enzyme families comprise the CDE structural superfamily. J Mol Biol, 408, 379-98.

Goetz, D. H., Holmes, M. A., Borregaard, N., Bluhm, M. E., Raymond, K. N., & Strong, R. K. (2002). The neutrophil lipocalin NGAL is a bacteriostatic agent that interferes with siderophore-mediated iron acquisition. Mol Cell, 10(5), 1033-1043.

Gonzalez-Flecha, B., & Demple, B. (1995). Metabolic sources of hydrogen peroxide in aerobically growing Escherichia coli. Journal of Biological Chemistry, 270(23), 13681–13687. https://doi.org/10.1074/jbc.270.23.13681.

Grabherr, R., Ernst, W., Oker-Blom, C. and Jones, I., 2001. Developments in the use of baculoviruses for the surface display of complex eukaryotic proteins. Trends in Biotechnology, 19(6), pp.231-236.

Gräslund, S., Sagemark, J., Berglund, H., Dahlgren, L.G., Flores, A., Hammarström, M., Johansson, I., Kotenyova, T., Nilsson, M., Nordlund, P. and Weigelt, J., 2008. The use of systematic N-and C-terminal deletions to promote production and structural studies of recombinant proteins. Protein Expression and Purification, 58(2), pp.210-221.

Grass, G., Franke, S., Taudte, N., Nies, D. H., Kucharski, L. M., Maguire, M. E., & Rensing, C. (2005). The metal permease ZupT from Escherichia coli is a transporter with a broad substrate spectrum. Journal of Bacteriology, 187(5), 1604–1611. https://doi.org/10.1128/JB.187.5.1604-1611.2005.

Grass, G., Grass, G., Franke, S., Franke, S., Taudte, N., Taudte, N., … Rensing, C. (2005). The Metal Permease ZupT from. Society, 187(5), 1604–1611. https://doi.org/10.1128/JB.187.5.1604.

Grass, G., Wong, M. D., Rosen, B. P., Ron, L., Rensing, C., & Smith, R. L. (2002). ZupT Is a Zn (II) Uptake System in Escherichia coli. Journal of Bacteriology, 184(3), 864–866. https://doi.org/10.1128/JB.184.3.864.

Grifantini, R., Frigimelica, E., Delany, I., Bartolini, E., Giovinazzi, S., Balloni, S., Agarwal, S., Galli, G., Genco, C. & Grandi, G. 2004. Characterization of a novel Neisseria meningitidis Fur and iron-regulated operon required for protection from oxidative stress: utility of DNA microarray in the assignment of the biological role of hypothetical genes. Mol Microbiol, 54, 962-79.

Grifantini, R., Sebastian, S., Frigimelica, E., Draghi, M., Bartolini, E., Muzzi, A., . . . Genco, C. A. (2003). Identification of iron-activated and -repressed Fur-dependent genes

by transcriptome analysis of Neisseria meningitidis group B. Proc Natl Acad Sci U S A, 100(16), 9542-9547. doi: 10.1073/pnas.1033001100.

Grifantini, R., Sebastian, S., Frigimelica, E., Draghi, M., Bartolini, E., Muzzi, A., Rappuoli, R., Grandi, G. & Genco, C. A. 2003. Identification of Iron-Activated And -Repressed Fur-Dependent Genes by Transcriptome Analysis Of Neisseria Meningitidis Group B. Proc Natl Acad Sci U S A, 100, 9542-7.

Griffith, K. L. & Wolf, R. E., JR. 2004. Genetic evidence for pre-recruitment as the mechanism of transcription activation by SoxS of Escherichia coli: the dominance of DNA binding mutations of SoxS. J Mol Biol, 344, 1-10.

Griffith, K.L., Shah, I.M. and E. Wolf Jr, R., 2004. Proteolytic degradation of Escherichia coli transcription activators SoxS and MarA as the mechanism for reversing the induction of the superoxide (SoxRS) and multiple antibiotic resistance (Mar) regulons. Molecular Microbiology, 51(6), pp.1801-1816.

Griffiths, W. J., Kelly, A. L., & Cox, T. M. (1999). Inherited disorders of iron storage and transport. Mol Med Today, 5(10), 431-438.

Grosse, C., Scherer, J., Koch, D., Otto, M., Taudte, N., & Grass, G. (2006). A new ferrous iron-uptake transporter, EfeU (YcdN), from Escherichia coli. Mol Microbiol, 62(1), 120-131. doi: 10.1111/j.1365-2958.2006.05326.

Große, C., Scherer, J., Koch, D., Otto, M., Taudte, N., & Grass, G. (2006). A new ferrous iron-uptake transporter, EfeU (YcdN), from Escherichia coli. Molecular Microbiology, 62(1), 120–131. https://doi.org/10.1111/j.1365-2958.2006.05326.x.

Guerinot, M. L. (1994). Microbial iron transport. Annual Review of Microbiology, 48, 743–772. https://doi.org/10.1146/annurev.micro.48.1.743.

Guilfoyle, A., Maher, M. J., Rapp, M., Clarke, R., Harrop, S. & Jormakka, M. 2009. Structural basis of GDP release and gating in G protein coupled Fe2+ transport. EMBO J, 28, 2677-85.

Guzman, L. M., Belin, D., Carson, M. J., & Beckwith, J. 1995. Tight regulation, modulation, and high-level expression by vectors containing the arabinose These include: Tight Regulation, Modulation, and High-Level Expression by Vectors Containing the Arabinose P BAD Promoter. Journal of Bacteriology, 177(14), 4121–4130. https://doi.org/0021-9193/95/$04.00+0.

Haemig, H.A., Moen, P.J. and Brooker, R.J., 2010. Evidence that highly conserved residues of transmembrane segment 6 of Escherichia coli MntH are important for transport activity. Biochemistry, 49(22), pp.4662-4671.

Hagelueken, G., Clarke, B.R., Huang, H., Tuukkanen, A., Danciu, I., Svergun, D.I., Hussain, R., Liu, H., Whitfield, C. and Naismith, J.H., 2015. A coiled-coil domain acts as a molecular ruler to regulate O-antigen chain length in lipopolysaccharide. Nature Structural & Molecular Biology, 22(1), p.50.

Hagelueken, G., Hoffmann, J., Schubert, E., Duthie, F. G., Florin, N., Konrad, L., Imhof, D., Behrmann, E., Morgner, N. & Schiemann, O. 2016. Studies on the X-Ray and Solution Structure of FeoB from Escherichia coli BL21. Biophys J, 110, 2642-2650.

Hahn, A., Parey, K., Bublitz, M., Mills, D.J., Zickermann, V., Vonck, J., Kühlbrandt, W. and Meier, T., 2016. Structure of a complete ATP synthase dimer reveals the molecular basis of inner mitochondrial membrane morphology. Molecular Cell, 63(3), pp.445-456.

Haikarainen, T., & Papageorgiou, A. C. 2010. Dps-like proteins: structural and functional insights into a versatile protein family. Cellular and Molecular Life Sciences: CMLS, 67(3), 341–51. https://doi.org/10.1007/s00018-009-0168-2.

Hanahan, D. (1983). Studies on transformation of Escherichia coli with plasmids. Journal of Molecular Biology, 166(4), 557–580. https://doi.org/10.1016/S0022-2836(83)80284-8.

Hantke K., Nicholson G., Rabsch W., and Winkelmann G., 2003 Salmochelins, siderophores of Salmonella enterica and uropathogenic Escherichia coli strains, are

recognized by the outer membrane receptor IroN. Proceedings of the National Academy of Science of the USA, 100: 3677–3682.

Hantke, K. 1987. Ferrous iron transport mutants in Escherichia coli K12. FEMS Microbiology Letters, 44(1), 53–57. https://doi.org/10.1111/j.1574-6968.1987.tb02241.x.

Hantke, K. 1997. Ferrous iron uptake by a magnesium transport system is toxic for Escherichia coli and Salmonella typhimurium. J Bacteriol, 179(19), 6201-6204.

Hantke, K. 2001. Iron and metal regulation in bacteria. Current Opinion in Microbiology, 4(2), 172–177. https://doi.org/10.1016/S1369-5274(00)00184-3.

Harrison, P. M., & Arosio, P. 1996. The ferritins: molecular properties, iron storage function and cellular regulation. Biochimica et Biophysica Acta (BBA)-Bioenergetics, 1275(3), 161-203.

Hashimoto, K., Nishi, H., Bryant, S. and Panchenko, A.R., 2011. Caught in self-interaction: evolutionary and functional mechanisms of protein homooligomerization. Physical Biology, 8(3), p.035007.

Hassett, D. J., Sokol, P. A., Howell, M. L., Ma, J. F., Schweizer, H. T., Ochsner, U., & Vasil, M. L. 1996. Ferric uptake regulator (Fur) mutants of Pseudomonas aeruginosa demonstrate defective siderophore-mediated iron uptake, altered aerobic growth, and decreased superoxide dismutase and catalase activities. Journal of Bacteriology, 178(14), 3996-4003.

Hattori, M., Jin, Y., Nishimasu, H., Tanaka, Y., Mochizuki, M., Uchiumi, T., Ishitani, R., Ito, K. & Nureki, O. 2009. Structural basis of novel interactions between the small-GTPase and GDI-like domains in prokaryotic FeoB iron transporter. Structure, 17, 1345-55.

Helenius, A. and Simons, K.A.I., 1975. Solubilization of membranes by detergents. Biochimica et Biophysica Acta (BBA)-Reviews on Biomembranes, 415(1), pp.29-79.

Helenius, A., McCaslin, D.R., Fries, E. and Tanford, C., 1979. [63] Properties of detergents. In Methods in Enzymology (Vol. 56, pp. 734-749). Academic Press.

Henle, E.S., Luo, Y. and Linn, S. 1996. Fe2+, Fe3+ and oxygen react with DNA derived radicals formed during iron mediated Fenton reactions. Biochemistry 35:12212-9.

Hentze, M. W., Muckenthaler, M. U., & Andrews, N. C. 2004. Balancing acts: molecular control of mammalian iron metabolism. Cell, 117(3), 285-297.

Herman, J.G., Merlo, A., Mao, L.I., Lapidus, R.G., Issa, J.P.J., Davidson, N.E., Sidransky, D. and Baylin, S.B., 1995. Inactivation of the CDKN2/p16/MTS1 gene is frequently associated with aberrant DNA methylation in all common human cancers. Cancer research, 55(20), pp.4525-4530.

Hidese, R., Mihara, H., Kurihara, T. & Esaki, N. 2014. Global Identification of Genes Affecting Iron-Sulfur Cluster Biogenesis and Iron Homeostasis. Journal of Bacteriology, 196, 1238-1249.

Higgs, P. I., Myers, P. S. & Postle, K. 1998. Interactions in the TonB-dependent energy transduction complex: ExbB and ExbD form homomultimers. J Bacteriol, 180, 6031-8.

Hilgenfeld, R. 1995. How do the GTPases really work? Nat Struct Biol, 2, 3-6.

Hornung, J.M., Jones, H.A. and Perry, R.D., 1996. The hmu locus of Yersinia pestis is essential for utilization of free haemin and haem-protein complexes as iron sources. Molecular Microbiology, 20(4), pp.725-739.

Hsueh, K. L., Yu, L. K., Chen, Y. H., Cheng, Y. H., Hsieh, Y. C., Ke, S. chu, … Huang, T. H. (2013). FeoC from Klebsiella pneumoniae contains a [4Fe-4S] cluster. Journal of Bacteriology, 195(20), 4726–4734. https://doi.org/10.1128/JB.00687-13.

Hückelhoven, R., 2004. BAX Inhibitor-1, an ancient cell death suppressor in animals and plants with prokaryotic relatives. Apoptosis, 9(3), pp.299-307.

Hung, K. W., Chang, Y. W., Eng, E. T., Chen, J. H., Chen, Y. C., Sun, Y. J., … Huang, T. huang. 2010. Structural fold, conservation and Fe(II) binding of the intracellular domain of prokaryote FeoB. Journal of Structural Biology, 170(3), 501–512. https://doi.org/10.1016/j.jsb.2010.01.017.

Hung, K.-W., Tsai, J.-Y., Juan, T.-H., Hsu, Y.-L., Hsiao, C.-D., & Huang, T.-H. (2012). Crystal structure of KpNFeoB/KpFeoC complex and the roles of FeoC in the regulation of Fe2+ transport by the bacterial Feo system. Journal of Bacteriology, (September). https://doi.org/10.1128/JB.01228-12.

Hwang, I., Chen, H.C. and Sheen, J., 2002. Two-component signal transduction pathways in Arabidopsis. Plant physiology, 129(2), pp.500-515.

Idris, M.I.A., 2014. A Comparison of Titrimetric and Instrumental Methods in Determination of Iron in Ferrous Sulphate Capsules (Doctoral dissertation, University of Gezira).

Imlay, J. A. & Fridovich, I. 1991. Assay of metabolic superoxide production in Escherichia coli. J Biol Chem, 266, 6957-65.

Imlay, J. A. & Linn, S. 1988. DNA damage and oxygen radical toxicity. Science, 240, 1302-9.

Imlay, J. A. 2013. The molecular mechanisms and physiological consequences of oxidative stress: lessons from a model bacterium. Nat Rev Microbiol, 11, 443-54.

Giustarini D1, Dalle-Donne I, Colombo R, Milzani A, Rossi R. 2008 Is ascorbate able to reduce disulfide bridges? A cautionary note. Biotechnology 10(5): 411-421.

Ito, K. and Akiyama, Y., 2005. Cellular functions, mechanism of action, and regulation of FtsH protease. Annu. Rev. Microbiol., 59, pp.211-231.

Guzman LM1, Belin D, Carson MJ, Beckwith J. 1995. Tight regulation, modulation, and high-level expression by vectors containing the arabinose PBAD promoter. J Bacteriol.177(14):4121-30

Jabado, N., Jankowski, a, Dougaparsad, S., Picard, V., Grinstein, S., & Gros, P. (2000). Natural resistance to intracellular infections: natural resistance-associated macrophage protein 1 (Nramp1) functions as a pH-dependent manganese transporter at the phagosomal membrane. The Journal of Experimental Medicine, 192(9), 1237–1248. https://doi.org/10.1084/jem.192.9.1237.

Jang, S. and Imlay, J.A., 2010. Hydrogen peroxide inactivates the Escherichia coli Isc iron-sulphur assembly system, and OxyR induces the Suf system to compensate. Molecular Microbiology, 78(6), pp.1448-1467.

Jaskula, J. C., Letain, T. E., Roof, S. K., Skare, J. T., & Postle, K. (1994). Role of the TonB amino terminus in energy transduction between membranes. Journal of Bacteriology, 176(8), 2326–2338.

Jeon, J., Kim, H., Yun, J., Ryu, S., Groisman, E. A., & Shin, D. (2008). RstA-promoted expression of the ferrous iron transporter FeoB under iron-replete conditions enhances Fur activity in Salmonella enterica. Journal of Bacteriology, 190(22), 7326–7334. https://doi.org/10.1128/JB.00903-08.

Johnson, Z.L., Cheong, C.G. and Lee, S.Y., 2012. Crystal structure of a concentrative nucleoside transporter from Vibrio cholerae at 2.4 Å. Nature, 483(7390), p.489.

Kammler, M., Schön, C., Hantke, K., Schon, C., & Hantke, K. (1993). Characterization of the ferrous iron uptake system of Escherichia coli. J. Bacteriol., 175(19), 6212–6219. Retrieved from http://jb.asm.org/content/175/19/6212.

Kashmir, Z. N. & Mankr, S. A. 2014. Free radicals and oxidative stress in bacteria.

Kawate, T. and Gouaux, E., 2006. Fluorescence-detection size-exclusion chromatography for precrystallization screening of integral membrane proteins. Structure, 14(4), pp.673-681.

Kehres, D. G., & Maguire, M. E. (2003). Emerging themes in manganese transport, biochemistry and pathogenesis in bacteria. FEMS Microbiology Reviews, 27(2–3), 263–290. https://doi.org/10.1016/S0168-6445(03)00052-4.

Kehres, D. G., Zaharik, M. L., Finlay, B. B. & Maguire, M. E. 2000. The Nramp proteins of Salmonella typhimurium and Escherichia coli are selective manganese transporters involved in the response to reactive oxygen. Mol Microbiol, 36, 1085-100.

Kelly, D.J., Quinn, P.C., Slater, A.M., Lee, K., Ge, L. and Pascalis, O., 2007. The other-race effect develops during infancy: Evidence of perceptual narrowing. Psychological Science, 18(12), pp.1084-1089.

Khan, A. G., Shouldice, S. R., Kirby, S. D., Yu, R. H., Tari, L. W. & Schryvers, A. B. 2007. High-affinity binding by the periplasmic iron-binding protein from Haemophilus influenzae is required for acquiring iron from transferrin. Biochem J, 404, 217-25.

Kihara, A., Akiyama, Y. and Ito, K., 1999. Dislocation of membrane proteins in FtsH-mediated proteolysis. The EMBO Journal, 18(11), pp.2970-2981.

Kim, H., Lee, H., & Shin, D. (2012). The FeoA protein is necessary for the FeoB transporter to import ferrous iron. Biochemical and Biophysical Research Communications, 423(4), 733–738. https://doi.org/10.1016/j.bbrc.2012.06.027

Kim, H., Lee, H., & Shin, D. (2013). The FeoC protein leads to high cellular levels of the Fe(II) transporter FeoB by preventing FtSH protease regulation of FeoB in Salmonella enterica. Journal of Bacteriology, 195(15), 3364–3370. https://doi.org/10.1128/JB.00343-13.

Kim, H., Lee, H., & Shin, D. (2015). Lon-mediated proteolysis of the FeoC protein prevents salmonella enterica from accumulating the Fe (II) transporter FeoB under high-oxygen conditions. Journal of Bacteriology, 197(1), 92–98. https://doi.org/10.1128/JB.01826-14.

Kingsley, R. A., Reissbrodt, R., Rabsch, W., Ketley, J. M., Tsolis, R. M., Everest, P., . . . Williams, P. H. (1999). Ferrioxamine-mediated Iron (III) utilization by Salmonella enterica. Appl Environ Microbiol, 65(4), 1610-1618.

Kingsley, R., Rabsch, W., Roberts, M., Reissbrodt, R., & Williams, P. H. (1996). TonB-dependent iron supply in Salmonella by alpha-ketoacids and alpha-hydroxyacids. FEMS Microbiol Lett, 140(1), 65-70.

Kohgo, Y., Ikuta, K., Ohtake, T., Torimoto, Y., & Kato, J. (2008). Body iron metabolism and pathophysiology of iron overload. Int J Hematol, 88(1), 7-15. doi: 10.1007/s12185-008-0120-5.

Kohlstaedt, M., Von Der Hocht, I., Hilbers, F., Thielmann, Y. and Michel, H., 2015. Development of a Thermofluor assay for stability determination of membrane proteins using the Na+/H+ antiporter NhaA and cytochrome c oxidase. Acta Crystallographica Section D: Biological Crystallography, 71(5), pp.1112-1122.

Komenda, J., Barker, M., Kuviková, S., de Vries, R., Mullineaux, C.W., Tichý, M. and Nixon, P.J., 2006. The FtsH protease slr0228 is important for quality control of photosystem II in the thylakoid membrane of Synechocystis sp. PCC 6803. Journal of Biological Chemistry, 281(2), pp.1145-1151.

Kosman, D.J., 2003. Molecular mechanisms of iron uptake in fungi. Molecular microbiology, 47(5), pp.1185-1197.

Koster, W. 2001. ABC transporter-mediated uptake of iron, siderophores, heme and vitamin B12. Res Microbiol, 152, 291-301.

Kotschwar, M., Harfst, E., Ohanjan, T. & Schumann, W. 2004. Construction and analyses of mutant ftsH alleles of Bacillus subtilis involving the ATPase- and Zn-binding domains. Curr Microbiol, 49, 180-5.

Kramarenko, G. G., Hummel, S. G., Martin, S. M. & Buettner, G. R. 2006. Ascorbate reacts with singlet oxygen to produce hydrogen peroxide. Photochem Photobiol, 82, 1634-7.

Krewulak, K. D., & Vogel, H. J. (2008). Structural biology of bacterial iron uptake. Biochim Biophys Acta, 1778(9), 1781-1804. doi: 10.1016/j.bbamem.2007.07.026.

Krieg, S., Huché, F., Diederichs, K., Izadi-Pruneyre, N., Lecroisey, A., Wandersman, C., Delepelaire, P. and Welte, W. (2009) Heme uptake across the outer membrane as revealed by crystal structures of the receptor–hemophore complex. Proc Natl Acad Sci USA. 106:1045-50.

Krogh, A., Larsson, B., Von Heijne, G. & Sonnhammer, E. L. 2001. Predicting transmembrane protein topology with a hidden Markov model: application to complete genomes. J Mol Biol, 305, 567-80.

Krzywda, S., Brzozowski, A.M., Verma, C., Karata, K., Ogura, T. and Wilkinson, A.J., 2002. The crystal structure of the AAA domain of the ATP-dependent protease FtsH of Escherichia coli at 1.5 Å resolution. Structure, 10(8), pp.1073-1083.

Kuby, J., 1997. Overview of the immune system. Immunology, 3, pp.3-24.

Kuhn, D.E., Baker, B.D., Lafuse, W.P. and Zwilling, B.S., 1999. Differential iron transport into phagosomes isolated from the RAW264. 7 macrophage cell lines transfected with Nramp1Gly169 or Nramp1Asp169. Journal of Leukocyte Biology, 66(1), pp.113-119.

Kunau, W.H., Beyer, A., Franken, T., Götte, K., Marzioch, M., Saidowsky, J., Skaletz-Rorowski, A. and Wiebel, F.F., 1993. Two complementary approaches to study peroxisome biogenesis in Saccharomyces cerevisiae: forward and reversed genetics. Biochimie, 75(3-4), pp.209-224.

Kunkel, T.A., 1985. Rapid and efficient site-specific mutagenesis without phenotypic selection. Proceedings of the National Academy of Sciences, 82(2), pp.488-492.

Kwok, E. Y., Severance, S. & Kosman, D. J. 2006. Evidence for iron channeling in the Fet3p-Ftr1p high-affinity iron uptake complex in the yeast plasma membrane. Biochemistry, 45, 6317-27.

Langer, T., 2000. AAA proteases: cellular machines for degrading membrane proteins. Trends in Biochemical Sciences, 25(5), pp.247-251.

Langklotz, S., Baumann, U. and Narberhaus, F., 2012. Structure and function of the bacterial AAA protease FtsH. Biochimica et Biophysica Acta (BBA)-Molecular Cell Research, 1823(1), pp.40-48.

Lansky, I.B., Lukat-Rodgers, G.S., Block, D., Rodgers, K.R., Ratliff, M. and Wilks, A., 2006. The cytoplasmic heme-binding protein (PhuS) from the heme uptake system of Pseudomonas aeruginosa is an intracellular heme-trafficking protein to the δ-regioselective heme oxygenase. Journal of Biological Chemistry, 281(19), pp.13652-13662.

Larsen, R. A., Letain, T. E., & Postle, K. (2003). In vivo evidence of TonB shuttling between the cytoplasmic and outer membrane in Escherichia coli. Mol Microbiol, 49(1), 211-218.

Larsen, R. A., Thomas, M. G., & Postle, K. (1999). Protonmotive force, ExbB and ligand-bound FepA drive conformational changes in TonB. Mol Microbiol, 31(6), 1809-1824.

Larson, J. A., Howie, H. L., & So, M. (2004). Neisseria meningitidis accelerates ferritin degradation in host epithelial cells to yield an essential iron source. Mol Microbiol, 53(3), 807-820. doi: 10.1111/j.1365-2958.2004.04169.

Latunde-Dada, G. O., Simpson, R. J., & McKie, A. T. (2006). Recent advances in mammalian haem transport. Trends in Biochemical Sciences, 31(3), 182-188.

Lau, C. K. Y., Ishida, H., Liu, Z., & Vogel, H. J. (2013). Solution structure of Escherichia coli feoA and its potential role in bacterial ferrous iron transport. Journal of Bacteriology, 195(1), 46–55. https://doi.org/10.1128/JB.01121-12.

Lau, C. K., Krewulak, K. D. & Vogel, H. J. 2016. Bacterial ferrous iron transport: the Feo system. FEMS Microbiol Rev, 40, 273-98.

Lau, C.K., Krewulak, K.D. and Vogel, H.J., 2015. Bacterial ferrous iron transport: the Feo system. FEMS Microbiology Reviews, 40(2), pp.273-298.

Le Brun, N. E., Crow, A., Murphy, M. E. P., Mauk, A. G., & Moore, G. R. (2010). Iron core mineralisation in prokaryotic ferritins. Biochimica et Biophysica Acta - General Subjects, 1800(8), 732–744. https://doi.org/10.1016/j.bbagen.2010.04.002.

Lee, J. W., & Helmann, J. D. (2007). Functional specialization within the fur family of metalloregulators. BioMetals, 20(3–4), 485–499. https://doi.org/10.1007/s10534-006-9070-7.

Lee, N. L., Gielow, W. O., & Wallace, R. G. (1981). Mechanism of araC autoregulation and the domains of two overlapping promoters, Pc and PBAD, in the L-arabinose regulatory region of Escherichia coli. Proceedings of the National Academy of Sciences of the United States of America, 78(2), 752–6. https://doi.org/10.1073/pnas.78.2.752.

Lee, N., Francklyn, C., & Hamilton, E. P. (1987). Arabinose-induced binding of AraC protein to araI2 activates the araBAD operon promoter. Proceedings of the National Academy of Sciences of the United States of America, 84(24), 8814–8. https://doi.org/10.1073/pnas.84.24.8814.

Leonhard, K., Herrmann, J.M., Stuart, R.A., Mannhaupt, G., Neupert, W. and Langer, T., 1996. AAA proteases with catalytic sites on opposite membrane surfaces comprise a proteolytic system for the ATP-dependent degradation of inner membrane proteins in mitochondria. The EMBO Journal, 15(16), pp.4218-4229.

Letain, T. E., & Postle, K. (1997). TonB protein appears to transduce energy by shuttling between the cytoplasmic membrane and the outer membrane in Escherichia coli. Mol Microbiol, 24(2), 271-283.

Letoffe, S., Heuck, G., Delepelaire, P., Lange, N., & Wandersman, C. (2009). Bacteria capture iron from heme by keeping tetrapyrrol skeleton intact. Proceedings of the National Academy of Sciences of the United States of America, 106(28), 11719–11724. https://doi.org/10.1073/pnas.0903842106.

Li, S.S.C., 2005. Specificity and versatility of SH3 and other proline-recognition domains: structural basis and implications for cellular signal transduction. Biochemical Journal, 390(3), pp.641-653.

Li, W., Joshi, S. R., Hou, G., Burdige, D. J., Sparks, D. L. & Jaisi, D. P. 2015. Characterizing phosphorus speciation of Chesapeake Bay sediments using chemical extraction, 31P NMR, and X-ray absorption fine structure spectroscopy. Environ Sci Technol, 49, 203-11.

Li, Z. and Demple, B., 1994. SoxS, an activator of superoxide stress genes in Escherichia coli. Purification and interaction with DNA. Journal of Biological Chemistry, 269(28), pp.18371-18377.

Li, Z. and Demple, B., 1996. Sequence specificity for DNA binding by Escherichia coli SoxS and Rob proteins. Molecular Microbiology, 20(5), pp.937-945.

Lippard S., and Berg M., (1994): Principles of Bioinorganic Chemistry. University Science Books: Mill Valley, CA, USA.

Litwin, C. M., & Calderwood, S. B. (1993). Role of iron in regulation of virulence genes. Clinical Microbiology Reviews, 6(2), 137-149.

Liu, D., Vleugel, M., Backer, C.B., Hori, T., Fukagawa, T., Cheeseman, I.M. and Lampson, M.A., 2010. Regulated targeting of protein phosphatase 1 to the outer kinetochore by KNL1 opposes Aurora B kinase. The Journal of Cell Biology, 188(6), pp.809-820.

Liu, H. and Naismith, J.H., 2008. An efficient one-step site-directed deletion, insertion, single and multiple-site plasmid mutagenesis protocol. BMC Biotechnology, 8(1), p.91.

Liu, X., Du, Q., Wang, Z., Zhu, D., Huang, Y., Li, N., Gu, L. (2011). Crystal structure and Biochemical features of EfeB/YcdB from Escherichia coli O157: ASP235 plays divergent roles in different enzyme-catalyzed processes. Journal of Biological Chemistry, 286(17), 14922–14931. https://doi.org/10.1074/jbc.M110.197780.

Liu, Y., & Imlay, J. a. (2013). Cell death from antibiotics without the involvement of reactive oxygen species. Science (New York, N.Y.), 339(6124), 1210–3. https://doi.org/10.1126/science.1232751.

Loewen, P. C., Switala, J. & Triggs-Raine, B. L. 1985. Catalases HPI and HPII in Escherichia coli are induced independently. Arch Biochem Biophys, 243, 144-9.

Loll, P.J., 2014. Membrane proteins, detergents and crystals: what is the state of the art?. Acta Crystallographica Section F: Structural Biology Communications, 70(12), pp.1576-1583.

Lorenzo, H.K., Susin, S.A., Penninger, J. and Kroemer, G., 1999. Apoptosis inducing factor (AIF): a phylogenetically old, caspase-independent effector of cell death. Cell death and Differentiation, 6(6), p.516.

Louvel, H., Saint Girons, I., & Picardeau, M. (2005). Isolation and characterization of FecA- and FeoB-mediated iron acquisition systems of the spirochete Leptospira biflexa by random insertional mutagenesis. Journal of Bacteriology, 187(9), 3249–3254. https://doi.org/10.1128/JB.187.9.3249-3254.2005.

Lua, R.C., Wilson, S.J., Konecki, D.M., Wilkins, A.D., Venner, E., Morgan, D.H. and Lichtarge, O., 2015. UET: a database of evolutionarily-predicted functional determinants of protein sequences that cluster as functional sites in protein structures. Nucleic Acids Research, 44(D1), pp.D308-D312.

Mak, A. F., Lai, W. M. & Mow, V. C. 1987. Biphasic indentation of articular cartilage-I. Theoretical analysis. J Biomech, 20, 703-14.

Makui, H., Roig, E., Cole, S. T., Helmann, J. D., Gros, P., & Cellier, M. F. M. (2000). Identification of the Escherichia coli K-12 Nramp orthologue (MntH) as a selective divalent metal ion transporter. Molecular Microbiology, 35(5), 1065–1078. https://doi.org/10.1046/j.1365-2958.2000.01774.x.

Manahan, S. (2000). Environmental chemistry. Environmental Chemistry, 8th ed, 743. Retrieved from http://www.chemistry.uoc.gr/courses/xhm405/01 Environmental Chemistry Manahan.

Marcoleta, A. E., Gutiérrez-Cortez, S., Hurtado, F., Argandoña, Y., Corsini, G., Monasterio, O., & Lagos, R. (2018). The Ferric uptake regulator (Fur) and iron availability control the production and maturation of the antibacterial peptide microcin E492. PloS One, 13(8), e0200835.

Marlovits, T. C., Haase, W., Herrmann, C., Aller, S. G., & Unger, V. M. (2002). The membrane protein FeoB contains an intramolecular G protein essential for Fe(II) uptake in bacteria. Proceedings of the National Academy of Sciences of the United States of America, 99(25), 16243–8. https://doi.org/10.1073/pnas.242338299.

Maruyama, Y., Ochiai, A., Mikami, B., Hashimoto, W., & Murata, K. (2011). Crystal structure of bacterial cell-surface alginate-binding protein with an M75 peptidase motif. Biochemical and Biophysical Research Communications, 405(3), 411–416. https://doi.org/10.1016/j.bbrc.2011.01.043.

Massé, E., & Gottesman, S. (2002). A small RNA regulates the expression of genes involved in iron metabolism in Escherichia coli. Proceedings of the National Academy of Sciences 99: 4620-4625.

Mattle, D., Zeltina, A., Woo, J.S., Goetz, B.A. and Locher. (2010) Two stacked heme molecules in the binding pocket of the periplasmicheme-binding protein HmuT from Yersinia pestis. J Mol Biol. 404:220-231.

Matzanke, B. F., Böhnke, R., Möllmann, U., Reissbrodt, R., Schünemann, V., & Trautwein, A. X. (1997). Iron uptake and intracellular metal transfer in mycobacteria

mediated by xenosiderophores. BioMetals, 10(3), 193–203. https://doi.org/10.1023/A:1018351728081

Maukonen, J. & Saarela, M. 2015. Human gut microbiota: does diet matter? Proc Nutr Soc, 74, 23-36.

Maurer, L. M., Yohannes, E., Bondurant, S. S., Radmacher, M. & Slonczewski, J. L. 2005. pH regulates genes for flagellar motility, catabolism, and oxidative stress in Escherichia coli K-12. J Bacteriol, 187, 304-19.

McCord, J.M., Keele, B.B. and Fridovich, I., 1971. An enzyme-based theory of obligate anaerobiosis: the physiological function of superoxide dismutase. Proceedings of the National Academy of Sciences, 68(5), pp.1024-1027.

McDonald, I., Sloan, G. C., Zijlstra, A. A., Matsunaga, N., Matsuura, M., Kraemer, K. E., Markwick, A. J. (2010). Rusty Old Stars: a Source of the Missing Interstellar Iron? The Astrophysical Journal, 717(2), L92–L97. https://doi.org/10.1088/2041-8205/717/2/L92.

Mchugh, J. P., Rodriguez-Quinones, F., Abdul-Tehrani, H., Svistunenko, D. A., Poole, R. K., Cooper, C. E. & Andrews, S. C. 2003. Global iron-dependent gene regulation in Escherichia coli. A new mechanism for iron homeostasis. J Biol Chem, 278, 29478-86.

McLuskey, K., Roszak, A., Zhu, Y., and Isaacs, N. 2009. Crystal structures of all-alpha type membrane proteins. European Biophysics Journal, http://www.springerlink.com/content/c785214508570616

Merrell, D. S., Butler, S. M., Qadri, F., Dolganov, N. A., Alam, A., Cohen, M. B., Calderwood, S. B., Schoolnik, G. K. & Camilli, A. 2002. Host-induced epidemic spread of the cholera bacterium. Nature, 417, 642-5.

Merrell, D.S. and Camilli, A., 2002. Acid tolerance of gastrointestinal pathogens. Current Opinion in Microbiology, 5(1), pp.51-55.

Mey, A. R., Wyckoff, E. E., Hoover, L. A., Fisher, C. R., & Payne, S. M. (2008). Vibrio cholerae VciB promotes iron uptake via ferrous iron transporters. Journal of Bacteriology, 190(17), 5953–5962. https://doi.org/10.1128/JB.00569-08.

Miethke, M., & Marahiel, M. A. (2007). Siderophore-Based Iron Acquisition and Pathogen Control. Microbiology and Molecular Biology Reviews, 71(3), 413–451. https://doi.org/10.1128/MMBR.00012-07.

Miethke, M., Monteferrante, C. G., Marahiel, M. A., & van Dijl, J. M. (2013). The Bacillus subtilis EfeUOB transporter is essential for high-affinity acquisition of ferrous and ferric iron. Biochimica et Biophysica Acta - Molecular Cell Research, 1833(10), 2267–2278. https://doi.org/10.1016/j.bbamcr.2013.05.027.

Miller, J.H., 1992. A short course in molecular genetics. Cold Spring Harbor Laboratory Press.

Mittal, P.K., 1972. Morphological and cytochemical studies in the vitellogenesis of crustaceans.

Moraes, I., Evans, G., Sanchez-Weatherby, J., Newstead, S. and Stewart, P.D.S., 2014. Membrane protein structure determination—the next generation. Biochimica et Biophysica Acta (BBA)-Biomembranes, 1838(1), pp.78-87.

Moraes, T. F., Yu, R. H., Strynadka, N. C. & Schryvers, A. B. 2009. Insights into the bacterial transferrin receptor: the structure of transferrin-binding protein B from Actinobacillus pleuropneumoniae. Mol Cell, 35, 523-33.

Morgan, J.K., Ortiz, J.A. and Riordan, J.T., 2014. The role for TolA in enterohemorrhagic Escherichia coli pathogenesis and virulence gene transcription. Microbial Pathogenesis, 77, pp.42-52.

Morgan, R.W., Christman, M.F., Jacobson, F.S., Storz, G. and Ames, B.N., 1986. Hydrogen peroxide-inducible proteins in Salmonella typhimurium overlap with heat shock and other stress proteins. Proceedings of the National Academy of Sciences, 83(21), pp.8059-8063.

Muller, R. 2016. Governance and Governmentality for Projects: Enablers, Practices, and Consequences, Taylor & Francis.

Müller, S. I., Valdebenito, M., & Hantke, K. (2009). Salmochelin, the long-overlooked catecholate siderophore of Salmonella. Biometals, 22(4), 691-695.

Murphy, E. R. & Payne, S. M. 2007. RyhB, an iron-responsive small RNA molecule, regulates Shigella dysenteriae virulence. Infect Immun, 75, 3470-7.

Nadadur, S. S., Srirama, K., & Mudipalli, A. (2008). Iron transport & homeostasis mechanisms: their role in health & disease. Indian Journal of Medical Research, 128(4), 533.

Naikare, H., Palyada, K., Panciera, R., Marlow, D., & Stintzi, A. (2006). Major role for FeoB in Campylobacter jejuni ferrous iron acquisition, gut colonization, and intracellular survival. Infection and Immunity, 74(10), 5433–5444. https://doi.org/10.1128/IAI.00052-06.

Nakajima, H., Takatani, N., Yoshimitsu, K., Itoh, M., Aono, S., Takahashi, Y. and Watanabe, Y., 2010. The role of the Fe-S cluster in the sensory domain of nitrogenase transcriptional activator VnfA from Azotobacter vinelandii. The FEBS Journal, 277(3), pp.817-832.

Nakayama, K.O.J.I., 1992. Nucleotide sequence of Streptococcus mutans superoxide dismutase gene and isolation of insertion mutants. Journal of Bacteriology, 174(15), pp.4928-4934.

Nam, W. (2007). High-valent iron(IV)-oxo complexes of heme and non-heme ligands in oxygenation reactions. Accounts of Chemical Research, 40, pp. 522–531. https://doi.org/10.1021/ar700027f.

Narberhaus, F., Obrist, M., Führer, F. and Langklotz, S., 2009. Degradation of cytoplasmic substrates by FtsH, a membrane-anchored protease with many talents. Research in Microbiology, 160(9), pp.652-659.

Neilands, J. B. (1982). Microbial envelope proteins related to iron. Annual Review of Microbiology, 36, 285–309. https://doi.org/10.1146/annurev.mi.36.100182.001441.

Neto, J. F. D., Braz, V. S., Italiani, V. C. S., & Marques, M. V. (2009). Fur controls iron homeostasis and oxidative stress defense in the oligotrophic alpha-proteobacterium Caulobacter crescentus. Nucleic Acids Res, 37(14), 4812-4825. doi: 10.1093/nar/gkp509.

Neugebauer, J.M., 1990. [18] Detergents: An overview. In Methods in enzymology (Vol. 182, pp. 239-253). Academic Press. Nitric Oxide. 2008 Nov;19(3):252-8. doi: 10.1016/j.niox.2008.07.003. Epub 2008 Jul 17.

Niwa, K., Kazama, K., Younkin, S.G., Carlson, G.A. and Iadecola, C., 2002. Alterations in cerebral blood flow and glucose utilization in mice overexpressing the amyloid precursor protein. Neurobiology of Disease, 9(1), pp.61-68.

Noinaj, N., Guillier, M., Barnard, T. J., & Buchanan, S. K. (2010). TonB-dependent transporters: regulation, structure, and function. Annu Rev Microbiol, 64, 43-60. doi: 10.1146/annurev.micro.112408.134247.

Nomura, A., Stemmermann, G. N., Chyou, P. H., Perez-Perez, G. I., & Blaser, M. J. (1994). Helicobacter pylori infection and the risk for duodenal and gastric ulceration. Annals of Internal Medicine, 120(12), 977–81. Retrieved from http://www.ncbi.nlm.nih.gov/pubmed/7741826.

Nonaka, G., Blankschien, M., Herman, C., Gross, C. A. & Rhodius, V. A. 2006. Regulon and promoter analysis of the E. coli heat-shock factor, sigma32, reveals a multifaceted cellular response to heat stress. Genes Dev, 20, 1776-89.

Nonaka, I., Von Krogh, G. and Voelpel, S., 2006. Organizational knowledge creation theory: Evolutionary paths and future advances. Organization Studies, 27(8), pp.1179-1208.

Nunoshiba, T., Hidalgo, E., Amabile Cuevas, C. F. & Demple, B. 1992. Two-stage control of an oxidative stress regulon: the Escherichia coli SoxR protein triggers redox-inducible expression of the soxS regulatory gene. J Bacteriol, 174, 6054-60.

Nystrom-Lahti, M., Wu, Y., Moisio, A. L., Hofstra, R. M., Osinga, J., Mecklin, J. P., … Peltomaki, P. (1996). DNA mismatch repair gene mutations in 55 kindreds with verified or putative hereditary non-polyposis colorectal cancer. Human Molecular Genetics, 5(6), 763–769. Retrieved from http://www.ncbi.nlm.nih.gov/htbin-post/Entrez/query?db=m&form=6&dopt=r&uid=8776590.

Ochsner, U. A., & Vasil, M. L. (1996). Gene repression by the ferric uptake regulator in Pseudomonas aeruginosa: cycle selection of iron-regulated genes. Proceedings of the National Academy of Sciences, 93(9), 4409-4414.

Okuno, M., Hamaguchi, H.O. and Hayashi, S., 2006. Magnetic manipulation of materials in a magnetic ionic liquid. Applied Physics Letters, 89(13), p.132506.

Okuno, T., Yamanaka, K. & Ogura, T. 2006. Flavodoxin, a new fluorescent substrate for monitoring proteolytic activity of FtsH lacking a robust unfolding activity. J Struct Biol, 156, 115-9.

Ollinger, J., Song, K. B., Antelmann, H., Hecker, M., & Helmann, J. D. (2006). Role of the Fur regulon in iron transport in Bacillus subtilis. Journal of Bacteriology, 188(10), 3664–3673. https://doi.org/10.1128/JB.188.10.3664-3673.2006.

Ortiz De Orue Lucana, D., Wedderhoff, I. & Groves, M. R. 2012. ROS-Mediated Signalling in Bacteria: Zinc-Containing Cys-X-X-Cys Redox Centres and Iron-Based Oxidative Stress. J Signal Transduct, 2012, 605905.

Ovchinnikov, A., Saparov, B., Xia, S.Q. and Bobev, S., 2017. The ternary alkaline-earth metal manganese bismuthides Sr2MnBi2 and Ba2Mn1–x Bi2 (x≈ 0.15). Inorganic Chemistry, 56(20), pp.12369-12378.

Ovchinnikov, S., Park, H., Varghese, N., Huang, P. S., Pavlopoulos, G. A., Kim, D. E., Kamisetty, H., Kyrpides, N. C. & Baker, D. 2017. Protein structure determination using metagenome sequence data. Science, 355, 294-298.

Oxenoid, K. and Chou, J.J., 2005. The structure of phospholamban pentamer reveals a channel-like architecture in membranes. Proceedings of the National Academy of Sciences, 102(31), pp.10870-10875.

Pace, C.N., Vajdos, F., Fee, L., Grimsley, G., and Gray, T. 1995. How to measure and predict the molar absorption coefficient of a protein. Protein Sci 4(11): 2411-2423.

Pandey, A. & Sonti, R. V. 2010. Role of the FeoB protein and siderophore in promoting virulence of Xanthomonas oryzae pv. oryzae on rice. J Bacteriol, 192, 3187-203.

Pankowski, A. & Mcminn, A. 2009. Development of immunoassays for the iron-regulated proteins ferredoxin and flavodoxin in polar microalgae (1). J Phycol, 45, 771-83.

Papp-Wallace, K. M., & Maguire, M. E. (2006). Manganese transport and the role of manganese in virulence. Annual Review of Microbiology, 60, 187–209. https://doi.org/10.1146/annurev.micro.60.080805.142149.

Paronetto, M. P., Miele, R., Maugliani, a, Borro, M., & Bonaccorsi di Patti, M. C. (2001). Cloning of Pichia pastoris Fet3: insights into the high affinity iron uptake system. Archives of Biochemistry and Biophysics, 392(1), 162–167. https://doi.org/10.1006/abbi.2001.2425.

Patzer, S. I., & Hantke, K. (2001). Dual repression by Fe^{2+}-Fur and Mn^{2+}-MntR of the mntH gene, encoding an NRAMP-like Mn^{2+} transporter in Escherichia coli. Journal of Bacteriology, 183(16), 4806–4813. https://doi.org/10.1128/JB.183.16.4806-4813.2001.

Pecqueur, L., D'autreaux, B., Dupuy, J., Nicolet, Y., Jacquamet, L., Brutscher, B., Michaud-Soret, I. & Bersch, B. 2006. Structural changes of Escherichia coli ferric uptake regulator during metal-dependent dimerization and activation explored by NMR and X-ray crystallography. J Biol Chem, 281, 21286-95.

Peng, E. D., Wyckoff, E. E., Mey, A. R., Fisher, C. R. & Payne, S. M. 2016. Nonredundant Roles of Iron Acquisition Systems in Vibrio cholerae. Infect Immun, 84, 511-23.

Pengelley, S.C., Chapman, D.C., Abbott, W.M., Lin, H.H., Huang, W., Dalton, K. and Jones, I.M., 2006. A suite of parallel vectors for baculovirus expression. Protein Expression and Purification, 48(2), pp.173-181.

Perez, A., Morrone, J.A., Simmerling, C. and Dill, K.A., 2016. Advances in free-energy-based simulations of protein folding and ligand binding. Current Opinion in Structural Biology, 36, pp.25-31.

Perry, R. D. & Brubaker, R. R. 1979. Accumulation of iron by yersiniae. J Bacteriol, 137, 1290-8.

Perry, R. D., Mier, I., & Fetherston, J. D. (2007). Roles of the Yfe and Feo transporters of Yersinia pestis in iron uptake and intracellular growth. BioMetals, 20(3–4), 699–703. https://doi.org/10.1007/s10534-006-9051-x.

Perry, R.J. and Ridgway, N.D., 2006. Oxysterol-binding protein and vesicle-associated membrane protein–associated protein are required for sterol-dependent activation of the ceramide transport protein. Molecular Biology of the Cell, 17(6), pp.2604-2616.

Petermann, I., Huebner, C., Browning, B.L., Gearry, R.B., Barclay, M.L., Kennedy, M., Roberts, R., Shelling, A.N., Philpott, M., Han, D.Y. and Ferguson, L.R., 2009. Interactions among genes influencing bacterial recognition increase IBD risk in a population-based New Zealand cohort. Human Immunology, 70(6), pp.440-446.

Peti, W. and Page, R., 2007. Strategies to maximize heterologous protein expression in Escherichia coli with minimal cost. Protein Expression and Purification, 51(1), pp.1-10.

Pohorille, A., Schweighofer, K. and Wilson, M.A., 2005. The origin and early evolution of membrane channels. Astrobiology, 5(1), pp.1-17.

Pomposiello, P. J. & Demple, B. 2001. Redox-operated genetic switches: the SoxR and OxyR transcription factors. Trends Biotechnol, 19, 109-14.

Porcheron, G., Garénaux, A., Proulx, J., Sabri, M. and Dozois, C.M., 2013. Iron, copper, zinc, and manganese transport and regulation in pathogenic Enterobacteria: correlations between strains, site of infection and the relative importance of the different metal transport systems for virulence. Frontiers in Cellular and Infection Microbiology, 3, p.90.

Porto, G. and De Sousa, M., 2007. Iron overload and immunity. World Journal of Gastroenterology: WJG, 13(35), p.4707.

Posey, J. E., & Gherardini, F. C. (2000). Lack of a role for iron in the Lyme disease pathogen. Science, 288(5471), 1651–1653. https://doi.org/10.1126/science.288.5471.1651.

Postle, K., & Larsen, R. A. (2007). TonB-dependent energy transduction between outer and cytoplasmic membranes. Biometals, 20(3-4), 453-465. doi: 10.1007/s10534-006-9071-6.

Privé, G.G., 2007. Detergents for the stabilization and crystallization of membrane proteins. Methods, 41(4), pp.388-397.

Rajasekaran, M. B., Nilapwar, S., Andrews, S. C., & Watson, K. A. (2010). EfeO-cupredoxins: Major new members of the cupredoxin superfamily with roles in bacterial iron transport. BioMetals, 23(1), 1–17. https://doi.org/10.1007/s10534-009-9262-z.

Raphael, B. H., & Joens, L. a. (2003). FeoB is not required for ferrous iron uptake in Campylobacter jejuni. Canadian Journal of Microbiology, 49(11), 727–731. https://doi.org/10.1139/w03-086.

Rath, A., Glibowicka, M., Nadeau, V.G., Chen, G. and Deber, C.M., 2009. Detergent binding explains anomalous SDS-PAGE migration of membrane proteins. Proceedings of the National Academy of Sciences, 106(6), pp.1760-1765.

Ratledge, C., & Dover, L. G. (2000). Iron metabolism in pathogenic bacteria. Annu Rev Microbiol, 54, 881-941. doi: 10.1146/annurev.micro.54.1.881.

Rawlings, A.E., 2016. Membrane proteins: always an insoluble problem? Biochemical Society Transactions, 44(3), pp.790-795.

Raymond, K.N. and Dertz, E.A., 2004. Biochemical and physical properties of siderophores. Iron transport in bacteria. ASM Press, Washington, DC, pp.3-17.

Reigstad, C.S., Hultgren, S.J. and Gordon, J.I., 2007. Functional genomic studies of uropathogenic Escherichia coli and host urothelial cells when intracellular bacterial communities are assembled. Journal of Biological Chemistry, 282(29), pp.21259-21267.Rhodobacter sphaeroides. Environmental Microbiology Reports, 11(2), 118-128.

Rigaud, J.L. and Lévy, D., 2003. Reconstitution of membrane proteins into liposomes. In Methods in Enzymology (Vol. 372, pp. 65-86). Academic Press.

Robey, M., & Cianciotto, N. P. (2002). Legionella pneumophila feoAB promotes ferrous iron uptake and intracellular infection. Infection and Immunity, 70(10), 5659–5669. https://doi.org/10.1128/IAI.70.10.5659-5669.2002.

Rosen, C.A., 1992. HIV regulatory proteins: potential targets for therapeutic intervention. AIDS Research and Human Retroviruses, 8(2), pp.175-181.

Rosen, R., Sacher, A., Shechter, N., Becher, D., Büttner, K., Biran, D., Hecker, M. and Ron, E.Z., 2004. Two-dimensional reference map of Agrobacterium tumefaciens proteins. Proteomics, 4(4), pp.1061-1073.

Rossi M., Fetherston J., Letoffe S., Carniel E., Perry R., and Ghigo J., (2001): Identification and characterization of the hemophore-dependent heme acquisition system of Yersinia pestis. Infection and Immunity, 69 (11): 6707-6717.

Runyen-Janecky, L. J., Reeves, S. A., Gonzales, E. G., & Payne, S. M. (2003). Contribution of the Shigella flexneri sit, iuc, and feo iron acquisition systems to iron acquisition in vitro and in cultured cells. Infection and Immunity, 71(4), 1919–1928. https://doi.org/10.1128/IAI.71.4.1919-1928.2003.

Russell, J.B., Diez-Gonzalez, F. and Jarvis, G.N., 2000. Potential effect of cattle diets on the transmission of pathogenic Escherichia coli to humans. Microbes and Infection, 2(1), pp.45-53.

Rzymski, P. & Ganz, T. 2018. Comment on "Serum Hepcidin and Soluble Transferrin Receptor in the Assessment of Iron Metabolism in Children on a Vegetarian Diet". Biol Trace Elem Res, 185, 252-254.

Sabri, M., Caza, M., Proulx, J., Lymberopoulos, M. H., Brée, A., Moulin-Schouleur, M., Dozois, C. M. (2008). Contribution of the SitABCD, MntH, and FeoB metal transporters to the virulence of avian pathogenic Escherichia coli O78 strain ??7122. Infection and Immunity, 76(2), 601–611. https://doi.org/10.1128/IAI.00789-07.

Sambrook J., (1989): Molecular Cloning; A Laboratory Manual (3rd Edition). Cold Spring Harbor Laboratory Press. New York.

Sambrook J., Fritsch F., and Maniatis T. (2001): Molecular cloning; A Laboratory Manual, Cold Spring Harbor Laboratory Press. New York.

Sastry, A. V., Gao, Y., Szubin, R., Hefner, Y., Xu, S., Kim, D., ... & Palsson, B. O. (2019). The Escherichia coli Transcriptome Consists of Independently Regulated Modules. bioRxiv, 620799.

Schaible, U. E., & Kaufmann, S. H. (2004). Iron and microbial infection. Nat. Rev. Microbiol., 2(1740–1526 (Print)), 946–953. https://doi.org/10.1038/nrmicro1116.

Seaver, L. C. & Imlay, J. A. 2001. Hydrogen peroxide fluxes and compartmentalization inside growing Escherichia coli. J Bacteriol, 183, 7182-9.

Seaver, L.C. and Imlay, J.A., 2004. Are respiratory enzymes the primary sources of intracellular hydrogen peroxide? Journal of Biological Chemistry, 279(47), pp.48742-48750.

Seddon, A.M., Curnow, P. and Booth, P.J., 2004. Membrane proteins, lipids and detergents: not just a soap opera. Biochimica et Biophysica Acta (BBA)-Biomembranes, 1666(1-2), pp.105-117.

Seo, S. W., Kim, D., Latif, H., O'brien, E. J., Szubin, R. & Palsson, B. O. 2014. Deciphering Fur transcriptional regulatory network highlights its complex role beyond iron metabolism in Escherichia coli. Nat Commun, 5, 4910.

Sestok, A. E., Linkous, R. O. & Smith, A. T. 2018. Toward a mechanistic understanding of Feo-mediated ferrous iron uptake. Metallomics, 10, 887-898.

Severance, S., Chakraborty, S. & Kosman, D. J. 2004. The Ftr1p iron permease in the yeast plasma membrane: orientation, topology and structure-function relationships. Biochem J, 380, 487-96.

Seyedmohammad, S., Born, D. and Venter, H., 2014. Expression, purification and functional reconstitution of FeoB, the ferrous iron transporter from Pseudomonas aeruginosa. Protein Expression and Purification, 101, pp.138-145.

Seyedmohammad, S., Fuentealba, N.A., Marriott, R.A., Goetze, T.A., Edwardson, J.M., Barrera, N.P. and Venter, H., 2016. Structural model of FeoB, the iron transporter from Pseudomonas aeruginosa, predicts a cysteine lined, GTP-gated pore. Bioscience Reports, 36(2), p.e00322.

Sherwood, R.A., Pippard, M.J. and Peters, T.J., 1998. Iron homeostasis and the assessment of iron status. Annals of Clinical Biochemistry, 35(6), pp.693-708.

Shortland, G.J. and Losty, H.C., 1997. Galactosaemia. Current Paediatrics, 7(2), pp.135-138.

Shultis, D.D., Purdy, M.D., Banchs, C.N. and Wiener, M.C., 2006. Outer membrane active transport: structure of the BtuB: TonB complex. Science, 312(5778), pp.1396-1399.

Singh, A., Severance, S., Kaur, N., Wiltsie, W. & Kosman, D. J. 2006. Assembly, activation, and trafficking of the Fet3p.Ftr1p high affinity iron permease complex in Saccharomyces cerevisiae. J Biol Chem, 281, 13355-64.

Siu, K.K., Sultana, A., Azimi, F.C. and Lee, J.E., 2013. Structural determinants of HIV-1 Vif susceptibility and DNA binding in APOBEC3F. Nature Communications, 4, p.2593.

Sjöstrand, D., Diamanti, R., Lundgren, C.A., Wiseman, B. and Högbom, M., 2017. A rapid expression and purification condition screening protocol for membrane protein structural biology. Protein Science, 26(8), pp.1653-1666.

Sjuts, H., Schreuder, H., Engel, C.K., Bussemer, T. and Gokarn, Y., 2019. Matching pH values for antibody stabilization and crystallization suggest rationale for accelerated development of biotherapeutic drugs. Drug Development Research. 1-9.

Skaar, E. P. 2010. The battle for iron between bacterial pathogens and their vertebrate hosts. PLoS Pathog, 6, e1000949.

Skamene, E., Schurr, E. & Gros, P. 1998. Infection genomics: Nramp1 as a major determinant of natural resistance to intracellular infections. Annu Rev Med, 49, 275-87.

Smagghe, B.J., Hoy, J.A., Percifield, R., Kundu, S., Hargrove, M.S., Sarath, G., Hilbert, J.L., Watts, R.A., Dennis, E.S., Peacock, W.J. and Dewilde, S., 2009. Correlations between oxygen affinity and sequence classifications of plant hemoglobins. Biopolymers: Original Research on Biomolecules, 91(12), pp.1083-1096.

Small, S. K., & O'Brian, M. R. (2011). The Bradyrhizobium japonicum frcB gene encodes a diheme ferric reductase. Journal of Bacteriology, 193(16), 4088-4094.

Smith, A., Hooper, N. I., Shipulina, N. & Morgan, W. T. 1996. Heme binding by a bacterial repressor protein, the gene product of the ferric uptake regulation (fur) gene of Escherichia coli. J Protein Chem, 15, 575-83.

Smith, A.T. and Sestok, A.E., 2018. Expression and purification of functionally active ferrous iron transporter FeoB from Klebsiella pneumoniae. Protein expression and purification, 142, pp.1-7.

Smith, M. A., & Bidochka, M. J. (1998). Bacterial fitness and plasmid loss: the importance of culture conditions and plasmid size. Canadian Journal of Microbiology, 44(4), 351–355. https://doi.org/10.1139/w98-020.

Spiro, S., & Guest, J. R. (1990). FNR and its role in oxygen-regulated gene expression in Escherichia coli. FEMS Microbiology Reviews, 6(4), 399–428. https://doi.org/http://dx.doi.org/10.1016/0378-1097(90)90690-R.

Sprang, S. R. 1997. G protein mechanisms: insights from structural analysis. Annu Rev Biochem, 66, 639-78.

Sprang, S. R. 2000. Conformational display: a role for switch polymorphism in the superfamily of regulatory GTPases. Sci STKE, 2000, pe1.

Sriram, N., Kalayarasan, S., Ashokkumar, P., Sureshkumar, A. and Sudhandiran, G., 2008. Diallyl sulfide induces apoptosis in Colo 320 DM human colon cancer cells: involvement of caspase-3, NF-κB, and ERK-2. Molecular and Cellular Biochemistry, 311(1-2), p.157.

Stetsenko, A. and Guskov, A., 2017. An overview of the top ten detergents used for membrane protein crystallization. Crystals, 7(7), p.197.

Stevenson, B., Wyckoff, E.E. and Payne, S.M., 2016. Vibrio cholerae FeoA, FeoB, and FeoC interact to form a complex. Journal of Bacteriology, 198(7), pp.1160-1170.

Stojiljkovic, I. & Hantke, K. 1992. Hemin uptake system of Yersinia enterocolitica: similarities with other TonB-dependent systems in gram-negative bacteria. EMBO J, 11, 4359-67.

Stojiljkovic, I., Cobeljic, M., & Hantke, K. (1993). Escherichia coli K-12 ferrous iron uptake mutants are impaired in their ability to colonize the mouse intestine. FEMS Microbiology Letters, 108(1), 111–115. https://doi.org/10.1111/j.1574-6968.1993.tb06082.x.

Storz, G., Christman, M.F., Sies, H. and Ames, B.N., 1987. Spontaneous mutagenesis and oxidative damage to DNA in Salmonella typhimurium. Proceedings of the National Academy of Sciences, 84(24), pp.8917-8921.

Storz, G., Tartaglia, L.A. and Ames, B.N., 1990. The oxyR regulon. Antonie Van Leeuwenhoek, 58(3), pp.157-161.

Storz, G. & Altuvia, S. 1994. OxyR regulon. Methods Enzymol, 234, 217-23.

Sturm, A., Schierhorn, A., Lindenstrauss, U., Lilie, H., & Brüser, T. (2006). YcdB from Escherichia coli reveals a novel class of Tat-dependently translocated hemoproteins. Journal of Biological Chemistry, 281(20), 13972–13978. https://doi.org/10.1074/jbc.M511891200.

Su Y., Chin K., Hung H., et al (2010): Structure of Stenotrophomonas maltophila FeoA complexed with zink: unique prokaryotic SH3-domain protein that possibly acts a bacterial ferrous iron-transport activating factor. Acta Crystallographica Section F, 66: 636–642.

Swaffield, J.C. and Purugganan, M.D., 1997. The evolution of the conserved ATPase domain (CAD): reconstructing the history of an ancient protein module. Journal of Molecular Evolution, 45(5), pp.549-563.

Takeshita, S., Sato, M., Toba, M., Masahashi, W., & Hashimoto-Gotoh, T. (1987). High-copy-number and low-copy-number plasmid vectors for lacZ??-complementation and chloramphenicol- or kanamycin-resistance selection. Gene, 61(1), 63–74. https://doi.org/10.1016/0378-1119(87)90365-9.

Takeyasu, K., Omote, H., Nettikadan, S., Tokumasu, F., Iwamoto-Kihara, A. and Futai, M., 1996. Molecular imaging of Escherichia coli F0F1-ATPase in reconstituted membranes using atomic force microscopy. FEBS letters, 392(2), pp.110-113.

Tartaglia, L. A., Storz, G. & Ames, B. N. 1989. Identification and molecular analysis of oxyR-regulated promoters important for the bacterial adaptation to oxidative stress. J Mol Biol, 210, 709-19.

Thompson, B.M., Binkley, J.M. and Stewart, G.C., 2011. Current physical and SDS extraction methods do not efficiently remove exosporium proteins from Bacillus anthracis spores. Journal of Microbiological Methods, 85(2), pp.143-148.

Tomoyasu, T., 1992. Development of the immunomagnetic enrichment method selective for Vibrio parahaemolyticus serotype K and its application to food poisoning study. Appl. Environ. Microbiol., 58(8), pp.2679-2682.

Tomoyasu, T., Yuki, T., Morimura, S., Mori, H., Yamanaka, K., Niki, H., Hiraga, S. and Ogura, T., 1993. The Escherichia coli FtsH protein is a prokaryotic member of a protein family of putative ATPases involved in membrane functions, cell cycle control, and gene expression. Journal of Bacteriology, 175(5), pp.1344-1351.

Tong, Y. and Guo, M., 2009. Bacterial heme-transport proteins and their heme-coordination modes. Archives of Biochemistry and Biophysics, 481(1), pp.1-15.

Torres AG, Redford P, Welch RA, Payne SM. 2001. TonB-dependent systems of uropathogenic Escherichia coli: aerobactin and heme transport and TonB are required for virulence in the mouse. Infection and immunity 69: 6179-85.

Torres, A. G., & Payne, S. M. (1997). Haem iron-transport system in enterohaemorrhagic Escherichia coli O157:H7. Mol Microbiol, 23(4), 825-833.

Touati, D. 2000. Iron and oxidative stress in bacteria. Arch Biochem Biophys, 373, 1-6.

Tsaneva, I. R. & Weiss, B. 1990. soxR, a locus governing a superoxide response regulon in Escherichia coli K-12. J Bacteriol, 172, 4197-205.

Tsolis, R. M., Bäumler, A. J., Heffron, F., & Stojiljkovic, I. (1996). Contribution of TonB- and Feo-mediated iron uptake to growth of Salmonella typhimurium in the mouse. Infection and Immunity, 64(11), 4549–4556.

Tulumello, D.V. and Deber, C.M., 2012. Efficiency of detergents at maintaining membrane protein structures in their biologically relevant forms. Biochimica et Biophysica Acta (BBA)-Biomembranes, 1818(5), pp.1351-1358.

Valdez, Y., Diehl, G. E., Vallance, B. A., Grassl, G. A., Guttman, J. A., Brown, N. F., Rosenberger, C. M., Littman, D. R., Gros, P. & Finlay, B. B. 2008. Nramp1 expression by dendritic cells modulates inflammatory responses during Salmonella Typhimurium infection. Cell Microbiol, 10, 1646-61.

Van Vliet, A. H., Ketley, J. M., Park, S. F. & Penn, C. W. 2002. The role of iron in Campylobacter gene regulation, metabolism and oxidative stress defense. FEMS Microbiol Rev, 26, 173-86.

Van Ho, A., Ward, D.M. and Kaplan, J., 2002. Transition metal transport in yeast. *Annual* Reviews in Microbiology, 56(1), pp.237-261.

Vasil, M. L. & Ochsner, U. A. 1999. The response of Pseudomonas aeruginosa to iron: genetics, biochemistry and virulence. Mol Microbiol, 34, 399-413.

Vedadi, M., Arrowsmith, C.H., Allali-Hassani, A., Senisterra, G. and Wasney, G.A., 2010. Biophysical characterization of recombinant proteins: a key to higher structural genomics success. Journal of Structural Biology, 172(1), pp.107-119.

Velayudhan, J., Hughes, N. J., McColm, A. A., Bagshaw, J., Clayton, C. L., Andrews, S. C., & Kelly, D. J. (2000). Iron acquisition and virulence in Helicobacter pylori: A major role for FeoB, a high-affinity ferrous iron transporter. Molecular Microbiology, 37(2), 274–286. https://doi.org/10.1046/j.1365-2958.2000.01987.x.

Von Heijne, G., 2006. Membrane-protein topology. Nature Reviews Molecular Cell Biology, 7(12), p.909.

Waldo, G.S., Standish, B.M., Berendzen, J. and Terwilliger, T.C., 1999. Rapid protein-folding assay using green fluorescent protein. Nature Biotechnology, 17(7), p.691.

Walker, J.E., Saraste, M., Runswick, M.J. and Gay, N.J., 1982. Distantly related sequences in the alpha-and beta-subunits of ATP synthase, myosin, kinases and other ATP-requiring enzymes and a common nucleotide binding fold. The EMBO journal, 1(8), pp.945-951.

Wandersman, C., & Stojiljkovic, I. (2000). Bacterial heme sources: the role of heme, hemoprotein receptors and hemophores. Curr Opin Microbiol, 3(2), 215-220.

Wang, W., Liu, X., Jiang, S., Wu, Y., Zhang, C., Liu, C., Rehman, U. and Mehmood, K., 2018. Influence of Iron Content on Microstructure and Magnetic Properties of SrLaCa n (FeO) Co. Journal of Superconductivity & Novel Magnetism, 31(1).

Wardrop, S.L. and Richardson, D.R., 1999. The effect of intracellular iron concentration and nitrogen monoxide on Nramp2 expression and non-transferrin-bound iron uptake. European Journal of Biochemistry, 263(1), pp.41-50.

Weaver, E. A., Wyckoff, E. E., Mey, A. R., Morrison, R., & Payne, S. M. (2013). FeoA and FeoC are essential components of the Vibrio cholerae ferrous iron uptake system, and FeoC interacts with FeoB. Journal of Bacteriology, 195(21), 4826–4835. https://doi.org/10.1128/JB.00738-13.

Wei, Y., & Murphy, E. R. (2016). Iron acquisition systems and their regulation. Frontiers in Cellular and Infection Microbiology, 6(February), 18. https://doi.org/10.3389/fcimb.2016.00018.

Weinberg, E. D. (1997). The Lactobacillus anomaly: total iron abstinence. Perspectives in Biology and Medicine, 40(4), 578-583.

Weinberg, E. D. 1978. Iron and infection. Microbiol Rev, 42, 45-66.

Weinstein, D. L., Holmes, R. K. & O'brien, A. D. 1988. Effects of iron and temperature on Shiga-like toxin I production by Escherichia coli. Infect Immun, 56, 106-11.

Weitl, F. L., Harris, W. R., & Raymond, K. N. (1979). Sulfonated catecholamide analogues of enterobactin as iron sequestering agents. J Med Chem, 22(11), 1281-1283.

White, I.M. and Fan, X., 2008. On the performance quantification of resonant refractive index sensors. Optics Express, 16(2), pp.1020-1028.

Woodman, A. G., Mah, R., Keddie, D., Noble, R. M. N., Panahi, S., Gragasin, F. S., Lemieux, H. & Bourque, S. L. 2018. Prenatal iron deficiency causes sex-dependent mitochondrial dysfunction and oxidative stress in fetal rat kidneys and liver. FASEB J, 32, 3254-3263.

Woodmansee, A. N., & Imlay, J. A. (2002). Reduced flavins promote oxidative DNA damage in non-respiring Escherichia coli by delivering electrons to intracellular free iron. Journal of Biological Chemistry, 277(37), 34055–34066. https://doi.org/10.1074/jbc.M203977200.

Wooldridge, K. G., & Van Vliet, A. H. (2005). Iron transport and regulation. Campylobacter molecular and cellular biology. Horizon Bioscience, Wymondham, United Kingdom, 293-310.

Wooldridge, K. G., & Williams, P. H. (1993). Iron uptake mechanisms of pathogenic bacteria. FEMS Microbiol Rev, 12(4), 325-348.

Wright, K.J., Seed, P.C. and Hultgren, S.J., 2007. Development of intracellular bacterial communities of uropathogenic Escherichia coli depends on type 1 pili. Cellular Microbiology, 9(9), pp.2230-2241.

Wu, J. and Weiss, B.E.R.N.A.R.D., 1992. Two-stage induction of the soxRS (superoxide response) regulon of Escherichia coli. Journal of Bacteriology, 174(12), pp.3915-3920.

Wyckoff, E. E., Mey, A. R., Leimbach, A., Fisher, C. F., & Payne, S. M. (2006). Characterization of ferric and ferrous iron transport systems in Vibrio cholerae. Journal of Bacteriology, 188(18), 6515–6523. https://doi.org/10.1128/JB.00626-06.

Yamamoto, K., Ishihama, A., Busby, S. J. & Grainger, D. C. 2011. The Escherichia coli K-12 MntR miniregulon includes dps, which encodes the major stationary-phase DNA-binding protein. J Bacteriol, 193, 1477-80.

Yeh, A.P., McMillan, A. and Stowell, M.H., 2006. Rapid and simple protein-stability screens: application to membrane proteins. Acta Crystallographica Section D: Biological Crystallography, 62(4), pp.451-457.

Yildirim, A.O., Bulau, P., Zakrzewicz, D., Kitowska, K.E., Weissmann, N., Grimminger, F., Morty, R.E. and Eickelberg, O., 2006. Increased protein arginine methylation in chronic hypoxia: role of protein arginine methyltransferases. American Journal of Respiratory Cell and Molecular Biology, 35(4), pp.436-443.

Yue, W.W., Grizot, S. and Buchanan, S.K., 2003. Structural evidence for iron-free citrate and ferric citrate binding to the TonB-dependent outer membrane transporter FecA. Journal of Molecular Biology, 332(2), pp.353-368.

Zellmeier, S., Zuber, U., Schumann, W. and Wiegert, T., 2003. The absence of FtsH metalloprotease activity causes overexpression of the σW-controlled pbpE gene, resulting in filamentous growth of Bacillus subtilis. Journal of Bacteriology, 185(3), pp.973-982.

Zhang, C., Xin, Y., Wang, Y., Guo, T., Lu, S., & Kong, J. (2015). Identification of a novel dye-decolorizing peroxidase, efeB, translocated by a twin-arginine translocation system in streptococcus thermophilus CGMCC 7.179. Applied and Environmental Microbiology, 81(18), 6108–6119. https://doi.org/10.1128/AEM.01300-15.

Zhao, Y., Ge, W., Kong, Y. and Zhang, C., 2003. Cloning, expression, and renaturation studies of reteplase. Journal of Microbiology and Biotechnology, 13(6), pp.989-992.

Zhao, Z., Peng, T., Oh, J.I., Glaeser, J., Weber, L., Li, Q. and Klug, G., 2019. A response regulator of the OmpR family is part of the regulatory network controlling the oxidative stress response of Rhodobacter sphaeroides. Environmental Microbiology Reports, 11(2), pp.118-128.

Zheng, G., Chen, J. and Zheng, W., 2012. Relative contribution of CTR1 and DMT1 in copper transport by the blood–CSF barrier: Implication in manganese-induced neurotoxicity. Toxicology and Applied Pharmacology, 260(3), pp.285-293.

Zheng, H., Wang, S., Qiao, X. & Feng, G. 2001. [A simple and reliable spectrophotometric method for quantification of pyridine nucleotides in serum]. Sheng Wu Yi Xue Gong Cheng Xue Za Zhi, 18, 412-5.

Zheng, M., Aslund, F. & Storz, G. 1998. Activation of the OxyR transcription factor by reversible disulfide bond formation. Science, 279, 1718-21.

Zheng, W., & Monnot, A. D. (2012). Regulation of brain iron and copper homeostasis by brain barrier systems: implication in neurodegenerative diseases. Pharmacology & Therapeutics, 133(2), 177-188.

Zucker, F.H., Stewart, C., dela Rosa, J., Kim, J., Zhang, L., Xiao, L., Ross, J., Napuli, A.J., Mueller, N., Castaneda, L.J. and Hewitt, S.R.N., 2010. Prediction of protein crystallization outcome using a hybrid method. Journal of Structural Biology, 171(1), pp.64-73.

Zughaier, S. M. & Cornelis, P. 2018. Editorial: Role of Iron in Bacterial Pathogenesis. Front Cell Infect Microbiol, 8, 344.

Zughaier, S. M., Kandler, J. L. & Shafer, W. M. 2014. Neisseria gonorrhoeae modulates iron-limiting innate immune defenses in macrophages. PLoS One, 9, e87688.

Zwilling, B. S., Kuhn, D. E., Wikoff, L., Brown, D. & Lafuse, W. 1999. Role of iron in Nramp1-mediated inhibition of mycobacterial growth. Infect Immunol, 67, 1386-92.